Satya Prakash Gupta *Editor*

Ion Channels and Their Inhibitors

Springer

Ion Channels and Their Inhibitors

Satya Prakash Gupta
Editor

Ion Channels and Their Inhibitors

Springer

Editor
Prof. Satya Prakash Gupta
Department of Applied Sciences
Meerut Institute of Engineering and Technology
Meerut 250005
India
spgbits@gmail.com

ISBN 978-3-642-19921-9 e-ISBN 978-3-642-19922-6
DOI 10.1007/978-3-642-19922-6
Springer Heidelberg Dordrecht London New York

Library of Congress Control Number: 2011931782

Cover design: eStudio Calamar S.L.

Printed on acid-free paper

Springer is part of Springer Science+Business Media (www.springer.com)

Preface

As is well known, ion channels are crucial components of living cells. The physiological function of ion channels had been observed long before they were known to exist. They figure in a wide variety of biological processes that involve changes in cells, such as cardiac, skeletal, and smooth muscle contraction, epithelial transport of nutrients and ions, T-cell activation, and pancreatic β-cell insulin release. Thus being the crucial components of living cells, ion channels are important targets of therapeutic agents. Historically, it has been challenging to develop drugs on this target class. A major issue with target-based ion channel drug development is identification of good small chemical leads for medicinal chemistry optimization to clinical candidate status. Thus, enough attention has been paid to the study of structure and functions of ion channels and their potential inhibitors. The present book compiles a few important articles authored by eminent workers in the field to cover some recent advances in the studies on the structure and functions of some ion channels, e.g., Na^+, K^+, Ca^{2+}, Cl^-, and their inhibitors. The book may be of great use to the students and scientists working in the area of molecular biology, biochemistry, physiology, and neurobiology.

The book contains 11 articles in total. Ion channels, in fact, are transmembrane proteins that selectively allow a given species of ion to pass through them. In Chap. 1 entitled *Structural and Functional Discrimination of Membrane Proteins*, Gromiha et al. discuss all aspects of these membrane proteins right from their structural discrimination to resulting functional discrimination and drug–target interactions. In Chap. 2, Bois et al. present the pharmacology of hyperpolarization-activated cyclic nucleotide-gated (HCN) channels. HCN channels generate and/or regulate neuronal and cardiac excitability. Several physiological roles have been ascribed to HCN channels which are the consequence of their particular biophysical properties. In Chap. 3 entitled *Advanced Molecular Modeling Techniques Applied to Ion Channels Blockers*, Hannongbua et al. describe some important advanced molecular modeling techniques used to design and develop the potent ion channel blockers. These techniques include 2D-, 3D-, and 4D-QSARs, ADMET prediction, molecular dynamics simulations, molecular docking, quantum chemical

calculations, and QM/MM calculations. These techniques have been widely applied to the drug design.

Of the various ion channels, sodium ion channels have been of great significance. An article on this with the title *Advances in Design and Development of Sodium Channel Blockers* has been exclusively written by Zuliani et al. to describe briefly the recent advances in the development of isoform-specific and state-selective sodium channel blockers and the medicinal chemistry involved, surveying the emerging therapeutic fields. Abnormal activity of sodium channels is related to several pathological processes, including cardiac arrhythmias, epilepsy, chronic pain, neurodegenerative diseases, and spasticity.

The potassium ion channels play no less important role in the human body. They constitute the important target for the development of antiarrhythmic agents. Therefore, in Chap. 5, You et al. have presented the development of potassium channel blockers as antiarrhythmic agents. Although there are a variety of potassium channels, scientists have developed immense interest in human *ether-a-go-go*-related gene (*hERG*) potassium channels due to their involvement in life-threatening cardiac arrhythmia. Therefore, an article on *hERG* channels has been presented by Singh and Sharma to describe their functions and dysfunctions, therapeutic agents modulating these channels, and associated QT prolongation. In the next article, Schiesaro and Ecker describe structure- and ligand-based approaches to develop models which shed light on the molecular basis of hERG channel inhibition and present an overview on recent approaches for prediction of hERG channel blockers. In continuation to this, an article on *Advances in Structure–Activity Relationship Studies on Potassium Channel Modulators* has been contributed by Sharma et al., highlighting the mode of functions of potassium ion channel modulators.

Calcium ions are a ubiquitous second messenger and their entry into the cytosol is mediated by multiple types of calcium channels, each with a distinct physiological role. They constitute an important target to develop drugs against several cardiovascular and noncardiovascular diseases, such as angina, hypertension, arrhythmias, asthma, dysmenorrhea, premature labor, cancer, epilepsy, and glaucoma. In Chap. 9, therefore, Hadjipavlou-Litina presents a vivid description of calcium ion channels, their subtypes, and their blockers, with detailed structure–activity relationships of blockers. N-type voltage-gated Ca^{2+} channels (NCCs) play dominant roles in neuropathic pain and cerebral ischemia. An article on this type of calcium ion channels, therefore, has been presented by Gopi Mohan et al. to mainly focus on their blockers and the pharmaceutical importance thereof.

Chloride ion channels have been found to play crucial roles in the development of human diseases, e.g., mutations in the genes encoding Cl^- channels lead to a variety of deleterious diseases in muscle, kidney, bone, and brain, including myotonia congenita, dystrophia myotonica, cystic fibrosis, osteopetrosis, and epilepsy, and similarly their activation is supposed to be responsible for the progression of glioma in the brain and the growth of malaria parasite in the red blood cells. Thus, the study of the structure, function, and blockers of Cl^- channels seems to be of great importance. The last article entitled *Chloride Ion Channels: Structure,*

Functions and Inhibitors, therefore, has been written by Gupta and Kaur to describe all important classes of Cl^- channels with a detail of their structures, functions, and inhibitors.

Thus, an attempt has been made to make the book an interesting reading by selecting the articles of varying taste for all those involved in research on ion channels and their blockers. As an editor of this book, I have greatly enjoyed reading all the articles and hope so will do all the readers. I gratefully acknowledge the enthusiasm of all the authors for contributing the excellent articles in this book.

Meerut, Uttar Pradesh, India Satya P. Gupta
June 2011

Contents

Contributors

Laura Amori Dipartimento Farmaceutico, Università degli Studi di Parma, V.le G.P. Usberti, 27/A, 43124 Parma, Italy, laura.amori@unipr.it

Jocelyn Bescond Institut de Physiologie et Biologie Cellulaires, UMR CNRS n°6187/Université de Poitiers, Bât B36, Pôle Biologie Santé, 1 rue Georges Bonnet, BP 633, 86022 Poitiers, France

Patrick Bois Institut de Physiologie et Biologie Cellulaires, UMR CNRS n°6187/ Université de Poitiers, Bât B36, Pôle Biologie Santé, 1 rue Georges Bonnet, BP 633, 86022 Poitiers, France, Patrick.Bois@univ-poitiers.fr

Warabhorn Boonyarat Department of Chemistry, Faculty of Science, Kasetsart University, Bangkok 10900, Thailand; Center of Nanotechnology, Kasetsart University, Bangkok 10900, Thailand

Aurelien Chatelier Institut de Physiologie et Biologie Cellulaires, UMR CNRS n°6187/Université de Poitiers, Bât B36, Pôle Biologie Santé, 1 rue Georges Bonnet, BP 633, 86022 Poitiers, France

Shu-An Chen Department of Computer Science and Engineering, Yuan Ze University, Chung-Li, Taiwan

Gerhard F. Ecker Pharmacoinformatics Research Group, Department of Medicinal Chemistry, University of Vienna, Althanstraße 14, 1090 Vienna, Austria, gerhard.f.ecker@univie.ac.at

Jean-François Faivre Institut de Physiologie et Biologie Cellulaires, UMR CNRS n°6187/Université de Poitiers, Bât B36, Pôle Biologie Santé, 1 rue Georges Bonnet, BP 633, 86022 Poitiers, France

M. Michael Gromiha Department of Biotechnology, Indian Institute of Technology (IIT) Madras, Chennai 600 036, Tamilnadu, India, gromiha@iitm.ac.in

Satya P. Gupta Department of Applied Sciences and Department of Pharmaceutical Technology, Meerut Institute of Engineering and Technology, Meerut 250005, India, spgbits@gmail.com

Dimitra Hadjipavlou-Litina Department of Pharmaceutical Chemistry, School of Pharmacy, Aristotle University of Thessaloniki, Thessaloniki 54124, Greece, hadjipav@pharm.auth.gr

Supa Hannongbua Department of Chemistry, Faculty of Science, Kasetsart University, Bangkok 10900, Thailand; Center of Nanotechnology, Kasetsart University, Bangkok 10900, Thailand, fscisph@ku.ac.th

Preet K. Kaur Department of Pharmaceutical Technology, Meerut Institute of Engineering and Technology, Meerut 250005, India

C. Gopi Mohan Department of Pharmacoinformatics, National Institute of Pharmaceutical Education and Research, Sector 67, S.A.S. Nagar 160 062 Punjab, India, cmohan@niper.ac.in, cgopimohan@yahoo.com

Jignesh Mungalpara Natural Products and Medicinal Chemistry Research Group, Department of Pharmacy, Faculty of Health Sciences, University of Tromsø, Tromsø, Norway

Yu-Yen Ou Department of Computer Science and Engineering, Yuan Ze University, Chung-Li, Taiwan

Ashish Pandey Department of Pharmacoinformatics, National Institute of Pharmaceutical Education and Research, Sector 67, S.A.S. Nagar, 160 062 Punjab, India

Yenamandra S. Prabhakar Medicinal and Process Chemistry Division, Central Drug Research Institute, CSIR, Lucknow 226 001, India, yenpra@yahoo.com

Mirko Rivara Dipartimento Farmaceutico, Università degli Studi di Parma, V.le G.P. Usberti, 27/A, 43124 Parma, Italy, mirko.rivara@unipr.it

Andrea Schiesaro Pharmacoinformatics Research Group, Department of Medicinal Chemistry, University of Vienna, Althanstraße 14, 1090 Vienna, Austria

Brij K. Sharma Department of Chemistry, S. K. Government College, Sikar 332 001, India

Shyam S. Sharma Department of Pharmacology and Toxicology, National Institute of Pharmaceutical Education and Research (NIPER), Sector- 67, S.A.S. Nagar, Punjab, 160062, India, sssharma@niper.ac.in

Jitendra N. Singh Department of Pharmacology and Toxicology, National Institute of Pharmaceutical Education and Research (NIPER), Sector- 67, S.A.S. Nagar, Punjab 160062, India

Prithvi Singh Department of Chemistry, S. K. Government College, Sikar 332 001, India

Witcha Treesuwan Institute of Food Research and Product Development, Kasetsart University, Bangkok 10900, Thailand

Xiaojian Wang School of Pharmacy, China Pharmaceutical University, Nanjing 210009, China

Qian Yang School of Pharmacy, China Pharmaceutical University, Nanjing 210009, China

Qidong You School of Pharmacy, China Pharmaceutical University, Nanjing 210009, China

Valentina Zuliani Dipartimento Farmaceutico, Università degli Studi di Parma, V.le G.P. Usberti, 27/A, 43124 Parma, Italy, valentina.zuliani@unipr.it

Structural and Functional Discrimination of Membrane Proteins

M. Michael Gromiha, Yu-Yen Ou, and Shu-An Chen

Contents

Abstract Membrane proteins perform diverse functions inside the cell including transporters, receptors, and channels. Ion channels are integral membrane proteins that regulate the flow of ions across the membranes and are categorized as a part of membrane transport proteins. In this article, we briefly outline the structure and

M.M. Gromiha (✉)
Department of Biotechnology, Indian Institute of Technology (IIT) Madras, Chennai 600 036, Tamilnadu, India
e-mail: gromiha@iitm.ac.in

S.P. Gupta (ed.), *Ion Channels and Their Inhibitors*,
DOI 10.1007/978-3-642-19922-6_1,

function of membrane proteins and their classifications. On the structural point of view, we discuss the available databases and methods for discriminating α-helical and β-barrel membrane proteins from globular proteins. In addition, different algorithms developed for identifying the membrane spanning segments are discussed. On the functional aspect, the discrimination of transporters from other membrane proteins is mentioned. Further, classification of transporters into different groups such as channels/pores, electrochemical and active transporters, as well as their six families is illustrated. The specific features of channels compared with porins are discussed along with the discrimination of channels and pores and the classification of channels and drug targets for channel proteins. In addition, a list of online resources for the databases and classifications of membrane proteins based on their structure and function is provided.

Keywords Channel • Function • Membrane protein • Structure • Transporter

Abbreviations

DAS	Dense alignment surface
HMM	Hidden Markov model
OMP	Outer membrane protein
PDB	Protein Data Bank
PSSM	Position-specific scoring matrices
RBF	Radial basis function
TCDB	Transport Classification Database
TMB	Transmembrane β-barrel
TMH	Transmembrane helical
TMS	Transmembrane strand

1 Introduction

Membrane proteins, which require to be embedded into the lipid bilayers, have amino acid sequences that will fold with a hydrophobic surface in contact with the alkane chains of the lipids and polar surface in contact with the aqueous phases on both sides of the membrane and the polar head groups of the lipids. Membrane proteins have become attractive targets for pharmaceutical agents and about 20–30% of protein sequences in genomes are identified as membrane proteins. On the structural aspect, they are of two kinds (1) transmembrane helical (TMH) and (2) transmembrane strand (TMS or outer membrane or transmembrane β-barrel, TMB) proteins. TMH proteins span the cytoplasmic membrane with α-helices [1], whereas TMS proteins traverse the outer membranes of Gram-negative bacteria with β-strands [2].

On the functional point of view, membrane proteins perform a variety of functions, including the transport of ions and molecules across the membrane, bind to small molecules at the extracellular space, recognize the immune system, cell–cell signaling and energy transducers. Transporters are one of the major classes of membrane proteins that span the cell membrane and form an intricate system of pumps and channels through which they deliver essential nutrients, eject waste products, and assist the cell to sense environmental conditions. Transporters represent a diverse group of proteins that differ in membrane topology, energy coupling mechanism, and substrate specificities [3, 4]. Transporters are generally classified into channels/pores, electrochemical and active transporters along with other minor classes, group translocators, transport electron carriers, accessory factors involved in transport and incompletely characterized transport systems [5].

The classifications of membrane proteins based on their structure and function are important problems toward the advancement of structural and functional genomics. In this review, we focus on various discrimination algorithms developed for the classification of membrane proteins based on their structures, TMH and TMS proteins as well as their functions, especially different classes and families of transporters. In the first part, we discuss the features of transmembrane proteins, algorithms for discriminating TMH proteins and predicting their membrane spanning regions. Further, we mention the principles of β-barrel membrane proteins along with discrimination/prediction methods. In the second part, the characteristic features of amino acid residues in different classes and families of membrane transporters will be outlined and the discrimination methods for classifying channels, pores, electrochemical and active transporters will be presented. Further, the subclassification of ion channels and drug–target interactions will be discussed.

2 Databases for Membrane Proteins Based on Their Structures

The three-dimensional structures of proteins and their complexes are complied in Protein Data Bank (PDB) [6]. Based on the PDB, several other databases have been developed for different sets of proteins, and specifically for membrane proteins. Tusnady et al. [7] developed a database of transmembrane proteins, PDBTM, which includes the sequences and structures of redundant and nonredundant α-helical and β-barrel membrane proteins along with their membrane spanning segments. Jeyasinghe et al. [8] compiled the structures of known membrane proteins, MPtopo and classified them into several groups, such as monotopic, GPCRs, rhodopsins, and β-barrel membrane proteins. They have included the PDB codes, structures, and their respective references. Ikeda et al. [9] developed a database of transmembrane protein topologies, TMPDB, which is based on the experimental evidences from X-ray crystallography, NMR spectroscopy, etc. These databases provide additional information on nonredundant structures, options to search the database

Table 1 List of databases related with membrane protein structure and function

Name	URL
PDB, Protein Data Bank	http://www.rcsb.org/
MPtopo	http://blanco.biomol.uci.edu/mptopo
TMPDB	http://bioinfo.si.hirosaki-u.ac.jp/~TMPDB/
PDBTM	http://pdbtm.enzim.hu/
TMBETA-GENOME	http://tmbeta-genome.cbrc.jp/annotation/
OMPdb	http://bioinformatics.biol.uoa.gr/OMPdb
TCDB	http://www.tcdb.org/
Ion channels	http://www.ionchannels.org/
TMFunction	http://tmbeta-genome.cbrc.jp/TMFunction/

based on the secondary structures, number of membrane spanning segments and keywords. In Table 1, we list the databases for the structure and function of membrane proteins.

3 Structural Discrimination of Membrane Proteins

3.1 Transmembrane Helical Proteins: Features

The folding environment of TMH proteins differs from that of soluble globular proteins due to the presence of relatively long hydrophobic helical segments that traverse the membrane matrix, around which the interaction of water is almost absent. The TMH proteins generally follow specific rules as listed below (1) the length of membrane spanning helices is about 20–30 residues, corresponding to the width of the apolar part of the membrane, (2) globular regions between membrane helices are generally short, (3) they have a specific distribution of positive charged amino acid residues known as "positive-inside rule" [10], (4) loop regions inside the membrane have more positive charged residues than that on outside, and (5) long globular regions follow inside-out topology, which is defined by the orientation of the helices with respect to the lipid bilayer. If the upper part of the helix is located in the periplasm and the lower part is located in cytoplasm, then the topology is "out" [11].

3.2 Discrimination of TMH Proteins and Predicting Their Membrane Spanning Regions

The analysis of protein three-dimensional structures in PDB shows that only 2% of protein structures are membrane proteins. This urges the necessity of developing methods to predict the three-dimensional structures of membrane proteins to bridge the gap between the number of solved structures of membrane proteins and their

sequences. The first step to achieve this goal is the successful prediction of membrane spanning regions in TMH proteins. Accordingly, several methods have been proposed to identify TMH proteins and predict their membrane spanning regions. Most of the methods use amino acid properties and machine-learning methods have also been developed for prediction.

3.2.1 Statistical Methods

The statistical methods are mainly based on hydrophobicity profiles, physicochemical properties, conformational parameters, and the combination of them.

Kyte and Doolittle [12] developed a hydrophobicity profile method for locating the membrane spanning helical segments in amino acid sequences. To identify membrane regions, they implemented a moving-window approach in which the hydrophobicity indices of the amino acid residues have been summed over a stretch of residues and took the average. If the average hydrophobicity for a segment exceeds a threshold, the segment has been suggested as a transmembrane helix. Eisenberg et al. [13] developed the helical hydrophobic moment as a measure of the amphiphilicity of α helix. This hydrophobic moment differed between transmembrane, and globular helices, and could thus be explored to predict transmembrane regions [14]. Jayasinghe et al. [15] attempted to improve hydropathy analysis by directly improving the hydropathy scales. The commonly used hydrophobicity scales neglect the thermodynamic constraints α-helices impose on transmembrane stability, and hence they have derived a whole-residue hydropathy scale from the Wimley–White experiments that took into account the backbone constraints.

Ponnuswamy and Gromiha [16] developed a surrounding hydrophobicity scale applicable to both globular and membrane proteins and proposed a "surrounding hydrophobicity profile" method for predicting transmembrane helices from the amino acid sequence of a protein. This profile is simply the plot of the surrounding hydrophobicity indices of the residues against their sequence numbers. In this plot, the hydrophobic and hydrophilic parts are distinguished by a horizontal line representing the average hydrophobicity value, which is obtained from the surrounding hydrophobicity values for all the amino acid residues in the sample set of proteins. The surrounding hydrophobicity profile thus constructed projects the transmembrane helices as a sequence of peaks and valleys above the average middle line (or with a few valleys crossing down the average line), and the other parts as peaks and valleys frequently crossing the middle line, of falling below the middle line. The criterion of a continuous sequence of 20–24 points above the average line with a maximum of two nonadjacent exceptions was used to determine the length of a predicted transmembrane helix.

Hirokawa et al. [17] developed a method, SOSUI, for discriminating transmembrane helical proteins and predicting their membrane spanning segments using the combination of a variety of physicochemical parameters. Specifically, the parameters, Kyte–Doolittle hydropathy index, amphiphilicity, relative and net charges, and protein length have been used to detect transmembrane α-helices.

von Heijne [10] introduced the concept of "positive-inside rule", which observes that regions of polytopic (multispanning) membrane proteins facing the cytoplasm are generally enriched in Arg and Lys residues, whereas translocated regions are largely devoid of these residues. This implies that the distribution of positively charged amino acids may also be a major determinant of the transmembrane topology of integral membrane proteins, and this concept has been used for predicting the membrane spanning segments [18].

Hofmann and Stoffel [19] analyzed the statistical preferences of amino acid residues using the sequence data available in SWISS-PROT database. Based on these preferences, a method, TMpred, has been proposed for predicting transmembrane helices using a combination of several weight matrices for scoring. Gromiha [20] developed a set of conformational parameters for the 20 amino acid residues in transmembrane helical proteins using the frequency of occurrence of amino acid residues in the transmembrane helical part of membrane proteins, and that in the whole complex in a set of 70 membrane proteins. Based on these conformational parameters, a simple algorithm has been formulated using a set of primary and secondary rules to predict the transmembrane α-helices in membrane proteins.

Juretic and colleagues integrated multiple scales for amino acids for the prediction of transmembrane regions and developed the method SPLIT [21, 22]. Pasquier et al. [23] proposed an algorithm, PRED-TMR, which uses a standard hydrophobicity analysis with an emphasis on the detection of potential helix ends. Using the propensities of amino acid residues at the termini of transmembrane helices, PRED-TMR compiles scores for the termini of each putative segment. The best prediction has been achieved by a scoring function obtained from the two termini scores, a hydropathy score and a length constraint.

Kitsas et al. [24] developed a method based on hydrophobicity properties and higher-order statistics for predicting the membrane spanning helices in membrane proteins. Ganapathiraju et al. [25] proposed a method, TMpro for predicting membrane spanning helical segments using multiple amino acid properties such as charge, polarity, aromaticity, size, and electronic properties as features.

3.2.2 Hidden Markov Models, Multiple Sequence Alignment and Machine-Learning Methods

Tusnady and Simon [26] suggested a method for topology prediction of helical transmembrane proteins, HMMTOP, based on the hypothesis that the localizations of the transmembrane segments and the topology are determined by the difference in the amino acid distributions in various structural parts of these proteins rather than by specific amino acid compositions of these parts. A hidden Markov model (HMM) with special architecture was developed to search transmembrane topology corresponding to the maximum likelihood among all the possible topologies of a given protein. This model distinguishes the five structural states: inside

nonmembrane region, inside TMH-cap, membrane helix, outside TMH-cap, and outside nonmembrane region.

Rost et al. [27] developed a method based on neural networks for identifying the location and topology of transmembrane α-helices. Further, the method has been refined by postprocessing the neural network output through a dynamic programming-like algorithm, similar to the one introduced by Jones et al. [28]. Persson and Argos [29] proposed a method based on multiple sequence alignment for predicting transmembrane helical segments and their topologies. They have used two sets of propensity values: one for the middle, hydrophobic portion and the other for the terminal regions of the transmembrane sequence spans. Average propensity values were calculated for each position along the alignment, with the contribution from each sequence weighted according to its dissimilarity relative to the other aligned sequences.

Although multiple sequence alignments improve prediction accuracy, there are no homologues in current databases for 20–30% of all proteins [30]. To overcome this situation, the so-called dense alignment surface (DAS) method was developed [31]. DAS is based on the scoring matrix originally introduced to improve alignments for G-protein-coupled receptors. It compares low-stringency dot-plots of the query protein against the background representing the universe of nonhomologous membrane proteins using the scoring matrix.

Nugent and Jones [32] developed a method based on support vector machines for predicting the topology of membrane proteins along with signal peptides and reentrant helices. Osmanbeyoglu et al. [33] utilized an active learning approach for predicting transmembrane helices in membrane proteins. Ahmed et al. [34] presented a new transmembrane helix topology prediction method that combines support vector machines, HMMs, and a widely used rule-based scheme.

Further, methods have been developed for predicting helix–helix interactions and modeling the three-dimensional structures of membrane proteins. Park and Helms [35] proposed a method to predict the assembly of transmembrane helices in polytopic membrane proteins using sequence conservation patterns. Fuchs et al. [36] developed a method for predicting the interacting helices and helix–helix contacts in polytopic membrane proteins using neural networks. Michino et al. [37] developed a protocol, FoldGPCR for modeling the transmembrane domains of G-protein-coupled receptors. Recently, de Brevern [38] reviewed the developments on the 3D modeling of membrane proteins. The general methodology composed of the following: (1) use of secondary structure prediction to complete the comparative modeling process, (2) perform refinement and assessment steps to a novel comparative modeling process, and (3) consider the helix–helix and helix–lipid interactions, and even build quaternary structures. However, the most important factor when proceeding to correct structural models is taking the experimental data into account.

The servers for identifying TMH proteins and predicting the membrane spanning helical segments are listed in Table 2.

Table 2 Web servers for transmembrane helix prediction

Name	URL
ALOM	http://psort.nibb.ac.jp/form.html
MPEx	http://blanco.biomol.uci.edu/mpex/
KD plot	http://fasta.bioch.virginia.edu/fasta/grease.htm
TMpred	http://www.ch.embnet.org/software/TMPRED_form.html
SPLIT	http://split.pmfst.hr/split/
TopPred	http://www.sbc.su.se/~erikw/toppred2/
PRED-TMR	http://o2.biol.uoa.gr/PRED-TMR/
SOSUI	http://sosui.proteome.bio.tuat.ac.jp/sosuiframe0.html
MEMSAT	http://bioinf.cs.ucl.ac.uk/psipred/psiform.html
PHDhtm	http://cubic.bioc.columbia.edu/predictprotein/
TMAP	http://bioinfo.limbo.ifm.liu.se/tmap/
DAS	http://www.sbc.su.se/~miklos/DAS/
HMMTOP	http://www.enzim.hu/hmmtop/
TMHMM	http://www.cbs.dtu.dk/services/TMHMM/
CoPreTHi	http://athina.biol.uoa.gr/CoPreTHi/
TMpro	http://linzer.blm.cs.cmu.edu/tmpro/ http://flan.blm.cs.cmu.edu/tmpro/

3.3 Transmembrane Strand Proteins: Features

Schultz [39] analyzed the structures of β-barrel membrane proteins and derived ten basic rules for understanding their folding and stability.

1. The number of β strands is even and the N and C termini are at the periplasmic barrel end.
2. The β-strand tilt is always around 45° and corresponds to the common β-sheet twist. Only one of the two possible tilt directions is assumed, and the other one is an energetically disfavored mirror image.
3. The shear number of an n-stranded barrel is positive and around n + 2, in agreement with the observed tilt.
4. All β strands are antiparallel and connected locally to their next neighbors along the chain, resulting in a maximum neighborhood correlation.
5. The strand connections at the periplasmic barrel end are short turns of a couple of residues.
6. At the external barrel end, the strand connections are usually long loops.
7. The β-barrel surface contacting the nonpolar membrane interior consists of aliphatic side chains forming a nonpolar ribbon with a width of about 22 Å.
8. The aliphatic ribbon is lined by two girdles of aromatic side chains, which have intermediate polarity and contact the two nonpolar–polar interface layers of the membrane.

9. The sequence variability of all parts of the β-barrel during evolution is high when compared with soluble proteins.
10. The external loops show exceptionally high sequence variability and they are usually mobile.

3.4 Discrimination of β-Barrel Membrane Proteins

Several methods have been proposed for discriminating TMBs from other folding types of globular and membrane proteins. These methods are broadly classified into two aspects: statistical analyses and machine-learning techniques.

3.4.1 Statistical Methods

The statistical methods are straightforward and these methods could explain their merits and limitations based on physical principles. In statistical methods, amino acid composition, residue pair preference and motifs have been mainly used for discrimination. In addition, hydrophobicity profiles, composition of residues in the membrane environment, and sequence alignments have been used for discriminating TMBs.

Gnanasekaran et al. [40] developed a structure-based sequence alignment method for discriminating TMBs and reported an accuracy of 80% for a limited number of proteins. Wimley [41] analyzed the architecture of 15 TMBs and proposed a method based on hydrophobicity for identifying TMBs in genomic sequences. It has been reported that this method correctly identified 75% of the TMBs. Liu et al. [42] analyzed the amino acid composition in the membrane spanning regions of 12 TMBs and applied the information for discrimination, which showed 85% accuracy when tested with 241 TMBs. We have proposed methods using the compositions of amino acids, residue pairs, and motifs [43–45]. In these methods, the compositions have been computed for both positive and negative datasets (TMS proteins and other globular/TMH proteins, respectively) and treated as standard compositions. For a new protein, we computed the composition and compared with standard compositions (positive and negative datasets). The test protein is assigned to TMB whether deviation is smallest from the standard composition for TMB and vice versa. The discrimination based on residue pair preference is explained below:

(1) Calculate the dipeptide composition for both globular ($Dipep_{glob}$) and TMBs ($Dipep_{TMB}$) and the difference between them ($\sigma_{TMB\text{-}glob}$); (2) for a new protein, X, calculate the dipeptide composition and give weights to the dipeptide composition with $\sigma_{TMB\text{-}glob}$; (3) calculate the sum of weighted dipeptide composition, and (4) the protein X is predicted to be an TMB if the total weighted dipeptide composition is positive and globular protein otherwise [44]. For a set of 377 TMBs and 674 globular proteins, this method correctly identified 357 TMBs (95%) and excluded 534 globular proteins (79%). The twofold cross validation test showed an average

accuracy of 91 and 73%, respectively, for correctly identifying TMBs and excluding globular proteins. The application of the method has been illustrated with Fig. 1.

It takes the amino acid sequence in the input and computes the residue pair preference and weighted composition. The weighted composition of the query protein is +89.16, and hence it is identified as an outer membrane protein or TMS protein.

3.4.2 Machine-Learning Techniques

Currently, machine-learning techniques are widely used for predicting several important factors in bioinformatics, including the secondary structures of proteins, solvent accessibility, protein–protein interactions, protein–nucleic acid interactions, etc. [46–50]. It has been reported that the machine-learning algorithms could achieve the highest level of accuracy. These methods include Bayes functions, Neural networks, Logistic functions, Support vector machines, Regression analysis, Nearest neighbor methods, Meta learning, Decision trees and Rules, etc. The details of all these methods have been explained in Gromiha and Suwa [51].

Martelli et al. [52] used 12 TMBs and developed a sequence-profile-based HMM for picking up the β-barrel membrane proteins and reported an accuracy of 84% in a set of 145 TMBs. Bagos et al. [53] developed an algorithm based on HMM for discriminating TMBs and reported an accuracy of 89% in a set of 133 TMBs. Natt et al. [54] used a set of 16 TMBs and proposed a method using the combination of neural networks and support vector machines for discrimination, which showed an average accuracy of 90% in a set of randomly selected 100 globular and 16 TMBs. Garrow et al. [55] proposed a modified k-nearest neighbor algorithm and reported an accuracy of 92.5% using weighted amino acids and evolutionary information. Gromiha and Suwa [51] analyzed the performance of different machine-learning techniques and found that there is no significant difference in performance between different machine-learning methods and most of the methods could discriminate TMBs with the accuracy in the range of 88–91% in a set of 1,088 proteins. Further, the usage of different adjustable parameters in these methods would make it possible for any method to perform better than the others.

They have further analyzed the applications of residue pair preferences and amino acid properties as descriptors for discriminating TMBs using machine-learning techniques [51, 56]. It has been observed that the usage of all the 400 residue pairs increased the accuracy up to 94.5% using support vector machines. Generally many parameters may cause the problem of overfitting, and hence Park et al. [56] selected few amino acids and residue pairs for discrimination. The combination of the compositions of 18 amino acid residues (except Ala and Glu) and 10 residue pairs (QA, DF, DA, KK, EF, NK, DR, YN, FF, and LI) improved the accuracy up to 93.9% for discriminating TMBs from other folding types of globular and membrane proteins.

Further, Gromiha and Suwa [51] applied 49 different physicochemical, energetic, and conformational parameters of amino acid residues for discriminating

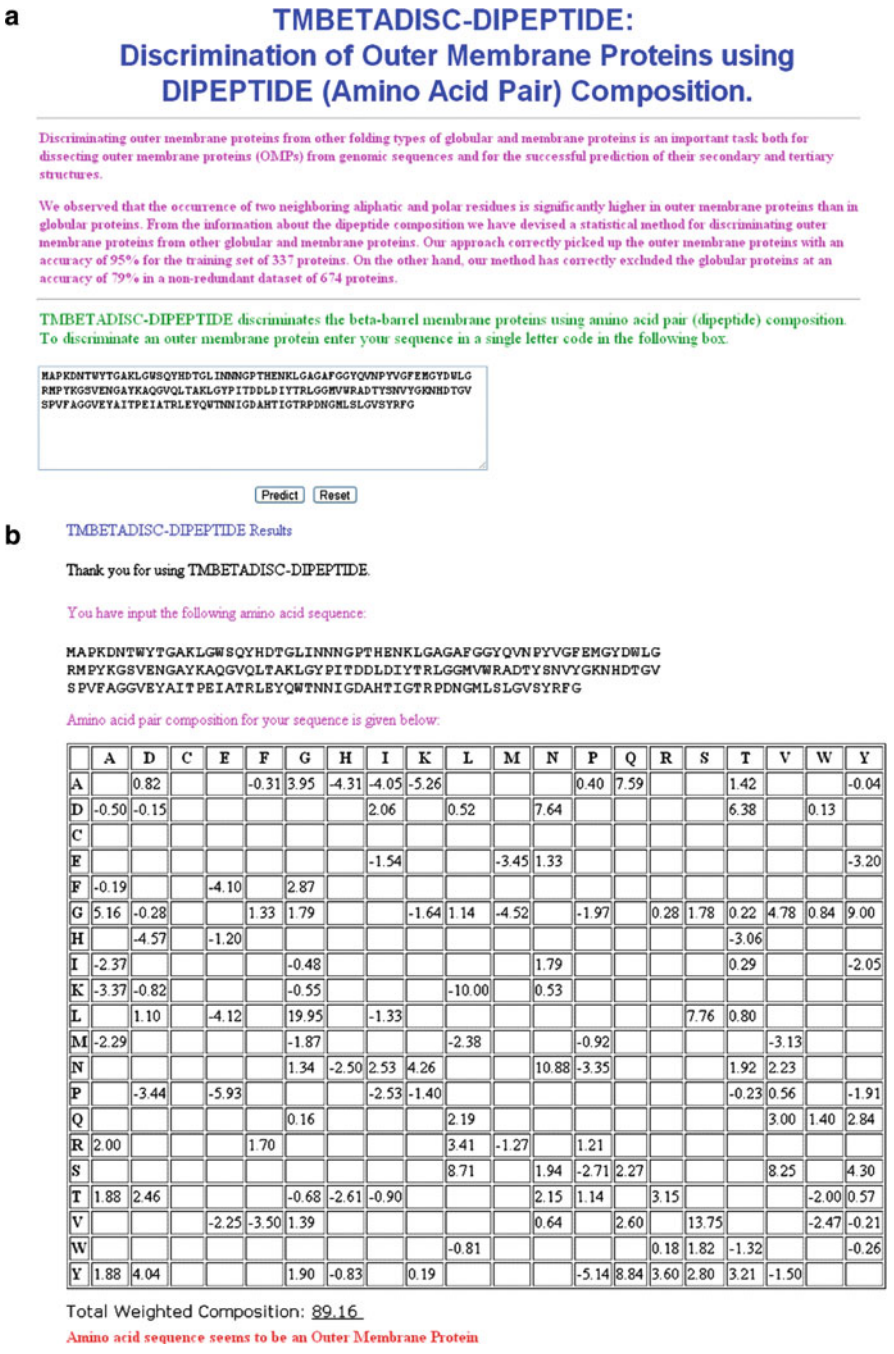

	A	D	C	E	F	G	H	I	K	L	M	N	P	Q	R	S	T	V	W	Y
A		0.82			-0.31	3.95	-4.31	-4.05	-5.26				0.40	7.59			1.42			-0.04
D	-0.50	-0.15						2.06		0.52		7.64					6.38		0.13	
C																				
E								-1.54			-3.45	1.33								-3.20
F	-0.19			-4.10		2.87														
G	5.16	-0.28			1.33	1.79			-1.64	1.14	-4.52		-1.97		0.28	1.78	0.22	4.78	0.84	9.00
H		-4.57		-1.20													-3.06			
I	-2.37					-0.48						1.79					0.29			-2.05
K	-3.37	-0.82				-0.55				-10.00		0.53								
L		1.10		-4.12		19.95		-1.33								7.76	0.80			
M	-2.29					-1.87				-2.38			-0.92					-3.13		
N						1.34	-2.50	2.53	4.26			10.88	-3.35				1.92	2.23		
P		-3.44		-5.93				-2.53	-1.40								-0.23	0.56		-1.91
Q						0.16				2.19								3.00	1.40	2.84
R	2.00				1.70					3.41	-1.27		1.21							
S										8.71		1.94	-2.71	2.27				8.25		4.30
T	1.88	2.46				-0.68	-2.61	-0.90				2.15	1.14		3.15				-2.00	0.57
V				-2.25	-3.50	1.39						0.64		2.60		13.75			-2.47	-0.21
W										-0.81					0.18	1.82	-1.32			-0.26
Y	1.88	4.04				1.90	-0.83		0.19				-5.14	8.84	3.60	2.80	3.21	-1.50		

Fig. 1 Discrimination of β-barrel membrane proteins using residue pair preference; (a) first page showing the input options (amino acid sequence); (b) the weighted dipeptide composition, total composition and predicted type of the query protein. In this example, the total weighted composition is +89.16 and the sequence is predicted to be a TMB protein

TMBs, and it could discriminate with the accuracy of 94.2% in a set of 1,088 proteins. This will also have the ability of correctly excluding 1,612 proteins belonging to 30 major folds of globular proteins with the accuracy of 99%. In addition, we have developed a method based on radial basis function (RBF) networks and position-specific scoring matrices (PSSM) profiles, which enhanced the accuracy of discriminating 268 TMBs and 1,045 non-TMBs to an accuracy of 96.4% [57].

The comparison of several statistical and machine-learning techniques for discriminating TMBs is presented in Table 3. We noticed that the accuracy is remarkably higher with machine-learning techniques than with statistical methods. Further, the statistical methods could correctly identify the TMBs, whereas the performance of machine-learning techniques is better for excluding globular and TMH proteins than identifying TMBs.

The online resources available for discriminating β-barrel membrane proteins are listed in Table 4.

Table 3 Comparison between statistical methods and machine learning techniques for discriminating β-barrel membrane proteins

Method	Parameters	Sensitivity	Specificity	Accuracy	Reference
Statistical	AAC	**89**	79	83	[43]
Statistical	Residue pairs	**95**	79	86	[44]
Statistical	Motifs	**96**	86	90	[45]
SVM	18 AA + 10 pairs	91	**95**	94	[56]
NN	49 Properties	81	**98**	94	[51]
RBF	PSSM profiles	89	**98**	96	[57]

18 AA: All amino acids except Ala and Glu
10 pairs: QA, DF, DA, KK, EF, NK, DR, YN, FF and LI
AAC amino acid composition

Table 4 Web servers for transmembrane strand prediction

Name	URL
PRED-TMBB	http://bioinformatics.biol.uoa.gr/PRED-TMBB
TMB-HUNT	www.bioinformatics.leeds.ac.uk/betaBarrel
TMBETA-DISC	http://psfs.cbrc.jp/tmbetadisc/
TMBETA-SVM	http://tmbeta-svm.cbrc.jp/
TMETADISC-RBF	http://rbf.bioinfo.tw/~sachen/OMP.html
ProfTMB	http://cubic.bioc.columbia.edu/services/proftmb/
TBBpred	http://www.imtech.res.in/raghava/tbbpred/
TMBETA-NET	http://psfs.cbrc.jp/tmbeta-net/
ConBBPRED	http://bioinformatics.biol.uoa.gr/ConBBPRED/
TMBpro	http://www.igb.uci.edu/servers/psss.html
TMBETAPRED-RBF	http://rbf.bioinfo.tw/~sachen/tmrbf.html
Freeman–Wimley algorithm	http://www.tulane.edu/~biochem/WW/apps.html

3.4.3 Genome-Wide Annotation of β-Barrel Membrane Proteins

The methods developed for discriminating β-barrel membrane proteins have been applied to detect such proteins in genomic sequences. Zhai and Saier [58] developed a β-barrel finder program based on secondary structure, hydropathy and amphipathicity parameters and used it for identifying TMBs in *Escherichia coli* genome. Berven et al. [59] proposed a program for identifying TMBs using two factors (1) C-terminal pattern typical of many integral β-barrel proteins and (2) integral β-barrel score based on the extent to which the sequence contains stretches of amino acids typical of transmembrane β-strands. Bigelow et al. [60] introduced a profile-based HMM for discriminating TMBs and suggested the probable TMBs in genomic sequences of 72 Gram-negative bacteria. The average occurrence of TMBs in genomes is predicted to be about 3%. Gromiha et al. [61] proposed a new approach for detecting TMBs in genomic sequences and the TMB finding pipeline is given below (Fig. 2). It includes the identification procedure using the residue pair preferences between TMBs and globular proteins and that between TMBs and TMH proteins [44] as well as elimination methods, which includes shorter sequences, TMH proteins using the program SOSUI [17], TMH and globular proteins that have more than 70% sequence identity and 80% coverage with known sequences and structures in Uniprot [62] and PDB [6], respectively, using the program, BLAST [63]. Further a database, TMBETA-GENOME has been developed for annotated TMBs in 275 genomic sequences, and it is available at http://tmbeta-genome.cbrc.jp/annotation/ [64]. Recently, Tsirigos et al. [65] developed a comprehensive database of integral β-barrel outer membrane proteins from Gram-negative bacteria, OMPdb, which contains 67,766 proteins, which are classified into 85 families, based on structural and functional criteria. It has cross-references to other databases, references to the literature, and annotation for sequence features, such as transmembrane segments and signal peptides.

Furthermore, OMPdb has the facility to browse the available data as well as to submit advance text searches and run BLAST queries against the database of protein sequences or domain searches against the collection of profile HMMs that represent the domain organization of each family. The database is available at http://bioinformatics.biol.uoa.gr/OMPdb.

3.5 Prediction of Membrane Spanning β-Strand Segments

Several statistical methods and machine-learning techniques have been proposed for predicting the membrane spanning segments of TMBs. As mentioned in the previous section, the performance of machine-learning techniques is better than that with statistical and knowledge-based methods. In addition, the inclusion of alignment profiles improved the accuracy significantly.

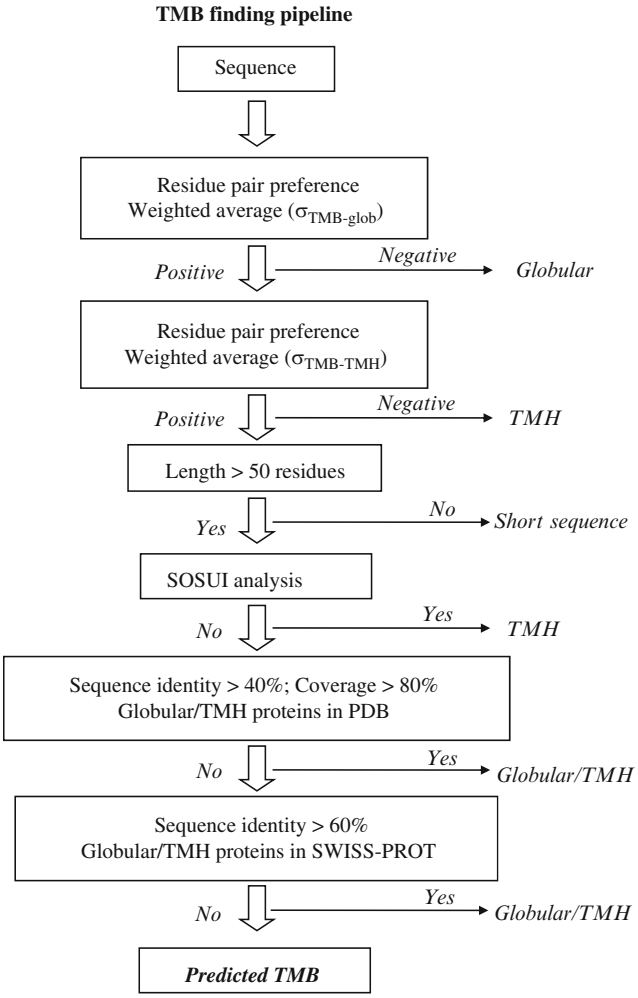

Fig. 2 Pipeline for detecting β-barrel membrane proteins in genomic sequences [61]

3.5.1 Statistical Methods

Paul and Rosenbusch [66] proposed an indirect method to predict transmembrane β-strands based on the elimination of turns in membrane. In their procedure, the amino acid residues have been divided into three groups: turn promoters, turn indifferent, and turn blockers. Turns have been identified as segments ≥3 residues, of which at least one in turn promoting and none in turn blocking. Segments between turns are considered to be membrane spanning segments and the longer stretches of residues between 6 and 18 are identified as potential β-strands.

Vogel and Jahnig [67] applied the concept of "amphipathicity of β-strands" to predict the transmembrane β-strands in TMBs. In this method, the mean

hydrophobicity of one side of an assumed membrane spanning β-strand is computed using the equation

$$H_{\beta}(i) = 1/5[h(i \pm 4) + h(i \pm 2) + h(i)],$$

where h(i) is the hydrophobicity of the residue based on Kyte and Doolittle [12]. An amphipathic β-strand is identified with a period of two residues, so that the criterion for prediction is $H_{\beta}(i) \geq 1.6$ and $H_{\beta}(i \pm 1) << 1.6$. The membrane spanning β-strands have been assigned with the minimal length of ten residues.

Gromiha and Ponnuswamy [68] used a "hydrophobicity profile method" for predicting the membrane spanning β-strand segments as described below (1) construct hydrophobicity profiles of window lengths 12, 6, and 1; (2) the high peaks in the profile correspond to transmembrane β-strands of around 12 residues, (3) the low peaks have been divided into seven overlapping six-residue segments and selected the segment showing the highest amphipathicity; and (4) the end residue is fixed when it breaks the amphipathic character (alternating high and low hydrophobicity) in the profile of window length one. This method has been successfully applied to predict the transmembrane segments of porin, maltoporin, ompA, and ompX, and we found a good agreement with experimental observations.

Gromiha et al. [69] developed a "rule-based approach" for predicting transmembrane β-strands using three features (1) preference of amino acid residues in membrane spanning β-strands (conformational parameters, β) and (2) hydrophobic character (H_p) (3) and amphipathicity. A set of five primary rules have been designed to assign the priority of each residue to be in transmembrane β-strand and four secondary rules to pick up the membrane spanning segments. The primary rules for assigning the priority of each residue, i, are: $\beta(i) > 1.0$ (average conformational parameter), $1/6 \sum_{i=1}^{6} \beta(i) > 1.0$, $H_p(i) > 13.34$ (average hydrophobicity), $1/6 \sum_{i=1}^{6} H_p(i) > 13.34$ and $1/2 \sum_{i=1}^{2} H_p(i) = 13.34 \pm 0.5$ (oscillating around the average hydrophobicity). If these conditions are satisfied, the priority is one and zero, otherwise. The secondary rules for picking up the membrane spanning segments are: if any residue has the priority of 5, two consecutive residues have the priority of 4 or three consecutive residues have the priority of ≥ 3, there is a possibility of a transmembrane β-strand segment around the residue(s). Extend the length in both directions so that there may not be two consecutive low priority residues (<3) or a residue of zero priority. If the segment is longer than 20 residues, cut into two smaller segments at the residue of highest hydrophobicity. The method has been applied to three different porins and the transmembrane β-strand segments are predicted with the accuracy of 82%. Recently, Freeman and Wimley [70] proposed a statistical method based on the physicochemical properties of experimentally characterized β-barrel membrane protein structures for predicting their membrane spanning segments.

3.5.2 Machine-Learning Techniques

Several machine-learning techniques including HMMs, support vector machines and neural networks have been widely used to predict the membrane spanning β-strands in TMBs. Jacoboni et al. [71] proposed a neural network method (B2TMPRED) for predicting the membrane spanning β-strands with 12 proteins and reported the residue accuracy of 69% using sequence information only. Further, they have raised the accuracy up to 78% by using the evolutionary information as input to the network. Bagos et al. [53] developed a method based on HMM (PRED-TMBB) and reported the residue accuracy of 84.2% in a set of 14 β-barrel membrane proteins. Bigelow et al. [60] proposed a method based on profile-based hidden Markov model (ProfTMB) for prediction. Natt et al. [54] used neural networks and support vector machines (TMMPred) for predicting the membrane spanning regions of TMBs. They obtained the accuracy of 70.4% with only sequence information and improved the accuracy up to 80.5% using the multiple sequence alignment obtained from PSI-BLAST. Gromiha et al. [72, 73] developed a neural network-based method (TMBETA-NET) and it could predict the membrane spanning regions of 13 TMBs with the accuracy of 73% using only the sequence information. In addition, our method would provide the probability of each residue to be in the transmembrane segment. Bagos et al. [74] combined different methods and proposed a consensus approach (ConBBPRED) for predicting membrane spanning β-strand segments.

Recently, we have developed a novel method for predicting the topology of β-barrel membrane proteins [75]. The procedure involves two steps (1) predicting the number of β-strand segments in TMH proteins and (2) predicting the residues in membrane spanning-strands. In the first step, we have developed a protocol to predict the number of β-strands in TMBs, and the flowchart is shown in Fig. 3.

The information about the total number of residues in a protein is sufficient to identify the β-barrel membrane proteins with 22 and 8 strands. For example, the proteins with more than 590 residues are predicted to have 22 β-strands. The number of β-strands is 8 if the number of residues in a protein is less than 200.

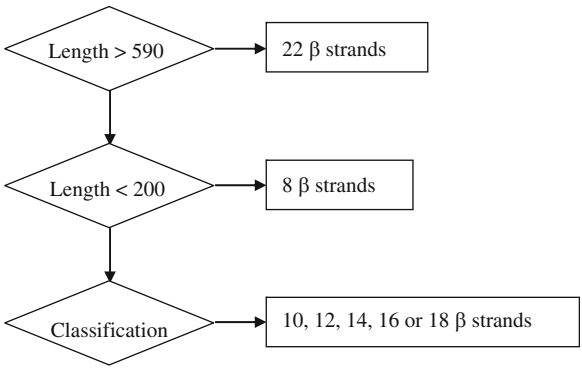

Fig. 3 Flowchart for predicting the number of β-strands in TMBs. Length denotes the total number of residues in a protein [75]

For proteins with the sequence length of 200–500 residues we have used RBF network and the compositions of specific amino acid residues (Ala, Asp, His, Tyr, and Val) for predicting the number of β-strands (10, 12, 14, 16, and 18). These five amino acids have been selected based on the highest performance obtained with the combination of amino acids using forward feature selection procedure. This method could correctly identify the number of strands in 27 of the 28 considered proteins and the leave-one-out cross-validation accuracy is 96%. In the second step, we have used PSSM profiles and RBF networks for predicting the membrane spanning segments. Our method could predict the membrane spanning residues with the accuracy of 87%. The sensitivity and specificity are 82% and 90%, respectively. We have developed a web server for predicting the membrane spanning β-strands for any β-barrel membrane protein and the details are presented in Fig. 4.

It takes the amino acid sequence in one letter format as the input and automatically omits gaps and numbers. The output provides the amino acid sequence of the protein along with the predicted membrane spanning β-strand regions. The prediction results are available at http://rbf.bioinfo.tw/~sachen/tmrbf.html.

The online resources available for predicting the membrane spanning segments of β-barrel membrane proteins are included in Table 4.

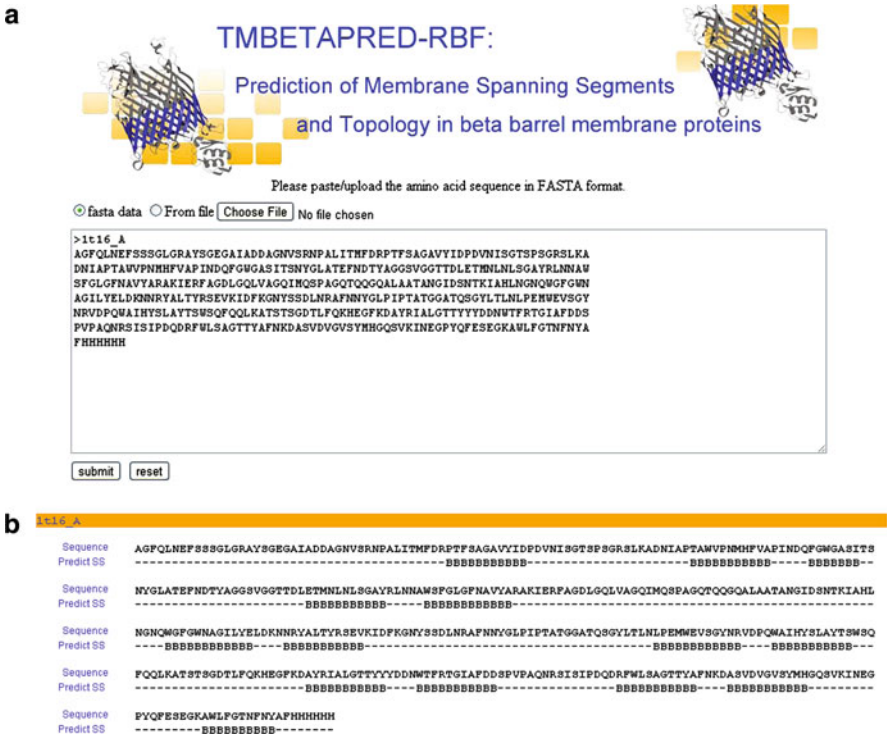

Fig. 4 Illustration for predicting the membrane spanning segments in β-barrel membrane proteins. (**a**) Input sequence in FASTA format; (**b**) predicted β-strand segments

4 Functional Discrimination of Membrane Proteins

In this section, we focus on the databases and methods developed for the classification of membrane proteins based on their functions. Specifically, we describe the methods to discriminate transporter proteins from other globular and membrane proteins along with the classification of transporters based on different classes and families including channels and pores.

4.1 Databases for Membrane Transporters and Functionally Important Residues in Membrane Proteins

Saier et al. [76] developed the Transporter Classification Database (TCDB), which contains sequence, structural, functional, and evolutionary information about transport systems from a variety of living organisms, based on the International Union of Biochemistry and Molecular Biology-approved transporter classification (TC) system. It is a curated repository for factual information compiled largely from published references. It uses a functional/phylogenetic system of classification, and currently encompasses about 5,000 representative transporters and putative transporters in more than 500 families.

Transport systems are classified on the basis of five components such as (1) transporter class (i.e., channel, carrier, primary active transporter, or group translocator), (2) transporter subclass which in the case of primary active transporters refers to the energy source used to drive transport, (3) transporter family, (4) subfamily, and (5) substrate or range of substrates transported. The browsing options available in TCDB are illustrated in Fig. 5. It also has the facility to retrieve data with several search options. TCDB is freely accessible at http://www.tcdb.org.

Gromiha et al. [77] developed the database TMFunction, which is a collection of experimentally observed functional residues in membrane proteins reported in the literature. Each entry includes the numerical values for the parameters IC50 (measure of the effectiveness of a compound in inhibiting biological function), Vmax (maximal velocity of transport), relative activity of mutants with respect to wild type protein, binding affinity, dissociation constant, etc., which are important for understanding the sequence–structure–function relationship of membrane proteins. In addition, they have provided information about name and source of the protein, Uniprot and PDB codes, mutational and literature information. Furthermore, TMFunction is linked with related databases and other resources. A web interface has been set up with different search and display options so that users have the ability to get the data in several ways. TMFunction is freely available at http://tmbeta-genome.cbrc.jp/TMFunction/. The usage of TMFunction is illustrated with the following example. The data obtained for the function “drug” and single mutants is shown in Fig. 6a. The terms: entry, protein, Uniprot ID, mutation,

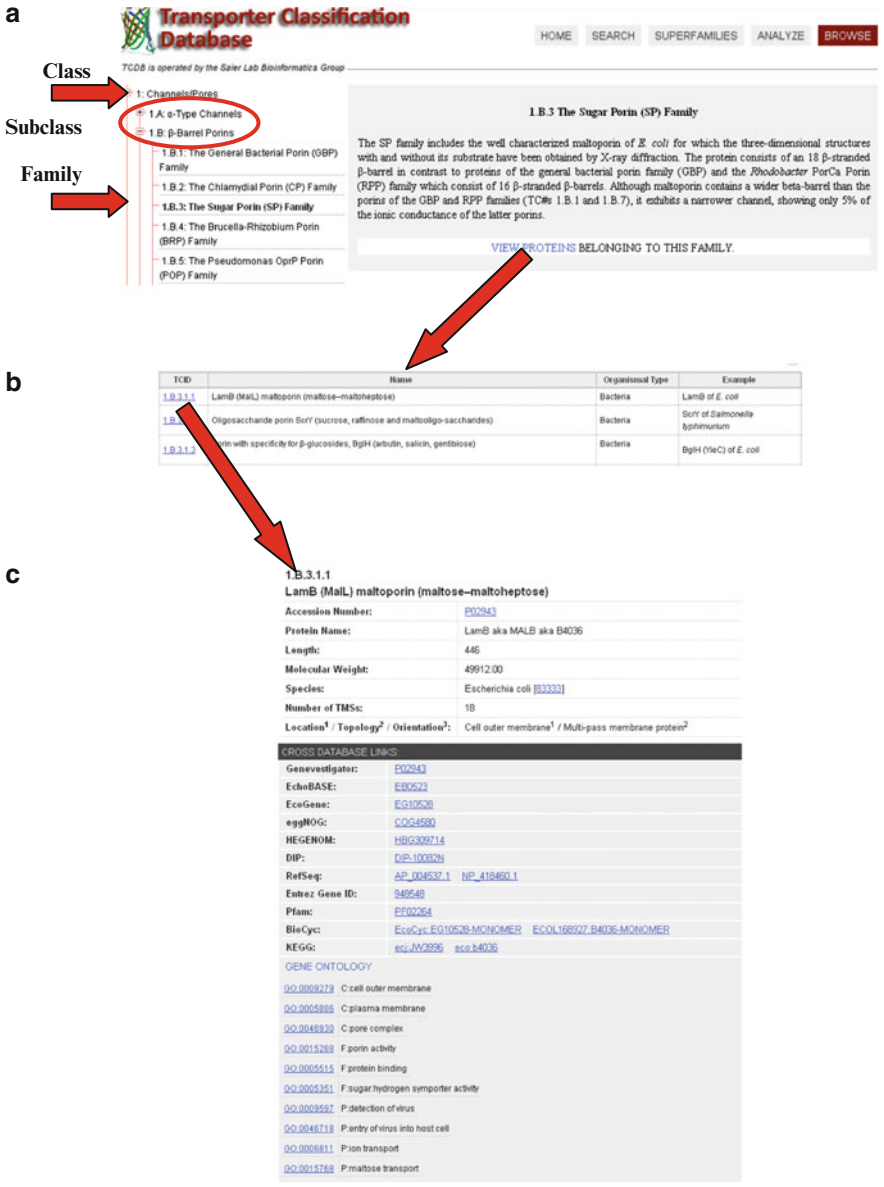

Fig. 5 Browsing data from Transport Classification Database. (**a**) Hierarchical representation of transporters, such as class, subclass and family; (**b**) proteins belonging to a specific family, sugar porin family; (**c**) details about a typical protein, LamB, maltoporin

parameter, data, function, experiments, and Pubmed ID have been selected for displaying the results (Fig. 6b). Fig. 6c shows the final results obtained with the search conditions and display options.

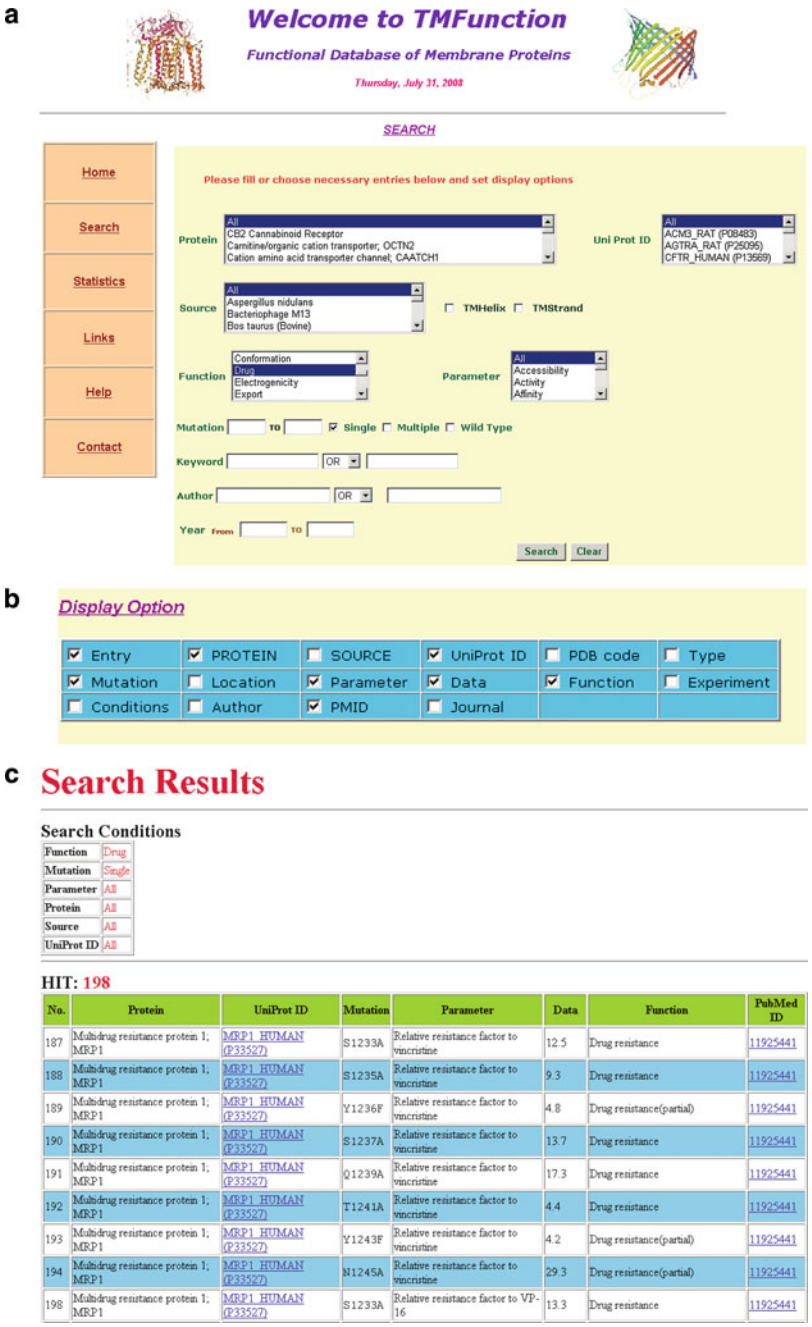

Fig. 6 An example of searching conditions, display options and results of TMFunction: (**a**) main menu for the search options in TMFunction. The items function (drug) and single mutants are selected for search as indicated by arrows; (**b**) display options in TMFunction. We have selected entry, protein, Uniprot ID, mutation, parameter, data, function, and PMID to show in the output; (**c**) part of the results obtained from TMFunction

Further, databases have been developed specifically for ion channels. Ion channels are transmembrane pores, which allow the passage of ions (charged particles) into and out of a cell down the electrochemical gradient. There are hundreds of different ion channels, and they are distinguished based upon their ion selectivity, gating mechanism, and sequence similarity. Ion channels can be voltage gated, ligand gated, pH gated, or mechanically gated. These gating criteria along with a combination of sequence similarity and ion selectivity further subdivide ion channels into several subtypes, voltage-gated potassium channels, voltage-gated sodium channels, voltage-gated calcium channels, chloride channels, ligand-gated channels, and so on. The ion channel activity for several genomes has been deposited in ion channels database, and it is available at http://www.ionchannels.org/.

4.2 Discrimination of Transporters from Other Globular and Membrane Proteins

The functional discrimination of membrane transporter proteins requires the knowledge about a query protein whether it is a transporter or a nontransporter. Hence, it is necessary to develop a method to discriminate transporters from other proteins. Several features have been tried for the discrimination and the important parameters are amino acid occurrence, amino acid properties and PSSM profiles. The amino acid occurrence could discriminate a set of 3,336 membrane nontransporters and 1,718 transporters with the fivefold cross-validation accuracy of 79.1% using k-nearest neighbor methods [78]. The sensitivity and specificity are 69.2 and 84.2%, respectively. Further a set of 5,048 proteins including membrane transporters, membrane nontransporters and globular proteins are discriminated with an accuracy of 78.7%. The method was also tested with equal number of transporters and nontransporters, which showed the accuracy in the range of 82–85%. We have developed a web server for discriminating transporters from other proteins and its utility is illustrated in Fig. 7. The server takes the amino acid sequence as input (Fig. 7a) and predicts the type of the protein as transporter or nontransporter using k-nearest neighbor (Fig. 7b). Li et al. [79] employed traditional homology-based methods to detect the transporters in a set of completed genomes and showed a recall and precision of 81.8% in yeast proteome.

4.3 Characteristic Features of Amino Acid Residues in Different Classes of Transporters

The three major classes of transporters are channels/pores, electrochemical and active transporters [5]. Channels/pores catalyze facilitated diffusion (by an energy-independent process) by passage through a transmembrane aqueous pore or channel

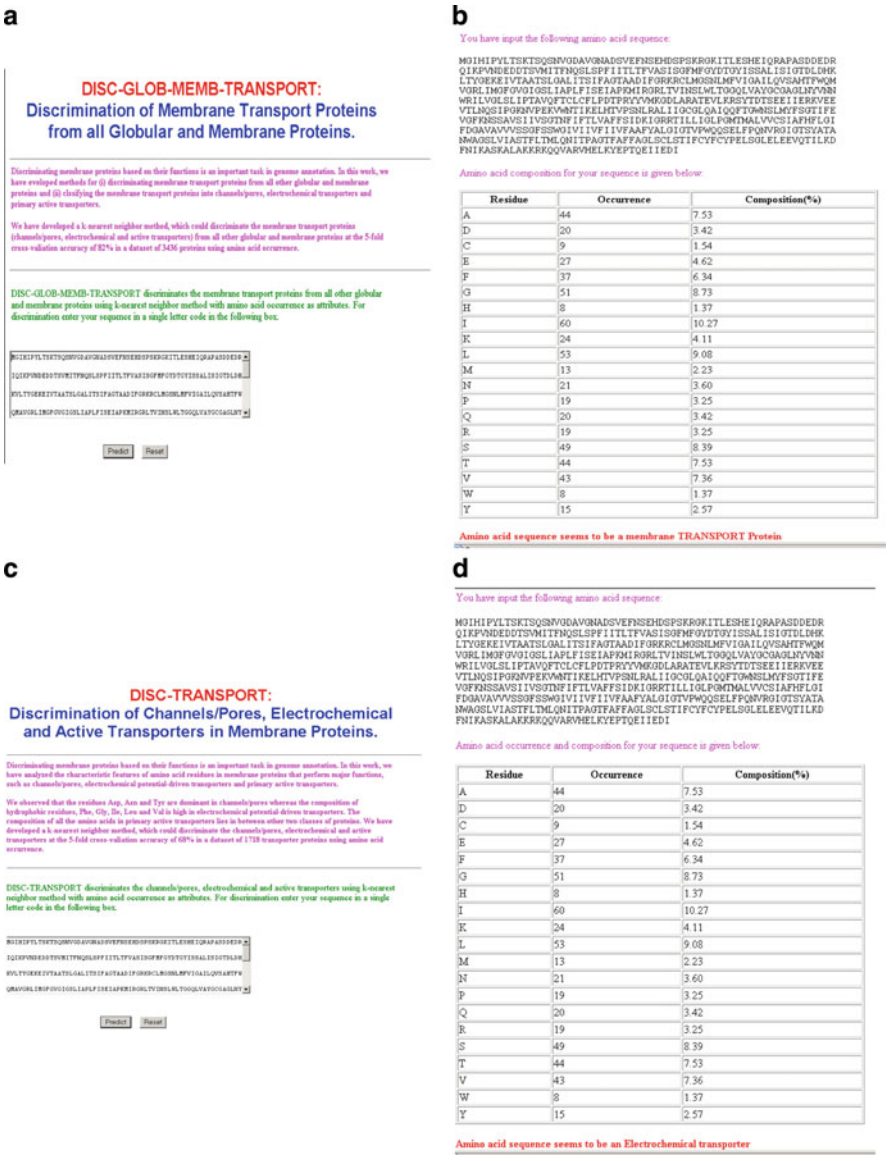

Fig. 7 Discrimination of membrane transporters and prediction of transporter class. (**a**) Input to discriminate transporters and nontransporters; (**b**) predicted type of the protein based on amino acid occurrence; (**c**) input amino acid sequence to predict the class of the transporter; (**d**) results showing the type of the transporter

without evidence for a carrier-mediated mechanism. Electrochemical transporters are the ones that utilize a carrier-mediated process. Active transporters use a primary source of energy to drive active transport of a solute against a concentration gradient.

The systematic analysis of amino acid residues in these transporters showed a preference of specific amino acid residues. The residue Asn is dominant in channels/pores among all the transporters. Interestingly, Asn plays an important role to the stability and function of β-barrel membrane proteins [43, 80]. Glu is another amino acid that shows the difference of more than one with electrochemical transporters. It has been showed that the residues Glu166 and Glu148 are important for the channel function in CIC chloride channel proteins [81]. The residues Phe and Leu are dominant in electrochemical transporters. In addition, the composition of Ala, Ile, Val, and Trp is higher in this class of proteins compared with other two transporters. Interestingly, in glycerol-3-phosphate transporter the space between helices 1 and 7 is filled by nine aromatic side chains and the occurrence of bulky aromatic residues helps to close the pore completely [82]. The higher occurrence of hydrophobic residues is due to the presence of long stretches of these residues in membrane spanning segments of α-helical membrane proteins.

4.4 Discrimination of Transporters Based on Different Classes and Families

We have utilized different machine-learning methods for discriminating channels/pores, electrochemical and active transporters [78]. We observed that the average accuracy of discriminating channels/pores, electrochemical and active transporters lies in the range of 56–64% for different machine-learning techniques. The highest accuracy of 64% is obtained for neural network-based method using fivefold cross-validation and jack-knife tests. Interestingly, this method has similar values for sensitivity and specificity, indicating the ability of picking up the specific class of transporters and eliminating others with similar accuracy. On the contrary, homology search-based methods such as BLAST could discriminate the three classes of transporters with an average accuracy of 51.5%. We have developed a web server for predicting the transporters into three classes. The server takes the amino acid sequence as input (Fig. 7c) and displays the predicted type of the transporter in the output (Fig. 7d). Recently, we have utilized PSSM profiles and amino acid properties for discriminating the three classes of transporters, channels/pores, electrochemical and active transporters and obtained an average accuracy of 78% in a test set of 118 proteins [83].

In addition, we have analyzed the influence of PSSM profiles and amino acid properties in six different families of transporters developed a method to discriminate them. We observed that the PSSM with amino acid properties could discriminate six different classes of transporters with an average accuracy of 69%, with an improvement of 8% over amino acid composition [83]. We have developed a strategy for the annotation of transporters in genomic sequences and it is depicted in Fig. 8. First our method classifies the query protein into transporter or nontransporter. For a transporter, it predicts the class as channels/pores, electrochemical or active

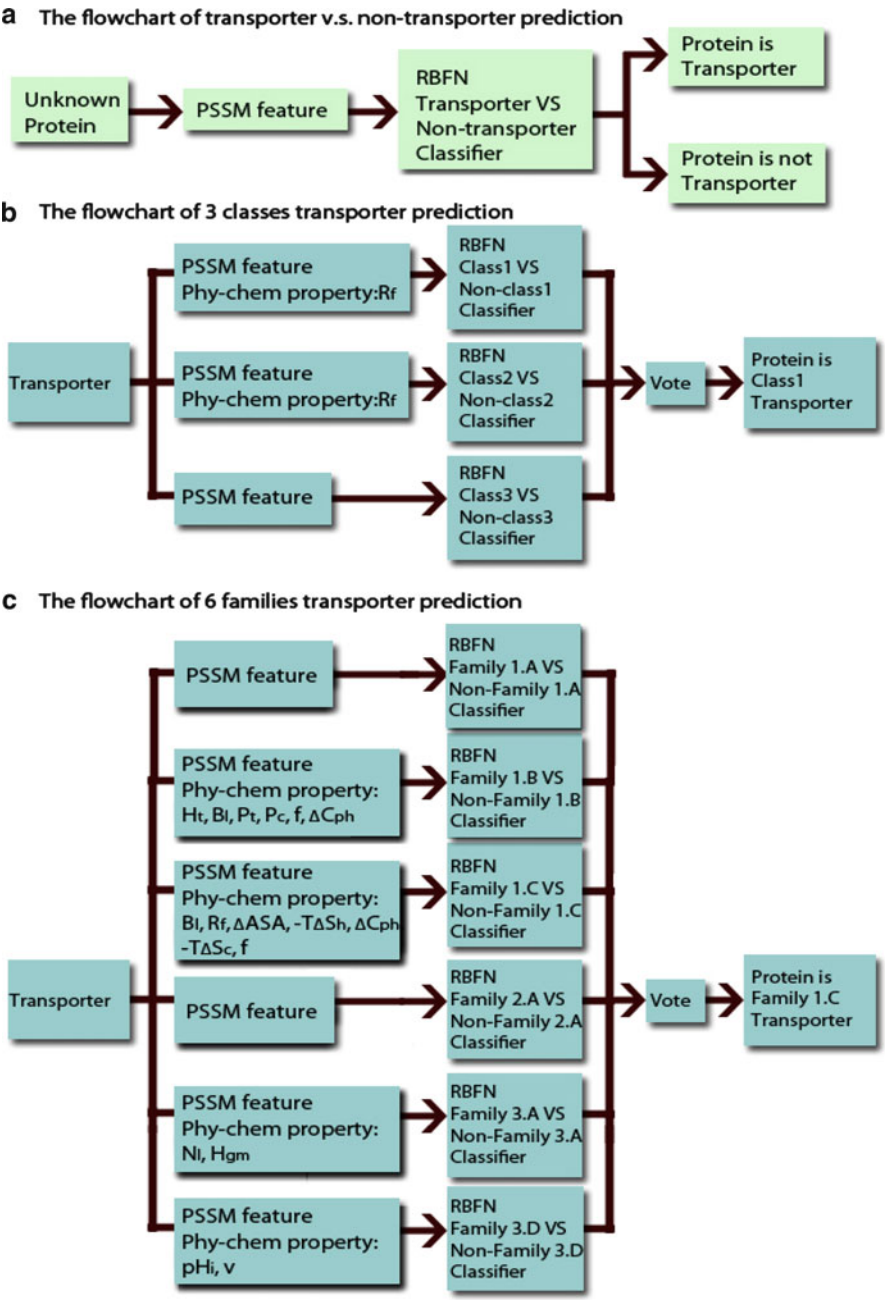

Fig. 8 Strategy to identify the class and family of a query protein

transporters and further classified into six families. Li et al. [84] utilized nearest neighbor algorithm to distinguish 484 transporter families and reported a fivefold cross validated accuracy of 72.3%.

4.5 Channels and Pores

In TCDB, channels and pores are grouped in the same class to include the transport systems that catalyze facilitated diffusion (by an energy-independent process) by passage through a transmembrane aqueous pore or channel without evidence for a carrier-mediated mechanism. However, channels have α-helical conformation, whereas pores have β-strands in their membrane spanning segments.

We have tested our method to discriminate channels and pores and the results obtained with amino acid composition are shown in Table 5. We found that most of the machine-learning methods discriminated the channels and pores with the accuracy in the range of 88–92%. The neural network and support vector machine showed the highest accuracy of 92.4%. The sensitivity and specificity are 93 and 92%, respectively using neural network. The achievement of high accuracy might be due to the difference in amino acid residues in the membrane spanning regions of α-helical and β-barrel membrane proteins. The α-helical membrane proteins are dominated with the stretches of hydrophobic residues, whereas the polar and charged resides are intervened in the membrane spanning segments of β-barrel membrane proteins.

Table 5 Discrimination of channels and pores using different machine learning approaches [78]

	Fivefold cross-validation		
Method	Sensitivity (%)	Specificity (%)	Accuracy (%)
Bayesnet	94.1	81.4	88.9
Naive Bayes	92.5	88.4	90.8
Logistic function	92.0	89.1	90.8
Neural network	93.0	91.5	92.4
RBF network	92.5	88.4	90.8
Support vector machines	95.2	88.4	92.4
k-nearest neighbor	89.8	86.8	88.6
Bagging meta learning	89.8	83.7	87.3
Classification via Regression	88.2	85.3	87.0
Decision tree J4.8	86.1	78.3	82.9
NBTree	90.9	83.7	88.0
Partial decision tree	87.2	79.1	83.9

Sensitivity = TP/(TP+FN); Specificity = TP/(TP+FP); Accuracy = (TP+TN)/(TP+TN+FP+FN)
TP, FP, TN and FN refer to the number of true positives, false positives, true negatives and false negatives, respectively

4.6 Discrimination of Different Classes of Ion Channel Proteins

Ion channels are integral membrane proteins that enable the passage of inorganic ions across cell membranes. They are key components for physiological functions and the evidence of ion channels for the role in diseases has been described in a special issue in Progress in Biophysics and Molecular Biology [85]. It has been mentioned that different types of ion channels voltage-gated potassium, calcium, sodium, and ligand-gated channels perform different functions. Hence, several methods have been proposed to discriminate the ion channels and classifying them into different groups. Saha et al. [86] developed a method based on support vector machines to discriminate ion channels and nonion channels and reported an accuracy of 89% to discriminate them. Further, the ion channels have been classified into potassium, sodium, calcium, and chloride channels with one against others and obtained an average accuracy of 97.8%. A web server, VGIchan has been developed for predicting and classifying voltage-gated ion channels, and it is available at www.imtech.res.in/raghava/vgichan/.

Recently, Lin and Ding [87] utilized a feature selection technique, analysis of variance and support vector machines to detect ion channels and classifying them. They showed an accuracy of 86.6% for discriminating ion channels and nonion channels. Further, voltage- and ligand-gated channels are distinguished with an accuracy of 92.6% and four types of channels (potassium, sodium, calcium, and anion) are classified with an accuracy of 87.8%.

5 Drug–Target Interactions

The identification of molecular target is a critical step in drug discovery and development. Ion channels are one of the most popular drug targets in various diseases including cardiovascular and central nervous systems. Hence, several bioinformatics methods have been developed to predict the potential drug targets with ion channels and other proteins. Yamanishi et al. [88] characterized four classes of drug–target interaction networks in humans involving enzymes, ion channels, G-protein coupled receptors and nuclear receptors and revealed significant correlations between drug structure similarity, target sequence similarity and the drug–target interaction network topology. The information on interaction between drugs and target proteins has been obtained from KEGG [89], BRENDA [90], SuperTarget [91], and DrugBank databases [92]. Further, they developed statistical methods to predict unknown drug–target interaction networks from chemical structure and genomic sequence information simultaneously on a large scale.

He et al. [93] developed the datasets for drug–target pairs (positive dataset) and non drug–target pairs (negative dataset) and utilized them for predicting drug–target interactions. The positive dataset contains a total of 4,797 drug–target

pairs, of which 2,719 for enzymes, 1,372 for ion channels, 630 for GPCRs, and 82 for nuclear receptors. The negative datasets were derived with the following steps (1) separated the pairs in the above positive dataset into single drugs and proteins, (2) recoupled these singles into pairs in a way that none of them occurs in the corresponding positive dataset, and (3) randomly picked the negative pairs thus formed until they reached the number two times as many as the positive pairs. The representative targets have been classified into 28 common groups based on their functional groups. A nearest neighbor algorithm has been used to identify the drug–target interaction pairs using different amino acid properties such as hydrophobicity, polarizability, polarity, secondary structure, normalized van der Waals volume, and solvent accessibility. This method showed a cross-validation accuracy of 85, 81, 78, and 86% for the drug target pairs with enzymes, ion channels, GPCRs, and nuclear receptors, respectively.

Huang et al. [94] developed a dataset of 1,268 approved human target proteins stored in DrugBank database and 7,252 nondrug targets. Among the dataset 31 and 16 ion channels were identified as ion channel target and ion-channel nontarget proteins. They utilized different properties of amino acid residues such as composition, hydrophobicity, polarity, polarizability and normalized van der Waals volume and RBF networks for discriminating the drug and nondrug targets. They showed that the drug and nondrug targets for the whole dataset can be discriminated with an accuracy of 85% and for the ion channel proteins with an accuracy of 84%.

6 Conclusions

This review is focused on the development of databases and prediction methods for understanding the structure and function of membrane proteins. The methods proposed for identifying transmembrane helical proteins and predicting their membrane spanning segments have been reviewed. The transmembrane helical proteins have a continuous stretch of hydrophobic residues in their membrane spanning segments, whereas membrane spanning β-strand segments in β-barrel membrane proteins have both polar and charged residues along with hydrophobic residues. The advances made for detecting such type of proteins in genomic sequences and predicting their membrane spanning β-strand segments have been discussed. On the functional front, the databases developed for transporters, ion channels and functionally important residues in membrane proteins have been outlined. Further, the discrimination methods for identifying membrane transporters and predicting transporters into three classes and six families have been described. In addition, recent methods for predicting the subclasses of ion channels as well as ion-channels–drug interactions have been explained. In essence, this comprehensive review provides the insights into understanding the structure and functions of membrane proteins along with ion channel proteins.

Acknowledgements This work was partially supported by Indian Institute of Technology Madras research grant (BIO/10-11/540/NFSC/MICH) to MMG.

References

1. White SH, Wimley WC (1999) Membrane protein folding and stability: physical principles. Ann Rev Biophys Biomol Str 28:319–365
2. Schulz GE (2003) Transmembrane beta-barrel proteins. Adv Protein Chem 63:47–70
3. Saier MH (2000) A functional-phylogenetic classification system for transmembrane solute transporters. Microbiol Mol Biol Rev 64(2):354–411
4. Ren QH, Chen KX, Paulsen IT (2007) TransportDB: a comprehensive database resource for cytoplasmic membrane transport systems and outer membrane channels. Nucleic Acids Res 35:D274–D279
5. Saier MH, Tran CV, Barabote RD (2006) TCDB: the transporter classification database for membrane transport protein analyses and information. Nucleic Acids Res 34:D181–D186
6. Berman H, Henrick K, Nakamura H, Markley JL (2007) The worldwide Protein Data Bank (wwPDB): ensuring a single, uniform archive of PDB data. Nucleic Acids Res 35:D301–D303
7. Tusnady GE, Dosztanyi Z, Simon I (2005) PDB_TM: selection and membrane localization of transmembrane proteins in the protein data bank. Nucleic Acids Res 33:D275–D278
8. Jayasinghe S, Hristova K, White SH (2001) MPtopo: a database of membrane protein topology. Protein Sci 10:455–458
9. Ikeda M, Arai M, Okuno T, Shimizu T (2003) TMPDB: a database of experimentally-characterized transmembrane topologies. Nucleic Acids Res 31:406–409
10. von Heijne G (1986) The distribution of positively charged residues in bacterial inner membrane proteins correlates with the trans-membrane topology. EMBO J 5:3021–3027
11. Chen CP, Rost B (2002) State-of-the-art in membrane protein prediction. Appl Bioinform 1:21–35
12. Kyte J, Doolittle RF (1982) A simple method for displaying the hydropathic character of a protein. J Mol Biol 157:105–132
13. Eisenberg D, Schwarz E, Komaromy M, Wall R (1984) Analysis of membrane and surface protein sequences with the hydrophobic moment plot. J Mol Biol 179:125–142
14. Eisenberg D, Weiss RM, Terwilliger TC (1982) The helical hydrophobic moment: a measure of the amphiphilicity of a helix. Nature 299:371–374
15. Jayasinghe S, Hristova K, White SH (2001) Energetics, stability, and prediction of transmembrane helices. J Mol Biol 312:927–934
16. Ponnuswamy PK, Gromiha MM (1993) Prediction of transmembrane helices from hydrophobic characteristics of proteins. Int J Pept Prot Res 42:326–341
17. Hirokawa T, Boon-Chieng S, Mitaku S (1998) SOSUI: classification and secondary structure prediction system for membrane proteins. Bioinformatics 14:378–379
18. von Heijne G (1992) Membrane protein structure prediction: hydrophobicity analysis and the positive-inside rule. J Mol Biol 225:487–494
19. Hofmann K, Stoffel W (1993) TMbase: a database of membrane spanning proteins segments. Biol Chem 347:166
20. Gromiha MM (1999) A simple method for predicting transmembrane alpha helices with better accuracy. Protein Eng 12:557–561
21. Juretić D, Lee B, Trinajstić N, Williams RW (1993) Conformational preference functions for predicting helices in membrane proteins. Biopolymers 33:255–273
22. Juretic D, Zucic D, Lucic B, Trinajstic N (1998) Preference functions for prediction of membrane-buried helices in integral membrane proteins. Comp Chem 22:279–294

23. Pasquier C, Promponas VJ, Palaios GA, Hamodrakas JS, Hamodrakas SJ (1999) A novel method for predicting transmembrane segments in proteins based on a statistical analysis of the SwissProt database: the PRED-TMR algorithm. Protein Eng 12:381–385
24. Kitsas IK, Hadjileontiadis LJ, Panas SM (2008) Transmembrane helix prediction in proteins using hydrophobicity properties and higher-order statistics. Comp Biol Med 38:867–880
25. Ganapathiraju M, Balakrishnan N, Reddy R, Klein-Seetharaman J (2008) Transmembrane helix prediction using amino acid property features and latent semantic analysis. BMC Bioinform 9:S4
26. Tusnady GE, Simon I (1998) Principles governing amino acid composition of integral membrane proteins: application to topology prediction. J Mol Biol 283:489–506
27. Rost B, Sander C, Casadio R, Fariselli P (1995) Transmembrane helices predicted at 95% accuracy. Protein Sci 4:521–533
28. Jones DT, Taylor WR, Thornton JM (1994) A model recognition approach to the prediction of all-helical membrane protein structure and topology. Biochemistry 33:3038–3049
29. Persson B, Argos P (1996) Topology prediction of membrane proteins. Protein Sci 5:363–371
30. Liu JF, Rost B (2001) Comparing function and structure between entire proteomes. Protein Sci 10:1970–1979
31. Cserzo M, Wallin E, Simon I, von Heijne G, Elofsson A (1997) Prediction of transmembrane alpha-helices in prokaryotic membrane proteins: the dense alignment surface method. Protein Eng 10:673–676
32. Nugent T, Jones DT (2009) Transmembrane protein topology prediction using support vector machines. BMC Bioinform 10:159
33. Osmanbeyoglu HU, Wehner JA, Carbonell JG, Ganapathiraju MK (2010) Active machine learning for transmembrane helix prediction. BMC Bioinform 11:S58
34. Ahmed R, Rangwala H, Karypis G (2010) TOPTMH: topology predictor for transmembrane alpha-helices. J Bioinform Comput Biol 8:39–57
35. Park Y, Helms V (2006) Assembly of transmembrane helices of simple polytopic membrane proteins from sequence conservation patterns. Proteins Struct Funct Bioinf 64:895–905
36. Fuchs A, Kirschner A, Frishman D (2009) Prediction of helix-helix contacts and interacting helices in polytopic membrane proteins using neural networks. Proteins Struct Funct Bioinf 74:857–871
37. Michino M, Chen JH, Stevens RC, Brooks CL (2010) FoldGPCR: structure prediction protocol for the transmembrane domain of G protein-coupled receptors from class A. Proteins Struct Funct Bioinf 78:2189–2201
38. de Brevern AG (2010) 3D structural models of transmembrane proteins. Meth Mol Biol 654:387–401
39. Schulz GE (2000) beta-Barrel membrane proteins. Curr Opin Struct Biol 10:443–447
40. Gnanasekaran TV, Peri S, Arockiasamy A, Krishnaswamy S (2000) Profiles from structure based sequence alignment of porins can identify beta stranded integral membrane proteins. Bioinformatics 16:839–842
41. Wimley WC (2002) Toward genomic identification of beta-barrel membrane proteins: composition and architecture of known structures. Protein Sci 11:301–312
42. Liu Q, Zhu YS, Wang BH, Li YX (2003) Identification of beta-barrel membrane proteins based on amino acid composition properties and predicted secondary structure. Comp Biol Chem 27:355–361
43. Gromiha MM, Suwa M (2005) A simple statistical method for discriminating outer membrane proteins with better accuracy. Bioinformatics 21:961–968
44. Gromiha MM, Ahmad S, Suwa M (2005) Application of residue distribution along the sequence for discriminating outer membrane proteins. Comp Biol Chem 29:135–142
45. Gromiha MM (2005) Motifs in outer membrane protein sequences: applications for discrimination. Biophys Chem 117:65–71
46. Rost B, Sander C (1993) Prediction of protein secondary structure at better than 70% accuracy. J Mol Biol 232:584–599

47. Ahmad S, Gromiha MM (2002) NETASA: neural network based prediction of solvent accessibility. Bioinformatics 18:819–824
48. Ahmad S, Gromiha MM, Sarai A (2003) Real value prediction of solvent accessibility from amino acid sequence. Proteins Struct Funct Genet 50:629–635
49. Ahmad S, Gromiha MM, Sarai A (2004) Analysis and prediction of DNA-binding proteins and their binding residues based on composition, sequence and structural information. Bioinformatics 20:477–486
50. Res I, Mihalek I, Lichtarge O (2005) An evolution based classifier for prediction of protein interfaces without using protein structures. Bioinformatics 21:2496–2501
51. Gromiha MM, Suwa M (2006) Influence of amino acid properties for discriminating outer membrane proteins at better accuracy. Biochim Biophys Acta 1764:1493–1497
52. Martelli PL, Fariselli P, Krogh A, Casadio R (2002) A sequence-profile-based HMM for predicting and discriminating β barrel membrane proteins. Bioinformatics 18:S46–S53
53. Bagos PG, Liakopoulos TD, Spyropoulos IC, Hamodrakas SJ (2004) A Hidden Markov Model method, capable of predicting and discriminating beta-barrel outer membrane proteins. BMC Bioinform 5:29
54. Natt NK, Kaur H, Raghava GPS (2004) Prediction of transmembrane regions of beta-barrel proteins using ANN- and SVM-based methods. Proteins Struct Funct Bioinf 56:11–18
55. Garrow AG, Agnew A, Westhead DR (2005) TMB-Hunt: a web server to screen sequence sets for transmembrane beta-barrel proteins. Nucleic Acids Res 33:W188–W192
56. Park KJ, Gromiha MM, Horton P, Suwa M (2005) Discrimination of outer membrane proteins using support vector machines. Bioinformatics 21:4223–4229
57. Ou YY, Gromiha MM, Chen SA, Suwa M (2008) TMBETADISC-RBF: discrimination of beta-barrel membrane proteins using RBF networks and PSSM profiles. Comp Biol Chem 32:227–231
58. Zhai YF, Saier MH (2002) The beta-barrel finder (BBF) program, allowing identification of outer membrane beta-barrel proteins encoded within prokaryotic genomes. Protein Sci 11:2196–2207
59. Berven FS, Flikka K, Jensen HB, Eidhammer I (2004) BOMP: a program to predict integral beta-barrel outer membrane proteins encoded within genomes of Gram-negative bacteria. Nucleic Acids Res 32:W394–W399
60. Bigelow HR, Petrey DS, Liu J, Przybylski D, Rost B (2004) Predicting transmembrane beta-barrels in proteomes. Nucleic Acids Res 32:2566–2577
61. Gromiha MM, Yabuki Y, Suwa M (2007) TMB finding pipeline: novel approach for detecting beta-barrel membrane proteins in genomic sequences. J Chem Inf Model 47:2456–2461
62. Bairoch A, Apweiler R, Wu CH, Barker WC, Boeckmann B, Ferro S, Gasteiger E, Huang HZ, Lopez R, Magrane M, Martin MJ, Natale DA, O'Donovan C, Redaschi N, Yeh LSL (2005) The universal protein resource (UniProt). Nucleic Acids Res 33:D154–D159
63. Altschul SF, Madden TL, Schaffer AA, Zhang JH, Zhang Z, Miller W, Lipman DJ (1997) Gapped BLAST and PSI-BLAST: a new generation of protein database search programs. Nucleic Acids Res 25:3389–3402
64. Gromiha MM, Yabuki Y, Kundu S, Suharnan S, Suwa M (2007) TMBETA-GENOME: database for annotated beta-barrel membrane proteins in genomic sequences. Nucleic Acids Res 35:D314–D316
65. Tsirigos KD, Bagos PG, Hamodrakas SJ (2011) OMPdb: a database of beta-barrel outer membrane proteins from Gram-negative bacteria. Nucleic Acids Res 39:D324–D331
66. Paul C, Rosenbusch JP (1985) Folding patterns of porin and bacteriorhodopsin. EMBO J 4:1593–1597
67. Vogel H, Jähnig F (1986) Models for the structure of outer-membrane proteins of Escherichia coli derived from Raman spectroscopy and prediction methods. J Mol Biol 190:191–199
68. Gromiha MM, Ponnuswamy PK (1993) Prediction of transmembrane beta strands from hydrophobic characteristics of proteins. Int J Pept Prot Res 42:420–431

69. Gromiha MM, Majumdar R, Ponnuswamy PK (1997) Identification of membrane spanning beta strands in bacterial porins. Protein Eng 10:497–500
70. Freeman TC, Wimley WC (2010) A highly accurate statistical approach for the prediction of transmembrane beta-barrels. Bioinformatics 26:1965–1974
71. Jacoboni I, Martelli PL, Fariselli P, De Pinto V, Casadio R (2001) Prediction of the transmembrane regions of beta-barrel membrane proteins with a neural network-based predictor. Protein Sci 10:779–787
72. Gromiha MM, Ahmad S, Suwa M (2004) Neural network-based prediction of transmembrane beta-strand segments in outer membrane proteins. J Comp Chem 25:762–767
73. Gromiha MM, Ahmad S, Suwa M (2005) TMBETA-NET: discrimination and prediction of membrane spanning beta-strands in outer membrane proteins. Nucleic Acids Res 33: W164–W167
74. Bagos PG, Liakopoulos TD, Hamodrakas SJ (2005) Evaluation of methods for predicting the topology of beta-barrel outer membrane proteins and a consensus prediction method. BMC Bioinform 6:7
75. Ou YY, Chen SA, Gromiha MM (2010) Prediction of membrane spanning segments and topology in beta-barrel membrane proteins at better accuracy. J Comp Chem 31:217–223
76. Saier MH, Yen MR, Noto K, Tamang DG, Elkan C (2009) The transporter classification database: recent advances. Nucleic Acids Res 37:D274–D278
77. Gromiha MM, Yabuki Y, Suresh MX, Thangakani AM, Suwa M, Fukui K (2009) TMFunction: database for functional residues in membrane proteins. Nucleic Acids Res 37:D201–D204
78. Gromiha MM, Yabuki Y (2008) Functional discrimination of membrane proteins using machine learning techniques. BMC Bioinform 9:135
79. Li HQ, Benedito VA, Udvardi MK, Zhao PX (2009) TransportTP: a two-phase classification approach for membrane transporter prediction and characterization. BMC Bioinform 10:418
80. Gromiha MM, Suwa M (2007) Current developments on beta-barrel membrane proteins: sequence and structure analysis, discrimination and prediction. Curr Prot Pept Sci 8:580–599
81. Dutzler R, Campbell EB, MacKinnon R (2003) Gating the selectivity filter in ClC chloride channels. Science 300:108–112
82. Huang YF, Lemieux MJ, Song JM, Auer M, Wang DN (2003) Structure and mechanism of the glycerol-3-phosphate transporter from *Escherichia coli*. Science 301:616–620
83. Ou YY, Chen SA, Gromiha MM (2010) Classification of transporters using efficient radial basis function networks with position-specific scoring matrices and biochemical properties. Proteins Struct Funct Bioinfo 78:1789–1797
84. Li HQ, Dai XB, Zhao XC (2008) A nearest neighbor approach for automated transporter prediction and categorization from protein sequences. Bioinformatics 24:1129–1136
85. Han J, Nilius B, Earm YE, Noble D (2010) Ion channels: growing evidence for the role in disease. Prog Biophys Mol Biol 103:1
86. Saha S, Zack J, Singh B, Raghava GPS (2006) VGIchan: prediction and classification of voltage-gated ion channels. Genomics Proteomics Bioinform 4:253–258
87. Lin H, Ding H (2011) Prediction of ion channels and their types. J Theor Biol 269(1):64–69
88. Yamanishi Y, Araki M, Gutteridge A, Honda W, Kanehisa M (2008) Prediction of drug-target interaction networks from the integration of chemical and genomic spaces. Bioinformatics 24: I232–I240
89. Kanehisa M, Goto S, Hattori M, Aoki-Kinoshita KF, Itoh M, Kawashima S, Katayama T, Araki M, Hirakawa M (2006) From genomics to chemical genomics: new developments in KEGG. Nucleic Acids Res 34:D354–D357
90. Schomburg I, Chang A, Ebeling C, Gremse M, Heldt C, Huhn G, Schomburg D (2004) BRENDA, the enzyme database: updates and major new developments. Nucleic Acids Res 32:D431–D433
91. Gunther S, Kuhn M, Dunkel M, Campillos M, Senger C, Petsalaki E, Ahmed J, Urdiales EG, Gewiess A, Jensen LJ, Schneider R, Skoblo R, Russell RB, Bourne PE, Bork P, Preissner R

(2008) SuperTarget and Matador: resources for exploring drug-target relationships. Nucleic Acids Res 36:D919–D922
92. Wishart DS, Knox C, Guo AC, Cheng D, Shrivastava S, Tzur D, Gautam B, Hassanali M (2008) DrugBank: a knowledgebase for drugs, drug actions and drug targets. Nucleic Acids Res 36:D901–D906
93. He ZS, Zhang J, Shi XH, Hu LL, Kong XY, Cai YD, Chou KC (2010) Predicting drug-target interaction networks based on functional groups and biological features. PLoS ONE 5:e9603
94. Huang C, Zhang RJ, Chen ZQ, Jiang YSA, Shang ZW, Sun P, Zhang XH, Li X (2010) Predict potential drug targets from the ion channel proteins based on SVM. J Theor Biol 262: 750–756

Pharmacology of Hyperpolarization-Activated Cyclic Nucleotide-Gated (HCN) Channels

Patrick Bois, Aurelien Chatelier, Jocelyn Bescond, and Jean-François Faivre

Contents

Abstract The current produced by hyperpolarization-activated cyclic nucleotide-gated (HCN) channels (termed I_f, cardiac pacemaker "funny" current, and I_h in neurons) is also considered a "pacemaker current" because it plays a key role in controlling the rhythmic activity of cardiac pacemaker cells and spontaneously firing neurons. The pacemaker current is an inward current activated by voltage hyperpolarization and modulated by intracellular cAMP. Voltage-dependent opening of these pacemaker channels is directly regulated by the binding of cAMP. The f-channels are encoded by four genes (HCN1–4) and are widely expressed throughout the heart and central nervous system. This article summarizes the structure, function, and regulation of these channels. Because of their relevance to cardiac pacemaker activity, f-channels are a natural target of drugs aimed at the pharmacological control of heart rate. In this regard, several agents developed for their

P. Bois (✉)
Institut de Physiologie et Biologie Cellulaires, UMR CNRS n°6187/Université de Poitiers, Bât B36, Pôle Biologie Santé, 1 rue Georges Bonnet, BP 633, 86022 Poitiers, France
e-mail: Patrick.Bois@univ-poitiers.fr

S.P. Gupta (ed.), *Ion Channels and Their Inhibitors*,
DOI 10.1007/978-3-642-19922-6_2,

capacity to selectively reduce heart rate act by specifically inhibiting f-channel function. Related compounds that could potentially be used for the treatment of diseases such as angina and heart failure are also discussed.

Keywords Brain • HCN • Heart • I_f • I_h • Ivabradine • Pacemaker

Abbreviations

CAD	Coronary artery disease
cAMP	Cyclic adenosine monophosphate
cGMP	Cyclic ganosine monophosphate
CNBD	Cyclic nucleotide binding domain
HCN	Hyperpolarization-activated cyclic nucleotide-gated I_h
HEK293	Human Embryonic Kidney 293 cells
I_f	Funny current
I_h	Hyperpolarization-activated current
Kv	Voltage-gated potassium channel
LTP	Long-term synaptic plasticity
MI	Myocardial Infarction
PKA	Protein Kinase A
PKC	Protein Kinase C
pS	Pico-Siemens
SAN	Sinoatrial node

1 Introduction

Noma and Irisawa [1] first reported the existence in sinoatrial node (SAN) tissue of a slow, time-dependent inward current that was activated by membrane hyperpolarization. This current has perplexed physiologists since it was first discovered. Initially, its properties were deemed exclusive, for which it has invariably been named I_h (h for hyperpolarization-activated), I_f (f for funny), or I_q (q for queer). Similar currents were later revealed in a diverse range of neuronal and nonneuronal cells, and today these currents are recognized as ubiquitous components of the nervous system. The current contributes to normal pacemaking activity in the sinoatrial and atrioventricular nodes in the atria, and Purkinje fibers in the ventricle [2, 3]. It also plays a role in abnormal spontaneous activity of cardiac myocytes under pathological conditions [4]. The pacemaker current also mediates repetitive firing in neurons and oscillatory activities in neuronal networks. In addition, this current acts to set the resting membrane potential of certain excitatory cells, and

may function in synaptic plasticity and the activation of sperm [5]. A notable characteristic feature of pacemaker channels is their modulation by cyclic nucleotides, i.e., cAMP and cGMP, independently of a phosphorylation process. In the 1990s, several cDNAs encoding pacemaker channels were isolated by molecular cloning [6–9]. On the basis of amino acid sequencing, four mammalian genes were revealed to code for members of the voltage-gated K (Kv) channel superfamily, and cyclic nucleotide-gated channels (see [10] for review). With regard to their dual properties, the channels were termed hyperpolarization-activated cyclic nucleotide-gated cation (HCN) channels. The four isoforms have diverse properties and variable expression patterns and can form functional heteromultimers with particular biophysical and regulatory properties.

Because of their fundamental role in cellular pacemaking, HCN channels are considered as relevant pharmacological targets, in particular with respect to the control of heart beat. A number of organic compounds have been described that block the pacemaker current in a relatively specific manner. Drug interactions and potential applications of their therapeutic use on the pacemaker current will be discussed below.

2 Molecular Structure

As described above, HCN channels belong to the family of cyclic-nucleotide gated channels and may be structurally related to voltage-sensitive potassium channels [11, 12]. Four main isoforms (see Fig. 1a), named HCN1 to HCN4, have been identified so far. The tissue distribution of HCN1, HCN2, HCN3 and HCN4 is heterogeneous, and specific expression of the different isoforms can be summarized briefly as follows: HCN1 is expressed in different regions of the central nervous system (olfactory bulb, cerebral cortex, hippocampus, superior colliculus, and cerebellum) and peripheral nervous system (dorsal root ganglion) [14]. HCN2 is present in most brain regions, with highest expression levels in the olfactory bulb, hippocampus, thalamus, and brain stem. HCN3 is widely expressed in the brain, but at low levels. HCN4 transcripts are selectively expressed in the thalamus and olfactory bulb. Besides expression in the peripheral and central nervous systems, HCN1, HCN2, and HCN4 are expressed in the heart with specific differences according to cardiac regions and species [15, 16].

All isoforms are composed of six transmembrane segments (see Fig. 1a, b) organized in a similar manner to other voltage-sensitive ion channels, i.e., voltage sensing located in the fourth segment and pore region between the fifth and the sixth segments. Voltage sensing is attributed to repetitive, positively charged amino acids (Lys and Arg) in the fourth segment, with activation or deactivation of the channel taking place according to changes in the transmembrane electrical field. While HCN channels are permeable to sodium and potassium, the pore region is characterized by a GYG sequence, which is generally considered to be a specific requirement for K channel selectivity. No clear explanation for this apparent contradiction has yet been provided. In addition to this classical transmembrane

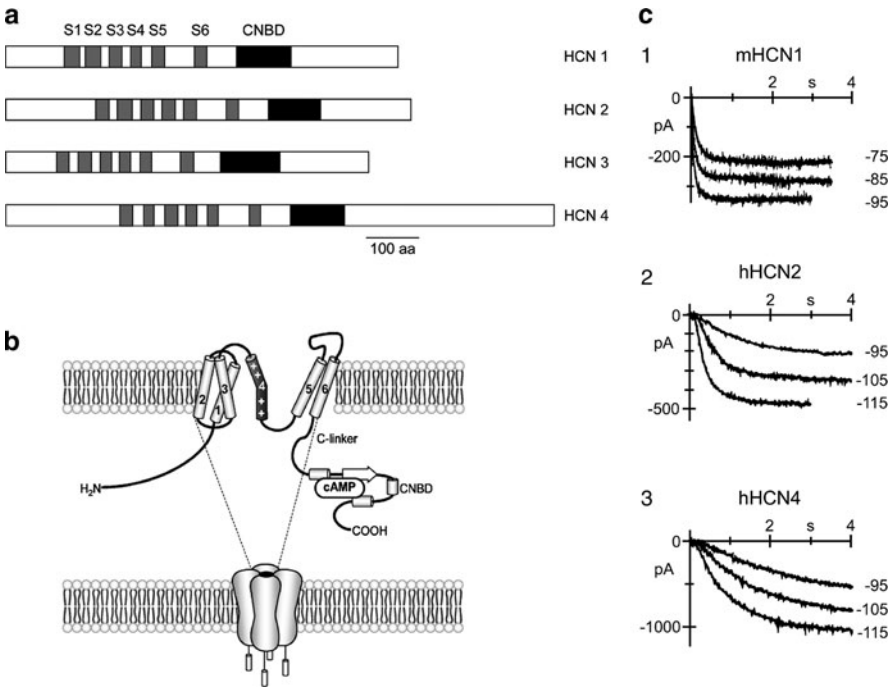

Fig. 1 (**a**) The four isoforms of the HCN family. The six transmembrane segments S1–S6 are numbered 1–6, CNBD indicates the cyclic nucleotide-binding domain. (**b**) HCN channels are tetramers. One monomer is composed of six transmembrane segments including the voltage sensor (S4) and the pore region between S5 and S6. The pore region contains the selectivity filter carrying the GYG motif. The COOH terminal channel domain is composed of the C-linker and the cyclic nucleotide-binding domain (CNBD). (**c**) Kinetic properties of the different HCN isoforms. Activation traces recorded on hyperpolarization to the indicated voltages of HEK-293 cells expressing mouse HCN1 (1), human HCN2 (2), and human HCN4 (3) channels (modified from [13])

voltage-dependent machinery, HCN proteins are characterized by a C-terminus domain, which contains consensus sequences able to bind with cyclic nucleotides (a 120 amino acid-long cyclic nucleotide binding domain, CNBD). From a functional point of view, as detailed below, channel activation is triggered by membrane hyperpolarization. The latter is facilitated by the prior binding of a cyclic nucleotide to the CNBD region. A high degree of conservation between the four HCN isoforms is observed in the transmembrane region, in the C-terminus CNBD, and in the peptide located between the sixth transmembrane domain and the CNBD (an 80 amino acid-long C-linker). In contrast, a high diversity is found in the N-terminal region and the C-terminal region downstream of the CNBD.

HCN subunits must assemble as tetramers, organized around the central pore region, to constitute functional channels. Biophysical and pharmacological properties depend on subunit composition and heterotetramerization may be necessary to constitute channels with current properties identical to native currents [17, 18].

3 Basic Biophysical Properties of HCN Channel Subtypes

An important feature of HCN channels is their activation by hyperpolarization. Generally, h-currents activate with hyperpolarizing steps to potentials negative to −50 to −70 mV. Unlike most other voltage-gated currents, I_h does not inactivate. Activation of I_h is preceded by a delay, resulting in a typical sigmoidal time course of onset. Several mechanisms have been described in the literature to explain the processes of I_h activation and deactivation that follow this delay [19]. The kinetic features of I_h require complex multi-state kinetic modeling based on the existence of distinct "delaying" and proper "gating" processes [20, 21]. Depending on the cell type, the kinetics of activation of the current are quite variable; these differences could reflect the diverse intrinsic activation properties of distinct HCN channel isoforms underlying the current and/or the experimental conditions, or even the cellular microenvironment of the HCN-channel [22].

All four HCN channel types (HCN1–4) display the principal biophysical properties of the native pacemaker current. Nevertheless, the biophysical properties vary according to experimental parameters and also diverge depending on the expression system or cell type. In general, the different isoforms differ from each other with respect to their voltage dependence and their degree of cAMP-dependent modulation. HCN2 has a more negative activation threshold than HCN1 and HCN4 [17, 20, 23]. The kinetics for voltage-dependent activation vary between the HCN channel subtypes (see Fig. 1c).

HCN1 is the fastest channel (time constant of 25–300 ms) depending on the voltage values employed [9, 24], while HCN4 is the slowest channel [25–27], displaying time constant values between a few hundred milliseconds at −140 mV up to several seconds at −70 mV. HCN2 and HCN3 activate with kinetics that range between those for HCN1 and HCN4 [9, 20, 23].

Evidence for the ion permeation properties of pacemaker channels is derived from experiments on Purkinje fibers and on isolated rabbit SA node myocytes [28, 29]. Ionic substitution experiments identified Na^+ and K^+ ions as carriers of the cardiac pacemaker f-current, with an Na^+/K^+ permeability ratio of 0.27 [28, 30]. Accordingly, HCN channels are more permeable to K^+ than to Na^+ (with permeability ratios of about 4:1 (see [16] for review). Despite this preference for K^+ conductance, h-channels carry an inward Na^+ current under physiological conditions. Moreover, the global conductance of the pacemaker current increases with external K^+ concentration [28]. It has been reported that HCN channels also display a very low permeability to Ca^{2+} [31, 32].

An ongoing discussion concerns the value of the single channel conductance of pacemaker channels [10]. Native channels recorded in isolated rabbit SAN myocytes have a very small single channel conductance estimated to be only 1 pS (see Fig. 2a) [29]. However, single channel currents recorded by Michels and coworkers [33] do not appear to be the same as those reported previously by DiFrancesco [29]. One difference is in the conductance, which for native pacemaker channels is nearly 20-fold higher than that previously reported. The

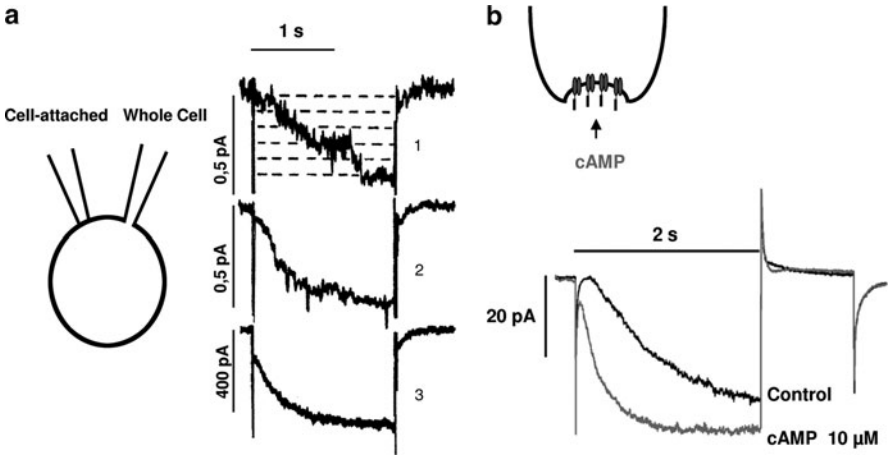

Fig. 2 (**a**) Representative recordings of pacemaker currents from whole-cell and cell-attached configurations. *1* – Single channel traces recorded from a cell-attached patch during hyperpolarization to −102 mV from a holding potential of −32 mV. *2* – Average of nine cell-attached traces. *3* – Whole-cell pacemaker current recorded with a second pipette during the same pulses (modified from [29]). (**b**) Action of cAMP on I_f activation in an inside-out macropatch. The I_f current was activated on hyperpolarization to −95 mV in a macropatch exposed to cAMP (10 µM) on the inside as represented in the *inset*

conductances reported for HCN isoforms are also very elevated (13- to 35-fold), and while the reason for this major discrepancy was not identified, it could be explained by the different cell preparations or experimental conditions (i.e., patch configurations) used. However, ensemble records shown by Michels and collaborators [33] for HCN isoforms and native h-current seem flat and do not divulge any time dependence, reflecting an instantaneous rather than a time-dependent behavior. Thus, it remains unclear whether pacemaker channels could exhibit two distinct conductances and/or different kinetics.

4 Role

As mentioned above, HCN channels generate and/or regulate neuronal and cardiac excitability. Several physiological roles have been ascribed to HCN channels, which are the consequences of their particular biophysical properties (see [16] for review).

In general, HCN channels engender and regulate neuronal and cardiac firing rates. Besides acting as a pacemaker, the HCN current also functions as a regulator of resting potential and membrane resistance. The current stabilizes the resting membrane potential because small hyperpolarizations activate the pacemaker channels, whose inward currents depolarize the cell. This depolarization, as a

consequence, deactivates the HCN channels, preventing continued departure from the resting potential. The h-channels possess an inherent negative-feedback property. On the contrary, neurotransmitters can influence rhythmic activity in both the heart and the nervous system by either increasing or decreasing the level of cAMP, which in turn directly modulates the activation kinetics and maximal current of HCN channels.

The pacemaker current is not only involved in principal rhythm generation but it also plays a key role in the regulation of heart rate by the autonomic nervous system. HCN channels are also implicated in several essential neuronal functions, which were described elegantly and in great detail by Biel et al. [16]. At least seven physiological roles have been ascribed to the h-current (1) in dendritic integration, (2) in the control of working memory, (3) in constraining hippocampal LTP (long-term synaptic plasticity), (4) in motor learning, (5) in synaptic transmission, (6) in resonance and oscillations, and (7) in the generation of thalamic rhythms.

5 Regulation

One of the most interesting characteristics of the pacemaker current is its regulation by cyclic nucleotides independently of a phosphorylation process. This mode of action of cAMP was first demonstrated by inside-out macro-patch f-current studies in rabbit SAN cells (see Fig. 2b) [34]. It was shown that cAMP directly binds to the inner face of the channel and facilitates the activation of I_h by shifting its voltage dependence of gating to more positive potentials. Further evidence of this direct regulation has been demonstrated using cAMP analogues. This study indicates that the channel's binding site may be structurally similar to the cyclic nucleotide binding site of olfactory receptor channels [35, 36]. The region implicated in ligand binding and the functional transfer of cAMP-mediated channel gating is located in the C-terminus [37, 38]. Wainger et al. [39] reported that deletion of the CNBD shifted the activation curves of HCN channels to more positive voltages by an amount similar to the maximal shift seen with saturating concentrations of cAMP. This indicates that cAMP binding enhances gating by removing a basal inhibitory action operated by the C-terminus. This mechanism had been previously suggested by Barbuti et al. [40]. cAMP shifts the $V_{1/2}$ value of human HCN2 and HCN4 channels to more positive voltages. In contrast, HCN1 and HCN3 are only weakly affected by cAMP [23, 37, 39]. All pharmacological agents or neurotransmitters, which are able to induce a change in the intracellular cAMP level modulate the h-current and consequently influence cellular pacemaking activity. For example, the adrenergic and cholinergic modulation of heart rate are directly related to the intracellular cAMP level, with cAMP acting as a major second messenger in f-channel regulation [20]. In the nervous system, serotonergic receptors in mammalian and crustacean motoneurons and in mammalian substantia nigra pars compacta neurons, as well as noradrenergic beta-receptors in neurons of the medial nucleus of the trapezoid body, and histaminergic H2 receptors in thalamic neurons

have been shown to modulate I_f via their modulation of intracellular cAMP levels (see [5, 16] for reviews). It has been reported that adenosine A1 receptors in thalamic and mesopontine neurons, and μ-opioïd receptors in nodose ganglion cells, are negatively coupled to adenylate cyclase, inducing a shift in the I_h activation curve [41, 42]. As is the case in neurons, I_f in the heart is enhanced by the stimulation of histamine H2 receptors and decreased by the action of adenosine [43, 44]. The current can also be regulated in both brain [45] and heart [46] by nitric oxide. This gas elevates cGMP levels by stimulation of soluble guanylate cyclase. Subsequent studies have suggested that I_h activity may also be regulated by protein phosphorylation and dephosphorylation [47]. A number of protein kinases have been implicated, including PKA [48, 49], PKC [48], and tyrosine kinases [50, 51]. It has also been shown that triiodothyronine (T3) enhances the pacemaker current in SA node cells isolated from rabbit heart by increasing maximal conductance without inducing a shift of the activation curve, signifying an overexpression of f-channels that possibly leads to the acceleration of the resting heart rate observed in hyperthyroïdism [52]. This overexpression has been corroborated by Pachuki et al. [53].

6 Pharmacology

6.1 Alinidine (ST567) and Clonidine

Alinidine (see Fig. 3 for chemical structure) is an antiarrhythmic drug that acts primarily on the sinus node. This *N*-allyl derivative of clonidine, a well-known α2 adrenoreceptor agonist, is a specific bradycardic agent. In the rabbit SAN, alinidine blocks I_f in the micromolar range [54]. This inhibition is associated with a reduced slope of slow diastolic depolarization and slightly prolonged action potential duration [55]. Experiments performed on sheep Purkinje fibers revealed that I_f inhibition by alinidine is a consequence of a decreased maximal conductance associated with a shift in the activation curve toward more negative potentials. These effects do not appear to be use- or frequency-dependent [56]. At present, despite its bradycardic action, alinidine is not used in therapy since it is not specific enough for I_f. Indeed, this drug also has inhibitory properties on other ionic currents as in the case, for example, of potassium and calcium conductances [54].

Recently, the α2 adrenoreceptor agonist clonidine was shown to have a direct inhibitory effect on I_f [57]. In that study, using knockout mice for the three α2 adrenoreceptors, the authors showed that clonidine induced bradycardia. Electrophysiological measurements in SAN cells confirmed that clonidine lowered the frequency of pacemaker potentials through I_f inhibition with an IC_{50} around 3 μM. HCN2 and HCN4 heterologously expressed in HEH293 cells present a similar sensitivity to clonidine, with an IC_{50} of 10 μM. This inhibition was associated with a shift in the activation curve toward more negative potentials.

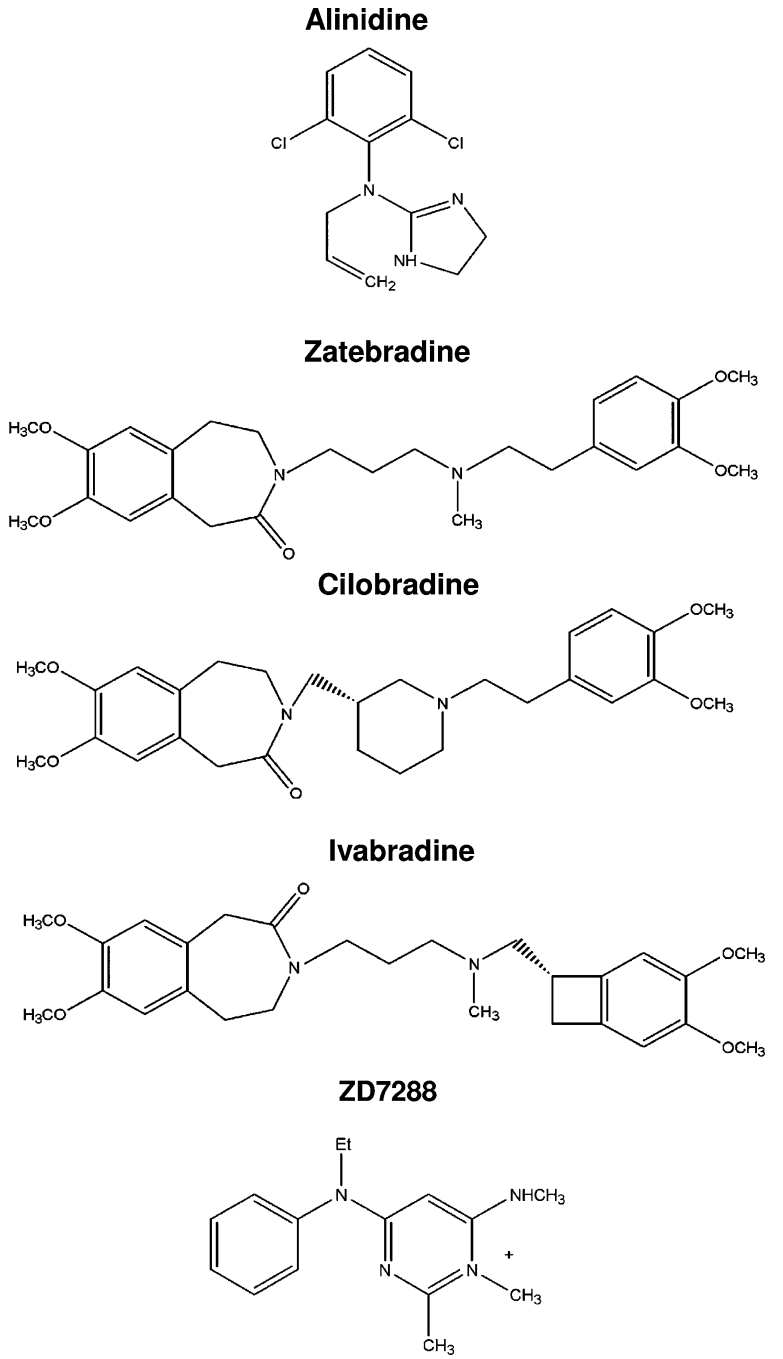

Fig. 3 Chemical structures of alinidine, zatebradine, cilobradine, ivabradine and ZD 7288

This study raises questions concerning the level of contribution of HCN channel inhibition in the bradycardic actions of clonidine observed in mouse. However, the IC_{50} for HCN2 and HCN4 seems very high to explain a major contribution of I_f inhibition in the therapeutic effects of clonidine in humans.

6.2 Zatebradine (UL-FS 49) and Cilobradine (DK-AH 269)

Zatebradine (UL-FS 49) and Cilobradine (DK-AH 269) (see chemical structures in Fig. 3) are bradycardic agents derived from structural modification of the calcium-antagonist verapamil. Both zatebradine and cilobradine cause a use-dependent block of I_f in cardiac Purkinje fibers, isolated SAN cells and the I_h current in nerve cells. More specifically, these compounds induce a concentration- and voltage-dependent inhibition of I_f, which slows diastolic depolarisation and decreases the spontaneous firing rate [58–63].

Cilobradine and zatebradine have a similar IC_{50} for the different HCN subtypes. However, use-dependent block kinetics depend on the isoform of the channel under consideration. Indeed, a study using the heterologous expression of HCN in HEK293 cells revealed that 5 μM cilobradine induces a tenfold faster use-dependent block for HCN3 and HCN4 than for HCN2 and HCN1 [63]. However, it is important to delve further into this apparent HCN isoform selectivity since the kinetics of block depend on protocol parameters such as the frequency and duration of hyperpolarizing pulses.

Interestingly, I_f recorded in murine SAN cells presents a similar use-dependent block compared to HCN4 [63]. Although cilobradine and zatebradine have similar use-dependent blocking properties, these drugs present a marked difference in their potency. Indeed, cilobradine blocks I_f and heterologously expressed HCN channels more effectively and faster than zatebradine [62, 63]. This is essentially a consequence of a slower dissociation rate associated presumably with a higher association rate.

To date, the binding site of zatebradine and cilobradine has not been fully elucidated. An investigation of the blocking mechanism of I_f by zatebradine in rabbit SAN cells indicates that this molecule blocks the channel by entering the open channel pore from the intracellular side for a distance of 39% of the membrane thickness [64]. Furthermore, a recent study using an alanine scanning mutagenesis approach revealed that mutations A425G or I432A in the S6 segment of HCN2 attenuated the block by cilobradine [65]. This block was even less effective in the double mutant I432A/A425G. These results indicate that cilobradine probably interacts with these specific residues of the S6 segment.

Besides its inhibitory action on I_f and I_h, zatebradine has been shown to block potassium currents [58, 66]. As a consequence, blocking the repolarizing current I_k in the myocardium would prolong the action potential in this tissue [67–69]. Furthermore, patients treated with zatebradine developed symptoms of visual disorders, which could be explained by the inhibitory effect of zatebradine on

retinal HCN channels [70–72]. These blocking characteristics on myocardial I_k and retinal I_h limit the possible clinical applications of zatebradine. Cilobradine appeared to be more specific than zatebradine without having any apparent effect on action potential shape when tested at low concentration on guinea-pig Purkinje fibers [62]. Experiments showed that cilobradine reduced heart rate in the rabbit without producing any negative inotropic effect, and reduced angina pectoris [73]. On that account, cilobradine might be an interesting candidate molecule for therapeutic approaches to combat cardiac diseases.

6.3 Ivabradine (S 16257)

Given that an elevated heart rate correlates with increased mortality in some cardiac diseases such as angina and heart failure, lowering heart rate is beneficial because of the reduced associated demand for oxygen and improvement in diastolic myocardial perfusion. To this extent, specific heart rate-reducing agents targeting f-channels were developed for their ability to slow heart rate by suppressing the rate of diastolic depolarization with limited side effects on action potential duration and inotropic state [74]. Among these "pure bradycardic agents", ivabradine (S 16257) [75], a compound with highly specific f-channel binding properties and typical reduction of I_f conductance, was the first I_f blocker used in clinical development and therapeutic application (see Fig. 3 for its chemical structure).

Patch-clamp studies on rabbit sinus node cells showed a selective use-dependent block of I_f in the same concentration range as that reducing the slope of spontaneous diastolic depolarisation [76, 77] (see Fig. 4a, b). Also, for concentrations close to the IC_{50} of I_f inhibition, no effect was observed on $I_{Ca,L}$, $I_{Ca,T}$, and I_{Kr}, suggesting a specific action of ivabradine on I_f in sinoatrial cells. In general, the ivabradine effect is comparable to that of zatebradine and cilobradine, since all of these drugs alter I_f by decreasing maximal conductance without changing the voltage dependence of current activation. This heart rate-reducing agent interacts with f-channels from the intracellular side [76]. Elegant studies performed on f-channels in SA node cells have provided further evidence for the precise blocking mechanism of ivabradine (for details see [77]). Ivabradine is an open-channel blocker with a block exerted when channels deactivate on depolarization (see Fig. 4c). This use-dependent property of ivabradine corresponding to drug accumulation during repetitive activity is clinically useful with respect to the better efficiency obtained at higher heart rates, when a bradycardic action is expected. The voltage-dependence of the block is a major property of ivabradine block facilitation by channel open/close cycling, with the block being stronger at depolarized voltages. The block of f-channels from the intracellular side and a better efficiency obtained at depolarized than at hyperpolarized voltages result from the chemical nature of ivabradine (positively charged at physiological pH by the presence of a quaternary ammonium ion). The action of ivabradine block can be described as "current"-dependent in that ivabradine blocks current flow by entering the pore and competing with permeating

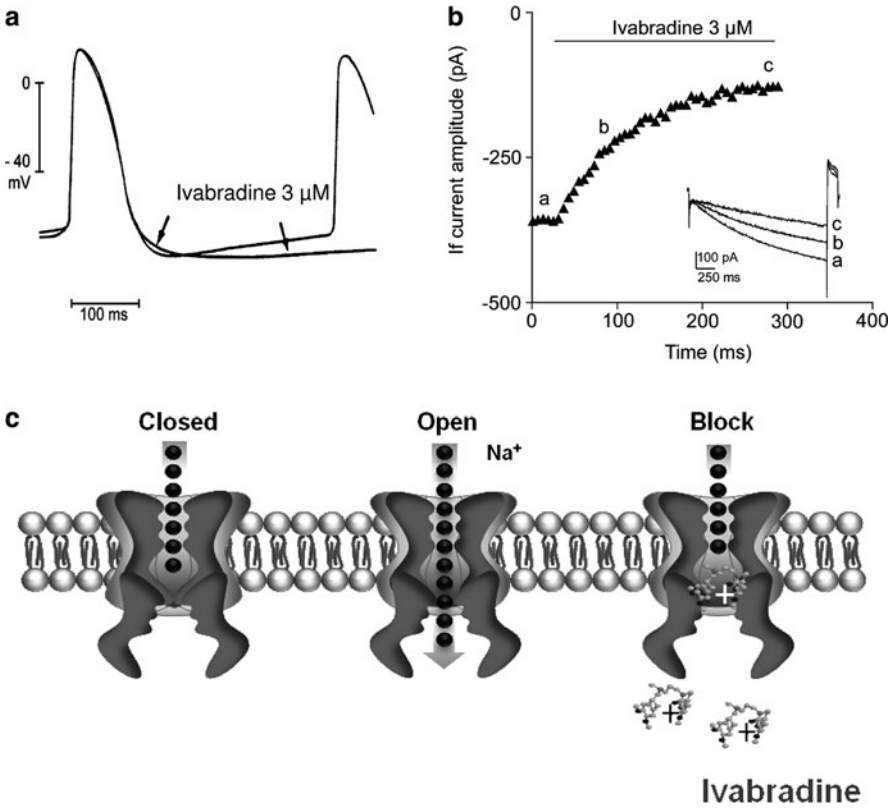

Fig. 4 (**a**) Recordings of spontaneous action potentials of rabbit sinus node preparation before and during ivabradine (3 µM) application (modified from [68]). (**b**) Use-dependent block of I_f by ivabradine (3 µM). Current was elicited by hyperpolarizing steps to −100 at 1/6 Hz. The graph plots the current–amplitude before and during ivabradine application. *Inset figures* show a set of three I_f traces specified on the graph (*a*, *b*, *c*). (**c**) Schematic representation of the specific mechanism of I_f channel blockade by ivabradine. Ivabradine enters the channel pore from the intracellular side of the channel and binds to a site in the ion permeation pathway

ions for a binding site along the permeation pathway when ions flow in the outward direction. Unblocking takes place when the current is inward during hyperpolarization. The dependence of block upon current flow was limited to HCN4, the predominant subtype present in the mammalian SAN, and is not significant for HCN1 [63, 78, 79]. This feature distinguishes the action of ivabradine from the other heart rate-reducing agents that reduce I_f in a voltage-dependent manner independently of the electrochemical gradient.

The anti-ischemic efficacy of ivabradine was initially established in pig and dog models mimicking exercise-induced angina pectoris [80–82], and was later confirmed in patients with stable angina [83, 84]. Ivabradine is, at present, the only member of the family of specific heart rate-reducing agents to have completed clinical assessment for the treatment of stable angina. Ivabradine has no side effects

on cardiac contractility and has potential for therapeutic use in patients with coronary artery disease (CAD). A large-scale, multicenter clinical trial (BEAUTI$_F$UL: the morBidity-mortality EvAlUaTion of the I_f inhibitor ivabradine in patients with coronary disease and left ventricular dysfunction) has evaluated the efficacy of ivabradine at reducing morbidity/mortality in patients with impaired left ventricular function [85, 86]. In these patients with a heart rate $\geq$70 bpm, ivabradine significantly reduces important coronary events such as myocardial infarction (MI) (by 36%) and coronary revascularisation (by 30%). Moreover, in a subgroup of patients with limited angina, the BEAUTI$_F$UL study showed that ivabradine (Procoralan) reduced the risk of the combination of primary endpoint-cardiovascular death, hospitalization for acute MI, or new or worsening heart failure by 24% in all angina patients, and by 31% in those with a heart rate $\geq$70 bpm. More recently, the Systolic Heart Failure Treatment with the If inhibitor ivabradine Trial (SHIFT) study has confirmed that high heart rate is a risk factor in heart failure, and the results support the importance of heart rate reduction with ivabradine for improvement of clinical outcomes in heart failure [87, 88]. Other ongoing clinical trials (SIGNI$_F$Y and VIVI$_F$Y) will allow a more precise analysis of the therapeutic action of ivabradine in CAD and acute coronary syndrome.

Although the f-current is the main ionic mechanism involved in the genesis and regulation of the spontaneous activity of SA node cells under physiological conditions, overexpression of pacemaker channels can be observed in pathological situations such as thyrotoxicosis, leading to sinus tachycardia [52, 53]. Overexpression of f-channels is also observed in rat hypertrophied myocytes [89] and in failing human heart [90]. Under these pathological conditions, I_f could be interacting with other mechanisms and thus contribute to the appearance of ventricular arrhythmias. In this way, we have reported that ivabradine inhibits the I_f current in atrial myocytes isolated from human right appendages with characteristics similar to those described previously in rabbit sinus node cells. In this human atrial tissue, the major HCN gene subtype detected was HCN2. The action of ivabradine could be beneficial in limiting the genesis of ectopic atrial arrhythmias, in which I_f may be involved [91].

Ivabradine could thus offer a new therapeutic strategy (or be a good candidate) to reduce these arrhythmias.

6.4 ZD 7288

ZD 7288 [4-(*N*-ethyl-*N*-phenylamino)-1,2-dimethyl-6-(methylamino) pyrimidinium chloride] (see chemical structure in Fig. 3), originally named ICI D7288, has been shown to reduce the I_f current in many different physiological preparations. In the heart, at concentrations lower than 1 μM, ZD 7288 was reported to decrease the spontaneous beating rate of guinea-pig isolated right atria with no effect on the contractile force of paced left atria [92]. This effect was attributed to a strong and specific inhibition of I_f at concentrations less than 1 μM [93]. ZD 7288 was

also shown to block the neuronal I_h current, although with less affinity than in cardiac cells [94, 95]. Precise mechanisms and molecular determinants of the effects of ZD 7288 have been the subject of continued efforts. In 2001, Shin and collaborators [96] characterized I_f blockade mechanisms by specific analysis of the effects of ZD 7288 on HCN1 expressed in HEK293 cells. They found that the blocking effects of ZD 7288 required channel opening and that the drug was trapped by closing of the channel. Interestingly, the ZD 7288 binding site has been located in the pore lining of the channel. A recent study by Cheng et al. mapped the binding site of ZD 7288 on HCN2 expressed in Xenopus oocytes [65]. Using site-directed mutagenesis, these authors reported that two amino acids located in the 6th transmembrane domain of the protein (Ala425 and Ile432) were determinant for the effect of the compound.

7 Conclusions and Future Directions

The hyperpolarization-activated cation current is clearly an important target for the treatment of stable angina in the heart. Modulation of I_h may also be a promising approach for the treatment of disease processes in the central and peripheral nervous systems. Several results suggest that HCN channels also play a prominent role in neuropathic pain (for recent review, see [97]). In this case, I_h blockers could be beneficial for analgesic therapy. Furthermore, the use of I_h blockers has also been implicated in epilepsy therapy [98]. However, given the complexity of the cellular mechanisms leading to these diseases, a clear notion for a rational design of antiepileptic I_h channel modulators has not yet emerged. Finally, HCN channels may contribute to the clinical actions of general anesthetics. Native neuronal I_h as well as heterologously expressed HCN channels are inhibited by clinically relevant concentrations of anesthetics [99–102]. In principle, existing blockers could be plausible molecular candidates. Nevertheless, these drugs inhibit all HCN isoforms with no apparent subtype selectivity and would also exert bradycardic effects. Ideal I_h neuronal blockers should not interfere with the function of sinoatrial HCN4 channels.

HCN isoforms could serve as new genetic targets in the modulation of cellular rhythmicity. For example, it was shown that HCN4 mutations underlie certain congenital cardiac arrhythmias such as the inherited form of the sick sinus syndrome [103]. Furthermore, it is essential to amplify the range of available therapeutic agents specifically targeting cardiac pacemaker channels, for instance. In this way, high affinity, subtype-specific HCN channel blockers must be developed. Moreover, one of the most important challenges in the coming years is the development of biological pacemakers, which may replace electronic devices. Indeed, pacemaker cells derived from stem cells and/or the stable in situ transfection of HCN channels represent a promising novel approach for the development of such pacemakers.

References

1. Noma A, Irisawa H (1976) Membrane currents in the rabbit sinoatrial node cell as studied by the double microelectrode method. Pflügers Arch 364:45–52
2. DiFrancesco D (1993) Pacemaker mechanisms in cardiac tissue. Annu Rev Physiol 55:455–472
3. DiFrancesco D (1995) The pacemaker current (I(f)) plays an important role in regulating SA node pacemaker activity. Cardiovasc Res 30:307–308
4. Opthof T (1998) The membrane current (I(f)) in human atrial cells:implications for atrial arrhythmias. Cardiovasc Res 38:537–540
5. Pape HC (1996) Queer current and pacemaker: the hyperpolarizationactivated cation current in neurons. Annu Rev Physiol 58:299–327
6. Gauss R, Seifert R, Kaupp UB (1998) Molecular identification of a hyperpolarization-activated channel in sea urchin sperm. Nature 393:583–587
7. Ludwig A, Zong X, Jeglitsch M et al (1998) A family of hyperpolarization-activated mammalian cation channels. Nature 393:587–591
8. Santoro B, Grant SG, Bartsch D et al (1997) Interactive cloning with the SH3 domain of N-src identifies a new brain specific ion channel protein, with homology to eag and cyclic nucleotide-gated channels. Proc Natl Acad Sci U S A 94:14815–14820
9. Santoro B, Liu DT, Yao H et al (1998) Identification of a gene encoding a hyperpolarization-activated pacemaker channel of brain. Cell 93:717–729
10. Kaupp UB, Seifert R (2001) Molecular diversity of pacemaker ion channels. Ann Rev Physiol 63:235–257
11. Craven KB, Zagotta WN (2006) CNG and HCN channels: two peas, one pod. Annu Rev Physiol 68:375–401
12. Yu FH, Yarov-Yarovoy V, Gutman GA et al (2005) Overview of molecular relationships in the voltage-gated ion channel superfamily. Pharmacol Rev 57:387–395
13. DiFrancesco D, Proenza C, Baruscotti M et al (2002) From funny current to HCN channels: 20 years of excitation. News Physiol Sci 17:32–37
14. Moosmang S, Biel M, Hofmann F, Ludwig A (1999) Differential distribution of four hyperpolarization-activated cation channels in mouse brain. Biol Chem 380:975–980
15. Robinson RB, Siegelbaum SA (2003) Hyperpolarization-activated cation currents: from molecules to physiological function. Annu Rev Physiol 65:453–480
16. Biel M, Wahl-Schott C, Stylianos M et al (2009) Hyperpolarization-activated cation channels: from genes to function. Physiol Rev 89:847–885
17. Altomare C, Terragni B, Brioschi C et al (2003) Heteromeric HCN1–HCN4 channels: a comparison with native pacemaker channels from the rabbit sinoatrial node. J Physiol 549:347–359
18. Much B, Wahl-Schott C, Zong X et al (2003) Role of subunit heteromerization and N-linked glycosylation in the formation of functional hyperpolarization-activated cyclic nucleotide-gated channels. J Biol Chem 278:43781–43786
19. DiFrancesco D (1984) Characterization of the pace-maker current kinetics in calf Purkinje fibres. J Physiol 348:341–367
20. Baruscotti M, Bucchi A, DiFrancesco D (2005) Physiology and pharmacology of the cardiac pacemaker ("funny") current. Pharm Ther 107:59–79
21. Altomare C, Bucchi A, Camatini E et al (2001) Integrated allosteric model of voltage gating of HCN channels. J Gen Physiol 117:519–532
22. Hofmann F, Biel M, Kaupp UB (2005) International union of pharmacology. LI. Nomenclature and structure-function relationships of cyclic nucleotide-regulated channels. Pharmacol Rev 57:455–462
23. Stieber J, Stockl G, Herrmann S et al (2005) Functional expression of the human HCN3 channel. J Biol Chem 280:34635–34643

24. Santoro B, Chen S, Luthi A et al (2000) Molecular and functional heterogeneity of hyperpolarization-activated pacemaker channels in the mouse CNS. J Neurosci 20:5264–5275
25. Ludwig A, Zong X, Stieber J et al (1999) Two pacemaker channels from human heart with profoundly different activation kinetics. EMBO J 18:2323–2329
26. Seifert R, Scholten A, Gauss R et al (1999) Molecular characterization of a slowly gating human hyperpolarization-activated channel predominantly expressed in thalamus, heart, and testis. Proc Natl Acad Sci U S A 96:9391–9396
27. Ishii TM, Takano M, Xie L et al (1999) Molecular characterization of the hyperpolarization-activated cation channel in rabbit heart sino-atrial node. J Biol Chem 274:12835–12839
28. DiFrancesco D (1981) A study of the ionic nature of the pace-maker current in calf Purkinje fibres. J Physiol 314:377–393
29. DiFrancesco D (1986) Characterization of single pacemaker channels in cardiac sino-atrial node cells. Nature 324:470–473
30. Frace AM, Maruoka F, Noma A (1992) External K^+ increases Na^+ conductance of the hyperpolarization-activated current in rabbit cardiac pacemaker cells. Pflügers Arch Eur J Physiol 421:97–99
31. Yu X, Duan KL, Shang CF et al (2004) Calcium influx through hyperpolarization-activated cation channels [I(h) channels] contributes to activity-evoked neuronal secretion. Proc Natl Acad Sci U S A 101:1051–1056
32. Yu X, Chen XW, Zhou P et al (2007) Calcium influx through If channels in rat ventricular myocytes. Am J Physiol Cell Physiol 292:C1147–C1155
33. Michels G, Er F, Khan I et al (2005) Single-channel properties support a potential contribution of hyperpolarization-activated cyclic nucleotide-gated channels and *If* to cardiac arrhythmias. Circulation 111:399–404
34. DiFrancesco D, Tortora P (1991) Direct activation of cardiac pacemaker channels by intracellular cyclic AMP. Nature 351:145–147
35. Bois P, Renaudon B, Baruscotti M et al (1997) Activation of f-channels by cAMP analogues in macropatches from rabbit sino-atrial node myocytes. J Physiol 501:565–571
36. Renaudon B, Bescond J, Bois P et al (1998) Nucleotide modulation of f-channel activity in rabbit sino-atrial node myocytes. Recept Channels 5:315–322
37. Viscomi C, Altomare C, Bucchi A et al (2001) C-terminus-mediated control of voltage and cAMP gating of hyperpolarization-activated cyclic nucleotide-gated channels. J Biol Chem 276:29930–29934
38. Wang J, Chen S, Siegelbaum SA (2001) Regulation of hyperpolarization-activated HCN channel gating and cAMP modulation due to interactions of COOH terminus and core transmembrane regions. J Gen Physiol 118:237–250
39. Wainger BJ, DeGennaro M, Santoro B et al (2001) Molecular mechanism of cAMP modulation of HCN pacemaker channels. Nature 411:805–810
40. Barbuti A, Baruscotti M, Altomare C et al (1999) Action of internal pronase on the f-channel kinetics in the rabbit SA node. J Physiol 520:737–744
41. Pape HC (1992) Adenosine promotes burst activity in guinea-pig geniculocortical neurons through two different mechanisms. J Physiol 447:729–753
42. Rainnie DG, Grunze HC, McCarley W et al (1994) Adenosine inhibition of mesopontine cholinergic neurons: implications for EEG arousal. Science 263:689–692
43. Satoh H (1993) Electrophysiological actions of adenosine and aminophylline in spontaneously beating and voltage-clamped rabbit sino-atrial node preparations. Naunyn Schmiedebergs Arch Pharmacol 347:197–204
44. Satoh H (1993) Modulation of automaticity by histamine and cimetidine in rabbit sino-atrial node cells. Gen Pharmacol 24:1213–1222
45. Pape HC, Mager R (1992) Nitric oxide controls oscillatory activity in thalamocortical neurons. Neuron 9:441–448
46. Musialek P, Lei M, Brown HF et al (1997) Nitric oxide can increase heart rate by stimulating the hyperpolarization-activated inward current, I(f). Circ Res 81:60–68

47. Yu H, Chang F, Cohen IS (1993) Phosphatase inhibition by calyculin A increases if in canine Purkinje fibers and myocytes. Pflügers Arch 422:614–616
48. Chang F, Cohen IS, DiFrancesco D et al (1991) Effects of protein kinase inhibitors on canine Purkinje fibre pacemaker depolarization and the pacemaker current if. J Physiol 440:367–384
49. Vargas G, Lucero MT (2002) Modulation by PKA of the hyperpolarization-activated current (Ih) in cultured rat olfactory receptor neurons. J Membr Biol 188:115–125
50. Accili EA, Redaelli G, DiFrancesco D (1997) Differential control of the hyperpolarization-activated current (If) by cAMP gating and phosphatase inhibition in rabbit sino-atrial node myocytes. J Physiol 500:643–651
51. Wu JY, Yu H, Cohen IS (2000) Epidermal growth factor increases I(f) in rabbit SA node cells by activating a tyrosine kinase. Biochim Biophys Acta 1463:15–19
52. Renaudon B, Lenfant J, Decressac S et al (2000) Thyroid hormone increases the conductance density of f-channels in rabbit sino-atrial node cells. Recept Channels 7:1–8
53. Pachuki J, Burmeister LA, Larsen PR (1999) Thyroid hormone regulates hyperpolarization-activated cyclic nucleotide-gated channel (HCN2) mRNA in the rat heart. Circ Res 85:498–503
54. Satoh H, Hashimoto K (1986) Electrophysiological study of alinidine in voltage clamped rabbit sino-atrial node cells. Eur J Pharmacol 121:211–219
55. Millar JS, Vaughan Williams EM (1983) Pharmacological mapping of regional effects in the rabbit heart of some new antiarrhythmic drugs. Br J Pharmacol 79:701–709
56. Snyders DJ, Van Bogaert PP (1987) Alinidine modifies the pacemaker current in sheep Purkinje fibers. Pflugers Arch 410:83–91
57. Knaus A, Zong X, Beetz N et al (2007) Direct inhibition of cardiac hyperpolarization-activated cyclic nucleotide-gated pacemaker channels by clonidine. Circulation 115:872–880
58. Goethals M, Raes A, Van Bogaert PP (1993) Use-dependent block of the pacemaker current I (f) in rabbit sinoatrial node cells by zatebradine (UL-FS 49). On the mode of action of sinus node inhibitors. Circulation 88:2389–2401
59. Raes A, Van de Vijver G, Goethals M et al (1998) Use-dependent block of Ih in mouse dorsal root ganglion neurons by sinus node inhibitors. Br J Pharmacol 125:741–750
60. Van Bogaert PP, Goethals M, Simoens C (1990) Use- and frequency-dependent blockade by UL-FS 49 of the if pacemaker current in sheep cardiac Purkinje fibres. Eur J Pharmacol 187:241–256
61. Van Bogaert PP, Raes A (1991) Use-dependent blockade of the If current by DK-AH3 in sheep Purkinje fibres: kinetic characteristics. Arch Int Pharmacodyn 310:191
62. Van Bogaert PP, Pittoors F (2003) Use-dependent blockade of cardiac pacemaker current (If) by cilobradine and zatebradine. Eur J Pharmacol 478:161–171
63. Stieber J, Wieland K, Stockl G et al (2006) Bradycardic and proarrhythmic properties of sinus node inhibitors. Mol Pharmacol 69:1328–1337
64. DiFrancesco D (1994) Some properties of the UL-FS 49 block of the hyperpolarization-activated current (i(f)) in sino-atrial node myocytes. Pflügers Arch 427:64–70
65. Cheng L, Kinard K, Rajamani R (2007) Molecular mapping of the binding site for a blocker of hyperpolarization-activated, cyclic nucleotide-modulated pacemaker channels. J Pharmacol Exp Ther 322:931–939
66. Valenzuela C, Delpón E, Franqueza L et al (1996) Class III antiarrhythmic effects of zatebradine. Time-, state-, use-, and voltage-dependent block of hKv1.5 channels. Circulation 94:562–570
67. Doerr T, Trautwein W (1990) On the mechanism of the "specific bradycardic action" of the verapamil derivative UL-FS 49. Naunyn Schmiedebergs Arch Pharmacol 341:331–340
68. Thollon C, Cambarrat C, Vian J et al (1994) Electrophysiological effects of S 16257, a novel sino-atrial node modulator, on rabbit and guinea-pig cardiac preparations: comparison with UL-FS 49. Br J Pharmacol 112:37–42

69. Perez O, Gay P, Franqueza L et al (1995) Electromechanical effects of zatebradine on isolated guinea pig cardiac preparations. J Cardiovasc Pharmacol 26:46–54
70. Gargini C, Demontis GC, Bisti S et al (1999) Effects of blocking the hyperpolarization-activated current (Ih) on the cat electroretinogram. Vis Res 39:1767–1774
71. Satoh TO, Yamada M (2002) Multiple inhibitory effects of zatebradine (UL-FS 49) on the electrophysiological properties of retinal rod photoreceptors. Pflügers Arch 443:532–540
72. Cervetto L, Demontis GC, Gargini C (2007) Cellular mechanisms underlying the pharmacological induction of phosphenes. Br J Pharmacol 150:383–390
73. Schmitz-Spanke S, Granetzny A, Stoffels B et al (2004) Effects of a bradycardic agent on postischemic cardiac recovery in rabbits. J Physiol Pharmacol 55:705–712
74. Simon L, Ghaleb B, Puybasset L et al (1995) Coronary and hemodynamic effects of S 16257, a new bradycardic agent, in resting and exercising conscious dogs. J Pharmacol Exp Ther 275:659–666
75. Thollon C, Bidouard JP, Cambarrat C et al (1997) Stereospecific in vitro and in vivo effects of the new sinus node inhibitor (+)-S 16257. Eur J Pharmacol 339:43–51
76. Bois P, Bescond J, Renaudon B et al (1996) Mode of action of bradycardic agent, S 16257, on ionic currents of rabbit sinoatrial node cells. Br J Pharmacol 118:1051–1057
77. Bucchi A, Baruscotti M, DiFrancesco D (2002) Current-dependent block of rabbit sino-atrial node I(f) channels by ivabradine. J Gen Physiol 120:1–13
78. Bucchi A, Tognati A, Milanesi R et al (2006) Properties of ivabradine-induced block of HCN1 and HCN4 pacemaker channels. J Physiol 572:335–346
79. Thollon C, Bedut S, Villeneuve N et al (2007) Use-dependent inhibition of hHCN4 by ivabradine and relationship with reduction in pacemaker activity. Br J Pharmacol 150:37–46
80. Monnet X, Ghaleb B, Colin P et al (2001) Effects of heart rate reduction with ivabradine on exercise-induced myocardial ischemia and stunning. J Pharmacol Exp Ther 299:1133–1139
81. Vilaine JP, Bidouard JP, Lesage L et al (2003) Anti-ischemic effects of ivabradine, a selective heart rate-reducing agent, in exercise-induced myocardial ischemia in pigs. J Cardiovasc Pharmacol 42:688–696
82. Monnet X, Colin P, Ghaleb B et al (2004) Heart rate reduction during exercise-induced myocardial ischaemia and stunning. Eur Heart J 25:579–586
83. Borer JS, Fox K, Jaillon P et al (2003) Ivabradine Investigators Group. Antianginal and antiischemic effects of ivabradine, an I(f) inhibitor, in stable angina: a randomized, double-blind, multicentered, placebo-controlled trial. Circulation 107:817–823
84. Tardif JC, Ford I, Tendera M et al (2005) INITIATIVE investigators. Efficacy of ivabradine, a new selective I(f) inhibitor, compared with atenolol in patients with chronic stable angina. Eur Heart J 26:2529–2536
85. Fox K, Ford I, Steg PG et al (2008) BEAUTIFUL investigators. Ivabradine for patients with stable coronary artery disease and left-ventricular systolic dysfunction (BEAUTIFUL): a randomised, double-blind, placebo-controlled trial. Lancet 372:807–816
86. Fox K, Ford I, Steg PG et al (2008) BEAUTIFUL investigators. Heart rate as a prognostic risk factor in patients with coronary artery disease and left-ventricular systolic dysfunction (BEAUTIFUL): a subgroup analysis of a randomised controlled trial. Lancet 372:817–821
87. Böhm M, Swedberg K, Komajda M et al (2010) SHIFT investigators. Heart rate as a risk factor in chronic heart failure (SHIFT): the association between heart rate and outcomes in a randomised placebo-controlled trial. Lancet 376:886–894
88. Swedberg K, Komajda M, Böhm M et al (2010) SHIFT investigators. Ivabradine and outcomes in chronic heart failure (SHIFT): a randomised placebo-controlled study. Lancet 376:875–885
89. Fernandez-Velasco M, Goren N, Benito G et al (2003) Regional distribution of hyperpolarization-activated current (If) and hyperpolarization-activated cyclic nucleotide-gated channel mRNA expression in ventricular cells from control and hypertrophied rat hearts. J Physiol 553:395–405

90. Cerbai E, Pino R, Porciatti F et al (1997) Characterization of hyperpolarization-activated current, (If), in ventricular myocytes from human failing heart. Circulation 95:558–571
91. El Chemaly A, Magaud C, Patri S et al (2007) The heart rate-lowering agent ivabradine inhibits the pacemaker current I(f) in human atrial myocytes. J Cardiovasc Electrophysiol 18:1190–1196
92. Marshall PW, Rouse W, Briggs I et al (1993) ICI D7288, a novel sinoatrial node modulator. J Cardiovasc Pharmacol 21:902–906
93. BoSmith RE, Briggs I, Sturgess NC (1993) Inhibitory actions of ZENECA ZD 7288 on whole-cell hyperpolarization activated inward current (If) in guinea-pig dissociated sinoatrial node cells. Br J Pharmacol 110:343–349
94. Gasparini S, DiFrancesco D (1997) Action of the hyperpolarization-activated current (Ih) blocker ZD 7288 in hippocampal CA1 neurons. Pflügers Arch 435:99–106
95. Harris NC, Constanti A (1995) Mechanism of block by ZD 7288 of the hyperpolarization-activated inward rectifying current in guinea pig substantia nigra neurons in vitro. J Neurophysiol 74:2366–2378
96. Shin KS, Rothberg BS, Yellen G (2001) Blocker state dependence and trapping in hyperpolarization-activated cation channels: evidence for an intracellular activation gate. J Gen Physiol 117:91–101
97. Jiang YQ, Sun Q, Tu HY et al (2008) Characteristics of HCN channels and their participation in neuropathic pain. Neurochem Res 33:1979–1989
98. Kitayama M, Miyata H, Yano M et al (2003) Ih blockers have a potential of antiepileptic effects. Epilepsia 44:20–24
99. Budde T, Coulon P, Pawlowski M et al (2008) Reciprocal modulation of I(h) and I(TASK) in thalamocortical relay neurons by halothane. Pflügers Arch 456:1061–1073
100. Chen X, Sirois JE, Lei Q et al (2005) HCN subunit-specific and cAMP-modulated effects of anesthetics on neuronal pacemaker currents. J Neurosci 25:5803–5814
101. Cacheaux LP, Topf N, Tibbs GR et al (2005) Impairment of hyperpolarization-activated, cyclic nucleotide-gated channel function by the intravenous general anesthetic propofol. J Pharmacol Exp Ther 315:517–525
102. Lyashchenko AK, Redd KJ, Yang J et al (2007) Propofol inhibits HCN1 pacemaker channels by selective association with the closed states of the membrane embedded channel core. J Physiol 583:37–56
103. DiFrancesco D (2010) The role of the funny current in pacemaker activity. Circ Res 106:255–271

Advanced Molecular Modeling Techniques Applied to Ion Channels Blockers

Supa Hannongbua, Witcha Treesuwan, and Warabhorn Boonyarat

Contents

Abstract Drug molecules which can block the function of ion channels are important in the treatment of several disorders which are all generally characterized by abnormal membrane excitability, that is autoimmune disorders, hypertension,

S. Hannongbua (✉)
Department of Chemistry, Faculty of Science, Kasetsart University, Bangkok 10900, Thailand
e-mail: fscisph@ku.ac.th

S.P. Gupta (ed.), *Ion Channels and Their Inhibitors*,
DOI 10.1007/978-3-642-19922-6_3,

cardiac arrhythmias and heart failure, Alzheimer's as well as Parkinson's diseases, and many others. Molecular Docking, Molecular Dynamics simulations, quantum chemical calculations, QM/MM calculations and 2D-, 3D- and 4D-QSAR, ADMET prediction have been widely used to drug discovery. In this article, we have highlighted the most recent applications of molecular modeling techniques to ion channels blockers and given the perspective.

Keywords Ion channels blockers • Molecular modeling • QSAR • ADMET • MD simulations • Docking • Quantum chemical calculations

Abbreviations

2D-QSAR	Two-dimensional quantitative structure–activity relationships
3D	Three dimensional
3D-QSAR	Three-dimensional quantitative structure–activity relationships
4D-QSAR	Four-dimensional quantitative structure–activity relationships
A	Activity
AChBP	Acetylcholine binding protein
ADMET	Absorption, distribution, metabolism, excretion, and toxicity
AEs	Adverse events
AgTX	Agitoxin
Aβ	β-Amyloid peptide
BD	Brownian dynamics
ChTX	Charybdotoxin
CoMFA	Comparative molecular field analysis
CoMSIA	Comparative molecular similarity indices analysis
DFT	Density functional theory
FDA	Food and drug administration
GA	Genetic algorithm
GABA	Gamma-aminobutyric acid
GlyR	Glycine receptor
hASIC	The human acid-sensing ion channel
HaTx1	Hanatoxin1
hERG	The human ether-a-go-go related gene
HF	Hartree Fock
KATP	ATP-sensitive potassium channels
KCOs	Potassium channel openers
Kir	The inwardly rectifying potassium channel
KITX	Kaliotoxin
Kv	Voltage-gated potassium channel
LBD	Ligand binding domain

LIE	Linear interaction energy
LQTS	The long QT syndrome
MD	Molecular dynamics
MEP	Molecular electrostatic potential
MM-PBSA	Molecular mechanics – Poisson Boltzmann/surface area
MP2	The second order Møller–Plesset perturbation theory
MTX	Maurotoxin
nAChR	Nicotinic acetylcholine receptor
NCIDS	National cancer institute diversity set
NMR	Nuclear magnetic resonance
PAAs	Phenylalkylamines
PB	Phasic block
PcTx1	Psalmotoxin 1
POPC	1-palmitoyl-2-oleoyl-sn-glycero-3-phosphocholine
QC	Quantum chemical calculations
QM/MM	Quantum mechanics/molecular mechanics
QSAR	Quantitative structure–activity relationships
RMSF	Root-mean-square fluctuations
RyR	Ryanodine receptor
TI	Thermodynamic integration
TTX	Tetrodotoxin
VGSCs	Voltage-gated sodium channels
Vpu	Viral protein U

1 Significance and Background

1.1 Ion Channels as Targets for Drugs

Ion channels are a subtype of integral transmembrane proteins (IDP). The determination of potassium channel structure by MacKinnon R. and co-workers [1] was the first to reveal that ions passing through the ion channel can induce different molecular signals. As these discoveries have had a significant impact on the scientific community, Peter Agre [2], for his earlier work on the related IDP, aquaporin, and Roderick MacKinnon were awarded the Nobel Prize in Chemistry in 2003.

Ion channels are found in every living cell. The channels are complex integral transmembrane proteins and function as a pathway for ion flow in and out of cells. These mechanisms lead to neurotransmission or signaling processes that can trigger or inhibit downstream physiological cell actions. Therefore, ion channels are associated with several diseases such as Alzheimer's disease, schizophrenia, epilepsy, anxiety disorders [3, 4], Parkinson's disease [5], cancer [6, 7], Lambert–Eaton myasthenic syndrome [8], and cardiovascular disease [9–11].

1.2 Type of Ion Channels

Ion channels, along with transporter proteins, display a huge diversity in terms of their structure and topology. Busch W. and co-workers were therefore able to establish the transporter classification system in 2002 to easily summarize structural information for researchers [12].

Ion channels can be classified by the nature of their gating mechanism, for instance, the voltage-gated ion channels, ligand-gated ion channels, and other gating ion channels. Voltage-gated ion channels are activated in response to depolarization of membrane potential [13]. When conformational change to the open state occurs, ions become permeable [14]. In the resting or closed channel state, repolarization of the membrane potential leads to reduced microscopic currents [15].

Voltage-gated ion channels show selectivity toward ions; Na^+, K^+, and Ca^{2+} channels (Figs. 1 and 2). Positively charged residues located on transmembrane segment S4 act as the voltage sensor leading to the alteration of gate currents and conformational change [16]. Ligand-gated ion channels mostly exist in pentamer. Several types of ligand-gated ion channels are found, however, the evolutionary tree of 106 sequences of ligand-gated ion channels had been generated by Ortells O. M. and co-workers in 1995 [17]. Ligand-gated ion channels are activated by

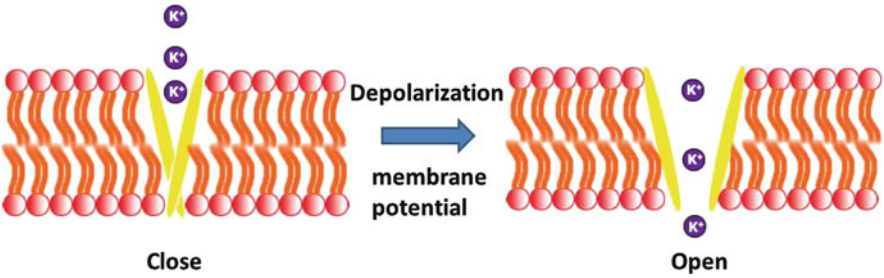

Fig. 1 An illustration of the voltage-gated potassium channel in closed and opened state

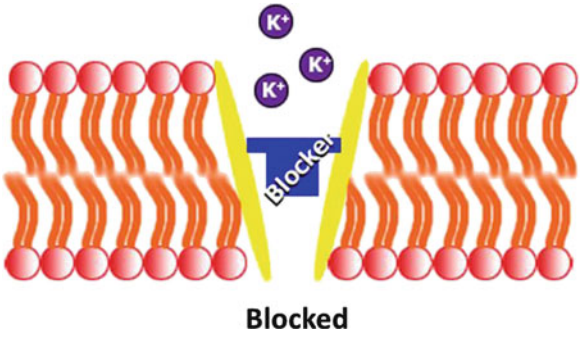

Fig. 2 An illustration of the voltage-gated potassium channel blocker such as R(+)-bupivacaine

specific molecules before the channel opens and ion flux. An example of ligand-gated ion channels is acetylcholine receptor (AChR), whereas acetylcholine is the gating molecule for Na^+ flow [18]. The binding site for ligands is located between the M2 subunit transmembrane region and extracellular loop C terminus [19].

1.3 Function of Ion Channels Blockers

Molecules that bind to ion channels resulting in the blockage of ion flux are termed ion channels blockers. The blockage of cellular signaling is important in pharmaceutical therapies including antitumor agent such as astemizole or imipramine [20], hypertension treatments [21] and decrease anti-inflammatory and bone resorption or Periodontal Disease [22].

Blockage of the voltage-gated potassium channel Kv1.3 found in the effective memory T cell (T_{EM}) is known to inhibit calcium signaling and cell proliferation [23]. Therefore, Kv1.3 blockers such as clofazimine have been used to treat sclerosis [24], graft-versus-host disease, cutaneous lupus, and pustular psoriasis [25]. The ion channel activity in the presence and absence of a blocker can be determined through the detection of the channel current using the patch clamp technique [26]. Recently, the anti-neuroexciting properties of novel Na^+ channel blocker was also assessed using whole-cell patch clamp recordings [27]. However, insight into the binding of blockers at the molecular level can be only obtained from computational methods at present.

1.4 Current Advanced Molecular Modeling Techniques Applied on Ion Channels Blockers

Computational research on the ion channels has grown dramatically since the first three-dimensional structure of the KcsA potassium channel was discovered in 1998 [1]. Molecular dynamics (MD) simulations of the KcsA potassium channel revealed the origin of the selectivity of the channel for Na^+ and K^+ ions of the channel. The complete solvation of the K^+ ions at the selectivity filter leads to the smaller passing energy barrier than Na^+ ions as large as 12 kT. Investigation on the thermodynamics using MD also suggested that the channel conductance is driven by the strength of the electrostatic interactions with ions and dipoles of residues rather than ion mobility itself [28].

In one of the earliest computational study of blockers, a simple molecular mechanics protocol with MMP2 parameters was used to optimize a series of 4-amino-*N*-phenylbenzamides followed by Monte Carlo (MC) simulations, which were compared with results from the maximal electroshock (MES) test. That study suggested that the high anticonvulsant activity required conformations where the

N-phenyl ring forms intermolecular hydrogen bonds to the backbone NH group and the orientation of the *ortho*-methyl substituent toward the backbone NH group [29].

That structural information at the molecular level can be obtained, which are helpful to understand the fundamental mechanism of chemical events occurring as these insights can aid the design of novel ion channels blockers. Several established approaches in computational chemistry include; quantum calculations, molecular simulations, molecular docking or screening and structure–activity relationship (SAR), which can prove highly beneficial during the pharmaceutical development process. The number of molecular modeling publications in the ion channel area is ~550 papers at present and ~60 for channel based on searches of the Scopus database (http://www.scopus.com). In this article, we focus on a number of significant modeling examples to exemplify the current state of the art in the field.

2 Molecular Docking of the Ion Channels Blockers

Molecular docking is of fundamentally importance in modern structure-based drug design due to its ability to predict accurate binding modes of a ligand inside a given receptor [30]. The method relies on sampling conformational space of the ligand within protein environment, driven by a conformational searching algorithm and a scoring function. Two popular searching strategies that have been proposed are incremental construction algorithm [31] and genetic algorithm (GA) [32]. A scoring function involves energetic calculations for ranking different poses of ligand, which are derived from either molecular mechanics [33–35] or empirical free energy [36].

The pharmaceutical major interested is to identify the interactions between blockers and protein channels. When the binding mechanism of blockers have not been solved yet, several questions remain unclear such as where is the most favorable binding site, how the blockers generally bind, which other types of ligand can bind, what are the key residues, etc. Molecular docking is an approach to answer to these questions. For instance, molecular docking has revealed the blocking site of Kir2.1 potassium channel [37], hERG potassium channel [38], GABA receptor [39], Torpedo nicotinic acetylcholine receptor [40], and suggested the binding conformation of the flexible blockers such as hanatoxin [41], bupivacaine [42], sertindole [43], and psalmotoxin-1 [44]. The key residues of the protein channel for the binding of ligands can be revealed when incorporating molecular docking with MD simulations [43, 45–47].

The molecular docking approach has a significant impact on high-throughput virtual screening to search for novel blockers of ion channels [48, 49]. Not only these characters were explored by molecular docking, but also new docking techniques for the ion channel blockers were introduced [50]. Moreover, molecular docking often generates the initial complex geometry used for later MD simulations.

2.1 Exploration of the Binding Sites on Ion Channels

The binding site of the ion channel can vary since the channel receptors usually have three domains; the extracellular-loop domain, the transmembrane domain, and the cytoplasmic domain. Molecular docking helps to predict the putative binding site or suggest novel interactions. For example, the cardiac inwardly rectifying K+ (Kir) channels, spermine is a blocker of the Kir2.1 potassium channel, which selected to bind in the cytoplasmic site surrounding by Asp255, Glu299, and Glu224, rather than the pore center in transmembrane domain [37]. On the contrary, carvedilol binds in the channel pore, where the binding site located at the cytosolic portion of inner helix containing Cys166, causing the carvedilol to preferably block Kir6.xs and Kir3.xs over the Kir2.xs [44].

When a combined method of docking followed by MD simulations can often allow greater insight, such as helping to identify multiple binding sites of the Kir6.2 channel and binding modes of imidazoline derivatives were revealed from docking/MD study when each blocker is accommodated in different site [51]. The open-state Kv1.5 actually contains two binding sites inside the channel pore for bupivacaine, which are at the selectivity filter (upper cavity) and a narrower ProValPro-bends (lower cavity) [42]. Putative binding site predicted by docking is confirmed by specific experiment. After amiloride and its derivatives were docked into the human acid-sensing ion channel (hASIC-1), the putative potential binding site was experimentally confirmed using whole-cell patch clamp [52]. A complex of the tarantula toxin PcTx1/hASIC-1a is first introduced by docking/MD technique. Moreover, novel binding recognition is also revealed when four domains participated in the binding but only two subunits of hASIC-1a directly interact with the PcTx1 [44].

For the Cys-loop family, when docking the γ-aminobutyric acid (GABA) into the specific site of the GABA receptor, the binding pocket is any region that supports cation–π interaction [39]. The glycine receptor (GlyR) is a target for ginkgolide A and ginkgolide X, where docking predicts that the putative binding site is formed by the 6′ M2, 2′, 10′ and 13′ residues, instead of only 6′ M2 residue [53]. Docking diverse molecules consisting of agonists and antagonists into α7-nAChR showed that the putative binding site consists of evolutionary conserved residues Ser34, Gln55, Ser146 and Tyr166. Virtual mutations of S34A/T/Y, G55A/E/N, S146A/T/Y, and Y166A/F/S generate class-specific residues that form H-bond to antagonists indicating the high sensitivity of ligand binding. In a large pocket such as that of the hERG potassium ion channel, where diverse molecule can bind and activate the gating mechanism, docking of propafenone derivatives into the closed and open state of the hERG provided the first insight into ligand binding [38].

2.2 Exploration of the Bound Blocker Conformation

Molecular docking can also be used to identify the blocker binding conformation to the ion channel. The gating modifier toxins such as Hanatoxin (HaTx1) bind

selectively to the carboxyl terminus of S3 segment (S3C) in voltage-gated potassium (Kv) channel and have been studied by Lou and co-workers. Docking of the helix drk1 S3C onto the HaTx1 generated several possibilities for the drk1 S3C orientation. The best energetic configuration revealed that the important region of interaction were the hydrophobic patch between drk1 and HaTx1. Therefore, the hydrophobic Val271, Tyr274, Leu275 and Val282 of drk1 S3C should be located at the boundary of membrane rather than located at the aqueous phase [41]. Movement of drk1 S3C toward S4 upon conformational change of Kv channel occurs after HaTx1 binding. Therefore, the structural roles of S3C-S4 proximity in interfering with S4 translocation were investigated by docking shaker with HaTx1 comparing with drk1. A significant movement of drk1 S3C, but not the Shaker S3C, in the direction presumably toward S4 during drk1 gating in the presence of HaTx1 was suggested [54].

Docking scorpion toxin – charybdotoxin (ChTX), kaliotoxin (KITX), and agitoxin (AgTX) – into the homology voltage-gated potassium channel (Kv1.3) explained the pore model when positioning two contacts of toxin residues: the side chain of Lys27 in its extended conformation into the central axis of the pore, and the side chain of Arg24 in close steric contact with the carboxyl group of Asp386 of the channel. The best conformation obtained after docking and minimization involved interaction with Asp386 of the channel i.e., Arg24 of the toxin forms a hydrogen bond with Asp386 of one subunit and Asn30 is in immediate contact with Asp386 of the opposing subunit in the tetramer [55].

Ten homology models of NR2B subunit in the NMDA receptor, composed of the R1-R2 domain in the open and closed conformation, were created prior to dock the ifenprodil. The binding pose of the ifenprodil antagonist for the NMDA receptors (glutamate-gated ion channels, iGluRs) was revealed at the atomic level by Marinelli and co-workers [56]. Further insight into the ifenprodil mechanism of action was discovered by MD simulations followed by MM-PBSA calculations, confirming that ifenprodil stabilized the closed conformation of the R1-R2 domain [56]. The significant structural conformation of ligand was revealed when agonists such as GABA and Muscimol were placed into the $GABA_A$ receptor model using distance-screen filtration in easyDock program. Calculation of the electrostatic potential complementarity is useful to discriminate multiple docked configurations especially for charged ligands. Muscimol has greater affinity than GABA because of its structural conformation, which sees the oxazolo ring sandwiched between the faces of Tyr181 and Tyr229 in the bound state [57].

2.3 Discovery of Novel Blockers by Virtual Screening

Novel blockers can be obtained from several approaches including high-throughput screening and combinatorial synthesis. A receptor-based virtual screening performed by docking is an additional method to search for either novel ligands or investigate novel binding pockets.

In the absence of a three-dimensional structure of nicotinic acetylcholine receptor (nAChR), crystal structures of acetylcholine binding protein (AChBP) from three species of sea snails: *Lymnaea stagnalis* (Ls); *Aplysia californica* (Ac); and *Bulinus truncates* (Bt) were used instead. Ligands from the National Cancer Institute Diversity Set (NCIDS) were docked into three species of AChBP using relaxed-complex method, which involved MD simulations and docking. These yielded 15 different conformations of the AChBP. Most ligands were found to bind behind the C-loop between two subunits. Novel blockers with significant potential were identified either for the common binding to all receptor conformations or were shown to selectively bind to specific receptor conformations [49]. Screening agonists against α7-nAChR using a combination of docking and MD simulations, and in conjunction with an analysis of hydrophobic/hydrophilic interactions, yielded seven compounds as possible leads for Alzheimer's disease therapy: gx-50, gx-51, gx-52, gx-180, open3d-99008, open3d-51265, open3d-60247 [58].

Sixteen agonists with known activity for homomeric α7 channels of nAChR were used to validate a simplified combination of docking, cluster analysis, and MM-PBSA method. Using the relative binding free energy from the structurally different compounds in test set, morpholine-containing compounds did not appear to improve the affinity at the α7-nAChRs while two novels structurally related analogues were predicted to have a high affinity for α7 subtype and were subsequently assayed in binding experiments [59]. A ligand-based virtual screening approach can also be useful to obtain novel blockers. ATP-sensitive potassium channels (K_{ATP} channels) are a target in the treatment of diabetes, where potassium channel openers (KCOs) such as the yanoguanidines, benzopyrans, and 1,2,4-thiadiazines stimulate potassium currents. 65,208 compounds were carefully assessed for chirality, protonation state, and tautomerism was filtered using the VolSurf procedure, which are descriptors related to the GRIND, FLAP, and TOPP approaches. While final 32 hits found, the top-ranked ligands from each methods could be different. Carosati and co-worker suggested that parallel application needed to enhance the probability of finding novel KCOs [48].

3 MD Simulations of Ion Channels Blockers

An MD simulation is a theoretical method to assess dynamic aspects associated with molecular systems. Whilst changing of the molecular coordinate is determined by motions including translation, rotation and vibration causing by atomic interactions, the energy function is the key factors driven atomic movement [60]. Several energy functions are available through simulation packages such as AMBER, CHARMM, Gromacs and Tripos force field. Therefore, the particular dynamics of a system like ease of and type of conformational changes as well as thermodynamic properties can be obtained from MD simulations making this technique popular for the biomolecule systems [61]. In this section, we discuss

aspects of MD simulations as applied to ion channels blockers. There are 71 unrelated structures of ion channels reported in the protein data bank. Species, mutation, and ligand complex differences can generate several hundred structures, for instance, few 3D structures were solved experimentally; voltage-gated potassium channel [1, 62–64], proton channel [65]; ligand-gated ion channels [66–69]; acid-sensing ion channel [70].

Because of the lack of suitable experimental structures, homology modeling is generally required before exploring the interactions between an ion channel blocker and its target. MD simulations are essential for the evaluation of these models of ion channels, while additional information can be associated from mutagenesis experiment. Gating or blocker binding mechanisms can also be revealed using MD simulations. MD simulations allow us to explore the configuration of the entire protein, thus demonstrate the conformational change of the channel gate, which is of course key to the function of ion channels. To observe the physiological properties of the ligand/ion channel complex, MD simulations are often used in conjunction with molecular docking methods.

3.1 Homology Modeling of Ion Channel Models

Acquiring crystallographic structures of ion channels is a major challenge due to the difficulty in obtaining suitable protein crystals for X-ray diffraction. Only a few proteins are available, for example, the bacterial KvAP channel [71] and the acetylcholine binding protein (AChBP) of *Lymnaea stagnalis* [68]. The unknown structures of targets, such as hERG potassium (Kv) channel, p7 of Hepatitis C, and β-amyloid aggregation, can only be studied using models derived from homology modeling and MD simulations. As the formation of the ion channel is generally based on protein–protein interactions, we have selected a small number of the systems to be reviewed, for example, bundles of tetramer, pentamer and hexamer, which are typically formed to function as the ion channel.

The β-amyloid peptide (Aβ) is proposed to aggregate into a tetramer or pentamer quaternary structure according to the favorable electrostatic interactions between the monomers. The model adopts a slightly distorted *C4* symmetry structure when monomers rotate their acidic face of itself to the basic face of neighboring monomer, driven by inter-subunit interaction with lysine, glutamic, aspartic, histidine, and tyrosine [72]. Viral protein U in HIV-1 (Vpu) exists in high stability homopentameric bundles where tryptophans residues are directed out of the pore facing the lipid layer [73]. Simulations of tetrameric bundles of hERG potassium channel provide good agreement with experimental observation [74]. A well-constructed model must be maintained the structural stability during 10 ns of simulations as indicated by the small root-mean-square fluctuations (RMSF) of the C_α atoms [47]. The benefit of these homology models is shown in docking technique, which is an important process in drug design [49]. Validation of the macrobiomolecular model is generally considered with the NOE from NMR

spectroscopy or compared to biochemical activity, however, for the uncomplexed channel model; channel conductance is used as the experimental reference [72]. The conductance value (g) as obtained from (1) depends on the resistivity (ρ), pore length (L), and pore radius (r):

$$g = 1/\left(R_{\mathrm{p}} + R_{\mathrm{A}}\right) = \pi r^2/[\rho(L + 0.5\pi r)]. \quad (1)$$

The unknown structures of the complex of blockers and ion channels can also be predicted by MD simulations. The initial configuration of the complex is usually obtained by molecular docking, before relaxation by MD simulations, as exemplified in the case of the homology complex model of human voltage-gated hERG potassium channel and its blockers [43]. When a poor scoring function from docking cannot discriminate strong and weak blockers of Sertindole and its derivatives against the open-state hERG channel, short MD simulations of 250 ps was found to helpfully remove steric and electrostatic clashes, yielding more reliable models [43]. The complex with top score from docking was sometimes selected before merging the model into the lipid bilayer followed by standard MD simulations [75]. The simulations not only relax the complex model but also help to reveal the key residues involved in the binding and blocking mechanism. Validation of the complex model can be achieved using relative thermodynamics properties and experimental affinities such as $\Delta\Delta G_{\mathrm{LIE}}$ versus $\Delta\Delta G_{\mathrm{IC50}}$ [43].

3.2 MD Simulations to Describe Ion Channel Blocking Mechanism

MD simulations not only help to elucidate aspects of the interaction between a blocker and an ion channel, but they can also help to describe the internal motions and thermodynamics properties of blocking process, revealing additional aspects of the blocking mechanism. Investigation of the voltage-gated potassium (Kv1) channel subtypes by the scorpion maurotoxin (MTX) was carried out by Brownian dynamics (BD) simulations at 500 K under rigid body conditions. Thus, this predicted that MTX preferred the Kv1.2 over Kv1.1 and Kv1.3 by 4–7 kcal/mol from the more favorable electrostatic interaction between triplet contacts. Critical residues associated with MTX blockage are all positively residues i.e. Lys23, Lys27, and Lys30, which interact with three negatively charged aspartic acid residues of Kv1.2 [76]. Novel blocking patterns of gambierol toxin against Kv1.5 potassium channel, which has not been reported from experiment, found that after the gambierol was docked into the Kv1.5 and the complex was inserted into POPC membrane with solvated waters, that the gambierol interacted with different subunits of Kv1.5 tetramer as described above, as well as residues of Thr480, Val505, Val512, Val516 [75].

Reportedly key residues in the experimentally undetermined model of the α7 nicotinic acetylcholine receptor we also predicted through MD simulations [47]. In

silico mutagenesis of the influential residue (Leu118) to a negative charge residue (glutamate or aspartate) and positive charge residue (lysine or arginine) was undertaken, with production MD simulations performed for 10 ns. The conformational changes in the binding pocket we investigated by taking a set of snapshots from each trajectory, with the re-docking of the agonist. The wild-type, L118E and L118D bound acetylcholine, however L118K and L118R did not.

The blocking process leads the ion channel to undergo a large conformational change. MD simulations have been used to assess the transition path between open and resting (close) state. The mammalian voltage-gated potassium channel Kv1.5 has a specific region that controls the open and close states, that is the ProValPro-type and Gly-type of bending hinge. A combination of homology, docking and MD simulations revealed that the blocker, R(+)-bupivacaine, selectively binds to the open-state of Kv1.5, for the K^+ ion occupancy state 0101, inside the pore at the ProValPro-type of bending hinge [42]. MD simulations also suggested that the ProValPro-bend appeared much more flexible than the Gly-bend, however, the open-state channel cannot turn to the close-state with bupivacaine bound. Important residues in the Kv1.5 for ligand recognition are hydrophobic amino residues; Val505, Ile508, Val512, and Val516 [45].

Almost blockers bind at the C-loop region of nicotinic acetylcholine receptor (nAChR) where the C-loop plays as the flexible gate outside the pore. The C-loop is known to have high flexibility and distinguished from other. The dynamics of C-loop region were captured within 5 ns of MD simulations in acetylcholine binding protein (AChBP) representing the nAChR. The C-loop has less movement when blockers bind inside the pocket, especially blockers contained aromatic substituents, which can form the cage stabilized in the C-loop region [49]. MD simulations also demonstrated that transition motion in gating of nAChR depend on the tilting of the M2 helices [77]. Selective binding of the blockers is supported by kinetics experiment when imipramine binds to the desensitized state of Torpedo AChR about fivefold higher affinity than the resting state [40]. Although some part of the channel shows high flexibility, there needs to be a very stable part also. Comparison of the stable and deformation of ligand binding domain (LBD) in Glycine receptor (GlyR), which is similar to the nAChR, from 500 ps MD simulations indicated fairly similar structure. This suggested that the β-sandwich core is relatively inflexible [78].

3.3 MD Simulation Protocols

Simulation results that provided an insight into the dynamics and other properties of the system depend on how well the initial models were generated and the choice of simulation protocol, which can be varied from each specific system. In this section, we review recent MD methodology applied on ion channel and blockers.

Partial atomic charge and force field parameters must first be assigned to a ligand [45]. Prior to the initial model, specific known state maybe loaded by carefully

placed K^+ ion and water in a specific site [37], for example, the 1010 state is where K^+ ions were present at the first and third positions of the selectivity filter [45]. The channel models are usually merged into lipid bilayer of 1-palmitoyl-2-oleoyl-sn-glycero-3-phosphocholine (POPC) and solvated by SPC or TIP3P water model [75]. After the channel is inserted into the lipid bilayer, counter ions and water should be added, that is 102 mmol/dm^3 ion concentration for Kir2.1 channel [37]. Without the lipid membrane, restraining forces need to be applied to the ion channel peptide backbone to maintain structural stability. High temperature of 700 K can be used [78]. In terms of solvation, a periodic cubic box is preferable to an octahedral box [78]. For the equilibration process, a restraint is usually applied on channel backbone or alpha carbon while temperature of the system is heated to 300 K [49]. If a simulation sphere is considered [45], multilevel restraint forces may be applied with a certain region such as a radius of 30–35 Å from the binding site and a force constant of 10 kcal/mol on the intermediate region and a force constant of 100 kcal/mol [42] on the outer 35 Å region. As the channel consists of bundles of transmembrane helices, constraints may be applied to keep the channel symmetry as C5 symmetry in the case of β-amyloid peptide (Aβ) for example [72]. The force field applied to simulate the channel can be the united atom Gromos-87 [42], OPLSAA [49] and AMBER99 [40]. In the production dynamics phase, bond constraint by SHAKE or LINCS algorithms is used [49]. After minimization with or without restraint, and equilibration at 300 K, the production phase was carried at 8–10 ns. MD simulations with the multiple time step method can be an alternative approach to study the binding between ligand and ion channel, where non-bonded interactions are divided into multiple regions. According to the multiple time step approach, time step of 1 and 2 fs are applied for intramolecular and intermolecular force, respectively, to observe the impramine/nAChR binding. Several energy evaluation methods are used in the biomolecular system such as thermodynamic integration (TI), molecular mechanic/Poisson Boltzmann surface area (MM/PBSA) and scoring function, however, to quantify the binding between blocker and the ion channel, are mostly determined by MD/LIE calculations [42, 43, 45] because of its compensation between simplicity and accuracy over others.

4 QSAR Study on Ion Channels Blockers

Quantitative structure–activity relationships (QSARs) [79] are mathematical model that describe the relationship between the structure and physical properties of chemicals and their biological activities. This method has been highly utilized in the drug design area. QSAR studies have been reported to identify important structural aspects associated with the inhibition of human ion channels blockers located in heart tissue [80–86]. The obtained results illustrate the applicability of binary QSAR methods for the classification of the *human ether-a-go-go* related gene (hERG) potassium channel blocker activities and for identification of potential toxicity risks [87]. The drug-related adverse events (AEs) were highly correlated

with known drug class warning, predicted of target activities of drug and specific subset of clinical indication for which the drug may have been prescribed [88] such as QT-prolonging drug [89], antidepressant [90], antiarrhythmic drugs [91], and chloroquine groups [92]. The advantages of QSAR are that they can reduce research time, cost and the numbers of animals required to study the properties and toxicity of chemicals. QSAR is useful for assessing the properties of that are experimentally very difficult to determine as well as being relatively easy to interpret, thereby allowing the decomposition of the terms involved to allow the design and prediction of novel chemicals. However, a disadvantage of all QSAR models are that an accurate prediction may not be possible if there are not enough compounds in the training datasets used to build the initial model. The advantages and disadvantages of 2D- and 3D-QSAR studies have been critically analyzed by comparing statistics [93]. For the prediction of the hERG-channel blockers affinities, 2D-QSAR seems to be more robust than 3D-QSAR [94].

4.1 Principle of QSAR Methodology

The QSAR models have been widely used in the field of pharmaceutical chemistry, toxicology, and agro chemistry. A QSAR is the mathematical model that describes the relationship between structure and physical properties of chemical and its activity. The general formula of QSAR model is shown in (2):

$$A \text{ or } P = f(\text{molecule structure}) \tag{2}$$

where A is Activity, P is Properties and $f(\ )$ is a function, which depend on the structure of chemical or molecular descriptors.

The QSAR technique has been described in the context of the development of the model to predict hERG inhibition [85]. Fragment-based QSAR descriptor methods such as support vector regression, partial least squares, and random forests [95] have been used. The alignment of molecules and active conformation selection were the successful 3D-QSAR model by CoMFA approach such as the development of antiarrhythmic drugs, the blockade of the rapidly and slowly activating/delayed rectifier K^+ currents has been specifically studied [91]. However, QSAR analysis was successfully performed using the lipophilicity adjusted hERG potency, $pIC_{50}^{hERG} - \text{Log } D$, to identify moieties [96].

4.2 2D-QSAR of Ion Channels Blockers

We have reviewed two-dimensional quantitative structure–activity relationship (2D-QSAR) models reported in the literature and discuss the nature of the models and the descriptors involved. The descriptors for 2D-QSAR [97] can also be

categorized according to their nature, such as constitutional, topological, geometrical, electrostatic, quantum-chemical, and thermodynamic descriptors. 2D-QSAR has been used on hERG channel blockers with diverse structures [94]. For example, for 2D-QSAR of Tocainide and Mexiletine were studied using lipophilic and basic molecular properties for voltage-gated sodium channels (VGSCs) [98]. 2D-QSAR modeling was carried out on ion channels blockers of the inactive form of the human skeletal muscle sodium channel isoform $Na_v1.4$. The chemometric analysis suggested that a pharmacophore hypothesis highlighting the structural characteristics needed for an enhanced phasic block (PB) activity. Thus, it appears that 2D-QSAR models can help in determining which parts of a molecule can be modified to increase (or decrease) affinity and efficacy, providing valuable guidance in the drug discovery process [99].

4.3 3D-QSAR of Ion Channels Blockers

The initial alignment of molecules is critical to the success of three-dimensional quantitative structure–activity relationships (3D-QSAR) model such as Comparative Molecular Fields Analysis (CoMFA). Therefore, in this regard, several attempts have been made to find the most appropriate molecular alignment to obtain more predictive models. Cavalli et al. (2002) attempted to develop a quantitative model correlating the 3D stereoelectronic characteristics of a set of molecules with hERG blocking activity [89]. They first considered an initial set of QT-prolonging drugs for which the hERG potassium channel blocking activity was measured on mammalian transfected cells. The models gave a general description of the molecular features associated with the QT-prolonging ability as well as a quantitative model to predict the hERG potassium channel blocking potential of new compounds. The CoMFA model presented an acceptable level of predictivity but cannot yet be proposed as a rapid and efficient in silico tool for the early identification of the long QT syndrome (LQTS) inducing activity. Furutani et al. (2009) demonstrated a 3D-QSAR model of antidepressants at the Kir4.1 channel, which suggested that their structures share common features including a hydrogen bond acceptor and positively charged moiety [90]. Additionally, they suggest that this charged moiety interacted with the inwardly rectifying potassium (Kir) 4.1 channel pore residues by hydrogen bond and ionic interactions, which account for preferential inhibitory action on Kir4.1 [100]. In particular, the presence of a polar negatively charged group was predicted to be important for the general pharmacophore associated with hERG blockage.

4.4 4D-QSAR of Ion Channels Blockers

In four-dimensional quantitative structure–activity relationships (4D-QSARs), each blocker is represented an ensemble of different conformations, orientations,

or protonation states [101]. The resultant 4D-QSAR models can be graphically displayed and used to virtually screen libraries of compounds [102]. 4D-QSAR methods were shown to perform better than CoMSIA and CoMFA in the past [103] because the CoMFA and CoMSIA models do not generalize beyond the molecules in the training set. This study was done to explore the relationships of molecular level physicochemical properties to in vivo antiarrhythmic activity [104]. These results suggested that the log *P* descriptor was of particular importance in the 4D-QSAR model, which was developed on a set of analogs ability to displace adsorbed Ca^{2+} ions.

5 ADMET Prediction of Ion Channels Blockers

Absorption, Distribution, Metabolism, Excretion and Toxicity is an acronym for key biological properties in the fields of pharmacokinetics, pharmacodynamics and pharmacology. An understanding of the relationships between important ADMET parameters and molecular structure and properties has been used to develop in silico models [105, 106]. This includes issues such as high plasma protein binding requiring extra studies for FDA approval [107]. The Meta-Drug system represents a prototype for integrative or ADMET systems that builds on the database- and network-building tools such as MetaCore [108, 109]. Studies reported the use of Gaussian process methods for the prediction of ADMET properties associated with the *human ether-a-go-go* related gene (hERG) channel inhibition [110].

The accumulated data make it possible to construct models for predicting the ADMET properties of compounds before structural modifications are made [111]. ADMET modeling was used to derive a quantitative relationship between channel blockers and physicochemical properties [112]. The computational models based on antiarrhythmics could have helped prevent some companies from selecting noncardiovascular drugs with hERG inhibitory activity [113] and is a cheaper alternative approach to in vitro and in vivo testing [114].

Thermodynamic descriptors describe the important features associated with hERG potassium channel blockers are hydrophobic groups, the number of aromatic rings and hydrogen bond acceptor [110]. Others also suggest that hERG inhibition increases with increasing molecular weight, log*P*, or both, with ionization state playing a beneficial or detrimental affect depending on the parameter in question [107]. Oprea et al. (2004) expected advances in this area, as more tailored ADMET prediction software that gives proper treatment to charge functional groups will yield improved predictivity [115]. An understanding of the profile of drug metabolism has increasingly become an important consideration in early stages of drug development and the profound effect of metabolism has been important drug properties as metabolic stability, toxicity, and drug–drug interactions [116]. Similarly, the prediction of molecules hERG channel activity is becoming increasingly important in the drug discovery process because blockade of the hERG channel may lead to life-threatening cardiac arrhythmias [117]. To identify ADMET properties, data relating to molecular structures tested in animal or human tissues in vitro or in vivo [103].

6 Quantum Chemical Calculations of Ion Channels Blockers

6.1 Applications of Ab-Initio and DFT Methods

Quantum chemical (QC) calculations while not so frequently used in drug discovery due to their computation costs are nonetheless important tools in computer-aided drug design research. The use of QC calculations provides a more accurate description of how molecules interact and their three-dimensional conformation, which in turn is important in determining their biological function. This approach can therefore also show the connecting link between experimentally determined structures and biological function.

QC calculations can be used to understand ion channels mechanism of action, hydrogen bonding, polarization effects, spectra, ligand binding and other fundamental processes both in normal and in aberrant biological contexts. With the advancement of parallel computing and progress in computer algorithm design, more realistic models of ion channel and its blockers are possible. For example, Density Functional Theory (DFT) based on B3LYP/6-31G (d,p) calculations were used for identification of the receptor site for the blocking of the voltage dependent K+ channels by protonated aminopyridines [118], and calculate the geometry of alkaloids obtained from *Aconitum* and *Delphinium* sp. [119]. Furthermore, specific DFT calculations of charged ryanodine receptor (RyR) calcium channel were used to study the binding energy and selectivity of Ca^{2+} versus monovalent cations [120].

The precise conformation of a blocker is important for binding to all receptors including ion channels. The complementarity of molecular surfaces and electrostatic potentials between ligand and the receptor site is essential for forming stable low binding energy complexes, as the total binding energy results from the local interactions between each part of the ligand and the surrounding protein. For instance, conformational properties and partial atomic charges of bupivacaine were determined from quantum chemical calculations at the HF/6-31G* level with inclusion of solvent effects. The binding of bupivacaine to the KcsA structure was found to prefer the closed channel state [121]. Another example can be appreciated by considering the Ab–initio Hartree–Fock molecular orbital calculations, which produced complete geometry optimizations on some phenylalkylamines (PAAs) [122].

In case of the Ca^{2+}–benzene complex, optimized in the gas phase using the Hartree–Fock model with the split valence 6-311G** basis set, it was found that the attraction between small metal cations and an aromatic residue would enhance single-channel conductance [123]. Another important example that demonstrates the utility of QC methods is in modeling the carbonyl oxygen atoms that surround permeating ions is the most important factor in determining ion selectivity rather than the size of the pore or the strength of the coordinating dipoles. Geometry optimizations were performed at the HF level using the 6-311G* basis set, and final interaction energy calculations were made using MP2/6-311G* with counterpoise

correction to minimize basis set superposition error [124]. Due to the large molecular system, HF/6-31G calculations coupled with intermolecular interaction calculations can be successfully applied to study mechanistic aspects of benzothiazepine class of calcium channel blockers. [125]

6.2 Applications of QM/MM Method

Due to the large size of ion channels, quantum chemical calculations of the type describe previously cannot be applied to the full protein-complex at present. However, recently more accurate molecular modeling of larger molecules, such as in molecular biology and surface chemistry, has become feasible due to developments in computational chemistry such as the hybrid quantum mechanics/molecular mechanics (QM/MM) technique. This method is becoming increasingly popular for modeling large molecular systems. In this approach, a large molecular system can be partitioned into a small model system for the chemically important active site, where a reaction or binding event occurs, and a large model system for chemically inactive part. The active site is treated at a high level of quantum calculation with more accurate methods, while the chemically inactive part is modeled using only a molecular mechanics method.

To discover insight into how the K^+ channel promotes ion conduction was provided by the structure of the KcsA potassium channel in complex with a monoclonal Fab antibody fragment at 2.0 Å resolution [126]. The electronic structure of the selectivity filter of KcsA potassium channel was investigated by density functional theory (DFT/BLYP) and QM/MM methods. The electronic distributions were then analyzed in terms of: (a) Wannier functions, (b) local dipole moments of cations and ligands and (c) atoms in molecules analysis on the electronic structure calculations obtained from the QM/MM simulations [127].

Another example is a cation–π interaction in ion channels that can discriminate sodium channels that are either sensitive to tetrodotoxin (TTX). This structure was further refined by a mixed-mode QM/MM optimization in which the Tyr401 side chain and TTX were treated at the QM level (HF/6–31G*), and the rest of the structure was treated at the MM level (OPLS2001 force field) with water represented as a continuum [123]. To address the question about the ionization state of the Glu71/Asp80 residues of the KcsA potassium channel, QM/MM simulation scheme was used where the two residues and their surroundings were treated by first principle MD while the rest of the protein and environment was described at the force-field level [128].

Moreover, QM/MM calculations can be used to compute the molecular electrostatic potential (MEP) inside the selectivity filter of the KcsA potassium channel. An effective procedure is proposed to refine the charge parameterization of a force field to reproduce a QM/MM reference potential along an MD trajectory [129]. More importantly, the QM/MM method has been successfully applied to assist the development of improved force fields for ion channel studies. QM/MM simulations

described the coordination numbers of K^+ and Na^+ ions in the KcsA channel [130]. However, this field of research has been opened for more accuracy of the parameterization of ion channels systems.

7 Outlook and Conclusion

Molecular modeling techniques are being used to understand aspects of the structures and interactions of ion channels and their blockers. As complex structures of ion channels and their blockers are not easily determined, there are opportunities for molecular modeling to be applied in novel ion channel blocker discovery. The QSAR approach is an important method to design for high potent blockers. MD simulations and combination of molecular docking are also useful approaches to obtain the ligand binding orientation, estimation of binding energies and ranking of virtual structures prior to syntheses. Moreover, with the high powerful of computer technology, the application of quantum chemical calculations is possible for large biomolecular systems such as ion channels. The combined quantum mechanics/molecular mechanics methods are also of interest for the mechanistic investigations. However, more accurate parameters for such system are needed for further development. Taken into account, molecular modeling methods, as reviewed above, should be helpful to suggestions for new and improved candidates for ion channels blockers discovery.

Acknowledgments The authors thank Prof. S. P. Gupta for his encouragement in writing this review. We would also like to thank the Thailand Research Fund (RTA5380010) and the National Center of Excellence in Petroleum, Petrochemical Technology and Advanced Materials for financial support. W.B. is grateful to Kasetsart University through the National Research University scholarship. We also express thanks to Dr. Matthew Paul Gleeson for valuable comments and proof reading the manuscript.

References

1. Doyle DA, Cabral JM, Pfuetzner RA, Kuo A, Gulbis JM, Cohen SL, Chait BT, MacKinnon R (1998) The structure of the potassium channel: molecular basis of K+ conduction and selectivity. Science 280:69–77
2. Preston GM, Carroll TP, Guggino WB, Agre P (1992) Appearance of water channels in Xenopus oocytes expressing red Cell CHIP28 protein. Science 256:385–387
3. Schapira M, Abagyan R, Totrov M (2002) Structural model of nicotinic acetylcholine receptor isotypes bound toacetylcholine and nicotine. BMC Struct Biol 2:1–8
4. Taly A, Corringer PJ, Guedin D, Lestage P, Changeux JP (2009) Nicotinic receptors: allosteric transitions and therapeutic targets in the nervous system. Nat Rev Drug Discovery 8:733–750
5. Lang F, Strutz-Seebohm N, Seebohm G, Lang UE (2010) Significance of SGK1 in the regulation of neuronal function. J Physiol 588:3349–3354

6. Aggarwal BB, Bhardwaj A, Aggarwal RS, Seeram NP, Shishodia S, Takada Y (2004) Role of resveratrol in prevention and therapy of cancer: preclinical and clinical studies. Anticancer Res 24:2783–2840
7. Yee NS, Zhou W, Lee M (2010) Transient receptor potential channel TRPM8 is over-expressed and required for cellular proliferation in pancreatic adenocarcinoma. Cancer Lett 297:49–55
8. David P, Martin-Moutot N, Leveque C, El Far O, Takahashi M, Seagar MJ (1993) Interaction of synaptotagmin with voltage gated calcium channels: a role in Lambert–Eaton myasthenic syndrome? Neuromuscul Disord 3:451–454
9. Li ZC, Zhang FQ, Song JC, Mei QB, Zhao DH (2002) Therapeutic effects of DCDDP, a calcium channel blocker, on chronic pulmonary hypertension in rat. J Appl Physiol 92:997–1003
10. Wang Q, Curran ME, Splawski I, Burn TC, Millholland JM, VanRaay TJ, Shen J, Timothy KW, Vincent GM, De Jager T, Schwartz PJ, Towbin JA, Moss AJ, Atkinson DL, Landes GM, Connors TD, Keating MT (1996) Positional cloning of a novel potassium channel gene: KVLQT1 mutations cause cardiac arrhythmias. Nat Genet 12:17–23
11. Das DK, Maulik N (2006) Cardiac genomic response following preconditioning stimulus. Cardiovasc Res 70:254–263
12. Busch W, Saier MH Jr (2002) The transporter classification (TC) system, 2002. Crit Rev Biochem Mol Biol 37:287–337
13. Catterall WA (1995) Structure and function of voltage-gated ion channels. Annu Rev Biochem 64:493–531
14. Marban E, Yamagishi T, Tomaselli GF (1998) Structure and function of voltage-gated sodium channels. J Physiol 508:647–657
15. Pathak MM, Yarov-Yarovoy V, Agarwal G, Roux B, Barth P, Kohout S, Tombola F, Isacoff EY (2007) Closing in on the resting state of the Shaker K+ channel. Neuron 56:124–140
16. Duclohier H (2009) Structure-function studies on the voltage-gated sodium channel. Biochim Biophys Acta Biomembr 1788:2374–2379
17. Ortells MO, Lunt GG (1995) Evolutionary history of the ligand-gated ion-channel superfamily of receptors. Trends Neurosci 18:121–127
18. Karlin A (2002) Emerging structure of the nicotinic acetylcholine receptors. Nat Rev Neurosci 3:102–114
19. Imoto K, Busch C, Sakmann B, Mishina M, Konno T, Nakai J, Bujo H, Mori Y, Fukuda K, Numa S (1988) Rings of negatively charged amino acids determine the acetylcholine receptor channel conductance. Nature 335:645–648
20. Teschemacher AG, Seward EP, Hancox JC, Witchel HJ (1999) Inhibition of the current of heterologously expressed HERG potassium channels by imipramine and amitriptyline. Br J Pharmacol 128:479–485
21. Ravens U (2010) Antiarrhythmic therapy in atrial fibrillation. Pharmacol Ther 128:129–145
22. Valverde P, Kawai T, Taubman MA (2005) Potassium channel-blockers as therapeutic agents to interfere with bone resorption of periodontal disease. J Dent Res 84:488–499
23. Ren YR, Pan F, Parvez S, Fleig A, Chong CR, Xu J, Dang Y, Zhang J, Jiang H, Penner R, Liu JO (2008) Clofazimine inhibits human Kv1.3 potassium channel by perturbing calcium oscillation in T lymphocytes. PLoS One 3:e4009
24. Rangaraju S, Chi V, Pennington MW, Chandy KG (2009) Kv1.3 potassium channels as a therapeutic target in multiple sclerosis. Expert Opin Ther Targets 13:909–924
25. Wulff H, Castle NA, Pardo LA (2009) Voltage-gated potassium channels as therapeutic targets. Nat Rev Drug Discovery 8:982–1001
26. Hamill OP, Marty A, Neher E (1981) Improved patch-clamp techniques for high-resolution current recording from cells and cell-free membrane patches. Pflugers Arch Eur J Physiol 391:85–100
27. Li CL, Yang BF, Zhang JH, Jiao JD, Li BX, Wu CF (2010) Effect of ANEPIII, a novel recombinant neurotoxic polypeptide, on sodium channels in primary cultured rat hippocampal and cortical neurons. Regul Pept 164:105–112

28. Allen TW, Kuyucak S, Chung SH (1999) Molecular dynamics study of the KcsA potassium channel. Biophys J 77:2502–2516
29. Duke NEC, Codding PW (1992) Molecular modeling and crystallographic studies of 4-amino-N-phenylbenzamide anticonvulsants. J Med Chem 35:1806–1812
30. Taylor RD, Jewsbury PJ, Essex JW (2002) A review of protein-small molecule docking methods. J Comput Aided Mol Des 16:151–166
31. Rarey M, Kramer B, Lengauer T, Klebe G (1996) A fast flexible docking method using an incremental construction algorithm. J Mol Biol 261:470–489
32. Morris GM, Goodsell DS, Halliday RS, Huey R, Hart WE, Belew RK, Olson AJ (1998) Automated docking using a Lamarckian genetic algorithm and an empirical binding free energy function. J Comput Chem 19:1639–1662
33. Cornell WD, Cieplak P, Bayly CI, Gould IR, Merz KM Jr, Ferguson DM, Spellmeyer DC, Fox T, Caldwell JW, Kollman PA (1995) A second generation force field for the simulation of proteins, nucleic acids, and organic molecules. J Am Chem Soc 117:5179–5197
34. Jorgensen WL, Tirado-Rives J (1988) The OPLS potential functions for proteins. Energy minimizations for crystals of cyclic peptides and crambin. J Am Chem Soc 110:1657–1666
35. Brooks BR, Bruccoleri RE, Olafson BD, States DJ, Swaminathan S, Karplus M (1983) CHARMM: a program for macromolecular energy, minimization, and dynamics calculations. J Comput Chem 4:187–217
36. Eldridge MD, Murray CW, Auton TR, Paolini GV, Mee RP (1997) Empirical scoring functions: I. The development of a fast empirical scoring function to estimate the binding affinity of ligands in receptor complexes. J Comput Aided Mol Des 11:425–445
37. Tai K, Stansfeld PJ, Sansom MSP (2009) Ion-blocking sites of the Kir2.1 channel revealed by multiscale modeling. Biochemistry 48:8758–8763
38. Thai KM, Windisch A, Stork D, Weinzinger A, Schiesaro A, Guy RH, Timin EN, Hering S, Ecker GF (2010) The hERG potassium channel and drug trapping: insight from docking studies with propafenone derivatives. ChemMedChem 5:436–442
39. Lummis SCR (2009) Locating GABA in GABA receptor binding sites. Biochem Soc Trans 37:1343–1346
40. Sanghvi M, Hamouda AK, Jozwiak K, Blanton MP, Trudell JR, Arias HR (2008) Identifying the binding site(s) for antidepressants on the Torpedo nicotinic acetylcholine receptor: [3H]2-azidoimipramine photolabeling and molecular dynamics studies. Biochim Biophys Acta Biomembr 1778:2690–2699
41. Lou KL, Huang PT, Shiau YS, Shiau YY (2002) Molecular determinants of the hanatoxin binding in voltage-gated K+ channel drk1. J Mol Recognit 15:175–179
42. Luzhkov VB, Nilsson J, Arhem P, Aqvist J (2003) Computational modelling of the open-state Kv1.5 ion channel block by bupivacaine. Biochim Biophys Acta Protein Proteonomics 1652: 35–51
43. Osterberg F, Aqvist J (2005) Exploring blocker binding to a homology model of the open hERG K+ channel using docking and molecular dynamics methods. FEBS Lett 579: 2939–2944
44. Pietra F (2009) Docking and MD simulations of the interaction of the tarantula peptide psalmotoxin-1 with ASIC1a channels using a homology model. J Chem Inf Model 49: 972–977
45. Ander M, Luzhkov VB, Aqvist J (2008) Ligand binding to the voltage-gated Kv1.5 potassium channel in the open state – docking and computer simulations of a homology model. Biophys J 94:820–831
46. Parthiban M, Shanmughavel P, Sowdhamini R (2010) In silico point mutation and evolutionary trace analysis applied to nicotinic acetylcholine receptors in deciphering ligand-binding surfaces. J Mol Med 16:1651–1670
47. Amiri S, Shimomura M, Vijayan R, Nishiwaki H, Akamatsu M, Matsuda K, Jones AK, Sansom MSP, Biggin PC, Sattelle DB (2008) A role for Leu118 of loop E in agonist binding to the 7 nicotinic acetylcholine receptor. Mol Pharmacol 73:1659–1667

48. Carosati E, Mannhold R, Wahl P, Hansen JB, Fremming T, Zamora I, Cianchetta G, Baroni M (2007) Virtual screening for novel openers of pancreatic K_{ATP} channels. J Med Chem 50:2117–2126
49. Babakhani A, Talley TT, Taylor P, McCammon JA (2009) A virtual screening study of the acetylcholine binding protein using a relaxed-complex approach. Comput Biol Chem 33:160–170
50. M'Barek S, Chagot B, Andreotti N, Visan V, Mansuelle P, Grissmer S, Marrakchi M, El Ayeb M, Sampieri F, Darbon H, Fajloun Z, De Waard M, Sabatier JM (2005) Increasing the molecular contacts between maurotoxin and Kv1.2 channel augments ligand affinity. Proteins 60:401–411
51. Zhang R, Wang Z, Ling B, Liu Y, Liu C (2010) Docking and molecular dynamics studies on the interaction of four imidazoline derivatives with potassium ion channel (Kir6.2). Mol Simul 36:166–174
52. Qadri YJ, Song Y, Fuller CM, Benos DJ (2010) Amiloride docking to acid-sensing ion channel-1. J Biol Chem 285:9627–9635
53. Jensen AA, Bergmann ML, Sander T, Balle T (2010) Ginkgolide X is a potent antagonist of anionic Cys-loop receptors with a unique selectivity profile at glycine receptors. J Biol Chem 285:10141–10153
54. Lou KL, Huang PT, Shiau YS, Liaw YC, Shiau YY, Liou HH (2003) A possible molecular mechanism of hanatoxin binding-modified gating in voltage-gated K+ channels. J Mol Recognit 16:392–395
55. Lipkind GM, Fozzard HA (1997) A model of scorpion toxin binding to voltage-gated K+ channels. J Membr Biol 158:187–196
56. Marinelli L, Cosconati S, Steinbrecher T, Limongelli V, Bertamino A, Novellino E, Case DA (2007) Homology modeling of NR2B modulatory domain of NMDA receptor and analysis of ifenprodil binding. ChemMedChem 2:1498–1510
57. Mokrab Y, Bavro VN, Mizuguchi K, Todorov NP, Martin IL, Dunn SMJ, Chan SL, Chau PL (2007) Exploring ligand recognition and ion flow in comparative models of the human GABA type A receptor. J Mol Graphics Modell 26:760–774
58. Gu RX, Gu H, Xie ZY, Wang JF, Arias HR, Wei DQ, Chou KC (2009) Possible drug candidates for Alzheimer's disease deduced from studying their binding interactions with alpha7 nicotinic acetylcholine receptor. Med Chem 5:250–262
59. Grazioso G, Pomè DY, Matera C, Frigerio F, Pucci L, Gotti C, Dallanoce C, Amici MD (2009) Design of novel α7-subtype-preferring nicotinic acetylcholine receptor agonists: application of docking and MM-PBSA computational approaches, synthetic and pharmacological studies. Bioorg Med Chem Lett 19:6353–6357
60. Adcock SA, McCammon JA (2006) Molecular dynamics: survey of methods for simulating the activity of proteins. Chem Rev 106:1589–1615
61. Karplus M, McCammon JA (2002) Molecular dynamics simulations of biomolecules. Nat Struct Biol 9:646–652
62. Zhou M, Morais-Cabral JH, Mann S, MacKinnon R (2001) Potassium channel receptor site for the inactivation gate and quaternary amine inhibitors. Nature 411:657–661
63. Jiang Y, Lee A, Chen J, Cadene M, Chait BT, MacKinnon R (2002) Crystal structure and mechanism of a calcium-gated potassium channel. Nature 417:515–522
64. Chen X, Wang Q, Ni F, Ma J (2010) Structure of the full-length Shaker potassium channel Kv1.2 by normal-mode-based X-ray crystallographic refinement. Proc Natl Acad Sci USA 107:11352–11357
65. Nishimura K, Kim S, Zhang L, Cross TA (2002) The closed state of a H+ channel helical bundle combining precise orientational and distance restraints from solid state NMR. Biochemistry 41:13170–13177
66. Jin R, Horning M, Mayer ML, Gouaux E (2002) Mechanism of activation and selectivity in a ligand-gated ion channel: structural and functional studies of GluR2 and quisqualate. Biochemistry 41:15635–15643

67. Nury H, Poitevin F, Van Renterghem C, Changeux JP, Corringer PJ, Delarue M, Baaden M (2010) One-microsecond molecular dynamics simulation of channel gating in a nicotinic receptor homologue. Proc Natl Acad Sci USA 107:6275–6280
68. Brejc K, Van Dijk WJ, Klaassen RV, Schuurmans M, Van Der Oost J, Smit AB, Sixma TK (2001) Crystal structure of an ACh-binding protein reveals the ligand-binding domain of nicotinic receptors. Nature 411:269–276
69. Bourne Y, Radic Z, Aráoz R, Talley TT, Benoit E, Servent D, Taylor P, Molgó J, Marchot P (2010) Structural determinants in phycotoxins and AChBP conferring high affinity binding and nicotinic AChR antagonism. Proc Natl Acad Sci USA 107:6076–6081
70. Gonzales EB, Kawate T, Gouaux E (2009) Pore architecture and ion sites in acid-sensing ion channels and P2X receptors. Nature 460:599–604
71. Jiang Y, Lee A, Chen J, Ruta V, Cadene M, Chait BT, MacKinnon R (2003) X-ray structure of a voltage-dependent K+ channel. Nature 423:33–41
72. Kim ST, Weaver DF (2000) Theoretical studies on Alzheimer's disease: structures of beta-amyloid aggregates. J Mol Struct – Theochem 527:127–138
73. Cordes FS, Kukol A, Forrest LR, Arkin IT, Sansom MSP, Fischer WB (2001) The structure of the HIV-1 Vpu ion channel: modelling and simulation studies. Biochim Biophys Acta Biomembr 1512:291–298
74. Hardman RM, Stansfeld PJ, Dalibalta S, Sutcliffe MJ, Mitcheson JS (2007) Activation gating of hERG potassium channels: S6 glycines are not required as gating hinges. J Biol Chem 282:31972–31981
75. Pietraa F (2008) Binding of ciguatera toxins to the voltage-gated Kv1.5 potassium channel in the open state. Docking of gambierol and molecular dynamics simulations of a homology model. J Phys Org Chem 21:997–1001
76. Fu W, Cui M, Briggs JM, Huang X, Xiong B, Zhang Y, Luo X, Shen J, Ji R, Jiang H, Chen K (2002) Brownian dynamics simulations of the recognition of the scorpion toxin maurotoxin with the voltage-gated potassium ion channels. Biophys J 83:2370–2385
77. Cheng X, Ivanov I, Wang H, Sine SM, McCammon JA (2007) Nanosecond-timescale conformational dynamics of the human α7 nicotinic acetylcholine receptor. Biophys J 93:2622–2634
78. Speranskiy K, Cascio M, Kurnikova M (2007) Homology modeling and molecular dynamics simulations of the glycine receptor ligand binding domain. Proteins 67:950–960
79. Ekins S, Crumb WJ, Sarazan RD, Wikel JH, Wrighton SA (2002) Three-dimensional quantitative structure-activity relationship for inhibition of human ether-a-go-go-related gene potassium channel. J Pharmacol Exp Ther 301:427–434
80. Pearlstein RA, Vaz RJ, Kang J, Chen X-L, Preobrazhenskaya M, Shchekotikhin AE, Korolev AM, Lysenkova LN, Miroshnikova OV, Hendrix J, Rampe D (2003) Characterization of HERG potassium channel inhibition using CoMSiA 3D QSAR and homology modeling approaches. Bioorg Med Chem Lett 13:1829–1835
81. Aronov AM, Goldman BB (2004) A model for identifying HERG K+ channel blockers. Bioorg Med Chem 12:2307–2315
82. Aronov AM (2005) Predictive in silico modeling for hERG channel blockers. Drug Discov Today 10:149–155
83. Cianchetta G, Li Y, Kang J, Rampe D, Fravolini A, Cruciani G, Vaz RJ (2005) Predictive models for hERG potassium channel blockers. Bioorg Med Chem Lett 15:3637–3642
84. Recanatini M, Poluzzi E, Masetti M, Cavalli A, Ponti FD (2005) QT prolongation through hERG K+ channel blockade: current knowledge and strategies for the early prediction during drug development. Med Res Rev 25:133–166
85. Diller DJ, Hobbs DW (2007) Understanding hERG inhibition with QSAR models based on a one-dimensional molecular representation. J Comput Aided Mol Des 21:379–393
86. Kramer C, Beck B, Kriegl JM, Clark T (2008) A composite model for hERG blockade. ChemMedChem 3:254–265
87. Thai K-M, Ecker GF (2008) A binary QSAR model for classification of hERG potassium channel blockers. Bioorg Med Chem 16:4107–4119

88. Matthews EJ, Kruhlak NL, Daniel Benz R, Sabaté DA, Marchant CA, Contrera JF (2009) Identification of structure-activity relationships for adverse effects of pharmaceuticals in humans: Part C: use of QSAR and an expert system for the estimation of the mechanism of action of drug-induced hepatobiliary and urinary tract toxicities. Regul Toxicol Pharmacol 54:43–65
89. Cavalli A, Poluzzi E, De Ponti F, Recanatini M (2002) Toward a pharmacophore for drugs inducing the long QT syndrome: insights from a CoMFA Study of HERG K+ channel blockers. J Med Chem 45:3844–3853
90. Furutani K, Ohno Y, Inanobe A, Hibino H, Kurachi Y (2009) Mutational and in silico analyses for antidepressant block of astroglial inward-rectifier Kir4.1 channel. Mol Pharmacol 75:1287–1295
91. Satuluri VSAK, Seelam J, Gupta SP (2009) A quantitative structure-activity relationship study on some series of potassium channel blockers. Med Chem 5:87–92
92. Furutani K, Hibino H, Inanobe A, Kurachi Y (2009) Compound-induced block of ion channel pore function: inward-rectifier potassium channels as a model. Mol Cell Pharmacol 75:1287–1295
93. van de Waterbeemd H (2008) Introduction. Advanced Computer-Assisted Techniques in Drug Discovery, Wiley-VCH Verlag GmbH
94. Yoshida K, Niwa T (2006) Quantitative structure – activity relationship studies on inhibition of HERG potassium channels. J Chem Inf Model 46:1371–1378
95. Song M, Clark M (2005) Development and evaluation of an in silico model for hERG binding. J Chem Inf Model 46:392–400
96. Shamovsky I, de Graaf C, Alderin L, Bengtsson M, Bladh H, Borjesson L, Connolly S, Dyke HJ, van den Heuvel M, Johansson H, Josefsson B-G, Kristoffersson A, Linnanen T, Lisius A, Mannikko R, Norden B, Price S, Ripa L, Rognan D, Rosendahl A, Skrinjar M, Urbahns K (2009) Increasing selectivity of CC chemokine receptor 8 antagonists by engineering nondesolvation related interactions with the intended and off-target binding sites. J Med Chem 52:7706–7723
97. Perkins R, Fang H, Tong W, Welsh WJ (2003) Quantitative structure-activity relationship methods: perspectives on drug discovery and toxicology. Environ Toxicol Chem 22:1666–1679
98. Carrieri A, Muraglia M, Corbo F, Pacifico C (2009) 2D- and 3D-QSAR of Tocainide and Mexiletine analogues acting as Nav1.4 channel blockers. Eur J Med Chem 44:1477–1485
99. Mungalpara J, Pandey A, Jain V, Mohan C (2010) Molecular modelling and QSAR analysis of some structurally diverse N-type calcium channel blockers. J Mol Model 16:629–644
100. Su B-H, M-y S, Esposito EX, Hopfinger AJ, Tseng YJ (2010) In silico binary classification QSAR models based on 4D-fingerprints and MOE descriptors for prediction of hERG blockage. J Chem Inf Model 50:1304–1318
101. Vedani A, Briem H, Dobler M, Dollinger H, McMasters DR (2000) Multiple-conformation and protonation-state representation in 4D-QSAR: the neurokinin-1 receptor system. J Med Chem 43:4416–4427
102. Krasowski MD, Hong X, Hopfinger AJ, Harrison NL (2002) 4D-QSAR analysis of a set of propofol analogues: mapping binding sites for an anesthetic phenol on the GABAA receptor. J Med Chem 45:3210–3221
103. Ekins S, Kortagere S, Iyer M, Reschly EJ, Lill MA, Redinbo MR, Krasowski MD (2009) Challenges predicting ligand-receptor interactions of promiscuous proteins: the nuclear receptor PXR. PLoS Comput Biol 5:e1000594
104. Klein CDP, Hopfinger AJ (1998) Pharmacological activity and membrane interactions of antiarrhythmics: 4D-QSAR/QSPR analysis. Pharm Res 15:303–311
105. van de Waterbeemd H, Gifford E (2003) ADMET in silico modelling: towards prediction paradise? Nat Rev Drug Discov 2:192–204
106. Shaikh SA, Jain T, Sandhu G, Latha N, Jayaram B (2007) From drug target to leads-sketching a physicochemical pathway for lead molecule design in silico. Curr Pharm Des 13:3454–3470

107. Gleeson MP (2008) Generation of a set of simple, interpretable ADMET rules of thumb. J Med Chem 51:817–834
108. Ekins S, Andreyev S, Ryabov A, Kirillov E, Rakhmatulin EA, Sorokina S, Bugrim A, Nikolskaya T (2006) A combined approach to drug metabolism and toxicity assessment. Drug Metab Dispos 34:495–503
109. Ekins S, Bugrim A, Brovold L, Kirillov E, Nikolsky Y, Rakhmatulin E, Sorokina S, Ryabov A, Serebryiskaya T, Melnikov A, Metz J, Nikolskaya T (2006) Algorithms for network analysis in systems-ADME/Tox using the MetaCore and MetaDrug platforms. Xenobiotica 36:877–901
110. Obrezanova O, Csanyi G, Gola JMR, Segall MD (2007) Gaussian processes: a method for automatic QSAR modeling of ADME properties. J Chem Inf Model 47:1847–1857
111. Li H, Zheng M, Luo X, Zhu W, Jiang H, Begley TP (2007) Drug Discovery and Development: Computational Approaches. Wiley Encyclopedia of Chemical Biology. John Wiley & Sons, Inc
112. Garg D, Gandhi T, Gopi Mohan C (2008) Exploring QSTR and toxicophore of hERG K+ channel blockers using GFA and HypoGen techniques. J Mol Graphics Modell 26:966–976
113. Ekins S (2003) In silico approaches to predicting drug metabolism, toxicology and beyond. Biochem Soc Trans 31:611–614
114. Kier L, Hall L (2005) The prediction of ADMET properties using structure information representations. Chem Biodivers 2:1428–1437
115. Oprea TI, Matter H (2004) Integrating virtual screening in lead discovery. Curr Opin Chem Biol 8:349–358
116. Li H, Yap C, Ung C, Xue Y, Li Z, Han L, Lin H, Chen Y (2007) Machine learning approaches for predicting compounds that interact with therapeutic and ADMET related proteins. J Pharm Sci 96:2838–2860
117. Nisius B, Goller AH (2009) Similarity-based classifier using topomers to provide a knowledge base for hERG channel inhibition. J Chem Inf Model 49:247–256
118. Muñoz-Caro C, Niño A (2002) The nature of the receptor site for the reversible K+ channel blocking by aminopyridines. Biophys Chem 96:1–14
119. Turabekova M, Rasulev B, Levkovich M, Abdullaev N, Leszczynski J (2008) Aconitum and Delphinium sp. alkaloids as antagonist modulators of voltage-gated Na+ channels: AM1/DFT electronic structure investigations and QSAR studies. Comput Biol Chem 32:88–101
120. Gillespie D (2008) Energetics of divalent selectivity in a calcium channel: the ryanodine receptor case study. Biophys J 94:1169–1184
121. Luzhkov VB, Nilsson J, Åhrem P, Åqvist J (2003) Computational modelling of the open-state Kv1.5 ion channel block by bupivacaine. Biochim Biophys Acta Protein Proteonomics 1652:35–51
122. Awasthi A, Yadav A (2007) Phenylalkylamines as calcium channel blockers. J Chem Sci 11:565–570
123. Santarelli VP, Eastwood AL, Dougherty DA, Ahern CA, Horn R (2007) Calcium block of single sodium channels: role of a pore-lining aromatic residue. Biophys J 93:2341–2349
124. Thomas M, Jayatilaka D, Corry B (2007) The predominant role of coordination number in potassium channel selectivity. Biophys J 93:2635–2643
125. Yadav A, Awasthi A, Rao NK (2009) Mechanistic aspects of benzothiazepines: a class of antiarrhythmic drugs. Eur J Med Chem 44:1–6
126. Zhou Y, Morais-Cabral JH, Kaufman A, MacKinnon R (2001) Chemistry of ion coordination and hydration revealed by a K+ channel-Fab complex at 2.0 Å resolution. Nature 414:43–48
127. Bucher D, Raugei S, Guidoni L, Dal Peraro M, Rothlisberger U, Carloni P, Klein ML (2006) Polarization effects and charge transfer in the KcsA potassium channel. Biophys Chem 124:292–301
128. Bucher D, Guidoni L, Rothlisberger U (2007) The protonation state of the Glu-71/Asp-80 residues in the KcsA potassium channel: a first-principles QM/MM molecular dynamics study. Biophys J 93:2315–2324

129. Bucher D, Guidoni L, Maurer P, Rothlisberger U (2009) Developing improved charge sets for the modeling of the KcsA K+ channel using QM/MM electrostatic potentials. J Chem Theory Comput 5:2173–21799
130. Bucher D, Rothlisberger U (2010) Molecular simulations of ion channels: a quantum chemist's perspective. J Gen Physiol 135:549–554

Advances in Design and Development of Sodium Channel Blockers

Valentina Zuliani, Laura Amori, and Mirko Rivara

Contents

Abstract The voltage-gated sodium channels (VGSCs) play a fundamental role in controlling cellular excitability. Abnormal activity of sodium channels is related to several pathological processes, including cardiac arrhythmias, epilepsy, chronic pain, neurodegenerative diseases, and spasticity. In view of this, VGSCs are considered important therapeutic targets for the treatment of these disorders. To date, nine functional VGSC isoforms have been identified and have a distinct pattern of expression within the human body. In addition, VGSC also have distinct electrophysiological profiles with differing activation and inactivation states. As

V. Zuliani (✉)
Dipartimento Farmaceutico, Università degli Studi di Parma, V.le G.P. Usberti, 27/A, 43124 Parma, Italy
e-mail: valentina.zuliani@unipr.it

S.P. Gupta (ed.), *Ion Channels and Their Inhibitors*,
DOI 10.1007/978-3-642-19922-6_4,

such, there is a concerted effort to develop not only isoform selective blockers, but also blockers that exhibit state selectivity, particularly to the inactivated state of the channel. This article provides a brief historical perspective and primarily focuses on recent advances in the development of isoform specific and state selective sodium channel blockers and the medicinal chemistry involved, surveying the emerging therapeutic fields.

Keywords Voltage-gated sodium channels • Blockers • Epilepsy • Pain • Migraine • Myotonic syndromes • Cardiovascular diseases • Neurodegenerative diseases • Psychiatric disorders • Cancer

Abbreviations

AEDs	Antiepileptic drugs
AFib	Atrial fibrillation
ALS	Amyotrophic lateral sclerosis
BD	Bipolar depression
BPD	Borderline personality disorder
BrS	Brugada syndrome
CAMs	Neural cell adhesion molecules
CIP	Congenital insensitivity to pain
CNS	Central nervous systems
CSD	Cortical spreading depression
DMC	Dilated cardiomyopathy
DRG	Dorsal root ganglion
FHM	Familial hemiplegic migraine
GEFS+	Generalized epilepsy with febrile seizures plus
HD	Huntington disease
IEM	Inherited erythromelalgia
IFM motif	Isoleucine, phenylalanine, and methionine
LAs	Local anesthetics
LQT-3	Long QT syndrome type 3
MS	Multiple sclerosis
PAMs	Potassium-aggravated myotonias
PCCD	Progressive cardiac conduction disease
PD	Parkinson disease
PEPD	Paroxysmal extreme pain disorder
PMC	Paramyotonia congenita
PNS	Peripheral nervous systems
PPs	Periodic paralyses
SIDS	Sudden infant death syndrome
SMEI	Dravet syndrome

SSS	Sick sinus syndrome
TCAs	Tricyclic antidepressants
TTX	Tetrodotoxin
VGSCs	Voltage-gated sodium channels

1 Introduction: A Brief Mention of All Ion Channels

Ion channels are membrane protein complexes allowing the passive flow of ions across biological membranes [1]. Differently from ion pumps, ion channels do not use the energy of ATP hydrolysis to transport ions against their electrochemical gradient. The majority of ion channels possess a pore loop, a region of the protein that repeatedly crosses the membrane to form the selectivity filter that discriminates among ion species. The passage of a specific ion takes place when the channel is open. The conformational change between closed and open state is called gating. Channel gating is controlled by multiple factors and ion channels can be classified according to which chemical or physical modulator controls their gating activity. The most common groups of channels are listed as follows:

- Voltage-gated channels [voltage-gated potassium channels, voltage-gated sodium channels, voltage-gated calcium channels], whose gating mechanism is guided by membrane potential
- Ligand-gated channels [nicotinic acetylcholine receptors (nAChRs), ionotropic glutamate receptors (NMDA, AMPA, Kainate), $GABA_A$ receptors, glycine strychinine-sensitive receptors (GlyR), ATP-gated P2X receptors, and the 5-HT_3 serotonin receptor], whose gating mechanism is guided by a ligand
- Mechanosensitive channels, for which gating occurs in response to variation in osmotic pressure and membrane curvature

By regulating ion fluxes, ion channels govern membrane potential and excitability, determine the shape of the action potential, trigger muscle contraction and exocytosis (through Ca^{2+} influx), keep cell volume under control and are involved in many other cellular processes. As a consequence to that, they play important roles in multiple physiological processes as nerve and muscle excitation, hormone secretion, cell proliferation, sensory transduction, learning and memory, regulation of blood pressure, salt and water balance, lymphocyte proliferation, fertilization, and cell death. Noteworthy, abnormalities in ion channel expression, structure and function are tightly related to pathological states present in a number of disorders. Therefore, we can conclude that due to their important functional roles, their membrane location, structural heterogeneity and the specific tissue expression of some channel types, ion channels represent interesting targets for drug discovery. In this chapter, we focus our attention on voltage-gated sodium channels (VGSCs).

2 Sodium Channels: Their Structure and Functions, Diseases Related to Na-Channels

2.1 VGSC Structure

VGSCs are a family of membrane proteins forming a pore, through which they selectively conduct sodium ions inward and outward cell's plasma membranes in response to variations of membrane potentials [2–4]. They are composed of a central α-subunit and of two auxiliary β-subunits; the former is endowed with characteristics, which make the channels fully functional, whereas the latter ones mediate the linkage of the α-subunit to the plasma membrane and influence biophysical properties of the channels [5]. The α-subunit is a large polypeptide of about 1,800 amino acids and of 260 kDa, which consists of four domains (I–IV or D1–D4), each developed through six α-helical transmembrane segments (S1–S6) as shown in Fig. 1. Toxin bindings on the external pore, mutational analysis and parallel studies carried on for voltage-gated potassium channels suggest that the four S5–S6 linkers, one from each domain, which are designed as P-loops, form the extracellular portion of the channel, a ring of suitable size and charge that works as the selectivity filter for sodium ions. There are evidences indicating that each S5–S6 loop contributes to the selectivity pore with a single crucial amino acid (aspartate from domain I, glutamate from domain II, lysine from domain III, and alanine from domain IV), all negatively charged. Similar to other ion channels, S6 segments, in each domain of VGSCs, form the cytoplasmic end of the ion pore. Mutagenesis studies have shown how local anesthetics (LA) have high affinity for the inactivated state of VGSCs due to their interaction with critical amino acid residues located on the inner portion of the pore, on S6 segments of domains I, III, and IV (Fig. 1) [6]. Antiarrythmic and antiepileptic sodium channel blockers also bind to the same site as LA [7, 8]. The S4 segments, one in each domain of the VGSC heterotetramer, contain positively charged amino acids regularly spaced along the α-helix and function as voltage sensors. Mutational analysis suggests that upon membrane depolarization the four S4 segments cross the membrane by an outward rotational movement and start the gating process by inducing the channel opening [9]. Site-directed antipeptide antibodies indicate that the intracellular loop between domain III and IV closes the cytoplasmic end of the pore of the VGSC α-subunit leading to the fast-inactivation of the channel (Fig. 1) [10, 11]. The *C* terminus of the α-subunit contributes to the stabilization of the VGSC inactivated state by influencing fast-inactivation and by binding interacting proteins [12, 13]. β-Subunits are transmembrane glycoproteins of about 35 kDa, playing an accessory role in VGSC functioning (Fig. 1). Four different subtypes have been identified so far (β1–β4), each one composed of a single α-helix stretching through the plasma membrane. β-Subunits are endowed with a short cytoplasmic *C* terminus and with a large extracellular *N* terminus, which resemble an immunoglobulin outer domain capable to bind external proteins and thereby is believed to influence VGSC migration. β-Subunits

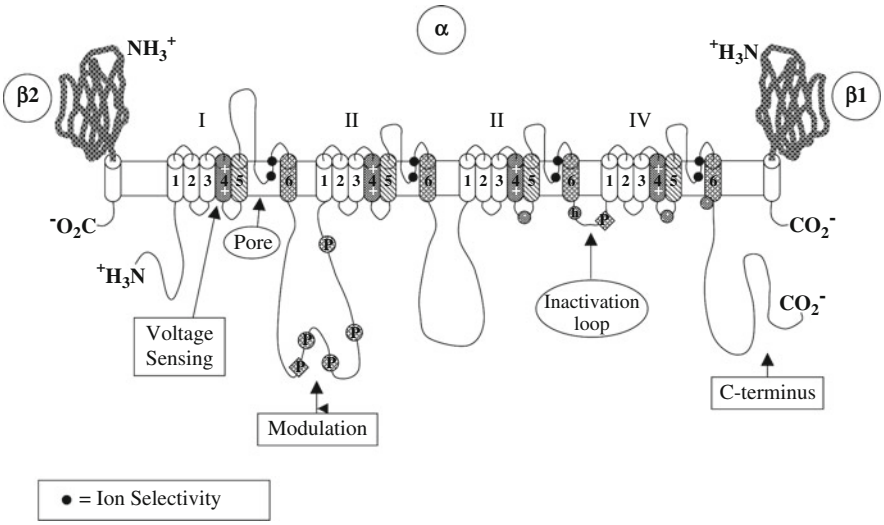

Fig. 1 VGSC subunit structure: VGSC α-subunit consists of four domains, I, II, III and IV, each one developed through six α-helical transmembrane segments, S1–S6 (cylinders 1–6). S4 segments in each domain contain positively charged amino acids and function as voltage sensors. *Black solid circles* represent negatively charged amino acids forming the ion selectivity loop. The intracellular loop between domain III (S6) and domain IV (S1) closes the cytoplasmic end of the channel pore leading to fast inactivation. P in *circles* and *diamonds* represents phosphorylation sites by kinases. Each VGSC β-subunit displays a large extracellular immunoglobuline-like N terminus. Reprinted with permission from [3]. Copyright 2000 Cell press

have similar primary structure to neural cell adhesion molecules (CAMs), whereas they share no homology with their counterparts of calcium and potassium channels. β1 and β3 covalently bind to the α-subunit by a disulfide bridge; conversely, β2 and β4 associate with the α-subunit only weakly.

2.2 VGSC Functions

The primary role of VGSCs is to trigger the rising phase of action potential in most excitable cells in mammals [3, 14]. The transition from a resting state (Fig. 2a), when the channel is closed, to an active state (Fig. 2b), when the channel is open and Na^+ ions can enter the pore, is called gating [2]. In the case of VGSCs, gating is governed by voltage signals. The highly conserved S4 transmembrane segments contain a motif of three positively charged amino acids (Fig. 1), which are exposed to the intracellular surface in the resting state and move outwardly in response to depolarization. Details on the S4 movement toward the outer face of the membrane are currently controversial. Nonetheless, it is commonly accepted that consequential conformational changes cause the pore to open [15, 16]. Within a few milliseconds after the channel opening, an inward Na^+ current is generated and

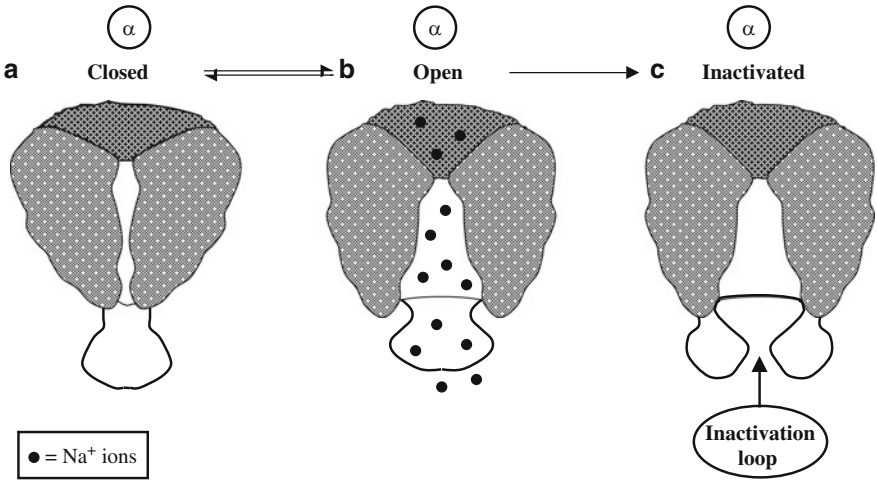

Fig. 2 VGSC functional states: (**a**) VGSC α-subunit in the resting state; (**b**) VGSC α-subunit in the active state, when an inward Na^+ current is generated; (**c**) VGSC α-subunit during fast inactivation, when the intracellular loop connecting domains III and IV closes the inner entrance of the conducting pore. Reprinted with permission from [4]. Copyright 2010 Elsevier

then the channel turns into a nonconductive inactivated state by a mechanism denominated fast inactivation. Immunohistochemical studies revealed a highly conserved intracellular loop connecting domains III and IV of the α-subunit (Fig. 1). Mutagenesis experiments suggest that a hydrophobic triad of amino acids (isoleucine, phenylalanine, and methionine) present in the loop, which is called IFM motif, play a crucial role in fast inactivation by closing the intracellular entrance of the conductive pore (Fig. 2c). Moreover, the *C* terminus of the α-subunit is likely to take part in the stabilization of the inactivated state. A number of evidences support the existence of functional coupling between activation and fast inactivation and indicate that the outward movement of the transmembrane segment S4 in domain IV is most likely the signal to initiate fast inactivation. A functionally and structurally different type of inactivation is slow inactivation. This kinetic process occurs during either prolonged depolarizing plateaus or high frequency repetitive firing and does not depend on the intracellular loop containing the IFM motif, but involves a significant conformational change of the channel. During slow inactivation, the channel continues to display residual conductance even at very positive membrane potentials [17].

2.3 VGSC α-Subunit Subtypes and Their Localization

Nine functional α-subunits, indicated as $Na_v1.1$–$Na_v1.9$, have been cloned and functionally expressed. *SCN1A–SCN5A* genes encode proteins $Na_v1.1$–$Na_v1.5$,

Table 1 VGSC α-subunit subtypes

VGSC α-subunit nomenclature	Gene	Tetrodotoxin sensitivity	Major tissue expression
$Na_v1.1$	*SCN1A*	TTXs	CNS, PNS
$Na_v1.2$	*SCN2A*	TTXs	CNS, PNS
$Na_v1.3$	*SCN3A*	TTXs	CNS, PNS
$Na_v1.4$	*SCN4A*	TTXs	Skeletal muscle
$Na_v1.5$	*SCN5A*	TTXr	Heart
$Na_v1.6$	*SCN8A*	TTXs	CNS, PNS
$Na_v1.7$	*SCN9A*	TTXs	PNS (SNS and PAs)
$Na_v1.8$	*SCN10A*	TTXr	PNS (PAs)
$Na_v1.9$	*SCN11A*	TTXr	PNS (PAs)
Na_x	*SCN6/7A*	Non-functional	Glia

CNS central nervous system; *PNS* peripheral nervous system; *PAs* primary afferent neurons; *SNS* sensory nervous system

whereas *SCN9A–SCN11A* genes codify proteins $Na_v1.6$–$Na_v1.9$ (Table 1). The expression of the various subtypes is both cell and tissue specific, and in some cases it changes during development [4]. $Na_v1.6$ is the main subunit expressed in mammalian brain during adulthood, but also $Na_v1.1$ and $Na_v1.2$ are present in axons and neuronal somata. $Na_v1.3$ subunits are expressed primarily in embryonic neurons in rodents, although they can be found in adult human brain for an extended period after embryogenesis. $Na_v1.4$ subunits are the main VGSC subtype expressed in the skeletal muscle, whereas $Na_v1.5$ subunits are located in cardiac muscle. Finally, proteins $Na_v1.7$–$Na_v1.9$ are present in peripheral primary sensory afferents. The nine α-subunits have been classified according to the dose of tetrodotoxin that blocks them. Namely, $Na_v1.1$–$Na_v1.4$, $Na_v1.6$ and $Na_v1.7$ are tetrodotoxin-sensitive (TTXs) as they are inhibited by nanomolar concentration of the toxin; conversely, $Na_v1.5$, $Na_v1.8$ and $Na_v1.9$ are tetrodotoxin-resistant (TTXr) as they require much higher concentrations to be blocked.

2.4 Diseases Related to VGSCs

Sodium channelopathies are inherited disorders caused by mutations in genes encoding VGSCs, which have proven to be particularly interesting as they provide significant insights into the physiological function of each VGSC and help clarifying molecular processes underlying normal and malfunctioning electrical excitability [18, 19]. Mutations in VGSC also provide medicinal chemists with useful cues, which could be treasured for the identification of selective modulators for different VGSC isoforms, as each channelopathy involves specific alterations either in the expression or in the function of individual channels. On the contrary, the present scenario urge scientists to search for specific blockers, since nonselective drugs induce undesired side effects [20]. Mutated VGSC genes have been found both in the central (CNS) and in the peripheral (PNS) nervous systems as well

Table 2 VGSC channelopathies

Mutated VGSC genes (subunits)	Effects of channelopathies	References
SCN1A ($Na_v1.1$)	Epilepsy, migraine, neuropsychiatric disorders	[20, 21, 55, 82]
SCN2A ($Na_v1.2$)	Epilepsy	[22]
SCN3A ($Na_v1.3$)	Epilepsy, pain	[25, 40, 41]
SCN4A ($Na_v1.4$)	Myotonic syndromes	[56–62]
SCN5A ($Na_v1.5$)	Cardiovascular diseases, cancer	[64–66]
SCN8A ($Na_v1.6$)	Neurodegenerative diseases	[73–76]
SCN9A ($Na_v1.7$)	Epilepsy, pain, cancer	[26, 45–51]
SCN10A ($Na_v1.8$)	Pain, neuropsychiatric disorders	[41, 45, 80, 81]
SCN11A ($Na_v1.9$)	Pain	[45]
SCN1B ($Na_v\beta1$)	Epilepsy, cardiac disorders	[23, 24, 34, 70]
SCN2B ($Na_v\beta2$)	Pain, cardiac disorders	[42, 70]
SCN3B ($Na_v\beta3$)	Cardiac disorders	[43, 70]
SCN4B ($Na_v\beta4$)	Cardiac disorders	[70]

as in heart, skeletal muscles and, recently, in certain types of cancer cells. Consequently, a number of disorders affecting different areas of the human body and ranging a wide spectrum of severity have been linked with mutated human VGSC genes. The clinical manifestations of these disorders depend primarily on the expression pattern of the mutant gene at the tissue level and the biophysical character of VGSC dysfunction at the molecular level (Table 2).

2.4.1 Epilepsy

Growing evidences suggest that abnormal VGSCs are involved in the pathophysiology of both acquired and inherited epilepsy. Hundred mutations in VGSC genes have been identified as responsible for inherited epileptic syndromes. Most epileptogenic mutations lie within *SCN1A* (encoding the $Na_v1.1$ α-subunit), whereas only a few are in *SCN2A* (encoding the $Na_v1.2$ α-subunit), in *SCN1B* (encoding the auxiliary β1-subunit), and possibly in *SCN3A* (encoding the $Na_v1.3$ α-subunit) and *SCN9A* (encoding the $Na_v1.7$ α-subunit) [4, 21–26]. $Na_v1.1$ mutations have been associated with generalized epilepsy with febrile seizures plus (GEFS+); they are missense mutations and are characterized by both a loss and a gain of function, depending on the type of cells where they are expressed [27]. Nonetheless, a loss of function has been found as the main effect induced by $Na_v1.1$ mutations, which leads to decreased Na^+ currents. For instance, severe myoclonic epilepsy of infancy or Dravet syndrome (SMEI), a more serious form of epilepsy related to *SCN1A* mutations, is mostly caused by $Na_v1.1$ loss of function [28], although it also exhibits biophysical defects due to persistent Na^+ current [29]. The apparently paradoxical link between VGSC loss of function and epilepsy could be explained by the evidence that $Na_v1.1$ is the predominant isoform in various types of inhibitory interneurons, such as hippocampal GABAergic interneurons [30, 31]. In fact, it is possible that malfunctioning VGSCs compromise the network inhibition by

reducing excitability of inhibitory interneurons, thus inducing epileptic seizures. Mutations in *SCN2A*, found in benign neonatal familial seizure, induce a mild clinical condition and convulsions that disappear into adulthood, in agreement with the transient expression of $Na_v1.2$ in myelinated axons of excitatory neurons early during postnatal development [32]. The related symptoms are generally associated with a decrease in channel density in the membrane, leading to a lower magnitude of whole-cell currents [33]. Mutations in *SCN1B* have been the first to be associated with GEFS+ [34]. Mutated β1-subunits are characterized by a reduced function, which impairs their modulation of α-subunits and probably decreases the level of channel expression in the membrane [23, 24, 34].

2.4.2 Pain

The perception of pain is a physiological process, which contributes to the maintenance of body integrity as it alerts to forthcoming harms. Nociception is the physiological system that conveys somatic information along the pain cascade from peripheral receptors to the spinal cord and to the brain, and can discriminate potentially damaging from innocuous stimuli. Conscious awareness of such sensorial signaling results into pain. Nociception is encoded by action potentials and specific VGSC subtypes are involved in their outset and propagation [35]. Abnormal expression and/or functioning of VGSCs, typical of certain inherited channelopathies, have been linked with inflammatory or neuropathic pain [35–37]. In contrast to inflammatory or nociceptive pain, which is caused by actual tissue damage or potentially tissue damaging stimuli, neuropathic pain is produced either by damage to, or pathological change in, the PNS or CNS, the system that normally signals pain. The key role of VGSCs in pain has been empirically confirmed by symptomatic relief in patients treated with sodium channel blockers [38, 39], but the nonspecific nature and side effects of existing blockers have limited their clinical utility. At least five subunits are expressed in human dorsal root ganglion (DRG) neurons, $Na_v1.7$, $Na_v1.8$, $Na_v1.9$, $Na_v1.1$, and $Na_v1.3$. Chronic injury to sensory neurons triggers neuropathic pain possibly due to the upregulation of embryonic $Na_v1.3$ in the somata and of $Na_v1.8$ in DRG neurons [40, 41], to an abnormal redistribution of $Na_v1.8$ and $Na_v1.9$ from the somata to the peripheral axon at the site of the lesion, and to the upregulation of β_2 and β_3 subunits [42, 43]. These changes induce spontaneous firing of nociceptive neurons at abnormally elevated frequencies and from ectopic sites. Upregulation of $Na_v1.3$ within second-order spinal cord dorsal horn neurons and third-order thalamic neurons seem to be involved in central neuropathic pain occurring after spinal cord injury. It is possible that the abnormal functioning of the VGSC subunit makes the host neurons hyperexcitable so that they act as pain amplifiers and generators [44]. There are strong evidences that $Na_v1.7$-1.9 contribute to inflammatory pain [45]. $Na_v1.7$ has recently gained particular interest in pain research as a genetic link has been found between the VGSC subtype and certain hereditary pain disorders in humans. In particular, dominant gain-of-function mutations in *SCN9A*, the gene that encodes

sodium channel $Na_v1.7$, cause two rare but extremely severe pain syndromes: inherited erythromelalgia (IEM) and paroxysmal extreme pain disorder (PEPD) [46–48]. In IEM, pain is localized to feet and hands and electrophysiological studies have linked painful states in this disorder with hyperpolarization of the mutated channel and to increased current magnitude. In contrast to IEM, PEPD-related pain affects mostly rectal but also ocular and mandibular areas and has been linked with delayed or absent inactivation of mutant channels. Congenital insensitivity to pain (CIP), a hereditary syndrome in which affected individuals are unable to experience pain, is characterized by recessive loss-of-function mutations in *SCN9A*. Noteworthy, CIP patients report normal sensory function, with the exception of impaired olfaction, and do not display any motor, cognitive, sympathetic, or gastrointestinal deficits [49–51].

2.4.3 Migraine

Familial hemiplegic migraine (FHM) is a severe autosomal dominant inherited headache characterized by visual aura and hemiparesis during attacks [52]. A large body of evidence indicates that cortical spreading depression (CSD) is the electrophysiologic event underlying migraine aura and possibly leading to headache [53]. CSD is a slowly propagating wave of transient neuronal and glial depolarization accompanied by increases in potassium ion concentrations, which can activate the meningeal trigeminovascular system and downstream pain pathways and thus cause headache [54]. FHM type 3 is associated with mutations in the *SCN1A* gene encoding the α-subunit of $Na_v1.1$ VGSCs [55]. The reported effects range from gain of function to complete loss of function and the pathogenic mechanisms have not been entirely clarified yet. Nonetheless, a current hypothesis suggests that mutated channels engender neuronal hyperexcitability, increased neurotransmitter release, and abnormal accumulation of extracellular potassium, contributing to CDS and thus to migraine [52].

2.4.4 Myotonic Syndromes

Sodium channelopathies involving skeletal muscles are characterized by mutations in *SCN4A* [56, 57]. Under physiologic conditions, muscular $Na_v1.4$ channels transform nerve stimulation into action potentials that trigger muscle contraction. Immediately after that, the sodium channel subunits undergo fast inactivation to prevent recurrent discharges and persistent depolarization of muscle fibers. The majority of *SCN4A* mutations, typical of myotonias and periodic paralysis, are located in regions of the $Na_v1.4$ channels associated with fast inactivation, and lead to an impairment of the channel ability to inactivate. Muscular disorders associated with sodium channelopathies include paramyotonia congenita (PMC), potassium-aggravated myotonias (PAMs), and periodic paralyses (PPs). Gain-of-function mutations in PMC and PAMs generate either altered channel gating, which

causes slower or incomplete inactivation, or enhanced $Na_v1.4$ activation [58]. Interestingly, low temperatures could worsen certain types of myotonias, by disrupting slow channel inactivation, and lead to flaccid paralysis [59, 60]. PPs are inherited sodium channelopathies, categorized as either hyper- or hypo-kalemic according to associated circulating potassium concentrations, which induce muscle weakness and transient inability to move. HyperPP is characterized by a strong depolarization leading to inactivation of $Na_v1.4$ channels and depolarization block, which cause paralysis. High potassium serum levels are a specific feature of hyperPP [61]. In contrast, hypoPP loss-of-function channel mutations induce $Na_v1.4$ channel inactivation, by stabilizing the inactivated state [62].

2.4.5 Cardiovascular Diseases

$Na_v1.5$, located in the sarcolemma of atrial and ventricular myocytes and the Purkinje fibers, is the VGSC subunits responsible for the large inward depolarizing currents (I_{Na}) occurring during phase 0 of the cardiac action potential. By doing so, I_{Na} regulate cardiac excitability and conduction velocity of electrical stimuli through the heart [63]. The importance of VGSC in the normal cardiac electrical function has been accentuated by the discovery of channelopathies linked with mutations in *SCN5A*, the gene encoding the cardiac $Na_v1.5$ subunits [64, 65]. These diseases include long QT syndrome type 3 (LQT-3), Brugada syndrome (BrS), progressive cardiac conduction disease (PCCD), dilated cardiomyopathy (DCM), sick sinus syndrome (SSS), atrial fibrillation (AFib), sudden infant death syndrome (SIDS), and overlap syndromes. LQT-3 is a condition where most *SCN5A* mutations typically disrupt fast inactivation of the sodium current, allowing for sodium channels to reopen, resulting in a persistent (or sustained) inward current during the action potential plateau phase [66]. Consequently, delayed repolarization and action potential prolongation occurs, and early after-depolarizations may subsequently trigger torsades de pointes and sudden death. Alternatively, certain mutated $Na_v1.5$ subunits less commonly cause LQT-3 through increased window current, reduced or destabilized slow inactivation, faster recovery from inactivation (causing increased sodium channel availability), and/or increased peak sodium current density. BrS is a familial disorder characterized by ventricular fibrillation sometime causing sudden cardiac death in otherwise healthy individuals at a relatively young age. Numerous *SCN5A* mutations displayed by BrS patients have been identified, most of which produce loss of function, either through decreased trafficking and membrane surface channel expression, or through altered channel gating properties. VGSC β-subunits are also expressed in the heart, where they play multiple roles. Briefly, β-subunits increase the density of Na^+ channels at the cell membrane, modulate their biophysical properties, and play a role in cell adhesion and recruitment of anchoring proteins such as ankyrins. Recently, mutated *SCN1B–SCN4B* have been found in sodium channelopathies displaying phenotypic cardiac disorders [67]. Besides being characteristic of mutated channels associated with genetic channelopathies, cardiac VGSC dysfunctions also occur in acquired

pathological states such as myocardial ischemia and heart failure, where they produce conduction disturbances and ventricular arrhythmias [65]. During both acute and chronic myocardial ischemia, local metabolic changes take place within the myocardium, which lead to inactivation of sodium currents and to consequent inhibition of cardiac excitability and electrical conduction. In particular, conduction slowing is considered a pro-arrhythmic factor [68, 69]. Cardiac electrophysiological properties, including changes in ion channels, are altered also in heart failure. In such condition, VGSC impaired functioning is part of a complex pathological network and may contribute to arrhythmogenesis by different pathways. For instance, sodium channel inability to inactivate, arising during heart failure, induces persistent sodium inward currents during zero phase, which may delay repolarization, prolong action potential duration, and alter intracellular sodium and calcium homeostasis, potentially predisposing to arrhythmogenesis [70]. In addition to increased inward current, loss of cardiac VGSCs may occur during heart failure, generating conduction slowing and ventricular reentrant arrhythmias [71].

2.4.6 Neurodegenerative Diseases

VGSCs have been proposed to play a role in processes involving either acute or progressive neuronal loss, typical of stroke, ischemia and neurodegenerative diseases such as amyotrophic lateral sclerosis (ALS), multiple sclerosis (MS), Parkinson disease (PD), and Huntington disease (HD) [72, 73]. It was hypothesized that in all those cases, characterized by a decreased energy supply, causing impaired activity of Na^+/K^+-ATP-depending pumps and membrane depolarization, there may be a greater persistent Na^+ conductance, most likely mediated by $Na_v1.6$ subunits. Na^+ overload inside the axon, combined to K^+ efflux, may lead to Ca^{2+} accumulation via reversal of the Na^+/Ca^{++} exchanger, thus triggering a pathogenic cascade, which ends with axonal injury and eventually with neuronal loss. An increase in the persistent Na^+ conductance, operating at rest in motor axons, is likely to contribute to the peripheral hyperexcitability in ALS, leading to the typical symptoms of cramps and fasciculations, and possibly causing abnormal glutamate release, which may have a major role in neurodegeneration [74, 75]. Moreover, VGSCs (in particular $Na_v1.5$ and $Na_v1.6$) are upregulated in activated microglia and microphages in models of autoimmune and inflammatory disorders, such as MS, and might be involved in the phagocytic ability or contribute to the migration of those cells, thus playing a role in the propagation of the inflammatory cascade [76, 77].

2.4.7 Psychiatric Disorders

VGSC blockers have displayed beneficial effects in the treatment of various psychiatric disorders such as bipolar depression (BD) and borderline personality disorder (BPD) [78, 79]. Lately, mutated sodium channels have been found in

patients suffering from certain psychiatric conditions, although those studies need to be confirmed by the analysis of a higher number of individuals. Preliminary data suggest that mutations in *SCN8A* may result in motor and cognitive deficits of variable expressivity and that *SCN8A* may be a potential susceptibility gene for bipolar disorder [80, 81]. Results from a recent study, carried on with subjects suffering from Dravet syndrome, a severe form of epilepsy often caused by mutations of *SCN1A* gene, are consistent with the hypothesis that *SCN1A* mutations can be responsible not only for epilepsy, but also for early and progressive severe mental impairment [82].

2.4.8 Cancer

Over the past decade, VGSCs have been reported to be involved in various types of cancer, such as breast cancer, prostate cancer, small and nonsmall cell lung cancer, lymphoma, mesothelioma, neuroblastoma, and cervical cancer [83, 84]. In particular, remarkable functional expression of VGSCs has been found in cancer cells with strong metastatic potential. For instance, $Na_v1.5$ subunit is highly expressed in human metastatic breast cancer cells [85]. The activity of that subunit is thought to enhance tumor invasiveness due to increased cysteine cathepsin activity [86]. A different VGSC subunit, $Na_v1.7$, is highly expressed in prostatic cancer, where it contributes to the metastatic cascade by potentiating cell migration [87, 88]. The functional expression of VGSCs might be an integral component of the metastatic process in both human small and nonsmall lung cancer cells, probably through their involvement in the regulation of intracellular sodium homeostasis [89, 90]. In summary, VGSCs could serve in cancer research both as novel markers of the metastatic phenotype and as potential new therapeutic targets.

3 Advances in the Development of Sodium Channel Blockers: A Few Introductory Lines

Many of the most common neurological disorders, such as epilepsy, migraine, neurodegeneration, and chronic pain, involve abnormalities in neuronal excitability. VGSCs play a fundamental role in originating the rising phase of cell membrane action potential and many experimental data indicate that the functional VGSCs could be implicated in the pathogenesis and/or the progression of such disorders. VGSC-interfering drugs have been used for decades to treat epileptic seizures, the most common disease related to abnormal neuronal excitability, and it has become evident that VGSC blockers could also be beneficial in the therapy of a broad range of disorders.

3.1 As Antiepileptic Drugs

Epilepsy is a very common neurological disease that affect about 0.5–1.0% of worldwide population [91]. It consists of a disorder of neuronal excitability, characterized by episodes of excessive synchronized neuronal activity. Electroencephalograms from patients suffering from epileptic disorders reveal two types of anomalous activity: interictal events, which are short asymptomatic episodes recurring periodically between seizures and consist of periods of relative inactivity, and ictal discharges, which are protracted abnormalities in neuronal activity [92]. Both ictal and interictal discharges are characterized by sustained firing of Na^+-dependent action potentials riding on a slow depolarized potential, mainly generated by synaptic ligand-gated cation currents [92]. It is possible to distinguish epilepsies based on the entity of seizures. In generalized seizures, the origin is in both hemispheres, while focal seizures involve only a portion of the brain, in particular structures in the temporal or frontal lobes. Current pharmacological approaches to the treatment of epilepsy try to control seizures, the major symptom of this pathological condition. Antiictogenic pharmacostrategies can free patients with established epilepsy from seizures, but in approximately one-third of all cases seizures cannot be controlled [93, 94]. In particular, voltage-gated ion channels are of great importance as targets for antiictogenic drugs. Sodium and calcium channels, in fact, regulate firing of action potentials and contribute to the paroxysmal depolarization shift, and they also regulate neurotransmitter release that is required for synaptic transmission [95].

3.1.1 VGSC Blockers for Epilepsy (AEDs)

The block of sodium channel currents is the most common and well-characterized mechanism of action of currently available AEDs. These drugs prevent the return of the channels to the active state by stabilizing the inactive form. The presynaptic and postsynaptic blockade of axonal sodium channels stabilizes neuronal membranes, blocks or prevents the potentiation of the electrical signal propagation, limits the maximal seizure activity and reduces the spread of seizures. The most used AEDs inhibit VGSCs at therapeutic concentrations; their capability to attenuate Na^+ currents is thought to be the main mechanism underlying their therapeutic efficacy [95]. All the drugs proposed for the therapy are potentially effective in the maximal electroshock seizure test, a model of tonic-clonic seizures that assesses the ability of AEDs to suppress seizures induced in normal rodents by electrical stimuli, and/or they are potentially effective in pentetrazol-treated rodents, a model used to identify drugs that are efficacious for absence seizures.

Phenytoin (Fig. 3): since its introduction in clinical practice, more than 70 years ago, phenytoin has been the major VGSC-specific AED in the treatment of partial and secondary generalized seizures. Its ability not to interfere with normal cognitive function conferred great importance to this drug in the treatment of epilepsies

[95]. Phenytoin is a weak blocker of VGSCs at hyperpolarized membrane potentials and low rates of channel activation, but its inhibitory action is greatly enhanced by sustained membrane depolarization and during high frequency channel activity [96]. As experimentally demonstrated, closed VGSCs, which are predominant at hyperpolarized membrane potentials, have a low affinity for phenytoin, whereas inactivated channel states, which are prevalent at depolarized holding potentials and during high frequency channel activation, bind phenytoin in low micromolar range [95, 96]. Voltage-dependent and frequency-dependent inhibition suggests a basis for the ability of phenytoin to suppress seizures while having minimum effects on cognition. According to this hypothesis, phenytoin only weakly suppresses Na^+ currents during the intervals between seizures, in which neurons depolarize transiently and fire single or short bursts of action potentials. Otherwise, during seizures, neurons have prolonged discharges of action potentials riding on sustained depolarizing episodes, which is the optimum condition for phenytoin inhibition of VGSC activity.

Carbamazepine (Fig. 3): carbamazepine, similar to phenytoin, inhibits VGSCs in a voltage-dependent and frequency-dependent manner at clinically relevant concentrations and it is one of the major AED for partial seizures and generalized tonic-clonic seizures but it is not effective against absence seizures [95]. The main mode of action of carbamazepine is to block sodium channels during rapid, repetitive, sustained neuronal firing. Hence, this drug might be more effective than phenytoin at inhibiting seizures characterized by relatively brief depolarizing shifts; this could explain the better responses of certain patients to phenytoin while others are more effectively treated with carbamazepine.

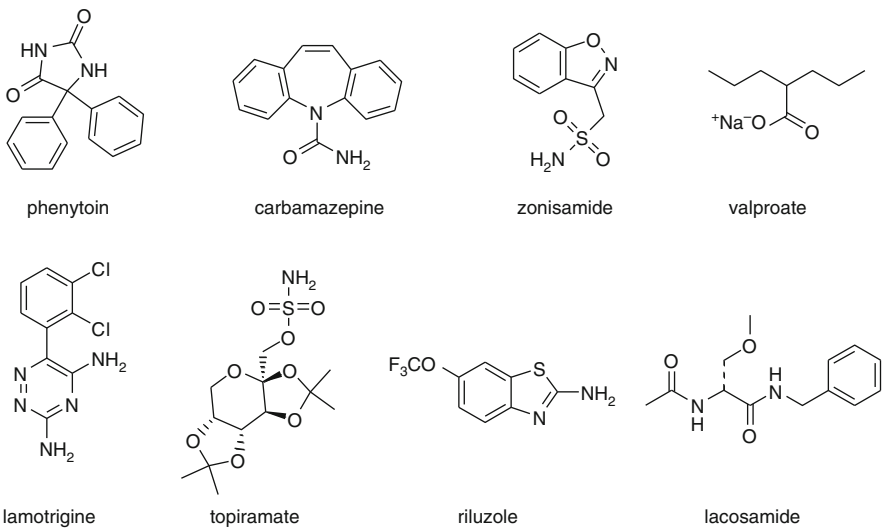

Fig. 3 Sodium channel blockers

Zonisamide (Fig. 3): zonisamide is chemically unrelated to any of the other AEDs. It was approved in the USA for the treatment of partial seizures in adults. The principle mechanism of action of zonisamide seems to be the block of the repetitive firing of VGSCs and the reduction of the T-type calcium currents. It is effective not only in adult focal epilepsies, but also it may represent an option in the difficult-to-treat epilepsy syndromes. Moreover, its favorable pharmacokinetic characteristics and its broad range of mechanism of action turns zonisamide into an important tool in combined therapy with other AEDs [95, 97].

Valproate (Fig. 3): valproate is an AED introduced in the 1970s, which has an exceptionally broad range of anticonvulsant efficacy: it is effective against partial and generalized tonic-clonic seizures, absence seizures, and myoclonic seizures [98]. The mechanism of action of valproate remains undefined, but it is evident that VGSCs are among the brain targets hit by the drug [98].

Lamotrigine (Fig. 3): lamotrigine represents an effective treatment for partial and generalized tonic-clonic seizures and also for the management of absence attacks in primary generalized epilepsies [95]. As for phenytoin, the demonstrated efficacy of lamotrigine in clinical practice is primarily due to its ability to block both in a voltage-dependent and in a frequency-dependent manner the VGSCs. However, its effectiveness cannot depend only on VGSC inhibition, but its capability to manage absences is probably due to its action on different targets [99, 100].

Topiramate (Fig. 3): topiramate is characterized by a phenytoin-like profile in maximal electroshock seizure and pentetrazol tests, and it presumably acts by depressing sustained repetitive firing and voltage-gated Na^+ currents [101]. However, topiramate antiepileptic effects may not depend exclusively on VGSCs blockade and it probably exerts its effect by others mechanisms, comprising the interaction with excitatory amino acid transmission [102, 103].

Riluzole (Fig. 3): riluzole was at first developed as an AED but approved for the treatment of amyotrophic lateral sclerosis. Its mechanism of action is most likely related to its antiglutamatergic properties; however, this drug has also been characterized as a classic VGSC blocker [104].

Lacosamide (Fig. 3): lacosamide is effective in patients with uncontrolled partial seizures and demonstrates an important efficacy in controlling seizure activity in several in vivo and in vitro models of epilepsy [105]. Lacosamide inhibits VGSCs by enhancing channel slow inactivation [106]. Voltage-clamp experiments have also revealed that this drug decreases the frequency of both inhibitory and excitatory postsynaptic currents without influencing membrane passive properties [107]. Therefore, lacosamide targets VGSCs, although with a different mechanism respect to phenytoin and carbamazepine.

3.2 As Pain-Relieving Drugs

Pain is a complex sensory phenomenon characterized according to duration (acute or chronic), intensity (mild, moderate, or severe), and type (nociceptive,

inflammatory, or neuropathic) [108, 109]. Chronic neuropathic pain may derive from a previous nerve or tissue damage or may have unknown etiology and seems to have no apparent utility [110–112]. Neuropathic pain occurs, at least, as a result of primary lesion or chronic dysfunction in PNS or CNS pathways. It becomes a pathophysiological condition that may persist indefinitely, also in absence of tissue damage or noxious input, and can manifest as hyperalgesia (increased sensitivity to normally painful stimulus) or allodynia (pain resulting from a normally sub-threshold physical stimulus) [113]. In other words, neuropathic pain is associated with severe painful sensory responses to innocuous or acute pain stimuli as well as to a painful sensation, often of long duration, with no particular trigger [111, 114, 115]. The most common forms of neuropathic pain have been not clearly understood; nonetheless they seem to involve important remodeling of pathways in both PNS and CNS [110, 111, 116]. In particular at the beginning of pain sensation, peripheral primary sensory afferent nerves are involved; specifically, those are medium-sized thinly myelinated Aδ-fibers and small unmyelinated C-fibers, which have their bodies in the dorsal root ganglia (DRG), that finally interface with the CNS [117]. DRGs are connections located in the spinal column, they comprise the cell body of sensory neurons which dendrites are situated in the skin, muscles, tendons, joints, and internal organs. These afferent fibers are responsible of sensation as touch, stretching, temperature, and pain [118]. Considering that chronic pain affects about 1.5 million people worldwide and that despite the numerous treatment options it is very difficult to practically achieve its handling, the possibility to discover new treatments for neuropathic pain represents a great challenge. In fact, to date, opioids are the best solution for the management of these syndromes; nevertheless, their use in long-term therapy is not a suitable choice due to their abuse potential and the wide range of side effects comprising low safety margins [111, 119, 120]. It has been established that sodium channels are essential for the capacity of DGR to transmit pain sensations. In fact, DRG neurons are characterized by a complex pattern of sodium currents: they express both TTX-R and TTX-S sodium currents characterized by a mixture of channels with slow and fast kinetics [121]. As a consequence to trauma or injury these neurons exhibit abnormal spontaneous activity and increased responses to a large variety of noxious stimuli. Consistent data support the fact that hyperexcitability and spontaneous firing are mediated by VGSCs.

3.2.1 VGSC Blockers for Neuropathic Pain

The current efforts to promote the use of sodium channel blockers in the treatment of neuropathic pain translate the merging of multiple advances in related scientific understanding. In fact, historically local anesthetics were used systemically to alleviate pain since 1944 and phenytoin was employed for trigeminal neuralgia in the early 1950s [122, 123]. In 1962 it was reported, for the same pathology, the use of the anticonvulsant carbamazepine [124]; although only in 1975 a common mechanism of action for these drugs, involving their ability to block sodium

channel currents, was recognized [125]. From early 1980s, it was demonstrated that sodium channel blockade contributes to the efficacy of amitriptyline and other tricyclic antidepressant used to treat pain [126–128], and the use of sodium channel blockers became a great focus of attention for the treatment of neuropathic pain [129–131]. Sodium channel blockers have currently been included not only in therapies controlling surgical pain, but they are also employed for the management of chronic pain conditions. In fact, there are several experimental evidences concerning the capacity of LA, tricyclic antidepressant and other sodium channel blockers to relieve neuropathic pain [132–136]. Anticonvulsant, antiarrythmics, LAs and tricyclic antidepressants are currently used to treat this pathology, by the virtue of their ability to modulate VGSCs. All the drugs currently used are sodium channel antagonists with analgesic properties acting as state-dependent blockers. Their actual efficacy is, to date, under investigation due to their low tolerability and to the numerous adverse effects observed. In fact, all the available sodium channel blockers used to treat chronic pain have shown severe tolerability limitations: the off-target adverse effects of these drugs made very narrow their therapeutic margin causing CNS liabilities as seizures, ataxia, confusion and sedation. For example, phenytoin is associated with rash, gingival hypertrophy, horizontal nystagmus, and teratogenicity, while carbamazepine can produce bone marrow suppression and tocainide can provoque bone marrow suppression and pulmonary fibrosis so it is no longer marketed in US. Mexiletine is poorly tolerated due to induced gastrointestinal upset and the sedative and anticholinergic side effects of tricyclic antidepressant can limit their therapeutic use. As a consequence to that, to maintain plasma therapeutic levels of sodium channel blockers a medical follow-up and often titration are necessary. Hereafter are presented the most interesting compounds recognized as useful drugs in the treatment of several chronic pain conditions.

Lamotrigine (Fig. 3): lamotrigine is clinically used for the treatment of epilepsy, schizophrenia, bipolar disorder and Huntington's chorea, and it is under evaluation for the treatment of neuropathic pain even if with often diverging results. For instance, a 2006 clinical trial, involving patients with neuropathic pain induced by chemotherapy did not show a significant difference between drug and placebo efficacy but, in a previous study, conducted in 2001 on patients suffering from diabetic neuropathy, lamotrigine showed a remarkable efficacy in pain control [137]. Again, in a similar study involving patients with spinal cord injury-induced neuropathic pain, lamotrigine was ineffective. In 2000 lamotrigine was used to treat HIV-associated neuropathy and it was effective only on patients exposed to neurotoxic antiretroviral therapy [138]. Lamotrigine was also effective in the treatment of post-stroke pain [139].

Topiramate (Fig. 3): topiramate has been used for the treatment of epilepsy, schizophrenia, bipolar disorder, and migraine. Recently, it has produced unclear results in the treatment of neuropathic pain; in particular, the results obtained from studies on diabetic neuropathy were not encouraging [140]. The most important drawback for the use of topiramate in the treatment of neuropathic pain is its broad and severe side effects such as dizziness, ataxia, speech disturbance, and visual impairment [140].

Ralfinamide (Fig. 4): while the ability of ralfinamide as analgesic is still under investigation, the result obtained in animal models for neuropathic pain is encouraging [141].

Lidocaine (Fig. 4): lidocaine is a local anesthetic of wide use and its intravenous injection has proven to be effective in reducing neuropathic pain [142] and diabetic pain [143]. It was also demonstrated that subcutaneous injection of this drug reduces cancer-related neuropathic pain in patients, who are insensitive to opioid treatment [144]. It is also important to highlight phenomenon that occurs in patients treated systemically with lidocaine. After brief exposures to the drug, patients report days or even weeks of pain relief. This observation is supported by data from animal models [133, 134].

Oxacarbazepine (Fig. 4): oxacarbazepine is a derivative of carbamazepine useful in the treatment of trigeminal neuralgia and diabetic neuropathies [145, 146]. Nevertheless, it seems to lack the severe side effects typically induced by carbamazepine; in fact, oxacarbazepine was developed to avoid hepatic enzyme induction while retaining anticonvulsant activity of carbamazepine [146, 147].

Amitriptyline and tricyclic antidepressants (TCAs) (Fig. 4): amitriptyline is a TCA recently used for neuropathic pain by virtue of its capability to block sodium channels [148]. It was demonstrated the drug capacity to relief patients from diabetic neuropathy and postherpetic neuralgia [135, 149, 150]. Moreover, a large number of TCAs are commonly used in the treatment of neuropathic pain and other chronic pain states [135, 151]. They bind, similar to LAs, to the inactivated state of VGSCs, although experimental evidences demonstrated that there are differences between the two classes of drugs to relieve pain [148].

Lacosamide (Fig. 3): lacosamide is a new anticonvulsant, which is thought to bind to a novel site of action that enhances slow inactivation. Lacosamide displays enhanced channel inhibition, and it has provided promising results in the treatment of painful diabetic peripheral neuropathy [106].

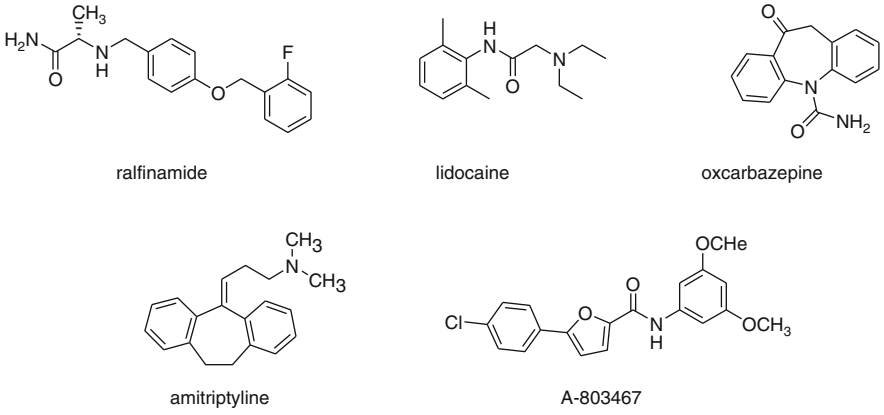

Fig. 4 Sodium channel blockers

A-803467 (Fig. 4): is a subtype selective blocker of Nav1.8 discovered by Abbott and Incagen [152]. In vivo, this compound reduces spontaneous and evoked firing of spinal dorsal horn neurons in spinal nerve ligated rats [153]. A-803467 is able to reduce pain in several animal models. The observation that this compound do not significantly alter motor coordination may provide the first experimental evidence that a subtype selectivity would translate into safer sodium channel blockers.

3.3 For the Treatment of Other Diseases

3.3.1 Migraine

As specified above, FHM3 is a rare subtype of FHM due to a mutation in SCN1A, the gene encoding for the voltage-gated $Na_V1.1$ channel [19, 154–156], and some sodium channels blockers (i.e., topiramate, carbamazepine, and lamotrigine) seems to be efficacious in the treatment of migraine, reducing aura and migraine attacks (Fig. 3) [4, 157, 158]. Nevertheless, the mechanism of action of these drugs in the treatment of this disease has to be clarified.

3.3.2 Myotonic Syndromes

Mutations in the gene encoding COC-1, a chloride channel, together with mutations in *SCN4A*, the gene encoding the α-subunit of the skeletal muscle sodium channel $Na_V1.4$ seem to be involved in the physiopathology of myotonic dystrophy [159–162]. At the moment it is impossible to cure the cause of the disorder and only symptomatic treatments are available, such as sodium channel blockers, that reduce the excitability of the cell membrane. Nevertheless, these drugs, such as procainamide, tocainide, mexiletine, flecainide, and phenytoin are not selective toward the $Na_V1.4$ VGSC isoform, and they could have serious side effects (Figs. 3 and 4) [163, 164]. Instead, several studies suggest that mexiletine is the agent of choice in the treatment of nondystrophic myotonia, even if its use is restricted by the side effects on cardiac functions, on the CNS and on the hematopoietic system [165–167]. Considering that sodium channels on cardiac and skeletal muscle tissues are different, there is the possibility to design use-dependent sodium channel blockers that preferentially block skeletal muscle isoforms. Many efforts have been made to develop this class of molecules but, so far, it has been impossible to obtain a pharmacological differentiation, even by synthesizing compounds more potent than mexiletine in vitro [168]. Similar, flecainide, an IC class antiarrythmic, improves myotonia, still retaining the same side effects observed for mexiletine. However, the drug seems useful in situations where mexiletine is less efficient [169–171]. Also, tocainide is among the few drugs clinically used for the symptomatic treatment of muscle hyperexcitability in myotonic syndromes, but with the

well-known side effects of this class of drugs [172, 173]. Several tocainide analogs were designed and synthesized to obtain novel potent voltage- and use-dependent skeletal muscle sodium channel blockers, also with the aim of identifying the structural requirements for ameliorating the therapeutic profile [174–177].

3.3.3 Cardiovascular Diseases

The ideal Na^+ blocker for the treatment of cardiac diseases should interact selectively with the $Na_V1.5$ isoform but, unfortunately, the sodium channel blockers in clinical use are neither isoform nor even channel selective [82, 178]. For example, class I antiarrhythmics, such as quinidine, procainamide, and disopyramide (class Ia agents) as well as lidocaine, mexiletine, tocainide and phenytoin (class Ib agents) and encainide, flecainide, moricizine, and propafenone (class Ic agents) are potentially pro-arrhythmic and with many other side effects due to their nonselective action, thus resulting contraindicated in several diseases (i.e., encainide is no longer used) (formulas of these molecules are reported in Figs. 3–6).

KC12292 (Fig. 7) is a thiadiazole derivative with antiischemic properties in the early stages of development [179]. This compound inhibits the inward peak I_{Na} also by inducing a reduction of the sustained component (or slowly or noninactivating) of sodium current [180]. These characteristics distinguish KC12291 from conventional VGSC blockers with no cardioprotective properties, making this molecule particularly promising for the treatment of ischemic conditions [181].

Ranolazine, approved in the USA by the FDA in 2006, is a new drug useful for the treatment of chronic angina pectoris in patients with ischemic heart disease [182, 183] (Fig. 7). It reduces the late I_{Na} and, consequently, it affects the sodium-

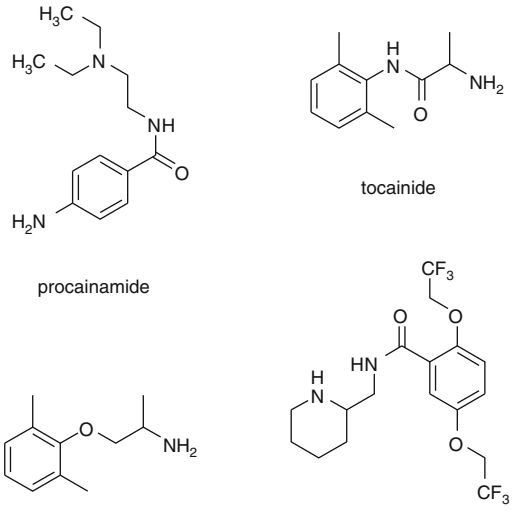

Fig. 5 Sodium channel blockers

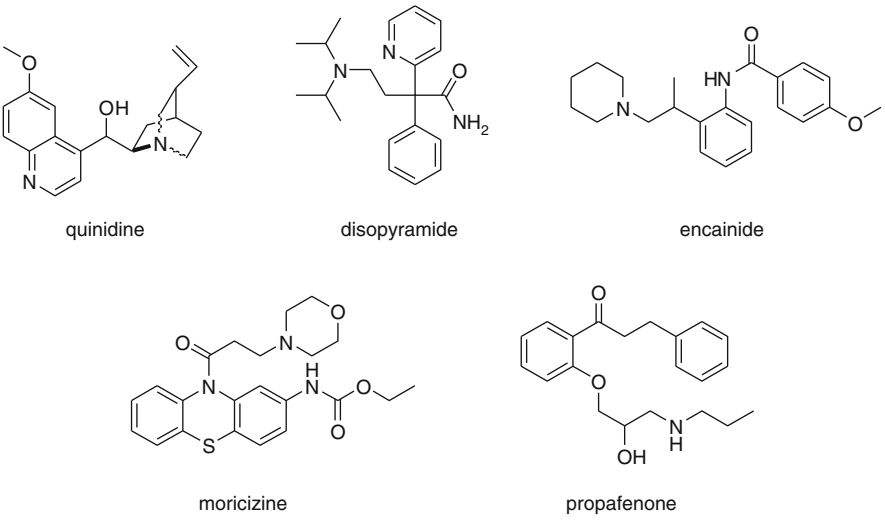

Fig. 6 Sodium channel blockers

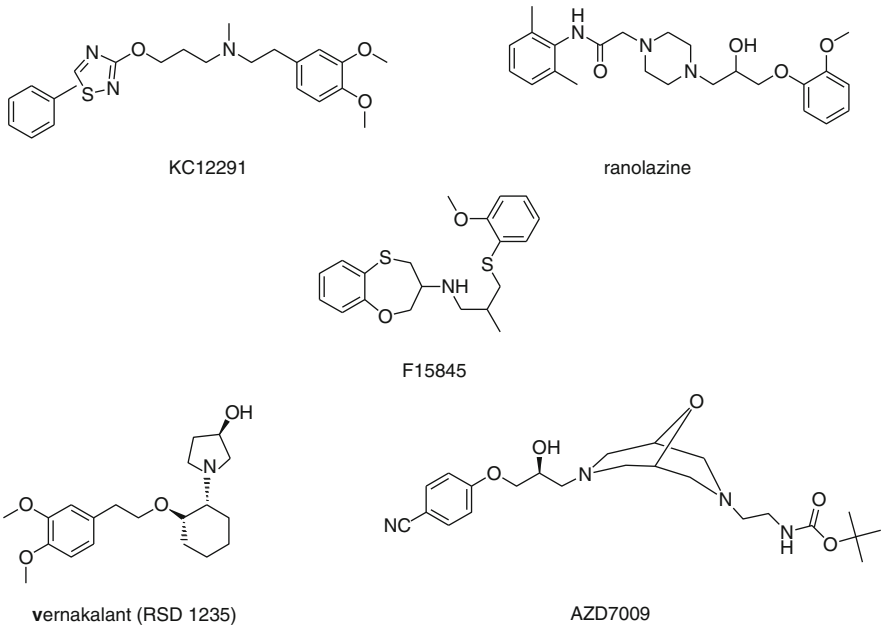

Fig. 7 Sodium channel blockers

dependent calcium channels, reducing calcium uptake via the sodium/calcium exchanger [184–187]. But ranolazine is only weakly potent against the persistent sodium current and it is poorly selective versus several potassium channels and, for these reasons, it is possible to suppose a combination of effects for this drug [188].

In contrast, F15845 is a benzoxathiepine derivative in phase II clinical trials for the treatment of angina that blocks selectively the sodium current (Fig. 7) [178, 189]. Moreover, it exerts short- and long-term cardioprotection after myocardial infarction and, at pharmacologically active doses, F15845 does not affect peak Na^+ current in normal polarized myocytes. This feature clearly distinguishes this promising compound from the commercially available $Na_V1.5$ blockers, as class I antiarrhythmics [188, 189].

RSD1235 (Vernakalant, Fig. 7) is a novel antiarrhythmic drug currently in clinical trials for the acute conversion of atrial fibrillation [190]. It achieves action potential interference through blockade of sodium and potassium currents, also having only minimal effects on ventricular repolarization at therapeutic concentrations [191, 192].

AZD7009 is a mixed ion channel blocker, acting on potassium and sodium currents, with electrophysiological effects predominantly on the atrial tissue (Fig. 7) [193].

3.3.4 Neurodegenerative Diseases

VGSCs are probably involved in the neurodegeneration that occur in several diseases, such as multiple sclerosis (MS), amyotrophic lateral sclerosis (ALS), Huntington, Parkinson, and Alzheimer disease.

Patients with MS often show both positive (pain and dysesthesia) and negative (paresis, ataxia, and hypesthesia) symptoms [194, 195]. Lidocaine and mexiletine are able to block the positive symptoms of MS, blocking Na^+ channels in a voltage- and frequency-dependent manner, thus acting selectively on fibers that mediate positive symptoms (Figs. 4 and 5) [196]. Moreover, several clinical trials regarding neuroprotection using VGSC blockers are under way; in particular, riluzole, topiramate, and lamotrigine are under investigation (Fig. 3) [197–199].

The mechanism leading to selective degeneration of motor neurons in ALS are far from being understood, but several hypotheses have been proposed, including altered functionality of VGSCs [200]. Riluzole is the drug used to treat ALS and it preferentially blocks TTX sensitive VGSCs, whose abnormal function is associated with damaged neurons (Fig. 3) [201, 202]. It seems that riluzole also exhibits a neuroprotective action in a model of Parkinson's disease in the rat [203]. This pathology is a degenerative disorder of the central nervous system that often impairs the sufferer's motor skills, speech, and other functions [204]. Other interesting sodium channel blockers in clinical trials for the treatment of this disease are remacemide and safinamide (Fig. 8) [205–207]. Another progressive neurodegenerative disorder is Huntington's disease, characterized by loss of muscle coordination, cognitive decline, and dementia [208]. Remacemide seems to improve motor function also in this pathology [209]. Finally, there are many evidences that β-subunits of VGSCs are sequentially processed by β-site amyloid precursor protein-cleaving enzyme (BACE1) and γ-secretase, and these results may provide new insights into the underlying pathology of Alzheimer disease [210].

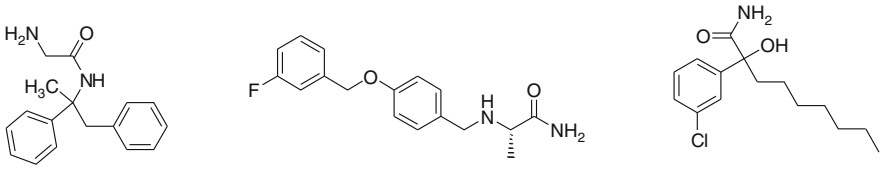

Fig. 8 Sodium channel blockers

3.3.5 Psychiatric Disorders

Several compounds among the anticonvulsant class have played a major role in therapeutic approaches to bipolar illness and other psychiatric disorders such as schizophrenia [95, 211, 212]. As specified in Sect. 2.4.7, genes encoding for different VGSCs seems to have a role in BPD and other psychiatric disorders; nevertheless, it is very difficult to believe that the block of sodium channels expressed in key regions of the limbic system is the only mechanism of action of these drugs and other candidate mechanisms should be explored [211].

Carbamazepine and lamotrigine are the only sodium channel blockers with a FDA indication for the treatment of psychiatric disorders (Fig. 3) [213]. In particular, carbamazepine was approved as a treatment for acute mania and depression in 2004, while lamotrigine has been approved as maintenance treatment of BPD and they seem also be efficacious for neuroleptic-resistant schizophrenia [214–218]. Other sodium channel blockers, such as oxcarbazepine, topiramate, and zonisamide stabilize mood in bipolar and schizoaffective disorders (Figs. 3 and 4) [219–222]. Finally, a Newron compound having sodium channel blocker properties, NW-3509, showed efficacy in a broad spectrum of rodent models of psychosis, mania, depression, and aggressiveness. Used in combination with current antipsychotics, NW-3509 may improve their efficacy allowing a decrease of both their dosage and side effects [223].

3.3.6 Cancer

Cancers are among the leading causes of death in the world, arising from genetic alterations and/or epigenetic changes [224–226]. At the moment, the therapeutic strategies available include the excision of the primary tumor, when cancer is at an early stage, followed by chemo- and/or radiotherapy. Nevertheless, this strategy is often not decisive, and it can lead to a reemergence of tumors after some years, followed by the develop of secondary tumors [84, 227]. This evolution is due to a process named “metastatic cascade,” in which cancer cells enter blood or lymph circulation and invade distant site, thus forming secondary tumors.

The ion channels are new attractive targets studied for cancer therapy and, in particular, VGSCs, that have been shown to be involved in different aspects of the

carcinogenic process, such as cell proliferation, resistance to apoptosis, cell migration or invasiveness [83, 84, 228, 229]. In fact, the expression of these channels is often altered in human cancers, as demonstrated by the biopsies of many epithelial tumors, where an overexpression of VGSCs has been found [230–233].

The use of VGSC blockers in the treatment of cancer appears to be very promising, especially considering the advantages of this therapy. In fact, they often act extracellularly, thus having limited metabolic effects and allowing an easier calibration of the treatment, together with an easier ability to test different structures in vitro [83]. Some examples of sodium channel inhibitors proven to affect tumor progression are the neurotoxin TTX that inhibits cell invasion in vitro in breast and prostate cancer cell lines, and phenytoin and α-hydroxy-α-phenylamides (Figs. 3 and 8), useful to treat prostate cancer by inhibiting cell proliferation [234–239]. However, it is difficult to imagine the use of an existing sodium channel blocker to treat cancer, because many of them (i.e., anticonvulsants or antidepressants) can cross the blood–brain barrier and almost all the small molecules so far known do not have selectivity between the different isoforms, thus causing many side effects. The main goal for the treatment of cancer by using sodium channel interfering drugs will be the discovery of new subtype-specific blockers, especially acting on the $Na_V1.5$ or $Na_V1.7$ isoforms, thus able to treat the disease though avoiding the occurrence of undesired side effects.

4 Conclusion

As indicated in the chapter, there is a wide range of VGSC pathologies, caused by mutations in sodium channel genes, bringing to altered function of membrane ion channels. The VGSC blockers, historically used to treat epilepsy, are now employed also for the treatment of other diseases, although with the consequence of many adverse side effects. As a matter of fact, these drugs are not able to discriminate between different channel subtypes, due to a high degree of sequence homology between them. Nevertheless, it has been proved that AEDs do not have serious side effects, for example, on the heart, and this is due to the existence of a state- and use-dependent block caused by certain small VGSC blockers. The design and synthesis of selective molecules will increase the therapeutic utility of VGSC modulators, especially considering that it is now possible to associate channel subtype mutations to specific disorders (i.e., $Na_V1.5$ in cardiac dysfunctions, $Na_V1.7$ in pain). In the last years, many new molecules have been designed with the aim to obtain subtype selective VGSC blockers, and to avoid the side effects affecting the safety profiles of nonselective drugs. Some among those compounds are now in clinical trials for the treatment of various disorders.

Certainly, Accademia and pharmaceutical industry have a great degree of interest in the search of new VGSC blockers, as demonstrated by the huge number of articles and patents published on this topic. In fact, it is now clear that VGSC modulators are endowed with an enormous and multifarious therapeutic potential.

References

1. Ashcroft FM (2006) From molecule to malady. Nature 440:440–447
2. Hodgkin AL, Huxley AF (1952) A quantitative description of membrane current and its application to conduction and excitation in nerve. J Physiol 117:500–544
3. Catterall WA (2000) From ionic currents to molecular mechanisms: the structure and function of voltage-gated sodium channels. Neuron 26:13–25
4. Mantegazza M, Curia G, Biagini G, Ragsdale DS, Avoli M (2010) Voltage-gated sodium channels as therapeutic targets in epilepsy and other neurological disorders. Lancet Neurol 9:413–424
5. Tseng TT, McMahon AM, Johnson VT, Mangubat EZ, Zahm RJ, Pacold ME, Jakobsson E (2007) Sodium channel auxiliary subunits. J Mol Microbiol Biotechnol 12:249–262
6. Ragsdale DS, McPhee JC, Scheuer T, Catterall WA (1994) Molecular determinants of state-dependent block of Na^+ channels by local anesthetics. Science 265:1724–1728
7. Yarov-Yarovoy V, Brown J, Sharp EM, Clare JJ, Scheuer T, Catterall WA (2001) Molecular determinants of voltage-dependent gating and binding of pore-blocking drugs in transmembrane segment IIIS6 of the Na(+) channel alpha subunit. J Biol Chem 276:20–27
8. Yarov-Yarovoy V, McPhee JC, Idsvoog D, Pate C, Scheuer T, Catterall WA (2002) Role of amino acid residues in transmembrane segments IS6 and IIS6 of the Na^+ channel alpha subunit in voltage-dependent gating and drug block. J Biol Chem 277:35393–35401
9. Stuhmer W, Conti F, Suzuki H, Wang X, Noda M, Yahadi N, Kubo H, Numa S (1989) Structural parts involved in activation and inactivation of the sodium channel. Nature 339:597–603
10. Vassilev PM, Scheuer T, Catterall WA (1988) Identification of an intracellular peptide segment involved in sodium channel inactivation. Science 241:1658–1661
11. Vassilev PM, Scheuer T, Catterall WA (1989) Inhibition of inactivation of single sodium channels by a site-directed antibody. Proc Natl Acad Sci USA 86:8147–8151
12. Mantegazza M, Yu FH, Catterall WA, Scheuer T (2001) Role of the C-terminal domain in inactivation of brain and cardiac sodium channels. Proc Natl Acad Sci USA 98:15348–15353
13. Abriel H, Kass RS (2005) Regulation of the voltage-gated cardiac sodium channel Nav1.5 by interacting proteins. Trends Cardiovasc Med 15:35–40
14. Yamaoka K, Vogel SM, Seyama I (2006) Na^+ channel pharmacology and molecular mechanisms of gating. Curr Pharm Des 12:429–442
15. DeCaen PG, Yarov-Yarovoy V, Sharp EM, Scheuer T, Catterall WA (2010) Sequential formation of ion pairs during activation of a sodium channel voltage sensor. Proc Natl Acad Sci USA 106:22498–22503
16. Paldi T, Gurevitz M (2010) Coupling between residues on S4 and S1 defines the voltage-sensor resting conformation in NaChBac. Biophys J 99:456–463
17. Goldin AL (2003) Mechanisms of sodium channel inactivation. Curr Opin Neurobiol 13:284–290
18. George LA Jr (2005) Inherited disorders of voltage-gated sodium channels. J Clin Invest 115:1990–1999
19. England S, de Groot MJ (2009) Subtype-selective targeting of voltage-gated sodium channels. Br J Pharmacol 158:1413–1425
20. Meisler MH, Kearney JA (2005) Sodium channel mutations in epilepsy and other neurological disorders. J Clin Invest 115:2010–2017
21. Catterall WA, Kalume F, Oakley JC (2010) $Na_V1.1$ channels and epilepsy. J Physiol 588:1849–1859
22. Scalmani P, Rusconi R, Armatura E, Zara F, Avanzini G, Franceschetti S, Mantegazza M (2006) Effects in neocortical neurons of mutations of the Na(v)1.2 Na^+ channel causing benign familial neonatal-infantile seizures. J Neurosci 26:10100–10109
23. Xu R, Thomas EA, Gazina EV, Richards KL, Quick M, Wallace RH, Harkin LA, Heron SE, Berkovic SF, Scheffer IE, Mulley JC, Petrou S (2007) Generalized epilepsy with febrile

seizures plus-associated sodium channel beta1 subunit mutations severely reduce beta subunit-mediated modulation of sodium channel function. Neuroscience 148:164–174
24. Patino GA, Claes LR, Lopez-Santiago LF, Slat EA, Dondeti RS, Chen C, O'Malley HA, Gray CB, Miyazaki H, Nukina N, Oyama F, De Jonghe P, Isom LL (2009) A functional null mutation of SCN1B in a patient with Dravet syndrome. J Neurosci 29:10764–10778
25. Holland KD, Kearney JA, Glauser TA, Buck G, Keddache M, Blankston JR, Glaaser IW, Kass RS, Meisler MH (2008) Mutation of sodium channel *SCN3A* in a patient with cryptogenic pediatric partial epilepsy. Neurosci Lett 433:65–70
26. Singh NA, Pappas C, Dahle EJ, Claes LR, Pruess TH, De Jonghe P, Thompson J, Dixon M, Gurnett C, Peiffer A, White HS, Filloux F, Leppert MF (2009) A role of *SCN9A* in human epilepsies, as a cause of febrile seizures and as a potential modifier of Dravet syndrome. PLoS Genet 5:e1000649
27. Tang B, Dutt K, Papale L, Rusconi R, Shankar A, Hunter J, Tufik S, Yu FH, Catterall WA, Mantegazza M, Goldin AL, Escayg A (2009) A BAC transgenic mouse model reveals neuron subtype-specific effects of a Generalized Epilepsy with Febrile Seizures Plus (GEFS+) mutation. Neurobiol Dis 35:91–102
28. Fujiwara T, Sugawara T, Mazaki-Miyazaki E, Takahashi Y, Fukushima K, Watanabe M, Hara K, Morikawa T, Yagi K, Yamakawa K, Inoue Y (2003) Mutations of sodium channel alpha subunit type 1 (SCN1A) in intractable childhood epilepsies with frequent generalized tonic-clonic seizures. Brain 126:531–546
29. Rhodes TH, Lossin C, Vanoye CG, Wang DW, George AL Jr (2004) Noninactivating voltage-gated sodium channels in severe myoclonic epilepsy of infancy. Proc Natl Acad Sci USA 101:11147–11152
30. Yu FH, Mantegazza M, Westenbroek RE, Robbins CA, Kalume F, Burton KA, Spain WJ, McKnight GS, Scheuer T, Catterall WA (2006) Reduced sodium current in GABAergic interneurons in a mouse model of severe myoclonic epilepsy in infancy. Nat Neurosci 9:1142–1149
31. Ragsdale DS (2008) How do mutant Nav1.1 sodium channels cause epilepsy? Brain Res Rev 58:149–159
32. Catterall WA, Goldin AL, Waxman SG (2005) International Union of Pharmacology. XLVII. Nomenclature and structure-function relationships of voltage-gated sodium channels. Pharmacol Rev 57:397–409
33. Misra SN, Khalig KM, George AL Jr (2008) Impaired NaV1.2 function and reduced cell surface expression in benign familial neonatal-infantile seizures. Epilepsia 49:1535–1545
34. Wallace RH, Wang DW, Singh R, Scheffer IE, George AL Jr, Phillips HA, Saar K, Reis A, Johnson EW, Sutherland GR, Berkovic SF, Mulley JC (1998) Febrile seizures and generalized epilepsy associated with a mutation in the Na^+-channel beta1 subunit gene *SCN1B*. Nat Genet 19:366–370
35. Dib-Hajj SD, Cummins TR, Black JA, Waxman SG (2007) From genes to pain: NaV1.7 and human pain disorders. Trends Neurosci 30:555–563
36. Lampert A, O'Reilly AO, Reeh P, Leffler A (2010) Sodium channelopathies and pain. Pflügers Arch Eur J Physiol 460:249–263
37. Cregg R, Momin A, Rugiero F, Wood JN, Zhao J (2010) Pain channelopathies. J Physiol 588:1897–1904
38. Rice AS, Hill RG (2006) New treatments for neuropathic pain. Annu Rev Med 57:535–551
39. Dworkin RH, O'Connor AB, Backonja M, Farrar JT, Finnerup NB, Jensen TS, Kalso EA, Loeser JD, Miaskowski C, Nurmikko TJ, Portenoy RK, Rice ASC, Stacey BR, Treede R-D, Turk DC, Wallace MS (2007) Pharmacologic management of neuropathic pain: evidence-based recommendations. Pain 132:237–251
40. Waxman SG, Kocsis JD, Black JA (1994) Type III sodium channel mRNA is expressed in embryonic but not adult spinal sensory neurons, and is reexpressed following axotomy. J Neurophysiol 72:466–470

41. He XH, Zang Y, Cheng X, Pang RP, Xu JT, Zhou X, Wei XH, Li YY, Xin WJ, Qin ZH, Liu XG (2010) TNF-alpha contributes to up-regulation of Nav1.3 and Nav1.8 in DRG neurons following motor fiber injury. Pain 151(2):266–279
42. Pertin M, Ji RR, Berta T, Powell AJ, Karchewski L, Tate SN, Isom LL, Woolf CJ, Gilliard N, Spahn DR, Decosterd I (2005) Upregulation of the voltage-gated sodium channel beta2 subunit in neuropathic pain models: characterization of expression in injured and non-injured primary sensory neurons. J Neurosci 25:10970–10980
43. Casula MA, Facer P, Powell AJ, Kinghorn IJ, Plumpton C, Tate SN, Bountra C, Birch R, Anand P (2004) Expression of the sodium channel beta3 subunit in injured human sensory neurons. Neuroreport 15:1629–1632
44. Waxman SG, Hains BC (2006) Fire and phantoms after spinal cord injury: Na^+ channels and central pain. Trends Neurosci 29:207–215
45. Dib-Hajj SD, Cummins TR, Black JA, Waxman SG (2010) Sodium channels in normal and pathological pain. Annu Rev Neurosci 33:325–347
46. Yang Y, Wang Y, Li S et al (2004) Mutations in *SCN9A*, encoding a sodium channel alpha subunit, in patients with primary erythermalgia. J Med Genet 41:171–174
47. Cummins TR, Dib-Hajj SD, Waxman SG (2004) Electrophysiological properties of mutant $Na_v1.7$ sodium channels in a painful inherited neuropathy. J Neurosci 24:8232–8236
48. Fertleman CR, Baker MD, Parker KA et al (2006) *SCN9A* mutations in paroxysmal extreme pain disorder: allelic variants underlie distinct channel defects and phenotypes. Neuron 52:767–774
49. Cox JJ, Reimann F, Nicholas AK et al (2006) An *SCN9A* channelopathy causes congenital inability to experience pain. Nature 444:894–898
50. Goldberg Y, Macfarlane J, Macdonald M, Thompson J, Dube MP et al (2007) Loss-of-function mutations in the Nav1.7 gene underlie congenital indifference to pain in multiple human populations. Clin Genet 71:311–319
51. Nilsen KB, Nicholas AK, Woods CG, Mellgren SI, Nebuchennykh M, Aasly J (2009) Two novel *SCN9A* mutations causing insensitivity to pain. Pain 143:155–158
52. Pietrobon D (2007) Familial hemiplegic migraine. Neurotherapeutics 4:274–284
53. Eikermann-Haerter K, Ayata C (2010) Cortical spreading depression and migraine. Curr Neurol Neurosci Rep 10:167–173
54. Bolay H, Reuter U, Dunn AK, Huang Z, Boas DA, Moskowits MA (2002) Intrinsic brain activity triggers trigeminal meningeal afferents in a migraine model. Nat Med 8:136–142
55. Dichgans M, Freilinger T, Eckstein G et al (2005) Mutation in the neuronal voltage-gated sodium channel *SCN1A* in familial hemiplegic migraine. Lancet 366:371–377
56. Platt D, Griggs R (2009) Skeletal muscle channelopathies: new insights into the periodic paralyses and nondystrophic myotonias. Curr Opin Neurol 22:524–531
57. Raja Rayan DL, Hanna MG (2010) Skeletal muscle channelopathies: nondystrophic myotonias and periodic paralysis. Curr Opin Neurol 23:466–476
58. Petitprez S, Tiab L, Chen L, Kappeler L, Rosler KM, Schorderet D et al (2008) A novel dominant mutation of the Nav1.4 alpha-subunit domain I leading to sodium channel myotonia. Neurology 71:1669–1675
59. Webb J, Cannon SC (2008) Cold-induced defects of sodium channel gating in atypical periodic paralysis plus myotonia. Neurology 70:755–761
60. Carle T, Fournier E, Sternberg D, Fontaine B, Tabti N (2009) Cold-induced disruption of Na^+ channel slow inactivation underlies paralysis in highly thermosensitive paramyotonia. J Physiol 587:1705–1714
61. Jurkat-Rott K, Lehmann-Horn F (2007) Genotype-phenotype correlation and therapeutic rationale in hyperkalemic periodic paralysis. Neurotherapeutics 4:216–224
62. Kuzmenkin A, Muncan V, Jurkat-Rott K, Hang C, Lerche H, Lehmann-Horn F, Mitrovic N (2002) Enhanced inactivation and pH sensitivity of Na(+) channel mutations causing hypokalaemic periodic paralysis type II. Brain 125:835–843

63. Balser JR (2001) The cardiac sodium channel: gating function and molecular pharmacology. J Mol Cell Cardiol 33:599–613
64. Amin AS, Asghari-Roodsari A, Tan HL (2010) Cardiac sodium channelopathies. Eur J Physiol 460:223–237
65. Remme CA, Bezzina CR (2010) Sodium channel (dys)function and cardiac arrhythmias. Cardiovasc Ther 28:287–294
66. Bennett PB, Yazawa K, Makita N, George AL (1995) Molecular mechanism for an inherited cardiac arrhythmia. Nature 376:683–685
67. Abriel H (2010) Cardiac sodium channel Nav1.5 and interacting proteins: physiology and pathophysiology. J Mol Cell Cardiol 48:2–11
68. Fozzard HA, Makielski JC (1985) The electrophysiology of acute myocardial ischemia. Annu Rev Med 36:275–284
69. Janse MJ, Wit AL (1989) Electrophysiological mechanisms of ventricular arrhythmias resulting from myocardial ischemia and infarction. Physiol Rev 69:1049–1169
70. Valdivia CR, Chu WW, Pu J, Foell JD, Haworth RA, Wolff MR, Kamp TJ, Makielski JC (2005) Increased late sodium current in myocytes from a canine heart failure model and from failing human heart. J Mol Cell Cardiol 38:475–483
71. Ufret-Vincenty CA, Baro DJ, Lederer WJ, Rockman HA, Quinones LE, Santana LF (2001) Role of sodium channel deglycosylation in the genesis of cardiac arrhythmias in heart failure. J Biol Chem 276:28197–28203
72. Stys PK (2005) General mechanisms of axonal damage and its prevention. J Neurol Sci 233:3–13
73. Waxman SG (2008) Mechanisms of disease: sodium channels and neuroprotection in multiple sclerosis-current status. Nat Clin Pract Neurol 4:159–169
74. Kiernan MC (2009) Hyperexcitability, persistent Na^+ conductances and neurodegeneration in amyotrophic lateral sclerosis. Exp Neurol 218:1–4
75. Vucic S, Kiernan MC (2010) Upregulation of persistent sodium conductances in familial ALS. J Neurol Neurosurg Psychiatry 81:222–227
76. Craner MJ, Damarjian TG, Liu S, Hains BC, Lo AC, Black JA, Newcombe J, Cuzner ML, Waxman SG (2005) Sodium channels contribute to microglia/macrophage activation and function in EAE and MS. Glia 49:220–229
77. Black JA, Liu S, Waxman SG (2005) Sodium channel activity modulates multiple functions in microglia. Glia 57:1072–1081
78. Bersudsky Y (2006) Phenytoin: an anti-bipolar anticonvulsant? Int J Neuropsychopharmacol 9:479–484
79. Zuliani V, Patel MK, Fantini M, Rivara M (2009) Recent advances in the medicinal chemistry of sodium channel blockers and their therapeutic potential. Curr Top Med Chem 9:396–415
80. Trudeau MM, Dalton JC, Day JW, Ranum LP, Meisler MH (2006) Heterozygosity for a protein truncation mutation of sodium channel SCN8A in a patient with cerebellar atrophy, ataxia, and mental retardation. J Med Genet 43:527–530
81. Wang Y, Zhang J, Liu B, Shao L, Wei Z, Li X, Ji J, Yang F, Wang T, Liu J, Wan C, Li B, Xu Y, Feng G, He L, He G (2010) Genetic polymorphisms in the SCN8A gene are associated with suicidal behavior in psychiatric disorders in the Chinese population. World J Biol Psychiatry. doi:10.3109/15622971003801936
82. Riva D, Vago C, Pantaleoni C, Bulgheroni S, Mantegazza M, Franceschetti S (2009) Progressive neurocognitive decline in two children with Dravet syndrome, de novo *SCN1A* truncations and different epileptic phenotypes. Am J Med Genet A 149A:2339–2345
83. Arcangeli A, Crociani O, Lastraioli E, Masi A, Pillozzi S, Becchetti A (2009) Targeting ion channels in cancer: a novel frontier in antineoplastic therapy. Curr Med Chem 16:66–93
84. Onkal R, Djamgoz MB (2009) Molecular pharmacology of voltage-gated sodium channel expression in metastatic disease: clinical potential of neonatal Nav1.5 in breast cancer. Eur J Pharmacol 625:206–219

85. Fraser SP, Diss JK, Chioni AM, Mycielska ME, Pan H, Yamaci RF, Pani F, Siwy Z, Krasowska M, Grzywna Z, Brackenbury WJ, Theodorou D, Koyutürk M, Kaya H, Battaloglu E, De Bella MT, Slade MJ, Tolhurst R, Palmieri C, Jiang J, Latchman DS, Coombes RC, Djamgoz MB (2005) Voltage-gated sodium channel expression and potentiation of human breast cancer metastasis. Clin Cancer Res 11:5381–5389
86. Gillet L, Roger S, Besson P, Lecaille F, Gore J, Bougnoux P, Lalmanach G, Le Guennec JY (2009) Voltage-gated sodium channel activity promotes cysteine cathepsin-dependent invasiveness and colony growth of human cancer cells. J Biol Chem 284:8680–8691
87. Grimes JA, Fraser SP, Stephens GJ, Downing JE, Laniado ME, Foster CS, Abel PD, Djamgoz MB (1995) Differential expression of voltage-activated Na^+ currents in two prostatic tumour cell lines: contribution to invasiveness in vitro. FEBS Lett 369:290–294
88. Mycielska ME, Fraser SP, Szatkowski M, Djamgoz MB (2003) Contribution of functional voltage-gated Na^+ channel expression to cell behaviors involved in the metastatic cascade in rat prostate cancer: II. Secretory membrane activity. J Cell Physiol 195:461–469
89. Onganer PU, Seckl MJ, Djamgoz MB (2005) Neuronal characteristics of small-cell lung cancer. Br J Cancer 93:1197–1201
90. Roger S, Rollin J, Barascu A, Besson P, Raynal PI, Iochmann S, Lei M, Bougnoux P, Gruel Y, Le Guennec JY (2007) Voltage-gated sodium channels potentiate the invasive capacities of human non-small-cell lung cancer cell lines. Int J Biochem Cell Biol 39:774–786
91. Sander JW (2003) The epidemiology of epilepsy revisited. Curr Opin Neurol 16:165–170
92. McCormick DA, Contreras D (2001) On the cellular and network bases of epileptic seizures. Annu Rev Physiol 63:815–846
93. Kwan P, Brodie MJ (2000) Early identification of refractory epilepsy. N Engl J Med 342:314–319
94. Dodson WE (2004) Definitions and classification of epilepsy. In: Shorvon S, Perucca E, Fish D, Dodson E (eds) The treatment of epilepsy. Blackwell Publishing, Oxford
95. Rogawski MA, Loscher W (2004) The neurobiology of antiepileptic drugs. Nat Rev Neurosci 5:553–564
96. Hille B (2001) Ionic channels of excitable membranes. Sinauer Associates Inc., Sunderland
97. Leppik IE (2004) Zonisamide: chemistry, mechanism of action, and pharmacokinetics. Seizure 13:S5–S9
98. Loscher W (2002) Basic pharmacology of valproate: a review after 35 years of clinical use for the treatment of epilepsy. CNS Drugs 16:669–694
99. Stefani A, Spadoni F, Siniscalchi A, Bernardi G (1996) Lamotrigine inhibits Ca^{2+} currents in cortical neurons: functional implications. Eur J Pharmacol 307:113–116
100. Zona C, Tancredi V, Longone P, D'Arcangelo G, D'Antuono M, Manfredi M, Avoli M (2002) Neocortical potassium currents are enhanced by the antiepileptic drug lamotrigine. Epilepsia 43:685–690
101. Shank RP, Maryanoff BE (2008) Molecular pharmacodynamics, clinical therapeutics, and pharmacokinetics of topiramate. CNS Neurosci Ther 14:120–142
102. Gryder DS, Rogawski MA (2003) Selective antagonism of GluR5 kainate-receptor-mediated synaptic currents by topiramate in rat basolateral amygdala neurons. J Neurosci 23:7069–7074
103. Qian J, Noebels JL (2003) Topiramate alters excitatory synaptic transmission in mouse hippocampus. Epilepsy Res 55:225–233
104. Pittenger C, Coric V, Banasr M, Bloch M, Krystal JH, Sanacora G (2008) Riluzole in the treatment of mood and anxiety disorders. CNS Drugs 22:761–786
105. Curia G, Biagini G, Perucca E, Avoli M (2009) Lacosamide: a new approach to target voltage-gated sodium currents in epileptic disorders. CNS Drugs 23:555–568
106. Errington AC, Stohr T, Heers C, Lees G (2008) The investigational anticonvulsant lacosamide selectively enhances slow inactivation of voltage-gated sodium channels. Mol Pharmacol 73:157–169
107. Errington AC, Coyne L, Stohr T, Selve N, Lees G (2006) Seeking a mechanism of action for the novel anticonvulsant lacosamide. Neuropharmacology 50:1016–1029

108. Julius D, Basbaum AI (2001) Molecular mechanism of nociception. Nature 413:203–210
109. Stucky CL, Gold MS, Zhang X (2001) Mechanism of pain. Proc Natl Acad Sci USA 98:11845–11846
110. Orza F, Boswell MV, Rosenberg SK (2000) Neuropathic pain: review of mechanisms and pharmacologic management. NeuroRehabilitation 14:15–23
111. Harden RN (2005) Chronic neuropathic pain. Mechanism, diagnosis and treatment. Neurologist 11:111–122
112. Zimmermann M (2001) Pathology of neuropathic pain. Eur J Pharmacol 429:23–37
113. Woolf CJ, Mannion RJ (1999) Neuropathic pain: aethiology, symptoms, mechanisms and management. Lancet 353:1959–1964
114. Hansson P (2002) Neuropathic pain: clinical characteristics and diagnostic workup. Eur J Pain 6:47–50
115. Jensen TS, Gottrup H, Sindrup SH, Bach FW (2001) The clinical picture of neuropathic pain. Eur J Pharmacol 429:1–11
116. Woolf CJ (2004) Dissecting out mechanism responsible for peripheral neuropathic pain: implications for diagnosis therapy. Life Sci 74:2605–2610
117. Lawson SN (2002) Phenotype and function of somatic primary afferent nociceptive neurones with C-, Aδ-, or Aα/β-fibres. Exp Physiol 87:239–244
118. Garcia-Poblete E, Fernandez-Garcia H, Moro-Rodriguez E, Catala-Rodriguez M, Rico-Morales ML, Garcia-Gomez-de-las-Heras S, Palomar-Gallego MA (2003) Sympathetic sprouting in dorsal root ganglia (DRG): a recent histological finding? Histol Histopathol 18:575–586
119. Eisenberg E, Mcnicol ED, Carr DB (2005) Efficacy and safety of opioid agonist in the treatment of neuropathic pain of nonmalignal origin: systematic review and meta-analysis of randomized controlled trials. JAMA 293:3043–3052
120. Trujllo KA (2002) The neurobiology of opiate tolerance, dependence and sensitization: mechanism of NMDA receptor-dependent synaptic plasticity. Neurotox Res 4:373–391
121. Kostyuk PG, Veselovsky NS, Tsyndrenko AY (1981) Ionic currents in the somatic membrane of rat dorsal root ganglion neurons-I. Sodium currents. Neuroscience 6:2423–2430
122. Bigelow N, Harrison I (1944) General analgesic effects of procaine. J Pharmacol Exp Ther 81:368–373
123. Lemoyne J (1950) Use of dimethyl-dithio-hydantoin in treatment of certain facial neuralgias. Ann Otolaryngol 67:626–628
124. Blom S (1962) Trigeminal neuralgia: its treatment with a new anticonvulsant drug (G-32883). Lancet 1:839–840
125. Vaughan Williams EM (1984) A classification of antiarrhythmic actions reassessed after a decade of new drugs. J Clin Pharmacol 24:129–147
126. Watson CP, Evans RJ, Reed K, Merskey H, Goldsmith L, Warsh J (1982) Amitriptyline versus placebo in postherpetic neuralgia. Neurology 32:671–673
127. Leijon G, Boivie J (1989) Central post-stroke pain – a controlled trial of amitriptyline and carbamazepine. Pain 36:27–36
128. Watson CP, Vernich L, Chipman M, Reed K (1998) Nortriptyline versus amitriptyline in postherpetic neuralgia: a randomized trial. Neurology 51:1166–1171
129. Boas RA, Covino BG, Shahnarian A (1982) Analgesic responses to i.v. Lignocaine. Br J Anaesth 54:501–505
130. Petersen P, Kastrup J (1987) Dercum's disease (adiposis dolorosa). Treatment of the severe pain with intravenous lidocaine. Pain 28:77–80
131. Kastrup J, Petersen P, Dejgard A, Angelo HR, Hilsted J (1987) Intravenous lidocaine infusion – a new treatment of chronic painful diabetic neuropathy? Pain 28:69–75
132. Araujo MC, Sinott CJ, Strichartz GR (2003) Multiple phases of relief from experimental mechanical allodynia by systemic lidocaine: responses to early and late infusion. Pain 103:21–29
133. Chaplan SR, Bach FW, Shafer SL, Yaksh TL (1995) Prolonged alleviation of tactile allodynia by intravenous lidocaine in neuropathic rats. Anesthesiology 83:775–785

134. Mao J, Price DD, Mayer DJ, Lu J, Hayes RL (1992) Intrathecal MK-801 and local nerve anesthesia synergistically reduce nociceptive behaviors in rats with experimental peripheral mononeuropathy. Brain Res 576:254–262
135. Max MB, Lynch SA, Muir J, Shoaf SE, Smoller B, Dubner R (1992) Effects of desipramine, amitriptyline and fluoxetine on pain in diabetic neuropathy. N Engl J Med 326:1250–1256
136. Strichartz GR, Zhou Z, Sinnott C, Khodorova A (2002) Therapeutic concentrations of local anesthetics unveil the potential role of sodium channels in neuropathic pain. In: Bock G, Goode JA (eds) Sodium channels and neuronal hyperexcitability. Wiley, New York
137. Harati Y, Gooch C, Swenson M, Edelman S, Greene D, Raskin P, Donofrio PD, Cornblath D, Sachdeo R, Siu CO, Kamin M (1998) Double-blind randomized trial of tramadol for the treatment of the pain of diabetic neuropathy. Neurology 50:1842–1846
138. Simpson DM, Olney R, McArthur JC, Khan A, Godbold J, Ebel-Frommer K (2000) A placebo-controlled trial of lamotrigine for painful HIV-associated neuropathy. Neurology 54:2115–2119
139. Vestergaard K, Andersen G, Gottrup H, Kristensen BT, Jensen TS (2001) Lamotrigine for central poststroke pain: a randomized controlled trial. Neurology 56:184–190
140. Raskin P, Donofrio PD, Rosenthal NR, Hewitt DJ, Jordan DM, Xiang J, Vinik AI (2004) Topiramate versus placebo in painful diabetic neuropathy: analgesic and metabolic effects. Neurology 63:865–873
141. Veneroni O, Maj R, Calabresi M, Faravelli L, Fariello RG, Salvati P (2003) Anti-allodynic effect of NW-1029, a novel Na^+ channel blocker, in experimental animal models of inflammatory and neuropathic pain. Pain 102:17–25
142. Ferrante FM, Paggioli J, Cherukuri S, Arthur GR (1996) The analgesic response to intravenous lidocaine in the treatment of neuropathic pain. Anesth Analg 82:91–97
143. Bach FW, Jensen TS, Kastrup J, Stigsby B, Dejgard A (1990) The effect of intravenous lidocaine on nociceptive processing in diabetic neuropathy. Pain 40:29–34
144. Devulder JE, Ghys L, Dhondt W, Rolly G (1993) Neuropathic pain in a cancer patient responding to subcutaneously administered lignocaine. Clin J Pain 9:220–223
145. Shorvon S (2000) Oxacarbazepine: a review. Seizure 9:75–79
146. Ambrosio AF, Soares-Da-Silva P, Carvalho CM, Carvalho AP (2002) Mechanism of action of carbamazepine and its derivatives, oxacarbazepine, BIA 2-093 and BIA 2-024. Neurochem Res 27:121–130
147. Tecoma ES (1999) Oxacarbazepine. Epilepsia 40:S37–S46
148. Sudoh Y, Cahoon EE, Gerner P, Wang GK (2003) Tricyclic antidepressants as long-acting local anesthetics. Pain 103:49–55
149. Turkington RW (1980) Depression masquerading as diabetic neuropathy. JAMA 243:1147–1150
150. Max MB, Schafer SC, Culnane M, Smoller B, Dubner R, Gracely RH (1988) Amitriptyline, but not lorazepam, relieves postherpetic neuralgia. Neurology 38:1427–1432
151. Bryson MH, Wilde MI (1996) Amitriptyline. A review of its pharmacological properties and therapeutic use in chronic pain states. Drugs Aging 8:459–476
152. Jarvis MF, Honore P, Shieh CC, Chapman M, Joshi S, Zhang XF, Kort M, Carroll W, Marron B, Atkinson R, Thomas J, Liu D, Krambis M, Liu Y, McGaraughty S, Chu KL, Roeloffs R, Zhong C, Mikusa JP, Hernandez G, Gauvin D, Wade C, Zhu C, Pai M, Scanio M, Shi L, Drizin I, Gregg R, Matulenko M, Hakeem A, Gross M, Johnson M, Marsh K, Wagoner PK, Sullivan JP, Faltynek CR, Krafte DS (2007) A-803467, a potent and selective Nav1.8 sodium channel blocker, attenuates neuropathic and inflammatory pain in the rat. Proc Natl Acad Sci USA 104:8520–8525
153. McGaraughty S, Chu KL, Scanio MJ, Kort ME, Faltynek CR, Jarvis MF (2008) A selective Nav 1.8 sodium channel blocker, A-803467 [5-(4-chlorophenyl)-N-(3,5-dimethoxyphenyl) furan-2-carboxamide] attenuates spinal neuronal activity in neuropathic rats. J Pharmacol Exp Ther 324:1204–1211

154. Castro MJ, Stam AH, Lemos C, de Vries B, Vanmolkot KR, Barros J, Terwindt GM, Frants RR, Sequeiros J, Ferrari MD, Pereira-Monteiro JM, van den Maagdenberg AMJM (2009) First mutation in the voltage-gated $Na_V1.1$ subunit gene SCN1A with co-occurring familial hemiplegic migraine and epilepsy. Cephalalgia 29:308–313
155. Diehgans M, Freilinger T, Eckstein G, Babini E, Lorenz-Depiereux B, Biskup S, Ferrari M, Herzog T, van den Maagdenberg AMJM, Pusch M, Strom T (2005) Mutation in the neuronal voltage-gated sodium channel SCN1A in familial hemiplegic migraine. Lancet 366:371–377
156. Gargus JJ, Tournay A (2007) Novel mutation confirms seizure locus SCN1A is also familial hemiplegic migraine. Pediatr Neurol 37:407–410
157. Kahlig KM, Rhodes TH, Pusch M, Freilinger T, Pereira-Monteiro JM, Ferrari MD, van den Maagdenberg AMJM, Diehgans M, George AC (2008) Divergent sodium channel defects in familial hemiplegic migraine. Proc Natl Acad Sci USA 105:9799–9804
158. Calabresi P, Galletti F, Rossi C, Sarchielli P, Cupini LM (2007) Antiepileptic drugs in migraine: from clinical aspects to cellular mechanism. Trends Pharmacol Sci 28:188–195
159. Mankodi A, Thornton CA (2002) Myotonic syndromes. Curr Opin Neurol 15:545–552
160. Harper PS (2001) Myotonic dystrophy. WB Saunders Company, London
161. Lehmann-Horn F, Kuther G, Ricker K, Grafe P, Ballanyi K, Rudel R (1987) Adynamia episodica hereditaria with myotonia: a noninactivating sodium current and the effect of extracellular pH. Muscle Nerve 10:363–374
162. Lehmann-Horn F, Rudel R, Ricker K (1987) Membrane defects in paramyotonia congenita (Eulenburg). Muscle Nerve 10:633–641
163. Dengler R, Rudel R (1979) Effects of tocainide on normal and myotonic mammalian skeletal muscle. Arzneimittelforschung 29:270–273
164. Streib EW (1986) Successful treatment with tocainide of recessive generalized congenital myotonia. Ann Neurol 19:501–504
165. Rüdel R (1994) Altered excitability of the muscle cell membrane. The non-dystrophic myotonias. In: Engel AG, Franzini-Armstrong C (eds) Myology. Mc Graw-Hill, New York
166. Trip J, Drost GG, van Engelen BGM, Faber GG (2006) Drug treatment for myotonia. Cochrane Database Syst Rev. doi:10.1002/14651858.CD004762.pub, John Wiley & Sons, Ltd
167. Hill RJ, Duff HJ, Sheldon RS (1988) Determinants of stereospecific binding of type I antiarrhythmic drugs to sodium channels. Mol Pharmacol 34:659–663
168. Franchini C, Carocci A, Catalano A, Cavalluzzi MM, Corbo F, Lentini G, Scilimati A, Tortorella P, Conte Camerino D, De Luca A (2003) Optically active mexiletine analogues as stereoselective blockers of voltage-gated Na^+ channels. J Med Chem 46:5238–5248
169. Desaphy J-F, De Luca A, Didonna MP, George AL Jr, Conte Camerino D (2004) Different flecainide sensitivity of $hNa_V1.4$ channels and myotonic mutants explained by state-dependent block. J Physiol 554:321–334
170. Rosenfeld J, Sloan-Brown K, George AL Jr (1997) A novel muscle sodium channel mutation causes painful congenital myotonia. Ann Neurol 42:811–814
171. Abriel H, Wehrens XHT, Benhorin J, Kerem G, Kass RS (2000) Molecular pharmacology of the sodium channel mutation D1790G linked to the long-QT syndrome. Circulation 102:921–925
172. Catalano A, Carocci A, Corbo F, Franchini C, Muraglia M, Scilimati A, De Bellis M, De Luca A, Conte Camerino D, Sinicropi MS, Tortorella V (2008) Constrained analogues of tocainide as potent skeletal muscle sodium channel blockers toward the development of antimyotonic agents. Eur J Med Chem 43:2535–2540
173. Herweg B, Steinberg JS (2000) Oral Antiarrhythmic drugs used for arrhythmia prevention. Card Electrophysiol Rev 4:255–261
174. Franchini C, Corbo F, Lentini G, Bruno G, Scilimati A, Tortorella V, Conte Camerino D, De Luca A (2000) Synthesis of new 2,6-prolylxylidide analogues of tocainide as stereoselective blockers of voltage-gated Na^+ channels with increased potency and improved use-dependent activity. J Med Chem 43:3792–3798

175. Talon S, De Luca A, De Bellis M, Desaphy J-F, Lentini G, Scilimati A, Corbo F, Franchini C, Tortorella P, Jockusch H, Conte Camerino D (2001) Increased rigidity of the chiral centre of tocainide favours stereoselectivity and use-dependent block of skeletal muscle Na^+ channels enhancing the antimyotonic activity in vivo. Br J Pharmacol 134:1523–1531
176. De Luca A, Talon S, De Bellis M, Desaphy J-F, Lentini G, Corbo F, Scilimati A, Franchini C, Tortorella P (2003) Optimal requirements for high affinity and use-dependent block of skeletal muscle sodium channel by N-benzyl analogs of tocainide-like compounds. Mol Pharmacol 64:932–945
177. De Bellis M, De Luca A, Lentini G, Carocci A, Corbo F, Franchini C, Conte Camerino D (2009) Newly synthesized mexiletine and tocainide analogues are potent use-dependent blockers of skeletal muscle sodium channels: potential implication for the antimyotonic activity. Neuromuscul Disord. doi:10.1016/j.nmd.2009.06.318
178. Le Grand B, Pignier C, Létienne R, Cuisiat F, Rolland F, Mas A, Vacher B (2008) Sodium late current blockers in ischemia reperfusion: is the bullet magic? J Med Chem 51:3856–3866
179. Saint DA (2008) The cardiac persistent sodium current: an appealing therapeutic target? Br J Pharmacol 153:1133–1142
180. Tamareille S, Le Grand B, John GW, Feuvray D, Coulombe A (2002) Anti-ischemic compound KC12291 prevents diastolic contracture in isolated atria by blockade of voltage-gated sodium channels. J Cardiovasc Pharmacol 40:346–355
181. John GW, Létienne R, Le Grand B, Pignier C, Vacher B, Patoiseau J-F, Colpaert FC, Coulombe A (2004) KC 12291: an atypical sodium channel blocker with myocardial antiischemic properties. Cardiovasc Drug Rev 22:17–26
182. Hayashida W, van Eyll C, Rousseau MF, Pouleur H (1994) Effects of ranolazine on left ventricular regional diastolic function in patients with ischemic heart disease. Cardiovasc Drugs Ther 8:741–747
183. Chaitman BR, Skettino SL, Parker JO, Hanley P, Meluzin J, Kuch J, Pepine CJ, Wang W, Nelson JJ, Hebert DA, Wolff AA (2004) Anti-ischemic effects and long-term survival during ranolazine monotherapy in patients with chronic severe angina. J Am Coll Cardiol 43:1375–1382
184. Belardinelli L, Shryock JC, Fraser H (2006) The mechanism of ranolazine action to reduce ischemia-induced diastolic dysfunction. Eur Heart J Suppl 8:A10–A13
185. Song Y, Shryock JC, Wu L, Belardinelli L (2004) Antagonism by ranolazine of the pro-arrhythmic effects of increasing I_{Na} in guinea pig ventricular myocytes. J Cardiovasc Pharmacol 44:192–199
186. Antzelevitch C, Belardinelli L, Zygmunt AC, Burashnikov A, Di Diego JM, Fish JM, Cordeiro JM, Thomas G (2004) Electrophysiological effects of ranolazine, a novel antianginal agent with antiarrhythmic properties. Circulation 110:904–910
187. Hale SL, Kloner RA (2006) Ranolazine, an inhibitor of the late sodium channel current, reduces postischemic myocardial dysfunction in the rabbit. J Cardiovasc Pharmacol Ther 11:249–255
188. Vié B, Sablayrolles S, Lètienne R, Vacher B, Darmellah MB, Feuvray D, Le Grand B (2009) 3-(R)-[3-(2-methoxyphenylthio-2-(S)-methylpropyl]amino-3,4-dihydro-2H-1,5-benzoxathiepine bromhydrate (F 15845) prevents ischemia-induced heart remodeling by reduction of the intracellular Na^+ overload. J Pharm Exp Ther 330:696–703
189. Vacher B, Pignier C, Lètienne R, Verscheure Y, Le Grand B (2009) F 15845 inhibits persistent sodium current in the heart and prevents angina in animal models. Br J Pharmacol 156:214–225
190. Finnin M (2010) Vernakalant: a novel agent for the termination of atrial fibrillation. Am J Health Syst Pharm 67:1157–1164
191. Orth PMR, Hesketh JC, Mak CKH, Yang Y, Lin S, Beatch GN, Ezrin AM, Fedida D (2006) RSD1235 blocks late I_{Na} and suppresses early afterdepolarizations and torsade de pointes induced by class III agents. Cardiovasc Res 70:486–496

192. Savelieva I, Camm J (2008) Antiarrhythmic drug therapy for atrial fibrillation: current anti-arrhythemic drugs, investigational agents and innovative approaches. Europace 10:647–665
193. Goldstein RN, Christion C, Carlson L, Waldo AL (2004) AZD 7009: a new antiarrhythmic drug with predominant effect on the atria effectively terminates and prevents reinduction of atrial fibrillation and flutter in the sterile pericarditis model. J Cardiovasc Electrophysiol 15:1444–1450
194. Osterman PO, Westerberg CE (1975) Paroxysmal symptoms in multiple sclerosis. Brain 98:189–202
195. Clifford DB, Trotter JL (1984) Pain in multiple sclerosis. Arch Neurol 41:1270–1272
196. Sakurai M, Kanazawa I (1999) Positive symptoms in multiple sclerosis: their treatment with sodium channel blockers, lidocaine and mexiletine. J Neurol Sci 162:162–168
197. Bechtold DA, Miller SJ, Dawson AC, Sun Y, Kapoor R, Berry D, Smith KJ (2006) Axonal protection achieved in a model of multiple sclerosis using lamotrigine. J Neurol 253:1542–1551
198. Kapoor R (2006) Neuroprotection in multiple sclerosis: therapeutic strategies and clinical trial design. Curr Opin Neurol 19:255–259
199. Comi G, Filippi M (2005) Clinical trials in multiple sclerosis: methodological issue. Curr Opin Neurol 9:220–229
200. Pieri M, Carunchio I, Curcio L, Mercuri NB, Zona C (2009) Increased persistent sodium current determines cortical hyperexcitability in a genetic model of amyotrophic lateral sclerosis. Exp Neurol 215:368–379
201. Song JH, Huang CS, Nagata K, Yeh JZ, Narahashi T (1997) Differential action of riluzole on tetrodotoxin-sensitive and tetrodotoxin-resistant sodium channels. J Pharmacol Exp Ther 282:707–714
202. Miller RG, Mitchell JD, Lyon M, Moore DH (2007) Riluzole for amyotrophic lateral sclerosis (ALS)/motor neuron disease (MND). Cochrane Database Syst Rev. doi:10.1002/14651858.CD001447.pub2 DOI:dx.doi.org
203. Barnéoud P, Mazadier M, Miquet J-M, Parmentier S, Dubédat P, Doble A, Boireau A (1996) Neuroprotective effects of riluzole on a model of Parkinson's disease in the rat. Neuroscience 74:971–983
204. Jankovic J (2008) Parkinson's disease: clinical features and diagnosis. J Neurol Neurosurg Psychiatry 79:368–376
205. Stocchi F, Vacca L, Grassini P, De Pandis MF, Battaglia G, Cattaneo C, Fardello RG (2006) Symptom relief in Parkinson disease by safinamide – biochemical and clinical evidence of efficacy beyond MAO-B inhibition. Neurology 67:S24–S29
206. Caccia C, Maj R, Calabresi M, Maestroni S, Faravelli R, Curatolo L, Salvati P, Fardello RG (2006) Safinamide from molecular targets to a new antiparkinson drug. Neurology 67: S18–S23
207. Parkinson Study Group (2001) A randomized, controlled trial of remacemide for motor fluctuations in Parkinson's disease. Neurology 56:455–462
208. Walker FO (2007) Huntington's disease. Lancet 369:218–228
209. Kieburtz K, Feigin A, McDermott M, Como P, Abwender D, Zimmerman C, Hickey C, Orme C, Claude K, Sotack J, Greenamyre JT, Dunn C, Shoulson I (1996) A controlled trial of remacemide hydrochloride in Huntington's disease. Mov Disord 11:273–277
210. Wong H-K, Sakurai T, Oyama F, Kaneko K, Wada K, Miyazaki H, Kurosawa M, De Strooper B, Saftig P, Nukina N (2005) β Subunits of voltage-gated sodium channels are novel substrates of β-site amyloid precursor protein-cleaving enzyme (BACE1) and γ-secretase. J Biol Chem 280:23009–23017
211. Post RM (2004) Differing psychotropic profiles of the anticonvulsants in bipolar and other psychiatric disorders. Clin Neurosci Res 4:9–30
212. Boylan LS, Devinsky O, Barry JJ, Ketter TA (2002) Psychiatric uses of antiepileptic treatments. Epilepsy Behav 3:S54–S59

213. Ettinger AB, Argoff CE (2007) Use of antiepileptic drugs for nonepileptic conditions: psychiatric disorders and chronic pain. Neurotherapeutics 4:75–83
214. Kowatch RA, Suppes T, Carmody TJ, Bucci JP, Hume JH, Kromelis M, Emslie GJ, Weinberg WA, Rush J (2000) Effect size of lithium, divalproex sodium, and carbamazepine in children and adolescents with bipolar disorder. J Am Acad Child Adolesc Psychiatry 39:713–720
215. Ketter TA, Kalali AH, Weisler RH (2004) A 6-month, multicenter, open-label evaluation of beaded, extended-release carbamazepine capsule monotherapy in bipolar disorder patients with manic or mixed episodes. J Clin Psychiatry 65:668–673
216. Calabrese JR, Bowden CL, Sachs GS, Ascher JA, Monaghan E, Rudd GD (1999) A double-blind placebo-controlled study of lamotrigine monotherapy in outpatients with bipolar I depression. J Clin Psychiatry 60:79–88
217. Calabrese JR, Bowden CL, Sachs G, Yatham LN, Behnke K, Mehtonen OP, Montgomery P, Ascher JA, Paska W, Earl N, DeVeaugh-Geiss J (2003) A placebo-controlled 18-month trial of lamotrigine and lithium maintenance treatment in recently depressed patients with bipolar I disorder. J Clin Psychiatry 64:1013–1024
218. Hosak L, Libiger J (2002) Antiepileptic drugs in schizophrenia: a review. Eur Psychiatry 17:371–378
219. Emrich HM (1990) Studies with (Trileptal) oxcarbazepine in acute mania. Int Clin Psychopharmacol 5:S83–S88
220. Grunze HC, Normann C, Langosch J, Schaefer M, Amann B, Sterr A, Schloesser S, Kleindienst N, Walden J (2001) Antimanic efficacy of topiramate in 11 patients in an open trial with an on-off-on design. J Clin Psychiatry 62:464–468
221. Kanba S, Yagi G, Kamijima K, Suzuki T, Tajima O, Otaki J, Arata E, Koshikawa H, Nibuya M, Kinoshita N (1994) The first open study of zonisamide, a novel anticonvulsant, shows efficacy in mania. Prog Neuropsychopharmacol Biol Psychiatry 18:707–715
222. Spina E, Perugi G (2004) Antiepileptic drugs: indications other than epilepsy. Epileptic Disord 6:57–75
223. Izzo E, Ieraci A, Meli S, Bortolato M, Frau R, Bini V, Salvati P, Anand R (2010) Adjuvant activity of the novel sodium channel blocker NW-3509 in combination therapy with antipsychotics. CINP – Hong Kong World Congress. https://www1.cinp-congress.org/guest/IDd3044a565c0d23/ID04773c0cfb0ea3/AbstractView?ABSID=8989
224. Edwards BK, Brown ML, Wingo PA, Howe HL, Ward E, Ries LA, Schrag D, Jamison PM, Jemal A, Wu XC, Friedman C, Harlan L, Warren J, Anderson RN, Pikle LW (2005) Annual report to the nation on the status of cancer, 1975–2002, featuring population-based trends in cancer treatment. J Natl Cancer Inst 97:1407–1427
225. Jemal A, Siegel R, Ward E, Hao Y, Xu J, Murray T, Thun MJ (2008) Cancer statistics, 2008. CA Cancer J Clin 58:71–96
226. Hanahan D, Weinberg RA (2000) The hallmarks of cancer. Cell 100:57–70
227. Vaidya KS, Welch DR (2007) Metastasis suppressors and their roles in breast carcinoma. J Mammary Gland Biol Neoplasia 12:175–190
228. Bacac M, Stamenkovic I (2007) Metastatic cancer cell. Annu Rev Pathol 3:221–247
229. Gillet L, Roger S, Bougnoux P, Le Guennec J-Y, Besson P (2010) Beneficial effects of omega-3 long-chain fatty acids in breast cancer and cardiovascular diseases: voltage-gated sodium channels as a common feature? Biochimie. doi:10.1016/j.biochi.2010.02.005
230. Roger S, Potier M, Vandier C, Besson P, Le Guennec J-Y (2006) Voltage-gated sodium channels: new targets in cancer therapy? Curr Pharm Des 12:3681–3695
231. Lang F, Föller M, Lang KS, Lang PA, Ritter M, Gulbins E, Vereninov A, Huber SM (2005) Ion channels in cell proliferation and apoptotic cell death. J Membr Biol 205:147–157
232. Schönherr R (2005) Clinical relevance of ion channels for diagnosis and therapy of cancer. J Membr Biol 205:175–184
233. Fiske JL, Fomin VP, Brown ML, Duncan RL, Sikes RA (2006) Voltage-sensitive ion channels and cancer. Cancer Metastasis Rev 25:493–500

234. Brackenbury WJ, Chioni AM, Diss JK, Djamgoz MB (2007) The neonatal splice variant of Na_V 1.5 potentiates *in vitro* invasive behaviour of MDA-MB-231 human breast cancer cells. Breast Cancer Res Treat 101:149–160
235. Anderson JD, Hansen TP, Lenkowski PW, Walls AM, Choudhury IM, Schenck HA, Friehling M, Hölll GM, Patel MK, Sikes RA, Brown ML (2003) Voltage-gated sodium channel blockers as cytostatic inhibitors of the androgen-independent prostate cancer cell line PC-3. Mol Cancer Ther 2:1149–1154
236. Brown ML, Zha CC, Van Dyke CC, Brown GB, Brouillette WJ (1999) Comparative molecular field analysis of hydantoin binding to the neuronal voltage-dependent sodium channel. J Med Chem 42:1537–1545
237. Sikes RA, Walls AM, Brennen WN, Anderson JD, Choudhury-Mukherjee I, Schenck HA, Brown ML (2003) Therapeutic approaches targeting prostate cancer progression using novel voltage-gated ion channel blockers. Clin Prostate Cancer 2:181–187
238. Rampe D, Murawsky MK, Gran J, Lewis EW (1998) The antipsychotic agent sertindole is a high affinity antagonist of the human cardiac potassium channel HERG. J Pharmacol Exp Ther 286:788–793
239. Laniado ME, Lalani EN, Fraser SP, Grimes JA, Bhagal G, Djamgoz MB, Abel PD (1997) Expression and functional analysis of voltage-activated Na^+ channels in human prostate cancer cell lines and their contribution to invasion *in vitro*. Am J Pathol 150:1213–1221

Potassium Channel Blockers as Antiarrhythmic Agents

Qidong You, Qian Yang, and Xiaojian Wang

Contents

Abstract This article highlights the development of potassium channel blockers as antiarrhythmic agents. The chemical structures, the structure–activity relationships (SARs) of related potassium channel blockers, and their possible binding modes reported so far in literatures and patents are summarized and evaluated.

Keywords Cardiac arrhythmic • Potassium channel blockers • SARs

Q. You (✉)
School of Pharmacy, China Pharmaceutical University, Nanjing 210009, China
e-mail: youqidong@gmail.com

S.P. Gupta (ed.), *Ion Channels and Their Inhibitors*,
DOI 10.1007/978-3-642-19922-6_5,

Abbreviations

AERP	Atrial effective refractory period
APD	Action potential duration
CHO	Chinese hamster ovary
ERP	Effective refractory period
HEK	Human embryonic kidney
I_{Kr}	Rapid delayed rectifier potassium channel currents
I_{Kur}	Ultrarapid delayed rectifier potassium current
IUPHAR	International union of basic and clinical pharmacology
TdP	Torsades de pointes
VERP	Ventricular effective refractory period

1 Introduction

Potassium channels, encoded by more than eighty genes, are one of the most diverse classes of cell membrane proteins that modulate cell membrane potential and excitability. Potassium channels are responsible for various neurological, cardiovascular, and other physiological processes. According to the International Union of Basic and Clinical Pharmacology (IUPHAR) criteria, potassium channels can be divided into four superfamilies, including voltage-gated potassium channels (K_v) [1], calcium-activated potassium channels (K_{Ca}) [2], inwardly rectifying potassium channels (K_{ir}) [3], and two-pore domain potassium channels (K_{2P}) [4].

The structures for the four potassium channel superfamilies are distinct. K_v and K_{Ca} channel families often possess six transmembrane domains (6-TM) and could be further subdivided into several conserved gene families. K_v channels are composed of *K_v1*, *K_v2*, *K_v3* and *K_v4* subunits that corresponding to four genes named *Shaker*, *Shab*, *Shaw*, and *Shal*, respectively, the silent K_v5, K_v6, K_v8, K_v9 subunits, namely KCNQ channels (K_v7), as well as the eag-like (K_v10–K_v12) subunits [5], while K_{Ca} channels are designated into BK_{Ca}, IK_{Ca}, and SK_{Ca} subfamilies [2]. K_{ir} channels contain four transmembrane regions (4-TM) that possess the property of inward rectification, which was evoked by hyperpolarizations from the potassium equilibrium potential and was responsible for the membrane potential and the potassium ion transportation across membranes [3]. The K_{2P} channel family is structurally distinct in which each subunit contains two pore-forming domains and four transmembrane segments. K_{2P} channels could be modulated by many physiological and chemical factors, and play a crucial role in setting the resting membrane potential and regulating cell excitability [4].

Among the four superfamilies potassium channels, voltage-gated potassium channels (K_v) expressed in both excitable cells and nonexcitable cells play key roles in the maintenance of cell action potential in cardiac myocytes. They are

usually closed at the resting potential of the cell, and opened on membrane depolarization, and are involved in the repolarization of the action potential and thus the electrical excitability of cardiac myocytes.

2 Biological Characterization of Potassium Channel Subtypes That Involved in Arrhythmic Diseases

The first crystallographic data of potassium channels was resolved on bacterial *KcsA* channel reported by R. MacKinnon who was honored for Nobel Prize in the year 2005 [6]. After that, the three-dimensional structures of calcium-activated potassium channel *MthK* [7], inwardly rectifying potassium channels $K_{ir}Bac$ [8], and voltage-gated potassium channels K_vAP [9] and $K_v1.2$ [10] have been reported.

To our knowledge, K_v1 (*shaker*) family channels have been extensively studied for their biological characteristics and electrophysiological features since they could be easily expressed in tool cells such as Chinese Hamster Ovary (CHO) or Human Embryonic Kidney (HEK). Taking $K_v1.2$ potassium channel as an example, mammalian K_v channels could be divided into three parts: extracellular region, membrane region, and cytoplasm region. In the extracellular and membrane region, K_v channels are assembled by the interactions of four identical or distinct α-subunits, which constituted to the pore forming of the channel. The cytoplasm region contains an auxiliary β-subunit that modified the functions of the pore-forming α-subunits as well as the T_1 auxiliary region, SH_3 binding domain, ball peptide, and other functional domain [11]. In *shaker* family K_v channel, one α subunit contains three parts. The core region is constituted of six transmembrane domains (6-TM) that coded by S1 to S6 in which S4 helix possess positive charges that is related to the gating actions. The other two parts is the N terminus and the C terminus. Among the 6-TM, the pore-forming region (P-region) located between S5 and S6 helix possesses a specific selectivity filter amino acid sequence (TVGYG) to form the potassium ion permeation pathway. Recently, the common structural features for the P-region in the *shaker* family K_v channels were summarized: First, the selectivity filter of the channel protein on the extracellular side of the pore is relatively conserved, while the inner pore between the selectivity filter and intracellular solution varies in its conformation [6, 9, 10, 12–14]; Besides, a highly conserved Pro-X-Pro triplet peptide sequence acts as the determinate factor for gating in *shaker* family K_v channels [15, 16]. It was concluded that the structural conservation of the selectivity filter underlies the conserved mechanism of selective ion conduction in potassium channels, while the variation of the inner pore structure relies on conformational changes between open- and close-state illustrates the structural diversities of potassium channels blockers (Fig. 1).

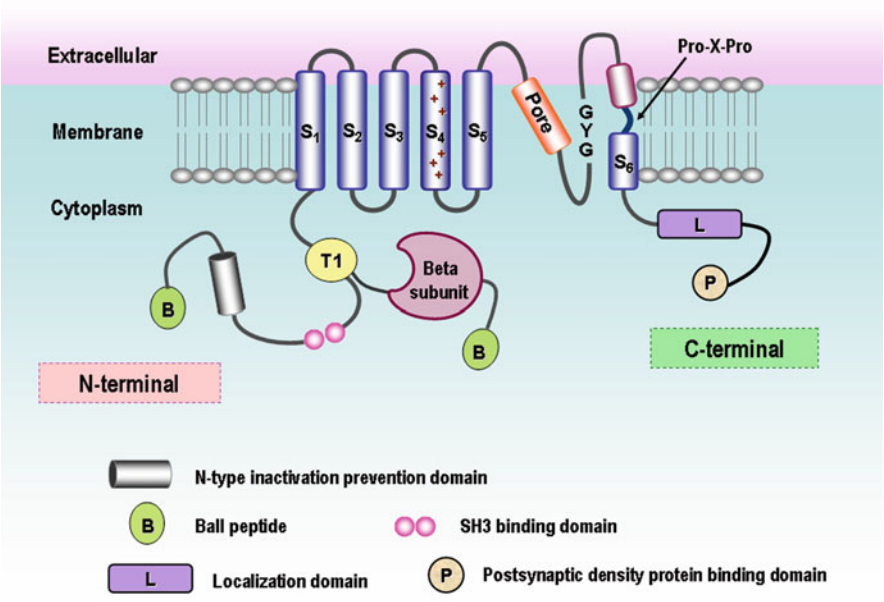

Fig. 1 Schematic illustration of *Shake* family K_v channels

3 The Chemical Structures and Structure–Activity Relationships (SARs) of Potassium Channel Blockers

3.1 Typical I_{Kr} (K_v11.1) *Blockers*

Ever since Quinidine was isolated from *Cinchona* bark and subsequently identified as effective agent for cardiac arrhythmia in the beginning of the twentieth century, antiarrhythmic drugs have been developed for over a hundred years. According to the Vaughan–William Scheme [17], potassium channel blockers belong to Class III antiarrhythmic agents, which mainly blocked the rapid delayed rectifier potassium channel currents (I_{Kr}, encoded by $K_v11.1$ gene which is usually called *h*ERG) [5, 18]. The electrophysiological properties of typical potassium channel blockers such as Propafenone [19], Flecainide [20], Sotalol [21], Dofetilide, and Ibutilide [22] are the prolongation of action potential duration (APD) and effective refractory period (ERP). However, the blockade of I_{Kr} would produce negative feedback on the ventricular repolarizations, which is widely considered as a critical risk factor of torsades de pointes (TdP) [23]. Therefore, clinical applications of typical Class III antiarrhythmic agents have decreased over the past decade because of its side effects called "proarrhythmia," which created more serious rhythm disorders than being treated.

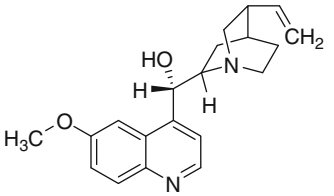

Quinidine

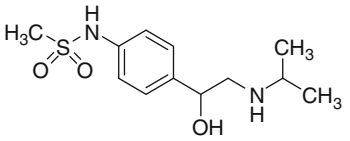

Sotalol

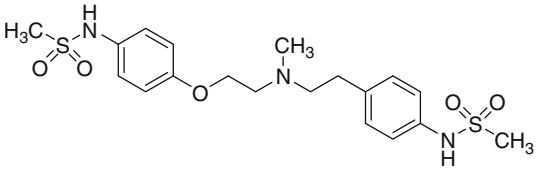

Dofetilide

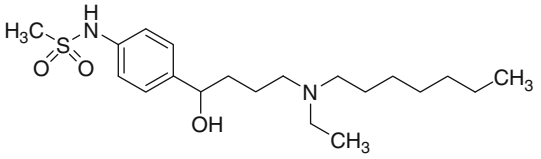

Ibutilide

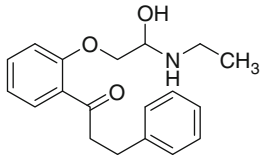

Propafenone

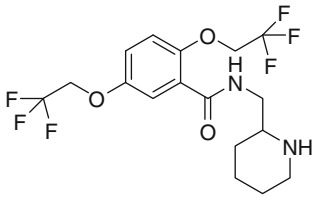

Flecainide

3.2 Multiple Ion Channel Blockers

During recent years, some multimechanism blockers were also applied in clinical treatment of arrhythmic diseases. The overall efficacy of these agents on several electronic current in cardiac myocytes may expand their therapy spectrum, although some detailed mechanisms are still controversial.

Amiodarone is approved by the Food and Drug Administration for the treatment of lethal ventricular arrhythmias but not for the management of atrial diseases.

Nonetheless, it is widely prescribed for this indication, although its severe side effects on thyroid should not be ignored. Dronedarone, a benzofuran derivative of Amiodarone [24], maintained the multiple electrophysiological properties of Amiodarone with reduced lipophilic and toxicity features. In the "Dronedarone Atrial Fibrillation study after Electrical Cardioversion" study, 270 AF patients were provided dronedarone daily (800, 1,200 or 1,600 mg) versus placebo, but the significant prolongation of the time to recurrent AF was only observed in 800 mg group [25]. The failure to see the dose-dependent phenomena might be related to the unwanted gastrointestinal effects at high dosage. However, the spontaneous to sinus rhythm was 5.8%, 8.2%, and 14.8% in the 800 mg, 1,200 mg, and 1,600 mg groups, while 3.1% for placebo, which showed a dose-effect correlation. Dronedarone is now marketed in the USA, Europe, and Canada, providing a safer, better tolerable modification to Amiodarone for the treatment of atrial disorders.

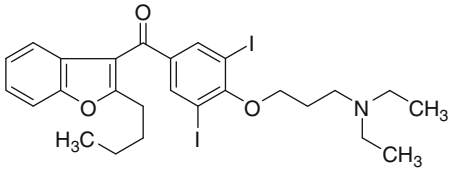

Amiodarone

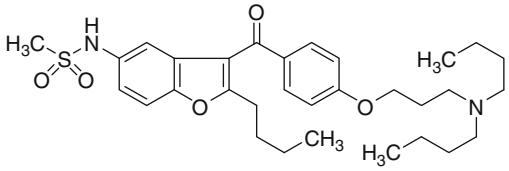

Dronedarone

3.3 K_v1.5 *Potassium Channel Blockers*

Current treatment of atrial diseases with Class III antiarrhythmic agents by blocking I_{Kr} in order to prolong the atrial effective refractory period (AERP) is often associated with ventricular proarrhythmia because of the excessive prolongation of ventricular effective refractory period (VERP) and action potential duration (APD). Therefore, atrial selective strategies were developed. Among *shaker* family K_v channels, cardiac $K_v1.5$ channel which is the molecular basis for the human cardiac ultrarapid delayed rectifier potassium current (I_{Kur}) has attracted much attention. Although $K_v1.5$ gene is also expressed at both mRNA and protein levels in human ventricle, its functional activities seem to be specific to the atrium, and the I_{Kur} currents have not yet been recorded in the human ventricle [26, 27]. Therefore, blockade of I_{Kur} may produce an atrial-selective increase in Phase I

repolarization and refractoriness [26, 28], which represents a promising approach to treat atrial disorders [29–31].

In 1993, Nattel reported the in vitro prolongation of APD in atrial myocytes by 50 μM of 4-Aminopyridine (4-AP) [26], which was then verified by follow-up electrophysiological and computational experiments [32–35]. During recent years, several pharmaceutical companies, including Icagen, Aventis, Merck, Eli Lilly, Procter & Gamble (P&G), and Bristol–Meyers Squibb (BMS), have focused on developing new structural types of $K_v1.5$ blockers [36, 37]. Many different types of $K_v1.5$ blockers have been designed and synthesized, and some of them are in clinical trials.

3.3.1 ICA-32 and Analogues

ICA-32 (**1**, $IC_{50} = 0.14$ μM) was designed and synthesized by Icagen without any pharmacological data published so far [38]. The framework of **1** contains a core heterocyclic ring as well as the upper and lower ring, which were connected by two flexible chain. Based on the structural analysis of **1**, researchers in P&G laboratories reported several series of analogues (Fig. 2), including thiazolidine-based derivatives [39], triazol derivatives [40], tetrazole derivatives [41], and 2-amino-2-imidazolidinone derivatives [42].

Thiazolidinone-Based Derivatives

In order to determine the contribution of vicinally substituted heterocycles in ICA-32 framework, Jackson et al. started from the thiazolidinone scaffold with two key structural modifications: (1) ketone instead of aldehyde-derived thiazolidinones and (2) incorporation of the carbonyl group rather than the

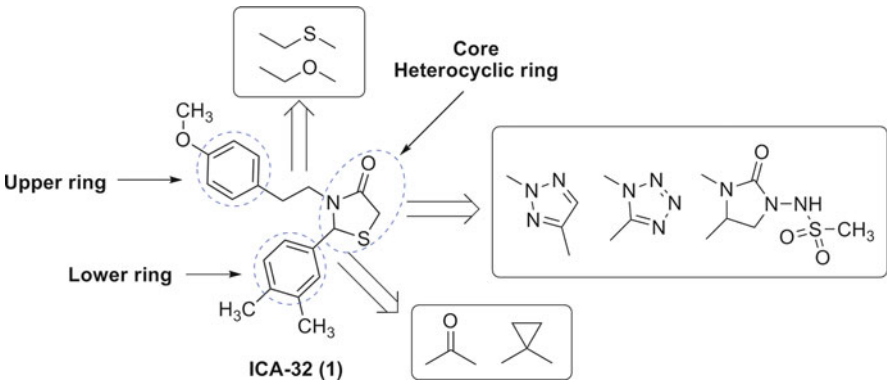

Fig. 2 Modification strategy towards ICA-32 (**1**)

heterocyclic ring in the linker to form acylthiazolidines. Compound **2** (IC_{50} = 0.09 μM) was obtained through replacing "–CH_2–" with "–O–" in the linker between core heterocyclic ring and the upper ring with the rationale of "me-too" strategy. However, these thiazoline compounds were rapidly metabolized. No parent compound remained after 30 min incubation with rat S9 microsomal fraction because of the oxidation of the sulfur atom in the heterocyclic ring [39].

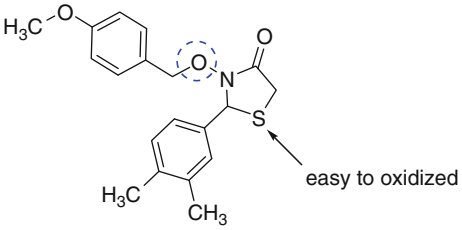

2

Triazol Derivatives

Based on the above results, 2,4-disubstituted-1,2,3-triazoles were synthesized to avoid the rapid metabolism induced by sulfur atom oxidation [40]. Among these compounds, compound **3** (IC_{50} = 0.29 μM) with ketone linker between heterocylic ring and lower ring was selected for further investigation. In the whole cell patch clamp experimentation, significantly decreased potency was observed at *h*ERG channel, $K_v1.3$ channel, and the L-type calcium channel. Moreover, 15 min infusion at a dose of 30 mg/kg in an anesthetized pig model resulted in an increase of 12% in the AERP, while the VERP remained unchanged.

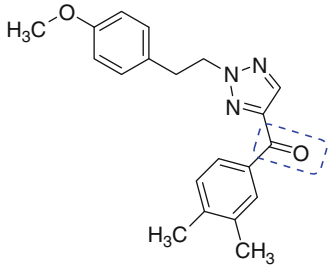

3

Tetrazole Derivatives

Except for triazol compounds, Wu described a replacement of the thiazolidinone scaffold of ICA-32 with a tetrazole framework [41]. Compound **4** containing

the cyclopropyl ring at the linker of the "lower" aromatic ring displayed potent in vitro blockade potency against $K_v1.5$ ($IC_{50} = 0.33$ μM) as well as atrial-selective prolongation of AERP in vivo. Besides, it lacked hemodynamic side effects.

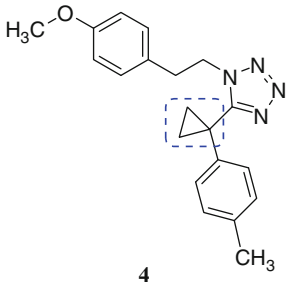

4

2-Amino-2-Imidazolidinone Derivatives

Recently, Blass et al. reported a series of 2-amino-2-imidazolidinone compounds to prevent the relative disposition of the aryl rings [42], the patents were also announced [43–45]. Among this series of compounds, KVI-020 (**5**) showed suitable physiochemical properties and was well tolerated in liver microsomal stability, caco-2 permeability and protein binding tests. Further in vivo evaluation showed that its pharmacokinetic and pharmaceutical properties were acceptable for late-stage preclinical development.

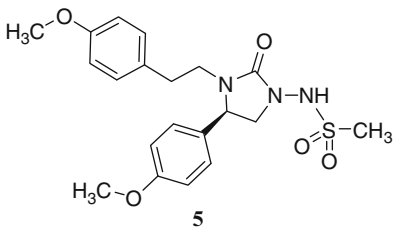

5

In brief, the core heterocyclic ring thiazolidinone of ICA-32 could be extended by its bioisosters including triazol, tetrazole, and imidazolidinone. However, the inadequate additions of hetero atom in the rings or linkers lead to the undesired metabolic and pharmacokinetic features, which hindered the future development of ICA-32 analogues. Till now only 2-amino-2-imidazolidinones is in development.

3.3.2 Tetrahydroindolone Derivatives

Considering the unacceptable pharmacokinetic profile of ICA-32 analogues, Wu and collaborators in P&G research laboratories developed another type

of $K_v1.5$ blockers based on tetrahydroindolone framework. However, only a few compounds showed inhibitory effects against $K_v1.5$. The in vivo assay of tetrahydroindolone-derived semicarbazones **6** ($IC_{50} = 0.13$ μM) showed an increase in right AERP by 18% at a dose of 30 mg/kg without increase in VERP [46]. To broaden the diversity of tetrahydroindolone-derived compounds, Fluxe et al. prepared isosteric tetrahydroindolone-derived carbamates. The most potent analogues, compound **7** ($IC_{50} = 0.07$ μM) showed over 450-fold selectivity against L-type calcium channel and *h*ERG channel ($IC_{50} > 30$ μM), in the meanwhile the interestingly low activities against calcium and *h*ERG channels were also consistent throughout the class [47].

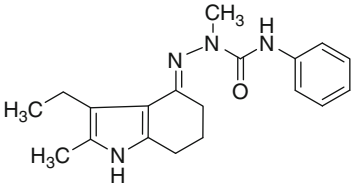

6

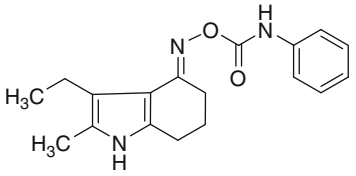

7

3.3.3 Aryl Sulfonamido Indane Derivatives

Aryl Sulfonamido Indanes and Tetrahydronaphthyls

Icagen and BMS reported a collection of aryl sulfonamido indanes and tetrahydronaphthyls with different amido region-isomers to determine the $K_v1.5$ pharmacophore [48–52]. It was reported that the (*1R*, *2R*) conformation of compound **8** has a selectively high IC_{50} of 0.03 μM against $K_v1.5$ with high selectivity over *h*ERG (inhibitory ratio: 37% at 10 μM), while the $K_v1.5$ inhibitory IC_{50} value of (*1S*, *2S*) conformation was only 0.76 μM. Aryl sulfonamido tetrahydronaphthyl compound **9** ($IC_{50} = 0.44$ μM) also showed good inhibitory effect against $K_v1.5$ channel. The modification of tetrahydronaphthyl scaffold lead to compound **10** ($IC_{50} = 0.20$ μM) and **11** ($IC_{50} = 0.24$ μM), which underlies the replaceable of rigid ring scaffold. However, the clinical trials of these compounds were suspended due to the poor aqueous solubility and low oral bioavailability. In this series, the chiral sulfonamide side chain was introduced, suggesting an asymmetry feature of

hydrogen bond acceptor in the binding site. On the contrary, they could provide evidences for the specification of the pharmacophore profiles.

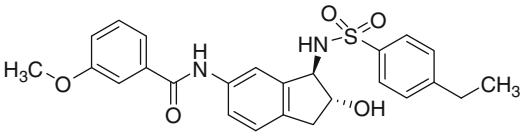

8

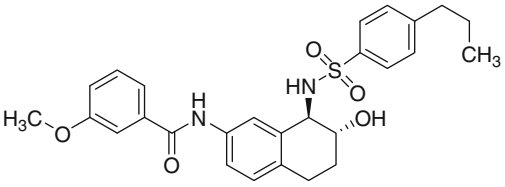

9

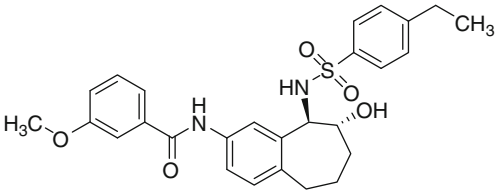

10

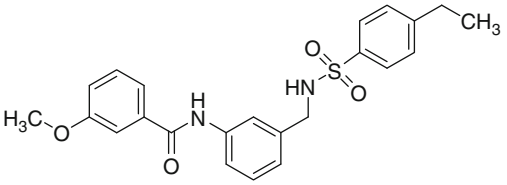

11

Benzopyran Sulfonamides

Considering that indane could be replaced by benzopyran, Lloyd and his co-workers suggested the benzopyran core as an acceptable scaffold for potent $K_v1.5$ blockers (compound **12**, $IC_{50} = 0.11$ μM). They explored different substituent in this scaffold, such as the amide at the 6-position of benzopyrane, the substituent on the phenyl ring of the phenyl sulfonamide, and modifications of the amino alcohol template, to discover several compounds with good potency of

$K_v1.5$ blocking and good selectivity over *h*ERG. The further modifications of the benzopyran derivatives are still ongoing [53].

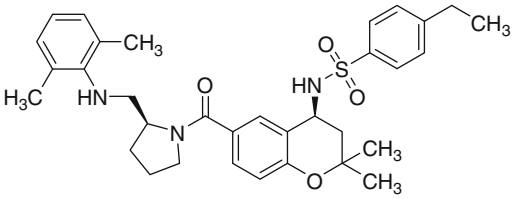

12

NIP-142 (**13**), a novel benzopyran derivative developed by Nissan, was able to moderately block $hK_v1.5$ current ($IC_{50} = 4.75$ μM) in a frequency-independent and dose-dependent manner [54]. Electrophysiological evaluation showed that NIP-142 decreased phase I notch and increased the height of phase II plateau without making any changes in APD [55]. Furthermore, NIP-142 could prolong AERP and APD through blockade of I_{KACh} [56]. Briefly, NIP-142 has distinct pharmacological properties from other classical antiarrhythmic agents, the overall biological features may possibly contribute to its antiarrhythmic profiles as a promising agent for the treatment of supraventricular arrhythmia [57].

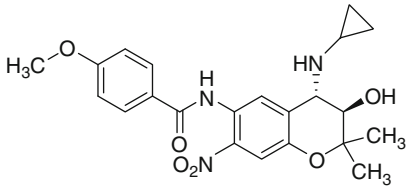

NIP-142 **(13)**

Pyrano-[2,3*b*]-Pyridines

Based on the above results, Finlay reported a series of pyrano-[2,3*b*]-pyridine compounds. However, the SARs of these compounds are differed from benzopyran series, and the activities of pyrano-[2,3*b*]-pyridines are generally lower than benzopyran compounds due to the introduction of polar groups. Among these compounds, only **14** ($IC_{50} = 0.39$ μM) showed moderate inhibitory effect against $K_v1.5$ channel [58].

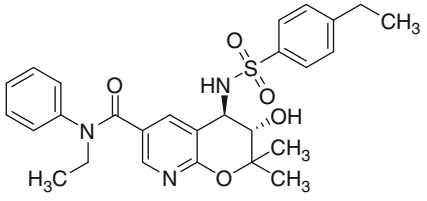

14

3.3.4 Quinoline or Isoquinoline Derivatives

In 2005, Merck laboratories announced the patents of the quinoline and isoquinoline derivatives (compounds **15** to **20**) as $K_v1.5$ blockers [59–67]. ISQ-1 (**15**), obtained by high-throughout screening approaches, was considered as lead compound [68]. The replacement of the dimethylaminomethyl moiety of ISQ-1 with a cyano group could neutralize the alkalinity of amine and increase its selectivity over *h*ERG potassium channel (**21**, $IC_{50} = 0.07$ μM). Then the optimization was continued to discover the ethanol amide compound **22**, an improved potent $K_v1.5$ blocker ($IC_{50} = 0.06$ μM) with excellent selectivity over *h*ERG (over 500-folds) and good pharmacokinetic properties (clearance 12 mL/min/kg; V_d 0.8 L/kg; oral bioavailability 21%). When being evaluated in an in vivo canine electrophysiological model in which I_{Kur} current is prominent in atrial repolarization [69], compound **22** ($IC_{50} = 0.06$ μM) exhibited atrial refractory period (ARP) prolongation without concomitant ventricular refractory period (VRP) prolongation. In consistent with these evidences, injection of compound **22** to anesthetized dogs leads to selective prolongation of AERP without side effect on VERP at any dose. Therefore, the reasonable combination of pharmacokinetic properties and in vivo effects solidified compound **22** as a promising atrial-selective agent for further investigation.

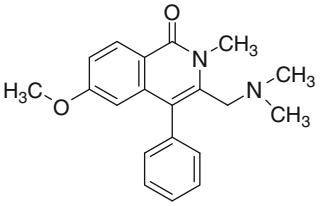

ISQ-1(**15**)

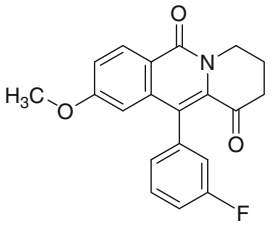

16

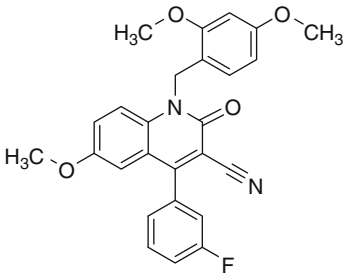

17

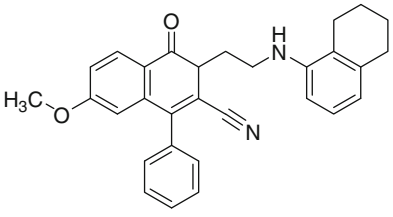

18

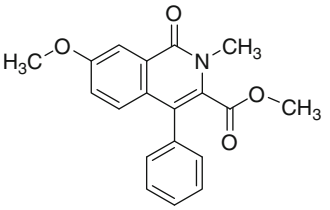

19

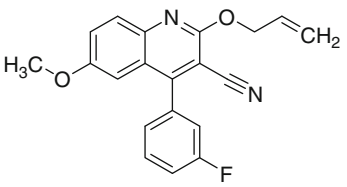

20

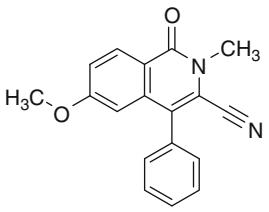

21

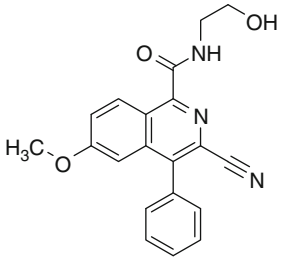

22

3.3.5 1, 1′-Disubstituted Biphenyl Compounds

Earlier in this century, Aventis started the rational design studies of selective $K_v1.5$ blockers. After analyzing the structural feature of reported $K_v1.5$ blockers including the above-mentioned aryl sulfonamido indanes and tetrahydronaphthyls, benzopyrans, thiazolidines, and quinolines, they concluded that the key structure features for effective $K_v1.5$ blocker were two to three appropriate hydrophobic points and flexible linkers between them. Then Peukert and collaborators launched the 2D similarity search using aryl sulfonamido indanes as template to obtain a 1,8-disubstituted naphthalene scaffold (**23**, $IC_{50} = 4.8$ μM). After chemical modification by replacing the framework with biphenyls, potent compounds AVE0118 (**24**, $IC_{50} = 1.1$ μM), S9947 (**25**, $IC_{50} = 0.4$ μM), S20951 (**26**, $IC_{50} = 1.2$ μM), and other analogues were obtained for further investigation. The SAR analysis of this kind of $K_v1.5$ blockers showed some interesting results: first, the introduction of pyridyl group in the side chains obtained higher activity than that of the phenyl ring, aliphatic amine or hydrophobic chains (**27**–**29**, $IC_{50} = 1.2$ μM, 2.2 μM, 3.3 μM, respectively); on the contrary, the substitution of amide group with sulfamide group that generally existed in the antiarrhythmic agents had slight influence on the inhibitory effect (**30**, $IC_{50} = 2.6$ μM) [70, 71].

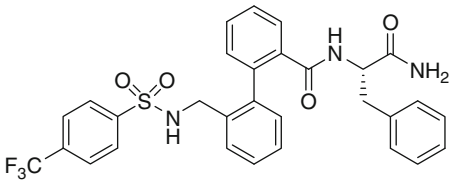

23

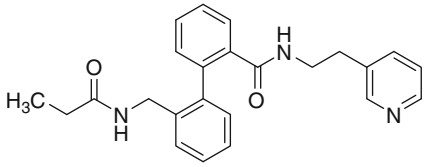

AVE-0118 **(24)**

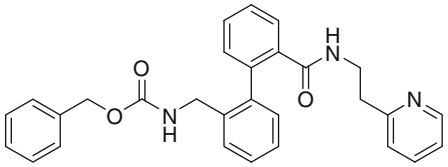

S9947 **(25)**

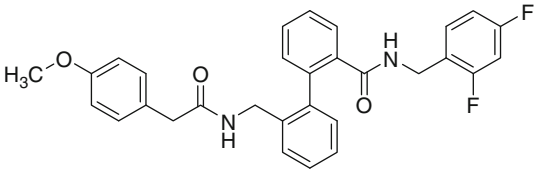

S20951 **(26)**

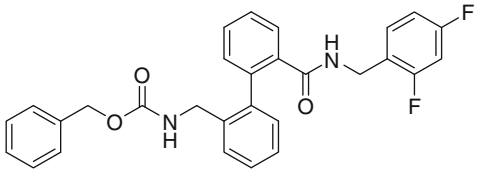

(27)

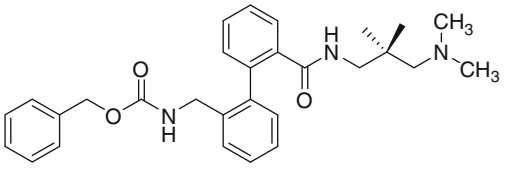

28

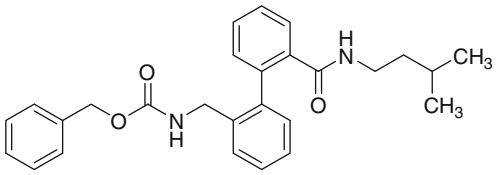

29

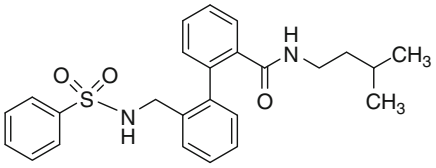

30

Among these series $K_v1.5$ blockers, AVE0118 (**24**) was able to decrease the steady-state $hK_v1.5$ current and prolong APD to enhance atrial contractility [72, 73]. Besides it can also prolong the atrial effective refractory period (AERP) in anesthetized pigs and conscious goats without any change on the QT interval of the ECG and any possibility of inducing TdP [74–76]. Recently, the micropuncture studies of atrial human tissues in chronic AF patients exhibited that AVE0118 could increase the plateau potential and prolong the APD by 20 ms at a concentration of 6 μM [77].

Another interesting compound, S9947 (**25**), could block the cloned human $K_v1.5$ channel current expressed in *Xenopus oocytes* and CHO cells with IC_{50} values of 0.6 μM and 0.4 μM, respectively [78]. Moreover, at a concentration of 3 μM, S9947 is served as sodium channel inhibitor since no influence on the upstroke of the action potential was observed [79]. S9947 could also prolonged rat ventricular action potential at both slow- and fast-pacing rates without any influence on *h*ERG channels. Being considered as multiple ion channel blockers, S9947 and S20951 (**26**) are thought to be prior to current available class III antiarrhythmic agents as their maximal APD prolongation at slow rates and minimal effects during tachycardia. Therefore, this series of blockers might have a superior antiarrhythmic profile in human atrial cells and could bear a promising strategy against AF [80].

3.3.6 Anthranilic Amide Derivatives

Researchers in Aventis established a three-hydrophobic-point pharmacophore model (Fig. 3) based on the biphenyl compounds **31** (IC_{50} = 0.2 μM) and **32** (IC_{50} = 2.8 μM). After 3D similarity search on Aventis in-house compound collection, Peukert et al. reported a new series of anthranilic amides as $K_v1.5$ blockers (**33**) [81]. The discovery of compound **33** (IC_{50} = 5.6 μM) was recognized as the application of an innovative scaffold hopping strategy [82] based on the

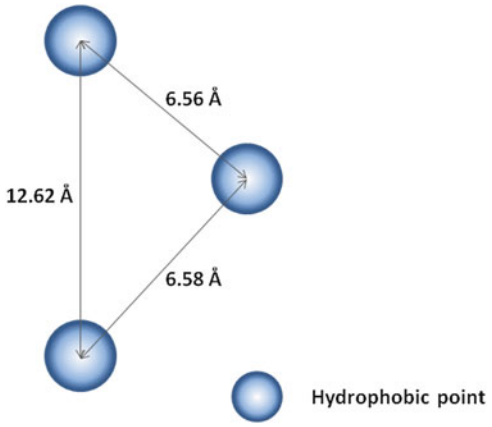

Fig. 3 A three hydrophobic point pharmacophore model for $K_v1.5$ blockers

pharmacophore model and biphenyl derivatives: the central phenyl moiety of compound **33** matches the middle hydrophobic center, and both ends of the side chains correspond to the remaining hydrophobic centers of the model.

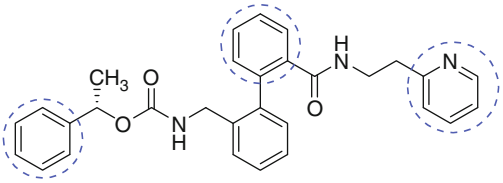

31

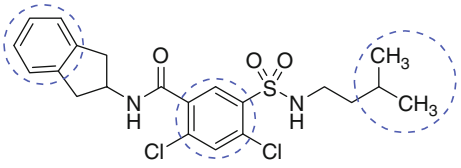

32

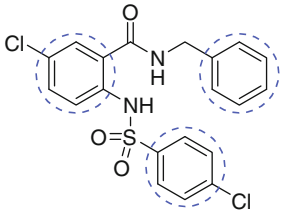

33

After the SAR analysis of different amide or sulfamide substitute groups, it was found that the blockade effects would be influenced by the steric and electrostatic effects of these substitutes [83]. The correlation between the inhibitory activities and the pK_a was observed. The p*K*a value decreased from 7.5 of compound **34** to 6.2 of compound **35** (1.21-fold), accompanied by the IC_{50} decreasing from 0.5 to 4 μM (eightfold). Otherwise, replacement of the acidic hydrogen by a methyl group (**36,** IC_{50} = 10 μM) resulted in further reduction of activity. These results suggest that the hydrogen might be involved in an intramolecular hydrogen bond with the carbonyl oxygen, which stabilizes a favorable active conformation. The replacement of methyl group of **36** to pyridine group lead to a potent $K_v1.5$ blockers S-0100176 (**37,** IC_{50} = 0.7 μM).

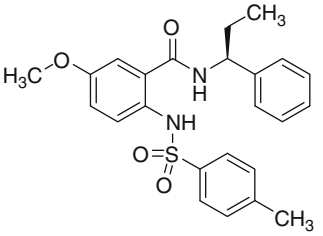

34

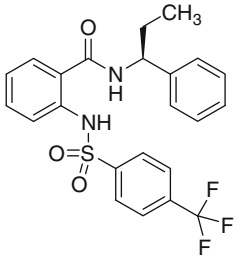

35

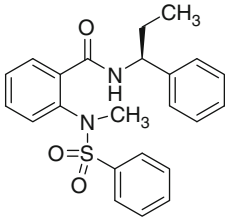

36

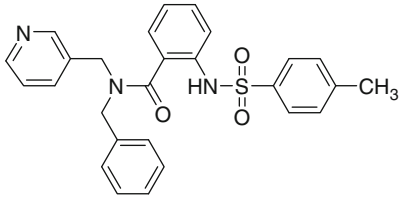

S-0100176 **(37)**

Based on the above results, Rezazadeh et al. reported a new $K_v1.5$ blockers, KN-93 (**38**, IC_{50} = 0.3 μM), which showed multiion channel blockade effect, including $K_v1.2$, $K_v1.4$, $K_v2.1$, $K_v3.2$, and $K_v4.2$, and also an inhibitor of Ca^{2+}/calmodulin-dependent protein kinase II (CAMK-II) [84].

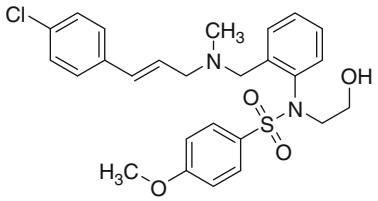

KN-93 **(38)**

3.3.7 Diisopropyl Amide Analogues

A novel type of blockers was discovered by Nanda et al. [85] through high-throughput screening of the Merck sample collection [85–88]. The lead compound **39** ($IC_{50} = 0.25$ μM) with a main functional group of *N*,*N*-diisopropyl amide was structurally distinct from recent disclosed cardiac channel antagonists. Based on the successful case in the structural modification from AVE0118 (**24**) to S9947 (**25**), the optimization strategy was focused on the two aryl rings. It was interesting that the replacement of either of the phenyl rings with a 3-pyridyl ring was well tolerated, but due to the different electrostatic interactions, incorporation of other pyridine isomers resulted in a significant decrease in potency. Compounds containing two pyridine rings, including those with retained single 3-pyridyl ring, would lose potency when compared with the 3-pyridyl and phenyl analogues. Substitute effects were also briefly investigated: the 3-bromophenyl or 4-cyanophenyl analogues exhibited better potency than the parent phenyls but the 2-cyano substitute group was not well tolerated.

The replacement of ester group in compound **39** by 2-fluorobenzyl urea leads to compound **40** ($IC_{50} = 0.15$ μM), which demonstrated the best potency against $K_v1.5$ at IC_{50} of 150 nM. This single active enantiomer was used for all further evaluation. No changes at any doses in VRP or QT interval in animal tests suggested a selective atrial effect of **40**. Moreover, compound **40** is also a P-glycoprotein (Pgp) substrate with low potential for central nervous system (CNS) exposure.

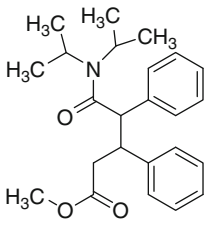

39 ($IC_{50} = 0.25$ μM)

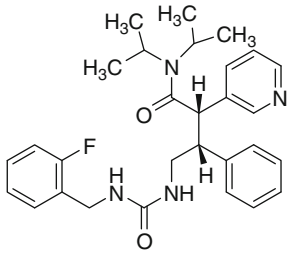

40 ($IC_{50} = 0.15$ μM)

3.3.8 Triarylethanolamine Derivatives

Recently, Beshore et al. in Merck laboratory reported triarylethanolamine analogue with enhanced positive ionizability to intervene π–cation interactions by introducing pyridinyl groups. Among these compounds, the most potent compound **41** (TAEA) reached an IC_{50} of 0.28 μM. However, further development was suspended due to CNS side effects [89].

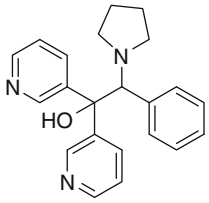

TAEA **(41)**

3.3.9 Pyrazolodihydropyrimidine Derivatives

In view of that, the L-type calcium antagonist Nifedipine was a weak blocker of $K_v1.5$ current, Vaccaro and co-workers developed a series of dihydropyrazolopyrimidine blockers [90]. The lead compound **42** showed moderate $K_v1.5$ blockade effect (IC_{50} = 1.1 μM) and L-type calcium channel inhibitory effect (IC_{50} = 6.1 μM). Compound **43** (IC_{50} = 0.16 μM) with piperazine group instead of ester group showed more potent inhibitory effect. Further modification showed that dihydropyrazolopyrimidines with a C_6 heterocycle substituent possessed high potency. The introduction of benzimidazole ring and the substituent in the 5-position of the dihydropyrazolopyrimidine ring produced **44** with an IC_{50} of 0.03 μM without significant blockade of other cardiac ion channels [91]. Then Lloyd et al. developed pyrrolidine amides of pyrazolodihydropyrimidine compound BMS34136 (**45**), which was chosen for further in vitro and in vivo evaluation [92].

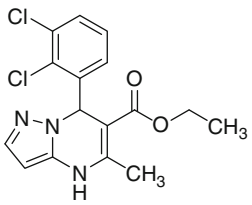

42

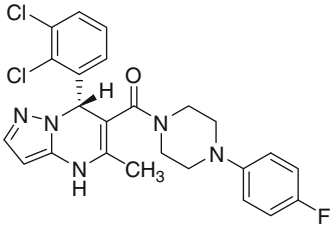

43

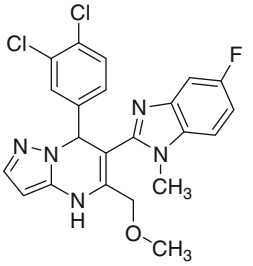

44

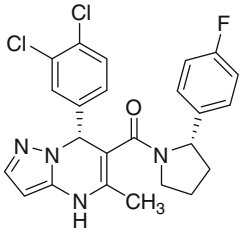

BMS34136 **(45)**

3.3.10 Common Structural Features for $K_v1.5$ Channel Blockers

For the molecular simulation of protein–ligand interaction, a commonly used method is to define three-dimensional arrangement of the structural and physicochemical features that are relevant to biological activity, or so-called pharmacophore identification. In the case of $K_v1.5$ blockers, prior reports had depicted a three-hydrophobic-pharmacophore model [71, 81]. However, the classic scaffold was not matched with novel blockers and was not in accordance with the development of binding mode analysis. The up-to-date four-center pharmacophore mapping for $K_v1.5$ blockers, including one aromatic ring, two hydrophobic points, and a hydrogen-bond acceptor, was derived from forty compounds with distinct structure types of $K_v1.5$ blockers (Fig. 4). This recognition model, together with the

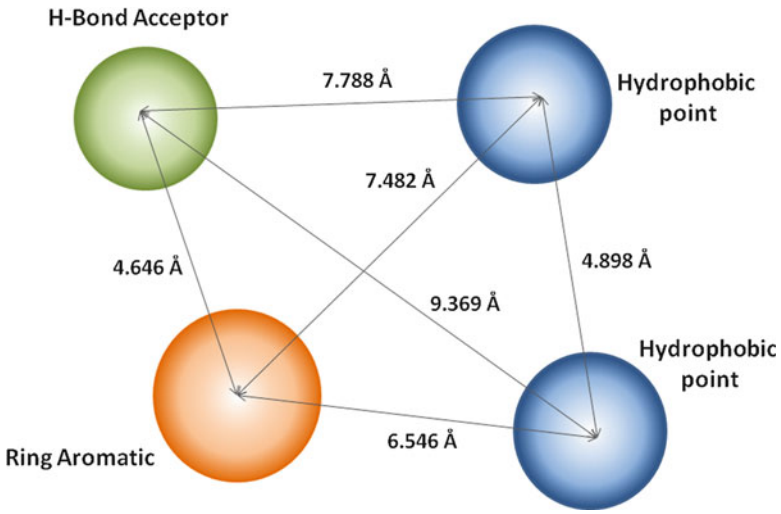

Fig. 4 Recently reported four point pharmacophore model for $K_v1.5$ blockers

postulated homology model for $K_v1.5$ potassium channel, will be used to guide designing new blockers with pre-determined blocking activity and selectivity [93].

3.4 *Other* $K_v1.5$ *Blockers in Clinical Trials*

3.4.1 Vernakalant (RSD-1235)

Vernakalant, a mixed sodium and potassium channel blockers [94, 95], is an atrial-selective antiarrhythmic drug developed by Cardiome Pharma and Astellas Pharma [96–98]. As simple three-hydrophobic-point $K_v1.5$ blockers, Vernakalant also shared similar framework with ICA-32 (**1**) but with better pharmacokinetic profiles. In this case, its stronger alkalinity triggers more interests for medicinal chemists. The phase I trial for controlled-release oral formulation of Vernakalant has been successfully completed in 2005. An oral formulation was then developed in phase II clinical phase as a chronic-use product for the maintenance of normal heart rhythm following the termination of AF symptom. This oral controlled-release formulation of Vernakalant was expected to help prevent or slow down the recurrence of Atrial Fibrillation (AF), and would be used as a follow-on therapy to intravenous Vernakalant. The safety and efficacy of intravenous Vernakalant in phase III study in approximately 120 AF patients from 30 centers in the USA, Canada and Europe [99] was carried out since 2005 and now Vernakalant is in pre-registration phase in American Food and Drug Administration (FDA).

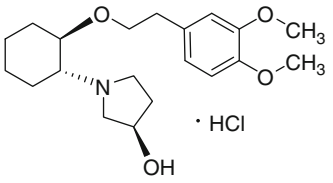

Vernakalant

3.4.2 AZD7009

AZD7009, developed by AstraZeneca, was highly potent in terminating atrial fibrillation and flutter in anesthetized dog model [100]. AZD7009 blocked both *h*ERG channel current ($IC_{50} = 0.6$ μM) and $hNa_v1.5$ channel current ($IC_{50} = 4.3$ μM). Persson et al. proposed that the combined current blockade underlies the prolongation of the refractoriness and the low proarrhythmic activity in vivo [101]. In the dilated rabbit atria, AZD7009 could increase AERP in a concentration dependent manner associated with effectively prevent AF induction and rapidly restore sinus rhythm [102]. In all, AZD7009 exhibited dose-dependent effects

in converting AF to sinus rhythm (SR) in AF patients with a lower risk of pro-arrhythmia [103].

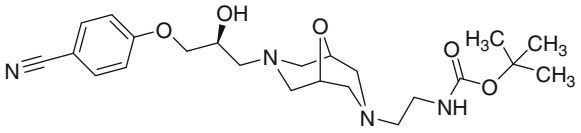

AZD7009

3.4.3 Azimilide

Azimilide is a novel class III antiarrhythmic agent, which is now in the pre-registration phase in FDA for arrhythmic disease. The prescription of Azimilide is still controversial. As I_{Kr}, I_{Ks} dual blockers, the I_{Ks} blockade effect may result in reduced TdP risk, however, the efficacy of Azimilide was inconsistent. The extensive testing of Azimilide in AF patients did not show any risk of increased mortality or morbidity, which might provide sense of comfort in prescribing it for high-risk patients [104]. But according to Pritchett's report in a large randomized clinical trials of post-infarct patients, Azimilide neither increased nor decreased mortality risk [105]. Otherwise, all the finished pharmacological evaluations did not demonstrate statistically significant efficacy in reducing the risk of arrhythmia recurrence in patients with heart disease, who suffered from atrial fibrillation and then converted to sinus rhythm [106].

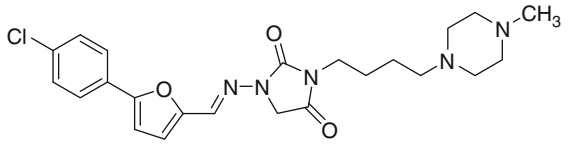

Azimilide

3.4.4 Tedisamil

Tedisamil is also a class III agent developed by Solvay Pharmaceuticals. It is now in pre-registration phase of AF therapy. As multiple potassium channels including I_{Kr}, I_{Ks}, I_{Kur}, I_{to}, and I_{KATP}, the agent could effectively terminate atrial fibrillation and flutter symptom, at 0.4 mg/kg and 0.6 mg/kg of intravenous tedisamil versus placebo, 41% and 51% conversion versus 7% with placebo were observed. However, QT prolongation and ventricular tachycardia were observed at high dose [107]. Accordingly, its utility for chronic treatment of AF might be limited by the combination of QT prolongation and sinus slowing that could result in TdP.

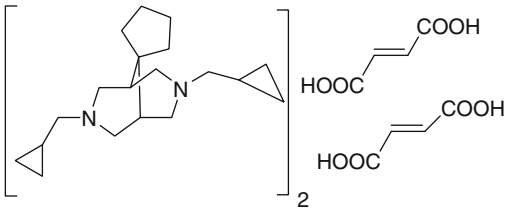

Tedisamil

4 Binding Mode Studies

Due to the absence of a determined 3D structure, researchers have to focus on the binding modes investigation of different blockers to the transmembrane region of $K_v1.5$ potassium channel by mutagenesis studies and computer modeling.

Through site-directed mutagenesis studies, the preliminary mode of ligand-$K_v1.5$ binding was disclosed. Multichannel blockers such as Quinidine, Bupivacaine and Benzocaine were located in a strong hydrophobic environment consisting of Thr507, Leu510 and Val514 of the S6 domain that lines the inner vestibule of the channel, and Thr479 near the selectivity filter, while Class I_a antiarrhythmic agent Disopyramide interacted with Val512 residue in the Pro-Val-Pro triplet amino acid region [108–110].

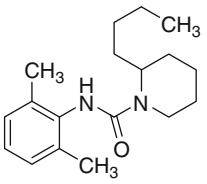

Bupivacaine

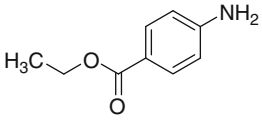

Benzocaine

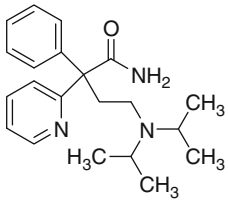

Disopyramide

Recently, selective $K_v1.5$ blockers such as S-0100176 (**37**) and AVE0118 (**24**) were employed in the mutagenesis studies as probes to explore the ligand–$K_v1.5$ interactions. It was concluded that residues including Thr479, Thr480, Val505, Ile508, and Val512 that faced the central cavity were involved in the interaction between **37** and $K_v1.5$ protein [111], whereas Thr479 and Thr480 in the selectivity filter, as well as Ile502, Val505, Ile508, Leu510, Val512, and Val516 in the S6 domain formed a hydrophobic network for **24** [112]. Compared with **37**, **24** was prone to contacting with the open-state channel and stretching its conformation to interact with critical hydrophobic Leu510, a residue predicted to face toward S6 helix and away from the central cavity to strengthen its binding ability, named "foot-in-the-door" phenomenon, while **37** was proposed to be trapped within the central cavity in the close state (Fig. 5).

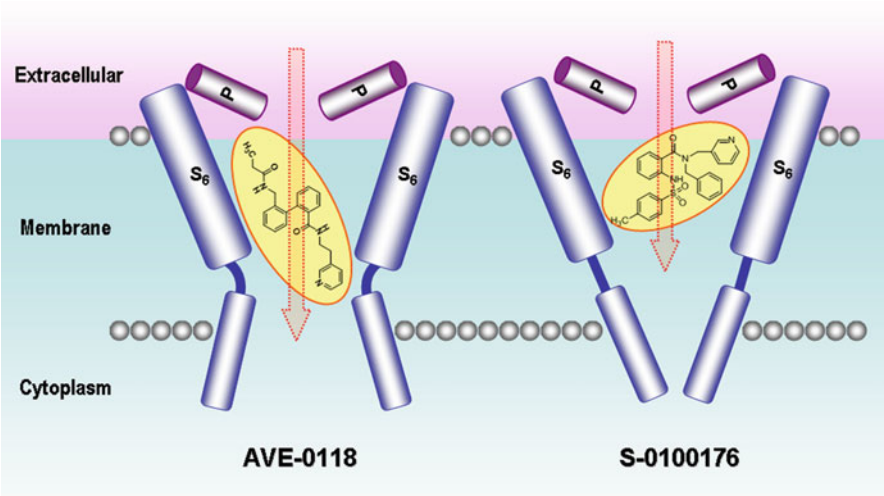

Fig. 5 The schematic binding mode of AVE0118 (**24**) and S-0100176 (**37**) with $K_v1.5$ channel

The prior computational work on $K_v1.5$ channel and ligands was carried out by Luzhkov et al. The homology model of $K_v1.5$ channel protein was built based on the crystal structure of KcsA potassium channel, which shared 54% sequence identity with $K_v1.5$ channel, even if KcsA lacks the highly conserved Pro-X-Pro motif in the S6 domain. S-0100176 (**37**) was used to validate the homology model. The docking results showed that the aromatic framework of **37** was located in a strong hydrophobic environment, where the pyridyl group faced downward to Ile508, the benzamide phenyl ring faced upward to Thr479 and Thr480, and the sulfonylamino moiety was close to Val505 while the toluene group was adjacent to Val512 [113].

Then Pirard and co-workers established a structure-based virtual screening protocol by using homology model of $K_v1.5$ potassium channel [114]. In addition, by using Catalyst program, a three-hydrophobic-point pharmacophore was established for the ligand-based virtual screening [71, 81]. The comparison was made and they concluded that structure-based strategy can be treated as complementary with the ligand-based virtual screening method because of a higher hit rate.

More recently, our research group developed $K_v1.5$ homology model based on the crystal structure of $K_v1.2$ potassium channel [10] since they shared 70% homology identity and highly conserved S5/H5/S6 domains. The validation of this homology model was carried out by the comparison of mutation data of S0100176 (**37**) and AVE0118 (**24**) reported by Decher et al. [111, 112] and KN-93 (**38**) reported by Fedida [84] through molecular docking. Further researches including the in silico prediction of $K_v1.5$ inhibitory effects and the design of selective agents for the treatment of atrial disorders are still ongoing [115].

5 Perspective

Most currently marketed drugs for cardiac arrhythmias are indiscriminate since that they all target ion channels especially *h*ERG channel in both atrial and ventricular myocytes, thus associated with life-threatening ventricular arrhythmias. For medicinal chemists, the molecular basis of the ligand–$K_v1.5$ channel interactions and its specific features should be deeply investigated when aiming at rational design of atrial-selective drugs.

$K_v1.5$ potassium channel is an interesting topic for medicinal chemists in recent years. Drug targeted cardiac $K_v1.5$ channels may have remarkably selectivity and safety advantages over current market drugs. Among the residues involved in ligand-$K_v1.5$ binding, Ile508 and Val512 are equivalent to Tyr652 and Phe656 of *h*ERG channel, thus underlie the possibility of hydrophobic interactions between blockers and $K_v1.5$ channel. Moreover, the physicochemical property difference between the hydrophobic residue Ile508 and Val512 of $K_v1.5$ channel and the aromatic Tyr652 and Phe656 of *h*ERG channel could provide an opportunity in differentiation of these two channels.

In conclusion, the rapid progress in physiology, pharmacology, biochemistry, genomics, and proteomics will significantly expedite the investigation of mechanism in cardiac diseases and the development of safe and effective drugs.

Acknowledgement The authors gratefully acknowledge financial support from the National Major Science and Technology Project of China (Innovation and Development of New Drugs, Grant No. 2008ZX09401-001 and 2009ZX09501-003), National 863 Program (Grant No.2007AA02Z307), and the Innovation Program for the Postgraduates in Jiangsu in 2007.

References

1. Nerbonne JM (1998) Regulation of voltage-gated K+ channel expression in the developing mammalian myocardium. J Neurobiol 37:37–59
2. Jensen BS, Strobaek D, Olesen SP et al (2001) The Ca^{2+}-activated K^+ channel of intermediate conductance: a molecular target for novel treatments? Curr Drug Targets 2:401–422
3. Minor DL Jr, Masseling SJ, Jan YN et al (1999) Transmembrane structure of an inwardly rectifying potassium channel. Cell 96:879–891
4. Ketchum KA, Joiner WJ, Sellers AJ et al (1995) A new family of outwardly rectifying potassium channel proteins with two pore domains in tandem. Nature 376:690–695
5. Warmke JW, Ganetzky B (1994) A family of potassium channel genes related to eag in Drosophila and mammals. Proc Natl Acad Sci USA 91:3438–3442
6. Roux B, MacKinnon R (1999) The cavity and pore helices in the KcsA K+ channel: electrostatic stabilization of monovalent cations. Science 285:100–102
7. Jiang Y, Lee A, Chen J et al (2002) Crystal structure and mechanism of a calcium-gated potassium channel. Nature 417:515–522
8. Kuo A, Gulbis JM, Antcliff JF et al (2003) Crystal structure of the potassium channel KirBac1.1 in the closed state. Science 300:1922–1926
9. Jiang Y, Lee A, Chen J et al (2003) X-ray structure of a voltage-dependent K+ channel. Nature 423:33–41

10. Long SB, Campbell EB, Mackinnon R (2005) Crystal structure of a mammalian voltage-dependent Shaker family K+ channel. Science 309:897–903
11. Yellen G (1998) The moving parts of voltage-gated ion channels. Q Rev Biophys 31:239–295
12. MacKinnon R (2004) Potassium channels and the atomic basis of selective ion conduction (Nobel Lecture). Angew Chem Int Ed Engl 43:4265–4277
13. Jiang Y, Lee A, Chen J et al (2002) The open pore conformation of potassium channels. Nature 417:523–526
14. Long SB, Campbell EB, Mackinnon R (2005) Voltage sensor of Kv1.2: structural basis of electromechanical coupling. Science 309:903–908
15. Hackos DH, Chang TH, Swartz KJ (2002) Scanning the intracellular S6 activation gate in the shaker K+ channel. J Gen Physiol 119:521–532
16. Lu Z, Klem AM, Ramu Y (2002) Coupling between voltage sensors and activation gate in voltage-gated K+ channels. J Gen Physiol 120:663–676
17. Hondeghem LM (2000) Classification of antiarrhythmic agents and the two laws of pharmacology. Cardiovasc Res 45:57–60
18. Sanguinetti MC, Jiang C, Curran ME et al (1995) A mechanistic link between an inherited and an acquired cardiac arrhythmia: HERG encodes the IKr potassium channel. Cell 81:299–307
19. Stroobandt R, Stiels B, Hoebrechts R (1997) Propafenone for conversion and prophylaxis of atrial fibrillation. Propafenone Atrial Fibrillation Trial Investigators. Am J Cardiol 79:418–423
20. Aliot E, Denjoy I (1996) Comparison of the safety and efficacy of flecainide versus propafenone in hospital out-patients with symptomatic paroxysmal atrial fibrillation/flutter. The Flecainide AF French Study Group. Am J Cardiol 77:66A–71A
21. Naccarelli GV, Wolbrette DL, Khan M et al (2003) Old and new antiarrhythmic drugs for converting and maintaining sinus rhythm in atrial fibrillation: comparative efficacy and results of trials. Am J Cardiol 91:15D–26D
22. Lombardi F, Borggrefe M, Ruzyllo W et al (2006) Azimilide vs. placebo and sotalol for persistent atrial fibrillation: the A-COMET-II (Azimilide-CardiOversion MaintEnance Trial-II) trial. Eur Heart J 27:2224–2231
23. Hancox JC, McPate MJ, El Harchi A et al (2008) The hERG potassium channel and hERG screening for drug-induced torsades de pointes. Pharmacol Ther 119:118–132
24. Khanderia U, Wagner D, Walker PC et al (2008) Amiodarone for atrial fibrillation following cardiac surgery: development of clinical practice guidelines at a university hospital. Clin Cardiol 31(1):6–10
25. Touboul P, Brugada J, Capucci A et al (2003) Dronedarone for prevention of atrial fibrillation: a dose-ranging study. Eur Heart J 24:1481–1487
26. Wang Z, Fermini B, Nattel S (1993) Sustained depolarization-induced outward current in human atrial myocytes. Evidence for a novel delayed rectifier K+ current similar to Kv1.5 cloned channel currents. Circ Res 73:1061–1076
27. Li GR, Feng J, Wang Z et al (1996) Adrenergic modulation of ultrarapid delayed rectifier K+ current in human atrial myocytes. Circ Res 78:903–915
28. Van Wagoner DR, Pond AL, McCarthy PM et al (1997) Outward K+ current densities and Kv1.5 expression are reduced in chronic human atrial fibrillation. Circ Res 80:772–781
29. Lip GY, Tse HF (2007) Management of atrial fibrillation. Lancet 370:604–618
30. Kaye DM, Krum H (2007) Drug discovery for heart failure: a new era or the end of the pipeline? Nat Rev Drug Discov 6:127–139
31. Conway E, Musco S, Kowey PR (2008) New horizons in antiarrhythmic therapy: will novel agents overcome current deficits? Am J Cardiol 102:12H–19H
32. Li GR, Feng J, Yue L et al (1996) Evidence for two components of delayed rectifier K+ current in human ventricular myocytes. Circ Res 78:689–696

33. Nattel S, Yue L, Wang Z (1999) Cardiac ultrarapid delayed rectifiers: a novel potassium current family of functional similarity and molecular diversity. Cell Physiol Biochem 9:217–226
34. Nygren A, Fiset C, Firek L et al (1998) Mathematical model of an adult human atrial cell: the role of K+ currents in repolarization. Circ Res 82:63–81
35. Courtemanche M, Ramirez RJ, Nattel S (1999) Ionic targets for drug therapy and atrial fibrillation-induced electrical remodeling: insights from a mathematical model. Cardiovasc Res 42:477–489
36. Brendel J, Peukert S (2002) Blockers of the Kv1.5 channel for the treatment of atrial arrhythmias. Expert Opin Ther Pat 12:1589–1598
37. Brendel J, Peukert S (2003) Blockers of the Kv1.5 channel for the treatment of atrial arrhythmias. Curr Med Chem Cardiovasc Hematol Agents 1:273–287
38. Yang Q, Du L, Wang X et al (2007) Strategies for atrial fibrillation therapy: focusing on I_{Kur} potassium channel. Expert Opin Ther Pat 17:1443–1456
39. Jackson CM, Blass B, Coburn K et al (2007) Evolution of thiazolidine-based blockers of human Kv1.5 for the treatment of atrial arrhythmias. Bioorg Med Chem Lett 17:282–284
40. Blass BE, Coburn K, Lee W et al (2006) Synthesis and evaluation of (2-phenethyl-2H-1,2,3-triazol-4-yl)(phenyl)methanones as Kv1.5 channel blockers for the treatment of atrial fibrillation. Bioorg Med Chem Lett 16:4629–4632
41. Wu S, Fluxe A, Sheffer J et al (2006) Discovery and in vitro/in vivo studies of tetrazole derivatives as Kv1.5 blockers. Bioorg Med Chem Lett 16:6213–6218
42. Blass BE, Fensome A, Trybulski E et al (2009) Selective Kv1.5 blockers: development of (R)-1-(methylsulfonylamino)-3-[2-(4-methoxyphenyl)ethyl]-4-(4-methoxypheny l)-2-imidazolidinone (KVI-020/WYE-160020) as a potential treatment for atrial arrhythmia. J Med Chem 52:6531–6534
43. Janusz JM, Hodson SJ, Bosch GK et al (2007) Imidazolidinone derivatives as Kv1.5 potassium channel inhibitors and their preparation, pharmaceutical compositions and use in the treatment of cardiac arrhythmia, WO 2007149874, Wyeth, USA, p 155
44. Blass BE, Janusz JM, Ridgeway JM et al (2009) Preparation of 4-imidazolidinones as Kv1.5 potassium channel inhibitors, WO 2009079630, Wyeth, John, and Brother Ltd., USA, p 51
45. Blass BE, Janusz JM, Wu S et al (2009) Preparation of 4-imidazolidinones as kv1.5 potassium channel inhibitors, WO 2009079624, Wyeth, John, and Brother Ltd., USA, p 208
46. Wu S, Fluxe A, Janusz JM et al (2006) Discovery and synthesis of tetrahydroindolone derived semicarbazones as selective Kv1.5 blockers. Bioorg Med Chem Lett 16:5859–5863
47. Fluxe A, Wu S, Sheffer JB et al (2006) Discovery and synthesis of tetrahydroindolone-derived carbamates as Kv1.5 blockers. Bioorg Med Chem Lett 16:5855–5858
48. Gross MF, Beaudoin S, McNaughton-Smith G et al (2007) Aryl sulfonamido indane inhibitors of the Kv1.5 ion channel. Bioorg Med Chem Lett 17:2849–2853
49. Beaudoin S, Reed AD, Gross M (2002) Preparation of N-indanyl sulfonamides as potassium channel inhibitors, WO 2002060874, Icagen Incorporated, USA, p 72
50. Gross M, Beaudoin S, Reed AD (2001) Preparation of N-heterocyclylmethyl indanediamines as potassium channel inhibitors, WO 2001046155, Icagen, Inc., USA, p 97
51. Beaudoin S, Gross MF, Reed AD et al (2002) Preparation of N-[(phenylsulfonylamino) tetrahydronaphthyl]cyclopropanecarboxamides as potassium channel inhibitors for treatment of cardiac arrhythmias, WO 2002008183, Icagen, Inc., USA, p 91
52. Reed AD, Gross MF, Beaudoin S (2002) Preparation of N-[(phenylsulfonylamino) tetrahydronaphthyl]-3-phenylbutanamides as potassium channel inhibitors for treatment of cardiac arrhythmias, WO 2002008191, Icagen, Inc., USA, p 98
53. Lloyd J, Atwal KS, Finlay HJ et al (2007) Benzopyran sulfonamides as Kv1.5 potassium channel blockers. Bioorg Med Chem Lett 17:3271–3275
54. Matsuda T, Masumiya H, Tanaka N et al (2001) Inhibition by a novel anti-arrhythmic agent, NIP-142, of cloned human cardiac K+ channel Kv1.5 current. Life Sci 68:2017–2024

55. Nagasawa H, Fujiki A, Fujikura N et al (2002) Effects of a novel class III antiarrhythmic agent, NIP-142, on canine atrial fibrillation and flutter. Circ J 66:185–191
56. Matsuda T, Ito M, Ishimaru S et al (2006) Blockade by NIP-142, an antiarrhythmic agent, of carbachol-induced atrial action potential shortening and GIRK1/4 channel. J Pharmacol Sci 101:303–310
57. Matsuda T, Takeda K, Ito M et al (2005) Atria selective prolongation by NIP-142, an antiarrhythmic agent, of refractory period and action potential duration in guinea pig myocardium. J Pharmacol Sci 98:33–40
58. Finlay HJ, Lloyd J, Nyman M et al (2008) Pyrano-[2,3b]-pyridines as potassium channel antagonists. Bioorg Med Chem Lett 18:2714–2718
59. Claremon DA, McIntyre CJ, Liverton NJ (2002) Preparation of isoquinolinone compounds as potassium channel inhibitors, WO 2002024655, Merck & Co., Inc., USA, p 96
60. Dinsmore CJ, Bergman JM (2005) Preparation of quinoline potassium channel inhibitors, WO 2005030792, Merck & Co., Inc., USA, p 64
61. Dinsmore CJ, Bergman JM, McIntyre CJ et al (2005) Preparation of isoquinolinone potassium channel inhibitors, WO 2005046578, Merck & Co., Inc., USA, p 54
62. Dinsmore CJ, Bergman JM, McIntyre CJ et al (2005) Preparation of isoquinoline derivatives as potassium channel inhibitors, WO 2005030726, Merck & Co., Inc., USA, p 56
63. Isaacs R, Dinsmore CJ, McIntyre CJ et al (2005) Preparation of isoquinoline derivatives as potassium channel inhibitors, WO 2005030727, Merck & Co., Inc., USA, p 48
64. Isaacs R, Dinsmore CJ, Trotter BW et al (2005) Preparation of isoquinoline derivatives as potassium channel inhibitors, WO 2005030729, Merck & Co., Inc., USA, p 114
65. Trotter BW, Claiborne C, Ponticello GS et al (2005) Preparation of isoquinoline derivatives as potassium channel inhibitors, WO 2005030791, Merck & Co., Inc., USA, p 56
66. Trotter BW, Isaacs R (2005) Preparation of quinazoline potassium channel inhibitors, WO 2005030217, Merck & Co., Inc., USA, p 48
67. Trotter BW, Nanda KK, Kett NR et al (2005) Preparation of isoquinoline derivatives as potassium channel inhibitors, WO 2005030130, Merck & Co., Inc., USA, p 115
68. Trotter BW, Nanda KK, Kett NR et al (2006) Design and synthesis of novel isoquinoline-3-nitriles as orally bioavailable Kv1.5 antagonists for the treatment of atrial fibrillation. J Med Chem 49:6954–6957
69. Fedida D, Eldstrom J, Hesketh JC et al (2003) Kv1.5 is an important component of repolarizing K+ current in canine atrial myocytes. Circ Res 93:744–751
70. Brendel J, Schmidt W, Below P (2001) Preparation of 2′-aminomethylbiphenyl-2-carboxamides as Kv1.5 potassium channel blockers, WO 2001025189, Aventis Pharma Deutschland G.m.b.H., Germany, p 125
71. Peukert S, Brendel J, Pirard B et al (2003) Identification, synthesis, and activity of novel blockers of the voltage-gated potassium channel Kv1.5. J Med Chem 46:486–498
72. de Haan S, Greiser M, Harks E et al (2006) AVE0118, blocker of the transient outward current (I(to)) and ultrarapid delayed rectifier current (I(Kur)), fully restores atrial contractility after cardioversion of atrial fibrillation in the goat. Circulation 114:1234–1242
73. Gogelein H, Brendel J, Steinmeyer K et al (2004) Effects of the atrial antiarrhythmic drug AVE0118 on cardiac ion channels. Naunyn Schmiedebergs Arch Pharmacol 370:183–192
74. Oros A, Volders PG, Beekman JD et al (2006) Atrial-specific drug AVE0118 is free of torsades de pointes in anesthetized dogs with chronic complete atrioventricular block. Heart Rhythm 3:1339–1345
75. Wirth KJ, Paehler T, Rosenstein B et al (2003) Atrial effects of the novel K(+)-channel-blocker AVE0118 in anesthetized pigs. Cardiovasc Res 60:298–306
76. Blaauw Y, Gogelein H, Tieleman RG et al (2004) "Early" class III drugs for the treatment of atrial fibrillation: efficacy and atrial selectivity of AVE0118 in remodeled atria of the goat. Circulation 110:1717–1724

77. Wettwer E, Hala O, Christ T et al (2004) Role of IKur in controlling action potential shape and contractility in the human atrium: influence of chronic atrial fibrillation. Circulation 110:2299–2306
78. Knobloch K, Brendel J, Peukert S et al (2002) Electrophysiological and antiarrhythmic effects of the novel IKur channel blockers, S9947 and S20951, on left vs. right pig atrium in vivo in comparison with the IKr blockers dofetilide, azimilide, dl-sotalol and ibutilide. Naunyn-Schmiedebergs Arch Pharmacol 366:482–487
79. Bachmann A, Gutcher I, Kopp K et al (2001) Characterization of a novel Kv1.5 channel blocker in Xenopus oocytes, CHO cells, human and rat cardiomyocytes. Naunyn Schmiedebergs Arch Pharmacol 364:472–478
80. Nattel S, Zeng FD (1984) Frequency-dependent effects of antiarrhythmic drugs on action potential duration and refractoriness of canine cardiac Purkinje fibers. J Pharmacol Exp Ther 229:283–291
81. Peukert S, Brendel J, Pirard B et al (2004) Pharmacophore-based search, synthesis, and biological evaluation of anthranilic amides as novel blockers of the Kv1.5 channel. Bioorg Med Chem Lett 14:2823–2827
82. Lloyd DG, Buenemann CL, Todorov NP et al (2004) Scaffold hopping in de novo design. Ligand generation in the absence of receptor information. J Med Chem 47:493–496
83. Brendel J, Boehme T, Peukert S et al (2002) Preparation of anthranilic acid amides as antiarrhythmics, WO 2002100825, Aventis Pharma Deutschland G.m.b.H., Germany, p 102
84. Rezazadeh S, Claydon TW, Fedida D (2006) KN-93 (2-[N-(2-hydroxyethyl)]-N-(4-methoxy benzenesulfonyl)]amino-N-(4-chlorocinnamyl)-N-methylbenzylamine), a calcium/calmodulin-dependent protein kinase II inhibitor, is a direct extracellular blocker of voltage-gated potassium channels. J Pharmacol Exp Ther 317:292–299
85. Nanda KK, Nolt MB, Cato MJ et al (2006) Potent antagonists of the Kv1.5 potassium channel: synthesis and evaluation of analogous N, N-diisopropyl-2-(pyridine-3-yl) acetamides. Bioorg Med Chem Lett 16:5897–5901
86. Trotter WB, Nanda KK, Wolkenberg S et al (2007) Heteroaryl compounds, processes for preparing them, pharmaceutical compositions containing them, and their use as potassium channel inhibitors, WO 2007050348, Merck & Co., Inc., USA, p 100
87. Wolkenberg S, Bilodeau MT, Nolt MB (2007) Preparation of (arylpyridinyl)dipyridinylethanol derivatives as potassium channel inhibitors, WO 2007050347, Merck & Co., Inc., USA, p 31
88. Trotter BW, Nanda KK, Wolkenberg SE et al (2007) Substituted butanamide derivatives as potassium channel inhibitors and their preparation, pharmaceutical compositions, and use in the treatment of cardiac arrhythmias and related diseases, WO 2007015775. Merck & Co., Inc., USA, p 65
89. Beshore DC, Liverton NJ, McIntyre CJ et al (2010) Discovery of triarylethanolamine inhibitors of the Kv1.5 potassium channel. Bioorg Med Chem Lett 20:2493–2496
90. Vaccaro W, Huynh T, Lloyd J et al (2008) Dihydropyrazolopyrimidine inhibitors of Kv1.5 (IKur). Bioorg Med Chem Lett 18:6381–6385
91. Lloyd J, Finlay HJ, Atwal K et al (2009) Dihydropyrazolopyrimidines containing benzimidazoles as Kv1.5 potassium channel antagonists. Bioorg Med Chem Lett 19: 5469–5473
92. Lloyd J, Finlay HJ, Vacarro W et al (2010) Pyrrolidine amides of pyrazolodihydropyrimidines as potent and selective Kv1.5 blockers. Bioorg Med Chem Lett 20:1436–1439
93. Yang Q, Du L, Tsai K-C et al (2009) Pharmacophore Mapping for Kv1.5 Potassium Channel Blockers. QSAR Comb Sci 28:59–71
94. Orth PM, Hesketh JC, Mak CK et al (2006) RSD1235 blocks late INa and suppresses early afterdepolarizations and torsades de pointes induced by class III agents. Cardiovasc Res 70:486–496
95. Fedida D, Orth PM, Chen JY et al (2005) The mechanism of atrial antiarrhythmic action of RSD1235. J Cardiovasc Electrophysiol 16:1227–1238

96. (2007) Vernakalant: RSD 1235, RSD-1235, RSD1235. Drugs R D 8:259–265
97. Billman GE (2003) RSD-1235. Cardiome. Curr Opin Investig Drugs 4:352–354
98. Fedida D (2007) Vernakalant (RSD1235): a novel, atrial-selective antifibrillatory agent. Expert Opin Investig Drugs 16:519–532
99. Roy D, Rowe BH, Stiell IG et al (2004) A randomized, controlled trial of RSD1235, a novel anti-arrhythmic agent, in the treatment of recent onset atrial fibrillation. J Am Coll Cardiol 44:2355–2361
100. Goldstein RN, Khrestian C, Carlsson L et al (2004) Azd7009: a new antiarrhythmic drug with predominant effects on the atria effectively terminates and prevents reinduction of atrial fibrillation and flutter in the sterile pericarditis model. J Cardiovasc Electrophysiol 15:1444–1450
101. Persson F, Carlsson L, Duker G et al (2005) Blocking characteristics of hERG, hNav1.5, and hKvLQT1/hminK after administration of the novel anti-arrhythmic compound AZD7009. J Cardiovasc Electrophysiol 16:329–341
102. Lofberg L, Jacobson I, Carlsson L (2006) Electrophysiological and antiarrhythmic effects of the novel antiarrhythmic agent AZD7009: a comparison with azimilide and AVE0118 in the acutely dilated right atrium of the rabbit in vitro. Europace 8:549–557
103. Crijns HJ, Van Gelder IC, Walfridsson H et al (2006) Safe and effective conversion of persistent atrial fibrillation to sinus rhythm by intravenous AZD7009. Heart Rhythm 3:1321–1331
104. Camm AJ, Pratt CM, Schwartz PJ et al (2004) Mortality in patients after a recent myocardial infarction: a randomized, placebo-controlled trial of azimilide using heart rate variability for risk stratification. Circulation 109:990–996
105. Pritchett EL, Marcello SR (2003) Azimilide for atrial fibrillation: clinical trial results and implications. Card Electrophysiol Rev 7:215–219
106. Pritchett EL, Kowey P, Connolly S et al (2006) Antiarrhythmic efficacy of azimilide in patients with atrial fibrillation. Maintenance of sinus rhythm after conversion to sinus rhythm. Am Heart J 151:1043–1049
107. Hohnloser SH, Dorian P, Straub M et al (2004) Safety and efficacy of intravenously administered tedisamil for rapid conversion of recent-onset atrial fibrillation or atrial flutter. J Am Coll Cardiol 44:99–104
108. Franqueza L, Longobardo M, Vicente J et al (1997) Molecular determinants of stereoselective bupivacaine block of hKv1.5 channels. Circ Res 81:1053–1064
109. Caballero R, Moreno I, Gonzalez T et al (2002) Putative binding sites for benzocaine on a human cardiac cloned channel (Kv1.5). Cardiovasc Res 56:104–117
110. Arechiga IA, Barrio-Echavarria GF, Rodriguez-Menchaca AA et al (2008) Kv1.5 open channel block by the antiarrhythmic drug disopyramide: molecular determinants of block. J Pharmacol Sci 108:49–55
111. Decher N, Pirard B, Bundis F et al (2004) Molecular basis for Kv1.5 channel block: conservation of drug binding sites among voltage-gated K+ channels. J Biol Chem 279:394–400
112. Decher N, Kumar P, Gonzalez T et al (2006) Binding site of a novel Kv1.5 blocker: a "foot in the door" against atrial fibrillation. Mol Pharmacol 70:1204–1211
113. Luzhkov VB, Nilsson J, Arhem P et al (2003) Computational modelling of the open-state Kv 1.5 ion channel block by bupivacaine. Biochim Biophys Acta 1652:35–51
114. Pirard B, Brendel J, Peukert S (2005) The discovery of Kv1.5 blockers as a case study for the application of virtual screening approaches. J Chem Inf Model 45:477–485
115. Yang Q, Fedida D, Xu H et al (2010) Structure-based virtual screening and electrophysiological evaluation of new chemotypes of Kv1.5 channel blockers. ChemMedChem 5:1353–1358

hERG Potassium Channels in Drug Discovery and Development

Jitendra N. Singh and Shyam S. Sharma

Contents

Abstract Potassium (K^+) channels play a central role in the electrical activity of excitable cells. Although there are variety of potassium channels, scientists have developed immense interest in human *ether-a-go-go*-related gene (*hERG*)

S.S. Sharma (✉)
Department of Pharmacology and Toxicology, National Institute of Pharmaceutical Education and Research (NIPER), Sector- 67, S.A.S. Nagar, Punjab, 160062, India
e-mail: sssharma@niper.ac.in

S.P. Gupta (ed.), *Ion Channels and Their Inhibitors*,
DOI 10.1007/978-3-642-19922-6_6,

potassium channels due to their involvement in life-threatening cardiac arrhythmia. *hERG* is *a* gene that encodes the pore-forming α-subunit of a voltage-gated potassium channel expressed in nervous and cardiac tissue including atrium, ventricles, purkinje fiber, SA node and AV node. Potassium flow through *hERG* channel plays an important role in action potential repolarization, particularly in ventricular muscle. Blockade of *hERG* potassium channel via pharmacological interventions or hereditary mutations of genes encoding the channel is associated with a prolongation of cardiac ventricular repolarization, that is long QT syndrome (LQTS), a disorder that predisposesindividuals to life-threatening arrhythmias and substantial risk of sudden death. Inherited or drug-induced mutations in *hERG* channel lead to disruption of delayed rectifier potassium current (IKr), increase in cardiac excitability subsequently torsades de pointes and sudden death. A large number of putative disease-causing mutations in *hERG* have been identified in affected families so far, yet mechanism behind these mutations is unspecified and undistinguished. Therefore, entire paradigm of drug discovery has shifted towards the safety of the new molecules to screen for potential cardiac arrhythmogenic effects. Non-clinical assays are not sensitive enough to accurately predict QT prolongation liabilities in humans. For this reason, International Conference on Harmonization (ICH) safety pharmacology S7B guidelines were proposed for new chemical entities. According to these guidelines, thorough studies (*in vitro* and *in vivo*) on QT are required for virtually all newly developed pharmaceutical agents. In this article, an overview on *hERG* channels, their functions and dysfunctions, therapeutic agents modulating these channels and associated QT prolongation, and assay have been discussed.

Keywords $K_v11.1$ • Long QT syndrome • Electrocardiogram • ICH • *Tdp* • Protein Trafficking • *hERG* assays

Abbreviations

CFTR	Cystic fibrosis transmembrane conductance regulator
cNBD	C-terminal cyclic nucleotide binding domain
DMSO	Dimethyl sulfoxide
EAD	Early after depolarization
ECG	Electrocardiogram
ER	Endoplasmic reticulum
EU	European Union
HEK	Human embroyonic kidney cells
hERG	Human *ether-a-go-go*-related gene
HSP	Heat shock protein
I	Current
ICH	International conference on harmonization
IK_i	Inward rectifier potassium current

IK_r	Delayed rectifier potassium current
IND	Investigational new drug approval
K^+	Potassium
K_v	Voltage-gated Potassium channel
$K_v11.1$	*hERG* Potassium channels
LQTS	Long QT syndrome
NCE	New chemical entity
PD	Pharmacodynamic
PK	Pharmacokinetic
QTc	QT interval correction
Rb^+	Rubidium
SERCA	Sarcoplasmic ER Ca^{2+}-ATPase
Tdp	Torsade de pointes
TEA^+	Tetraethyl ammonium
TMO	Trimethyl amineoxide
VSD	Voltage sensing domain
WT	Wild type

1 Introduction

Potassium (K^+) channels are the most widely distributed type of ion channel and are found in virtually all living organisms. They have been considered to be the third largest group of the signaling molecule after protein kinase and G-protein-coupled receptors. K^+ channels control the membrane potential (frequency and shape of action potential), secretion of hormones (insulin secretion from β cells of pancreas) and neurotransmitters by altering the excitability. Their activity may be regulated by different voltage-gated ions (sodium and calcium), neurotransmitters and different signaling pathways stimulated by potassium ions. K^+ channels have been characterized and classified into four structural types based on their activation and their transmembrane domains (TMs): (a) Ca^{2+}-activated K^+ channels (K_{ca}) having 6 or 7 TM in each α-subunit and open in response to the presence of calcium ions or other signaling molecules, (b) inwardly rectifying potassium channel (K_{ir}) having 2 TM and passes current (positive charge) more easily in the inward direction, (c) Tandem pore domain potassium channel (K_{2P}) having 4 TM and 2 pores and are constitutively open and possess high basal activation and (d) Voltage-gated potassium channel (K_v) having 6 TM and open or close in response to changes in transmembrane voltage (for details, please see flowchart).

Voltage-gated potassium channel (K_v) in human is encoded by 40 genes and divided into 12 subfamilies. K_v channel was first cloned in drosophila shaker channel. All mammalian K_v channels consist of four α-subunits, each containing six transmembrane α-helical segments, S1–S6 and a membrane-reentering P-loop, which are arranged circumferentially around a central pore as homotetramers or heterotetramers (Fig. 1). This ion conduction pore is lined by four S5–P–S6

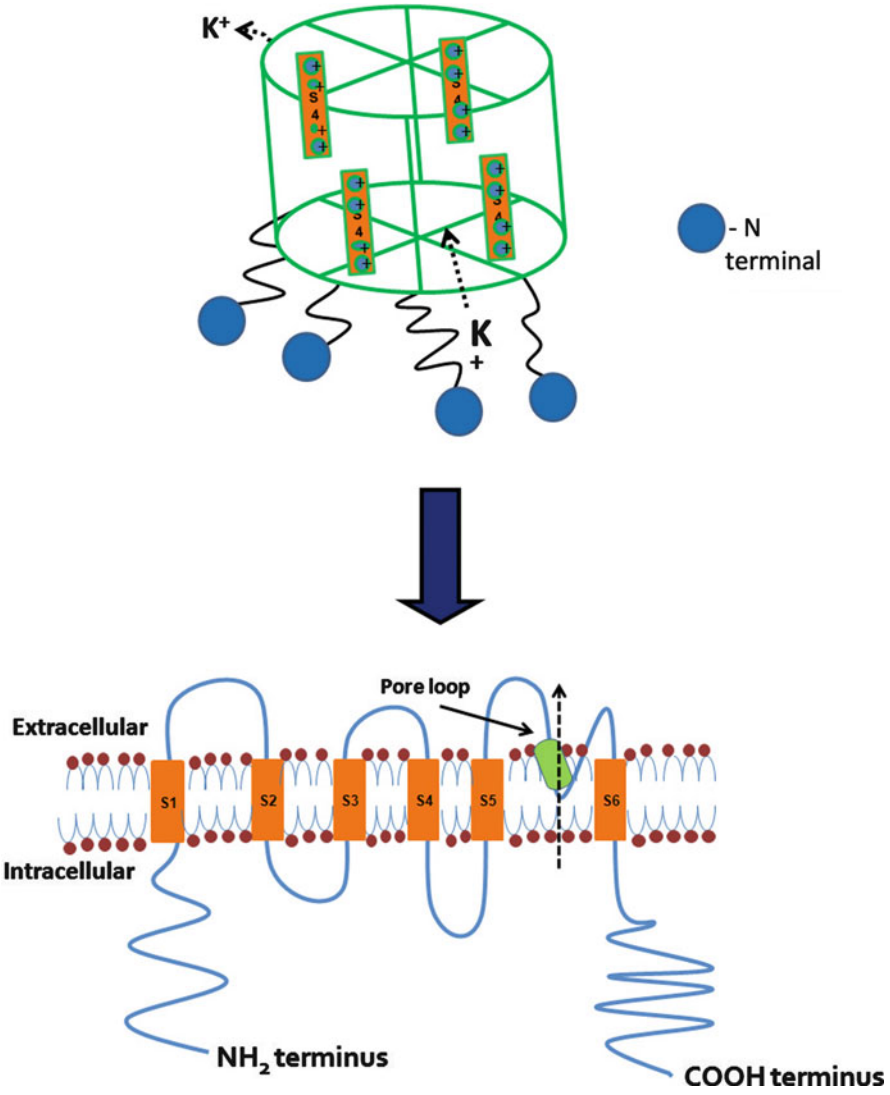

Fig. 1 Schematic diagram of *hERG* K^+ channel. Structure of the different regions of *hERG* K^+ channel has been shown with their different subunits, which are involved in QT prolongation

sequences. The four S1–S4 segments, each containing four positively charged arginine residues in the S4 helix, act as voltage sensor domains and "gate" the pore by "pulling" on the S4–S5 linker [1, 2]. All the 40 genes that encode the K_v channels in the human genome have been cloned and their biophysical properties have been characterized. However, it often remains a challenge to determine precisely which channel underlies a K^+ current in a native tissue. This is because, within subfamilies, such as the K_{v1} and K_{v7} families, the α-subunits can

heteromultimerize relatively freely, resulting in a wide range of possible channel tetramers with different biophysical and pharmacological properties. The properties of K_v channel α-subunit complexes can be further modified by association with intracellular β-subunits. As voltage-gated K^+ channels play important parts in defining the action potential waveform, modulators of these channels are expected to have therapeutic utility. Under conditions in which action potential firing is decreased (specifically, in depression and cognitive dysfunction), K_v channel blockers should restore normal firing. By contrast, K_v channel activators should be useful to reduce pathological hyperexcitability (specifically, in epilepsy and pain) by reducing action potential firing. In addition to this "mixing and matching" of α- and β-subunits, K_v channel properties can be further modified by phosphorylation, dephosphorylation, ubiquitylation, and palmitoylation [3]. Although a number of K^+ channels contribute to the process of action potential in cardiac tissue, voltage-gated K^+ channels 7.1 (commonly known as K_v7.1 or KCNQ1) and K_v11.1 (commonly known as *hERG* and KCNH2) play important role in cardiac repolarization, especially in the later phases of the action potential owing to its unique kinetics (Flowchart).

1.1 hERG K^+ Channels

Upon depolarization, in the ascending phase of the action potential, K_v 11.1 opens rapidly, but K^+ flux is quickly terminated by channel inactivation. Following repolarization, release of inactivation is fast and is followed by slow deactivation. In this way, the channel is active during the depolarization of the action potential and during part of the diastolic phase of the cardiac cycle. In the later phase, membrane potential is set at values at which driving force for K^+ flux is low, but K^+ conductance buffers incoming depolarizations [4, 5]. Therefore, K_v11.1 has a pivotal role in setting the duration of effective refractory period of cardiac action potential. Mutations in K_v11.1 can cause LQTS type 2 because deficient K_v11.1 function reduces repolarization and increases the possibility of torsades de pointes (*Tdp*), ventricular fibrillation and sudden death. The considerable interest of pharmaceutical industry in K_v11.1 is due to the involvement of this channel in drug-induced or acquired LQTS [6, 7]. The *hERG* inhibitors which inhibit the *hERG* channels includes astemizole, dofetilide and imipramine, while some of the *hERG* activators which activate *hERG* channel include NS1643, NS3623, PD307243, A935142 and RPR26024 [8].

1.2 Structure of hERG K^+ Channels

A detailed crystal structure for *hERG* K^+ channel is not yet available, so structural details for this channel are based on analogy with other ion channels, computer models, and pharmacology and mutagenesis studies. Fundamentally, *hERG* K^+

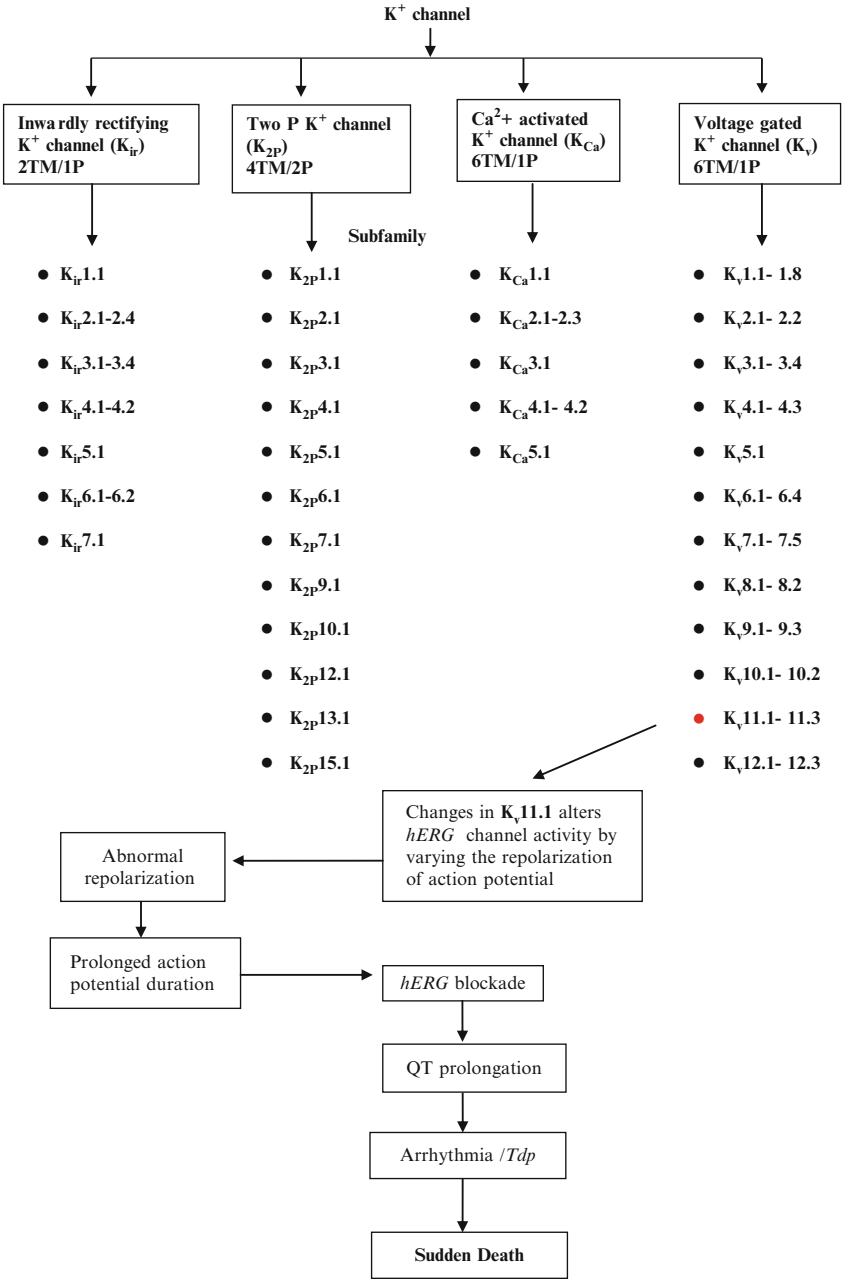

Flowchart Classification of the K^+ channels on the basis of IUPHAR and role of *hERG* channel causing QT prolongation and sometimes *Tdp*. A standardized nomenclature for K^+ channels has been proposed by NC-IUPHAR subcommittees on K^+ channels. They have been grouped into different families and subfamilies based on their structure and function. The relevant group/family is given for each subfamily

channel is a homotetramer having each of its subunit consisting of six transmembrane α-helices viz. S1-S6 and a pore helix situated between S5 and S6 through which ion conduction takes place (Fig. 1). Voltage sensing domains (VSDs) are integral components of *hERG* ion channels. The S1–S4 transmembrane domains from each subunit form the VSD, which move within the membrane in response to transmembrane voltage and regulate opening and closing of pore of voltage-gated K^+ channel [9, 10]. Between S5 and S6 helices, there is an extracellular loop (known as "the turret") and the pore loop, which begins and ends extracellularly but loops into the plasma membrane; the pore loop for each *hERG* subunits in one channel face into the ion-conducting pore and are adjacent to the corresponding loops of three other subunits and together they form selectivity filter region of the channel pore [11]. In addition to these transmembrane regions, *hERG* has intracellular N-terminal and C-terminal domains. The N-terminal region contains a Per–Arnt–Sim (PAS) domain, where they play important role in deactivation of the channel. The C-terminal tail contains a cyclic nucleotide binding domain (CNBD) whose function is not well characterized. Binding of cAMP to this domain has relatively little effect on gating [12]. However, this region is still an important consideration with respect to arrhythmogenesis since mutations in this region have been shown to cause trafficking defects [13, 14].

1.3 Functions and Dysfunctions of hERG K^+ Channels

hERG K^+ channel plays a key role in regulation of cardiac excitability and maintenance of normal cardiac rhythm. One-third of all cases of congenital long QT syndrome (LQTS) are primarily caused by mutation in *hERG*. In addition, *hERG* channel protein is the molecular target for almost all drugs that cause acquired form of long QT syndrome. Due to significance of *hERG* gating kinetics in both normal and abnormal cardiac function, much of the work has focused on understanding the voltage-dependent molecular rearrangements of channel protein [15]. *hERG* kinetic is distinct showing slow activation and rapid voltage-dependent inactivation resulting into outflow of small current through these channels. This is of importance in maintenance of plateau phase in cardiac action potential. In phase 3, a sharp outflow of K^+ current takes place as a result of quick recovery of channels from inactivated state. The current then decreases slowly until stimulus for second action potential arrived. Sequence alignments and hydropathy plots recommend that the overall structure of the VSD is homologous to that of other K_v channels, and it is suggested that S4 helix is loosely packed and most likely lipid exposed, much as it is presented in the crystal structure of $K_v1.2$. *hERG* channel dysfunction arising out of mutation may have adverse effects on cardiac electrical activity, and therefore its understanding may be helpful for knowing the correct functioning of $K_v11.1$ and designing proper therapy to avoid it. Till date about 300 mutations have been reported in $K_v11.1$ channel. Mechanisms of mutations mainly due to reduced or defective gating or synthesis or trafficking or ion permeation or single channel

conductance are described [16–18]. The genetic mutations reduce *hERG* channel function, which could have a deleterious effect on cardiac electrical activity. These mutations will not only contribute to a better understanding of channels functioning, but also form the basis of developing therapies aimed at correcting *hERG* channel dysfunction. The magnitude of *hERG* current in a cardiac myocyte is mainly determined by total number of channels on the plasma membrane, probability that any given channel is open and conductance of a single channel.

1.4 hERG Protein Trafficking

hERG channel biogenesis involves synthesis of a core-glycosylated monomer in the endoplasmic reticulum (ER) (135 kD band on western blot) followed by co-assembly into a tetramer that is subsequently transported to the Golgi. In the Golgi-complex glycosylation occurs resulting in the addition of sugar moieties to each subunit [19]. Therefore, western blot analysis of *hERG* channels expressed in mammalian cells gives two bands at 135 kD (ER) and 155 kD (Golgi and plasma membrane) if the channels are properly assembled and trafficked to the plasma membrane but only one band (135 kD) appear if they do not traffick from the ER. Mutations that affect either subunit assembly in the ER or trafficking from the ER to the plasma membrane will result in a trafficking failure. To date there are very few studies that have addressed the molecular basis of subunit assembly and domain interactions in *hERG* [20, 21].

Various approaches have been used to restore normal *hERG* trafficking *in vitro* and *in vivo* under different physiological and pathological conditions. Especially the trafficking-deficient mutations have become a focus of interest recently, since most of these mutations give rise to channel proteins capable of conducting IK_r current when intracellular trafficking is restored *in vitro* [22]. Mutations that affect either subunit assembly in ER or trafficking from ER to plasma membrane will result in a trafficking failure. *hERG* channel proteins are synthesized in the ER then it is transported to the cell surface of the Golgi apparatus. During this process, *hERG* proteins undergo two crucial steps of glycosylation. Initially newly synthesized immature *hERG* channels undergo asparagine (N)-linked core glycosylation in the ER. Consecutively, immature proteins are transported to Golgi apparatus, where complex glycosylation occurs. Finally, the fully glycosylated form of the *hERG* wild-type (WT) channel is inserted into the cell membrane [23, 24]. Misfolded and incompletely assembled proteins are common side products of protein synthesis in the ER. Analysis of the *hERG* sequence showed a putative ER retention signal present in the C terminus of *hERG*. Despite its presence in wild-type *hERG* proteins, these channels are not trafficking deficient. The C-terminal 104 amino acids mask and inactivate this retention signal in wild-type channels and that truncation of the C terminus leads to exposure of the R-G-R sequence, resulting in mistrafficking [25, 26]. In mammalian cells, another of quality control mechanisms consist of ER-associated and cytoplasmic chaperones. Identified two

cytosolic chaperones, heat shock protein (Hsp 70 and Hsp 90), interact dynamically with immature core-glycosylated ER-resident form of *hERG*, thereby forming a transient complex. During protein synthesis, large portions of the *hERG* protein are exposed to cytoplasm and thus possible binding partners for chaperones. These partners include N-terminal Per, Arnt and Sim (PAS) domain, the putative C-terminal ER retention signal R-G-R and the C-terminal cyclic nucleotide binding domain (cNBD), whereas small parts of the *hERG* tetramer point towards ER lumen [27]. The role of Golgi apparatus within the machinery is required for normal protein processing. During maturation in Golgi apparatus, *hERG* proteins associate with GM130/golgin-95, a Golgi-associated protein that is involved in vesicular transport [25, 28, 29]. The changes in temperature have opposing effect on activation and inactivation of channel. In voltage-dependent activation causes hyperpolarizing shift while inactivation results in depolarizing shift. The majority of identified trafficking-deficient mutants have been shown to be temperature-sensitive. The temperature-dependent induction of channel folding and processing in *hERG* R752W has been shown to be accompanied by a reduction in Hsp70 and Hsp90 association as well as by reduced synthesis and trafficking process [30]. The improved channel folding at lower temperatures might be due to an increased ER retention time at lower temperatures. In addition, reversal of the mutant's effects on *hERG* currents could be due to inhibition of proteasomal degradation at reduced incubation temperatures [19, 31].

Few studies have investigated the effects of a transcriptional regulator (4-phenylbutyrate) on *hERG* channel maturation. Despite markedly enhanced synthesis of mutant *hERG* R752W protein at 37°C upon application of 4-phenylbutyrate, transport of the mature protein to the cell surface could not be restored, indicating that the quality control machinery held the mutant protein in the ER, until it underwent degradation. Furthermore, in a study of five patients with *hERG* R752W-associated long QT syndrome treated with 4-phenylbutyrate (19 g/day) for 1 week; a dose that has proven successful in cystic fibrosis transmembrane conductance regulator (CFTR) rescue *in vivo*, cardiac repolarization was not significantly improved. These results suggested that enhanced protein expression may not be sufficient in restoring protein transport. Although data are limited, additional factors such as prolonged ER retention time and/or interactions with molecular or pharmacological chaperones seem to be required for successful rescue of *hERG* LQT2 mutants [2, 29, 32].

Chemical chaperones such as glycerol, dimethyl sulfoxide (DMSO), and trimethyl amine oxide (TMO) are believed to stabilize protein conformations during their maturation and restoration of trafficking by chemical chaperones such as glycerol has been indicated for hypomorphic *hERG* N470D channels. However, *hERG* R752W trafficking could not be corrected by incubation with glycerol indicating that rescue by chemical chaperones depends on the severity of mutation in *hERG*, which is determined by the protein domain affected by a mutation and by properties of introduced amino acid residue. Further investigations (e.g., mutagenesis studies on the effects of different amino acid substitutions at a certain position) need to be carried out to distinguish between

amino acid- and domain-related success and failure of chemical chaperones. Finally, the high concentrations of chemical chaperones required for restoration of protein trafficking (e.g., 10% glycerol) restrict their clinical use [33, 34]. In another sense, trafficking of mutant G601S and F805C channels was restored by application of sarcoplasmic/ER Ca^{2+}-ATPase (SERCA) inhibitor thapsigargin, which did not cause *hERG* current inhibition. It is speculated that in this mechanistically different case, alterations in the activity of calcium-dependent chaperone proteins in the ER promote the relocation of intracellular *hERG* protein to the cell surface. The underlying mechanism requires an intact Golgi apparatus. Further studies are required to investigate the precise mechanism of rescue by thapsigargin and to identify the chaperones involved in this rescue pathway [35].

Pharmacological rescue of trafficking-deficient *hERG* mutants appears to be the most promising approach. It has been revealed that trafficking of some Class 4 *hERG* mutants (e.g., *hERG* T65P, *hERG* N470D, *hERG* G601S) can be restored by application of high-affinity *hERG* channel ligands (i.e., inhibitors) such as methanesulfonanilide, and E4031, antihistamines agents such as astemizole and terfenadine, or gastrointestinal prokinetic drug such as cisapride. In contrast, attempts to rescue mutant *hERG* A561V, *hERG* R752W, *hERG* F805C or *hERG* R823W channels by incubation of pharmacological chaperones failed, suggesting that these channels represent a group of *hERG* LQT2 mutants, which is resistant to pharmacological rescue. More recently, the molecular determinants and the binding site for *hERG* channel ligand serving as pharmacological chaperones have been investigated. Nonetheless, pharmacological restoration of *hERG* channel maturation with high-affinity inhibitors of *hERG* currents requires application of the drug to the culture medium for a certain incubation time, followed by removal of the *hERG*-blocking drug prior to electrophysiological measurements, which prevents their clinical use [36–38]. Trafficking defects are present in a significant group of *hERG* mutants associated with LQT2. Since many of the trafficking-deficient channels give rise to functional channels when inserted into the cell membrane, restoration of normal channel trafficking is an attractive strategy for treating patients carrying Class 4 *hERG* mutations [39]. Among the strategies investigated to date, pharmacological restoration of *hERG* maturation with low-affinity channel antagonists seems to be most promising. However, limitations may derive from the fact that in each LQTS patient, the underlying mutation needs to be analyzed and characterized *in vitro* and the efficacy of specific therapies should be evaluated for each individual mutation prior to treatment [40–42].

2 QT Interval Prolongation and Torsade De Pointes

Lengthening of ventricular repolarization (Figs. 2 and 3) is known to be a risk factor for development of *Tdp*, a form of ventricular tachycardia thought to be initiated by an early after depolarization (EAD). *Tdp* is a potentially lethal arrhythmia that develops as a consequence of amplification of electrical heterogeneities intrinsic to

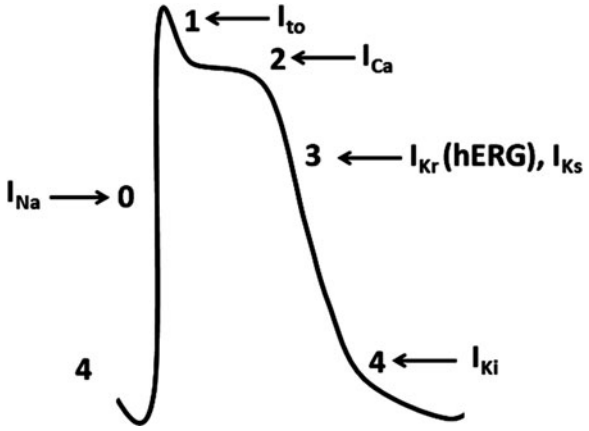

Fig. 2 Schematic diagram of an action potential recorded from a myocyte and involvement of Na^+ (I_{Na}), K^+ (I_{Kr}, I_{Ks}, and I_{Ki}) and Ca^{2+} (I_{Ca}) ion channel currents, which underlie each of its phases (0, 1, 2, 3, and 4). The cardiac electric events are outcome of different biologically important ionic pumps, exchangers and, most importantly, voltage-gated ion channels. The cardiac action potential recorded from either an atrial or a ventricular human myocyte can be classified into five distinct phases. (a) The phase 0, phase 0, or action potential upstroke, is generated by the rapid, transient influx of Na^+ into myocytes via Na^+ channels (inward current: I_{Na}). (b) Phase 1 describes the early repolarization process and is mediated by the efflux of K^+ from the cell through the opening of a distinct K^+ channel. The transient outward current (I_{to}) contributes to the termination of the upstroke of the action potential by causing an early phase of rapid repolarization. (c) Phase 2, or plateau of the action potential, is essentially because of the entry of extracellular Ca^{2+} into the cells through L-type Ca^{2+} channels (inward current: I_{Ca}). (d) Phase 3 describes the late repolarization process and is mediated by the efflux of K^+ from the cell through the opening of distinct K^+ channels. Two distinct K^+ channels contribute to Phase 3 repolarization [I_{Kr} or *hERG* current and I_{Ks}] by opposing Ca^{2+} influx during the plateau phase. (e) Phase 4, resting potential, is maintained by the inward rectifier (I_{Ki}). Besides maintaining phase 4, the inward rectifier also plays a prominent role in the final repolarization process in many species, although to a lesser extent in the human heart and clamps the cardiac myocyte at its resting potential [144, 145]

ventricular myocardium. Heterogeneity in development of prolongation of action potential and early after depolarizations results in a myocardium that is vulnerable to reentrant excitation, the probable immediate cause of *Tdp* in human [43].

2.1 QT Interval Correction (QTc)

The QT interval (Fig. 3) and heart rate have an inverse, non-linear relationship, which varies among and within species. Thus, change in heart rate exerts an effect on QT interval, which can confound the assessment of effect of test substance on ventricular repolarization and the QT interval [44]. Therefore, the interpretation of data from *in vivo* test systems should take into account the effect of coincident changes in heart rate. There are two important situations where variability in heart

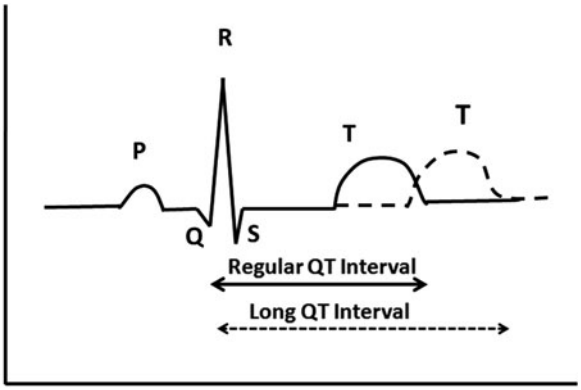

Fig. 3 A schematic diagram of electrocardiogram (ECG), recorded at the body surface, represents series of waves generated by electrical events of different chambers and conduction pathways within the heart. A typical ECG tracing of a normal heart beat consists of P wave, QRS complex and T wave [44]. P wave is the electrical signature of current that causes atrial contraction. Both the left and right atria contract simultaneously. The change in shape of P wave may indicate atrial problems. The QRS complex corresponds to the current that causes contraction of the left and right ventricles, which is much more forceful than that of the atria and involves more muscle, thus resulting in a greater ECG deflection. The Q wave represents the small horizontal current as action potential travels through interventricular septum. The R and S waves indicate contraction of the myocardium. The T wave represents the repolarization of the ventricles. The ST segment connects QRS complex and T wave. This segment lasts about 0.08 s and is usually level with the PR segment. The QT interval (time from the beginning of the QRS complex to the end of T wave) of the ECG is a measure of the duration of ventricular depolarization and repolarization [146]. Ventricular repolarization, determined by duration of cardiac action potential, is a complex physiological process. It is the net result of activities of many membrane ion channels and transporters. Under physiological conditions, the functions of these ion channels and transporters are highly interdependent. The activity of each ion channel or transporter is affected by multiple factors including, but not limited to, intracellular and extracellular ion concentrations, membrane potential, cell-to-cell electrical coupling, heart rate and autonomic nervous system activity. The rapidly and slowly activating components of I_{Kr} and I_{Ks} seem to have the most influential role in determining the duration of the action potential and the QT interval [147–150]

rate among animals occurs which is either difference in autonomic tone or effects of test substances on heart rate ideally. QT interval data obtained after administration of a test substance should be compared with control and baseline data at similar heart rates. When the heart rate variability is not due to the test substance, it can be reduced by acclimatization, or by use of anesthetized animal models [45].

2.2 Drug-Induced QT Prolongation

Drug-induced QT prolongation and the accompanying proarrhythmic risk are major regulatory concerns in drug development [44]. Drugs that delay ventricular repolarization and prolong. QT interval are associated with an increased risk of

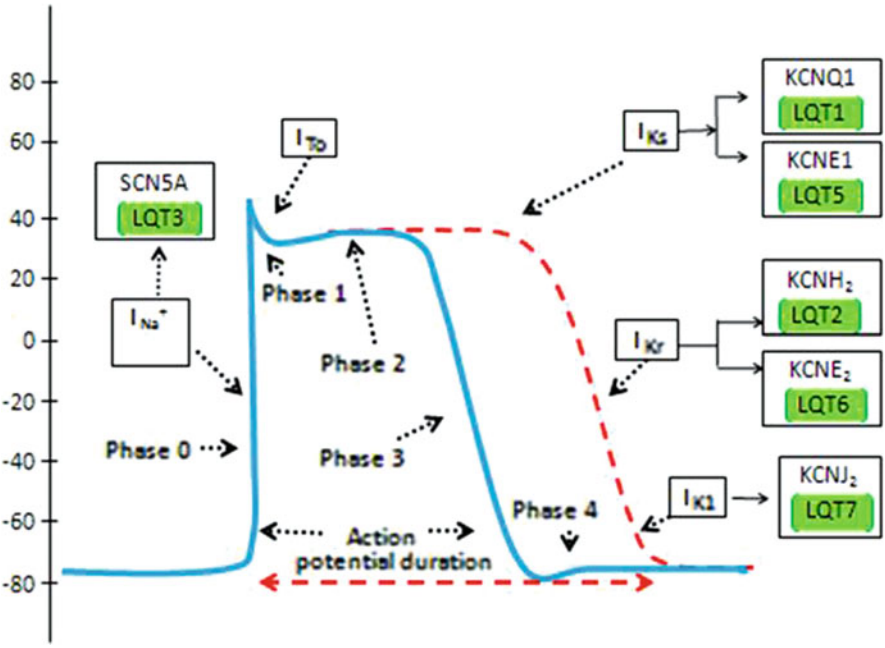

Fig. 4 Schematic diagram of a ventricular action potential showing effects of long QT syndrome by pharmacological inhibitors of voltage-gated K^+ channel 7.1 ($K_v7.1$; also known as KCNQ1) or $K_v11.1$ (also known as *hERG* or KCNH2) on action potential duration by alteration of the different gene, which alters the ion channel currents, in different phases (0, 1, 2, 3 and 4)

life-threatening ventricular tachyarrhythmia, in particular *Tdp*. Cardiac repolarization is a complex physiological process terminating the cardiac action potential and it results from the activities of multiple membrane ion channels and transporters. These ion channels and transporters interact through membrane potential and intra/or extra-cellular ionic concentrations, but are also affected by systemic factors including hormone regulation, metabolic state and autonomic nervous tone. Prolongation of action potential can result from inhibition of one or more of outward K^+ currents or by increasing inward currents (Na^+ or Ca^{2+}). Since IK_r plays a key role in repolarization of cardiac action potential, selective inhibition of this current slows repolarization and this is manifested as a prolongation of the QT interval on the ECG (Figs. 3 and 4). It is now widely accepted that the blockade of IK_r current by drugs is at least in part responsible for their proarrhythmic effect; however, this risk may be modulated by blocking other channels [46]. The spectrum of drugs associated with *Tdp* involves antiarrhythmic drugs, non-antiarrhythmic cardiovascular drugs and non-cardiovascular drugs (Table 1). Only 26% cases were associated with cardiac agents out of the 2,194 cases reported to the American Food and Drug Administration regarding *Tdp*. The other drug classes with proarrhythmic adverse effects are central nervous compounds comprising 22%, antiinfectives 19% and antihistamines 12%. Class-III antiarrhythmic drugs such as sotalol, dofetilide

Table 1 List of *hERG* K^+ channels ($K_v11.1$) activators

Name	Structures
PD307243	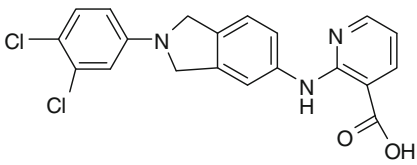
NS3623	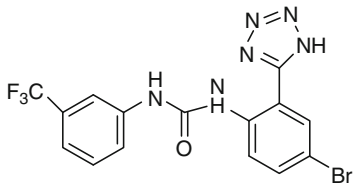
NS1643	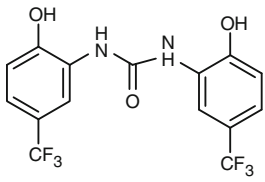
A935142	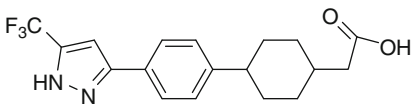
RPR26024	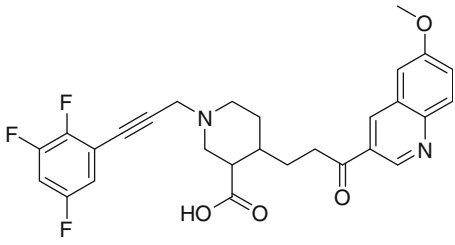

and ibutilide prolong cardiac repolarization mainly by reducing outward repolarizing potassium currents, notably IK_r at the level of single myocytes [47].

The exact incidence of drug-induced *Tdp* in general population is unknown. Most of our understandings of incidence, risk factors and drug interaction of

proarrhythmic drugs are derived from epidemiological studies, anecdotal case reports and clinical studies during drug development and post-marketing surveillance. The awareness of drug-induced *Tdp* in last few years has resulted in increase in the number of spontaneous reports. Nevertheless, the absolute total number remains very low, although it has been suggested that the system of spontaneous reporting under-reports the true incidence of serious adverse reactions by a factor of at least 10 [48]. Between 1983 and December 1999, 761 cases of *Tdp*, of which 34 were fatal, were reported to the World Health Organization Drug Monitoring Centre by the member states. WHO data provide an insight into the incidence of *Tdp* on most commonly reported proarrhythmic drugs. However, such a reporting system is undermined by the widely variable content and clinical information between different countries and sources. It is also compounded by various factors such as the patient's underlying disease, whether adverse drug reaction is well known or has not been previously described and the amount of attention paid by the medical community on a specific adverse drug reaction [49, 50].

3 *hERG* K^+ Channels as a Therapeutic Target

hERG potassium channels are essential for normal electrical activity in the heart. Inherited mutations in the *hERG* gene cause long QT syndrome, a disorder that predisposes individuals to life-threatening arrhythmias. Arrhythmia can also be induced by a blockage of *hERG* channels by a surprisingly diverse group of drugs. This side effect is a common reason for drug failure in preclinical safety trials. Insights gained from the crystal structures of other potassium channels have helped our understanding of block of *hERG* channels and the mechanisms of gating [51]. Many drugs have been withdrawn from the market and a large number of promising compounds have been stopped during development due to suspected or confirmed adverse events, including fatalities. Cardiac, hepatic and hematological abnormalities are the major causes of withdrawal of drugs or restriction in their labeling. Among these unintended effects, drug-induced arrhythmogenic death is the most dramatic. The common cause of the withdrawal or restriction of drugs produced delayed ventricular repolarization and the prolongation of QT interval associated with fatal polymorphic ventricular tachycardia, or *Tdp*. A convergence of data obtained from clinicians, basic electrophysiologists and geneticists who have studied the congenital long QT syndrome (also characterized by *Tdp*) has resulted in some understanding of the mechanisms, whereby drugs may cause this type of arrhythmia. Guidelines, which are still evolving, are aimed at predicting whether a new drug carries this risk. Paradoxically, however, increased knowledge has also illuminated the fact that the current predictors of this serious side effect are imperfect, both for individual patients and for populations of patients who are exposed to a given drug. Thus, although clinicians, members of regulatory bodies and drug developers, may be able to predict that a given drug may carry some risk, they can neither assess nor quantify it accurately [23, 52, 53].

Inhibition of the *hERG* channel can increase the QT interval and the likelihood of arrhythmias. If untreated, this undesired QT prolongation can lead to *Tdp* and may be fatal. Genetic mutations in the *hERG* channel can result in LQTS, a disorder in which the patient has a substantial risk of sudden death due to an arrhythmia known as *Tdp* [43]. Several drugs have recently been withdrawn as a result of multiple fatalities connected to *hERG* blockade. It is becoming increasingly necessary to assess a compound's effect on *hERG* channel activity at the initial stages of drug discovery process. High-throughput methods, such as rubidium (Rb^+) flux, make it possible to perform this *hERG* assessment during lead generation and optimization [54].

IK_r is important in determining the timing of electrical repolarization of the action potential in ventricular myocyte. Typically, an LQTS patient will have no clinical signs except prolongation of QT interval on the electrocardiogram (ECG) and the patient will appear otherwise healthy, having no other symptoms except some patients will suffer from occasional syncope [7, 55, 56]. The *hERG* channel has been shown to be the target antiarrhythmic drugs (e.g., amiodarone, sotalol and dofetilide; Table 2), which reduce the risk of re-entrant arrhythmias by prolonging the AP duration and the refractory period without slowing conduction velocity in the myocardium. *hERG* also promiscuously interacts with many other drugs, and it is the inadvertent target of myriad non-cardiac drugs [37, 57], a phenomenon that can under some circumstances lead to severe fatalities including acquired LQTS and its concomitant risk of sudden death. As a result, since the mid-1990s a wide variety of drugs found to be spoiled by this safety issue they have been reclassified or withdrawn from the market. Intensive efforts in drug development are continuing to root out compounds that might also suffer from this problem [13].

4 *hERG* K^+ Channels Activators and Inhibitors Which Alters QT Interval

The recent discovery of several structurally diverse *hERG* activators could be an immense breakthrough in treating the clinical conditions with *hERG* targets. Some of the compounds have been described as activators (Table 1) i.e., RPR260243, PD-118057, NS 1463, NS 3623 and mallotoxin [58, 59]. First, QT prolongation is associated with those drugs that predictably prolong QT interval. They are used to treat arrhythmias and include quinidine, procainamide, terfenadine, amiodarone, sotalol and dofetilide (Class I drugs). Second, those drugs which have been shown to prolong the QT interval, often at elevated serum concentrations may produce arrhythmias (Class II such as amitriptyline, cisapride, erythromycin, pimozide and thioridazine). There are a large number of drugs with limited or minimal ability to prolong the QT interval (Table 2) (Class III).

All of these drugs associated with QT prolongation could interact based on pharmacodynamic (PD) and/or pharmacokinetic (PK) mechanisms. Following

Table 2 List of *hERG* K^+ channel inhibitors causing QT prolongation and sometimes *Tdp* along with their chemical structure, year of approval/withdrawal by FDA and medical indication

Drug	Structure	Year of FDA approval	Year of FDA withdrawal	Medical indication
Amiodarone	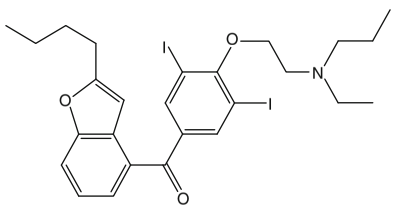	1985	2006	Cardiac arrhythmia
Bepridil	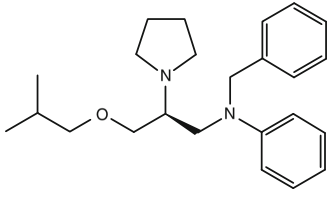	2005	2007	Angina pectoris
Mibefradil	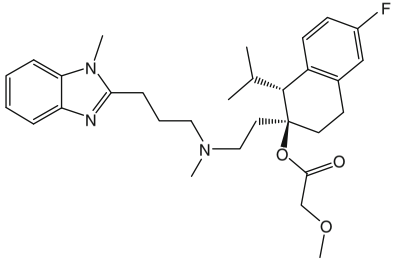	1997	1998	Hypertension and angina pectoris

(continued)

Table 2 (continued)

Drug	Structure	Year of FDA approval	Year of FDA withdrawal	Medical indication
Prenylamine	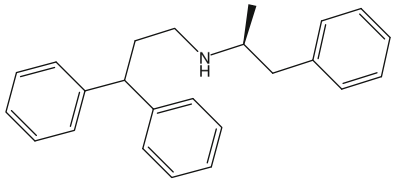	–	1988	Angina pectoris
Mesoridazine	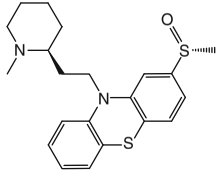	–	2004	Schizophrenia
Pimozide	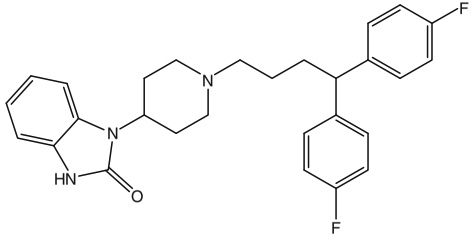	1965	2005	Schizophrenia

Rispiridone	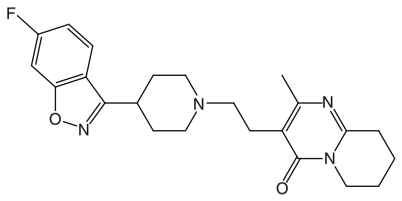	1994	2004	Schizophrenia
Sertindole	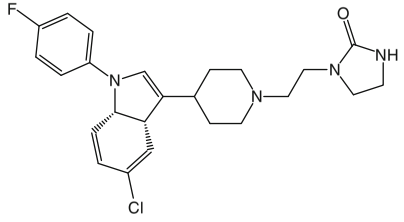	1995	1998	Schizophrenia
Fluoxetine	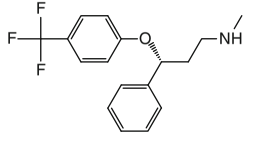	1987	–	Depression, obsessive compulsive disorder

(continued)

Table 2 (continued)

Drug	Structure	Year of FDA approval	Year of FDA withdrawal	Medical indication
Astemizole	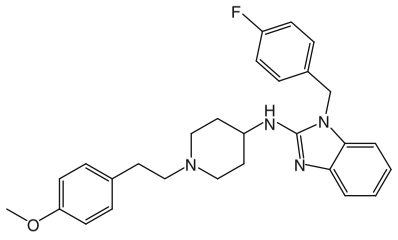	1988	1999	Allergic rhinitis
Terfenadine	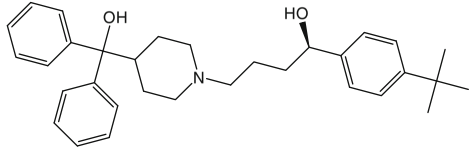	1985	1998	Allergic rhinitis
Grepafloxacin	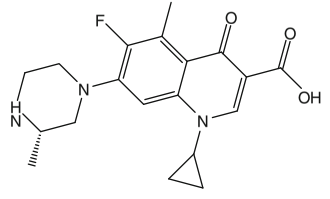	1997	1999	Bacterial infection

Cisapride	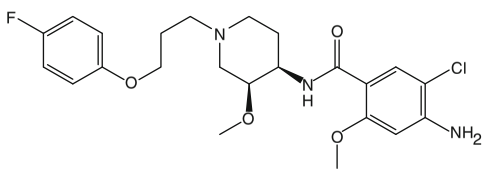	1993	2000	GI disorders; heartburn
Terodiline	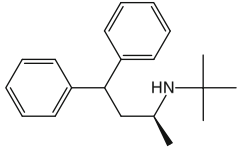	1971	1991	Bladder incontinence
Domperidone	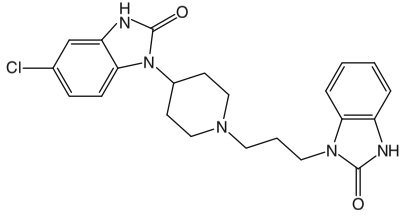	–	2001	Nausea and psychosis, promotes lactation

(continued)

Table 2 (continued)

Drug	Structure	Year of FDA approval	Year of FDA withdrawal	Medical indication
Levacetyl-methadol	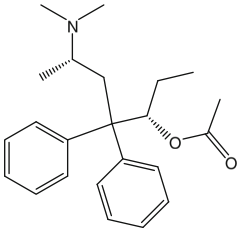	1993	2001	Opiate dependence
Methadone	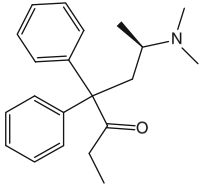	1947	2008	Pain control
Ketoconazole	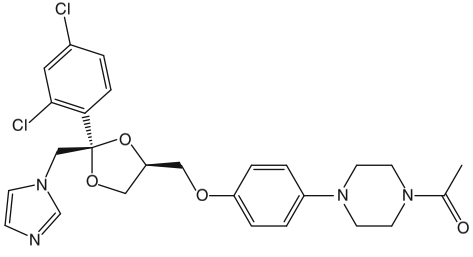	1981	–	Fungal infections

Fluconazole	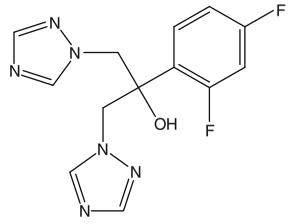	2003	–	Systemic fungal infection
Nelfinavir	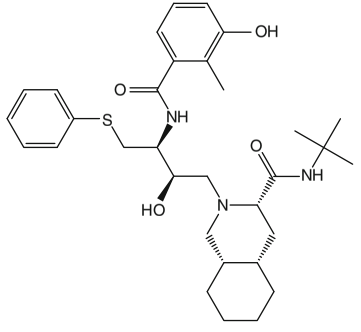	1997	–	HIV infection
E-4031	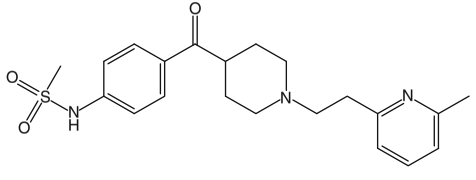	Banned by US FDA	Banned by US FDA	No medical indication. Use only for research purpose

general approaches are considered to minimize the QT prolongation associated with drug interaction. Combinations of drugs such as two drugs from Class I (PD interaction) quinidine plus dofetilide or a Class I drug plus a Class II drug when there is also a PK interaction (PD plus PK), for example quinidine with thioridazine should be avoided. The combinations can be recommended when benefit outweighs the risk, a Class I drug plus Class II drug when there is no PK interaction (PD only) e.g., procainamide with cisapride. Within Class II drugs when there is also a PK interaction (PD plus PK) such as erythromycin with cisapride should be avoided. Class II drugs when there is no PK interaction (PD only) e.g., amitriptyline plus cisapride combinations of Class III drugs may result in increased QT prolongation should be avoided. Patients with pre-existing QT prolongation, prolonged baseline QT, abnormally prolonged QT interval, QTc during drug and T-wave lability changes during drug treatment are probably at increased risk of developing arrhythmias. Patients with the risk factors including bradycardia, female sex, genetics (gene mutations in cardiac ion transport), heart disease (heart failure, ischemia), electrolyte disturbances (hypocalcemia, hypokalemia, hypomagnesemia and hypothyroidism) cardiac hypertrophy and increased age should be monitored carefully and therapy with alternative agents posing no risk for delayed repolarization should be considered [60–62]. Terfenadine and ketoconazole are most widely used positive reference drugs in non-clinical cardiac repolarization safety studies. Study reports have suggested the effects of terfenadine, ketoconazole alone and their combination on QT prolongation using conscious guinea pigs and QT were recorded using a telemetry system. Neither terfenadine nor ketoconazole produced any effect on the respiratory rate (RR), QT intervals, heart rate (HR). However, a combination of terfenadine and ketoconazole significantly prolonged RR and QT intervals and decreased HR in a time-dependent manner [63].

4.1 hERG Activators

RPR260243: (3R,4R)-4-[3-(6-methoxyquinolin-4-yl)-3-oxo-propyl]-1-[3-(2,3,5-trifluoro-phenyl)-prop-2-ynyl]-piperidine-3-carboxylic acid), is a novel activator of *hERG*. By using patch-clamp electrophysiology, it dramatically slowed current deactivation when applied to cells which were stably expressing *hERG* (Table 1) [58].

PD-118057: After RPR260243, another potent *hERG* channel enhancers i.e., 2-{4-[2-(3,4-dichloro-phenyl)-ethyl]-phenylamino}-benzoic acid (PD-118057) was reported, which increases the peak tail *hERG* current in human embryonic kidney cells [59]. PD-118057 did not affect the voltage dependence and kinetics of gating parameters, nor did it require open conformation of the channel. In isolated guinea pig cardiomyocytes, PD-118057 showed no major effect on I_{Na}, I_{Ca} and I_K. PD-118057 shortened the action potential duration and QT interval in arterially perfused rabbit ventricular wedge preparation in a concentration-dependent manner (Table 1).

NS1643: A diphenylurea compound i.e., 1,3-bis-(2-hydroxy-5-trifluoromethyl-phenyl)-urea (NS1643) also increases the activity of *hERG* channels expressed in *Xenopus laevis* oocytes. NS1643 (Table 1) (EC_{50}-10.5 μM) increased both steady-state and tail current at all voltages tested in the *hERG* expressed in *Xenopous* and *hERG* channels expressed in mammalian HEK 293 cells [64]. In guinea pig cardiomyocytes, NS1643 significantly activated delayed rectifier potassium current and decreased the action potential duration. This effect were reversed after application of the specific *hERG* channel inhibitor 4′-[[1-[2-(6-methyl-2-pyridyl)ethyl]-4-piperidinyl]carbonyl]-methanesulfonanilide (E-4031).

NS3623*:* N-(4-bromo-2-(1H-tetrazol-5-yl)-phenyl)-*N*′-(3′-trifluoromethylphenyl) urea (NS3623) also has the ability to activate *hERG* channels expressed in Xenopus oocytes. Exposure of NS3623 affects the voltage-dependent release from inactivation, resulting in a half-inactivation voltage is rightward-shifted in *Xenopus* oocytes [65]. Moreover, the compound affects the time constant of inactivation, leading to a slower onset of inactivation of the macroscopic *hERG* currents [65]. Application of NS3623 to *hERG* mutants did not result in increased *hERG* current. In contrast, applications of NS3623 to the mutant F656M have shown to increase *hERG* current to a larger extent as compared with wild-type *hERG*1 channels. NS3623 (Table 1) also has the ability to shorten action potential durations in guinea pig papillary muscle.

Mallotoxin: Mallotoxin (MTX) is recently introduced as a naturally occurring *hERG* channel activator. MTX increases both step and tail *hERG* currents. MTX leftward shifted the voltage dependence of *hERG* channel activation to less depolarized voltages [66]. MTX also increased *hERG* deactivation time constants without altering the half-maximal inactivation voltage of *hERG* channel, but it reduced the slope of voltage-dependent inactivation curve. All of these factors contribute to the enhanced activity of *hERG* channels. Application of MTX increases the flow of potassium ions through *hERG* channels (Table 1).

4.2 hERG Inhibitors

Amiodarone: Amiodarone is an antiarrhythmic drug used to treat ventricular and supraventricular (atrial) arrhythmias, the IC_{50} is around 0.7 μM. It prolongs QT of cardiac ECG (Table 2). It shows beta-adrenoreceptor and potassium channel blocking action on sinoatrial and atrioventricular node, which increases effective refractory period via sodium and potassium channel that subsequently reduce conduction of cardiac action potential. So it may lead to polymorphic ventricular arrhythmia [67].

Astemizole: A non-sedating and selective H1-receptor antagonist, astemizole, causes acquired long QT syndrome (Table 2). Astemizole blocks the rapidly activating delayed rectifier K^+ current I_{Kr} and the *hERG* K^+ channels that underlie it. The principal metabolite is desmethylastemizole and norastemizole. Desmethylastemizole

and astemizole cause equipotent block of *hERG* channels and these are among the most potent *hERG* channel antagonists so far. Because desmethylastemizole becomes a dominant compound in serum, it is confirmed that it becomes the principal cause of long QT syndrome observed in patients following astemizole ingestion. Norastemizole block of *hERG* channels is comparatively weaker; thus the risk of producing ventricular arrhythmias may be lower [27]. IC_{50} for astemizole on *hERG* expressed in Xenopus oocytes is 69 nM to 0.33 μM; in HEK cell; 0.9–22 nM and in the guinea pig/ventricular myocytes approximately 1.5 nM were reported [68].

Bepridil: It is a non-selective calcium channel blocker used to treat angina pectoris. It improves left ventricular performance and is found to be effective as monotherapy for treatment of patients with exertional angina. Its use is associated with increased exercise capacity and decreased angina frequency and nitroglycerine consumption as well as improved LV systolic and diastolic performance at rest and during peak exercise (Table 2). Bepridil produces prominent bradycardia-dependent QT prolongation with special attention in patients having structural heart disease [69].

Cisapride: Cisapride (IC_{50}, 0.02 μM) is a widely used prokinetic agent and has attracted much recent attention because of reports of QT prolongation and *Tdp* (Table 2). Approximately 23 cases of QT prolongation associated with cisapride were reported to the Food and Drug Administration from 1993 to 1996 with four deaths and 16 resuscitated cardiac arrests [48]. Many of the patients were also taking imidazole or a macrolide antibiotic, which could inhibit the P-450 CYP3A4 isoenzyme responsible for cisapride metabolism [70–72].

Domperidone: Several cases of QT prolongation and ventricular tachyarrhythmia have been reported with domperidone, a gastrokinetic and antiemetic agent available worldwide but still under investigation in the USA (Table 2). Although electrolyte disturbances such as hypokalemia could account for some of these events, it possesses cardiac electrophysiological effects predisposing some patients to proarrhythmia. These effects are observed at clinically relevant concentrations of the drug [73, 74].

E-4031: It is a methanesulfonanilide, class III antiarrhythmic drug that was initially reported to prolong cardiac action potential duration and block I_{Kr} in ventricular cells at submicromolar concentration (Table 2). E-4031 is a specific blocker of *hERG* K^+ channels in heterologous systems, cardiac cells and cardiac preparations [75].

Fluconazole: Fluconazole, a commonly used azole antifungal drug, can induce QT prolongation, which may lead to *Tdp* and sudden death (Table 2). It is indicated that fluconazole may cause acquired LQTS and ventricular arrhythmia through a direct inhibition of *hERG* current and by disrupting *hERG* protein trafficking and the mutations Y652 and F656 may be obligatory determinants in inhibition of *hERG* current for fluconazole [76, 77].

Fluoxetine*:* Fluoxetine, a selective serotonin reuptake inhibitor, is widely used as an antidepressant compound (Table 2) [78]. Recent studies revealed that the complex pharmacological profile of fluoxetine includes various additional effects, such as inhibition of muscular and neuronal nicotinic acetylcholine receptors, blockade of

monoamine oxidase A and B [79] and reduction of neuronal $K_v1.1$ potassium and sodium currents [80]. It has been suggested that fluoxetine might inhibit the K^+-induced serotonin release by decreasing the voltage-dependent Ca^{2+} entry into nerve terminals [81]. Furthermore, it had been demonstrated that delayed rectifier K^+ channels and Na^+ channels in human corneal epithelium are blocked by fluoxetine [82] and, finally, inhibitory effects of fluoxetine on cardiac Ca^{2+} and Na^+ channels. Selective serotonin reuptake inhibitor antidepressant drugs are generally believed to cause fewer proarrhythmic side effects compared with tricyclic antidepressants [83]. However, serious concerns have been raised by case reports of tachycardia and syncope associated with fluoxetine treatment [84]. In addition, a patient with markedly prolonged QTc interval due to fluoxetine has been reported, whereas previous experimental and clinical studies did not reveal any prolongation of the QTc interval [85]. But still the QTc prolongation seen during application of fluoxetine suggests that cardiac repolarization might be affected by this drug. Repolarization of cardiac ventricular myocyte is mainly due to outward potassium currents [86].

Grepafloxacin: It is well known to prolong cardiac repolarization and has been reported to increase the QT interval by an average of 10 ms in clinical trials at therapeutic doses (Table 2). Grepafloxacin was withdrawn from the market because of concerns over QT interval prolongation and rare cases of ventricular arrhythmia, including torsades de pointes, in patients receiving the drug [87, 88].

Ketoconazole: Ketoconazole is a synthetic antifungal drug and blocker of potassium rectifier current, which prolongs the QT interval (Table 2). It has been associated with QT prolongation and *Tdp* when co-administered with QT interval prolonging drugs (e.g., astemizole, terfenadine). Oral dose of 50 mg/kg terfenadine with ketoconazole 200 mg/kg combination results in immediate QT prolongation but none of them alone increased QT prolongation in telemetred conscious guinea pigs orally [63]. There is a pharmacokinetic component, both compounds use the same cytochrome-P450 metabolic pathway, resulting in an increase in plasma concentration of terfenadine. The voltage- and time-dependent characteristics of *hERG* blockade by ketoconazole indicated dependence of block on channel gating, ruling out a significant role for closed-state channel inhibition. Thus, ketoconazole accesses *hERG* channel pore-cavity on channel gating and S6 residue F656 is an important determinant of ketoconazole binding [63, 89, 90]. However, ketoconazole can block potassium currents mediated by *hERG* and $K_v1.5$, another cardiac potassium channel. The IC_{50} were reported 15.5–49 μM in Xenopus oocytes and approximately 2.5 μM in cat ventricular myocytes [90].

Levacetylmethadol: Opioids have capability to block *hERG* current in patients with or without any cardiac abnormalities and are responsible for QT interval prolongation (Table 2). Levacetylmethadol is a metabolite of methadone, causes *Tdp*, and its use requires electrophysiographic screening before treatment and during titrations. It is indicated as a second-line regimen drug for the treatment and management of opioid dependence if patients fail to respond to drugs such as methadone or buprenorphine [91].

Macrolides (erythromycin): Macrolides are a group of closely related compounds characterized by a macrocyclic lactone ring to which sugars are attached.

In contrast, little is known about the effects of these macrolides on the *hERG* channel [92]. They have been widely used as effective antibiotics against gram-positive organisms [93]. In fact, it is also the most thoroughly characterized with respect to effects on cardiac repolarization that seems to be mediated by cardiac potassium channel blockade [94–96]. The cardiac adverse effects of macrolides, especially erythromycin (Table 2) have been reported elsewhere [93]. It is also the most thoroughly characterized with respect to the effects on cardiac repolarization that seems to be mediated by cardiac potassium channel blockade [94–96]. With increasing reports of QT prolongation and arrhythmias associated with these drugs is by inhibiting *hERG* channels [97, 98].

Mesoridazine: Mesoridazine is used to treat the symptoms of schizophrenia and reduce restlessness, anxiety and tension. It can also reduce hyperactivity and uncooperativeness. Mesoridazine has been shown to prolong the QT interval in a dose-related manner which increases the risk of life-threatening arrhythmias such as *Tdp* and sudden death consequently its use in schizophrenia has been restricted (Table 2). Its use in other psychiatric disorders was abandoned after it was felt that there was an unacceptable balance of risks and benefits as a result of its cardiotoxic potential and it is no longer available in many countries [99].

Methadone: It is a synthetic opioid, used medically as an analgesic, antitussive and maintenance antiaddictive for use in patients on opioids (Table 2). Methadone inhibits the cardiac potassium channel *hERG* and can cause a prolonged QT interval. Methadone is chiral but its therapeutic activity is mainly due to (R)-methadone. Whole-cell patch-clamp experiments using cells expressing *hERG* showed that (S)-methadone blocked the *hERG* current 3.5-fold more potently than (R)-methadone [100–102].

Mibefradil: It is a calcium channel blocker that selectively blocks T-type calcium channel, useful in cardiovascular conditions such as hypertension, angina, or heart pain and congestive heart failure. It is also reported to cause QT prolongation and *Tdp* by blocking *hERG* potassium channel in concentration-dependent manner [103]. Also, K_vLQT1 is inhibited by bepridil and mibefradil, explains that Ikr is that sensitive target to most of the calcium channel blockers, which further depicts the proarrhythmic effect of these drugs (Table 2). Shortly following its introduction, mibefradil was withdrawn from the US market because of potentially harmful interactions with other drugs (e.g., amiodarone, quinidine, sotalol, erythromycin, desimipramine and thioridazine), which collectively prolong QT interval [104].

Nelfinavir: It is a potent HIV protease inhibitor class of antiretroviral drug that causes unpredicted adverse effects by changing elements of normal cellular metabolism (Table 2). Drug-induced QT prolongation is usually caused by block of *hERG* potassium channels and nelfinavir shown to cause dose-dependent blockade as heterologously expressed in HEK293 cells *in vitro*. Block by lopinavir of repolarizing IKr channels in neonatal mouse cardiac myocytes suggests that protease inhibitors could predispose individuals to QT prolongation and *Tdp* [105].

Pimozide: It is well another known antipsychotic which causes QT prolongation and *Tdp*. Forty cases (16 deaths) of serious cardiac reactions (predominantly

arrhythmias) of QT prolongation and ventricular tachyarrhythmia have been reported with pimozide by Committee on Safety of Medicines from 1971 to 1995, which is a potent neuroleptic useful in the management of motor and phonic tics associated with Tourette syndrome. The effects of pimozide on monophasic action potential duration were increased and concentration-dependent block of the rapid component of the delayed rectifier potassium current and tail current was decreased [106–109]. Pimozide possesses cardiac electrophysiological effects similar to those of class III antiarrhythmic drugs (Table 2). These effects are concentration dependent and observed at recommended dosages of the drug. Since pimozide is strongly metabolized by CYP3A4, special care should be taken to avoid potential pharmacokinetic interactions leading to high plasma levels of pimozide and proarrhythmia.

Prenylamine: It is a calcium channel blocker, which is used as a vasodilator in the treatment of angina pectoris. It has been shown to partially metabolize to amphetamine and can cause false positives for it in drug tests. Prenylamine also appears to act as a vesicular monoamine transporter inhibitor and has been demonstrated to deplete vesicular monoamine neurotransmitter stores similarly to reserpine (Table 2). It is well known fact that long use of prenylamine causes LQTS, ventricular premature beats and short run of ventricular tachyarrhthmia with *Tdp* pattern [110].

Risperidone: It is commonly used for the treatment of psychosis. Risperidone exerts antagonistic effects on 5-hydroxytryptamine (5-HT_2), dopamine (D_2), α-adrenoceptors and histamine (H_1) receptors. In contrast with other antipsychotics such as haloperidol and chlorpromazine, it allows a clear improvement of the quality of life of patients by a reduction in specific extrapyramidal effects [111]. Risperidone has been implicated in several cases of QT interval lengthening, the majority of them occurring with risperidone over-dosage [112]. However, to our knowledge, no case of *Tdp* was reported with risperidone at therapeutic doses. In most of the cases, QT prolongation by non-cardiac drugs such as risperidone involved a reduction of repolarizing K^+ currents, particularly the rapid component of delayed rectifier current IK_r. At cellular level, this results in prolongation of cardiac action potential duration [113]; 0.3 mM risperidone reduced by about 50% the IK_r current in rabbit ventricular myocytes and 0.1 mM risperidone lengthened significantly action potential duration recorded both in rabbit Purkinje fiber and in ventricular myocardium [114, 115]; 3 mM risperidone prolongs the action potential duration at 90% repolarization recorded in ventricular guinea pigs myocardium by about 27% [116] and 10 mM risperidone also prolonged the final action potential repolarization by about 20% in guinea pigs papillary muscle and by about 10% in isolated cardiac canine myocyte, concurrently with a reduction of IK_r current [117, 118]. In *hERG* cloned channel that expresses K^+ channel underlying IK_r in human heart, risperidone showed blockade of this channel at IC_{50} value of 1.6 μM, 0.39 μM, and 0.15 μM [119]. IK_r and IK_s have also been described in human atrial myocyte [120] but not in all myocytes and with only relatively small densities in comparison with the densities of potassium currents. In clinical practice, adverse effects of QT prolonging drugs can be prevented by not exceeding the

recommended dose; by restricting the dose in patients with pre-existing heart disease or other risk factors; and by avoiding concomitant administration of drugs that inhibit drug metabolism or excretion, prolong the QT interval, or produce hypokalaemia [121]. When the patient develops *Tdp*, the offending drug should be stopped and electrolyte abnormalities corrected [60].

Sertindole: Sertindole is a new indolylpiperidine antipsychotic agent, which has nanomolar affinities for dopamine D_2, serotonin 5-HT_2 and α-1 adrenergic receptors (Table 2). Sertindole blocked the *hERG* currents on two cloned human cardiac potassium channels, *hERG* and $K_v1.5$, in a stably transfected mammalian cell lines with an IC_{50} value at 14 nM. Sertindole enhanced the rate of current decay during these prolonged voltage steps and displayed a positive voltage dependence. Sertindole was approximately 1,000-fold less active at blocking $K_v1.5$ displaying an IC_{50} value of 2.1 μM. Sertindole is a high affinity antagonist of the human cardiac potassium channel *hERG* and blockade underlies the prolongation of QT interval [122].

Terfenadine: It is a second generation of histamine receptor antagonists ($IC_{50} = 56.0$ nmol/l), widely used as non-sedating antihistamines that differ pharmacologically from first-generation antihistamines by having preferential affinity for peripheral H_1 receptors versus the brain H_1 and cholinergic receptors (Table 2) [123]. Terfenadine at 0.3 mg/kg (IV) produced no effect on QT interval, but at 1 and 3 mg/kg, it significantly prolonged QT interval in dogs [124]. In guinea pig, 10 mg/kg IV infusion also results in QT prolongation.

Terodiline: Terodiline is used to treat urinary incontinence (Table 2). It was removed from the market in 1991 for proarrhythmia. Terodiline depresses the action potential plateau and induces triangulation without affecting action potential duration (APD_{90}). The triangulation ratios (normalized ratio of APD_{50} over APD_{90}) for terodiline were 0.94 and 0.59 for 1.0 and 10 μM. However, at supratherapeutic concentrations, preclinical data predict risk of QT prolongation. It is suggested that *hERG* block and triangulation are among multiple factors that must be considered in preclinical cardiac safety assessments [125, 126].

In addition to *hERG* inhibitors discussed above, several other drugs including chloroquine, chlorpromazine, disopyramide, dofetilide, droperidol, halofentrine, haloperidol, ibutilide, pentamidine, probucol, procainamide, quinidine, sotalol, thioridazine, and sparfloxacine have potential to produce QT prolongation.

5 Cardiovascular Safety and Guidelines

Accurately assessing the pro-arrhythmic potential of drug candidates should be done early in preclinical development to avoid the economic and public health consequences of late-stage failures of drug candidates, unfavorable labeling, and withdrawals of approved products. Regulatory authorities are focusing on safety issues associated with drugs where there is evidence of QT interval prolongation risk. The underlying basis for this stance is the observation that most drugs

associated with *Tdp* prolong the QT interval, though it should be noted that not all drugs known to prolong QT interval have been connected with *Tdp*. Although a variety of *in vitro* and *in vivo* experimental models are available for assessing the QT prolongation and proarrhythmic potential of drug candidate, no single preclinical model has been proven to be a predictive surrogate for human heart, that is clinical exposure. Recognizing this need, pharmaceutical regulatory agencies worldwide together with industry and academic scientists have developed guidance urging an integration of several assays in hope that their combination will provide a superior measure of true proarrhythmic risk. There are two documents developed by the working group under ICH. One guideline is dealing with the non-clinical strategy and another with clinical approach. Both recognize that the field of drug-induced alterations in ventricular repolarization and proarrhythmia will undergo changes as researchers are continuously gathering data, which in turn should adjust the guidelines [127, 128].

5.1 Preclinical Guidelines

1. Safety Pharmacology Studies for Human Pharmaceuticals (ICH S7A) ICH S7A describes the "core battery" of methods used to characterize the safety pharmacology profile of a compound. The goal of the ICH S7A guideline is to describe studies designed to assess the effects of drug molecule on vital physiological functions prior to first testing in man. The undone business of ICH S7A guideline, namely, the description of studies to assess the proarrhythmic potential of drugs through the prolongation of repolarization, was left for a secondary guideline, ICH S7B [129].
2. The Non-Clinical Evaluation of Potential for Delayed Ventricular Repolarization (QT Interval Prolongation) by Human Pharmaceuticals (ICH S7B). Unlike ICH S7A, ICH S7B heralds a new era for pharmaceutical industry since it now sets out how to address safety concerns of a new chemical entity (NCE), in relation to adverse reactions on ventricular repolarization, topic that has vexed industry and regulatory authorities for many years. This guideline applies to NCEs for human use and marketed pharmaceuticals when appropriate (e.g., when adverse clinical events, a new patient population, or new route of administration raises concerns not previously addressed). The objectives of the ICH S7B studies are to identify the potential of a test substance and its metabolites to delay ventricular repolarization and relate the extent of delayed ventricular repolarization to the concentrations of a test substance and its metabolites.

The study results can be used to elucidate the mechanism of action and, when considered with other information, estimate risk for delayed ventricular repolarization and QT interval prolongation in humans [130]. These guidelines describe a non-clinical testing strategy for assessing the potential of a test substance to delay ventricular repolarization. These guidelines also include information concerning non-clinical assays and integrated risk assessments. The assessment of the effects of

pharmaceuticals on ventricular repolarization and proarrhythmic risk is the subject of active investigation. The ICH S7B guideline, in the primary non-clinical testing strategy for assessing evidence of the risk of compounds to prolong the QT interval, has recommended the use of an *in vitro* IKr assay that evaluates the effects on IKr or the ionic current through a native or expressed IKr channel protein, such as that encoded by *hERG* and an *in vivo* QT assay that measures indices of ventricular repolarization, such as QT interval [129, 131].

5.2 Clinical Guidelines

In 2005, the International Conference on Harmonization released a document ICH E-14 concerning the clinical evaluation of QT and/or QTc interval prolongation and proarrhythmic potential for non-antiarrhythmic drugs. The guideline calls for a clinical thorough QT/QTc study (typically conducted in healthy volunteers), which is intended to determine whether a drug has a threshold pharmacological effect on cardiac repolarization, as detected by QT/QTc interval prolongation [132]. The ICH E-14 recommendations are generally applicable not only to new drugs that have systemic bioavailability but also to approved drugs when a new dose, route of administration, or target population that may result in an increased risk is explored. According to ICH E14 guideline, every drug should receive an extensive electrocardiographic evaluation in man. Although the guideline acknowledges the fact that QT prolongation is a poor marker for proarrhythmic risk, it postulates that there is a rough correlation between the mean degree of QT prolongation and the observed clinical proarrhythmic events [128]. Furthermore, non-clinical and especially proarrhythmic assays will be able to estimate whether concurrent observations of non-clinical and clinical repolarization delay is likely to impose a risk of *Tdp*. This also reflects the point that proarrhythmic conclusions should not be drawn from neither preclinical nor clinical QT studies. The objective of the guideline is to offer recommendations regarding the design, execution, analysis, and interpretation of a clinical study to evaluate the potential of a drug to delay cardiac repolarization [129, 133].

6 *hERG* Assay to Predict QT Prolongation

6.1 In Silico Methods

An alternative approach that can be applied during the earliest stages of the drug design and discovery process is *in silico* prediction of *hERG* channel blockade, based on pharmacophore models and knowledge of the drug-binding site of *hERG* channels. This approach is controversial because it has a significant potential for

false-positive and false-negative findings with respect to QT prolongation, the clinically relevant endpoint. *In silico hERG* -SAR assay is best for investigations within chemical class. The advantages of this approach include ability to rationalize predictions based on structural similarity to, as well as presence or absence of specific pharmacophore features shared by known *hERG* blockers [134, 135]. Computer modeling of electrophysiological information is an important technique for organizing and integrating generated data. The role of *in silico* modeling in predicting *Tdp* arrhythmia is likely to become increasingly important, as a vast amount of data needs to be exploited. An important strength of computer models is to reach down to the genetic level connecting the physiome with the genome [136, 137].

6.2 *In Vitro Assay*

Numerous structurally and functionally unrelated drugs block the *hERG* K^+ channel. *hERG* channels are involved in cardiac action potential repolarization and reduced function of *hERG* lengthens ventricular action potentials, prolongs the QT interval in an electrocardiogram and increases the risk for potentially fatal ventricular arrhythmias. To reduce the risk of investing resources in a drug candidate that fails preclinical safety studies because of QT prolongation, it is important to screen compounds for activity on *hERG* channels early in the lead optimization process [7, 11]. A number of *hERG* assays are available, ranging from high-throughput binding assays on stably expressed recombinant channels to very time-consuming electrophysiological examinations in cardiac myocyte. Depending on the number of compounds to be tested, binding assays or functional assays measuring membrane potential or Rb^+ flux, combined with electrophysiology on a few compounds, can be used to efficiently develop the structure–function relationship of *hERG* interactions. The inhibition of the *hERG*-encoded potassium channel can lead to prolongation of the cardiac action potential-manifested as a prolongation of QT interval on the ECG. Although QT interval prolongation is not dangerous per se, in a small percentage of cases, it is associated with a potentially fatal arrhythmia, that is *Tdp*. This channel type is pharmacologically promiscuous, so many compounds have caused QT interval prolongation in man, and this has led to drugs being withdrawn from the market following evidence of *Tdp*. From a drug discovery perspective, focusing as early as possible on screening out *hERG* activity is important. Retrospective analysis of *hERG* potency versus clinical incidence of *Tdp* suggests provisional safety margins that could be used as target values by medicinal chemists [129, 138]. Large safety margins will not always be possible; however and in such circumstances, if the risk-benefit ratio still favors developing the compound, a pre-clinical assessment of the likelihood that any QT interval prolongation will or will not lead to *Tdp* in man may be important. An isolated rabbit heart model of arrhythmia shows promise in this respect, based on a comparison of clinical data with that obtained from this assay. Clinical guideline (E14) suggests that

irrespective of the pre-clinical data, a thorough clinical ECG study will be required at some point during development [56, 139].

6.3 *Electrophysiological Studies Using Mammalian Cell Lines*

Some of the emerging methods involving channel proteins and isolated cells include automated patch clamp, *hERG* assay under pathophysiological conditions, pharmacodynamic interactions at the *hERG* channel, test for stereoselectivity, expression of *hERG* protein on the cell surface and effects on other cardiac ion channels can be good approaches to predict the risk of QT prolongation. Emerging automated patch-clamp methodologies promise to greatly enhance screening efficiency. It has the potential to become valuable high-throughput (HTP) screen during lead identification/optimization. PD interactions at *hERG* channel may involve binding at active or allosteric interactions. The effects can be synergistic or antagonistic. Test for stereoselectivity can be considered if racemate of NCEs is used. Effects on other cardiac ion channels can also be assessed if *hERG* block at relevant concentrations does not translate into effects on action potential duration/QT or if non-*hERG* effects on APD and ECG are seen [11, 32, 140].

6.4 *In Vivo Methods*

Beat-to-beat variability, T-wave morphology, effects on autonomic tone and intracardiac accumulation and metabolism are some of the emerging foci of research involving preclinical *in vivo* studies. Conscious anesthetized non-rodents are increasingly being studied using parameters derived from *in vitro* proarrhythmia indices. It is hoped that these models will give rise to better surrogate markers such as beat-to-beat variability and T-wave morphology. The latter has the potential to become a highly predictive for human torsadogenesis hence can be used for safety margin calculation [124, 141]. Effects on autonomic tone may be investigated on a case by case basis, while intra-cardiac accumulation, transporters and metabolism can be considered if effects on repolarization are unexpectedly seen at doses that should have high enough safety margin according to *hERG* assay [13, 142, 143].

7 Strategies to Tackle QT Prolongation Associated with *hERG* Inhibitors

Tdp is typically not seen during the development of a new drug until the filing of IND (Investigational New Drug Approval), which includes testing in typically less than 5,000 patients during clinical phase I–III. Following registration, evidence of

torsadogenic potential of a new drug can accumulate during post-marketing; a much higher number of patients are exposed over longer periods of time, including patients with risk factors, cardiovascular diseases, co-medication, metabolic impairment and genetically determined enhanced susceptibility. The role of inherited disturbances of the "rhythmome" (genes involved in the regulation of cardiac rhythm) is increasingly better understood. It is estimated that 5% of patients with drug-induced *Tdp* are silent carriers of gene mutations of cardiac ion channels. In other words, we know which drugs are associated with *Tdp* and something of how these drugs act to produce *Tdp*, but we do not understand individual patient variability very well. Safety biomarkers, identified via pharmacogenetic testing of patients with *Tdp*, help to characterize these individual liabilities for *Tdp?* The repolarization reserve of the human heart is difficult to quantify, but it is the result of a redundancy of physiological mechanisms. It is likely that risk factors and/or genetic alterations in the target population reduce the repolarization reserve of the heart and this leads in rare and specific cases to *Tdp*. Following this concept, it may be questionable to use healthy young animals with an intact repolarization reserve to predict the torsadogenic potential that occurs in very rare cases under specific conditions in man. It appears difficult to mimic the different conditions that may be involved in the initiation of *Tdp* in man. On the contrary, rare, poorly understood side effects occur with many highly effective drugs and the withdrawal of these medications from the market would probably harm more patients than it would help. Our partial understanding of the mechanisms underlying *Tdp* is a two-edged sword. On the one hand, drug safety has been improved: we are unlikely to see more new drugs that unexpectedly result in a high risk of *Tdp* after they have reached the market. On the other hand, as the molecular markers of risk for this and other unusual actions of drugs are elucidated, there is a great risk of paralyzing the drug development process in what is probably a fruitless effort to develop drugs that are entirely devoid of adverse effects.

8 Summary

After the discovery of role of voltage-gated potassium channels particularly *hERG* channels in the QT interval, there is no doubt that the level of awareness and understanding of the problems of drug-induced QT interval prolongation has progressed tremendously over last decade. ICH S7A, S7B and E-14 guidelines have been framed to avoid reaching any drug to the market, which has the potential to cause QT prolongation and ventricular arrthymia. We hope that ongoing rapid genetic advances will allow populations at higher risk to be identified, so that detection of risk becomes a practical means of screening. Hence, together with regulatory authorities, the pharmaceutical industry needs to identify the criteria needed to demonstrate the predictive value of new tests in such a way as to mitigate the need for a clinical assessment of *Tdp* potential.

Acknowledgements Authors thank the Department of Pharmaceuticals, Ministry of Chemical and Fertilizers, Govt. of India, New Delhi and CSIR, New Delhi for the financial support. Moreover, authors are thankful of Mr. Shivsharan Balbhim Kharatmal for his critical help in preparation of this article.

References

1. Swartz KJ (2004) Towards a structural view of gating in potassium channels. Nat Rev Neurosci 5:905–916
2. Bezanilla F (2008) How membrane proteins sense voltage. Nat Rev Mol Cell Biol 9:323–332
3. Zamponi GW, Feng ZP, Zhang L et al (2009) Scaffold-based design and synthesis of potent N-type calcium channel blockers. Bioorg Med Chem Lett 19:6467–6472
4. Hancox JC, McPate MJ, El Harchi A et al (2008) The hERG potassium channel and hERG screening for drug-induced torsades de pointes. Pharmacol Ther 119:118–132
5. Gussak I, Litwin J, Kleiman R et al (2004) Drug-induced cardiac toxicity: emphasizing the role of electrocardiography in clinical research and drug development. J Electrocardiol 37:19–24
6. Durdagi S, Subbotina J, Lees-Miller J et al (2010) Insights into the molecular mechanism of hERG1 channel activation and blockade by drugs. Curr Med Chem 17:3514–3532
7. Witchel HJ (2010) Drug-induced hERG Block and Long QT Syndrome. Cardiovasc Ther 1–9
8. Zareba W (2007) Drug induced QT prolongation. Cardiol J 14:523–533
9. Abbott GW, Roepke TK (2009) HERG biosynthesis: the positive influence of negative charge. Am J Physiol Heart Circ Physiol 296:H1211–H1212
10. Ahrendt E, Braun JE (2010) Channel triage: emerging insights into the processing and quality control of hERG potassium channels by DnaJA proteins 1, 2 and 4. Channels (Austin) 4:335–336
11. Mannikko R, Overend G, Perrey C et al (2010) Pharmacological and electrophysiological characterization of nine, single nucleotide polymorphisms of the hERG-encoded potassium channel. Br J Pharmacol 159:102–114
12. Cui J, Melman Y, Palma E et al (2000) Cyclic AMP regulates the HERG K(+) channel by dual pathways. Curr Biol 10:671–674
13. Thomsen MB, Volders PG, Beekman JD et al (2006) Beat-to-Beat variability of repolarization determines proarrhythmic outcome in dogs susceptible to drug-induced torsades de pointes. J Am Coll Cardiol 48:1268–1276
14. Pages G, Torres AM, Ju P et al (2009) Structure of the pore-helix of the hERG K(+) channel. Eur Biophys J 39:111–120
15. Alabi AA, Bahamonde MI, Jung HJ et al (2007) Portability of paddle motif function and pharmacology in voltage sensors. Nature 450:370–375
16. Perrin MJ, Subbiah RN, Vandenberg JI et al (2008) Human ether-a-go-go related gene (hERG) K+ channels: function and dysfunction. Prog Biophys Mol Biol 98:137–148
17. Antzelevitch C (2007) Ionic, molecular, and cellular bases of QT-interval prolongation and torsade de pointes. Europace 9(Suppl 4):iv4–iv15
18. Baumgartner D, Scholl-Burgi S, Sass JO et al (2007) Prolonged QTc intervals and decreased left ventricular contractility in patients with propionic acidemia. J Pediatr 150:192–197, 197.e1
19. Zhou Z, Gong Q, Ye B et al (1998) Properties of HERG channels stably expressed in HEK 293 cells studied at physiological temperature. Biophys J 74:230–241
20. Li X, Xu J, Li M (1997) The human delta1261 mutation of the HERG potassium channel results in a truncated protein that contains a subunit interaction domain and decreases the channel expression. J Biol Chem 272:705–708

21. Gong Q, Keeney DR, Robinson JC et al (2004) Defective assembly and trafficking of mutant HERG channels with C-terminal truncations in long QT syndrome. J Mol Cell Cardiol 37:1225–1233
22. Obers S, Staudacher I, Ficker E et al (2010) Multiple mechanisms of hERG liability: K+ current inhibition, disruption of protein trafficking, and apoptosis induced by amoxapine. Naunyn Schmiedebergs Arch Pharmacol 381:385–400
23. Staudacher I, Schweizer PA, Katus HA et al (2010) hERG: protein trafficking and potential for therapy and drug side effects. Curr Opin Drug Discov Devel 13:23–30
24. Schmitt N, Calloe K, Nielsen NH et al (2007) The novel C-terminal KCNQ1 mutation M520R alters protein trafficking. Biochem Biophys Res Commun 358:304–310
25. Chen J, Chen K, Sroubek J et al (2010) Post-transcriptional control of human ether-a-go-go-related gene potassium channel protein by alpha-adrenergic receptor stimulation. Mol Pharmacol 78:186–197
26. Mosley CA, Myers SJ, Murray EE et al (2009) Synthesis, structural activity-relationships, and biological evaluation of novel amide-based allosteric binding site antagonists in NR1A/NR2B N-methyl-D-aspartate receptors. Bioorg Med Chem 17:6463–6480
27. Wang L, Dennis AT, Trieu P et al (2009) Intracellular potassium stabilizes human ether-a-go-go-related gene channels for export from endoplasmic reticulum. Mol Pharmacol 75:927–937
28. Anumonwo JM, Horta J, Delmar M et al (1999) Proton and zinc effects on HERG currents. Biophys J 77:282–298
29. Chen J, Sroubek J, Krishnan Y et al (2009) PKA phosphorylation of HERG protein regulates the rate of channel synthesis. Am J Physiol Heart Circ Physiol 296:H1244–H1254
30. Vandenberg JI, Varghese A, Lu Y et al (2006) Temperature dependence of human ether-a-go-go-related gene K+ currents. Am J Physiol Cell Physiol 291:C165–C175
31. Milnes JT, Witchel HJ, Leaney JL et al (2010) Investigating dynamic protocol-dependence of hERG potassium channel inhibition at 37 degrees C: Cisapride versus dofetilide. J Pharmacol Toxicol Methods 61:178–191
32. Afrasiabi E, Hietamaki M, Viitanen T et al (2010) Expression and significance of HERG (KCNH2) potassium channels in the regulation of MDA-MB-435S melanoma cell proliferation and migration. Cell Signal 22:57–64
33. Gustina AS, Trudeau MC (2009) A recombinant N-terminal domain fully restores deactivation gating in N-truncated and long QT syndrome mutant hERG potassium channels. Proc Natl Acad Sci USA 106:13082–13087
34. Hancox JC, James AF (2008) Refining insights into high-affinity drug binding to the human ether-a-go-go-related gene potassium channel. Mol Pharmacol 73:1592–1595
35. Delisle BP, Underkofler HA, Moungey BM et al (2009) Small GTPase determinants for the Golgi processing and plasmalemmal expression of human ether-a-go-go related (hERG) K+ channels. J Biol Chem 284:2844–2853
36. Hancox JC, Witchel HJ, Varghese A (1998) Alteration of HERG current profile during the cardiac ventricular action potential, following a pore mutation. Biochem Biophys Res Commun 253:719–724
37. Ganapathi SB, Kester M, Elmslie KS (2009) State-dependent block of HERG potassium channels by R-roscovitine: implications for cancer therapy. Am J Physiol Cell Physiol 296: C701–C710
38. Jiang M, Zhang M, Maslennikov IV et al (2005) Dynamic conformational changes of extracellular S5-P linkers in the hERG channel. J Physiol 569:75–89
39. Babij P, Askew GR, Nieuwenhuijsen B et al (1998) Inhibition of cardiac delayed rectifier K+ current by overexpression of the long-QT syndrome HERG G628S mutation in transgenic mice. Circ Res 83:668–678
40. Perrin MJ, Kuchel PW, Campbell TJ et al (2008) Drug binding to the inactivated state is necessary but not sufficient for high-affinity binding to human ether-a-go-go-related gene channels. Mol Pharmacol 74:1443–1452

41. Potet F, Petersen CI, Boutaud O et al (2009) Genetic screening in *C. elegans* identifies rho-GTPase activating protein 6 as novel HERG regulator. J Mol Cell Cardiol 46:257–267
42. Ritchie TJ, Macdonald SJ (2009) The impact of aromatic ring count on compound developability – are too many aromatic rings a liability in drug design? Drug Discov Today 14:1011–1020
43. Sanguinetti MC, Mitcheson JS (2005) Predicting drug-hERG channel interactions that cause acquired long QT syndrome. Trends Pharmacol Sci 26:119–124
44. Singh JN, Kumar S, Berhe AH et al (2007) QT prolongation: paradigm shift in drug discovery and development. Curr Res Inform Pharm Sci 8:6–12
45. Pollard CE, Abi Gerges N, Bridgland-Taylor MH et al (2010) An introduction to QT interval prolongation and non-clinical approaches to assessing and reducing risk. Br J Pharmacol 159:12–21
46. Ponte ML, Keller GA, Di Girolamo G (2010) Mechanisms of drug induced QT interval prolongation. Curr Drug Saf 5:44–53
47. Roden DM (2004) Drug-induced prolongation of the QT interval. N Engl J Med 350:1013–1022
48. Wysowski DK, Bacsanyi J (1996) Cisapride and fatal arrhythmia. N Engl J Med 335:290–291
49. Shah RR (2005) Drugs, QT interval prolongation and ICH E14: the need to get it right. Drug Saf 28:115–125
50. Drolet B, Simard C, Roden DM (2004) Unusual effects of a QT-prolonging drug, arsenic trioxide, on cardiac potassium currents. Circulation 109:26–29
51. Mathie A (2010) Ion channels as novel therapeutic targets in the treatment of pain. J Pharm Pharmacol 62:1089–1095
52. Stary A, Wacker SJ, Boukharta L et al (2010) Toward a consensus model of the HERG potassium channel. ChemMedChem 5:455–467
53. Shimizu W, Moss AJ, Wilde AA et al (2009) Genotype-phenotype aspects of type 2 long QT syndrome. J Am Coll Cardiol 54:2052–2062
54. Chartrand E, Arnold AA, Gravel A et al (2010) Potential role of the membrane in hERG channel functioning and drug-induced long QT syndrome. Biochim Biophys Acta 1798:1651–1662
55. Larsen AP, Olesen SP, Grunnet M et al (2010) Pharmacological activation of IKr impairs conduction in guinea pig hearts. J Cardiovasc Electrophysiol 21:923–929
56. Witchel HJ (2010) Emerging trends in ion channel-based assays for predicting the cardiac safety of drugs. IDrugs 13:90–96
57. Hong HK, Park MH, Lee BH et al (2010) Block of the human ether-a-go-go-related gene (hERG) K+ channel by the antidepressant desipramine. Biochem Biophys Res Commun 394:536–541
58. Kang J, Chen XL, Wang H et al (2005) Discovery of a small molecule activator of the human ether-a-go-go-related gene (HERG) cardiac K+ channel. Mol Pharmacol 67:827–836
59. Zhou J, Augelli-Szafran CE, Bradley JA et al (2005) Novel potent human ether-a-go-go-related gene (hERG) potassium channel enhancers and their in vitro antiarrhythmic activity. Mol Pharmacol 68:876–884
60. Yang HT, Sun CF, Cui CC et al (2009) HERG-F463L potassium channels linked to long QT syndrome reduce I(Kr) current by a trafficking-deficient mechanism. Clin Exp Pharmacol Physiol 36:822–827
61. Thai KM, Windisch A, Stork D et al (2010) The hERG potassium channel and drug trapping: insight from docking studies with propafenone derivatives. ChemMedChem 5:436–442
62. Yap YG, Camm AJ (1999) Arrhythmogenic mechanisms of non-sedating antihistamines. Clin Exp Allergy 29(Suppl 3):174–181
63. Rajput SK, Singh JN, Sharma SS (2010) Evaluation of terfenadine and ketoconazole-induced QT prolongation in conscious telemetered guinea pigs. Pharmacol Rep 62:683–688

64. Hansen RS, Diness TG, Christ T et al (2006) Activation of human ether-a-go-go-related gene potassium channels by the diphenylurea 1,3-bis-(2-hydroxy-5-trifluoromethyl-phenyl)-urea (NS1643). Mol Pharmacol 69:266–277
65. Hansen RS, Diness TG, Christ T et al (2006) Biophysical characterization of the new human ether-a-go-go-related gene channel opener NS3623 [N-(4-bromo-2-(1H-tetrazol-5-yl)-phenyl)-N′-(3′-trifluoromethylphenyl)urea]. Mol Pharmacol 70:1319–1329
66. Zeng H, Lozinskaya IM, Lin Z et al (2006) Mallotoxin is a novel human ether-a-go-go-related gene (hERG) potassium channel activator. J Pharmacol Exp Ther 319:957–962
67. Lazzara R (1989) Amiodarone and torsade de pointes. Ann Intern Med 111:549–551
68. Zhou Z, Vorperian VR, Gong Q et al (1999) Block of HERG potassium channels by the antihistamine astemizole and its metabolites desmethylastemizole and norastemizole. J Cardiovasc Electrophysiol 10:836–843
69. Sadanaga T, Ogawa S (2007) Bepridil produces prominent bradycardia-dependent QT prolongation in patients with structural heart disease. J Electrocardiol 40:426–431
70. Barrows B, Cheung K, Bialobrzeski T et al (2009) Extracellular potassium dependency of block of HERG by quinidine and cisapride is primarily determined by the permeant ion and not by inactivation. Channels (Austin) 3:239–248
71. Kamiya K, Niwa R, Morishima M et al (2008) Molecular determinants of hERG channel block by terfenadine and cisapride. J Pharmacol Sci 108:301–307
72. Paakkari I (2002) Cardiotoxicity of new antihistamines and cisapride. Toxicol Lett 127: 279–284
73. Drolet B, Rousseau G, Daleau P et al (2000) Domperidone should not be considered a no-risk alternative to cisapride in the treatment of gastrointestinal motility disorders. Circulation 102: 1883–1885
74. Claassen S, Zunkler BJ (2005) Comparison of the effects of metoclopramide and domperidone on HERG channels. Pharmacology 74:31–36
75. Michael G, Dempster J, Kane KA et al (2007) Potentiation of E-4031-induced torsade de pointes by HMR1556 or ATX-II is not predicted by action potential short-term variability or triangulation. Br J Pharmacol 152:1215–1227
76. Esch JJ, Kantoch MJ (2008) Torsades de Pointes ventricular tachycardia in a pediatric patient treated with fluconazole. Pediatr Cardiol 29:210–213
77. Han S, Zhang Y, Chen Q et al (2010) Fluconazole inhibits hERG K(+) channel by direct block and disruption of protein trafficking. Eur J Pharmacol 650(1):138–144
78. Stark P, Fuller RW, Wong DT (1985) The pharmacologic profile of fluoxetine. J Clin Psychiatry 46:7–13
79. Leonardi ET, Azmitia EC (1994) MDMA (ecstasy) inhibition of MAO type A and type B: comparisons with fenfluramine and fluoxetine (Prozac). Neuropsychopharmacology 10: 231–238
80. Alvarez PA, Pahissa J (2010) QT alterations in psychopharmacology: proven candidates and suspects. Curr Drug Saf 5:97–104
81. Stauderman KA, Gandhi VC, Jones DJ (1992) Fluoxetine-induced inhibition of synaptosomal [3H]5-HT release: possible Ca(2+)-channel inhibition. Life Sci 50:2125–2138
82. Rae JL, Rich A, Zamudio AC et al (1995) Effect of Prozac on whole cell ionic currents in lens and corneal epithelia. Am J Physiol 269:C250–C256
83. Backer JM, Wjasow C, Zhang Y (1997) In vitro binding and phosphorylation of insulin receptor substrate 1 by the insulin receptor. Role of interactions mediated by the phosphotyrosine-binding domain and the pleckstrin-homology domain. Eur J Biochem 245: 91–96
84. Rajamani S, Eckhardt LL, Valdivia CR et al (2006) Drug-induced long QT syndrome: hERG K+ channel block and disruption of protein trafficking by fluoxetine and norfluoxetine. Br J Pharmacol 149:481–489
85. Varriale P (2001) Fluoxetine (Prozac) as a cause of QT prolongation. Arch Intern Med 161:612

86. Sanguinetti MC (1990) Na+1-activated and ATP-sensitive K+ channels in the heart. Prog Clin Biol Res 334:85–109
87. Bischoff U, Schmidt C, Netzer R et al (2000) Effects of fluoroquinolones on HERG currents. Eur J Pharmacol 406:341–343
88. Kang J, Wang L, Chen XL et al (2001) Interactions of a series of fluoroquinolone antibacterial drugs with the human cardiac K+ channel HERG. Mol Pharmacol 59:122–126
89. von Moltke LL, Greenblatt DJ, Duan SX et al (1994) In vitro prediction of the terfenadine-ketoconazole pharmacokinetic interaction. J Clin Pharmacol 34:1222–1227
90. Dumaine R, Roy ML, Brown AM (1998) Blockade of HERG and Kv1.5 by ketoconazole. J Pharmacol Exp Ther 286:727–735
91. Krantz MJ, Rowan SB, Schmittner J et al (2007) Physician awareness of the cardiac effects of methadone: results of a national survey. J Addict Dis 26:79–85
92. Weiss R, Mevissen M, Hauser DS et al (2002) Inhibition of human and pig ureter motility in vitro and in vivo by the K(+) channel openers PKF 217-744b and nicorandil. J Pharmacol Exp Ther 302:651–658
93. Katapadi K, Kostandy G, Katapadi M et al (1997) A review of erythromycin-induced malignant tachyarrhythmia–torsade de pointes. A case report. Angiology 48:821–826
94. Antzelevitch C, Sun ZQ, Zhang ZQ et al (1996) Cellular and ionic mechanisms underlying erythromycin-induced long QT intervals and torsade de pointes. J Am Coll Cardiol 28: 1836–1848
95. Rampe D, Murawsky MK (1997) Blockade of the human cardiac K+ channel Kv1.5 by the antibiotic erythromycin. Naunyn Schmiedebergs Arch Pharmacol 355:743–750
96. Drici MD, Knollmann BC, Wang WX et al (1998) Cardiac actions of erythromycin: influence of female sex. JAMA 280:1774–1776
97. Sekkarie MA (1997) Torsades de pointes in two chronic renal failure patients treated with cisapride and clarithromycin. Am J Kidney Dis 30:437–439
98. Woywodt A, Grommas U, Buth W et al (2000) QT prolongation due to roxithromycin. Postgrad Med J 76:651–653
99. Su Z, Martin R, Cox BF et al (2004) Mesoridazine: an open-channel blocker of human ether-a-go-go-related gene K+ channel. J Mol Cell Cardiol 36:151–160
100. Eap CB, Crettol S, Rougier JS et al (2007) Stereoselective block of hERG channel by (S)-methadone and QT interval prolongation in CYP2B6 slow metabolizers. Clin Pharmacol Ther 81(5):719–728
101. Maremmani I, Pacini M, Cesaroni C et al (2005) QTc interval prolongation in patients on long-term methadone maintenance therapy. Eur Addict Res 11:44–49
102. Routhier DD, Katz KD, Brooks DE (2007) QTc prolongation and torsades de pointes associated with methadone therapy. J Emerg Med 32:275–278
103. Chouabe C, Drici MD, Romey G et al (2000) Effects of calcium channel blockers on cloned cardiac K+ channels IKr and IKs. Therapie 55:195–202
104. Chouabe C, Drici MD, Romey G et al (1998) HERG and KvLQT1/IsK, the cardiac K+ channels involved in long QT syndromes, are targets for calcium channel blockers. Mol Pharmacol 54:695–703
105. Anson BD, Weaver JG, Ackerman MJ et al (2005) Blockade of HERG channels by HIV protease inhibitors. Lancet 365:682–686
106. Drolet B, Rousseau G, Daleau P et al (2001) Pimozide (Orap) prolongs cardiac repolarization by blocking the rapid component of the delayed rectifier potassium current in native cardiac myocytes. J Cardiovasc Pharmacol Ther 6:255–260
107. Kongsamut S, Kang J, Chen XL et al (2002) A comparison of the receptor binding and HERG channel affinities for a series of antipsychotic drugs. Eur J Pharmacol 450:37–41
108. Kang J, Wang L, Cai F et al (2000) High affinity blockade of the HERG cardiac K(+) channel by the neuroleptic pimozide. Eur J Pharmacol 392:137–140
109. Cubeddu LX (2009) Iatrogenic QT abnormalities and fatal arrhythmias: mechanisms and clinical significance. Curr Cardiol Rev 5:166–176

110. Grenadier E, Keidar S, Alpan G et al (1980) Prenylamine-induced ventricular tachycardia and syncope controlled by ventricular pacing. Br Heart J 44:330–334
111. Sanguinetti MC, Chen J, Fernandez D et al (2005) Physicochemical basis for binding and voltage-dependent block of hERG channels by structurally diverse drugs. Novartis Found Symp 266:159–166; discussion 166–170
112. Ando K, Sugiyama A, Takahara A et al (2007) Analysis of proarrhythmic potential of antipsychotics risperidone and olanzapine in anesthetized dogs. Eur J Pharmacol 558: 151–158
113. Haverkamp W, Breithardt G, Camm AJ et al (2000) The potential for QT prolongation and pro-arrhythmia by non-anti-arrhythmic drugs: clinical and regulatory implications. Report on a Policy Conference of the European Society of Cardiology. Cardiovasc Res 47:219–233
114. Gluais P, Bastide M, Grandmougin D et al (2004) Risperidone reduces K+ currents in human atrial myocytes and prolongs repolarization in human myocardium. Eur J Pharmacol 497: 215–222
115. Gluais P, Bastide M, Caron J et al (2002) Risperidone prolongs cardiac action potential through reduction of K+ currents in rabbit myocytes. Eur J Pharmacol 444:123–132
116. Botchway AN, Turner MA, Sheridan DJ et al (2003) Electrophysiological effects accompanying regression of left ventricular hypertrophy. Cardiovasc Res 60:510–517
117. Magyar J, Banyasz T, Bagi Z et al (2002) Electrophysiological effects of risperidone in mammalian cardiac cells. Naunyn Schmiedebergs Arch Pharmacol 366:350–356
118. Brown K, Levy H, Brenner C et al (1993) Overdose of risperidone. Ann Emerg Med 22:1908–1910
119. Sanguinetti MC, Jiang C, Curran ME et al (1995) A mechanistic link between an inherited and an acquired cardiac arrhythmia: HERG encodes the IKr potassium channel. Cell 81:299–307
120. Wang J, Best PM (1994) Characterization of the potassium channel from frog skeletal muscle sarcoplasmic reticulum membrane. J Physiol 477(Pt 2):279–290
121. Yap YG, Camm J (2000) Risk of torsades de pointes with non-cardiac drugs. Doctors need to be aware that many drugs can cause qt prolongation. BMJ 320:1158–1159
122. Zimbroff DL, Kane JM, Tamminga CA et al (1997) Controlled, dose-response study of sertindole and haloperidol in the treatment of schizophrenia. Sertindole Study Group. Am J Psychiatry 154:782–791
123. Simons FE, Simons KJ (1994) The pharmacology and use of H1-receptor-antagonist drugs. N Engl J Med 330:1663–1670
124. Tashibu H, Miyazaki H, Aoki K et al (2005) QT PRODACT: in vivo QT assay in anesthetized dog for detecting the potential for QT interval prolongation by human pharmaceuticals. J Pharmacol Sci 99:473–486
125. Martin RL, Su Z, Limberis JT et al (2006) In vitro preclinical cardiac assessment of tolterodine and terodiline: multiple factors predict the clinical experience. J Cardiovasc Pharmacol 48:199–206
126. Davis AS (1998) The pre-clinical assessment of QT interval prolongation: a comparison of in vitro and in vivo methods. Hum Exp Toxicol 17:677–680
127. Dumotier BM, Georgieva AV (2007) Preclinical cardio-safety assessment of torsadogenic risk and alternative methods to animal experimentation: the inseparable twins. Cell Biol Toxicol 23:293–302
128. Towart R, Linders JT, Hermans AN et al (2009) Blockade of the I(Ks) potassium channel: an overlooked cardiovascular liability in drug safety screening? J Pharmacol Toxicol Methods 60:1–10
129. Pugsley MK (2005) Methodology used in safety pharmacology: appraisal of the state-of-the-art, the regulatory issues and new directions. J Pharmacol Toxicol Methods 52:1–5
130. Anonymous (2000) The European Agency for the Evaluation of Medicinal Product. Human Medicine Evaluation Unit. ICH Topic S7. Safety Pharmacology Studies for Human Pharmaceuticals. Note for Guidance on Safety Pharmacology Studies in Human Pharmaceuticals. (CPMP/ICH/539/00)

131. Friedrichs GS, Patmore L, Bass A (2005) Non-clinical evaluation of ventricular repolarization (ICH S7B): results of an interim survey of international pharmaceutical companies. J Pharmacol Toxicol Methods 52:6–11
132. Anonymous (2005) ICH Harmonised Tripartite Guideline, The Non-clinical Evaluation of the Potential for Delayed Ventricular Repolarization (QT Interval Prolongation) by Human Pharmaceuticals S7B. Recommended for adoption at step 4 of the ICH process on12 May 2005 by the ICH Steering Committee. ICH; http://www.ich.org/
133. Shah RR (2005) Drugs, QTc interval prolongation and final ICH E14 guideline: an important milestone with challenges ahead. Drug Saf 28:1009–1028
134. Aronov AM, Goldman BB (2004) A model for identifying HERG K+ channel blockers. Bioorg Med Chem 12:2307–2315
135. Doddareddy MR, Klaasse EC, Shagufta et al (2010) Prospective validation of a comprehensive in silico hERG model and its applications to commercial compound and drug databases. ChemMedChem 5:716–729
136. Fenu LA, Teisman A, De Buck SS et al (2009) Cardio-vascular safety beyond hERG: in silico modelling of a guinea pig right atrium assay. J Comput Aided Mol Des 23:883–895
137. Su BH, Shen MY, Esposito EX et al (2010) In silico binary classification QSAR models based on 4D-fingerprints and MOE descriptors for prediction of hERG blockage. J Chem Inf Model 50:1304–1318
138. Nilsson MF, Danielsson C, Skold AC et al (2010) Improved methodology for identifying the teratogenic potential in early drug development of hERG channel blocking drugs. Reprod Toxicol 29:156–163
139. Suter W (2006) Predictive value of in vitro safety studies. Curr Opin Chem Biol 10:362–366
140. Ducroq J, Moha ou Maati H, Guilbot S et al (2009) Dexrazoxane protects the heart from acute doxorubicin-induced QT prolongation: a key role for I(Ks). Br J Pharmacol 159: 93–101
141. Toyoshima S, Kanno A, Kitayama T et al (2005) QT PRODACT: in vivo QT assay in the conscious dog for assessing the potential for QT interval prolongation by human pharmaceuticals. J Pharmacol Sci 99:459–471
142. Takahara A, Sasaki R, Nakamura M et al (2009) Clobutinol delays ventricular repolarization in the guinea pig heart: comparison with cardiac effects of HERG K+ channel inhibitor E-4031. J Cardiovasc Pharmacol 54:552–559
143. Cheng HC, Incardona J (2009) Models of torsades de pointes: effects of FPL64176, DPI201106, dofetilide, and chromanol 293B in isolated rabbit and guinea pig hearts. J Pharmacol Toxicol Methods 60:174–184
144. Roden DM (2004) Human genomics and its impact on arrhythmias. Trends Cardiovasc Med 14:112–116
145. Lazzerini PE, Capecchi PL, Laghi-Pasini F (2010) Anti-Ro/SSA antibodies and cardiac arrhythmias in the adult: facts and hypotheses. Scand J Immunol 72:213–222
146. Morganroth J (2007) Evaluation of the effect on cardiac repolarization (QTc interval) of oncologic drugs. Ernst Schering Res Found Workshop (59):171–184
147. Brembilla-Perrot B, Beurrier D, Terrier de la Chaise A (1994) Criteria of QRS duration in relationship to the age of myocardial infarction. Herz 19:235–242
148. Lehmann MH, Suzuki F, Fromm BS et al (1994) T wave "humps" as a potential electrocardiographic marker of the long QT syndrome. J Am Coll Cardiol 24:746–754
149. Miyazaki H, Tagawa M (2002) Rate-correction technique for QT interval in long-term telemetry ECG recording in beagle dogs. Exp Anim 51:465–475
150. Holzgrefe HH, Cavero I, Gleason CR (2007) Analysis of the nonclinical telemetered ECG: impact of logging rate and RR bin width in the dog and cynomolgus monkey. J Pharmacol Methods 56:34–42

Prediction of hERG Channel Inhibition Using In Silico Techniques

Andrea Schiesaro and Gerhard F. Ecker

Contents

Abstract Drug-induced long QT syndrome still represents a major risk for late-stage clinical failure of drug candidates. One of the main factors inducing long QT is inhibition of cardiac hERG channels. Early prediction of potential hERG

G.F. Ecker (✉)
Pharmacoinformatics Research Group, Department of Medicinal Chemistry, University of Vienna, Althanstraße 14, Vienna, 1090, Austria
e-mail: gerhard.f.ecker@univie.ac.at

S.P. Gupta (ed.), *Ion Channels and Their Inhibitors*,
DOI 10.1007/978-3-642-19922-6_7,

inhibitory activity of hits and lead compounds thus is of major importance in the drug discovery and development process. Both structure- and ligand-based approaches were used to develop models, which shed light on the molecular basis of hERG channel inhibition. In this article, an overview on recent approaches for prediction of hERG channel blockers has been provided.

Keywords hERG • Pharmacophore • QSAR • Classification • Homology model • Docking

Abbreviations

ADMET	Absorption, distribution, metabolism, elimination and toxicity
AUC	Area under the curve
CCR	Chemokine receptor
CoMFA	Comparative molecular field analysis
CoMSIA	Comparative molecular similarity indices analysis
CPG-NN	Counter-propagation neural network
CSD	Cambridge structural database
eag	Ether-a-go-go
ECG	Electrocardiogram
hERG	Human ether-a-go-go-related-gene K^+ channel
ISA	Iterative simulated annealing
KNN	*k* Nearest neighbor
LDA	Linear discriminant analysis
LIE	Linear interaction energy
LMS	Least median squares
LQTs	Long QT syndrome
LSER	Linear solvation energy relationship
MD	Molecular dynamics
PCA	Principal component analysis
PLS	Partial least squares
PLS-DA	Partial least squares discriminant analysis
PNN	Probabilistic neural network
QA	Quaternary ammonium
QSAR	Quantitative structure-activity relationship
RF	Random forest
ROC	Receiver operating characteristic
S	Transmembrane domain
SA	Simulated annealing
SAR	Structure-activity relationship
SOM	Self-organizing maps
SVM	Support vector machine
SVR	Support vector regression
TdP	Torsade de Pointes

1 Introduction

The ensemble of properties, which describe absorption, distribution, metabolism, elimination and toxicity (ADMET) are of utmost importance for the drug discovery process. In light of the studies on antitarget proteins responsible for poor ADMET properties of drug candidates, many high-throughput methods have been developed for early identification of compounds with a bad ADMET profile. In the past decade, many strategies were developed to screen libraries of compounds and to assess the risk of a bad ADMET profile. There is overwhelming evidence that the inhibition of the hERG potassium channel is directly correlated with a lethal arrhythmia called Torsade de Points. Thus, the discovery of unwanted interactions between compounds under development and the hERG channel is a killing criteria. One of the main challenges of antitarget proteins such as hERG, cytochrome P-450, P-glycoprotein and serum albumin is their polyspecificity. Even though the binding sites of many hERG blockers were indentified through docking into homology models, the molecular basis of the hERG polyspecificity is not clear yet. Due to the lack of crystal structures, ligand-based approaches were developed to predict the hERG activity of candidate compounds. Recent studies show that a combination of different methodologies, such as 2D- and 3D-QSAR with pharmacophore modeling and classification algorithms was quite successful and might be a powerful tool in the in silico screening of compound libraries. In this chapter, we will present selected in silico models developed to predict hERG channel blockers.

2 Long QT Syndrome

The cardiac action potential is composed of five phases. Phase 0 is characterized by rapid depolarization due to an inward Na^+ current. This phase is followed first by an initial short repolarization (phase 1) due to an outward K^+ current and then by a plateau (phase 2), which is characterized by a slow repolarization rate. During the plateau phase, an inward Ca^{2+} current is balanced by an outward K^+ current. In phase 3 of the cardiac action potential, the rapid and the slow delayed rectifier K^+ (I_{Kr} and I_{Ks}, respectively) determine the repolarization of the myocyte with its membrane potential to the resting state (phase 4). A long cardiac action potential is a safeguard mechanism that prevents the onset of potentially dangerous arrhythmias. However, this mechanism is not perfect, as a delay of cardiac repolarization prolongs the QT time.

Through the electrocardiogram is possible to register the electrical activity of the heart. The P wave registers the atrial depolarization, followed by the QRS complex, which registers the ventricular depolarization. The T wave finally corresponds to the ventricular repolarization. During the interval between the Q and T waves (QT interval), which is a measure of repolarization duration, the heart is refractory to new excitations. A delay in ventricular repolarization is registered in the ECG as

a prolonged QT interval. The Long QT syndrome (LQTs) is associated with increased risk of occurrence of potentially lethal arrhythmias called Torsade de Pointes (TdP). The LQTs is estimated to affect 1 person every 5,000–10,000 people [1]. The LQTs is mostly due to mutations of the hERG channel, a potassium-selective voltage-gated channel that conducts the I_{Kr} current, and to the KCNQ1 channel that encodes the Kv7.1 channel, which is responsible for the I_{Ks} current. Up to now, there are almost 300 mutations known to affect the hERG potassium channel.

Many classes of compounds known to block the hERG potassium channel prolong the QT interval and thus also might be involved in potentially dangerous arrhythmias such as TdP [2–21].

3 Structure of the hERG Channel

The name of the hERG potassium channel origins from the human homologous gene ether-a-go-go (eag) found in *Drosophila melanogaster*. The human-related ether-a-go-go-related gene is also called KCNH2 according to the new nomenclature, and the protein encoded is often referred to as hERG, even if the official annotation according to the new nomenclature name is Kv11.1.

The hERG potassium channel has a tetrameric architecture, where each subunit is formed by six transmembrane domains (S1–S6). Up to date two forms of hERG are known, hERG1a and hERG1b, which can form a homo- or hetero-tetrameric structure with different kinetic proprieties. Each subunit is formed by a voltage-sensing transmembrane domain (S1–S4), and the K^+-selective pore (S5–S6), which is responsible for the K^+ conduction.

The K^+ channel can be divided into three regions: the K^+-selectivity filter, the central cavity and the inner pore [22]. The K^+-selectivity filter is a narrow cylinder built to mimic perfectly an aqueous environment and to conduct specifically K^+ ions. The highly conserved signature sequence in the Kv channels (Thr/Ser-Val-Gly-Tyr/Phe-Gly) at the C-terminal end of the selectivity filter is responsible for the creation of the aqueous environment. The hydroxyl groups of Thr as well as the carbonyl groups of the other four amino acids form several octahedral binding sites, which coordinate the K^+ ions analogous to a water filled environment. The diameter of the cylinder is too large for the Na^+ ions and thus they cannot be well coordinated, so they stay in the aqueous environment where the water molecules coordinate the ions.

The central cavity is a wide water-filled pore located below the selectivity filter, whose size changes in the open and in the closed conformation.

The inner pore is located at the cytoplasmatic side of the membrane and connects the central cavity with the cytoplasm of the cell. It consists of two concentric rings made by four Tyr652 and four Phe656. The four Phe656 form the first ring located at the cytoplasmatic side of the hERG channel. The four Tyr652 build the second ring, which faces the central cavity. These two concentric rings are considered the main

feature responsible for the polyspecificity of the hERG channel, mainly due to the possibility to make multiple and compound specific interactions. In the closed conformation, the S6 domains intersect at the cytoplasmatic side of the channel, closing the inner pore and preventing the flow of K^+ ions. During channel activation, the S6 domains rotate outward, opening the inner pore and allowing ions to flow.

The hERG channel and other K^+-channels contain a PAS domain on the cytoplasmic N-terminus, [23] which is involved in protein-protein interactions. Although the function of the PAS domain in the hERG channel is not understood, mutagenesis studies show that disruption of this domain reduces the outward current and prolongs the QT interval [24].

Also, the role of the C terminus domain is not yet completely clarified, although a cAMP-binding domain is located there. cAMP accelerates the deactivation kinetics of the hERG channel [25].

4 Ligand-Based Approaches

4.1 Pharmacophore Models

Several pharmacophore models have been published up to date. They provide a powerful tool for the identification of potential hERG blockers by virtual screening of compound databases. Some pharmacophore models were already reviewed elsewhere [26, 27].

Morgan and Sullivan [28] analyzed a set of class III antiarrhythmic drugs. In the pharmacophore model, the charged nitrogen is linked by 1–3 atoms to two features, which might be an aromatic ring or an alkyl moiety. A third feature, consisting of a para-substituted ring, is linked with the charged nitrogen through a chain of 1–4 atoms. The model derived by Ekins et al. [29] was generated from a training set of 15 compounds taken from the literature. The pharmacophore model contains one positive ionizable feature connected with four hydrophobic moieties. A "constructionist approach" was used by Cavalli et al. [30] to develop a pharmacophore model. The crystal structure of astemizole was used as template on which molecules with similar geometry were aligned, leading to the addition of new pharmacophoric features, which were not present in the previous pharmacophore. To the initial pharmacophore consisting of a basic nitrogen (N) and two aromatic features (C0 and C1), a fourth feature defined by the aromatic ring (C2) of an astemizole derivative was added. Thus, the charged nitrogen group (N) is connected to three aromatic groups (C0–C2). The authors noted that all the hERG blockers tested have the C0 feature, while some molecules lack the C1 or C2 moieties. They also found that a polarizable function in C0, such as a carboxylic or a sulfonamidic group, may also influence the activity.

Pearlstein et al. [21] developed a "drain plug" model through a combination of hERG homology modeling and the CoMSIA analysis of 22 sertindole derivatives and 10 structurally diverse hERG inhibitors. The analysis of the hERG homology model reveals a "drain plug" picture, which is complementary to the shape of the cavity, where the amino acids responsible for the interactions are located. The "drain plug" pharmacophore model consists of two aromatic groups that can interact with Phe656, and a basic nitrogen that might interact with Tyr652. They also suggest that a hydrophobic or an aromatic substituent in this portion of the molecule might improve the potency of hERG blockers through the interaction with Tyr652.

Aronov et al. [31] used a set of 85 hERG blockers to develop three hypotheses of three-point pharmacophores. The first two hypotheses are in agreement with the C0–N–C2 and C0–N–C1 pharmacophores published by Cavalli et al. [30]. In the third pharmacophore model, there is a hydrogen bond acceptor feature placed between the charged nitrogen and the aromatic ring, at a distance of 1.8–3.7 Å from the latter one. Similarly, Testai et al. [32] found that an acceptor feature is normally placed within 4–6 Å from an ionizable center.

Aronov et al. [33] also used the pharmacophore elucidation module implemented in MOE to analyze an in-house dataset of 194 uncharged compounds. At the beginning, two-point queries are generated and used to make more complex *n*-point queries through a "build up" method. Two five-point pharmacophore models containing three hydrophobic/aromatic features and two hydrogen bond acceptors were selected from all generated pharmacophore models. These two five-point pharmacophore models, which differ only in the position of one of the hydrogen bond acceptors, were merged into a six-point pharmacophore. The two five-point pharmacophores were able to correctly classify 78% and 69% of potent hERG blockers of the dataset. The six-point pharmacophore matched 21% ($IC_{50} < 10\ \mu M$) and 44% ($IC_{50} < 30\ \mu M$) of hERG blockers and 4% of nonblockers. Applying a ClogP > 1 cutoff, the number of false-positives was reduced in all three models.

Crumb et al. [34] developed a qualitative pharmacophore model through the analysis of 11 antipsychotic drugs. The model, which consists of one aromatic query surrounded by three hydrophobic moieties, is matched by the most potent hERG blockers present in the dataset.

A collection of 1,075 hERG inhibitors was used by Johnson et al. [35] to develop a series of pharmacophore and QSAR models. As seen in previous studies, the basic nitrogen, which is placed 6–9 Å apart from a centroid of an aromatic ring, was found to be an important feature for hERG blockers. In the second pharmacophore model, the effect on the activity of the basic nitrogen is attenuated by the presence of two hydrogen bond acceptors and a lipophilic group. This might be a useful hint for development of compounds without reduced hERG blocking activity. In the third pharmacophore, the aromatic rings are placed at the opposite side of the molecule and are separated by 14 bonds. In the fourth model, the aromatic ring feature is coupled with a hydrogen bond moiety. The fifth pharmacophore model consists of two aromatic rings placed within 6–13 Å from two hydrogen bond donors.

With the aim to subdivide specific and nonspecific hERG blockers in a dataset of 113 compounds, Kramer et al. [36] developed a method where pharmacophore and QSAR techniques are combined. SA15 (sertindole analogue), clemastine, tolterodine, and haloperidol were used to build the first pharmacophore model. Similar to other published models, it contains a positive ionizable nitrogen feature connected to two aromatic/hydrophobic features, one of which is in close proximity with a hydrophobic spot. The model was tested against the entire dataset and 51 compounds matched the pharmacophore. The potent hERG blockers astemizole, cisapride, flunarizine, and sertindole, which match the first pharmacophore model, were used to develop a more specific model. Differently from the first pharmacophore, in this model the hydrophobic queries are directly connected with the charged nitrogen. The second model is similar to the one obtained by Cavalli et al. [30].

Through the analysis of 56 compounds using Catalyst Garg et al. [37] generated seven models. The most predictive pharmacophore model consists of one hydrophobic group (HP), one aromatic ring (RA) and one hydrogen bond acceptor lipid group (HBAl), which are three important features for potent hERG blockers. This model was able to find 22 of the 25 potent blockers in the dataset, showing to be capable to distinguish between potent and nonpotent blockers.

With the aim to avoid the potentially lethal hERG blockage of chemokine receptor antagonists, Shamovsky et al. [38] analyzed the influence of four classes of fragments on the hERG inhibition. They obtained two pharmacophore models. The first pharmacophore model consists of one aromatic ring, one basic center, two hydrogen bond donors, and one hydrogen bond acceptor. The fragments that match this pharmacophore increase the hERG blocking potency even if they decrease the lipophilicity of the compounds. In the second pharmacophore model there are two aromatic rings connected with a basic nitrogen. Here, the fragments that match this pharmacophore increase the hERG potency by increasing the lipophilicity of the compounds.

Coi et al. [39] generated a "toxicophore" using the docking poses of compounds docked in the hERG channel in the closed state. The analysis of the interactions of the lowest-energy poses with the hERG channel shows that there are several hot spots in the binding site: Ser624 (E), Gly657 (I), the region around Phe656 (H), and four cavities in the region around Tyr652 (C). The docking pose of the potent hERG blocker astemizole was used as "template" to generate the toxicophore. The analysis of the poses of astemizole, haloperidol, ritanserine, R59022, cisapride, spiperone, 8-hydroxy-DPAT, sotalol, quinidine, trifluperidol, and tetracaine, allowed the identification of the features needed to interact with the hERG channel: (a) the optimal distance between the protonated nitrogen and an hydrogen-bond acceptor is 4.5 Å; (b) aromatic rings located in I or in E. Moreover, the authors suggest that also hydrophobic interactions with the amino acids located in C and/or H should be avoided. To evaluate the toxicophore, 18 known hERG blockers/nonblockers were docked into the homology model of the hERG channel in the closed state. The results confirmed that the toxicophore is able to distinguish between hERG inhibitors and noninhibitors.

In summary, the pharmacophore models suggest that the hERG blockers are characterized by the presence of a protonated nitrogen linked with two or three hydrophobic and/or aromatic moieties. The only exception is the pharmacophore model obtained by Aronov et al., which was generated solely by uncharged molecules. This indicated that the development of uncharged compounds is not a safe way to avoid unwanted inhibition of the hERG channel. The charged nitrogen atom, the hydrophobic and the aromatic features might interact with the amino acids Tyr652 and Phe656. Some pharmacophore models suggest also that hydrogen-bond donor and/or acceptor groups might play an important role for hERG inhibition, probably by interaction with Thr623, Ser624, or Ser649.

4.2 3D-QSAR

The first 3D-QSAR model for prediction of hERG blockers was developed by Ekins et al. [29] through the analysis of 15 molecules with Catalyst. These compounds are characterized by the presence of one ionizable feature and four hydrophobic moieties. The pharmacophore shows the presence of one ionizable feature surrounded by four hydrophobic features. The 3D-QSAR model shows a high correlation with an r^2 of 0.90, and also a good performance in the prediction of the activity of the external test set, with an r^2 of 0.83. The ability of the model to correctly rank the hERG blockers according to their IC_{50} values achieved a Spearman's rank coefficient of 0.76 and 0.77 for the training and the test set, respectively. The excellent performance of the model for both qualitative prediction and quantitative ranking of hERG inhibitors indicates that it is a suitable tool to discover potential hERG blockers.

Cavalli et al. [30] developed a 3D-QSAR model through the analysis of 31 hERG blockers using the CoMFA technique. For most of the molecules, the 3D structure was retrieved from the Cambridge Structural Database (CSD) or by adding substituents to the crystallographic structure. Three-dimensional structures of additional molecules were generated with SYBYL. The alignment of the molecules was performed using the previously generated pharmacophore. The model shows a good predictive performance with $r^2 = 0.95$ and $q^2 = 0.74$. In a further validation using a test set of compounds not involved in the model generation, an r^2 of 0.74 was achieved. The comparison of the pharmacophore and the CoMFA models shows that the pharmacophoric features C1 and C2 are sterically favorable regions, while C0 is influenced by the steric and electrostatic properties of the compounds. In particular an increased volume in C0 will decrease the activity, while an opposite effect is predicted for charged groups.

Through the application of the CoMSiA technique, 22 sertindole analogues and a set of 10 structurally different hERG blockers were analyzed by Pearlstein et al. [21]. The best model reached a q^2 of 0.571. Docking studies performed in a homology model of the hERG channel in the open state could explain the pharmacophore and the CoMSiA models.

In total 882 compounds were used by Cianchetta et al. [40] to develop a GRIND-based model. Four probes representing hydrophobic interactions (DRY), hydrogen bond acceptor (sp^2 carbonyl oxygen), hydrogen bond donor (neutral flat amide NH), and the molecular shape (TIP) were used to calculate the GRIND descriptors. The correlation between the GRIND descriptors and the pIC_{50} values of the hERG blockers was analyzed through multivariate techniques such as principal component analysis (PCA) and partial least squares (PLS). The dataset was subdivided into two subsets characterized by the presence or absence of a basic nitrogen atom. The 338 hERG blockers, which form the subset of compounds without a charged nitrogen, were subdivided into a training set of 322 compounds and a test set of 16 molecules. The model obtained resulted in four latent variables and showed an r^2 of 0.76 and a q^2 of 0.72. The 544 compounds that constitute the charged nitrogen database were split into a training set of 518 molecules and in a test set of 26 compounds. The model obtained from the PLS regression analysis had three latent variables yielding an r^2 of 0.77 and a q^2 of 0.74. The descriptors involved in the two models were practically identical. The authors suggest that this might indicate that the charged and noncharged compounds share the same binding mode. The two models differ in terms of distance between the edge of the molecule and the space between a hydrophobic MIF and a hydrogen bond donor group. In the first case, the distance for the optimum space between the two fields generated is 25 Å for the noncharged molecules and 29 Å for the charged compounds. In the second case, the DRY/hydrogen bond distance for the noncharged compounds is 14 Å, while for the charged molecules it is 21 Å. Statistical analysis shows that in both models a hydrogen bond moiety close to the edge of the molecules plays an important role.

Johnson et al. [35] analyzed 1,075 compounds through a combination of physicochemical and pharmacophoric descriptors. Least median squares (LMS) regression was used to analyze the 925 compounds of the training set and the resulting model shows an r^2 of 0.65 and a q^2 of 0.66. In a further test using 1,679 compounds, the model showed an r^2 of 0.54. These compounds were then clustered based on Daylight Fingerprint Tanimoto using the average linkage method and a similarity cutoff of 0.7. In the largest cluster, the model achieved an r^2 of 0.32. However, when only the compounds in the training set with a Tanimoto similarity greater than 0.65 were considered, the r^2 for the validation set increased to 0.72.

With the aim to develop a model able to discriminate between hERG inhibitors and noninhibitors, Li et al. [41] combined pharmacophore-based GRIND descriptors and support vector machine (SVM) techniques. Four GRIND probes representing hydrophobic interactions (DRY), hydrogen bond acceptors (sp^2 carbonyl oxygen), hydrogen bond donors (NH neutral flat amide), and molecular shape descriptors (TIP) were used. From a library of 495 compounds, only the 192 molecules with IC_{50} values lower than 40 μM were considered. The model generated from the PLS analysis consists of three latent variables and shows a rather poor r^2 of 0.34 and a q^2 of 0.07. The analysis of the predicted versus the experimental pIC_{50} shows that the IC_{50} of sertindole derivatives is overestimated. A better model with $r^2 = 0.57$ and $q^2 = 0.41$ was obtained considering only the hERG blockers with an IC_{50} value lower than 32 nM and by removing the sertindole

derivatives. The analysis of the influence of the descriptors highlights that the descriptor related to two hydrogen donor atoms placed at a distance of 9 Å has the highest principal component coefficient. This descriptor is encoded by the charged nitrogen atom. Also, the descriptors related to the presence of a hydrogen bond acceptor and a hydrogen bond donor (6 Å or 9.5 Å apart), to the presence of the hydrophobic moiety and a hydrogen bond donor (9 Å or 16 Å apart) and to the hydrogen bond donor and one of the edges of the molecule (10 Å or 17.5 Å apart), show a high correlation with biological activity. These data are in agreement with the model published by Cianchetta et al. [40].

In a recent study, Kramer et al. [36] reported a predictive QSAR model able to distinguish between specific and nonspecific binding. 113 compounds from the literature were split into six groups of equal activity range. From the 113 compounds, 15 molecule were randomly selected as validation set. The remaining 98 compounds were divided into a training set of 75 molecules and a test set of 23 molecules. The uncharged forms of the compounds were used to calculate 1D-, 2D-, and 3D-descriptors such as the molecular electrostatic potential (MEP), the local ionization energy (IEL), the local electron affinity (EAL), the local polarizability (POL), and the Shannon entropies (SHANI and SHANE). The first model was obtained using a combination of ε-SVR and multiple linear regression descriptor selection. An r^2 of 0.81 for the training set was obtained by using EALmax, EALmin, POLmin, SHANIbar, Naryl, shapeQ2, and shapeQ4 descriptors. The model shows a good performance also for the validation set with an r^2 of 0.70, while the q^2 is 0.50. In the second model the Naryl, shape and EALmin descriptors were selected. The statistical analysis of this model resulted in an r^2 for the training, test and validation set of 0.64, 0.61, and 0.62, respectively. The Naryl descriptor encodes for the number of aromatic rings in the molecule, and its selection highlights that the potency of the blockers is correlated with the number of aromatic rings. The shape descriptors are a measure of the shape similarity with astemizole, cisapride and sertindole. They have a positive sign, indicating that the more the shape of the molecule is similar to those of one of the three compounds cited above, the higher is the probability of the compound to be a potent blocker. The EALmin descriptor has a positive value, which might suggest that the potency of the hERG blockers is decreased if the minimum electron affinity decreases. Additional six models were generated, all of them showing quite satisfactory performance. These six models describe a specific or an unspecific binding type. In general, the models suggest that the affinity of the blockers is correlated with the similarity of the compounds with the three hERG inhibitors cited above, and with the number of aromatic rings present. To decrease the hERG potency, it is necessary to introduce electronegative moieties, such as carbonyl groups, as indicating by the EALmin descriptor.The Positive coefficient of the ClogP indicates that decreasing the lipophilicity of the compounds might also lead to a hERG affinity decrease. In addition, the number of hydrogen-bond donors is negatively correlated with the potency, probably due to the desolvation penalty that cannot be compensated by the hydrogen–bond interactions with the amino acids facing the central cavity of the hERG channel.

Ermondi et al. [42] reported a GRIND-based 3D-QSAR model generated by the ALMOND software. They used the 31 hERG blockers that Cavalli et al. [30] used to develop the CoMFA model, and six compounds as a test set. The descriptors were calculated using probes that represent the hydrophobic interaction (DRY), hydrogen bond acceptor properties (sp^2 carbonyl oxygen), hydrogen bond donor properties (neutral flat amide NH), and molecular shape (TIP probe). The PLS analysis resulted in a model with three latent variables, which shows an r^2 of 0.93 and a q^2 of 0.69. The analysis of the model suggests that the presence of aromatic rings on the edges of the molecule, hydrogen bond donor moieties not related to the basic nitrogen, hydrogen bond acceptors far from the aromatic rings and placed at the same distance of the hydrogen bond donors from the aromatic group, increase the potency of the hERG blockers. The 37 molecules were also analyzed using the DRY-DRY GRIND descriptors. Interestingly, the PC1 discriminates between the potent blockers and the weak blockers. In particular, it highlighted that the potent blockers have two or more hydrophobic regions far away from each other. The ALMOND model was compared with the CoMFA model obtained by Cavalli et al. [30]. Both models show a comparable predictivity and have problems to predict the activity of lipophilic hERG blockers. In the ALMOND model, there is a second hydrophobic feature, which is missing in the CoMFA model, probably due to the different calculation methods for hydrophobic interactions.

The 3D-QSAR techniques, such as Catalyst, CoMFA, CoMSiA, and ALMOND have proven to be a powerful tool for hERG potency prediction. Together with the pharmacophore models, 3D-QSAR shed light on the molecular determinants that characterize hERG inhibitors, and provided insights for the potential binding mode of blockers. The 3D-QSAR models further underline the importance of a basic nitrogen, of a hydophobic/aromatic moieties, and of a hydrogen bond donor and acceptor groups.

4.3 2D-QSAR

Although 3D-QSAR techniques are a powerful resource in the drug discovery process and 3D-models can be very useful to discover compounds, which potentially block the hERG channel, they suffer from limitations due to the requirement of conformational sampling alignment (CoMFA, CoMSiA).

Aptula et al. [43] developed a 2D-QSAR model based on the stepwise regression analysis using the hydrophobicity corrected for ionization (logD) and the maximum diameter for the molecules (Dmax) as descriptors. The model, based on 19 molecules, shows a good internal and external validation with an r^2 of 0.87 and a q^2 of 0.73. The analysis of 81 hERG blockers highlights that the most active compounds have a Dmax $>$ 18 Å, indicating that the cavity of the hERG channel is big enough to accommodate large compounds.

Keserü et al. [44] developed a QSAR model for a series of 55 hERG inhibitors. The model consists of five descriptors, such as ClogP, molar refractivity, partial

negative surface area, polarizability (Volsurf W2), and hydrophobicity (Volsurf D3). It shows a good performance with an r of 0.97. The five descriptors indicate that lipophilic, polarizable compounds with a basic moiety and a large size might interact with the hERG channel. The model was evaluated with a test set of 13 compounds, and gained an r value of 0.75. In a second test, the model was evaluated in the ability to classify 82 active and nonactive compounds selected from the World Drug Index. The molecules of the dataset with an $IC_{50} < 1$ μm were considered as actives. The model showed a good performance classifying correctly 83% of the blockers and 82% of the nonblockers. Also, a hologram QSAR model was generated using the same data set. The model shows an excellent performance with an r value of 0.98. The test set achieved an r value of 0.90, indicating that the model has also a high predictive power. For the active compounds of the World Drug Index, the model was able to correctly classify 81% of the molecules. The HQSAR model was further tested against 743 compounds approved in the World Drug Index, where it achieved a low rate of false positive (18%).

Five QSAR models with a q^2 ranging from 0.65 to 0.90 were developed by Fioravanzo et al. [45], where 29 compounds from a training set and 30 compounds from a test set were analyzed through PLS and PCA techniques with EVA and DRAGON descriptors.

Song et al. [46] used a combination of fragment-based descriptors, support vector regression (SVR), partial least squares (PLS) and random forest (RF) to develop a QSAR model to predict the activity of hERG blockers. Seventy-one compounds were initially used to calculate and identify fragment descriptors correlated with hERG inhibition. Subsequently, they were used to build SVR, PLS, and RF models. Nineteen compounds served as test set. The best performance was achieved by the SVR model with an r^2 of 0.91 and a q^2 of 0.64. The model showed also a good performance for the test set with an r^2 of 0.85. The analysis of the fragment descriptors highlights that lipophilic fragments have a positive impact on the hERG activity, while hydrophilic moieties generally decrease the binding affinity. Fluorine and methane sulfonamide are two exceptions on this general rule. The two moieties, despite their hydrophilic nature, are positively related with the hERG activity. The model also reveals that tertiary amines are important for drug binding.

The role of the nitrogen atom on the hERG activity of compounds was studied by Zolotoy et al. [47]. They found that a tertiary amino group is present in 84% of the hERG channel blockers with $IC_{50} < 1$ μM. In 73% of the inhibitors with 1 μM $< IC_{50} < 10$ μM the charged nitrogen is located at the periphery of the compounds. In 84% of the weak blockers, the amine is primary, secondary, or neutral.

The CODESSA program was used by Coi et al. [48] to study a series of hERG blockers. Two experiments were performed. In the first experiment, the compounds of the dataset were divided into 55 and 27 molecules for the training and test set, respectively. The first model showed an r^2 of 0.77 using 12 descriptors. The training and the test set used to generate the second model contained 64 and 18 compounds, respectively. The best model selected for this sets showed an r^2 of 0.74 using nine descriptors. The analysis of the descriptors selected in the two models highlighted

that the relative number of double bonds (RNDBs), the factorized molecular volume (MV/XYZB), the relative number of carbon atoms (RNCAs) and the relative negative charge (RNCG) are the most important descriptors. The first two descriptors are negatively correlated with the pIC_{50}, highlighting that the hydrophobicity and the proprieties related to the volume of the molecules increase the potency of the hERG blockers. These two descriptors might explain why the ideal hERG blocker candidates are hydrophobic molecules with a large size, as in the case of some potent hERG blockers such as MK-499 and astemizole. On the contrary, small molecules with high globularity lacking hydrophobic moieties normally show a lower ability to block the hERG channel.

Yoshida et al. [49] analyzed 104 compounds collected from the literature. The model included the topological polar surface area (TPSA), the octanol/water partition coefficient (ClogP), the largest value in the distance matrix (diameter) and the summed surface area of atoms with partial charges from −0.25 to 0.20 (PEOE_VSA-4). They also introduced an indicator variable (Cell) indicating whether the drugs were tested in the hERG channels expressed in HEK cells (value of 0), or in CHO cells (value of 1). In the most significant model the statistical analysis showed an r^2 of 0.70 and a q^2 of 0.67. The interactions between the hERG channel and the blockers occur in the inner cavity. Many studies show that the size of the cavity is big enough to accommodate large compounds, and this is fully in agreement with the positive coefficient of the diameter descriptor. The Positive coefficient for the PEOE_VSA-4 descriptor might be explained by the interactions with amino acids such as Thr623, Ser624, Ser649, and Tyr652, which are capable to form hydrogen bond interactions. The pore region has a hydrophobic nature due to the high number of hydrophobic amino acids, thus the potency of the drugs increase with the ClogP of the molecules. In contrast, increasing the hydrophilicity of the compounds, represented by the TPSA descriptor, decrease hERG potency.

Seierstad et al. [50] reported a combination of models based on neural network ensembles with different representations of the structural properties. For 439 compounds, six sets of descriptors were calculated using DirectedDiversity, comprising 117 Kier-Hall (KH) topological indices, 142 Ghose–Crippen atom types, 166 Isis keys, 150 atom pair descriptors, 49 electrotopologic state descriptors, six common medicinal chemistry descriptors, and 146 2D descriptors calculated with the Molecular Operating Environment (MOE) package. To select the descriptors, different feature selection algorithms were employed comprising four filter-based ones such as PCA, correlation with response variable, difference in distribution between actives and inactives, training error of single-feature models, and two wrapper-based such as Forward stepwise selection and Simulated annealing. The neural network and neural network ensemble models were obtained from tenfold cross-validation procedures. The authors found that the "neural network ensembles have greater generalization ability and are less susceptible to the particular choice of training and test sets" showing that this methodology is a powerful tool for hERG prediction. In the filter-type technique, the PCA showed the best performance, although the simulated annealing reached the highest r^2 value. The 2D model,

which is based on 20 descriptors selected through the simulated annealing technique, shows an r^2 of 0.76. The model, tested with an external validation set of 40 compounds, achieves an r^2 of 0.52. Each of the 20 descriptors was used alone to build a model and the cross-validation r^2 values were calculated. As in many other models, the top scoring descriptors, such as AlogP and L-10-L (which describe two hydrophobic moieties separated by a chain of the atoms) shows that hydrophobic interactions and π–stacking are important for hERG blocking. The highest r^2 value was obtained with the model generated using only the descriptor F-C_1sp^2 (fluorines connected to sp^2 carbons). The importance of this group might depend on its ability to form strong π–stacking interactions. The Goose-Crippen atom type O in phenol, enol and carboxyl OH shows a negative correlation with the hERG inhibition. It is noteworthy that two of the three compounds, which show the largest error contain a carboxylic moiety, thus the model seems to underestimate its contribution to the decrease of hERG inhibition.

Ekins et al. [51] showed that also recursive partitioning models can be applied for early discovery of potential hERG blockers. Ninety-nine compounds from literature sources were used to develop two models using the ChemTree software package. In the first model 99 compounds were used to generate 100 random models using 564 path length molecular descriptors. The model showed a good IC_{50} correlation with an r^2 of 0.90, but the prediction of the 35 compounds of the validation test set resulted in an r^2 of 0.33. In the second model, 134 compounds were used to generate 694 path length descriptors, which were employed in the generation of 100 random models. The second model showed a lower r^2 value (0.85).

Leong et al. [52] used a combination of pharmacophore modeling and SVMs to predict the potency of hERG blockers. The model obtained from the 26 compounds of the training set had an r^2 of 0.97, while for the 13 compounds of the validation test set the q^2 value was 0.94.

Recently, Gavaghan et al. [53] studied 1,312 compounds through the combination of D-optimal onion design, PLS, and PCA techniques. The molecular descriptors calculated with the software packages Selma, DRONE, and VolSurf were integrated with fragment-based descriptors, which were used to calculate base level PLS models from each descriptor set. The scores generated from the base level PLS models were combined and used as descriptors in the upper level hierarchical PLS models. The best hierarchical PLS model generated from 13 descriptors and a training set of 436 compounds showed a q^2 of 0.59. The model was tested with an additional external test set of 7,520 compounds, composed of 4,813 actives and 2,707 inactives. Unfortunately, the model was unable to distinguish between potent, moderate, and nonactive blockers.

Recently, a dataset of 68 compounds collected from the literature was used by Garg et al. [37] to perform a 2D-QSTR analysis based on S_sNH2 (primary amines), JX (Balaban index), Kappa-3 (third order of Kier shape index), ADMET_PPB (tendency to bind to plasma protein), Atype_O_57 (atom type Oin phenol, enol, carboxyl OH), Atype_O_59 (atom type O in Al-O-Al) and Atype_H_46 (atom type H attached to Csp^0_3) descriptors. The model shows a good prediction ability achieving an r^2 of 0.84 and a q^2 of 0.78. In a validation

with an external test set of 12 molecules, the QSTR model shows an r^2 value of 0.70. The importance of the Kappa-3 descriptor might indicate that the molecular shape can play a role in the hERG interaction. The S_sNH2 descriptor highlights that the presence of a primary amine group increases hERG inhibition. The Balaban index is inversely correlated with hERG potency, indicating that it might be possible to decrease the activity of hERG blockers by increasing the branching of the molecule. All the A-type descriptors are negatively correlated with the inhibition of the hERG channel. This suggests that hERG potency decreases by adding electronegative groups.

Shamovsky et al. [38] studied hERG selectivity of four classes of chemokine receptor (CCR) ligands. In this study, the baseline lipophilicity relationship (BLR) approach was used to increase the hERG selectivity of compounds. Mathematically, the BLR is:

$$\mathrm{pIC}_{50} = a \times \log D - k \times \Delta G_{\mathrm{intr}} + \mathrm{const}, \tag{1}$$

pIC_{50} = potency of the compound; a = hydrophobicity factor of the binding site; D = n-octanol/water partition coefficient; ΔG_{intr} = intrinsic binding energy nonrelated with the desolvation; k = coefficient equal to $(2.303 \times RT)^{-1}$.

The term $a \times \log D$ is the lipophilicity driven component of potency caused by desolvation. The second term $-k \times \Delta G_{\mathrm{intr}}$ is the intrinsic potency, which depends on the molecular interactions of the ligand with the target. When the hERG selectivity of the compound (C) is taken into consideration, the equation becomes:

$$\mathrm{pIC}_{50}^{\mathrm{C}} - -\mathrm{pIC}_{50}^{\mathrm{hERG}} = \left(\mathrm{pIC}_{50}^{\mathrm{C}} - a^{\mathrm{hERG}} \times \log D\right) + k \times \Delta G_{\mathrm{intr}}^{\mathrm{hERG}} + \mathrm{const} \tag{2}$$

The term $k \times \Delta G_{\mathrm{intr}}^{\mathrm{hERG}}$ does not depend on the interactions with the primary target. The term $\left(\mathrm{pIC}_{50}^{\mathrm{C}} - a^{\mathrm{hERG}} \times \log D\right)$ (lipophilicity-adjusted primary potency) is independent on the hERG binding affinity. The lipophilicity-adjusted hERG potency $\left(\mathrm{pIC}_{50}^{\mathrm{hERG}} - a^{\mathrm{hERG}} \times \log D\right)$ was used in a fragment-based QSAR analysis to identify moieties that form important nonhydrophobic interactions with the hERG channel. The fragment-based QSAR analysis in a given chemical series ranks the fragments according to their contribution to the hERG potency. The regression analysis using (1) shows that a^{hERG} is close to one for all four classes of compounds. This means that if the lipophilicity increases by one unit, also the hERG potency increases. Further analysis of (1) indicates that the lipophilicity has a stronger influence on hERG potency than on hERG selectivity. This renders it quite difficult to enhance the hERG selectivity by decreasing the lipophilicity, suggesting that it is easier to improve the hERG selectivity by increasing the lipophilicity-adjusted primary potency value.

In a follow-up study, Shamovsky et al. [54] used 464 CCR8 antagonists and 8 hERG mutants to increase the selectivity of the compounds toward the hERG channel. A 2D fragment-based QSAR analysis performed on a subset of 25 spirocyclic CCR8 antagonists revealed that bulky and rigid substituents decrease the hERG affinity due to van der Waals clashes with Phe656.

Based on a dataset of 67 compounds, 50 in the training set and 17 in the test set, Roy et al. [55] combined the extended topochemical atom (ETA) indices for diverse hERG blockers and non-ETA-descriptors with factor analysis followed by multiple linear regression, stepwise regression, and PLS, to develop QSTR models. The best model was obtained combining ETA and non-ETA descriptors (r^2 of 0.619 and a q^2 of 0.546). The model indicates that the hERG affinity is increased by enlarging the size of the molecule and increasing the electron richness, while the presence of a carboxylic group and an aliphatic tertiary nitrogen is detrimental for the hERG activity, which, under the light of all models discussed so far, seems quite unlikely.

Due to their simplicity, the 2D-QSARs were extensively applied to develop models able to predict hERG potency. Interestingly, some 2D-descriptors provided structural information of the central cavity of the hERG channel, suggesting that it can accommodate large molecules. The 2D-descriptors also provided some interesting insight into the characteristics of hERG blockers, indicating that the nature and the charge of the nitrogen atom might have a strong influence on the potency.

4.4 1D-QSAR

A new QSAR technique was proposed by Diller et al. [56, 57] to analyze 230 compounds collected from the literature. To minimize the variation on the IC_{50} values due to the use of different cell lines, the data were corrected by introducing a correction factor for each cell type to obtain a match of the data measured in HEK cells. Through the projection of the atoms of the molecules onto one dimension using multidimensional scaling, the structures were described as a 1D string of atoms. Six descriptors were employed to generate the model: Size (number of heavy atoms), C-Aliph-Estate (the electro-topological state of the atom if the atom is a carbon not in an aromatic ring), C-Arom-Estate (the electro-topological state of the atom if the atom is a carbon in an aromatic ring), N-Acc-Estate (10 minus the Estate of the atom if the atom is a nitrogen with a free lone pair), N-Don-Estate (the electro-topological state of a nitrogen with an attached hydrogen), and O-Estate (the electro-topological state of the atom if the atom is an oxygen). The statistical analysis of the model showed a correlation coefficient of 0.68 for the training (189 compounds) and of 0.76 for the test (41 compounds) set, respectively. The descriptors that mainly contribute to hERG inhibition were the N-Acc E-state and the C-Arom-Estate, revealing the importance of the basic nitrogen and the aromatic ring.

The same QSAR technique based on 1D-descriptors was used by Diller et al. [58]. The one dimensional representation of the molecules was achieved by multidimensional scaling from 2D topological descriptors. To generate the model, six descriptors were used: the number of heavy atoms, E-state key for aliphatic carbons, E-state key for aromatic carbons, E-state key for nitrogen atoms with a free lone pair, E-state key for nitrogen atom with an attached hydrogen and E-state key for oxygen atoms. The IC_{50} values of 230 compounds collected from the

literature were corrected as previously described. The analysis of the contribution of the descriptors revealed the positive contribution of the E-state key of the aromatic carbon and of the nitrogen atom with a free lone pair. In particular, the model indicates that a separation of 9–10 bonds between two phenyl rings increases hERG affinity. This is consistent with previously published pharmacophore models, which indicates the importance of the presence of a tertiary amine linked with two aromatic rings. The final model achieved the mean absolute errors of 0.62 and 0.62 for the training set (189 compounds) and test set (41 compounds). Different from other publications, the authors used the mean absolute errors as performance measure, which makes it complicated to compare their model with the results already published.

The 1D-, 2D-, and 3D- QSAR models discussed highlight the importance of the basic nitrogen and of the hydrophobic and aromatic groups for strong hERG blockers. To reduce hERG affinity, the QSAR models suggest to reduce the number of aromatic rings, to modulate the pKa of the basic nitrogen, and to reduce the lipophilicity of the molecule. It is noteworthy that the compounds with a carboxylic group are unlikely to be hERG blockers.

4.5 Classification Models

To discover potential hERG blockers classification techniques became an important and powerful tool. Although they do not need accurate IC_{50} values, it is necessary to set up a threshold, which defines if the compounds are considered as active or as inactive.

Bains et al. [59] chose an IC_{50} of 1 μM as threshold to define hERG blockers and nonblockers. Tobita et al. [60] used thresholds of 1 μM and 40 μM to classify active and inactive compounds. Roche et al. [61], Dubus et al. [62], Ekins et al. [51], Thai et al. [63–65], and Chekmarev et al. [66] classified the hERG blockers into three different classes: low IC_{50} (lower than < 1 μM, blockers), medium IC_{50} (between 1 and 10 μM), and high IC_{50} (higher than > 10 μM, nonblockers). Doddareddy et al. [67] used the cutoff values of $IC_{50} < 3$ μM, 6 μM and 10 μM to define hERG inhibitors, and of >30 μM for the hERG inactives. O'Brien et al. [68] selected the value of 20 μM to define hERG inhibitors. Sun et al. [69] and Jia et al. [70] defined a compound as hERG blocker if it has an IC_{50} value lower than 30 μM. Buyck et al. [71] used the threshold of 130 nM to define if the compounds are hERG blockers or not. Catana et al. [72] used an IC_{50} of 40 μM as a cutoff to define the separation between hERG blockers and nonblockers. Li et al. [41] used the threshold values of 1 μM, 5 μM, 10 μM, 20 μM, 30 μM, and 40 μM. Some approved drugs have an IC_{50} value between 1 and 10 μM. Typically, a drug is considered safe if the IC_{50} value is higher than 10 μM [53]. To assess the safety of compounds also the ration between the free therapeutic plasma concentration and the hERG IC_{50} has to be considered. Generally, a molecule with a margin greater than 30-fold between the free therapeutic plasma concentration and the hERG IC_{50} is regarded as safe [73].

Roche et al. [61] employed different techniques such as self-organizing maps (SOM), PCA, PLS, and supervised neural networks to develop predictive models based on 1,258 descriptors to classify 472 compounds. The substructure analysis performed with LeadScope did not highlight any moieties exclusive for blockers or for nonblockers, although some weak trends could be noted. In 57% of the nonblockers and in 30% of the blockers, two hydrogen-bond donors separated by six bonds were present. In 20% of the nonblockers and in 2% of the blockers, a benzenesulfonyl groups was found. In 49% of hERG inhibitors, the 1-R-4-alkyl-benzene moiety was found. The best prediction performance was achieved with the neural network model, which was able to correctly classify 93% of the nonblockers and 71% of the blockers (95 compounds validation test set). The prediction method was additionally used to analyze virtual combinatorial libraries to demonstrate its applicability for shaping compounds libraries toward low probability to contain potential hERG blockers. The structures based on scaffold one (Fig. 1) have a structural moiety common to many hERG inhibitors, while the molecules based on scaffold two are designed to be nonblockers. The prediction highlights that in the library of compounds based on scaffold one there are 58% of potential hERG blockers, while in the second library the possibility to have hERG blockers decreases to 0.1%.

Bains et al. [59] applied evolutionary programming with fragment-based descriptors to predict hERG inhibition. The resulting model shows an accuracy of 85–90% for the classification of blockers and nonblockers. The model was generated calculating 618 fragment- and nonfragment-based descriptors on 124 compounds randomly partitioned in 70:30:24 for training, generalization, and validation data sets. Ten different partitions and subsequently 10 runs for each partition were performed to generate a "consensus model" based on the average of the prediction of the ten best generalizing models. The partition with the best performance over the data sets was selected. Through a meta-SAR analysis, 30 descriptors related to hERG inhibition were identified. Inspection of the selected descriptors revealed that the presence of a secondary or tertiary amino group, of one or more aromatic rings and of a five-membered nitrogen heterocycle increases the potency of hERG blockers. The model also shows that the presence of negatively ionizable groups such as COOH and of oxygens as H-bond acceptors is detrimental for hERG inhibition. Analysis of the 60 most correlated descriptors with hERG blockade provided a pharmacophore model similar to the already published ones. It consists of a nitrogen atom in the center to which an aromatic and a hydrophobic feature are attached, separated by a linker of 4–5 and 1–2 carbon atoms, respectively. This pharmacophore model highlights again the importance of the presence of a secondary or tertiary amino group linked with two hydrophobic or aromatic

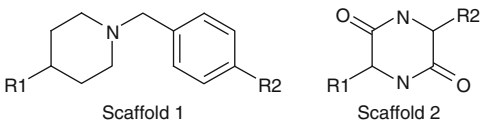

Fig. 1 Chemical scaffolds of the combinatorial libraries

features, which might interact with the aromatic amino acids Phe656 and Tyr652. The model also suggests that the amino group should be located asymmetrically between the hydrophobic or aromatic features, to interact optimally with the hERG channel.

A set of linear solvation energy relationship (LSER) descriptors were used by Yap et al. [74] to develop an SVM-based classification using a training set of 271 compounds collected from the ArizonaCERT, Micromedex, *Drug Information Handbook*, Meyler's side Effect of Drugs, and from the work of De Ponti and the American Hospital Formulary Service. The model obtained was validated using leave-one-out and Y-randomization methods and model was further tested with an independent validation set of 78 compounds. Furthermore, the prediction accuracy was compared with those obtained from other classification methods such as *k* nearest neighbor (KNN), probabilistic neural network (PNN), and C4.5 decision tree. The SVM classification model shows a higher performance than the other three classification methods, reaching a prediction accuracy of 97.4% and 84.6% for the blockers and nonblockers and an overall accuracy of 91%.

Tobita et al. [60] also generated an SVM model, which achieved a prediction accuracy of 90% and 95% with two different test sets. To build the discriminant models they used 73 compounds from the literature for which 57 2D descriptors from the MOE software package, and 51 molecular fragment-count descriptors taken from the MACCS key set were calculated. The SVM implemented in the WEKA software package was used to develop two different discriminant models using IC_{50} values of 1 μM and 40 μM to define blockers and nonblockers. The accuracy of the two models to correctly classify the inhibitors and the noninhibitors was evaluated through tenfold cross validation. The model shows an accuracy of prediction of 70% when it was tested with an external dataset of 827 compounds using a threshold 1 μM. In both models, the most accurate classification was achieved selecting eight descriptors. For the model with a threshold of 40 μM the descriptors selected were five 2D descriptors (SlogP, PEOE_VSA6, PEOE_VSA + 1, SMR_VSA5, DIAMETER), and three fragment-count descriptors (number of NH_2 fragments, which is correlated with the possible number of hydrogen bond sites, ACH_2CH_2A and A$A!A$A related to flexibility/hydrophobicity of the molecule and the presence of two rings connected by a bond respectively). The fragment ACH_2CH_2A also suggests that the presence of a long chain might play an important role for potent hERG blockers. In the models with a threshold of 1 μM, the descriptors indentified as important were three 2D descriptors (VSA_BASE, PEOE_Vsa0, SMR_VSA0), and five molecular fragment-count descriptors (OAAAO, ACH_2AAACH_2A, Nnot%A%A, ACH_2AACH_2A and eight-membered or larger rings). The descriptors selected by the two models are basically different. In the model with the IC_{50} value of 40 μM, the 2D descriptors selected are measures of global properties of the compounds, while in the model with the IC_{50} value of 1 μM they are related to a particular structure of the hERG blockers. This highlights that nonpotent hERG blockers need to satisfy some general properties such as the DIAMETER and the SlogP, while for potent blockers the presence of certain structural fragments is important. The analysis of molecular fragments shows that

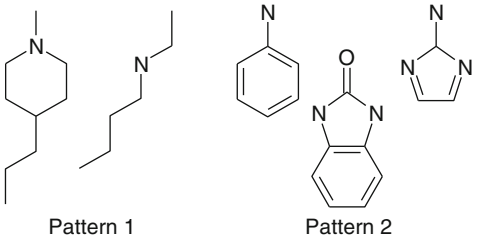

Fig. 2 Fragments related to strong hERG inhibition

the descriptors selected for the threshold at 1 μM are specific cases of the descriptors selected for the threshold at 40 μM. The fragments ACH_2AACH_2A and ACH_2AAACH_2A are related to the global descriptor SlogP. The fragment Nnot %A%A is a specific case of the A$A!A$A fragment. Two fragment patterns (pattern1 and pattern2) (Fig. 2), common to many potent blockers, were discovered through the mapping of the descriptors selected with the threshold at 1 μM. The fragments of pattern1 are related to the ACH_2AACH_2A and ACH_2AAACH_2A fragments, while the fragments of pattern2 are characterized by a nitrogen atom bound to an aromatic ring.

A series of 246 descriptors and the naïve Bayes classification technique were used by Sun et al. [69] A training set of 1,979 compounds from Roche and generic molecular descriptors and fingerprint-based descriptors were used to generate a classification model. The model achieved an ROC accuracy of 0.87. The model, tested with an external dataset, predicted correctly 58 out of 66 molecules. The fingerprint-based naïve Bayes model was built using FCFP_6, a 2D-descriptor where each heavy atom of the molecule is described by a string of extended connectivity values, together with physicochemical descriptors such as AlogP, molecular weight, number of hydrogen bond donors and acceptors, and number of rotatable bonds. The model achieved an ROC accuracy of 0.93, indicating that the classification accuracy of the fingerprint-based model is higher than the one of the atom-typing model. The predictive accuracy of both models is similar, as shown by the predictions of the 66 compounds of the test set. Analysis of the most important atom-types indicates that some particular fragments might play an important role for hERG inhibition. The presence of acidic groups abolishes hERG blocking, while basic groups such as piperidines and piperazines are important for hERG blockage. They also observed that compounds, which branch immediately after an aromatic moiety have the tendency to be hERG blockers.

SVMs combined with the pharmacophore-based GRIND descriptors were used by Li et al. [41] to design a classification model. To generate the GRIND descriptors, 495 compounds were docked into a homology model of the hERG channel in the open state. For every molecule the best scoring pose was selected to calculate the pharmacophoric GRIND descriptors, which were combined with the SVM to generate classification models using cutoff values of 1 μM, 5 μM, 10 μM, 20 μM, 30 μM, and 40 μM. Four probes were selected to calculate the pharmacophore-based GRIND descriptors: DRY (representing the hydrophobic interactions), O sp^2 carbonyl oxygen (representing H-bond acceptor), NH neutral

flat amide (representing H-bond donor) and TIP probe (representing molecular shape descriptors). The model obtained using a threshold of 40 μM showed the best performance. It classified correctly 283 out of 343 nonblockers and 83 out of 152 blockers, with an overall accuracy of 74%. For the external test set composed of 66 compounds from the WOMBAT-PK database, the model achieved an overall accuracy of 72%, with a correct prediction of 85% and 36% of blockers and nonblockers, respectively. In an additional test using 1,877 compounds from the PubChem database, the model correctly classified 107 out of 187 inhibitors and 1,271 out of 1,690 inactives.

Thai et al. [65] developed two Binary QSAR models for the prediction of hERG blockers using two sets of descriptors, 32 P_VSA descriptors, and 11 relevant 2D descriptors such as hydrophobic descriptors (SlogP, a_hyd, SlogP_VSA7, Q_VSA_HYD, PEOE_VSA_HYD), diameter, atom counts (a_heavy), bond counts (opr_nrot), subdivided surface areas (SMR_VSA5), as well as Kier and Hall connectivity indices (chi1v_C, chi0_C). A dataset of 313 compounds collected from the literature was divided into three classes based on the IC_{50} value: class 1 with $IC_{50} < 1$ μM (low IC_{50}), class 2 with $IC_{50} \geq 10$ μM (high IC_{50}), and class 3 with IC_{50} in the range 1–10 μM. To generate the training and test sets, 184 2D descriptors were calculated on the 313 molecules of the dataset and combined with the pIC_{50} to perform a diverse subset selection, which resulted in 240 compounds for the training set and 73 structures for the test set. A second dataset was generated removing the compounds containing carboxylic moieties. The best Binary QSAR model with a cutoff at 1 μM (MODEL I) was obtained using 11 relevant 2D descriptors and removing the compounds with carboxylic groups from the training and test sets. The model showed a total accuracy of 0.85 for the training set and 0.94 for the test set. The best Binary QSAR model with a threshold at 10 μM (MODEL II) was also based on the dataset without compounds containing carboxylic groups. The model achieved a total accuracy of 0.83 for the training set and of 0.75 for the test set, respectively. Due to the difficulty to correctly classify compounds with IC_{50} values in the range of 1–10 μM, new training and test sets were generated omitting the molecules that belong to this class. The Binary QSAR based on 11 relevant 2D descriptors (MODEL III) showed a total accuracy of 0.87 for the training set and of 0.93 for the test set. All three models were further tested with an external test set of 58 compounds taken from the literature and showed a good performance, with a total accuracy of 0.84, 0.78, and 0.86 for MODEL I, MODEL II and MODEL III, respectively.

Counter-propagation neural network (CPG-NN) was used by Thai et al. [64] to develop classification models using 285 compounds collected from the literature and 2 sets of 2D descriptors, one based on 32 P_VSA descriptors and the other on 11 relevant descriptors. Based on the IC_{50} values, the compounds were divided into three classes: class 1 ($IC_{50} \geq 10$ μM), class 2 (10 μM $\leq IC_{50} < 1$ μM) and class 3 ($IC_{50} < 1$ μM). The dataset was split into training and test sets by random division (80:20 and 50:50), or by diverse subset selection (80:20 and 50:50). The best CPG-NN classification performance, obtained with a 3D output layer combined with 11 selected 2D descriptors, reached a total accuracy of 0.93–0.95 for the training set

and 0.83–0.85 for the test set, respectively. In particular, this model was able to correctly classify high, moderate, and weak hERG inhibitors with an accuracy of 0.93 for class 1, 0.97 for class 2, and 0.96 for class 3. Using only one output layer, the CPG-NN was also used to predict hERG affinity. The model based on 11 relevant descriptors showed highest performance with an r^2 of 0.87 for the training and the test set.

A new series of fragment/pharmacophore descriptors combined with SVM and Random Forest (RF) was applied by Catana et al. [72] to develop classification models for a dataset of 561 compounds. An external test set of 1,895 molecules from the PubChem was used to validate the model. Each molecule was hashed into different fragments. Subsequently, each fragment was mapped back onto the dataset compounds, numbered, and a C-fragment descriptor was calculated. The value of the "comprehensive fragment" descriptor (CF) is calculated by summing the contribution of each atoms of the fragment. This implies that the values of each CF descriptor differs for each molecule. The following descriptors were calculated: E-state (CF_E-state_*), AlogP (CF_AlogP_*), MR (CF_MR_*), positive Gasteiger partial charges (CF_GC_P_*), negative Gasteiger partial charges (CF_GC_N-*), the van der Waals surface area positively charged (CF_VSA_P_*), the van der Waals surface area negatively charged (CF_VSA_N_*), the van der Waals surface area (CF__VSA_*), the van der Waals surface area with a positive AlogP (CF_VSA_AlogP_P_*), the van der Waals surface are with a negative AlogP (CF_VSA_AlogP_N_*). In addition, pharmacophore fingerprints implemented in MOE were used to generate a new set of descriptors (CP_*) using the approach described above. The model generated by RF using the CF_Estate_*, CF_VSA_P_*, CF_VSA_N_*, and CF_GA_N_* and some 2D MOE descriptors showed an overall accuracy of 0.79 with a precision of 62.2% and 92.3% for true active and inactive compounds, respectively. For the external test set, the model correctly predicted 105 of 193 inhibitors and 1,408 of 1,702 inactives. The model created using the SVM based on the C-pharmacophore descriptors showed a poor performance for the classification of hERG blockers (78 out of 193 compounds were correctly predicted). Conversely, the good result achieved in the prediction of hERG inactives indicates that this model might be used to select nonblockers.

In a recent study, in silico Binary QSAR and CPG-NN were used by Thai et al. [63] to classify hERG blockers and nonblockers. The models were built using a dataset of 243 compounds with SIBAR descriptors calculated on the basis of four reference sets: 24 diverse drugs obtained from Sköld et al. [75], 20 hERG blockers, 20 hERG nonblockers, and 20 compounds divided in 10 blockers and 10 nonblockers. The SIBAR descriptors were calculated from 11 selected descriptors from a total number of 184 2D descriptors, 86 VolSurf descriptors, 50 3D "inductive" QSAR descriptors (related to atomic electronegativity, covalent radii and intramolecular distances) and 32 P_VSA descriptors. The Binary QSAR models were generated using 16 SIBAR descriptors and threshold values of 1 μM and 10 μM. The best classification model was obtained with the 11 hERG relevant descriptors using the 20 most diverse hERG blockers as reference set (total accuracy of 0.85–0.88 for the training set and 0.73–0.92 for the test set). The CPG-NN

models were built using the dataset divided into class 1 (low hERG activity), class 2 (high hERG activity) and class 3 (medium hERG activity). The dataset compounds were divided into the training set by random selection (80:20) or by diverse subset selection (80:20). The architecture of the CPG-NNs was designed with 3 output layers representing the classes 1–3. The CPG-NN models were trained with 16 different sets of descriptors. The CPG-NN model obtained using the set of 11 hERG relevant descriptors and the reference set of 20 diverse inhibitors showed the best performance, reaching a total accuracy of 0.73–0.74 for the test set and 0.92–0.93 for the training set. The best Binary QSAR and CPG-NN models were validated using 1,806 compounds published in the PubChem compound library and 58 compounds collected from the literature. With the threshold value of 1 μM, the Binary QSAR model achieved the total accuracy of 0.93. The CPG-NN model correctly classified 68% of the compounds in class 1, 100% of the compounds in class2 and 75% of class 3.

Jia et al. [70] designed a classification model using an SVM and the atom type as molecular descriptors. The model yielded an overall accuracy of 99.59% for the 977 compounds of the training set and of 94% for the 66 compounds of the test set. The use of the atomic molecular descriptors makes the classification model easy to interpret. The most important atom-type descriptors were the N16 (nitrogen atom in an aliphatic ring), C17 (unsubstituted carbon atom next to the N16 in a ring), H4 (acidic hydrogen) and M12 (number of aromatic rings). The nitrogen of the N16 descriptor was usually protonated, and it was found in hERG blockers 308 times out of 322 times of the total occurrence of the descriptor. The C17 descriptor was found 1,635 times of which 1,318 times it was associated with hERG inhibitors. The H4 descriptor was found in 60 structures of which only 5 were hERG positives, in agreement with the fact that negatively charged compounds are normally nonblockers. The M12 descriptor occurred 2,581 times. Only 94 out of 535 molecules containing 3 aromatic rings were hERG inactive, while 14 out 19 compounds containing one aromatic ring were nonblockers.

New descriptors generated from the Shape Signature method were used by Checkmarev et al. [66] in combination with *k* nearest neighbors (*k*-NN), SVMs, and Kohonen self-organizing maps (SOM) to create classification models. The models were built based on a dataset of 83 compounds divided into strong binders ($IC_{50} < 1$ μM) and weak binders ($IC_{50} > 10$ μM). Two different sets of molecular descriptors were calculated, one based only on molecular shape and the other one based on molecular shape and polarity. The SVM models showed a better performance than the *k*-NN with an overall accuracy of 69–74% and of 66–67%, respectively.

4.5.1 Decision Trees

The decision tree approach was chosen by several groups to classify hERG blockers and nonblockers. The ClogP, MR and p*K*a were used by Buyck et al. [71].

Compounds were categorized as hERG inhibitors when the following three conditions are satisfied: clogP $\geq$ 3.7, $-110 \leq$ MR $<$ 176 and p*K*a $\geq$ 7.3.

A Neural Network model based on the E-state keys and Barnard 4096-bit fingerprints, and a Bayesian model based on FCFP_6, AlogP, Molecular Weight, and the counts of hydrogen bond acceptors and donors descriptors were used by O'Brien et al. [68] to generate a consensus model. The models were built using a dataset of 58.963 compounds randomly divided (80:20) to obtain a training and a test set of 46.967 and 11.996 compounds, respectively. The Neural Network model shows slightly better results than the Bayesian model with 85% vs. 82% of compounds correctly classified. To improve the ability to correctly classify the compounds the Neural Network and the Bayesian models were combined. The "recover +ve" classifies the compound as hERG blockers if one of the models predicts it to be positive. The "recover −ve" classifies a compound as negative if one of the models predicts it to be negative. With this classification model the number of false positives increases. The "consensus model" classifies a compound as positive or negative if both models agree. The model correctly classifies 91% of hERG blockers and 87% of hERG nonblockers. With the "consensus model" the rates of false positive and false negative are reduced compared to the Neural Network and Bayesian models.

A total of 155 descriptors such as physicochemical, topological, SMARTS strings and SIMAST descriptors were computed on a dataset of 264 compounds by Gepp et al. [76] to generate two decision trees composed by a maximum of eight branches. The first descriptor used in the two partitioning models is the pharmacophoric string PHARM$, which correctly classifies 71% of the compounds in both models and only 13 compounds were misclassified as false positives. The two models are identical in the two subsequent layers, which contain the descriptors HACSUR (ratio of surface of hydrogen-bond acceptor atoms to total surface), T1E (topological electronic index using the number of nonhydrogen atoms), HY (number of hydrogen atoms), DIPDENS (dipolar density) and T2E (topological electronic index using the number of bonds between nonhydrogen atoms). The differences between the two models start from the fourth layer. The first model contains seven branches and the last fourth layers contain the descriptors HLSURF (ratio of surface on halogen atoms to total surface), MDE23 (molecular distance-edge vector λ_{23}), MR, CHBBA (covalent hydrogen-bond basicity), logP, QSUMN (sum of atomic charges on nitrogen atoms), and MGHBD (minimal geometric distance between two hydrogen-bond donor atoms). In the second partitioning model, the SIMAST descriptor (fingerprint similarity compared to astemizole) is used in many branches instead of the MR and logP, and the QSUM- (sum of negative ESP charges) replaces the MR in the fifth layer. The first and the second partitioning models achieve overall accuracies for the training set of 91.7% and 93.2%, and of 76% and 80% for the test set.

Recursive partitioning models were developed by Dubus et al. [62]. They used 203 molecules from the Aureus Pharma database, 32 P_VSA descriptors and 23 uncorrelated relevant descriptors selected from 184 2D-descriptors calculated with the Molecular Operating Environment (MOE) software. Model1 used an

active/inactive boundary of 1 μM. Classification accuracy for the training set of 96% and 97.5%, and of 74% and 81% for the test set was achieved by the model using the relevant and P_VSA descriptors, respectively. In detail the models correctly classified 94% of the strong blockers, while the precision for classification of the weak blockers decreased to 63% for the relevant descriptors model and to 74% for the P_VSA model. Noteworthy, the misclassified molecules mainly showed an IC_{50} between 1 and 10 μM.

In a study performed by Ekins et al. [51] recursive partitioning, Sammon nonlinear mapping and Kohonen self-organizing maps were investigated with the aim to analyze the performance of these techniques individually or in a consensus approach. The recursive partitioning model was built using a training set of 99 compounds providing an r^2 of 0.90. Interestingly, the performance of the test set of 35 compounds was improved (from a r^2 value of 0.33–0.83) when the Tanimoto index was introduced to filter the molecules according to their similarity to those used in the training set. The Sammon nonlinear mapping and Kohonen self-organizing maps models were generated using a dataset of 93 compounds and 8 descriptors selected with the PCA technique from more than 150 descriptors. The eight descriptors selected are the Wiener index (a measure of molecular branching), the topological Balaban index (provides information on the connectivity and branching of the molecule and is related to the hydrophobic interaction of the molecule), number of H-bond donors, hydrophilicity index and electrotopological state indices (CH_2, CH and >N, which provide information on the topology, polarity and hydrogen bonding capabilities of the compound). These descriptors suggest that the topology of the molecule plays an important role for hERG inhibition. The 93 molecules of the training set were divided in three classes based on their activity: class0 ($IC_{50} < 1$ μM), class1 ($1 < IC_{50} < 10$ μM), and class2 ($IC_{50} > 10$ μM). The analysis of the nonlinear map generated with the Sammon nonlinear mapping technique revealed that the compounds of the classes 0 and 2 were mapped in two different areas. The compounds of class 1 were mapped in a wide area of the map overlapping the areas occupied by class 0 and 2, resulting in a poor prediction ability. The model predicts correctly 86% and 100% of the compounds in the classes 0 and 2, giving an overall classification accuracy of 95%. As happened for the Sammon nonlinear mapping, also in the map generated with the Kohonen self-organizing map the molecules belonging to class 0 and 2 were mapped in distinct areas, while the area occupied by compounds belonging to class 1 overlapped the sites of the other two classes. The method correctly classified 86% and 79% of the compounds belonging to class 0 and 2, respectively. A consensus analysis performed using the three methods resulted in 86% of the compounds correctly classified in the classes 0 and 2. The consensus approach did not improve the results obtained with the individual methods.

Doddareddy et al. [67] designed 24 binary models by using Linear Discriminant Analysis (LDA) and SVMs to classify 2.644 compounds. Four molecular fingerprint descriptors belonging to the extended connectivity fingerprints (ECFPs) and to the functional class fingerprints (FCFPs) were chosen. Four representative models out of 24 were selected for further validation. The four classification models yielded

overall accuracies of 82–86% for the training set and 83–85% for the test set. The selected models were further tested by using the PubChem database. The models showed a poor predictivity in the classification of the test set compounds, with only 78 out of 193 compounds correctly classified. In addition, 50 compounds from the Cambridge database that were predicted as hERG blockers and 10 compounds that were predicted as nonblockers by two or more models were selected for experimental validation. Of the 50, 18 predicted hERG inhibitors showed more than 50% displacement of astemizole, while all the predicted nonblockers were found to be inactive.

The SOM was used by Hidaka et al. [77] to classify the compounds using structural information. First, 37 compounds were divided into three classes depending on whether the activity (pIC_{50}) was below 5, between 5 and 7, or higher than 7. The analysis of the map obtained reveals that the potent blockers and the inactive compounds occupy two different areas, while the compounds with the intermediate activity overlap the two areas. The same method was then applied to the public available dataset. They divided this database into active ("Hit") and inactive compounds. The "Hit" molecules were subdivided into compounds that cause hERG blockade between 20 and 30%, between 30 and 50%, and more than 50%. Considering only the "Hit" compounds they established a line which divides the map into two parts: hERG positive and hERG negative areas. All compounds that block the hERG channel by more than 50% are mapped in the area of the hERG positive potential, with the exception of one false negative.

4.6 Matched Molecular Pairs

In a recent and interesting study, Papadatos et al. [78] applied the matched molecular pairs technique to three large data sets: hERG (76.266 compounds), solubility (94.053 compounds), and lipophilicity (180.440 compounds) to find the most frequent modifications of the molecules. The matched molecular pair analysis of the hERG database identified 15 frequent transformations. These modifications are related to only one or two heavy atoms, except for the substitution of a hydrogen atom with a phenyl ring. In 9 transformations out of 15, the modifications have only a small or no effect for the hERG affinity of the compounds. According to previous results, they found that replacing a hydrogen atom with a hydroxy group is detrimental for the hERG affinity in 45% of the cases, while replacing a hydrogen atom with a phenyl ring increases the hERG inhibition in 65% of the cases. The use of context descriptors, such as reduced graphs, Murcko frameworks and Daylight fingerprints, as well as more local descriptors such as localized RG nodes and atom environments, highlights significant trends that are not evident when only the matched molecular pairs technique is used. For example, considering the substitution of a hydrogen atom with a methoxy group the global distribution indicates that the possibilities to reduce or to improve the hERG affinity are more or less identical. However, if one takes into account the reduced graph node the scenario appears to

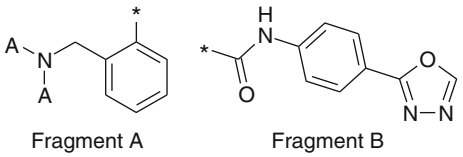

Fig. 3 Fragments found in hERG blockers. The asterisk indicates the attachment point

be more complex. The possibility to reduce the hERG affinity increases if the transformation is adjacent to an aliphatic chain. The opposite effect is obtained if the transformation is next to a hydrogen-bond acceptor in an aromatic ring. On the contrary, if the transformation is adjacent to an aromatic ring the hERG inhibition is not affected. These results are related to the possibility to form hydrogen-bonds by the oxygen atom of the methoxy group. In the case of the substitution of a methyl group with a fluorine atom, the global distribution indicates that this might result in an increase or a decrease of the hERG affinity. The presence of the fragment A (Fig. 3) is correlated with the increase of hERG potency. The analysis of the global distribution shows that replacing the cyclohexyl with the phenyl group can reduce or improve hERG potency. The cyclohexyl >> phenyl transformation in the fragment B (Fig. 3) increases the probability to obtain a more potent hERG blocker. This result is due to the increased lipophilicity and hydrophobicity of the molecule, and to the reduced ability to form hydrogen-bonds of the adjacent amidic carbonyl. These three examples show the importance to include contextual information in the drug discovery process to develop compounds with a good toxicological profile.

5 Structure-Based Approaches

5.1 Homology Models of the hERG Channel

Up to date there is no crystal structure of the hERG channel and most of our knowledge comes from studies on the Shaker channel (Kv1.1) and on mammalian channels (Kv1.2), KcsA, MthK, and KvAP. Since the eukaryotic and prokaryotic pores are closely related, it appears reasonable to use the crystal structures of KcsA (pdb codes 1BL8 [79], 1K4C [80] and 1R3J [81]) and of KirBac1.1 (1P7B [82]) to build homology models of the hERG channel in the closed state, or MthK (1LNQ [83]) and KvaP (1ORQ [84]) for the open state. It has to be noted that the degree of the pore opening varies in the crystal structures, from the closed state (KcsA) to the open state (KvaP), up to an even more open state in MthK. These different degrees in pore opening might represent different gating properties of the K^+ channel, or different snapshots in the gating trajectory. The first homology models of hERG channel were discussed also in several reviews [26, 27, 85–87].

Many groups modeled the hERG channel in the closed state using as template the crystal structures of KcsA (1BL8 or 1K4C) [4–6, 11, 12, 88–94], as well as of MthK (1LNQ) [11, 21, 49, 88, 89, 94]. The homology models of the hERG channel

Table 1 Published homology models of the hERG potassium channel in the closed and open state

References	Template	Homology model/docking
[6]	KcsA (1BL8)	Insight II/FLOG
[5]	KcsA (1BL8)	MOE/FLOG
[21]	MthK (1LNQ)	Modeller
[4]	KcsA (1BL8)	QUANTA/CHARMm/Manual docking
[119]	KcsA (1BL8)	SWISS-MODEL/Chimera
[12]	KcsA (1BL8)	Modeller v6.0/GOLD
[11]	KcsA (1BL8), MthK (1LNQ)	Insight II/FlexiDock
[89]	KcsA (1K4C), MthK (1LNQ)	PRIME/Glide
[105]	KcsA (1BL8)	Modeller v6.0/GOLD
[98]	KvaP (1ORQ)	SWISS-MODEL/AutoDock 3.0
[88]	KcsA (1BL8), MthK (1LNQ)	Insight II/FlexiDock
[97]	KvaP (1R3J)	Modeller v.8.0/GOLD v.2.2
[49]	MthK (1LNQ)	MOE/Glide
[99]	KvaP (1ORQ)	PRIME/Glide 3.0
[120]	Kv1.2 (2A79)	SWISS-MODEL/AutoDock 3.0
[90]	KcsA (1BL8)	SWISS-MODEL/ZDOCK
[95]	KvaP (1ORQ)	Modeller v6.0/Sievgene
[96]	KvaP (1ORQ)	Modeller
[100]	KcsA (1BL8), Kv1.2 (2A79)	QUANTA/Manual docking
[39]	KcsA (1BL8)	Insight II/DOCK v.5.2
[121]	KcsA (1BL8)	Moloc/Manual docking
[91]	KcsA (1K4C), KvaP (1ORQ)	Modeller v.7.7/GOLD v.3.0.1
[92]	KcsA (1BL8)	Modeller v.7.7/Insight II/GOLD v.3.1
[116]	KcsA (1BL8)	Insight II/Manual docking
[93]	KcsA (1BL8)	Modeler v6.0/GOLD
[94]	MthK (1LNQ), KvaP (1ORQ), KcsA (1BL8)	Modeler v.6.2 and Modeler v.7.7/ GOLD v.3.0
[117]	MthK (1LNQ)	Modeler v.8.2
[38]	Kcsa (1R3J)	Insight II/Glide
[104]	KcsA (1BL8)	Insight II/FLOG
[102]	KcsA (1K4C)	Modeller/FlexX
[118]	KcsA (2BOB, 2HjF and 2HVK)	Modeller/GOLD

in the open state were constructed with the crystal structures of KvaP (1ORQ, or 1R3J) [91, 94–99] and Kv1.2 (2A79) [100] used as template (Table 1).

5.2 hERG Inhibition and Drug Trapping

In 1969, Armstrong [101] demonstrated that the channel opening is a necessary condition to obtain the inhibition of the voltage gated K^+ channel by a small quaternary ammonium (QA) ion. Normally, the QA interferes with the channel gating upon repolarization causing a slow deactivation due to the impossibility to close the activation gate in a mechanism called “foot-in-the-door.” In a few words,

the activation gate cannot close until the inhibitor dissociates from the hERG channel. Armstrong noted that the channel block due to small QA compounds, such as tetraethylammonium, did not show interference with the deactivation rate, suggesting that these compounds might be trapped in the hERG channel in the closed state. A molecule can only be trapped only if it is small enough to fit into the central cavity. If the molecule is charged, it cannot leave the central cavity through the hydrophobic environment of the inner pore or through the membrane, hence the block is irreversible until the channel reopens. Mitcheson et al. [3] used the potent hERG blocker MK-499 and the hERG mutant D540K to test the trapping hypothesis. This mutant of the hERG channel has the particular characteristic to open in response to hyperpolarization. They observed that the channel reopening during the hyperpolarization allowed the recovery from the block of MK499, as postulated by the trapping hypothesis. Moreover, the observation that molecules with large size such as MK499 (7×20 Å) can be trapped, suggests that the hERG channel has a central cavity bigger than the one of the Shaker K^+ channel. The Shaker K^+ channel is blocked by tetraethylammonium (6.9 Å of diameter), but it cannot trap MK499.

5.2.1 Case Studies: Propafenone Derivatives Trapping

Docking studies combined with alanine scanning of the amino acids facing the central cavity were performed to investigate the molecular determinants of hERG inhibition by propafenone, as well as the amino acids involved in the drug trapping [11]. The mutagenesis data showed that propafenone's inhibition of hERG was strongly dependent on the interactions between the compound and the amino acid Phe656, while it was not affected by mutations of Tyr652, Thr623, Ser624, Val625, Gly648 or Val659. The analysis of recovery from the propafenone block showed that the compound was not released faster from the mutant channels T652A, V625A, and S624A than from the wild-type channel. Only in the case of F656A the recovery from the block is slightly faster. These results suggest that only the mutation F656A slightly reduces the interaction of propafenone with the hERG channel in the closed state. Their results also indicate that the mutagenesis data are better rationalized with the docking poses obtained with the hERG channel in the open state. Almost all of the top ranked poses form π–stacking interactions with two Phe656 of adjacent subunits. The model of the hERG channel in the open state suggests that the four Phe656 are highly accessible to the compound, whereas in the closed-state model the space between the Phe656 units is reduced, making it impossible for propafenone to form π–stacking interactions with Phe656. This indicates that there are gating-induced changes in the position of Phe656 side chains.

In a recent study, Thai et al. [102] used five propafenone derivatives to perform a systematic analysis of use-dependency and recovery from the block of the hERG channel. The pose of propafenone docked into the hERG channel in the closed state predicts that the phenyl ring forms π–stacking interactions with Tyr652, that the

Thr623 makes hydrogen-bonds with the hydroxy group and the protonated nitrogen atom, and that Ser624 forms hydrogen-bonds with the hydroxy moiety. The pose of propafenone docked into the homology model of the hERG channel in the open state shows π–stacking interactions between the phenyl ring and Tyr652, and that the hydroxyl and the carbonyl group as well as the ether oxygen form hydrogen-bonds with Thr623 and two Ser624 of adjacent subunits, respectively. The docking pose of propafenone into the hERG channel in the open state shows that the protonated nitrogen moves in the direction of the cytoplasm. This indicates that the propafenone moves upward when the hERG channel closes. The other trapped compound, the piperidine analogue, shows a similar poses. The poses of nontrapped propafenone derivatives bearing a 2,3-dimethylphenyl-1-piperazinyl ring docked into the hERG open state, predict that the carbonyl group and the ether oxygen form two hydrogen-bonds with Ser624 of different subunits. The conformation of the nontrapped compounds is similar to the pose of propafenone, with the substituent located into the inner pore. The nontrapped 1-[4-{3-[4-(2,3-dimethylphenyl)piperazin-1-yl]-2-hydroxypropoxy}-phenyl]ethanone makes a π–cation interactions with Phe656, and a hydrogen-bond with Ser624. Like the other nontrapped molecule, the 2,3-dimethylphenyl ring is placed in the inner pore. Even if the compound has a smaller volume than propafenone due to the lack of the second phenyl ring, the molecule is not trapped. These poses indicate that electrostatic interactions are important for drug trapping, because the protonated nitrogen is pushed up during the channel gating. Witchel et al. [11] indicated that the amino acid Phe656 plays an important role in the interaction with propafenone, while the mutations of other amino acids to alanine do not affect the hERG block. In this study, the results suggest that also the amino acids Thr623 and Ser624 might interact with propafenone. The main structural difference between trapped and nontrapped compounds is the bulkiness of the substituent attached to the protonated nitrogen atom, which is larger in the nontrapped ones. In light of this consideration, the authors suggest that the size of the substituent might be one of the contributing factors playing a role in the drug trapping/nontrapping. In detail, all these results indicate that the compounds that are small enough and that can alter the conformation can be trapped, in contrast to compounds with a bulky substituent that can prevent the closure of the activation gate with a "foot-in-the-door" like mechanism.

5.3 Amino Acids Involved in hERG Inhibition

At the base of the hERG channel, two concentric rings formed by four Tyr652 and four Phe656 are located. The ring formed by the four Phe656 is placed near the cytoplasm, whereas the ring made by four Tyr652 face the central cavity. These two rings can make hydrophobic, π–stacking and π–cation interactions, explaining the polyspecificity of the hERG channel.

Several authors studied the physicochemical properties responsible for interactions with Tyr652 and Phe656 with the ligands. Fernandez et al. [103] studied the

nature of the interactions of MK-499, terfenadine and cisapride with the amino acids Tyr652 and Phe656. They observed that the mutation of Phe656 to Trp, Tyr, Met, Leu or Ile altered the block of MK-499, cisapride and terfenadine only slightly. In contrast, the mutation of Phe656 to the polar amino acids Arg, Glu, Ser, and Thr, or to small amino acids such as Ala and Gly increased the IC_{50}. All together these results indicate that the most important physicochemical feature of Phe656 is the hydrophobic volume and not the aromaticity. Mutation of Tyr652 to Phe or Trp did not influence significantly the sensitivity of hERG to Mk-499, terfenadine and cisapride, indicating that the hydroxyl group of Tyr652 is not essential for the interaction with hERG blockers. The IC_{50} of MK-499, terfenadine and cisapride dramatically increased when Tyr652 was mutated to Ile, Val, Ala, Thr, Gln, and Glu. All together these results highlight that the aromaticity at position Tyr652 is an important feature for hERG inhibition by these three potent blockers.

Mitcheson et al. [6] found that the hERG block mediated by MK-499 was affected by mutations of Thr623, Ser624, Val625, Gly648, Tyr652, Phe656, and Val659. The experiments performed on terfenadine and cisapride supported the interactions with Tyr652 and Phe656, but not the interaction with Val625. Same results were obtained by Karczewski et al. [104] for MK-499, its enantiomers, and its analogs obtained replacing the hydroxyl group with a hydrogen or an amine group. In contrast, the carbonyl analog was insensitive to the Phe656Ala mutation. This result indicates that the carbonyl oxygen interacts with the hERG channel.

The reduction of sensitivity due to the mutation of Thr623, Ser624, and Val625 to alanine was observed also for clofilium and ibutilide. Sanchez-Chapula et al. [5] determined that the binding site for the weak blocker chloroquine is formed by Tyr652 and Phe656. In contrast to previous results [103], they found that the mutation Tyr652Phe was detrimental for the affinity, indicating that the hydroxyl group is essential for the inhibition of the hERG channel mediated by chloroquine.

Mutation of the Phe656 and Tyr652 to alanine reduce the binding affinity of the potent blockers MK-499, terfenadine, cisapride [6, 9], clofilium, ibutilide [12, 105], thioridazine [106], and of the weak blockers chloroquine [5], nifekalant, bepridil [8], maprotiline [107], and mianserin [108] indicating the importance of the presence of aromatic amino acids in this position.

In contrast to these results, hERG channel block mediated by some blockers was almost insensitive to the mutations of Tyr652 and/or Phe656 to alanine. The inhibition of hERG channels by fluvoxamine was only partially attenuated by the Phe656Ala mutation [109]. Mutation of Phe656 to alanine did not affect the hERG block by dronedarone and amiodarone [110]. Tyr652Ala mutation showed a modest effect on the block mediated by dronedarone, while it had a more marked effect on the amiodarone binding. All these data suggest that neither Tyr652 nor Phe656 interact with dronedarone, while Tyr652 might be part of the amiodarone-binding site. Mutation of Tyr652 to alanine did not affect the hERG block by erythromycin, and mutation of Phe656 to alanine had only a weak effect on the inhibition [88].

An interesting study of Shamovsky et al. [54] analyzed the contribution of the desolvation component of hERG potency and the nondesolvation-related

interactions with the hERG channel. They used 25 3,9-diazaspiro-[5.5]undecane analogs and 8 hERG mutants. The PLS discriminant analysis (PLS-DA) revealed that the desolvation component of hERG potency increases the block of the mutants Tyr652Ala and Tyr652Phe, while the Thr623Ser and Ser624Thr mutants are less sensitive to inhibitors. These results suggest that the desolvation component of hERG potency is related to the lipophilicity of the compounds. Within the nondesolvation-related interactions with the hERG channel the Thr623Ser, Ser624Thr, Tyr652Ala, Phe656Met, Phe656Thr, and Phe656Trp mutants increase hERG potency. This indicates that the lipophilic substituents cannot fit into the inner pore due to clashes with Phe656. This hypothesis is confirmed by docking studies on the homology model of hERG in the closed state, which predicts that the molecules cannot fit well at the level of the four Phe656. All together these results suggest that bulky and rigid substituents are detrimental for the hERG affinity.

5.4 Hydrogen Bonds with Ser624, Thr623 or Val625?

The amino acids Thr623, Ser624 and Val625 lie at the top of the inner cavity. Dougherty et al. [111] mutated the amino acids facing the hERG pore to determine the binding efficacy of astemizol, dofetilide, haloperidol, risperidone, droperidol, pimozide, loxapine, amoxapine, imipramine, fluphenazine, trifluprom azine, *cis*-flupenthixol, and amperozide. Astemizole showed an increased IC_{50} value with the double flourinated Phe relative to the single flourinated Phe and the Tyr652Phe mutants, indicating that Tyr652 interacts with astemizole through π–stacking and/or π–cation interactions. The mutation of Phe656 into the two flourinated phenylalanines did not affect hERG channel block. This suggests that Phe656 may not be involved in the binding of astemizole, or that it forms hydrophobic interactions. Mutation of Thr623 to the nonnatural amino acid Thr623-(OH) led only to slight increase of the binding affinity, while the Thr623Val mutant is less sensitive to astemizole. The Ser624Thr mutation slightly decreased the astemizole hERG block, while the affinity for the hERG channel was lost in the Ser624Ala mutation. These results show the importance of the hydroxy group of Ser624.

Perry et al. [12] used site-directed mutagenesis to investigate the interactions of clofilium and ibutilide with hERG channel. The authors performed an alanine scanning of the amino acids of the S6 domain facing the pore of the hERG channel. The results show that both blockers were affected by mutation of the amino acids Thr623, Ser624, Val625, Gly648, Tyr652, Phe656, and Val659 to alanine.

Using the same method, Kamiya et al. [8] determined that the binding site of the hERG blockers E-4031 and dofetilide consists of the amino acids Thr623, Ser624, Val625, Tyr652, Phe656 and Val659. The same effect was obtained for the hERG blocker nifekalant, except for the Val659Ala mutation that did not affect the hERG inhibition and for the Ile655Ala that reduced channel block. The Thr623, Ser624, Val625 and Phe656 mutations reduced the block of the hERG channel by bepridil.

Using alanine scanning, Kamiya et al. [9] showed that amino acids Thr623, Ser624, Tyr652 and Phe656 play an important role in hERG inhibition by terfenadine and cisapride.

Finally, Hosaka et al. [95] applied a site-directed mutagenesis to analyze the interactions between nifekalant and amino acids in the pore region of hERG. The mutation of Thr623, Val625, Gly648, Tyr652 and Phe656 to alanine abolished the block of the hERG channel. The mutant Val625Ala disrupted the K^+ selectivity. This indicates that the side chain of Val625 might be essential for the stability of the selectivity filter structure, hence the mutant Val625Ala might perturb the surface of the inner cavity reducing indirectly the affinity for nifekalant. The homology model of the hERG channel in the open state showed that Gly648 was not part of the pore channel, so the reduction of the hERG block was due to an indirect action.

5.5 Role of Gly648

Siebrands et al. [112] created the hERG mutants T623A, S624A, V625A, G648A, Y652A, Y652T, F656A and F656T by site-direct mutagenesis to analyze the interactions between bupivacaine and the hERG channel. All the mutants abolished the channel block by bupivacaine. The mutation of Gly648 to alanine might lead to a reorientation of the amino acids in the S6 domain, thus indirectly reducing the affinity for the blocker.

5.6 Which Subunits Are Involved in Drug Binding?

Recently it was investigated which subunits of the hERG channel are involved in the interaction with the blockers [113, 114]. Myokai et al. [113] constructed seven tandem dimers with single or double mutations (Y652A and/or P656A) to test which mutations affect the binding of cisapride. The results brought to light that the binding site of cisapride consists of several subunits. Combining the voltage dependence of the cisapride block, the steady-state block, mutagenesis and kinetic data, it was suggested that cisapride binds at first to the low-affinity binding site formed by the two Phe656 of opposite subunits. Only when the voltage-dependent conformational changes reorient the residues in the pore, cisapride binds to the high-affinity binding site constituted by the two Tyr652 of adjacent subunits and Phe656.

Imai et al. [114] constructed the tandem dimers mutating the amino acids Ser624, Tyr652, and Phe656 of opposite subunits to investigate the binding site of cisapride, E-4031 and terfenadine. The inhibition curves of the mutant channels revealed that cisapride and E-4031 interact with Tyr652 and Phe656 of adjacent subunits and with Ser624, while terfenadine interacts with Tyr652 and Phe656 of

opposite subunits but not with Ser624. Based on the results of the inhibition curves, the three compounds were docked into homology models of the hERG channel in the open state. The docking pose of cisapride shows π–π interaction between one aromatic ring of the molecule and Tyr652, and CH–π interaction between the Tyr652 of adjacent subunits and the methylene group near the protonated nitrogen in the piperidine ring. The second aromatic ring of the molecule forms π–stacking interactions with Phe656, and the carbonyl oxygen interacts via hydrogen bond with Ser624. The docking pose of E-4031 indicates that the aromatic rings form π–π interactions with herringbone geometry with two Tyr652 of adjacent subunits, that the pyridine ring makes a hydrogen-bond with Ser624, and that the methyl group in the methansulfonamide moiety forms a CH–π interaction with the amino acid Phe656. The pose of terfenadine shows that the two terminal aromatic rings and the second benzene ring of the benzhydryl moiety interact with Tyr652 and Phe656 through π–π interaction with herringbone geometry. Based on these interactions, the introduction of an electron withdrawing group, or the introduction of a bulky substituent, which disrupts the interactions with Tyr652 and Phe656, can lead to a terfenadine derivative with an attenuated hERG binding affinity. The docking poses of cisapride, E-4031 and terfenadine proposed in this study, in contrast to a previous study [103], highlighted that π–cation interactions might not always play a dominant role, and that π–π interactions with herringbone geometry and CH–π interactions could be important in the hERG-blocker complex formation.

5.7 *Influence of Para-Substituents on the Phenyl Ring*

Mutagenesis data and docking studies suggest that the *para*-substituent of phenyl rings in inhibitors forms polar interactions with Thr623 and Ser624[12]. To test this hypothesis, a structure activity relationship of ibutilide derivatives was performed to analyze the influence on the IC_{50} of different *para*-substituents [105]. The IC_{50} of ibutilide analogs measured on wild-type hERG channels showed a rank order of nitro > chlorine > amine > amide. Similar results were obtained also with dofetilide derivatives. These results are in agreement with the 3D-CoMSiA and the 3D-pharmacophore models developed by Cavalli et al. [30], which indicated the importance of a polar or a polarizable region close to an aromatic ring. All these information suggest that it is possible to reduce the hERG potency by modifying the nature of the substituent in the *para* position of phenyl rings and thereby develop compounds with a better toxicological profile.

The docking poses of clofilium and the nitro analog show that the *para*-substituent interacts with Thr623 and Ser624 and that the phenyl ring forms π–stacking interaction with Tyr652. The ethyl group attached to the protonated nitrogen, which is placed in the center of the central cavity, forms hydrophobic interactions with Tyr652. The second ethyl group present in some docked inhibitors may form hydrophobic interactions with a second Tyr652. The docking poses indicate that

bulky substituents in *para* position prevent to adopt the conformations of clofilium and its nitro analog. The pose of clofilium predicts that the chlorine atom forms hydrogen–bond interactions with Ser624. In the proposed binding conformation of ibutilide, the *para*-substituent interacts with Thr623, Ser624, and the phenyl ring forms π–stacking interaction with Tyr652. The amide analog cannot adopt the binding mode of ibutilide and interacts with Thr623 and Ser624, probably due to the lack of the sulfonyl and of the hydroxyl groups. The interactions with Tyr652 are weak, and this explains the low affinity of the amide analog for the hERG channel. In all four compounds, the tail makes hydrophobic interactions with Phe656.

5.8 Two or Three Binding Interactions?

Mutagenesis studies of the S6 domain identified Tyr652 and Phe656 as important sites of interaction. These results led to propose that the charged nitrogen atom may form π–cation interactions with Tyr652 or Phe656, and that the aromatic moieties of the blockers can make π–stacking interactions with the amino acids cited above. Choe et al. [97] suggested a model with three key interactions: hydrogen–bond interaction between the protonated nitrogen atom and the carbonyl oxygen of Thr623; π–stacking interactions between an aromatic ring and Tyr652; hydrophobic interaction between an hydrophobic moiety of the blocker and Phe656. To test the three key interactions model, 69 known hERG blockers were divided into eight binding types and further subdivided into two groups based on the number of interactions with the hERG channel (two or three) predicted by the model. Consistent with the three key interactions model, the different distribution of pIC_{50} values between the two groups reveals that the blockers can form three interactions, and that the compounds, which are predicted to form more interactions show a higher mean pIC_{50} value.

5.9 Docking Studies and Prediction of hERG Binding Affinity

Rajamani et al. [89] developed a two-state binding affinity model to predict the IC_{50} values of potential hERG blockers. Homology models of the hERG channel in the closed and open states were constructed using as template the crystal structures of KcsA and MthK, respectively. Initially, the S6 helix of the reference closed-state model was rotated to match MthK S6 helix, and subsequently the channel was closed rotating the S6 helix by 1°. The partial open-state model (10° translation away from the reference model) and the fully open state (19° translation away from the reference model) were used to dock 32 hERG inhibitors. The best pose for each ligand was then minimized within the channel, and finally the minimized pose

(bound state) was extracted and minimized in water (free state) to obtain the reference electrostatic and van der Waals energies. The difference in the computed energy values (Δele and Δvdw) between the bound and the free states were used to derive linear regression fits to the experimental pIC_{50}. The estimated interaction energy was used to establish the preference of each ligand for one of the two states. The computed pIC_{50} values of the 21 ligands that prefer to bind the open-state model were predicted with an RMSD of 1.2 [$pIC_{50Open} = -0.166(\Delta vdw) + 0.002(\Delta ele)$]. For the 11 compounds that preferentially interact with the partially open-state model, the pIC_{50} values were calculated with an RMSD of 0.85 [$pIC_{50Closed} = -0.155(\Delta vdw) + 0.0004(\Delta ele)$]. Given the fact that both models had essentially the same coefficients for the (Δvdw) term, a single model was generated combining the energies for each ligand docked into its best fit state. Plotting the experimental versus computed pIC_{50} values five outliers were identified. The model obtained [$pIC_{50Combined} = -0.163(\Delta vdw) + 0.0009(\Delta ele)$] omitting those five outliers showed an RMSD of 0.56 and an r^2 of 0.82. The equation reveals that the most important contribution to the hERG affinity arises from Δvdw, in agreement with the previous observations, which indicated that hydrophobicity and aromaticity were the most important physicochemical features of Phe656 and of Tyr652, respectively [103].

Österberg et al. [98] used molecular dynamics (MD) simulations and the linear interaction energy (LIE) method to calculate the binding affinity of six sertindole analogues docked into the homology model of the hERG channel in the open state. For each ligand, the pose with the lowest energy was selected from the two or three best clusters, and was submitted to molecular dynamics (MD) simulations. The K^+ ions can occupy the selectivity filter with the 1010 (K^+–H_2O–K^+–H_2O) or with the 0101 (H_2O–K^+–H_2O–K^+) configurations. The binding free energies for hERG indicated that the 1010 is the most favorable conformation. The higher value of binding free energies obtained with the 0101 configuration is due to the electrostatic repulsion between the basic nitrogen of the blocker and the K^+ ion facing the central cavity. The plot of the calculated LIE free energies versus the experimental values shows a good correlation between these two terms.

Also, Farid et al. [99] obtained a good correlation between the predicted and the experimental ligand binding free energy of four sertindole analogs. The compounds were docked into the homology model of the hERG channel in the open state using the induce-fit protocol. The correlation between the Extra Precision (XP) scoring in Glide and the experimental binding affinity shows an r^2 of 0.95. The analysis of the terms of the Extra Precision (XP) scoring indicates that the Glide-XP lipophilic contact and the Glide-XP van der Waals energy terms are favorable for hERG inhibitors, while the Glide-XP penalty for buried polar groups term is unfavorable.

The GOLD docking software was used to dock 56 known blockers into a closed-state model [92]. For each ligand, the best pose was selected and the docking GOLDScore fitness was used to derive a linear regression fit to the experimental pIC_{50}. The model achieved an r^2 of 0.60 and a q^2 of 0.56, demonstrating that it can be used to predict the binding affinity of hERG inhibitors.

5.10 Case Studies: Docking Studies and Improvement of the Selectivity

A structure-activity relationship combined with docking studies was used by Price et al. [115] to reduce the hERG affinity in a series of CCR5 antagonists. Docking of the lead compound into a homology model of the hERG channel in the closed state revealed that the benzimidazole group fits perfectly to the lipophilc region described by the four Tyr652. This result suggested that it was possible to reduce the affinity of the compounds for the hERG channel by replacing the benzimidazole moiety with other moieties. This led to the discovery of maraviroc, a potent CCR5 antagonist, which does not interact with the hERG channel.

Micheli et al. [100] performed an interesting study on the combination of docking experiments with structure-activity relationship (SAR) to improve the affinity of a series of 1,2,4-Triazol-3-yl-thiopropyl-tetrahydrobenzazepines with the dopaminergic receptor D_3 and to avoid the interaction with the hERG channel. The compounds were docked manually into homology models of the hERG channel in the closed and the open state. The docking experiments predict that the lead compound assumes a U-conformation, probably due to interactions with Tyr652, Phe656 and intramolecular π–stacking interaction. The pose shows that the charged nitrogen atom and the quinoxaline ring form hydrogen-bonds with serines in the pore of the hERG channel. Based on the docking results, two strategies were used to tackle hERG liability. In the first one the hydrophilicity of the compounds was increased. This strategy led to a compound highly selective for the D_3 receptor and with a reduced affinity for the hERG channel. The second strategy was to reduce the π interactions between the isoxazolyl group and the hERG channel breaking the coplanarity between the isoxazolyl and the benzazepine moieties. This strategy led to a reduction of hERG activity, without affecting the D_3 potency.

Also, Dinges et al. [116] used a combination of SAR and docking results to develop KDR kinase inhibitors with an optimized hERG profile. One kinase inhibitor was manually docked into a model of the hERG channel in the closed state. The best fit was obtained by orienting the compound parallel to the pore of the channel, with the acetylenic ether group oriented toward the cytoplasmatic side of the hERG channel. The pose predicts that the 1,4-dihydroindeno [1,2-*c*]pyrazole forms π–stacking interactions with Phe656, that the charged nitrogen atom on the *N*-methylpiperazine moiety can make π–cation interactions with Tyr652, and that the external nitrogen forms a hydrogen-bond with Ser624. Based on this pose three strategies were developed. The first strategy consisted on the modification of the basic side chain. This approach led to compounds with a reduced hERG affinity, but the antitumoral efficacy was compromised. In the second strategy the polarity of the acetylenic chain was increased. This led to molecules with an attenuated hERG activity, but also the KDR affinity was reduced, except for the compound bearing the glycol ether moiety that inhibited 76% tumor growth in the MX-1 tumor xenograft model. The third approach used the introduction of groups that disrupt electronically or sterically the π–stacking interaction between the

1,4-dihydroindeno [1,2-*c*]pyrazole and Phe656. The substitution of the methylene bridge with a carbonyl group reduced the hERG affinity, without affecting the KDR inhibitions.

In a recent study, Levoin et al. [117] combined homology modeling and docking to refine a homology model of the H_3 receptor. The model of the H_3 receptor was optimized in three different ways: ten independent molecular dynamics simulations of the proteins embedded in the membrane; ten independent simulated annealing (SA) runs with the most active compound of ten clusters obtained from the training set of inhibitors of each protein; iterative simulated annealing (ISA) with a rigid potent compound. The ligands were docked in the refined models and subsequently the first ranked pose of each ligand was selected, and the affinity with the protein was assessed using the DOCK_SCORE, Ligscore1-2, PLP1-2, Jain, PMF, and Ludi_1-3 scoring functions. The performance of the prediction was then evaluated using the ROC curve and the area under the curve (AUC). The best performing model in the screening of the training set compounds was the one refined via the ISA method, which achieved an AUC value of 0.73. Similar results were obtained with the test set, where the model showed an AUC of 0.71. To predict also the interactions with antitarget proteins, the same procedure was applied to refine the homology models of hERG and CYP2D6. Also in these cases, the refinement process leads to a better performance of the homology models by producing an AUC > 0.69 for both antitarget proteins.

Recently, Shamovsky et al. [38] used a combination of pharmacophore modeling, QSAR and docking to develop a successful lead optimization strategy that overcomes the undesirable interactions with hERG. The aim of the docking experiments performed on a homology model of the hERG channel in the closed state was to explain the intrinsic hERG binding. To achieve this aim two compounds, which represent extreme cases of intrinsic hERG binding were docked into the homology model of hERG. The compound A (Fig. 4) makes cooperative hydrogen–bond interactions with Ser624, whereas the compound B forms cooperative π–stacking interactions with Tyr652. The docking poses suggest that also the amino acids Leu622, Ser649, and Phe656 are involved in the intrinsic interactions between the hERG channel and the blockers.

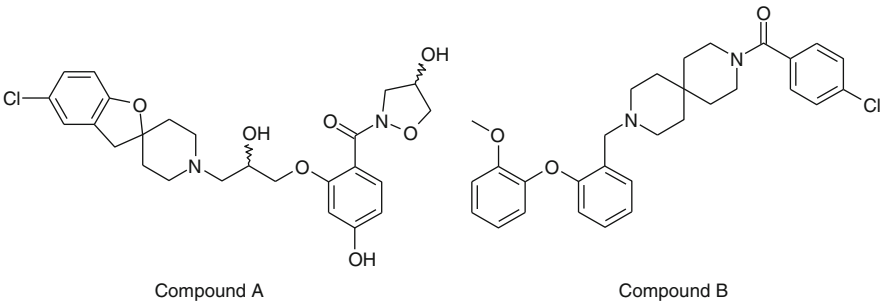

Fig. 4 2D structure of the two compounds docked in hERG channel

5.11 Orthogonal Binding Site?

In contrast to the accepted idea that the blockers bind the hERG channel longitudinally to the z axis, Zachariae et al. [118] proposed an orthogonal binding site. During MD simulations of a homology model of the hERG channel in the closed state the four Tyr652 adopted a "down conformation" with the aromatic ring plane pointing into the central cavity. The "down conformation," which is stabilized by the interactions with Phe656, opens a way to the membrane. This can explain why the cavity size of hERG in the closed state is larger than the vestibule of KcsA and can accommodate bulky compounds, such as MK-499 [3]. Docking studies performed on several compounds such as dofetilide, terfenadine, and cisapride, and previously published pharmacophore models [28–30, 33] corroborate this model. The pose of dofetilide suggests that the charged nitrogen atom is close to the K^+ binding site, and that the two aromatic rings form π–stacking interactions with two Tyr652 of opposite subunits. The binding position of terfenadine shows that the two neighboring aromatic rings of the molecule interact with two Tyr652 of adjacent subunits. In the case of cisapride, the two phenyl rings interact with two opposite Tyr652.

5.12 Docking Results

The main goal of the docking technique is to model the molecules in the binding site and to find the bound conformation of the compounds as close as possible to the crystal poses, allowing the analysis of the interactions between the ligand and the target protein.

Mitcheson et al. [6] docked MK-499 into a closed state homology model of the hERG channel. The analysis of the poses shows that the p-CN phenyl ring and the benzopyran form π–stacking interactions with Phe656 and Tyr652, while the methanesulfonanilide moiety is placed into the pocket delimited by Gly648, Thr623 and Ser624.

Karczewski et al. [104] docked MK-499 into a homology model of the hERG channel in the closed state. The docking poses of MK-499 predict that the hydroxyl group forms a hydrogen-bond with Ser624, but the contribution of this interaction to the complex stabilization is modest due to the distance between the two hydroxy oxygens (3.4 Å). In the docking pose of the carbonyl analog the distance between the oxygen of the side chain of Ser624 and the one of the substituent is 3.0 Å. This indicates that the hydrogen-bond between the carbonyl analog and Ser624 is stronger than the previously discussed one, which might explain the insensitivity to the Phe656Ala mutation.

Two possible binding modes of chloroquine were proposed by Sanchez-Chapula et al. [5]. In the first binding mode, the molecule forms π–stacking interactions with Phe656 on three subunits, as well as a hydrogen-bond with Ser649, while the

diethyl groups of the tail of the molecule form hydrophobic interactions with Tyr652. In the second binding pose, the quinoline group makes π–stacking interactions with Tyr652 and Phe656. The nitrogen atom attached to the quinoline forms a hydrogen-bond with Ser649 and the ethyl group attached to the charged nitrogen interacts with Tyr652 through hydrophobic interactions.

The aligned inhibitors used to generate the CoMSiA model of Pearlstein et al. [21] were docked into a homology model of the hERG channel in the open state. The proposed binding mode suggests that the Phe656 forms π–stacking interactions with an aromatic ring, that a second hydrophobic group can interact with another Phe656, and that the charged nitrogen atom makes π–cation interactions with Tyr652. The tail region of the blockers reaches into the pore region that extends from Tyr652 to the selectivity filter.

Moreno et al. [4] studied the effect of irbesartan on hERG, KvLQT1 + minK, hKv1.5 and Kv4.3 channels using the patch clamp technique. The homology models of hERG and hKv1.5 channels in the closed state were generated using the KcsA crystal structure as template. The pose obtained from manual docking of ibersartan shows that the blocker forms a hydrogen-bond and π–stacking interactions with Tyr652, π–stacking interactions with Phe656 and van der Waals interactions with Thr623.

The pose of clofilium proposed by Perry et al. [12] shows π–stacking interactions between the Tyr652 and the phenyl ring of the molecule, in addition to the hydrophobic interactions of the aliphatic tail of clofilium with Phe656 and the interactions of the chlorine with Thr623, Ser624, and Val625.

Duncan et al. [88] docked erythromycin into a model of the hERG channel in the open state. All the poses with low energy interact with Phe656, while the interaction with Tyr652 is prevented by the large size of the molecule that restricts the ability of erythromycin to move up into the inner cavity. The docking poses obtained with a model of the closed state shows high energy values due to steric clashes, indicating that the molecule cannot fit into the closed-state channel. Visual inspection reveals that the molecule is too large for the central cavity of the hERG channel in the closed state.

Yoshida et al. [49] docked the hERG blocker pimozide into an open-state model to examine the correspondence between the molecular determinants derived from the 2D-QSAR model with the 3D structure of the channel. The docking pose suggests that the fluorine atoms and the carbonyl group of pimozide forms hydrogen bond interactions with Ser649 and Ser624, respectively.

Hosaka et al. [95] performed a flexible docking of nifekalant into an open-state model. Consistent with the mutagenesis data, docking simulations suggest that the entire molecule is placed in the central cavity surrounded by Thr623, Ser624, Tyr652, and Phe656 of different subunits and located in close vicinity to Ser649.

Österberg et al. [98] docked a series of sertindole analogs into a homology model of the hERG channel in the open state. The docking pose of sertindole suggests that the carbonyl oxygen forms a hydrogen bond with the water molecule located in the selectivity filter. The imidazolidinone group makes good interactions with Thr623

and Ser624. Interestingly, the charged nitrogen is almost superposed to the crystallographic position of the K^+ ion in KvaP.

Farid et al. [99] used the induce-fit docking protocol to dock 12 known hERG blockers into hERG channel models in the open and closed state. S-terfenadine interacts with four Tyr652 and two Phe656. It forms T-shaped interactions with four of the six aromatic amino acids. The docking results show that the poses of R- and S-terfenadine are similar. S-terfenadine interacts simultaneously with four Tyr652 and two Phe656. The replacement of a T-shape interaction with a parallel one is the only important difference between the S-and R-terfenadine. S-terfenadine forms hydrogen-bonds with the backbone oxygen of the amino acid Leu622, and with the side chains of Ser624 and Ser649. R-terfenadine makes four hydrogen-bonds, three of them are with Ser624 of different subunits and the fourth one is with Tyr652. Also, the poses of (+)-cisapride and (−)-cisapride are similar. (+)-cisapride interacts with three Tyr652 and two Phe656, making two T-shaped interactions with the Tyr652 on opposite subunits, and a parallel interaction with one Phe656. The pose predicts also that the piperidine NH forms a hydrogen-bond with Ser624. The only difference between (+)-cisapride and (−)-cisapride is that the interaction with Phe656 is replaced by an interaction with Tyr652. MK-499 interacts simultaneously with four aromatic amino acids (two Tyr652 and two Phe656). The molecule is predicted to be near Thr623, Ser624, Ser649, and Ala653, with which it can interact. The aliphatic chain of S-ibutilide interacts with three Tyr652 and one Phe656. The phenyl ring forms a T-shaped interaction with Tyr652. The methanesulfonanilide group and the basic nitrogen are predicted to make hydrogen-bonds with two Ser624 of adjacent subunits. The pose of R-ibutilide is a mirror image of the one of S-ibutilide. Clofilium makes simultaneous interactions with four Tyr652 and three Phe656. The pose predicts one T-shaped interaction with Tyr652 and two with Phe656. Sertindole interacts with three Tyr652, two of which make T-shaped interactions. The docking pose shows also interactions with one Phe656. The pose of sertindole A5 predicts the interactions with two Tyr652 and one Phe656. It makes T-shaped interactions with one Tyr652 and one Phe656. The pose predicts also a hydrogen-bond between the backbone oxygen of Thr623 and the dimethylamine NH group. Sertindole A1-A4 interact with Tyr652 and Phe 656. Moreover, it makes hydrogen-bonds with Ser649 and with the backbone oxygen of Leu622.

Masetti et al. [91] constructed a homology model of the hERG channel in the open and in the closed state. Subsequently, the two models were embedded in a membrane bilayer, solvated, and the system was neutralized. Both models were subjected to molecular dynamics simulations of 5 ns. The docking of astemizole into the hERG channel in the closed state could not provide any reasonable pose. Reliable binding poses were identified only when astemizole was docked into snapshots of MD simulations of the hERG channel in the open state. The top ranked pose shows that the benzimidazole ring forms π–stacking interactions with Tyr652 and parallel displaced interactions with Phe656 of the same subunit. The *p*-fluorophenyl interacts with Tyr652 through parallel displaced interactions. The pose predicts also a possible hydrogen-bond between the fluorine atom and

Ser624, and the charged nitrogen atom of the piperidine ring forms a π–cation interaction with Phe656. The *p*-methoxybenzene ring is shown to be exposed to the cytoplasm.

The pose of terfenadine reported by Du et al. [92] shows that the *t*-butylphenyl moiety forms hydrophobic interactions with the amino acids Ser649, Tyr652, Ala653, and Phe656, whereas the diphenylmethanol group makes hydrophobic interactions with Ser624, Ser649 and Tyr652. The phenyl ring of the hERG blocker ibutilide is predicted to form hydrophobic interactions with Thr623, whereas the alkyl chain makes hydrophobic interactions with Thr623, Ser649, Tyr652, Ala653 and Phe656. Furthermore, the nitrogen atom of the methylsulfonamide moiety can form a hydrogen-bond with Thr623.

Singleton et al. [93] docked a series of dofetilide derivatives bearing a fluorescent group into a hERG channel homology model of the closed state. The poses highlight that the compounds lie in the inner pore, where they interact with Tyr652 and Phe656. The polycyclic conjugated dyes occupy the central cavity.

Models of hERG channel in the open and closed state were generated by Stansfeld et al. [94] using as template the structure of MthK, KvaP, and KcsA. As the models showed only partial agreement with mutagenesis data, a series of KcsA-based intermediate models were generated rotating the four S6 domains. To obtain homology models where the Phe656 can interact with the blockers also a series of intermediate models, which simulate the channel opening, were created. The docking poses of compounds E-4031, dofetilide, ibutilide, and dronedarone show that the methanesulphonamide makes hydrogen-bonds with Thr623 and Ser624. A phenyl ring is predicted to form π–stacking interactions with Tyr652. The methanesulphonamide MK-499 does not interact with the amino acids Thr623 and Ser624. The pose of dronedarone predicts that the charged nitrogen atom is placed in the same position of the K^+ identified in the inner pore in the KvaP crystal structure. The docking pose of fluvoxamine suggests that the protonated nitrogen is placed below Phe656, whereas the trifluoromethyl group lies in the central cavity and shows hydrogen–bond interactions with Thr623 and Ser624. The poses of propafenone and vesnarione make π–stacking interactions with Tyr652. For propafenone, it is also predicted that the charged nitrogen atom is placed between the Phe656 residues, with which it can form π–cation interactions. The pose of terfenadine indicates that this compound interacts with Tyr652 and Phe656. In the case of clofilium and cisapride the molecules make π–stacking interactions with Tyr652, whereas the polar groups interact with the amino acids Thr623 and Ser624. In the docking poses of quinidine and chloroquine, the basic nitrogen is placed above Phe656 and the ring system forms π–stacking interactions with Tyr652.

In summary, numerous docking studies have been conducted and they support findings from QSAR and mutation studies. However, with respect to prediction of strong hERG binders, docking definitely suffers from the still unsolved issue of proper binding free energy calculations. In addition, the channel is quite flexible and compounds might bind to the closed, semiopen and/or open states. This renders hERG binding prediction solely based on docking quite risky.

6 Conclusions

Within this review, we presented ligand-based and structure-based approaches to predict the potential risk of compounds for binding to the hERG potassium channel in a strength, which might lead to Torsades de Points. Although numerous studies have been conducted and most of them exhibit good to excellent predictivity, this issue still is not completely resolved. QSAR studies definitely suffer from the small chemical space the training compounds are covering, which renders generalization of the models difficult. Although pharmacophore models and docking could overcome this general drawback of QSAR approaches, they very often do not take into account the plasticity of the channel. Finally, channel opening and closing is a dynamic process and interaction with drugs can occur at any step. Thus, in an industrial setup, high throughput biological testing and repeated lead optimization cycles are still the method of choice to get rid of unwanted hERG activity. Finally, there is increasing evidence that, in addition to hERG, other cardiac ion channels are involved in TdP. Thus, prediction of the final clinical outcome on the organismic level will require integrated approaches, as for example, pursued by large EU-projects such as the Virtual Physiological Human Network of Excellence (http://www.vph-noe.eu) or the eTox project, which aims at prediction of the toxicological profiles of small molecules in early stages of the drug development pipeline (http://193.146.190.66/etox-web/index.html).

Acknowledgments Andrea Schiesaro is grateful for financial support by the University of Vienna under the framework of the PhD program "Molecular Drug Target" and for support from the Innovative Medicines Initiative (eTox, 115002).

References

1. Gene Connection for the Heart. http://www.fsm.it/cardmoc/
2. Witchel HJ, Hancox JC (2000) Familial and acquired long qt syndrome and the cardiac rapid delayed rectifier potassium current. Clin Exp Pharmacol Physiol 27:753–766
3. Mitcheson JS, Chen J, Sanguinetti MC (2000) Trapping of a methanesulfonanilide by closure of the HERG potassium channel activation gate. J Gen Physiol 115:229–240
4. Moreno I, Caballero R, Gonzalez T et al (2003) Effects of irbesartan on cloned potassium channels involved in human cardiac repolarization. J Pharmacol Exp Ther 304:862–873
5. Sanchez-Chapula JA, Navarro-Polanco RA, Culberson C et al (2002) Molecular determinants of voltage-dependent human ether-a-go-go related gene (HERG) K+ channel block. J Biol Chem 277:23587–23595
6. Mitcheson JS, Chen J, Lin M et al (2000) A structural basis for drug-induced long QT syndrome. Proc Natl Acad Sci USA 97:12329–12333
7. Mitcheson JS (2008) hERG potassium channels and the structural basis of drug-induced arrhythmias. Chem Res Toxicol 21:1005–1010
8. Kamiya K, Niwa R, Mitcheson JS et al (2006) Molecular determinants of HERG channel block. Mol Pharmacol 69:1709–1716
9. Kamiya K, Niwa R, Morishima M et al (2008) Molecular determinants of hERG channel block by terfenadine and cisapride. J Pharmacol Sci 108:301–307

10. Stork D, Timin EN, Berjukow S et al (2007) State dependent dissociation of HERG channel inhibitors. Br J Pharmacol 151:1368–1376
11. Witchel HJ, Dempsey CE, Sessions RB et al (2004) The low-potency, voltage-dependent HERG blocker propafenone–molecular determinants and drug trapping. Mol Pharmacol 66: 1201–1212
12. Perry M, de Groot MJ, Helliwell R et al (2004) Structural determinants of HERG channel block by clofilium and ibutilide. Mol Pharmacol 66:240–249
13. Arias C, Gonzalez T, Moreno I et al (2003) Effects of propafenone and its main metabolite, 5-hydroxypropafenone, on HERG channels. Cardiovasc Res 57:660–669
14. Katchman AN, Koerner J, Tosaka T et al (2006) Comparative evaluation of HERG currents and QT intervals following challenge with suspected torsadogenic and nontorsadogenic drugs. J Pharmacol Exp Ther 316:1098–1106
15. Kiehn J, Thomas D, Karle CA et al (1999) Inhibitory effects of the class III antiarrhythmic drug amiodarone on cloned HERG potassium channels. Naunyn Schmiedebergs Arch Pharmacol 359:212–219
16. Mergenthaler J, Haverkamp W, Huttenhofer A et al (2001) Blocking effects of the antiarrhythmic drug propafenone on the HERG potassium channel. Naunyn Schmiedebergs Arch Pharmacol 363:472–480
17. Paul AA, Witchel HJ, Hancox JC (2002) Inhibition of the current of heterologously expressed HERG potassium channels by flecainide and comparison with quinidine, propafenone and lignocaine. Br J Pharmacol 136:717–729
18. Sanchez-Chapula JA, Ferrer T, Navarro-Polanco RA et al (2003) Voltage-dependent profile of human ether-a-go-go-related gene channel block is influenced by a single residue in the S6 transmembrane domain. Mol Pharmacol 63:1051–1058
19. Schwoerer AP, Blutner C, Brandt S et al (2007) Molecular interaction of droperidol with human ether-a-go-go-related gene channels: prolongation of action potential duration without inducing early afterdepolarization. Anesthesiology 106:967–976
20. Clancy CE, Kurokawa J, Tateyama M et al (2003) K+ channel structure-activity relationships and mechanisms of drug-induced QT prolongation. Annu Rev Pharmacol Toxicol 43:441–461
21. Pearlstein RA, Vaz RJ, Kang J et al (2003) Characterization of HERG potassium channel inhibition using CoMSiA 3D QSAR and homology modeling approaches. Bioorg Med Chem Lett 13:1829–1835
22. Sanguinetti MC, Tristani-Firouzi M (2006) hERG potassium channels and cardiac arrhythmia. Nature 440:463–469
23. Morais Cabral JH, Lee A, Cohen SL et al (1998) Crystal structure and functional analysis of the HERG potassium channel N terminus: a eukaryotic PAS domain. Cell 95:649–655
24. Chen J, Mitcheson JS, Tristani-Firouzi M et al (2001) The S4-S5 linker couples voltage sensing and activation of pacemaker channels. Proc Natl Acad Sci USA 98:11277–11282
25. Cui J, Melman Y, Palma E et al (2000) Cyclic AMP regulates the HERG K(+) channel by dual pathways. Curr Biol 10:671–674
26. Thai KM, Ecker GF (2007) Predictive models for HERG channel blockers: ligand-based and structure-based approaches. Curr Med Chem 14:3003–3026
27. Aronov AM (2008) Tuning out of hERG. Curr Opin Drug Discov Devel 11:128–140
28. Morgan TK Jr, Sullivan ME (1992) An overview of class III electrophysiological agents: a new generation of antiarrhythmic therapy. Prog Med Chem 29:65–108
29. Ekins S, Crumb WJ, Sarazan RD et al (2002) Three-dimensional quantitative structure-activity relationship for inhibition of human ether-a-go-go-related gene potassium channel. J Pharmacol Exp Ther 301:427–434
30. Cavalli A, Poluzzi E, De Ponti F et al (2002) Toward a pharmacophore for drugs inducing the long QT syndrome: insights from a CoMFA study of HERG K(+) channel blockers. J Med Chem 45:3844–3853

31. Aronov AM, Goldman BB (2004) A model for identifying HERG K+ channel blockers. Bioorg Med Chem 12:2307–2315
32. Testai L, Bianucci AM, Massarelli I et al (2004) Torsadogenic cardiotoxicity of antipsychotic drugs: a structural feature, potentially involved in the interaction with cardiac HERG potassium channels. Curr Med Chem 11:2691–2706
33. Aronov AM (2006) Common pharmacophores for uncharged human ether-a-go-go-related gene (hERG) blockers. J Med Chem 49:6917–6921
34. Crumb WJ Jr, Ekins S, Sarazan RD et al (2006) Effects of antipsychotic drugs on I(to), I (Na), I (sus), I (K1), and hERG: QT prolongation, structure activity relationship, and network analysis. Pharm Res 23:1133–1143
35. Johnson SR, Yue H, Conder ML et al (2007) Estimation of hERG inhibition of drug candidates using multivariate property and pharmacophore SAR. Bioorg Med Chem 15: 6182–6192
36. Kramer C, Beck B, Kriegl JM et al (2008) A composite model for HERG blockade. ChemMedChem 3:254–265
37. Garg D, Gandhi T, Gopi Mohan C (2008) Exploring QSTR and toxicophore of hERG K+ channel blockers using GFA and HypoGen techniques. J Mol Graph Model 26:966–976
38. Shamovsky I, Connolly S, David L et al (2008) Overcoming undesirable HERG potency of chemokine receptor antagonists using baseline lipophilicity relationships. J Med Chem 51: 1162–1178
39. Coi A, Massarelli I, Testai L et al (2008) Identification of "toxicophoric" features for predicting drug-induced QT interval prolongation. Eur J Med Chem 43:2479–2488
40. Cianchetta G, Li Y, Kang J et al (2005) Predictive models for hERG potassium channel blockers. Bioorg Med Chem Lett 15:3637–3642
41. Li Q, Jorgensen FS, Oprea T et al (2008) hERG classification model based on a combination of support vector machine method and GRIND descriptors. Mol Pharm 5:117–127
42. Ermondi G, Visentin S, Caron G (2009) GRIND-based 3D-QSAR and CoMFA to investigate topics dominated by hydrophobic interactions: the case of hERG K+ channel blockers. Eur J Med Chem 44:1926–1932
43. Aptula AO, Cronin MT (2004) Prediction of hERG K+ blocking potency: application of structural knowledge. SAR QSAR Environ Res 15:399–411
44. Keseru GM (2003) Prediction of hERG potassium channel affinity by traditional and hologram qSAR methods. Bioorg Med Chem Lett 13:2773–2775
45. Fioravanzo E, Cazzolla N, Durando L et al (2005) General and independent approaches to predict HERG affinity values. Internet Electron J Mol Des 4:625–646
46. Song M, Clark M (2006) Development and evaluation of an in silico model for hERG binding. J Chem Inf Model 46:392–400
47. Zolotoy AB, Plouvier BP, Beatch GB et al (2003) Physicochemical determinants for drug induced blockade of HERG potassium channels: effect of charge and charge shielding. Curr Med Chem Cardiovasc Hematol Agents 1:225–241
48. Coi A, Massarelli I, Murgia L et al (2006) Prediction of hERG potassium channel affinity by the CODESSA approach. Bioorg Med Chem 14:3153–3159
49. Yoshida K, Niwa T (2006) Quantitative structure-activity relationship studies on inhibition of HERG potassium channels. J Chem Inf Model 46:1371–1378
50. Seierstad M, Agrafiotis DK (2006) A QSAR model of HERG binding using a large, diverse, and internally consistent training set. Chem Biol Drug Des 67:284–296
51. Ekins S, Balakin KV, Savchuk N et al (2006) Insights for human ether-a-go-go-related gene potassium channel inhibition using recursive partitioning and Kohonen and Sammon mapping techniques. J Med Chem 49:5059–5071
52. Leong MK (2007) A novel approach using pharmacophore ensemble/support vector machine (PhE/SVM) for prediction of hERG liability. Chem Res Toxicol 20:217–226

53. Gavaghan CL, Arnby CH, Blomberg N et al (2007) Development, interpretation and temporal evaluation of a global QSAR of hERG electrophysiology screening data. J Comput Aided Mol Des 21:189–206
54. Shamovsky I, de Graaf C, Alderin L et al (2009) Increasing selectivity of CC chemokine receptor 8 antagonists by engineering nondesolvation related interactions with the intended and off-target binding sites. J Med Chem 52:7706–7723
55. Roy K, Ghosh G (2009) QSTR with extended topochemical atom (ETA) indices. 13. Modelling of hERG K+ channel blocking activity of diverse functional drugs using different chemometric tools. Mol Simulat 35:1256–1268
56. Diller DJ, Wang N, Delisle RK et al (2006) WO Patent WO2006055918
57. Diller DJ, Wang N, Delisle RK et al (2006) US Patent US20060206269
58. Diller DJ, Hobbs DW (2007) Understanding hERG inhibition with QSAR models based on a one-dimensional molecular representation. J Comput Aided Mol Des 21:379–393
59. Bains W, Basman A, White C (2004) HERG binding specificity and binding site structure: evidence from a fragment-based evolutionary computing SAR study. Prog Biophys Mol Biol 86:205–233
60. Tobita M, Nishikawa T, Nagashima R (2005) A discriminant model constructed by the support vector machine method for HERG potassium channel inhibitors. Bioorg Med Chem Lett 15:2886–2890
61. Roche O, Trube G, Zuegge J et al (2002) A virtual screening method for prediction of the HERG potassium channel liability of compound libraries. Chembiochem 3:455–459
62. Dubus E, Ijjaali I, Petitet F et al (2006) In silico classification of HERG channel blockers: a knowledge-based strategy. ChemMedChem 1:622–630
63. Thai KM, Ecker GF (2009) Similarity-based SIBAR descriptors for classification of chemically diverse hERG blockers. Mol Divers 13:321–336
64. Thai KM, Ecker GF (2008) Classification models for HERG inhibitors by counter-propagation neural networks. Chem Biol Drug Des 72:279–289
65. Thai KM, Ecker GF (2008) A binary QSAR model for classification of hERG potassium channel blockers. Bioorg Med Chem 16:4107–4119
66. Chekmarev DS, Kholodovych V, Balakin KV et al (2008) Shape signatures: new descriptors for predicting cardiotoxicity in silico. Chem Res Toxicol 21:1304–1314
67. Doddareddy MR, Klaasse EC, Shagufta et al. Prospective validation of a comprehensive in silico hERG model and its applications to commercial compound and drug databases. ChemMedChem 5:716–729
68. O'Brien SE, de Groot MJ (2005) Greater than the sum of its parts: combining models for useful ADMET prediction. J Med Chem 48:1287–1291
69. Sun H (2006) An accurate and interpretable bayesian classification model for prediction of HERG liability. ChemMedChem 1:315–322
70. Jia L, Sun H (2008) Support vector machines classification of hERG liabilities based on atom types. Bioorg Med Chem 16:6252–6260
71. Buyck C, Tollenaere J, Engels M et al (8–13 Sep. 2002) The 14th European Symposium on QSARs. Bournemouth, UK
72. Catana C (2009) Simple idea to generate fragment and pharmacophore descriptors and their implications in chemical informatics. J Chem Inf Model 49:543–548
73. Redfern WS, Carlsson L, Davis AS et al (2003) Relationships between preclinical cardiac electrophysiology, clinical QT interval prolongation and torsade de pointes for a broad range of drugs: evidence for a provisional safety margin in drug development. Cardiovasc Res 58: 32–45
74. Yap CW, Cai CZ, Xue Y et al (2004) Prediction of torsade-causing potential of drugs by support vector machine approach. Toxicol Sci 79:170–177
75. Skold C, Winiwarter S, Wernevik J et al (2006) Presentation of a structurally diverse and commercially available drug data set for correlation and benchmarking studies. J Med Chem 49:6660–6671

76. Gepp MM, Hutter MC (2006) Determination of hERG channel blockers using a decision tree. Bioorg Med Chem 14:5325–5332
77. Hidaka S, Yamasaki H, Ohmayu Y et al (2010) Nonlinear classification of hERG channel inhibitory activity by unsupervised classification method. J Toxicol Sci 35:393–399
78. Papadatos G, Alkarouri M, Gillet VJ et al (2010) Lead optimization using matched molecular pairs: inclusion of contextual information for enhanced prediction of HERG inhibition, solubility, and lipophilicity. J Chem Inf Model 50:1872–1886
79. Doyle DA, Morais Cabral J, Pfuetzner RA et al (1998) The structure of the potassium channel: molecular basis of K+ conduction and selectivity. Science 280:69–77
80. Zhou Y, Morais-Cabral JH, Kaufman A et al (2001) Chemistry of ion coordination and hydration revealed by a K+ channel-Fab complex at 2.0 A resolution. Nature 414:43–48
81. Zhou Y, MacKinnon R (2003) The occupancy of ions in the K+ selectivity filter: charge balance and coupling of ion binding to a protein conformational change underlie high conduction rates. J Mol Biol 333:965–975
82. Kuo A, Gulbis JM, Antcliff JF et al (2003) Crystal structure of the potassium channel KirBac1.1 in the closed state. Science 300:1922–1926
83. Jiang Y, Lee A, Chen J et al (2002) Crystal structure and mechanism of a calcium-gated potassium channel. Nature 417:515–522
84. Jiang Y, Lee A, Chen J et al (2003) X-ray structure of a voltage-dependent K+ channel. Nature 423:33–41
85. Jalaie M, Holsworth DD (2005) QT interval prolongation: and the beat goes on. Mini Rev Med Chem 5:1083–1091
86. Recanatini M, Poluzzi E, Masetti M et al (2005) QT prolongation through hERG K(+) channel blockade: current knowledge and strategies for the early prediction during drug development. Med Res Rev 25:133–166
87. Aronov AM (2005) Predictive in silico modeling for hERG channel blockers. Drug Discov Today 10:149–155
88. Duncan RS, Ridley JM, Dempsey CE et al (2006) Erythromycin block of the HERG K+ channel: accessibility to F656 and Y652. Biochem Biophys Res Commun 341:500–506
89. Rajamani R, Tounge BA, Li J et al (2005) A two-state homology model of the hERG K+ channel: application to ligand binding. Bioorg Med Chem Lett 15:1737–1741
90. Yi H, Cao Z, Yin S et al (2007) Interaction simulation of hERG K+ channel with its specific BeKm-1 peptide: insights into the selectivity of molecular recognition. J Proteome Res 6: 611–620
91. Masetti M, Cavalli A, Recanatini M (2008) Modeling the hERG potassium channel in a phospholipid bilayer: molecular dynamis and drug docking studies. J Comput Chem 29: 795–808
92. Du L, Li M, You Q et al (2007) A novel structure-based virtual screening model for the hERG channel blockers. Biochem Biophys Res Commun 355:889–894
93. Singleton DH, Boyd H, Steidl-Nichols JV et al (2007) Fluorescently labeled analogues of dofetilide as high-affinity fluorescence polarization ligands for the human ether-a-go-go-related gene (hERG) channel. J Med Chem 50:2931–2941
94. Stansfeld PJ, Gedeck P, Gosling M et al (2007) Drug block of the hERG potassium channel: insight from modeling. Proteins 68:568–580
95. Hosaka Y, Iwata M, Kamiya N et al (2007) Mutational analysis of block and facilitation of HERG current by a class III anti-arrhythmic agent, nifekalant. Channels (Austin) 1:198–208
96. Tseng GN, Sonawane KD, Korolkova YV et al (2007) Probing the outer mouth structure of the HERG channel with peptide toxin footprinting and molecular modeling. Biophys J 92:3524–3540
97. Choe H, Nah KH, Lee SN et al (2006) A novel hypothesis for the binding mode of HERG channel blockers. Biochem Biophys Res Commun 344:72–78

98. Osterberg F, Aqvist J (2005) Exploring blocker binding to a homology model of the open hERG K+ channel using docking and molecular dynamics methods. FEBS Lett 579: 2939–2944
99. Farid R, Day T, Friesner RA et al (2006) New insights about HERG blockade obtained from protein modeling, potential energy mapping, and docking studies. Bioorg Med Chem 14: 3160–3173
100. Micheli F, Bonanomi G, Blaney FE et al (2007) 1,2,4-triazol-3-yl-thiopropyl-tetrahydrobenzazepines: a series of potent and selective dopamine D(3) receptor antagonists. J Med Chem 50:5076–5089
101. Armstrong CM (1969) Inactivation of the potassium conductance and related phenomena caused by quaternary ammonium ion injection in squid axons. J Gen Physiol 54:553–575
102. Thai KM, Windisch A, Stork D et al (2010) The hERG potassium channel and drug trapping: insight from docking studies with propafenone derivatives. ChemMedChem 5:436–442
103. Fernandez D, Ghanta A, Kauffman GW et al (2004) Physicochemical features of the HERG channel drug binding site. J Biol Chem 279:10120–10127
104. Karczewski J, Wang J, Kane SA et al (2009) Analogs of MK-499 are differentially affected by a mutation in the S6 domain of the hERG K+ channel. Biochem Pharmacol 77:1602–1611
105. Perry M, Stansfeld PJ, Leaney J et al (2006) Drug binding interactions in the inner cavity of HERG channels: molecular insights from structure-activity relationships of clofilium and ibutilide analogs. Mol Pharmacol 69:509–519
106. Milnes JT, Witchel HJ, Leaney JL et al (2006) hERG K+ channel blockade by the antipsychotic drug thioridazine: an obligatory role for the S6 helix residue F656. Biochem Biophys Res Commun 351:273–280
107. Kiesecker C, Alter M, Kathofer S et al (2006) Atypical tetracyclic antidepressant maprotiline is an antagonist at cardiac hERG potassium channels. Naunyn Schmiedebergs Arch Pharmacol 373:212–220
108. Scherer D, von Lowenstern K, Zitron E et al (2008) Inhibition of cardiac hERG potassium channels by tetracyclic antidepressant mianserin. Naunyn Schmiedebergs Arch Pharmacol 378: 73–83
109. Milnes JT, Crociani O, Arcangeli A et al (2003) Blockade of HERG potassium currents by fluvoxamine: incomplete attenuation by S6 mutations at F656 or Y652. Br J Pharmacol 139: 887–898
110. Ridley JM, Milnes JT, Witchel HJ et al (2004) High affinity HERG K(+) channel blockade by the antiarrhythmic agent dronedarone: resistance to mutations of the S6 residues Y652 and F656. Biochem Biophys Res Commun 325:883–891
111. Dougherty DA, Lester HA, Nowak MW (2006) US Patent US20060084102
112. Siebrands CC, Friederich P (2007) Structural requirements of human ether-a-go-go-related gene channels for block by bupivacaine. Anesthesiology 106:523–531
113. Myokai T, Ryu S, Shimizu H et al (2008) Topological mapping of the asymmetric drug binding to the human ether-a-go-go-related gene product (HERG) potassium channel by use of tandem dimers. Mol Pharmacol 73:1643–1651
114. Imai YN, Ryu S, Oiki S (2009) Docking model of drug binding to the human ether-a-go-go potassium channel guided by tandem dimer mutant patch-clamp data: a synergic approach. J Med Chem 52:1630–1638
115. Price DA, Armour D, de Groot M et al (2006) Overcoming HERG affinity in the discovery of the CCR5 antagonist maraviroc. Bioorg Med Chem Lett 16:4633–4637
116. Dinges J, Albert DH, Arnold LD et al (2007) 1,4-Dihydroindeno[1,2-c]pyrazoles with acetylenic side chains as novel and potent multitargeted receptor tyrosine kinase inhibitors with low affinity for the hERG ion channel. J Med Chem 50:2011–2029
117. Levoin N, Calmels T, Poupardin-Olivier O et al (2008) Refined docking as a valuable tool for lead optimization: application to histamine H3 receptor antagonists. Arch Pharm (Weinheim) 341:610–623

118. Zachariae U, Giordanetto F, Leach AG (2009) Side chain flexibilities in the human ether-a-go-go related gene potassium channel (hERG) together with matched-pair binding studies suggest a new binding mode for channel blockers. J Med Chem 52:4266–4276
119. Frenal K, Xu CQ, Wolff N et al (2004) Exploring structural features of the interaction between the scorpion toxinCnErg1 and ERG K+ channels. Proteins 56:367–375
120. Gomez-Varela D, Contreras-Jurado C, Furini S et al (2006) Different relevance of inactivation and F468 residue in the mechanisms of hEag1 channel blockage by astemizole, imipramine and dofetilide. FEBS Lett 580:5059–5066
121. Waldhauser KM, Brecht K, Hebeisen S et al (2008) Interaction with the hERG channel and cytotoxicity of amiodarone and amiodarone analogues. Br J Pharmacol 155:585–595

Advances in Structure–Activity Relationship Studies on Potassium Channel Modulators

Brij K. Sharma, Prithvi Singh, and Yenamandra S. Prabhakar

Contents

Abstract Ion channels are part of cell membranes. They control the influx and efflux of ions such as sodium, potassium, calcium, or chloride, as well as ligands of several biochemical processes. Due to this, they play important role in a variety of diseases ranging from the cardiovascular, nervous, immune and endocrine systems to the cancer metastasis. Moreover, a number of chemicals and genetic disorders disrupt functioning of ion channels, which in turn can lead to aggrieved situations. This makes ion channels as potential targets in drug discovery programs. However, because of ion channels' ubiquitous nature and high variability even within a given family, identification of drugs acting via them with specificity and high therapeutic value is a challenge! With a brief introduction to the fundamental aspects of ion channels, the review chapter explored the structure-activity advancements made on some potassium channel modulators namely, benzodiazepines, cromakalim analogues, benzothiadiazines, khellinone derivatives and other related chemical

Y.S. Prabhakar (✉)
Medicinal and Process Chemistry Division, Central Drug Research Institute, CSIR, Lucknow 226 001, India
e-mail: yenpra@yahoo.com

S.P. Gupta (ed.), *Ion Channels and Their Inhibitors*,
DOI 10.1007/978-3-642-19922-6_8,

prototypes. Also, attempts were made to analyze the scope of these and other ion channel modulators in addressing the challenges faced in the chemotherapy of various diseases.

Keywords Potassium ion channel modulators • QSAR • Molecular modeling • Benzodiazepine • Benzopyrans • Benzothiazine • Benzothiadiazine • Khellinone derivatives • Benzotriazoles • Benzimidazolones • Benzanilides

Abbreviations

3D-MoRSE	3D Molecule representation of structures based on electron diffraction
ABC	ATP-binding cassette
ADMET	Absorption, distribution, metabolism, elimination and toxicity
ATP	Adenosine triphosphate
BK-channels	Big K^+-channels
CFTR	Cystic fibrosis transmembrane conductance regulator
CODESSA	Comprehensive descriptors for structural and statistical analysis
CoMSIA	Comparative molecular similarity analysis
CP-MLR	Combinatorial protocol in multiple linear regression
EC_{50}	Half maximal effective concentration
G/PLS	Genetic partial least squares
GFA	Genetic function approximation
GRIND	Grid-independent descriptors
hERG	Human ether-à-go-go-related gene
HOMO	Highest occupied molecular orbital
IC_{50}	Half maximal inhibitory concentration
I_K	Cardiac rectifier potassium ion current
I_{Kr}	Rapidly activating ion current
I_{Ks}	Slowly activating ion current
KATP	ATP-sensitive K^+-channel
K_{ir}/IRK	Inwardly rectifying K^+-channel
Kv	Voltage-gated K^+-channel
LUMO	Lowest unoccupied molecular orbital
MLR	Multiple linear regression
MOPAC	Molecular orbital partial atomic charge
PCA	Principal component analysis
PCO	Potassium (K^+)-channel opener
PCR	Principle components in multiple linear regression
PLS	Partial least square
QSAR	Quantitative structure–activity relationship

QSTR	Quantitative structure–toxicity relationship
RASMC	Rat aortic smooth muscle cells
WHIM	Weighted holistic invariant molecular descriptors

1 Introduction

Ion channels are part of cell membranes. They are pore-forming proteins embedded in the membranes that surround all biological cells. Depending on the type of channel, they regulate the flow of specific ions such as sodium, potassium, calcium, or chloride by means of voltage gradient across the membrane [1]. Of the different approaches to categorize ion channels, the most acceptable one appears to be the way the ion channels are regulated. Accordingly, they can be divided into three main groups as (a) the voltage-gated channels (e.g., the sodium and potassium channels of the nerve axons and nerve terminals), (b) the extracellular ligand-activated channels (e.g., neurotransmitter regulated channels i.e., GABA and glycine receptor channels) and (c) the intracellular ligand-gated ion channels (e.g., the cystic fibrosis transmembrane conductance regulator – CFTR, ATP-binding Cassette – ABC superfamily and ion channels of sense perception). In all living organisms, potassium channels are the most widely distributed and control diverse cellular functions, which include shaping action potentials in excitable cells (e.g., neurons and cardiac muscle) and secretion of hormones (e.g., insulin release from beta-cells in the pancreas) [2–4]. They are formed from four protein subunits, either a homotetramer complex of C_4 symmetry or a heterotetrameric complex of pseudo C_4 symmetry, with a central ion conducting pore [5–8]. Depending upon the function, the potassium channels may be put in four major classes [1, 9] as (a) calcium-activated potassium channel, (b) inwardly rectifying potassium channel (K_{ir} or IRK), (c) tandem pore domain potassium channel and (d) voltage-gated potassium channels. As the name indicates, the calcium-activated potassium channels open in response to Ca^{2+} and/or other signaling ligands. The blocking of these channels increases intracellular calcium. The K_{ir} channel passes positive current into the cell and play important role in regulating neuronal activity via establishing the resting membrane potentials of the cell. They are found in variety of cells, which include cardiac, kidney, leukocytes, neurons and endothelial. The tandem pore domain potassium channels are two-pore-domain potassium channels. They are also known as "leak channels" [10] and set the negative membrane potential of neuron. When open, they allow potassium ions to cross the membrane very fast. These channels are regulated via G-proteins, oxygen tension, pH, etc. The voltage-gated potassium channels are transmembrane potassium channels sensitive to voltage changes in the cell's membrane. During action potentials, they play a vital role in returning the depolarized cell to a resting state.

Ion channels play important role in a variety of diseases ranging from the cardiovascular nervous, immune and endocrine systems to the cancer metastasis [11–16]. Also, number of chemical entities as well as genetic disorders can disrupt

the functioning of ion channels, which in turn lead to aggrieved situations [17]. This makes them as potential targets in drug discovery programs. However, because of ion channels' ubiquitous nature and high variability even within a given family, identification of drugs acting via them with specificity and high therapeutic value is a challenge. This article discusses some of the recent advances made in quantitative structure–activity relationship (QSAR) and modeling studies in the optimization of various potassium channel modulators acting on different targets.

2 QSAR and Modeling Studies

Barring the accidental discoveries, identification and design of a ligand (or inhibitor) for any given biological target is a complex process. Also, the drug research and development is an interdisciplinary task of many areas, which include chemical, biological, clinical, chemo- and bio-informatics. In this scenario, the quantitative structure–activity relationship (QSAR) and modeling studies offer rationales to make educated choice of biomolecular requirements by bridging the chemical features and the activity phenomena.

The QSAR and modeling studies discussed in this article involved a variety of physicochemical, quantum chemical, topological and topographical descriptors from various sources such as Hansch and Leo's monograph [18], Molecular Orbital Partial Atomic Charge (MOPAC) [19], ChemDraw's property/descriptor database [20], Comprehensive Descriptors for Structural and Statistical Analysis (CODESSA) [21, 22] and DRAGON [23], for the parameterization of the chemical structure. Most of the studies reviewed have involved 2D-QSAR approaches for the rationalization of the biological function. They include simple Multiple Linear Regression (MLR), Principle Components Regression (PCR), Partial Least Square (PLS) [24], Genetic Function Approximation (GFA) [25], Genetic Partial Least Squares (G/PLS) [26], Combinatorial Protocol in Multiple Linear Regression (CP-MLR) [27], Discriminant and Cluster Analysis. Some of the reported works also involved 3D-approaches in deriving the QSAR models. These approaches were identified in the discussion of concerned models.

Most of the QSAR results presented in this article were validated through various techniques such as leave one out, leave many out and external test sets. For all regression equations, the statistics were reproduced as reported in the original source. Briefly, in regression statistics n is the number of compounds in the dataset, r is the correlation coefficient, Q^2 is cross-validated r^2 from leave-one/many out procedure, s is the standard error of the estimate and F is the F-ratio between the variances of calculated and observed activities. The values given in the parentheses of regression equation are the standard errors (without arithmetic sign) or 95% confidence limits (with $\pm$ arithmetic sign) of the regression coefficients. Also for each study, wherever applicable, the QSAR methodology and the contributing or modeling descriptors were highlighted and discussed to pull out the essence of the investigation.

The succeeding sections of this review summarize QSAR studies carried out on different chemical scaffolds in modulating the activity of various potassium ion channels. Each section is identified with the leading chemical scaffold. Most of the articles reviewed belong to preceding 5–7 years. They provide critical inputs for modulating the biological endpoints of chemical entities in terms of the potential structural modifications.

2.1 Benzodiazepine Derivatives

Late 1990s has seen considerable research activity in the discovery of chemical prototypes, which can activate or block the potassium channels [12]. In antiarrhythmic agents, Class I agents interfere with sodium channels, Class II agents (β blockers) are anti-sympathetic nervous system agents and Class III agents interfere with potassium (K^+) efflux [28]. The cardiac arrhythmia suppression trial has shown that treatment of arrhythmias with Class I agents lead to higher deaths than with placebo [29]. This has prompted a search for compounds, which exert antiarrhythmic effects through other pathways. The Class III antiarrhythmic agents work through delaying repolarization of cardiac myocytes. The cardiac rectifier potassium ion current, I_K, contributes to repolarization in two kinetically distinct ways namely, a rapidly activating ion current I_{Kr} and a slowly activating ion current component I_{Ks}. Selective blockade of either I_{Kr} or I_{Ks} would lead to a prolongation of the refractory period. A selective blocking of I_{Ks} is more safer than blocking I_{Kr} channel [30, 31]. While benzodiazepines were probed as cholecystokinin-B receptor antagonists, some analogues markedly increased the electrocardiographic QT interval in dogs. Thus, benzodiazepines were further explored as potential blocker of I_{Ks}. This has led to (R)-2-(2,4-trifluoromethyl)-N-[2-oxo-5-phenyl-1-(2,2,2-trifluoroethyl)-2,3-dihydro- 1H-benzo[e][1,4]diazepin-3-yl]acetamide (L-768,673) (**1**; X = F_3CCH_2 and Y = CH_2-2,4-diCF_3-Ph), an orally active, potent and selective I_{Ks} blocking agent [32].

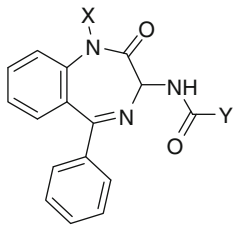

1

In view of its importance, Gupta and coworkers [33] have investigated the rationale behind the I_{Ks} blocking activity of these benzodiazepine derivatives (**1**) with simple molecular connectivity indices (1). In these compounds, X is either alkyl, fluoroalkyl, alkylamine or hydrogen, and Y is substituted aryls and cyclohexyls linked through methylene/ethylene spacers.

$$\log(1/IC_{50}) = 0.064(\pm\ 4.211) + 3.524(\pm\ 2.652)^{1}\chi^{v}_{Y} - 0.486(\pm\ 0.398)(^{1}\chi^{v}_{Y})^{2} + 0.485(\pm\ 0.428)^{1}\chi^{v}_{X} - 1.710(\pm\ 0.672)I_{1} + 0.927(\pm\ 0.531)I_{R}$$
$$n = 23, r = 0.913, Q^{2} = 0.58, s = 0.46, F = 17.03, (^{1}\chi^{v}_{Y})_{opt} = 3.63. \quad (1)$$

In (1), the I_1 and I_R are indicator variables. The I_1 has been used to account for the amine character of Y-substituents ($I_1 = 1$) and zero otherwise. The I_R takes a value of 1 for R-configuration and zero for any other configuration (S or RS). In the equation, the negative coefficient of I_1 suggests that a Y-substituent with amine character is not favorable for the activity. The positive effect of I_R suggests that R-configuration is favorable for the activity. Also, the equation suggests that 3.36 is the optimum value for the first-order valence molecular connectivity index of Y ($^{1}\chi^{v}_{Y}$). The first-order valence molecular connectivity index of X ($^{1}\chi^{v}_{X}$) is linearly and positively correlated with the activity. In these compounds $^{1}\chi^{v}$ and calculated log*P* are highly correlated ($r = 0.73$). In view of this, it is suggested that I_{Ks} blocking activity of the benzodiazepine derivatives may be influencing through the hydrophobic character of the molecules [33].

2.2 *Benzopyrans*

Cromakalim is a potential potassium channel-opener (PCO). It is a compound of benzopyran (chromane) class. It has marked myorelaxant activity resulting from the smooth muscle K_{ATP} channels [34]. It activates K_{ATP} channels [35, 36] and thereby causes plasma membrane hyperpolarization and reduction in cell excitability. The active isomer is levcromakalim (**2**). The pharmacological profile of cromakalim attracted the attention of several groups to discover other chemotypes as potential potassium channel-openers. Cromakalim being a benzopyran class of compound, benzopyran scaffold has gained considerable attention in the modulation of potassium channels activity.

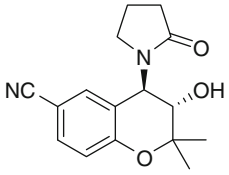

2

2.2.1 6-Substituted Benzopyrans

In one of the early modeling studies, Mannhold and coworkers have investigated the 6-substituted benzopyrans (**3**) as potassium channel activators [37]. These

compounds were evaluated for their relaxant potency in rat aorta and trachea. The chemical space of the compounds was parameterized using the Log*P*, heat of formation, ionization potential, dipole moment, HOMO, LUMO, electronegativity, hardness, polarity and GRID based 3D-interaction energy maps [37]. The models were derived using principal component analysis (PCA) and partial least-squares (PLS) analysis. A 3-component PLS model has explained 81 and 82% variance, respectively, in the aortic and the tracheal responses of the compounds. The models have suggested a direct bearing of 6-substituents on the receptor site, presumably via dipolar interactions. Apart from this, electronegativity, heat of formation, substituent size, lipophilicity, low minimum energies were identified as the dominant molecular properties in the PLS components in explaining the biological response of these compounds [37].

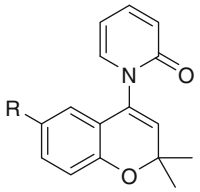

3

In an attempt to offer simpler QSAR models, Agrawal et al. [38] have reinvestigated Mannhold et al.'s data [37] in stepwise regression with distance-based topological indices, negentropy and molecular redundancy indices. This has resulted in the following 4-parameter model to explain the relaxant activity (rat trachea; EC_{50}) of the compounds.

$$\begin{aligned} \mathrm{pEC}_{50} &= -1.4982 + 3.7015(\pm\ 0.9099)J + 5.2400(\pm\ 1.8987)\mathrm{MRI} \\ &\quad + 2.1840 \times 10^{-4}\left(\pm\ 1.7955 \times 10^{-4}\right)W - 1.2294(\pm\ 0.1522)I_{p1} \\ n &= 28, r = 0.9406, s = 0.3254, F = 44.143. \end{aligned} \tag{2}$$

In this equation, J is distance-based topological index, MRI is molecular information content, W is Wiener index and I_{p1} is an indicator parameter. The negative coefficient of I_{p1} suggested that 'oxy' substitution at R (6-position) is not favorable for the activity. The positive regression coefficients of J, MRI and W indicated that an increased information content of these descriptors can improve the activity [38]. Even though some information is lost from Mannhold et al.'s model, Agrawal et al.'s attempt has offered much simpler rationale for the activity of the compounds.

2.2.2 4,6-Disubstituted-2,2-Dimethylchroman Derivatives

The PCOs have definite role in insulin secretion from the pancreas. Cromakalim provokes the relaxation of smooth muscles and/or the inhibition of endocrine

releases [39, 40]. However, cromakalim is poorly active as an inhibitor of insulin secretion [41, 42]. Therefore, in order to discover potent pancreatic β-cell selective PCOs, Sebille et al. [43] synthesized 4,6-disubstituted-2,2-dimethylchromans (**4**), structurally related to cromakalim, and evaluated them for insulin secretion from rat pancreatic islets and on the contractile activity of rat aorta rings.

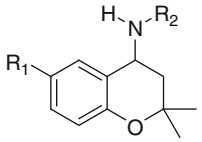

4

In an attempt to rationalize the activity of these compounds (**4**), Sharma et al. [44] have carried out a QSAR study with CP-MLR feature selection approach for optimum models. This study has identified following equations for the contractile activity of KCl-depolarized rat aorta rings (pED_{50}, where ED_{50} is the concentration in moles per liter for 50% inhibition against the K_{ATP} channel) of the compounds.

$$\begin{aligned} pED_{50} &= 60.747 - 55.466(12.333)\text{MATS4m} + 12.837(2.649)\text{MATS1p} \\ &\quad + 0.598(0.141)C - 040 \\ n &= 25, r = 0.876, Q^2 = 0.672, s = 0.338, F = 23.072. \end{aligned} \tag{3}$$

$$\begin{aligned} pED_{50} &= 24.913 - 65.976(10.109)\text{X2}A - 2.207(0.499)\text{GGI7} \\ &\quad + 7.881(1.724)\text{MATS4p} \\ n &= 25, r = 0.872, Q^2 = 0.672, s = 0.343, F = 22.287. \end{aligned} \tag{4}$$

$$\begin{aligned} pED_{50} &= -5.694 + 31.396(5.011)\text{PW3} - 3.111(0.678)\text{GGI8} \\ &\quad + 10.219(2.501)\text{MATS1p} + 1.330(0.585)\text{GATS5p} \\ n &= 25, r = 0.899, Q^2 = 0.722, s = 0.314, F = 21.076. \end{aligned} \tag{5}$$

In these equations, MATS1p, MATS4p, MATS4m and GATS5p are 2D autocorrelation descriptors [23]. MATS1p and MATS4p are the Moran autocorrelation of topological structure with path length (*lag*) 2 and 4, respectively, in the graph weighted by atomic polarizabilities. GATS5p is the Geary autocorrelation of *lag* 5 weighted by atomic polarizabilities. The regression coefficients of these descriptors indicate that the higher path lengths rich in polarizability content would be favorable for the improvement of activity. The descriptor MATS4m is Moran autocorrelation of *lag* 4 in the graph weighted by atomic masses. The negative regression coefficient associated with this descriptor suggests that a lower path length rich in atomic mass would be beneficial. The descriptors GGI7 and GGI8 are Galvez topological charge indices of orders 7 and 8, respectively. They represent the seventh and eighth eigenvalues, respectively, of the corrected adjacency matrix of

a molecule. A lower value for these descriptors is required to improve the myorelaxant activity. The descriptors X2A and PW3 represent topological class. The X2A is the average connectivity index chi-2. It encodes information about size, branching, cyclization, unsaturation and heteroatom content in a molecule. Small value for this descriptor would enhance the activity. The PW3 is path/walk Randic shape index of order 3. A higher value of this index would be beneficiary to the activity. The C-040 represents the count of structural fragments having carbon atoms attached to the hetero atom by single or multiple bonding and one valence is satisfied by an alkyl group [R-C(=X)-X′/R-C#X where X and X′ are heteroatoms, and -, = and # represent single, double and triple bonds, respectively]. In the molecules, a structural feature of this kind is helpful in augmenting the activity. Collectively, all these observations provided the detailed structural requirements in these compounds (**4**) for the myorelaxant activity.

2.2.3 Chromanol Derivatives

Chromanols (**5**) are closely related to cromakalim and inspired the researchers to explore them as potential K_{ATP}-channel blockers. Gerlach et al. investigated them for their potassium channel blocking activity (IC_{50}) using human I_{Ks} channel expressed in *Xenopus oocytes* [45]. The R_1 in these analogues is either methyl, ethyl, or butyl group. The

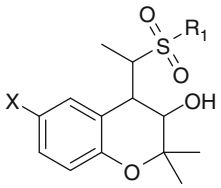

5

X-substituent on the aryl moiety has variations in terms of CN, F, Cl and alkoxy groups. Gupta et al. [46] discovered following elegant linear models for the potassium channel blocking activity of these analogues in terms of the hydrophobic constant of X-substituent and indicator parameters I_{CN} and I_{Cf}.

$$\begin{aligned} \log(1/\mathrm{IC}_{50}) &= 5.441(\pm\ 0.263) + 0.760(\pm\ 0.226)\pi_{\mathrm{X}} \\ n &= 17, r = 0.880, s = 0.42, F = 51.53. \end{aligned} \tag{6}$$

$$\begin{aligned} \log(1/\mathrm{IC}_{50}) &= 5.642(\pm\ 0.268) + 0.514(\pm\ 0.203)\pi_{\mathrm{X}} - 0.732(\pm\ 0.453)I_{\mathrm{CN}} \\ &\quad + 0.585(\pm 0.312)I_{\mathrm{Cf}} \\ n &= 17,\ r = 0.961, Q^2 = 0.87, s = 0.26,\ F = 52.80. \end{aligned} \tag{7}$$

Equations (6) and (7) clearly indicated the favorable role of hydrophobicity for the activity. In (7), the parameter I_{CN} was assigned a value of 1 for X = CN and the

parameter I_{Cf} a value of 1 for the compounds with configuration (3R,4S). The regression coefficient of I_{CN} indicated the unfavorable nature of the CN group for the activity. It was suggested that CN being more electronic in nature may contribute less towards the hydrophobic interaction. The positive coefficient of I_{Cf} suggested the favorable role of (3R,4S) configuration of the chiral centres in the compound over any other configuration [46].

The chromanol derivatives as shown by **6** and **7** were also explored as K_{ATP}-channel blockers [47, 48]. In the series of **6**, R_1 is an aryl or heteroaryl moiety, R_2 is CN, CCH, NO_2 or H, and X is NCN, O, or S group/atom [47]. For the compounds belonging to **7**, R_1 is aryl or heteroaryl moiety and R_2 is an alkylester [48]. They are reported to possess vasorelaxant activity. The QSAR of these compounds was investigated using first-order valence molecular connectivity index and hydrophobic parameters [49]. Interestingly, vasorelaxant activity of these benzopyran derivatives (**6** and **7**) was found to have highly significant correlations with the first-order valence molecular connectivity index ($^1\chi^v$) of the compounds (8–11). In both the series of compounds, the negative coefficient of $^1\chi^v$, which defines the shape and size of the molecule, indicated that bulky molecules may not be advantageous for the activity.

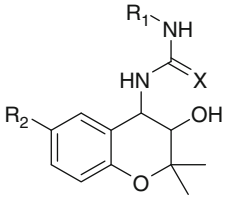

6

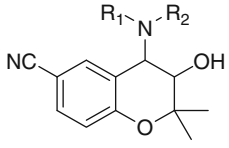

7

QSAR for **6**

$$\log(1/IC_{50}) = 14.990(\pm\ 3.257) - 1.093(\pm\ 0.387)^1\chi^v$$
$$n = 12, r = 0.893, s = 0.28, F = 39.52. \tag{8}$$

$$\log(1/IC_{50}) = 16.866(\pm 3.154) - 1.330(\pm 0.382)^1\chi^v + 0.461(\pm 0.414)I_1$$
$$n = 12, r = 0.939, s = 0.23, F = 33.53. \tag{9}$$

QSAR for **7**

$$\log(1/IC_{50}) = 6.021(\pm 1.381) - 0.288(\pm 0.275)^1\chi^v$$
$$n = 8, r = 0.723, s = 0.43, F = 6.57. \tag{10}$$

$$\log(1/IC_{50}) = 6.436(\pm 0.607) - 0.318(\pm 0.116)^1\chi^v - 0.725(\pm 0.325)I_2$$
$$n = 8, r = 0.968, s = 0.17, F = 37.18. \tag{11}$$

In (9), I_1 is an indicator parameter defined for the presence of halogen in R_1 ($I_1 = 1$) and zero otherwise. Its positive regression coefficient suggested the favorable contribution of halogens when present as part of R_1 group. In (11), the indicator variable I_2 represents an R_2-substituent containing COOEt moiety. Its negative coefficient suggested that an R_2-substituent with a specific COOEt moiety is detrimental to the activity. These equations have suggested importance of the steric factors in modulating the activity of these compounds [49].

2.3 Benzothiazine Derivatives

Benzothiazine skeleton is closely related to benzopyran scaffold. Several 1, 4-benzothiazine derivatives (**8**) were reported to show K_{ATP}-channel opening activity [50]. In **8**, R_2 is Br, NO_2, CN or CF_3 and R_1 in most of the compounds is a five- or six-membered heterocyclic moiety. The n has a value of zero to two. The K_{ATP}-channel opening activity of these derivatives was evaluated as the smooth muscle relaxing effect evoked on endothelium-denuded aortic rings precontracted with 20 mM KCl and was expressed as pEC50. Additionally, the binding affinities (pK_D values) of these derivatives were also measured in rat aortic smooth muscle cells (RASMC) and cardiomyocytes of the rat using [^{3}H]P1075 as a radioligand. Carosati et al. have reported a 3D-QSAR study of these 1,4-benzothiazine analogues [51]. The study divulged high correlation between binding data (pK_D) and pEC_{50} values for relaxation indicating the close similarities between cardiac K_{ATP}-channels and aortic smooth muscle K_{ATP}-channels.

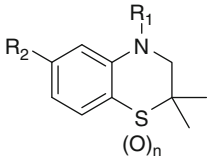

8

The 3D QSAR model was developed using GRid-Independent descriptors (GRIND) [52]. The molecular interaction fields (MIFs) were generated using GRID probes namely DRY (hydrophobic), N1 (hydrogen bond donor interaction), O (hydrogen bond acceptor interaction) and TIP (shape description). In PLS analysis, two latent variables were found to be optimum for modeling all the three biological responses of these compounds. The 3D-QSAR model of smooth muscle relaxation has explained 97% variance in the activity ($r^2 = 0.97$, $Q^2 = 0.69$, SDEC = 0.37, SDEP = 1.18). Also, the models for RASMC-binding ($r^2 = 0.94$, $Q^2 = 0.66$, SDEC = 0.34, SDEP = 0.78) and cardiomyocytes-binding ($r^2 = 0.94$, $Q^2 = 0.64$, SDEC = 0.29, SDEP = 0.73) have shown equal significance. The study has revealed that the carbonyl on the substituent at N-4, the hydrogen bond acceptor at C-6, the five-membered ring at N-4, and the geminal

dimethyl groups in **8** may be the main pharmacophoric features for all three activities of all the derivatives of **8**. It is suggested that these features closely match the K_{ATP}-channel binding requirements and are responsible for the muscle relaxation potencies [51]. The study has provided a composite rationale for three related biological endpoints of these compounds.

Satuluri and Gupta [49] have correlated the vasorelaxant activity of these benzothiazine derivatives (**8**) with *C*log*P* of the compounds and two indicator variables (I_3 and I_4) (12). In (12), *C*log*P* alone accounted for 44% of the variance in the activity.

$$\begin{aligned} \mathrm{pEC50} &= 7.653(\pm 1.508) + 0.916(\pm 0.474) C\log P - 1.098(\pm 1.012) I_3 \\ &\quad - 2.743(\pm 1.014) I_4 \\ n &= 15, r = 0.946, Q^2 = 0.80, s = 0.84,\ F = 31.35. \end{aligned} \tag{12}$$

Here, the indicator variable I_3 is defined for an R_1-substituent, which is 2-oxo-pyrrilidinyl group and I_4 is defined for an R_2-substituent, which is simply bromine. The regression coefficients of both these indicators suggested the unfavorable nature of R_1- and R_2- substituents for the activity. The results of 2D- and 3D-QSAR are in agreement with each other. However, the 2D-models provided fundamental explanation to the activity of the analogues. Additionally, as Satuluri and Gupta have investigated both benzopyran (**6** and **7**) and benzothiazine (**8**) derivatives, their findings have led to suggest that in benzopyran derivatives the steric factors may be more crucial for the activity, whereas in benzothiazine derivatives the hydrophobic property appears to be prominently influencing the activity [49]. This study has vividly explained the structural requirement for the K_{ATP}-channel blockers by making use of the fundamental descriptors involved in the equations.

2.4 Benzothiadiazine 1,1-Dioxide Derivatives

Boverie and coworkers have investigated different 3-alkylamino-4*H*-1,2, 4-benzothiadiazine 1,1-dioxides (**9**) for the pancreatic and vascular (rat aorta) K_{ATP} channel opening activity [53–55]. In these compounds (**9**), R_3 substituent represents various alkyl and aminoalkyl moieties and R_6 and R_7 represent the groups such as halo, nitro, alkylesters, alkyl and aminoalkyl. For these compounds, inhibition of glucose-induced insulin secretion (evaluated on isolated rat pancreatic islets) is reported in terms of IC_{50}, and myorelaxant effect on the contractile activity of KCl-depolarized rat aorta rings is reported in terms of EC_{50}. For these compounds, Sharma et al. [56] developed QSAR models (13 and 14), showing the dependence of activities on hydrophobic, steric and some indicator parameters.

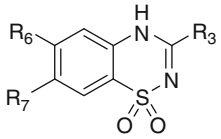

9

$$\begin{aligned} \mathrm{pIC}_{50}(\text{pancreas}) &= 6.455 - 1.254(\pm 0.28)C\log P(\mathrm{R}_3) - 2.184(\pm 0.86)\mathrm{Vw}(\mathrm{R}_7) \\ &\quad + 0.454(\pm 0.14)I_3 + 0.505(\pm 0.16)I_6 \\ n &= 23, r = 0.920, Q^2 = 0.765, s = 0.223, F = 24.66. \end{aligned} \tag{13}$$

$$\begin{aligned} \mathrm{pEC}_{50}(\text{rat aorta}) &= 3.772 + 0.837(\pm 0.37)\pi_6 + 1.443(\pm 0.35)\pi_7 \\ n &= 20, r = 0.900, Q^2 = 0.737, s = 0.307, F = 36.27. \end{aligned} \tag{14}$$

Equation (13) suggested that the R_3- and R_7-substituents may face the steric problem. Thus, it suggested that the bulky substituents, which also affect the hydrophobicity, may not be advantageous for the activity. However, the positive coefficients of the indicator variables I_3 and I_6, where the former is for an aminoisopropyl substituent at the 3-position and the latter for a chloro substituent at the 6-position, indicate that such substituent would be beneficial to the pancreatic activity of the compounds. The myorelaxant effect on rat aorta rings (EC_{50}) of the compounds was shown to be positively correlated with hydrophobic constants of R_6 and R_7 substituents (14) signifying the importance of hydrophobic property of these substituents in modulating the activity of the compounds. These equations suggest the substructural requirement in this class of compounds for K_{ATP} channel modulation.

In a further study, Sharma et al. enlarged the scope of preceding QSAR model for myorelaxant effects [56] by including more benzothiadiazine-dioxide derivatives [54, 55] in the analysis. The enlarged QSAR of all the compounds was reinvestigated in CP-MLR with topological descriptors from DRAGON software. The following equation was found to be the best model for the myorelaxant activity of the compounds [57].

$$\begin{aligned} \mathrm{pEC}_{50}(\text{rat aorta}) &= 3.927 - 1.581(0.342)\mathrm{Mor24u} + 0.875(0.126)\mathrm{Mor04m} \\ &\quad - 0.387(0.096)\mathrm{Mor10m} + 0.843(0.216)\mathrm{Mor13e} \\ &\quad + 2.159(0.688)\mathrm{G3u} + 0.151(0.018)\mathrm{L1m} \\ n &= 57, r = 0.844, Q^2 = 0.628, s = 0.428, F = 20.69. \end{aligned} \tag{15}$$

The descriptors emerged in above model Mor24u, Mor04m, Mor10m and Mor13e belong to 3D MoRSE (3D molecule representation of structures based on electron diffraction) class. These descriptors are based on the idea of obtaining information from the 3D atomic coordinates by the transformations used in electron diffraction studies for preparing theoretical scattering curves. These descriptors in

model are indicative of the role for atomic mass (*m*) and the Sanderson atomic electronegativity (*e*) in electron diffraction signals. Unweighted 3D-MoRSE electron diffraction signal number 24 (Mor24u) and atomic mass weighted 4th signal (Mor04m) contributed negatively to the activity, whereas atomic mass weighted 10th signal (Mor10m) and Sanderson atomic electronegativity weighted 13th signal contributed positively to the activity.

The G3u (3rd component symmetry directional WHIM index/unweighted) and L1m(1st component size directional WHIM index/weighted by atomic masses) belong to WHIM (weighted holistic invariant molecular descriptors) class descriptors. They are geometrical descriptors based on statistical indices, calculated on the projections of the atoms along principal axes. These descriptors are built in such a way as to capture relevant molecular 3D information regarding molecular size, shape, symmetry and atom distribution with respect to invariant reference frames. Calculation of WHIM descriptors involves the eigenvalues of the weighted covariance matrix of the molecular atomic coordinates. Each eigenvalue represents a dispersion measure (i.e., the weighted variance) of the projected atoms along the considered principal axis, thus accounting for the molecular size along that principal direction. They describe the molecular shape. Interpretability of these descriptors is relatively complex but they encode refined structural information for the activity.

2.5 *Khellinone Derivatives*

The voltage-gated potassium channel Kv1.3 is linked with the activation of human T cells and therefore pursued as an important target in the treatment of T-cell-mediated autoimmune diseases such as multiple sclerosis [58–60]. Khellinone (**10**; $R_1 = R_2 = Me$), a naturally occurring benzofuran derivative isolated from *Ammi visnaga*, weakly blocks Kv1.3 with an EC_{50} of 45 μM [61]. In this background, Baell and coworkers prepared

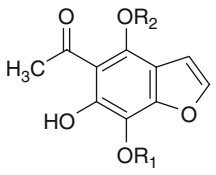

10

a variety of khellinone derivatives as promising Kv1.3-blockers [61, 62]. The effectiveness of the compounds in blocking Kv1.3 was assayed on L929 cells stably expressing mKV1.3. Keeping the importance of these derivatives in view, Gupta and coworkers [46, 63] attempted to rationalize the potassium channel (Kv1.3) blocking activity of these compounds with the physicochemical and steric parameters. For 4,7-alkoxy khellinone derivatives (**10**) [62], the Kv1.3 channel

blocking activity (EC_{50}) was reported to be correlated with the sum of hydrophobic constants of R_1- and R_2-substituents ($\Sigma\pi$) and the surface tension parameter st of the whole molecule (16) [46].

$$\log(1/EC_{50}) = -3.178(\pm 2.544) + 2.661(\pm 0.851)\Sigma\pi - 0.541(\pm 0.171)(\Sigma\pi)^2 + 0.119(\pm 0.041)\text{st}$$
$$n = 12,\ r = 0.942,\ Q^2 = 0.67,\ s = 0.14,\ F = 20.86,\ \Sigma\pi_o = 2.46. \quad (16)$$

In this equation, the second-degree term in $\Sigma\pi$ has suggested 2.46 as the optimum value for hydrophobic property of R_1- and R_2-substituents ($\Sigma\pi_o = 2.46$). The equation has suggested that hydrophobicity and surface tension are important properties for the potassium channel blocking activity of the compounds.

The khellinone derivatives shown in **11a** and **11b** are closely related positional isomers of each other. They were formed by replacing the 4- and 7-alkoxy groups of khellinone with substituted benzyloxy groups [62].

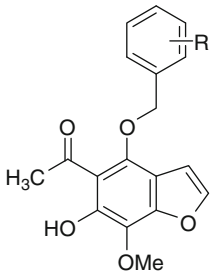

11a

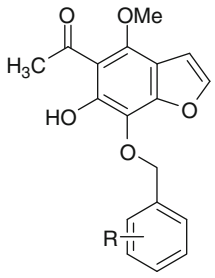

11b

Satuluri et al. [46] correlated the Kv1.3 channel blocking activity of these derivatives with the Verloop's STERIMOL parameters B_1 (minimum width of the substituent) and L (length) and indicator variables as shown by (17) and (18) for **11a** and **11b,** respectively.

$$\log(1/EC_{50}) = 5.205(\pm 0.665) + 0.696(\pm 0.392)B_1 - 0.137(\pm 0.061)L + 0.290(\pm 0.186)I_P$$
$$n = 19,\ r = 0.852,\ Q^2 = 0.43,\ s = 0.17,\ F = 13.20. \quad (17)$$

$$\log(1/EC_{50}) = 5.111(\pm 0.811) + 1.001(\pm 0.453)B_1 - 0.173(\pm 0.064)L - 0.325(\pm 0258)I_O$$
$$n = 16,\ r = 0.915,\ Q^2 = 0.71,\ s = 0.17,\ F = 20.58. \quad (18)$$

These equations suggested that the width parameter B_1 is favorable for the potassium channel blocking activity of the compounds. However, the negative

coefficient of L (length parameter) indicated that lengthy substituents would produce a negative effect on the activity. It was therefore suggested that the phenyl ring substituents may be involved in some kind of van der Waals interactions with the active site of the receptor with some steric restrictions due to the length. In these equations, I_P and I_O are indicator parameters for *para*- and *ortho*-substituents of 4- and 7- benzyloxy groups of khellinone derivatives, respectively. These indicators were given a value of one for the presence of substituent and zero for the absence. The regression coefficients of these indicator parameters suggested that a *para*-substituent is favorable in 4-benzyloxy series (**11a**) and an *ortho*-substituent unfavorable in 7-benzyloxy analogues (**11b**) [46].

For a different series of khellinone derivatives studied by Baell et al. [61], Saini et al. [63] had derived (19) correlating Kv1.3 channel blocking activity of the compounds with calculated hydrophobicity (*C*log*P*), calculated molar refractivity (CMR), polarizability (Pol) and a structural indicator (I_2). This correlation had suggested a clear

$$\begin{aligned}\log(1/\mathrm{EC}_{50}) = {} & -0.327(\pm 2.078) + 1.700(\pm 1.310)C\log P \\ & - 0.155(\pm 0.138)(C\log P)^2 - 0.755(\pm 0.431)\mathrm{CMR} \\ & + 0.242(\pm 0.101)\mathrm{Pol} - 1.705(\pm 0.962)I_2 \\ n = 22,\ r = 0.937,\ Q^2 = 0.82,\ s = 0.29,\ F = 22.96,\ & (C\log P)_{\mathrm{o}} = 5.48.\end{aligned} \tag{19}$$

role of fundamental physicochemical parameters in modulating the activity of the compounds. While CMR suggested steric restrictions, Pol and *C*log*P* pointed out the positive effects of polarizability and hydrophobicity of the molecules on their activity. However, the *C*log*P* was shown to have an optimum value of 5.48. Baell et al. [61] had also made a similar observation.

2.6 Benzotriazole, Benzimidazolone and Benzanilide Derivatives

The Big Potassium channels (BK channels) typically show large conductance of potassium ions through the cell membrane. They are calcium-activated potassium channels [64]. They open in response to increase in cytosolic Ca^{2+} concentration and membrane depolarization. This leads to an increased K^+ efflux, which in turn triggers the rapid hyperpolarization of the excitatory membranes and reduces Ca^{2+} influx via voltage- dependent Ca^{2+} channels. BK channels are involved in a variety of cellular functions, which include action potential repolarization, neuronal excitability, neurotransmitter release, hormone secretion, etc. In several pathological conditions caused by cell hyperexcitability, such as asthma, urge incontinence and bladder spasm, gastric hypermotility, neurological and psychiatric disorders, BK channels offer convenient handle to manage them clinically [65, 66]. In view of

their clinical utility, Coi et al. [67] have carried out an exhaustive QSAR study on the BK channel opening profile of several benzotriazole, benzimidazolone and benzanilide derivatives sharing a large common sub-structure among them (**12**). The minimum common hyper-structure space of these analogues is schematically shown in **12**. On this (hyper-structure template), R, R_1 and R_2 may be functionalized alkyl and aryl moieties, and X is satisfied by CH, CO, N, or even absent depending on the chemical class.

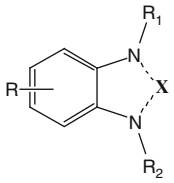

12

For all the compounds, the BK channel opening potency was measured in terms of IC_{50}, the concentration of the compound to evoke 50% reduction of the contractile tone induced by KCl 20 mM. Coi et al. [67] had derived the following QSAR rationale for the activity of these compounds involving a heuristic procedure available in CODESSA [21].

$$\begin{aligned}
\mathrm{pIC_{50}} = {} & -33.700 - 0.216(\text{Max } n - n \text{ repulsion for a C} - \text{N bond}) \\
& + 0.588(\text{Kier flexibility index}) + 11.500(\text{Min atomic orbital electronic population}) \\
& + 6.870(\text{ZX Shadow}/\text{ZX Rectangle}) + 2.550(\text{Average bond order of a O atom}) \\
& + 75.300(\text{Max valence of a H atom}) - 8.170(\text{Max valence of a O atom}) \\
& + 520.000(\text{HACA} - 2/\text{TMSA}) + 31.400(\text{Min partial charge for a C atom}) \\
& - 5.17(\text{YZ Shadow}/\text{YZ Rectangle}) + 29.500(\text{Max partial charge for a H atom}) \\
& + 0.033(\text{ZX Shadow}) - 0.049(\text{HACA} - 1) \\
n = 66, \;\; & r^2 = 0.73, \;\; Q^2 = 0.56, \;\; r^2_{\text{Test}} = 0.91. \qquad (20)
\end{aligned}$$

The molecular features emerged in this model are from topological (Kier flexibility index), geometrical (ZX Shadow/ZX Rectangle, YZ Shadow/YZ Rectangle and ZX Shadow), electrostatic (HACA-2/TMSA, minimum partial charge for a C atom, and maximum partial charge for a H atom) and quantum-chemical (maximum n-n repulsion for a C-N bond, minimum atomic orbital electronic population, average bond order of a O atom, maximum valence of a H atom, maximum valence of a O atom, and HACA-1) classes of CODESSA molecular descriptors. Further information of these descriptors can be found from [21, 22]. These descriptors provided some basis for improving the BK channel opening activity of the compounds. This study showed how a diverse chemical space can be unified into single scaffold space in explaining the biological response of all compounds.

2.7 *hERG K^+ Modulators*

The hERG (human ether-à-go-go-related gene) potassium channel (Kv11.1) plays a vital role in maintaining normal electrical activity in the heart [17]. It mediates the repolarizing I_{Kr} current in the cardiac action potential. The intended or unintended inhibition of electrical conductance of hERG K^+ channel either by drugs or by gene-mutation can cause serious disorder called long QT syndrome. Even several clinically useful and approved drugs are known to show a tendency to inhibit hERG K^+ channel conductance and thereby cause arrhythmias, and create a risk of sudden death. For drug-induced QT prolongation, the increase in the duration of repolarization through blockade of outward K^+ current is responsible. Thus, hERG inhibition is an important anti-target, which must be avoided during drug development [68].

The primary structural components in hERG are found to be a positively charged S4 helix and a P-loop. Different hERG-ligand modeling studies have suggested that Phe-656 and Tyr-652 residues are involved in hydrophobic interactions and Thr-623 and Ser-624 residues modulate the binding potency through the polar tails of hERG blockers [69–72]. Also, results from some studies have favored multiple pharmacophore models to explain the binding of high- and low-affinity ligands [73, 74]. The in silico modeling studies of Borosy group [75, 76] on hERG channel blockers have pointed out a five-point pharmacophore (hydrogen bond donor, hydrogen bond acceptor, two aromatic rings, and a hydrophobic aliphatic chain) model for the most active molecules and a four-point pharmacophore model for the less potent agents. The results from Ekins et al. also favored a five centered pharmacophore model, where a positive center has separated from four hydrophobes at distances 5.2, 6.2, 6.8 and 7.5 Å [77]. Cavalli et al. constructed another pharmacophore model having three aromatic moieties connected through a nitrogen function (tertiary amine) at distances of 5.2–9.1, 5.7–7.3 and 4.6–7.6 Å [78]. These authors have also reported several geometrical parameters such as angles, angle between the planes, and the height above the planes of the pharmacophore.

Apart from the above reported findings on hERG, a CoMSIA study was reported making use of its high affinity ligand. Sertindole (**13**) is an antipsychotic drug and blocks hERG with high affinity [79]. Pearlstein et al. [80] carried out, using SYBYL 6.7.2 Tripos Inc. [81], a CoMSIA modeling of the hERG inhibitory activity of 22 sertindole analogues together with ten assorted compounds. These authors found a complementary

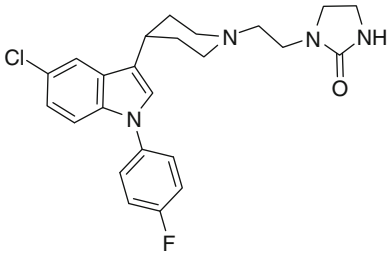

13

Table 1 Compounds used in deriving 2D-QSAR and pharmacophore model of hERG K^+ channel blockers [82]

Compounds			
Amiodarone	Domperidone	Moxifloxacin	Terfenadine
Amitryptiline	Droperidol	N-desmethyl-clozapine	Thioridazine
Astemizole	E-4031	Ofloxacin	Vardenafil
Azimilide	Flecainide	Olanzapine	Verapamil
Bepridil	Gatifloxacin	Ondansetron	Ziprasidone
Chloroquine	Granisetron	Perhexiline	Acrivastine
Chlorpheniramine	Grepafloxacin	Phenobarbital	Amsacrine
Chlorpromazine	Halofentrine	Phenytoin	Cocaine
Ciprofloxacin	Haloperidol	Pimozide	Desmethylastemizole
Cisapride	Imipramine	Propafenone	Desmethylcarboxyloratadine
Clozapine	Lidocaine	Pyrilamine	Fentanyl
Clozapine-N-oxide	Loratadine	Queitiapine	Fexofenadinec
Desipramine	Lumefantrine	Quinidine	Ketoconazole
Diltiazem	Mesoridazine	Risperidone	Lidoflazine
Diphenhydramine	Mibefradil	Sertindole	Meperidine
Dofetilide	Mizolastine	Sparfloxacin	Tadalafil
Dolasetron	Mefloquine	Spironolactone	Cetrizine

relationship between the CoMSIA model and the hERG homology model built from the crystal structure of the open bacterial MthK potassium channel [80]. The CoMSIA and the hERG homology models led Pearlstein et al. to suggest that (a) aromatic moieties optimally provide hydrophobicity and get involved in π-stacking with Phe 656 side chain, (b) basic nitrogen facilitates π-cation interaction with Try 652, and (c) the ion pore diameter and depth act as constrains for the inhibitor interaction [80].

Garg et al. [82] have modeled the hERG K^+ channel blocking activity of diverse molecules (Table 1) selected from literature using Cerius2 and Catalyst software [83]. The activity of these compounds (IC_{50}) against hERG K^+ channels was expressed in mammalian cells lines. In Cerius2, using several electrotopological, thermodynamic, ADMET, graph theoretical and physicochemical properties, the 2D-quantitative structure–toxicity relationship (2D-QSTR) was derived for the hERG K^+ channel blocking activity of the compounds (Table 1).

$$\begin{aligned} \mathrm{pIC}_{50} &= 2.04746 + 0.18227\mathrm{kappa3} - 1.61453\ \mathrm{Atype\_O\_57} + 0.251155\ \mathrm{S\_sNH2} \\ &\quad - 1.97268\ \mathrm{JX} - 0.969258\ \mathrm{Atype\_O\_59} + 0.61608\ \mathrm{ADMET\_PPB} \\ &\quad - 0.063453\ \mathrm{Atype\_H\_46} \\ n &= 56,\ r^2 = 0.837,\ Q^2 = 0.776,\ \mathrm{BS}r^2 = 0.838 \pm 0.001,\ \mathrm{LOF} = 0.5, \\ &\quad \mathrm{PRESS} = 16.06, r^2_{\mathrm{pred}} = 0.701. \end{aligned} \tag{21}$$

The presence of topological descriptor, kappa3 (The Kier and Hall kappa shape index of order 3), shows the importance of shape in exhibiting hERG K^+ channel

inhibitory activity. The electrotopological descriptor S_sNH2 stands for sum descriptor for nitrogen bonded to two hydrogens and one single bond and has indicated that more number of features, such as nitrogen containing heterocyclic moieties, are beneficial to the inhibitory activity. The descriptor ADMET_PPB corresponds to likelihood of binding of the molecule to plasma proteins in the threshold of 90-95%. The descriptor JX (Balaban index) reflects upon the relative connectivity and effective size of the carbon chain to which multiple methyl groups are attached. Here, an increase in number of methyl groups decreases the activity. The Atype descriptors are thermodynamic descriptors, which define the presence of the particular type of atom in the molecule. The negative contribution of descriptor Atype_H_46 (hydrogen attached to Csp_3^0) illustrates that inhibitory activity decreases with increase in the hydrophobicity associated with this hydrogen. Likewise Atype_O_57 and Atype_O_59 descriptors also showed a negative contribution to activity. Here the 'O' in Atype_O_57 represents oxygen in phenol, enol, and carboxyl OH and Atype_O_59 refers to oxygen in Al–O–Al (Al = aliphatic). The negative contribution of Atype thermodynamic descriptors and that of topological Balaban index JX to inhibitory activity advocate that electronegative groups in the ligand decrease the affinity for hERG K^+ channels.

Garg et al. [82] have further used these compounds (Table 1) in HypoGen of Catalyst to generate the toxicophore models. This has led to the identification of three important features for hERG K^+ channel blockers. These features were identified as (a) hydrophobic group, (b) ring aromatic group and (c) hydrogen bond acceptor lipid group. The most predictive hypothesis has best explained the activity and showed a low RMS deviation as well as high cost difference. Also, both 2D-QSTR and toxicophore models have optimally predicted the hERG K^+ channel blocking activity of test set compounds [82]. Thus, this study has helped in understanding the hERG K^+ channels affinity for different compounds (Table 1), and provided inputs to overcome the adverse structural features responsible for the binding affinity and addressed the ways to mitigate the undesirable side effects.

3 Conclusions

Potassium ion channels play important role in a variety of diseases having direct bearing on the quality of life. Cardiovascular, nervous, immune and endocrine systems are a few critical organs/ systems among many others, which are affected by these ion channels. In this background, maintenance of stasis of the ion channels is curial for the health. Because the ion channels are ubiquitous in nature and highly variable even within a given family, identification of drugs acting through them with specificity and high therapeutic value is a challenge. From a broad perspective, several of the chemical scaffolds discussed in this article share a large structure space, at the same time each one has distinctly responded at the target in eliciting the biological response. In this scenario, QSAR and modeling studies offer fast

initial estimates of the structural and functional requirements of the optimum modulators. In this article studies expounded under benzopyrans and hERG K^+ modulators provide a glimpse of the role of QSAR and modeling approaches in lead alteration and optimization. Advancements in retro-QSAR methodologies could further help in translating the in silico results to wet laboratories.

Acknowledgements Authors thank Director, CDRI for extending the library facility and Dr. Shreekant Deshpande, Faculty of Pharmacy, Hygia Institute of Pharmaceutical Education and Research, Lucknow, for critical reading of the draft manuscript (CDRI communication No. 8062).

References

1. Hille B (1992) Ionic channels of excitable membranes, 2nd edn. Sinauer Associates, Sunderland, MA
2. Camerino DC, Tricarico D, Desaphy JF (2007) Ion channel pharmacology. Neurotherapeutics 4:184–198
3. Verkman AS, Galietta LJ (2009) Chloride channels as drug targets. Nat Rev Drug Discov 8:153–171
4. Camerino DC, Desaphy JF, Tricarico D et al (2008) Therapeutic approaches to ion channel diseases. Adv Genet 64:81–145
5. Doyle DA, Cabral JM, Pfuetzner RA et al (1998) The structure of the potassium channel: molecular basis of K^+ conduction and selectivity. Science 280:69–77
6. Catterall WA (1993) Structure and modulation of Na^+ and Ca^{2+} channels. Ann NY Acad Sci 707:1–19
7. Mackinnon R (1991) Determination of the subunit stoichiometry of a voltage-activated potassium channel. Nature 350:232–235
8. Mackinnon R, Aldrich RW, Lee AW (1993) Functional stoichiometry of Shaker potassium channel inactivation. Science 262:757–759
9. Rudy B (1988) Diversity and ubiquity of K channels. Neuroscience 25:729–749
10. Goldstein SAN, Wang KW, Ilan N et al (1998) Sequence and function of the two P domain potassium channels: implications of an emerging superfamily. J Mol Med 76:13–20
11. Shieh C-C, Coghlan M, Sullivan JP et al (2000) Potassium channels: molecular defects, diseases and therapeutic opportunities. Pharmacol Rev 52:557–593
12. Coghlan MJ, Carroll WA, Gopalakrishnan M (2001) Recent developments in the biology and medicinal chemistry of potassium channel modulators: update from a decade of progress. J Med Chem 44:1627–1653
13. Conti M (2004) Targeting K^+ channels for cancer therapy. J Exp Ther Oncol 4:161–166
14. Jahangir A, Terzic A (2005) K_{ATP} channel therapeutics at the bedside. J Mol Cell Cardiol 39:99–112
15. Kaczorowski GJ, McManus OB, Priest BT et al (2008) Ion channels as drug targets: the next GPCRs. J Gen Physiol 131:399–405
16. Sandhiya S, Dkhar SA (2009) Potassium channels in health, disease & development of channel modulators. Indian J Med Res 129:223–232
17. Sanguinetti MC, Tristani-Firouzi M (2006) hERG potassium channels and cardiac arrhythmia. Nature 440:463–469
18. Hansch C, Leo A (1979) Substituent constants for correlation analysis in. Wiley-Interscience, New York
19. Stewart JJP (2004) Optimization of parameters for semiempirical methods IV: extension of MNDO, AM1, and PM3 to more main group elements. J Mol Model 10:155–164
20. CS Chem3D Ultra® Cambridge Soft Corporation, Cambridge, USA

21. Katritzky AR, Lobnov V, Karelson M (1994) CODESSA (Comprehensive Descriptors for Structural and Statistical Analysis) University of Florida,Gainesville, FL. http://www.codessa-pro.com
22. Katritzky AR, Perumal S, Petrukhin R et al (2001) Codessa-based theoretical QSPR model for hydantoin HPLC-RT lipophilicities. J Chem Inf Comput Sci 41:569–574
23. DRAGON software version 3.0 (2003) Todeschini R, Consonni V, Mauri A, Pavan M, Milano, Italy. http://disat.unimib.it/chm/Dragon.htm
24. Wold S, Ruhe A, Wold H et al (1984) The collinearity problem in linear regression. The partial least squares (PLS) approach to generalized inverses. SIAM J Sci Stat Comp 5:735–743
25. Rogers D, Hopfinger AJ (1994) Application of genetic function approximation to quantitative structure-activity relationships and quantitative structure-property relationships. J Chem Inf Comput Sci 34:854–866
26. Cerius^2 Version 4.10 (2005) Accelrys Inc, San Diego, USA. http://www.accelrys.com/cerius2
27. Prabhakar YS (2003) A combinatorial approach to the variable selection in multiple linear regression: analysis of Selwood et al. data set – a case study. QSAR Comb Sci 22:583–595
28. Vaughan Williams EM (1984) A classification of antiarrhythmic actions reassessed after a decade of new drugs. J Clin Pharmacol 24:129–147
29. Echt DS, Liebson MD, Mitchell LB et al (1991) Mortality and morbidity in patients receiving encainide, flecainide, or placebo. The Cardiac Arrhythmia Suppression Trial. N Engl J Med 324:781–788
30. Jurkiewicz NK, Sanguinetti MC (1993) Rate-dependent prolongation of cardiac action potentials by a methanesulfonanilide class III antiarrhythmic agent. Specific block of rapidly activating delayed rectifier K^+ current by dofetilide. Circ Res 72:75–83
31. Hondeghem LM (1992) Development of class III antiarrhythmic agents. J Cardivasc Pharmacol 20:S17–S22
32. Selnick HG, Liverton NJ, Baldwin JJ et al (1997) Class III antiarrhythmic activity in vivo by selective blockade of the slowly activating cardiac delayed rectifier potassium current IKs by (R)-2-(2,4-trifluoromethyl)-N-[2-oxo-5-phenyl-1-(2,2,2- trifluoroethyl)-2,3-dihydro-1H-benzo[e][1,4]diazepin-3-yl]acetamide. J Med Chem 40:3865–3868
33. Gupta SP, Paleti A, Mekapati SB et al (2005) A quantitative structure-activity relationship study on some Na^+ and K^+ channel blockers: role of molecular connectivity index. Lett Drug Des Discov 2:287–290
34. Edwards G, Weston A-H (1993) The pharmacology of ATP-sensitive channels. Annu Rev Pharmacol Toxicol 33:597–637
35. Wickenden AD (2002) K^+ Channels as therapeutic drug targets. Pharmacol Ther 94:157–182
36. Mannhold R (2004) K_{ATP} channel openers: structure-activity relationships and therapeutic potential. Med Res Rev 24:213–266
37. Mannhold R, Cruciani G, Weber H et al (1999) 6-Substituted benzopyrans as potassium channel activators: synthesis, vasodilator properties, and multivariate analysis. J Med Chem 42:981–991
38. Agrawal VK, Singh J, Gupta M et al (2006) QSAR studies on benzopyran potassium channel activators. Eur J Med Chem 41:360–366
39. Lebrun P, Devreux V, Hermann M et al (1989) Similarities between the effects of pinacidil and diazoxide on ionic and secretory events in rat pancreatic islets. J Pharmacol Exp Ther 250:1011–1018
40. Quast U (1993) Do the K^+ channel openers relax smooth muscle by opening K^+ channels? Trends Pharmacol Sci 14:332–337
41. Petit P, Hillaire-Buys D, Mir A-K et al (1992) Differential effects of cromakalim on pancreatic vascular resistance and insulin secretion in vitro. Fundam Clin Pharmacol 6:185–190
42. Lebrun P, Antoine M-H, Devreux V et al (1990) Paradoxical inhibitory effect of cromakalim on 86Rb outflow from pancreatic islet cells. J Pharmacol Exp Ther 255:948–954

43. Sebille S, de Tullio P, Becker B et al (2005) 4,6-Disubstituted 2,2-dimethylchromans structurally related to the K(ATP) channel opener cromakalim: design, synthesis, and effect on insulin release and vascular tone. J Med Chem 48:614–621
44. Sharma S, Prabhakar YS, Singh P et al (2008) QSAR study about ATP-sensitive potassium channel activation of cromakalim analogues using CP-MLR approach. Eur J Med Chem 43:2354–2360
45. Gerlach U, Brendel J, Lang H-J et al (2001) Synthesis and activity of novel and selective IKs-channel blockers. J Med Chem 44:3831–3837
46. Satuluri VSAK, Seelam J, Gupta SP (2008) A quantitative structure-activity relationship study on some series of potassium channel blockers. Med Chem 5:87–92
47. Atwal KS, Grover GJ, Ahmed SZ et al (1993) Cardioselective anti-ischemic ATP-sensitive potassium channel openers. J Med Chem 36:3971–3974
48. Rovnyak GC, Ahmed SZ, Ding CZ et al (1997) Cardioselective antiischemic ATP-sensitive potassium channel (K_{ATP}) openers. 5. Identification of 4-(N-aryl)-substituted benzopyran derivatives with high selectivity. J Med Chem 40:24–34
49. Satuluri VSAK, Gupta SP (2008) A QSAR study on some series of ATP-sensitive potassium channel openers. Lett Drug Des Discov 5:173–177
50. Cecchetti V, Calderone V, Tabarrini O et al (2003) Highly potent 1,4-benzothiazine derivatives as K (ATP)-channel openers. J Med Chem 46:3670–3679
51. Carosati E, Lemoine H, Spogli R et al (2005) Binding studies and GRIND/ALMOND-based 3D QSAR analysis of benzothiazine type K_{ATP}-channel openers. Bioorg Med Chem 13:5581–5591
52. Pastor M, Cruciani G, McLay I et al (2000) GRid-INdependent descriptors (GRIND): a novel class of alignment-independent three-dimensional molecular descriptors. J Med Chem 43:3233–3243
53. de Tullio P, Boverie S, Becker B et al (2005) 3-Alkylamino-4H-1,2,4-benzothiadiazine 1,1-dioxides as ATP-sensitive potassium channel openers: effect of 6,7-disubstitution on potency and tissue selectivity. J Med Chem 48:4990–5000
54. de Tullio P, Becker B, Boverie S et al (2003) Toward tissue-selective pancreatic B-cells K_{ATP} channel openers belonging to 3-alkylamino-7-halo-4*H*-1,2,4-benzothiadiazine 1,1-dioxides. J Med Chem 46:3342–3353
55. Boverie S, Antoine M-H, Somers F et al (2005) Effect on K(ATP) channel activation properties and tissue selectivity of the nature of the substituent in the 7-and the 3-position of 4*H*-1,2,4-benzothiadiazine 1,1-dioxides. J Med Chem 48:3492–3503
56. Sharma BK, Sharma SK, Singh P et al (2008) Quantitative structure-activity relationship study of ATP-sensitive potassium channel openers: derivatives of 3-alkylamino-4*H*-1,2, 4-benzothiadiazine 1,1-dioxide. J Enzyme Inhib Med Chem 23:1–6
57. Sharma BK, Sharma SK, Pilania P et al (2009) A quantitative structure-activity relationship study of ATP-sensitive potassium channel openers: the derivatives of 3-alkylamino-4*H*-1,2, 4-benzothiadiazine 1,1-dioxide. Int J Chem Sci 7:655–671
58. Wulff H, Calabresi PA, Allie R et al (2003) The voltage-gated Kv1.3 K^+ channel in effector memory T cells as new target for MS. J Clin Invest 111:1703–1713
59. Beeton C, Barbaria J, Giraud P et al (2001) Selective blocking of voltage-gated K^+ channels improves experimental autoimmune encephalomyelitis and inhibits T cell activation. J Immunol 166:936–944
60. Beeton C, Wulff H, Barbaria J et al (2001) Selective blockade of T lymphocyte K^+ channels ameliorates experimental autoimmune encephalomyelitis, a model for multiple sclerosis. Proc Natl Acad Sci USA 98:13942–13947
61. Baell JB, Gable RW, Harvey AJ et al (2004) Khellinone derivatives as blockers of voltage-gated potassium channel Kvl.3: synthesis and immunosuppressive activity. J Med Chem 47:2326–2336
62. Harvey AJ, Baell JB, Toovey N et al (2006) A new class of blockers of the voltage-gated potassium channel Kv1.3 via modification of the 4- or 7-position of khellinone. J Med Chem 49:1433–1441

63. Saini L, Gupta SP, Satuluri VSAK (2009) A QSAR study on some series of sodium and potassium channel blockers. Med Chem 5:570–576
64. Yuan P, Leonetti MD, Pico AR et al (2010) Structure of the human BK channel Ca^{2+}-activation apparatus at 3.0 A resolution". Science 329:182–186
65. Calderone V (2002) Large-conductance, Ca^{+2}-activated K^+ channels: function, pharmacology and drugs. Curr Med Chem 9:1385–1395
66. Wu S-N (2003) Large-conductance Ca^{2+}-activated K^+ channels: physiological role and pharmacology. Curr Med Chem 10:649–661
67. Coi A, Fiamingo FL, Livi O et al (2009) QSAR studies on BK channel activators. Bioorg Med Chem 17:319–325
68. Zunkler BJ (2006) Human ether-a-go-go-related (HERG) gene and ATP-sensitive potassium channels as targets for adverse drug effects. Pharmacol Ther 112:12–37
69. Wang Q, Bowles NE, Towbin JA (1998) The molecular basis of long QT syndrome and prospects for therapy. Mol Med Today 4:382–388
70. Rajamani R, Tounge BA, Li J et al (2005) A two-state homology model of the hERG K^+ channel: application to ligand binding. Bioorg Med Chem Lett 15:1737–1741
71. Song M, Clark M (2006) Development and evaluation of an in silico model for hERG binding. J Chem Inf Model 46:392–400
72. Aronov AM (2006) Common pharmacophores for uncharged human ether-a-go-go-related gene (hERG) blockers. J Med Chem 49:6917–6921
73. Sanchez-Capula JA, Salinas-Stefanon E, Torres-Jacome J et al (2001) Blockade of currents by the antimalarial drug chloroquine in feline ventricular myocytes. J Pharmacol Exp Ther 297:437–445
74. Ficker E, Obejero-Paz CA, Zhao S et al (2002) The binding site for channel blockers that rescue misprocessed human long QT syndrome type 2 ether-a-go-go-related gene (HERG) mutations. J Biol Chem 277:4989–4998
75. Borosy AP, Keseru K, Penzes I et al (2000) 3D QSAR study of class I antiarrhythmics. J Mol Struct THEOCHEM 503:113–129
76. Matyus P, Borosy AP, Varro A et al (1998) Development of pharmacophores for inhibitors of the rapid component of the cardiac delayed rectifier potassium current. Int J Quantum Chem 69:21–30
77. Ekins S, Crumb WJ, Sarazan RD et al (2002) Three-dimensional quantitative structure-activity relationship for inhibition of human ether-a-go-go-related gene potassium channel. J Pharmacol Exp Ther 301:427–434
78. Cavalli A, Poluzzi E, De Ponti F et al (2002) Toward a pharmacophore for drugs inducing the long QT syndrome: insights from a CoMFA study of HERG K^+ channel blockers. J Med Chem 45:3844–3853
79. Rampe D, Murawsky MK, Grau J et al (1998) The antipsychotic agent sertindole is a high affinity antagonist of the human cardiac potassium channel HERG. J Pharmacol Exp Ther 286:788–793
80. Pearlstein RA, Vaz RJ, Kang J et al (2003) Characterization of HERG potassium channel inhibition using CoMSiA 3D QSAR and homology modeling approaches. Bioorg Med Chem Lett 13:1829–1835
81. SYBYL 6.7.2 Tripos Inc., 1699 S. Hanley Rd., St. Louis, MO 631444 USA
82. Garg D, Gandhi T, Mohan CG (2008) Exploring QSTR and toxicophore of Herg K^+ channel blockers using GFA and HypoGen techniques. J Mol Graph Model 26:966–976
83. Catalyst, Version 4.10 A. (2005). San Diego, Inc., CA, USA

Calcium Ion Channels and Their Blockers

Dimitra Hadjipavlou-Litina

Contents

Abstract Calcium is a ubiquitous second messenger. Calcium entry into the cytosol is mediated by multiple types of calcium channels each with a distinct physiological role. There exist five different types of voltage-dependent Ca^{2+} channel. The calcium ion channel blocking agents are a chemically, pharmacologically, and therapeutically heterogeneous group of drugs. Most calcium channel blockers decrease the force of contraction of the myocardium resulting in a decrease in blood pressure. Representative classes include: (a) dihydropyridines and (b) nondihydropyridines. Structure–activity relationship studies and the structural features that are characterized as prerequisite for the calcium ion channel-blocking activity indicate that the presence of a C-4 phenyl group is a preferential requirement to optimize the biological activity. Steric hindrance is shown to be significant. No relationship of activity is indicated with electronic or lipophilic properties.

Keywords Calcium ion channels • Calcium channel blockers • Therapeutic potential • Structure–activity relationships

D. Hadjipavlou-Litina (✉)
Department of Pharmaceutical Chemistry, School of Pharmacy, Aristotle University of Thessaloniki, Thessaloniki 54124, Greece
e-mail: hadjipav@pharm.auth.gr

S.P. Gupta (ed.), *Ion Channels and Their Inhibitors*,
DOI 10.1007/978-3-642-19922-6_9,

Abbreviations

DHPs	Dihydropyridines
HVA	High-voltage-activated
LCC	L-type Ca^{2+} ion channels
LSSVM	Least squares support vector machine
QSAR	Quantitative SAR structure–activity relationships
QTMS	Quantum topological molecular similarity
SAR	Structure–activity relationships
VDCCs	Voltage-dependent calcium channels

1 Introduction

1.1 Calcium Ion Channels

Calcium is essential in all living organisms and a ubiquitous second messenger. The influx of calcium ions into cells is involved in numerous intracellular events. Calcium entry into the cytosol is mediated by multiple types of calcium channels and ligand-dependent calcium channel, each with a distinct physiological role [1]. Ca^{2+} channels are hetero-oligomeric protein complexes consisting of a pore-forming a1-subunit, one out of at least four b-subunits (b1–b4), an a2/d-subunit, and in skeletal muscle of an additional g-subunit [2, 3]. The auxiliary channel subunits, in particular the b-subunits, modulate voltage dependence, expression density and kinetics of the channels. Calcium ion channels were first identified by Fatt and Katz in crustacean muscle when they left the Na^{+} out of their bathing medium and found that the muscle still generated action potential [4]. Fatt and Ginsborg investigated in detail the significance of this observation [5]. In continuation, Hagiwara and Byerly [6] studied in depth the calcium conductance in various invertebrate tissues.

Calcium channels have major roles in both normal functioning and in pathologies affecting neuronal, neurosecretory and muscle cells [7]. It has become apparent that in several tissues, including certain cardiac muscle cells and subsequently, neurons and other excitable cells, there are two types of calcium ions channels. One is activated by small depolarization and shows rapid voltage-dependent inactivation; this is termed "low-voltage-activated," or "T" (for transient). The second is activated by large depolarization and is termed "high-voltage-activated" (HVA). At least five different types of voltage-dependent Ca^{2+} channel (VDCCs) exist in electrically excitable mammalian cells. Biophysical and pharmacological studies have identified four subtypes of high-voltage-activated (HVA) calcium channels that are encoded by a family of seven different a1 subunit proteins (Cav) as L, N, P, Q, R or T-types. L-type (Cav1.1–Cav1.4), N-type (Cav2.2), P/Q-type (Cav2.1), and R-type (Cav2.3) as well as low-voltage-activated

calcium channels, called T-type, encoded by three distinct α1 subunit proteins (Cav3.1–Cav3.3). The N, P, Q, and R type channels have all been shown to play key roles in neurotransmitter release [8–10]. N-Type calcium channels are located at presynaptic terminals throughout neurons and directly mediate spinal transmission of pain signals from the peripheral to the central nervous system. L-type Ca^{2+} ion channels (LCCs) mediate muscle contraction, hormone secretion and transcriptional events supporting learning and memory. Different subclasses of L-channels exist, which may contribute to tissue selectivity. T-type calcium channels are known to be implicated in pathogenesis of epilepsy and neuropathic pain [11, 12]. Unlike other types of calcium channels, T-type calcium channels comprise only a pore-forming a1 subunit that is different from the calcium channel subtypes [13, 14]. Three different genes encode the a1 subunit of T-type calcium channels, termed a1G, a1H, and a1I, respectively, each with its own distinct functional and pharmacological profile [15, 16].

Calcium ions are required for contraction of skeletal muscle and heart, release of neurotransmitters and hormones, induction of cell death, activation of various protein kinases and signaling cascades [17] for the cell cycle regulation [8, 18–21] and cellular proliferation and for the activation of early genes, which leads the cell into G1 phase. In contrast, Ca^{2+} ion channels in inflammatory cells, such as lymphocytes, mast cells, and neutrophils, are activated regardless of their membrane potential [22] and are known as store operated calcium ion channels. They have been shown to play important roles in the pathogenesis and exacerbation of inflammatory and autoimmune diseases [23–26].

Depletion of intracellular calcium arrests the cell cycle in the G0/G1 and S interphases [27], whereas regulation of the changes in intracellular calcium has been proposed to be through a T-type calcium channel [28]. This is considered to be important to control the cell cycle signaling pathway and to manage certain pathophysiological diseases, where the cell cycle is aberrant.

2 Calcium Ion Channel Blockers

2.1 Mechanism of Action

The calcium ion channel blocking agents are a chemically, pharmacologically and therapeutically heterogeneous group of drugs. L-type Ca^{2+} channels are sensitive to numerous agonist and antagonist drugs that modulate the Ca^{2+} flow. The interaction of an ion channel blocker with its receptor sites depends on whether the channel is in a resting (closed), open (activated), or inactivated (closed) conformational state. Calcium channel blockers work by blocking voltage-gated calcium channels in cardiac muscle and blood vessels. The mechanism underlying the clinically important use of calcium channel blockers is thought to be mediated by L-class ("slow channels") of voltage-gated calcium ions channels, which are abundant in

cardiac and smooth muscle. They block the entry of calcium into the muscle cells of the heart and the arteries. By blocking the entry of calcium, calcium channel blockers decrease the contraction of the heart and dilate the arteries. This may partially explain their rather selective effects on the cardiovascular system.

Calcium channel blockers are primarily used for treating cardiac arrythmia and pulmonary hypertension and for prevention of reperfusion injury as well as atherosclerosis (particularly the lipophilic agents). They also slow the rate at which calcium passes into the heart muscle and into the vessel walls. This relaxes the vessels. The relaxed vessels let blood flow more easily through them, thereby lowering blood pressure. Unlike β-blockers, calcium channel blockers do not decrease the responsiveness of the heart.

Different classes of Calcium channel blockers bind to different sites on the a1-subunit. Recent clinical evidence in patients with microvascular disease suggests that blockade of the T-type calcium ion channel has additional benefit. Blockade of these channels slows the sinus rate and prolongs atrioventricular nodal conduction, in addition to causing vasodilation, without adverse negative inotropic or positive chronotropic cardiac actions [29, 30].

Recently, some of the classical L-type calcium channel blockers were found to have a potent inhibitory activity against the N-type as well. The N-type channel has been shown to play a significant role in the pathophysiological processes of stroke and neuropathic pain [31–33], in addition to physiological regulation. Over the last decade, synthetic efforts have focused on the development of both peptidic and nonpeptidic-based small molecule N-type calcium channel blockers for analgesia or neuroprotection.

2.2 *Classification of Calcium Ion Channel Blockers*

- Dihydropyridines (DHPs)
- Nondihydropyridines:
  - Phenylalkylamines
  - Benzothiazepine
- Nonselective (Fig. 1)

All the above-mentioned blockers differ not only in their basic chemical structure, but also in their relative selectivity toward cardiac versus vascular L-type calcium channels. All of them bind reversibly with the L-type Calcium channel, but each class binds to different binding sites of the same channel in a stereoselective manner and with dissociation constants in the nanomolar range (0.1–50 nM). Verapamil binds to the V binding site. Diltiazem binds to the D binding site in the L-type Ca^{2+} channel. However, it shows cardiovascular effects similar to those of verapamil. Calcium channel antagonists block the inward movement of calcium by binding to the L-type calcium channels in the heart and in smooth muscle of the peripheral vasculature.

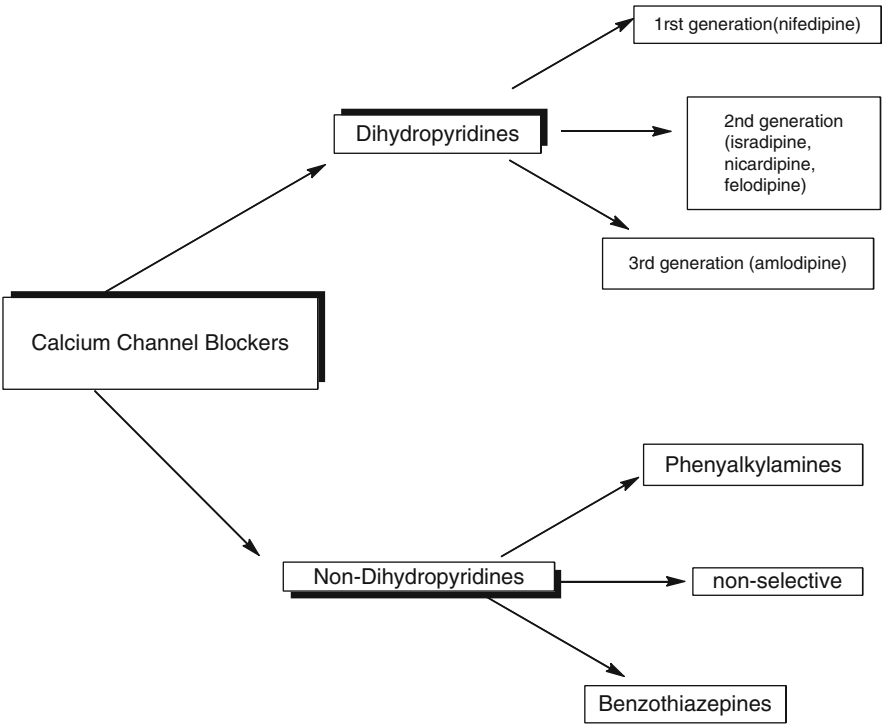

Fig. 1 Classification of calcium channel blockers

Furthermore, there are other classes of drugs that have overlapping effects as calcium ion channel blockers: angiotensin inhibitors, β-blockers, and nitrates.

2.2.1 Dihydropyridines Calcium Ion Channel Blockers (Partial Agonists, Antagonists, Dual-Acting Agents)

This class is easily identified by the suffix "-dipine." First generation calcium channel blockers (nifidepine), all block L-type calcium channels and all are competitive antagonists, whereas second and third generation analogs are either slow-release or long-acting formulations (amlodipine or felodipine) [34] (Fig. 2).

A number of molecules and their trade names (in alphabetical order), belonging to this class are given below:

Amlodipine (Norvasc), Aranidipine (Sapresta), Azelnidipine (Calblock), Barnidipine (HypoCa), Benidipine (Coniel), Cilnidipine (Atelec, Cinalong, Siscard), Clevidipine (Cleviprex), Efonidipine (Landel), Felodipine (Plendil), Lacidipine (Motens, Lacipil), Lercanidipine (Zanidip), Manidipine (Calslot, Madipine), Nicardipine (Cardene, Carden SR), Nifedipine (Procardia, Adalat),

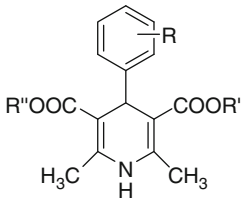

Fig. 2 General structure of 1,4-dihydropyridines

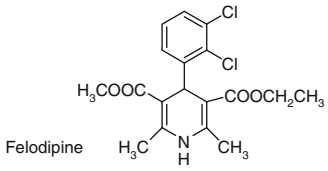

Felodipine

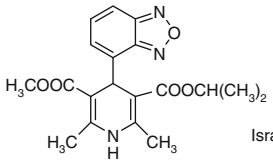

Isradipine

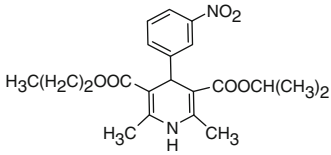

Nimodipine (*S*)

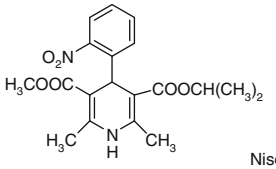

Nisoldipine

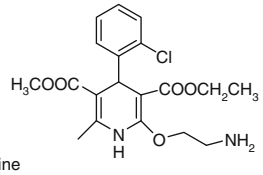

Amlodipine

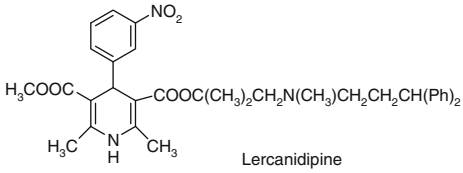

Lercanidipine

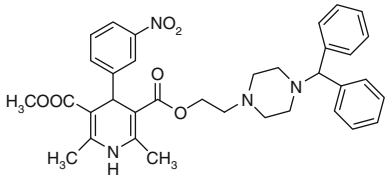

Manidipine

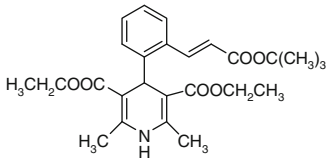

Lacidipine

Fig. 3 Analogs of nifedipine

Nilvadipine (Nivadil), Nimodipine (Nimotop), Nisoldipine (Baymycard, Sular, Syscor), Nitrendipine (Cardif, Nitrepin, Baylotensin), Pranidipine (Acalas).

Nifedipine. Nifedipine is the lead compound, which was first successfully introduced for the treatment of coronary angina in Germany at the beginning of 1975. Major disadvantage of its use is the short plasma half-life. The consequence is multiple daily administrations to achieve blood pressure control (Fig. 3).

Analogs of Nifedipine. Following the introduction of nifedipine into the market, a number of analogs were prepared starting from its structure, which were characterized by a short duration of pharmacological action. All of these belong to the first generation dihydropyridines. Among these, felodipine, isradepine, nimodepine, nisoldipine, amlodipine, lercanidipine and manidipine have emerged as novel therapeutic agents.

Felodipine. Felodipine is a very potent calcium antagonist, which reduces both systolic and diastolic blood pressures in a dose-related manner. The activity is exerted through a specific binding to the dihydropyridine site. It increases the secretion of potassium, calcium, and magnesium. Since this drug is mainly metabolized by the liver, patients under therapy with felodipine should avoid cytochrome P450 3A4 and 1A2 isoform inhibitors, such as grapefruit juice, which induce interference with the hepatic metabolism of felodipine. Concerning the structural characteristics, in this analog the *ortho*- nitro group in the aryl moiety has been replaced by 1, 2-dichloro group (Fig. 3).

Isradipine. It is used either alone or in combination with diuretics in the treatment of hypertension. It presents high calcium antagonist activity together with oral bioavailability (90–95%). However, the hepatic first-pass effect reduces it to 15–24%. Although isradipine showed antiatheromatic activity in a number of experimental models, clinical studies in patients failed to confirm these findings (Fig. 3).

Nimodipine (*S*). It is an asymmetric structural analog of nifedipine. The pharmacological activity is exerted through its ability to bind to the α1 subunit of the L-type calcium channel. Nimodipine is lipophilic, which enables it to cross the blood–brain barrier and achieve effective drug concentration. It shows a preferential binding activity at the cerebral vessels. Thus, it has been widely used for the treatment of neurological disorders such as stroke of the subarachnoid hemorrhagic type (Fig. 3).

Nisoldipine. This nifedipine analog is at least five to ten times more potent than the "parent" molecule on arterial smooth muscle and it can be used for the treatment of hypertension. Due to its massive hepatic metabolism, it is currently used for once daily administration (Fig. 3).

Amlodipine. It presents a long kinetic half-life and thus is characterized as a long-acting blocker. Its hepatic first pass is less than that of the other analogs. Another interesting aspect is its antiatheromatic properties, which can be further increased by combination with statins (Fig. 3).

Lercanidipine. It is a molecule with high lipophilicity, which explains its long duration of action. It is used in the treatment of hypertension and angina, and it is especially indicated in elderly patients. It is one of the last dihydropyridines introduced into the market (Fig. 3).

Manidipine. It is a potent and selective analog toward the renal vasculature, making it particularly helpful for the therapy of renovascular hypertension (Fig. 3).

Dihydropyridines appeared as both blockers and activators of L-type calcium ions channels [35]. They possess significant selectivity toward vascular versus myocardial cells and therefore have a greater vasodilatory effect with respect to

other calcium blockers. They also show a minor negative inotropic effect, atrioventricular blockade or neurohormonal activation [36–38], which often limit their therapeutic use. They do not show any significant direct effect on the heart. All seem effective in the clinical situation and they are well tolerated. Their oral bioavailability is low. Their in vivo metabolism after oral administration is due to oxidation of the 1, 4-dihydropyridine ring by the cytochrome P450 3A4 isoform to an aromatic pyridine ring and to oxidative cleavage of the carboxylic esters. The derivatives are insoluble in water and light sensitive. For the most lipophilic analogs, the side effects (such as ankle edema) seem less pronounced, most likely due to their slow onset of activity.

Structure Activity–Relationships: Essential Structural Features and Physicochemical Properties

Glossmann et al. [39] reported that dihydropyridines containing 3, 5-dicarboxylic acid esters might exhibit a spectrum of activity toward the calcium channel somewhere between the extremes of antagonism and agonism. Attempts were made to differentiate in the mechanisms of their agonist and antagonist activities. Höltje and Marrer [40] using quantum mechanical calculations demonstrated that the molecular potential of a single receptor site was reduced by interaction with calcium channel activators and increased by interaction with calcium channel blockers. Matowe et al. [41] described the pharmacological properties of AK-2–38 (Fig. 4), a C-4 2-pyridinyl analog that exhibited twice the potency of nifedipine on smooth muscle and partial agonism on cardiac muscle. Compounds with the above properties are known as "dual cardioselective calcium-channel agonist–smooth muscle selective calcium-channel antagonists" or "third-generation dihydropyridines" [42] (Fig. 4).

Structure–activity relationship (SAR) studies of dual-acting agents revealed that although C-4 2-pyridinyl isomer acts as a dual agent, the 3-pyridinyl and 4-pyridinyl isomers are calcium-channel agonists on both heart and smooth muscle [43]. From the above, it is obvious that the position of the pyridinyl nitrogen-free electron pair and/or charge distribution on the pyridinyl might be important parameters of calcium-channel agonist–antagonist modulatory effects [44]. In addition, dihydropyridines possessing a C-4-appropriate thienyl isomeric substituent also exhibit desirable calcium-modulating effects [45].

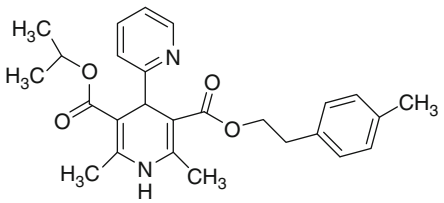

Fig. 4 Structure of AK-2-38

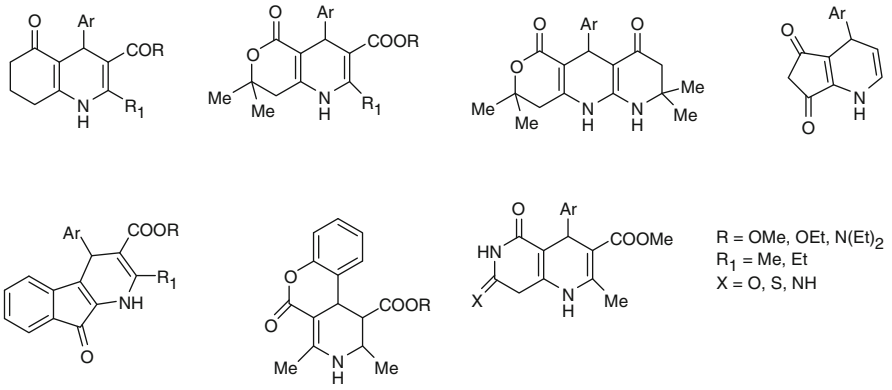

Fig. 5 Derivatives containing dihydropyridine core into condensed ring systems

Fig. 6 Hexahydroquinolines, fluroquinolines, indenopyridines and lactones

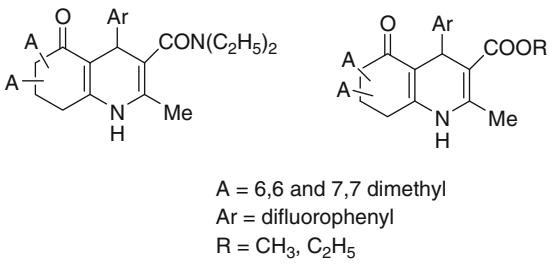

Fig. 7 Nitroimidazoles

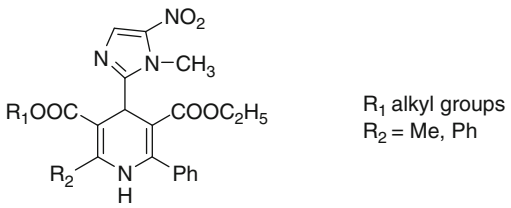

Other studies indicate that dual-acting derivatives can be obtained by the introduction of the dihydropyridine core into condensed ring systems (Fig. 5) [46].

Racemic hexahydroquinolines, fluroquinolines, indenopyridines, and lactones (Fig. 6) exhibit calcium-antagonistic effects on smooth muscle and positive inotropic activity [46, 47].

A series of compounds resulting from the replacement of nitrophenyl in Nifedipine analogs with its bioisoster 1-methyl-5-nitroimidazole (Fig. 7), presented [48–52] calcium channels antagonistic activities. A valuable QSAR model was obtained by using constitutional and topological indices from which it is obvious that nonrotable groups resulted in increasing calcium channel blocker activity [53].

Antagonists of the nifedipine type are flexible molecules, in which the C-4-aryl moiety and the C-3 and C-5 ester substituents can rotate and the conformation of the 1, 4-dihydropyridine ring can change [54]. The exact stereochemical and/or

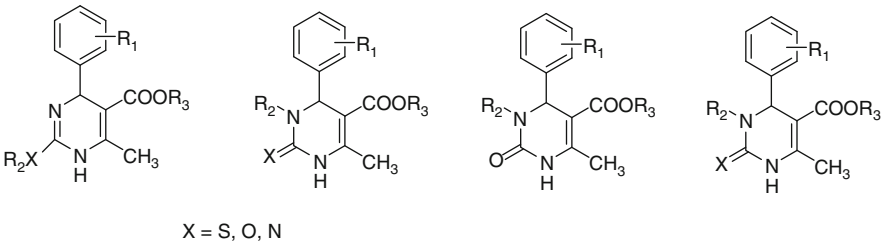

Fig. 8 Dihydropyrimidine analogues

conformational requirements for calcium-channel antagonist–agonist modulation activity are still not well defined [40, 55]. To study in detail the structure–activity relationships of unsymmetrical molecules and to find the effects of absolute stereochemistry on biological activity, Atwal et al. [56–59] studied four different series of dihydropyrimidine analogs (Fig. 8). The latter were found to highly imitate dihydropyridines and to adopt in solid state molecular conformation similar to the reported conformation of dihydropyridines.

Gupta in a QSAR analysis [60] showed that almost all those characteristics that are essential for the activity of 1,4-dihydropyridines are also essential for the activity of dihydropyrimidine analogs: conformation of the molecule, the relative orientation of the aryl ring with respect to the pyrimidine ring, and some substituents capable of forming the hydrogen bonds with the receptor but less bulky in nature, and high molar refractivity of the molecule.

The following structural features are characterized as prerequisite for the calcium ions channel-blocking activity:

(a) The nature and position of C-4-aryl ring substituents: optimizes activity. Phenyl group is preferred. The pseudoaxial conformation of C-4 aryl ring is also important [61–63].
(b) The 1, 4-dihydropyridine ring is essential for activity because it is necessary for hydrogen bonding. Substitution at the N-1 position or the use of oxidized (piperidine) or reduced (pyridine) ring systems greatly diminish activity [61]. Nifedipine and related analogs have been shown to exist in a boat conformation [64]. Protonation of the dihydropyridine ring nitrogen results in a slight deviation of the boat-like conformer of the protonated dihydropyridines from the planarity producing a twist-like conformation [65].
(c) C-3 and C-5 substituents modulate activity and tissue selectivity [43, 63]. Asymmetrical substituents in C-3 and C-5 alter the activity [48]. The electronic features of the oxygen of the carboxyl ester group influenced biological activity. Carbonyl oxygen participates in hydrogen bonding with the receptor [66]. X-ray structural investigations indicate that at least one ester must be in the *cis* arrangement, which is necessary for hydrogen bonding to the receptor [54]. Molecular orbital conformational calculations suggest that both carboxy groups are preferentially oriented in a plane that intersects the plane of the dihydropyridine ring with an angle of between 308 and 608 [66]. Based on

the orientation of the individual carbonyl groups of the C-3 and C-5 ester substituents with respect to the dihydropyridine ring double bond, three different conformations are possible for the ester groups: *trans*/*trans*, *cis*/*cis* and enantiomeric *cis*/*trans*, and *trans*/*cis* arrangements [65]. Furthermore, it has been suggested that syn-periplanar carbonyl groups might be a common feature of dihydropyridines calcium-channel antagonists and that an antiperiplanar carbonyl group, such as the lactone group in the rigid compounds, might be prerequisite for calcium-channel agonist activity [63].

(d) When the esters at C-3 and C-5 are different, C-4 carbon becomes chiral and stereoselectivity between enantiomers is presented [67].

(e) Modified activity can be obtained by altering the changes at C-2 and C-6 substituents. The receptor can tolerate different changes [63, 67].

(f) In unsymmetrical dihydropyridines, C-4 is a chiral center. It was suggested that calcium-channel modulation (antagonist versus agonist activity) is dependent on the absolute configuration at C-4, whereby the orientation of the 4-aryl group (*R* versus *S*-enantiomer) acts as a "molar switch" between antagonist and agonist activity [40, 55, 68]. The replacement of large lipophilic groups by small ester groups presenting a negative potential (e.g., nitro group) will be the point of chirality for the C-4. The resulting individual enantiomers will have exactly the opposite biological response [54]. Instead of blocking the entry of calcium into cardiac and vascular muscle, these derivatives will enhance it. Thus, these derivatives are characterized as "calcium agonists" or "calcium-channel activators" [54].

Coburn et al. [45] applied a Hansch analysis to a series of 45 4-phenyl-substituted dihydropyridines (Fig. 2). They concluded that the biological activity is dependent on the lipophilic, as well as the electronic and steric properties of the substituents on 4-phenyl dihydropyridines analogs of nifedipine [45].

Hemmateenejad et al. [63, 69] examined the same data set, using multiple linear regressions combined with genetic algorithm for variable selection and an artificial neural network model combined with principal component analysis for dimension reduction and genetic algorithm for factor selection. The resulting equations suggested that the electronic properties of the atoms belonging to the backbone of the molecules as well as the conformation of the molecules affect the binding of these molecules with their receptor.

In 2008, Hemmateenejad et al. [62] evaluated a novel type of electronic descriptors called quantum topological molecular similarity (QTMS) indices for describing the quantitative effects of molecular electronic environments on the antagonistic activity of the same dihydropyridine derivatives. QTMS theory produces a matrix of descriptors, including bond (or structure) information in one dimension and electronic effects in another dimension, for each molecule. The significant effects of chemical bonds on the antagonistic activity were identified by calculating variable important in projection (VIP). It was obtained that those belongings to the substituted 4-phenyl ring represent high influence on the biological activity.

Mahmoudian and Richard [70] conducted a Hansch analysis on a subset of 4-phenyl-substituted dihydropyridines (Fig. 2) and found that bulky and lipophilic groups at the *ortho*-position and *ortho*-bulky groups with high Hammet electronic constant (σ) at the *meta*-position of the 4-phenyl ring increase the activity.

From a Hansch analysis for a series of *ortho*-analogs (Fig. 2), [66] steric hindrance of the substituents (as Verloop parameter B_1) was shown to be significant for the calcium ion channel blocking activity. No relationship was indicated for either electronic or lipophilic properties. Since the biological response increases as B_1 increases, steric hindrance in the *ortho*-position is required to fix the dihydropyridine core into a favorable conformation in which the aromatic moiety is approximately perpendicular to the dihydropyridine ring.

A QSAR study was applied on a large number of 4-phenyl-substituted nifedipine analogs (Fig. 2) [71] by the combination of substituent constants and molecular descriptors. QSAR analysis showed that a dominant steric effect (as V_w van der Waals volume) can be produced from the para position [71]. For all mono-para substituted analogs, the bulky substituents will be dentrimental to the activity, and this was also shown by Berntsson and Wold [72] in a study on the binding affinity of a small set of compounds. The same researchers had observed that the activity will be increased by the presence of electron withdrawing substituents on the ring. It was found that the activity of *meta*-substituted analogs is affected by both steric and electronic parameters, whereas the hydrophobic and electronic parameters of the *para*-substituted analogs affect the activity. Hansch analysis has been applied for nifedipine analogs containing nitroimidazolyl, phenylimidazolyl, and methylsulphonyl-imidazolyl groups at the C-4 position and different ester substituents at C-3 and C-5 positions of the ring. The results showed that Hammett's electronic and hydrophobic properties are highly correlated with the biological activity [73].

In a series of sulfonylindolizines (Fig. 9), Gupta et al. [74] recently showed, through a QSAR study, that the presence of different heterocyclic rings in different compounds could affect the activity altering the conformations of the receptor through their steric properties.

In 2009, Miri et al. [75] synthesized a novel group of bis-1, 4-dihydropyridines using the condensation of *n*-alkyl diacetoacetate ($n = 2$–7) with methyl-3-aminocrotonate and nitrophenylaldehyde (Fig. 10).

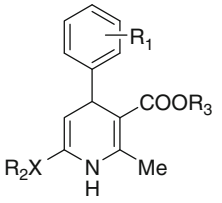

R_1 = NO_2, Cl, CF_3
R_2 = Me, $CH_2CH_2N(CH_3)Bn$, CH_2Ph, CH_2CHCH_2, $CH_2CH_2N(CH_3)_2$
R_3 = Me, Et, iPr, sBu, $CH_2CH_2N(CH_3)Bn$

Fig. 9 Sulfonylindolizines

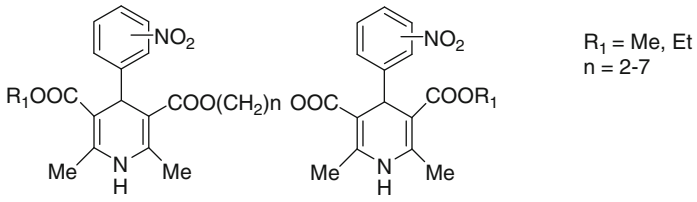

Fig. 10 Bis-1,4-dihydropyridines

Their biological results were used in quantitative structure–activity relationship studies utilizing multiple linear regression analysis. For this purpose, a wide range of descriptors were used such as quantum chemical, topological, functional, electronic, and constitutional. A total of 120 descriptors were calculated for each molecule. Most of these compounds were less active compared with nifedipine. Increase in steric hindrance resulted decrease in activity. The quantitative structure–activity relationship study indicated that the activity was related to the electrostatic and topological parameters and the distance between two C-5 esteric groups of 1, 4-dihydropyridine rings.

Partial least squares [76], principal component analysis [77] and the gene expression programming were employed [78], using theoretically derived descriptors for different DHPs analogs. In addition, the quantum chemical QSAR study indicated the importance of electronic features of the dihydropyridine derivatives for receptor binding [79].

Yao et al. [80] used the least squares support vector machine (LSSVM) algorithm to develop quantitative and classification models for a series of 1, 4-dihydropyridine calcium channel antagonists [81], as a potential screening mechanism. Each compound was represented by calculated structural descriptors that encode constitutional, topological, geometrical**,** electrostatic, quantum-chemical features. The heuristic method was then used to search the descriptor space and select the descriptors responsible for activity. Quantitative modeling resulted in a nonlinear, seven-descriptor model based on LSSVM with mean-square errors 0.2593, a predicted correlation coefficient 0.8696, and a cross-validated correlation coefficient 0.8167. In the linear model, there were two topological descriptors, one geometric descriptor, three quantum chemical descriptors and one electrostatic descriptor.

Compared with classical QSAR investigations, 3D QSAR approaches yield better results. A 3D QSAR study (comparative molecular field analysis and comparative molecular similarity studies) of 4-phenyl-substituted dihydropyridines indicated unfavorable steric interactions for bulky moieties in the *para*-position of the phenyl ring and that bulky substituents are favorable in *ortho*- and *meta*-positions. The best combination is obtained when the bulky substituents at *ortho* - or *meta*- positions produce negatively charged electrostatic potential. From these studies was indicated that repulsive electronic interaction with binding-site residue

or to the potential of electron-deficient 4-aryl moieties behaved as electron acceptors in charge transfer mechanism [82].

X-ray as well as (Q)SAR analyses of several series of dihydropyridine analogs [68] resulted that the torsion angle of the bond between the aryl and the 1, 4-dihydropyridine ring is fixed by lactone bridges of different chain lengths. These findings were used in a lead optimization program from which a second generation analog, *lacidipine,* with a sustained duration of action, potency, and selectivity was derived [83] (Fig. 3). In *lacipidine*, the ester group is the bulky *tert*-butyl moiety. It is a competitive calcium ions antagonist with high lipophilicity. Its pharmacological profile was studied extensively both in vitro and in vivo. Furthermore, it was found to present antioxidant activity [84] equipotent to vitamin E in many tests. Lacidipine also showed a direct protective effect on the vasculature at non-anti-hypertensive doses, indicating that its high lipophilic character combined with antioxidant ability, selectivity, potency, significant antiatheromatic activity, and sustained duration of action might be beneficial for elderly patients [85, 86].

2.2.2 Nondihydropyridines

Phenylalkylamines

Phenylalkylamines [87] are thought to access calcium ion channels from the intracellular side, although this evidence is not well defined. The drugs of this class are relatively selective for myocardium. They reduce myocardial oxygen demand and reverse coronary vasospasm, and they are often used to treat angina. They present minimal vasodilatory effects compared to dihydropyridines. Thus, their major mechanism of action is causing negative inotropy.

Representative agents belonging to this class are: verapamil (Calan, Isoptin) and gallopamil (Procorum, D600) (Fig. 11).

Verapamil is the most widely used phenylalkylamine. It mainly gets access to the binding domain when the channel is open. As an organic cation, it blocks the channel by interfering with Ca^{2+} ion binding to the extracellular mouth of the pore and slows the recovery of channels from inactivation. Once bound to the open state, it can promote the inactivated channel conformation. Verapamil has two enantiomers with different kinetics and activity. The (*S*) isomer is more active but has a shorter half-life and lower bioavailability than the (*R*) isomer. The higher proportion of (*S)* isomer that is available is the major reason why *intravenous* verapamil has more cardiac effects for a given serum concentration than oral verapamil.

The more active methoxyverapamil (gallopamil) is also licensed for clinical use in some countries.

Verapamil analogs were subjected to a QSAR analysis from which was found that along with the electronic property, the size of the substituents (molecular volume of the ring substituents) will also be important for their activity [88].

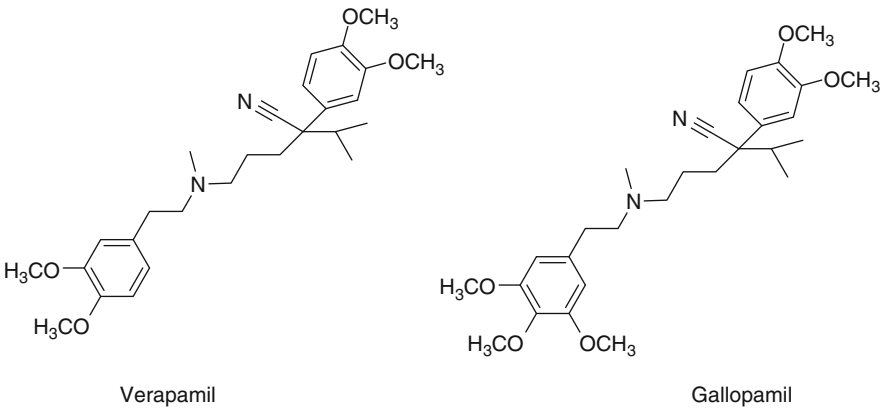

Fig. 11 Structures of verapamil and gallopamil

Fig. 12 Diltiazem and analogs

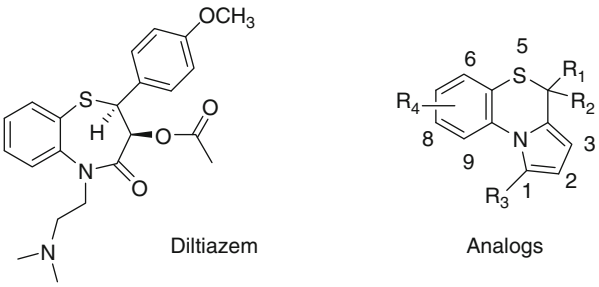

Benzothiazepines

Benzothiazepines in terms of selectivity for vascular calcium ion channels consist an intermediate class between phenylalkylamines and dihydropyridines. Since they have both cardiac depressant and vasodilator activities, they are able to reduce arterial pressure without producing the same degree of reflex cardiac stimulation caused by dihydropyridines.

Diltiazem (cardizem) and clentiazem are the main representatives of this class of calcium ion channel blockers (Fig. 12).

Diltiazem, a 1,5-benzothiazepine, has affinity for the L-type calcium channels like the other calcium ion channel blockers, but it is less potent on the peripheral smooth muscle than on myocardial tissue. This weak selectivity produces negative chronotropic and inotropic effects that reduce the myocardial oxygen demand [89].

Negative inotropic potency of 60 benzothiazepine-like calcium entry blockers, Diltiazem analogs, was successfully modeled using Bayesian regularized genetic neural networks (BRGNNs) and 2D autocorrelation vectors. The analysis of the network inputs pointed out to the electronegativity and polarizability 2D topological distributions at substructural fragments of sizes 3 and 4 as the most relevant features governing the nonlinear modeling of the negative inotropic potency.

A comparative molecular field analysis (CoMFA) [90] made for a series of Diltiazem-like channel blockers suggested that they can interact with the receptor as its negative charge site, two hydrogen–bonding sites and three hydrophobic regions. Campiani and co-researchers [91] also suggested that substitution on the fused phenyl ring (R_4) and the double substitution at C4 were beneficial to the activity as well as the substitution of the electron withdrawing group in the fused phenyl ring. In addition, the substituted phenyl ring at C4 and the basic side chain at C1 on the pyrrole ring were found to constitute two important pharmacophores [91] (Fig. 12).

Two more pharmacophores were also identified by Kimball [92]: the basic nitrogen and the phenyl methyl ethers. In particular, the selective chronotropic and inotropic activity of new compounds might open new perspectives in the search for more effective drugs for the control of cardiac arrhythmias and led attention to the synthesis of novel Diltiazem-like calcium channels blockers [72, 93–95].

2.2.3 Nonselective Calcium Ions Channel Blockers: T-Type Calcium Channel Blockers-Structure–Activity Relationships – Molecular Features

Mibefradil ($IC_{50} = 1.34 \pm 0.49$ μM; Posicor ™), bepridil, fluspirilene, and fendiline are considered as *nonselective* calcium blockers (Fig. 13).

Furthermore, *Mibefradil* is an important example of the selective T-type calcium channel blockers and it has been used as the first selective T-type calcium channel blocker in treatment of hypertension and stable angina [4, 19, 96, 97]. Depending on the cell type, mibefradil blocks T-type calcium channels 10–30 times more potently than L-type calcium channels [98]. In addition, mibefradil is highly tissue selective, relaxing smooth muscle without inducing reflex tachycardia, or having much effect on cardiac chronotropy or inotropy [99, 100]. *Mibefradil* because of potential harmful interactions with other drugs [101] has been withdrawn from the US market (May 1998) very shortly. Continuous structure–activity relationship studies on 3, 4-dihydroquinazoline series led to the synthesis of KYS05090 [102] (Fig. 14), which is a very potent blocker ($IC_{50} = 41 \pm 1$ nM) against T-type calcium channel and also is as potent as doxorubicin against some human cancer cells without acute toxicity [103, 104].

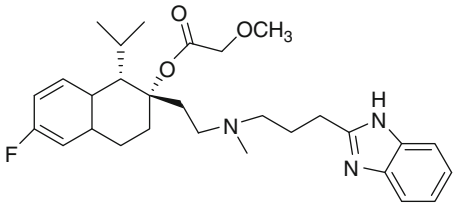

Fig. 13 Mibefradil

Fig. 14 KYS05090

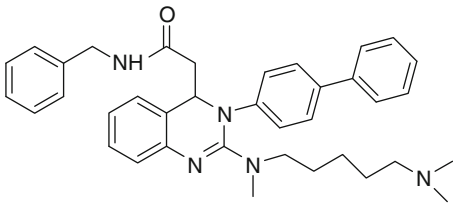

Lee et al. [105] performed 3D QSAR studies on a set of 42 3,4-dihydroquinazolines using a comparative molecular field similarity indices analyses (CoMSIA) method, to find out the pharmacophore elements for T-type calcium channel blocking activity. The derived 3D QSAR model provided good predictivity for the training set ($q^2 = 0.642$, $r^2 = 0.874$) and the test set (r^2 pred $= 0.884$) and can be used for the design of new chemical entities with high T-type calcium channel blocking activity.

A set of 24 isoxazolyl compounds potent T-type calcium channel blockers served to establish Comparative molecular field analysis (CoMFA) and comparative molecular similarity indices analysis (CoMSIA) [106]. CoMFA and CoMSIA contour maps were used to analyze the structural features of the ligands accounting for the activity in terms of positively contributing physicochemical properties: steric, electrostatic, hydrophobic, and hydrogen bonding fields. All CoMFA and CoMSIA models gave cross-validated r^2 (q^2) value of more than 0.5 and conventional r^2 value of more than 0.85.

As a result, the efforts for the discovery of new T-type calcium channel blockers have been intensified [105–108].

2.2.4 Differences Among Calcium Ion Channel Blockers Side Effects

Calcium ion channel blockers differ in their duration of action, the process by which they are eliminated from the body and most importantly, in their ability to affect heart rate and contraction. Some of them e.g., *amlodipine*, have very little effect on heart rate and contraction so they are safer to use in individuals who have heart failure or bradycardia. *Verapami*l and *diltiazem* have the greatest effects on the heart and reduce the strength and rate of contraction.

2.2.5 Side Effects

Many unwanted effects are related to the vasodilatory effects of Ca^{2+} channel blockers, such as flushing, headache, dizziness, and hypotension. DHPs frequently cause edema and ankle swelling upon chronic use. Worsening of angina has also been observed with dihydropyridines. This is most likely due to their pronounced

effect on coronary resistance resulting in coronary steal in the presence of hypoperfused regions. It may also be caused by the reactive sympathetic activation with increase in heart rate and cardiac oxygen consumption.

Epidemiological and case–control studies suggested that Ca^{2+} channel blockers cause increased risk for myocardial infarction, cancer and gastrointestinal bleeding. The increased cardiovascular morbidity was again associated with short-acting dihydropyridines and fast release forms of verapamil and diltiazem.

3 Conclusion

Calcium channel blockers inhibit calcium uptake, block smooth muscle contraction and bind to the receptor sites associated with the voltage-dependent calcium ion channels. All these activities have been found to be mutually correlated [109]. Different linear and nonlinear methods have been used in QSAR studies to obtain additional and more precise physicochemical parameters that are important for the biological activity of calcium ion channel blockers and for the design of more selective molecules [110].

Even today, the studies on the calcium channel blockers remained centered around the dihydropyridines. QSAR studies of 4-phenyl-substituted dihydropyridines indicate unfavorable steric interactions for bulky moieties in the *para*-position of the phenyl ring and that bulky substituents are favorable in *ortho*- and *meta*-positions. The best combination is obtained when the bulky substituents at *ortho*- or *meta*- positions produce negatively charged electrostatic potential. Further, investigation and studies are still needed to delineate the physicochemical parameters implicated in the case of the nondihydropyridines.

References

1. Zamponi GW (1998) Antagonist binding sites of voltage-dependent calcium channels. Drug Dev Res 42:131–143
2. Catterall WA (1994) Molecular properties of a superfamily of plasma-membrane cation channels. Curr Opin Cell Biol 6:607–615
3. Walker D, De Waard M (1998) Subunit interaction sites in voltage-dependent Ca^{2+} channels: role in channel function. Trends Neurosci 21(4):148–154
4. Fatt P, Katz B (1953) The electrical properties of crustacean muscle fibres. J Physiol 120:171–204
5. Fatt P, Ginsborg BL (1958) The ionic requirements for the production of action potentials in crustacean muscle fibres. J Physiol 142:516–543
6. Hagiwara S, Byerly L (1981) Calcium channel. Annu Rev Neurosci 4:69–125
7. Dolphin AC (2006) A short history of voltage-gated calcium channels. Br J Pharmacol 147(suppl 1):S56–S62

8. Barton ME, Eberle EL, Shannon HE (2005) The antihyperalgesic effects of the T-type calcium channel blockers ethosuximide, trimethadione, and mibefradil. Eur J Pharmacol 521:79–85
9. Coulter DA, Huguenard JR, Prince DA (1989) Calcium currents in rat thalamocortical relay neurons: kinetic properties of the transient, low-threshold current. Ann Neurol 25:582–593
10. Coulter DA, Huguenard JR, Prince DA (1990) Differential effects of petit mal anticonvulsants and convulsants on thalamic neurones: GABA current blockade. Br J Pharmacol 100:800–806
11. Nelson MT, Todorovic SM (2006) The role of T-type calcium channels in epilepsy and pain. Curr Pharm Des 12:2189–2197
12. Perez-Reyes E (2003) Molecular physiology of low-voltage-activated T-type calcium channels. Physiol Rev 83:117–161
13. Catterall WA, Perez-Reyes E, Snutch TP, Striessnig J (2005) International union of Pharmacology. XLVII. Nomenclature and structure-function relationships of voltage-gated sodium channels. Pharmacol Rev 57:411–425
14. McRory JE, Santi CM, Hamming KSC, Mezeyova J, Sutton KG, Baillie DL, Stea A, Snutch TP (2001) Molecular and functional characterization of a family of rat brain T-type calcium channels. J Biol Chem 276:3999–4011
15. Shin H-S, Cheong E-J, Choi S, Lee J, Na HS (2008) T-type Ca^{2+} channels as therapeutic targets in the nervous system. Curr Opin Pharmacol 8:33–41
16. Ertel EA, Campbell KP, Harpold MM, Hofmann F, Mori Y, Perez-Reyes E, Schwartz A, Snutch TP, Tanabe BL, Tsien RW, Catterall WA (2000) Nomenclature of voltage-gated calcium channels. Neuron 25:533–535
17. Doering D, Zamponi G, Connolly TM, Barrow JC, Triggle DJ, Snutch TP (2006) Voltage-gated ion channels as drug targets. Wiley-VCH, Weinhiem
18. McDonough SI, Bean BP (1998) Mibefradil inhibition of T-type calcium channels in cerebellar Purkinje neurons. Mol Pharmacol 54:1080–1087
19. Mishra SK, Hermsmeyer K (1994) Selective inhibition of T-type Ca^{2+} channels by Ro 40–5967. Circ Res 75:144–148
20. SoRelle R (1998) Withdrawal of Posicor from market. Circulation 98:831–832
21. Flatters SJL (2005) T-type calcium channels: a potential target for the treatment of chronic pain. Drugs Future 30:573–580
22. Hoth M (1995) Calcium and barium permeation through calcium release-activated calcium (CRAC) channels. Pflugers Arch 430(3):315–322
23. Hoth M, Penner R (1992) Depletion of intracellular calcium stores activates a calcium current in mast cells. Nature 355:353–356
24. Lewis RS, Cahalan MD (1995) Potassium and calcium channels in lymphocytes. Annu Rev Immunol 13:623–653
25. Clementi E, Meldolesi J (1996) Pharmacological and functional properties of voltagemi independent Ca^{2+} channels. Cell Calcium 19:269–279
26. Geiszt M, Kapus A, Nemet K, Farkas L, Ligeti E (1997) Regulation of capacitative Ca^{2+} influx in human neutrophil granulocytes. Alterations in chronic granulomatous disease. J Biol Chem 272:26471–26478
27. Clapham DE (1995) Calcium signaling. Cell 80:259–268
28. Gray LS, Perez-Reyes E, Gamorra JC, Haverstick DM, Shattock M, McLatchie L, Harper J, Brooks G, Heady T, Macdonald TL (2004) The role of voltage gated T-type Ca^{2+} channel isoforms in mediating "capacitative" Ca^{2+} entry in cancer cells. Cell Calcium 36(6):489–497
29. Portegies MC, Schmitt R, Kraaij CJ, Braat SHJG, Gassner A, Hagemeijer F, Ponzenel H, Prager G, Viersma JW, VanderWall EE, Kleinbloesem CH, Lie KI (1991) Lack of negative inotropic effects of the new calcium antagonist Ro 40–5967 in patients with stable angina pectoris. J Cardiovasc Pharmacol 18:746–751

30. Cremers B, Flesch M, Sudkamp M, Bohm M (1997) Effects of the novel T-type calcium channel antagonist mibefradil on human myocardial contractility in comparison with nifedipine and verapamil. J Cardiovasc Pharmacol 29:692–696
31. Sheng ZH, Rettig J, Cook T, Catterall WA (1996) Calcium-dependent interaction of N-type calcium channels with the synaptic core complex. Nature 379:451–454
32. Saegusa H, Kurihara T, Zong S, KazunoA MY, Nonaka T, Han W, Toriyama H, Tanabe T (2001) Suppression of inflammatory and neuropathic pain symptoms in mice lacking the N-type Ca^{2+} channel. EMBO J 20:2349–2356
33. Cox B, Denyer J (1998) Patents N-type calcium channel blockers in pain and stroke. Expert Opin Ther Pat 8:1237–1250
34. Munikumar RD, Hee KJ, Joo HC, Yong SC, Hun YK, Moon HC, Ae NP (2004) 3D QSAR studies on T-type calcium channel blockers using CoMFA and CoMSIA. Bioorg Med Chem 12:1613–1621
35. Catterall WA, Striessnig J (1992) Receptor sites for Ca^{2+} channel antagonists. Trends Pharmacol Sci 13:256–262
36. Opie LH, Frishman WH, Thadani U (1999) Calcium channel antagonists (calcium entry blockers). In: Opie LH (ed) Drugs for the heart, 4th edn. Saunders WB, Philadelphia
37. Abernethy DR, Schwartz JB (1999) Calcium-antagonist drugs. N Engl J Med 341:1447–1457
38. Thadani U (1999) Management of stable angina pectoris. Curr Opin Cardiol 14:349–358
39. Glossmann H, Ferry DR, Goll A, Striessnig J, Zernig G (1985) Calcium channels and calcium channel drugs: recent biochemical and biophysical findings. Arzneimittelforschung 35:1917–1935
40. Höltje H-D, Marrer S (1987) A molecular graphics study on structure-action relationships of calcium-antagonistic and agonistic 1,4-dihydropyridines. J Comput Aided Mol Des 1:23–30
41. Matowe WC, Akula M, Knaus EE, Wolowyk MW (1989) AK-2–38, a nifedipine analogue with potent smooth muscle calcium antagonist action and partial agonist effects on isolated guinea pig left atrium. Proc West Pharmacol Soc 32:305–307
42. Vo D, Nguyen JT, McEwen CA, Shan R, Knaus EE (2002) Syntheses, calcium channel agonist-antagonist modulation effects, and nitric oxide release studies of [3-(benzenesulfonyl)furoxan-4-yloxy]alkyl 1,4-dihydro-2,6-dimethyl-5-nitro-4-(2-trifluoromethylphenyl, benzofurazan-4-yl, 2-, 3-, or 4-pyridyl)-3-pyridinecarboxylates. Drug Dev Res 56:1–16
43. Vo D, Matowe WC, Ramesh M, Iqbal N, Wolowyk MW, Howlett SE, Knaus EE (1995) Syntheses, calcium channel agonist-antagonist modulation activities, and voltage-clamp studies of isopropyl 1, 4-dihydro-2,6-dimethyl-3-nitro-4-pyridinylpyridine-5-carboxylate racemates and enantiomers. J Med Chem 38:2851–2859
44. Vo D, Wolowyk MW, Knaus EE (1992) Synthesis and cardioselective beta-adrenergic antagonist activity of quinolyloxypropanolamines. Drug Des Discov 9:69–78
45. Coburn RA, Wierzba M, Suto MJ, Solo AJ, Triggle AM, Triggle DJ (1988) 1,4-Dihydropyridine antagonist activities at the calcium channel: a quantitative structure–activity relationship approach. J Med Chem 31:2103–2107
46. Safak C, Simsek R (2006) Fused 1,4-dihydropyridines as potential calcium modulatory compounds. Mini Rev Med Chem 6:747–755
47. Rose U, Drager M (1992) Synthesis, configuration, and calcium modulatory properties of enantiomerically pure 5-oxo-1, 4, 5, 6, 7, 8-hexahydroquinoline-3-carboxylates. J Med Chem 35:2238–2243
48. Miri R, Javidnia K, Sarkarzadeh H, Hemmateenejad B (2006) Synthesis, study of 3D structures, and pharmacological activities of lipophilic nitroimidazolyl-1,4-dihydropyridines as calcium channel antagonist. Bioorg Med Chem 14:4842–4849
49. Miri R, Niknahad H, Vazin A, Azarpira A, Shafiee A (2002) Synthesis and smooth muscle calcium channel antagonist effects of new derivatives of 1,4-dihydropyridine containing nitroimidzolyl substituent. DARU 10:130–136

50. Miri R, Niknahad H, Vesal G, Shafiee A (2002) Synthesis and calcium channel antagonist activities of 3-nitrooxyalkyl, 5-alkyl1,4-dihydro-2,6-dimethyl-4-(1-methyl-5-nitro-2-imidazolyl)-3,5-pyridinedicaboxylates. Farmaco 57:123–128
51. Shafiee A, Miri R, Dehpour AR, Solimani F (1996) Syntheses and calcium channel antagonist activity of nifedipine containing imidazolyl substitutent. Pharm Sci 2:541–543
52. Miri R, Javidnia K, Kebriaie-Zadeh A, Niknahad H, Shaygani N, Semnanian S, Shafiee A (2003) Synthesis and evaluation of pharmacological activities of 3,4-dialkyl1,4-dihydro-2,6-dimethyl- 4-nitroimidazole-3,5-pyridine dicarboxylates. Arch Pharm Pharm Med Chem 336:422–428
53. Miri R, Javidnia K, Mirkhani H, Hemmateenejad B, Sepeher Z, Zalpour M, Behzad T, Khoshneviszadeh M, Edraki N, Mehdipour AR (2007) Synthesis, QSAR and calcium channel modulator activity of new hexahydroquinoline derivatives containing nitroimidazole. Chem Biol Drug Des 70:329–336
54. Goldmann S, Stoltefuss J (1991) 1, 4-Dihydropyridines: effects of chirality and conformation on the calcium antagonist and agonist activities. Angew Chem Int Ed 30:1559–1578
55. Jauk B, Pernat T, Kappe CO (2000) Design and synthesis of a conformationally rigid mimic of the dihydropyrimidine calcium channel modulator SQ 32,926. Molecules 5:227–239
56. Atwal KS, Rovnyak GC, Schwartz J, Morelan S, Hedberg A, Gougoutas JZ, Malley MF, Floyd DM (1990) Dihydropyrimidine calcium channel blockers: 2-heterosubstituted 4-aryl-1,4-dihydro-6- methyl-5-pyrimidinecarboxylic acid esters as potent mimics of dihydropyridines. J Med Chem 33:1510–1515
57. Atwal KS, Rovnyak GC, Kimball SD, Floyd DM, Moreland S, Swanson BN, Gougoutas JZ, Schwartz J, Smillie KM, Malley MF (1990) Dihydropyrimidine calcium channel blockers. II. 3- Substituted-4-aryl-1, 4-dihydro-6-methyl-5-pyrimidinecarboxylic acid esters as potent mimics of dihydropyridines. J Med Chem 33:2629–2635
58. Atwal KS, Swanson BN, Unger SE, Floyd DM, Moreland S, Hedberg A, O'Reilly BC (1991) Dihydropyrimidine calcium channel blockers. 3. 3-carbamoyl-4-aryl-1,2,3,4-tetrahydro-6-methyl- 5-pyrimidinecarboxylic acid esters as orally effective antihypertensive agents. J Med Chem 34:806–811
59. Rovnyak GC, Atwal KS, Hedberg A, Kimball SD, Moreland S, Gougoutas JZ, O'Reilly BC, Schwartz J, Malley MF (1992) Dihydropyrimidine calcium channel blockers. 4. Basic 3-substituted-4-aryl-1, 4-dihydropyrimidine-5-carboxylic acid esters. Potent antihypertensive agents. J Med Chem 35:3254–3263
60. Gupta SP, Veerman A, Bagar P (2000) Quantitative structure–activity relationship studies on some series of calcium channel blockers. Mol Divers 8:357–363
61. Harrold M (2002) Angiotensin converting enzyme inhibitors, antagonist and calcium channel blockers. In: Lemke TL, Williams D (eds) Foye's principles of medicinal chemistry. Lippincott Williams & Wilkins, Baltimore, MD
62. Mohajeri A, Hemmateenejad B, Mehdipour A, Miri R (2008) Modeling calcium channel antagonistic activity of dihydropyridine derivatives using QTMS indices analyzed by GA-PLS and PC-GAPLS. J Mol Graph Model 26:1057–1065
63. Mojarrad JS, Miri R, Knaus EE (2004) Design and synthesis of methyl 2-methyl-7, 7-dihalo-5- phenyl-2-azabicyclo [4.1.0] hept-3-ene-4-carboxylates with calcium channel antagonist activity. Bioorg Med Chem 12:3215–3220
64. Dagnino L, Li-Kwong-Ken MC, Wolowyk MC, Wynn H, Triggle CR, Knaus EE (1986) Synthesis and calcium channel antagonist activity of dialkyl 1,4-dihydro-2,6-dimethyl-4-(pyridinyl)-3,5- pyridinedicarboxylates. J Med Chem 29:2524–2529
65. Hemmateenejad B, Miri R, Safarpour MA, Khoshneviszadeh M, Edraki N (2005) Conformational analysis of some new derivatives of 4-nitroimidazolyl-1,4-dihydropyridine-based calcium channel blockers. J Mol Struct Theochem 717:139–152
66. Mahmoudian M, Richards W (1986) A conformational distinction between dihydropyridine calcium agonists and antagonists. J Chem Soc Chem Commun 10:739–741

67. Handrock R, Herzig S (1996) Stereoselectivity of Ca^{2+} channel block by dihydropyridines: no modulation by the voltage protocol. Eur J Pharmacol 309:317–321
68. Rovnyak GC, Kimball SD, Beyer B, Cucinotta G, DiMarco JD, Gougoutas J, Hedberg A, Malley M, McCarthy JP (1995) Calcium entry blockers and activators: conformational and structural determinants of dihydropyrimidine calcium channel modulators. J Med Chem 38:119–129
69. Hemmateenejad B, Safarpour MA, Miri R, Taghavi F (2004) Application of *ab initio* theory to QSAR study of 1,4-dihydropyridine-based calcium channel blockers using GA-MLR and PC-GA-ANN procedures. J Comput Chem 25:1495–1503
70. Mahmoudian M, Richards WGA (1990) Quantum chemical study of structure–activity relationships of dihydropyridine calcium antagonists. J Sci Technol IR Iran 1:261–265
71. Gaudio AC, Korolkovas A, Takahata Y (1994) Quantitative structure–activity relationships for 1, 4 -dihydropyridine calcium channel antagonists (nifedipine analogues): a quantum chemical/classical approach. J Pharm Sci 83:1110–1115
72. Berntsson P, Wold S (1986) Comparison between X-ray crystallographic data and physicochemical parameters with respect to their information about the calcium channel antagonist activity of 4-phenyl-1,4-dihydropyridines. Quant Struct Act Relat 5:45–50
73. Hemmateenejad B, Miri R, Akhond M, Shamsipur M (2002) Quantitative structure–activity relationship study of recently synthesized 1, 4-dihydropyridine calcium channel antagonists. Application of the Hansch analysis method. Arch Pharm Weinheim 335:472–480
74. Gupta SP, Mathur AN, Nagappa AN, Kumar D, Kumaran S (2003) A quantitative structure–activity relationship study on a novel class of calcium entry blockers:1-[{4-(aminoalkoxy) phephenyl} sulphonyl] Indolizines. Eur J Med Chem 38:867–873
75. Miri R, Javidnia K, Hemmateenejad B, Tabarzad M, Jafarpour M (2009) Synthesis, evaluation of pharmacological activities and quantitative structure–activity relationship studies of a novel group of bis(4-nitroaryl-1,4-dihyropyridine). Chem Biol Drug Des 73:225–235
76. Hemmateenejad B, Miri R, Akhond M, Shamsipur M (2002) QSAR study of the calcium channel antagonist activity of some recently synthesized dihydropyridine derivatives. An application of genetic algorithm for variable selection in MLR and PLS methods. Chemometr Intell Lab Syst 64:91–99
77. Hemmateenejad B, Akhond M, Miri R, Shamsipur M (2003) Genetic algorithm applied to the selection of factors in principal component-artificial neural networks: application to QSAR study of calcium channel antagonist activity of 1,4-dihydropyridines (nifedipine analogous). J Chem Inf Comput Sci 43:1328–1334
78. Si HZ, Wang T, Zhang Ke Jun, De Hua Z, Fane Bo Tao (2006) QSAR study of 1, 4-dihydropyridine calcium channel antagonists based on gene expression programming. Bioorg Med Chem 14:4834–4841
79. Safarpour MA, Hemmateenejad B, Miri R, Jamali M (2004) Quantum chemical-QSAR study of some newly synthesized 1,4-dihydropyridine calcium channel blockers. QSAR Comb Sci 22:997–1005
80. Yao X, Liu H, Zhang R, Liu M, Hu Z (2005) QSAR and classification study of 1,4-dihydropyridine calcium channel antagonists based on least squares support vector machines. Mol Pharm 2:348–356
81. Costa MCA, Gaudio AC, Takahata Y (1997) A comparative study of principal component and linear multiple regression analysis in SAR and QSAR applied to 1,4-dihydropyridine calcium channel antagonists (nifedipine analogues). J Mol Struct Theochem 394:291–300
82. Schleifer KJ, Tot E (2002) CoMFA, CoMSIA and GRID/GOLPE studies on calcium entry blocking 1,4-dihydropyridines. Quant Struct Act Rel 21:239–248
83. Kawada T, Hsiao-Tung S, Nakazawa M, Imai S (2000) In vitro effects of the new calcium antagonist lacidipine. Jpn J Pharmacol 62:289–296
84. Van Amsterdam FTM, Roveri A, Maiorino M, Ratti E, Ursini F (1992) Lacidipine: a dihydropyridine calcium antagonist with antioxidant activity. Free Redic Biol Med 12:183–187

85. Lupo E, Locher R, Weisser B, Vetter W (1994) In vitro antioxidant activity of calcium antagonists against LDL oxidation compared with α-tocopherol. Biochem Biophys Res Commun 203:1803–1808
86. Berkels R, Breitenbach T, Bartels H, Taubert D, Roesenkranz A, Klaus W, Roesen R (2005) Different antioxidative potencies of dihydropyridine calcium channel modulators in various models. Vascul Pharmacol 42:145–152
87. Hockerman GH, Peterson BZ, Johnson BD, Catterall WA (1997) Molecular determinants of drug binding and action on L-type calcium channels. Annu Rev Pharmacol Toxicol 37:361–396
88. Manhold R, Steiner R, Hass W, Kaufman R (1978) Investigations on the structure–activity relationships of verapamil. Naunyn Schmiedebergs Arch Pharmacol 302:217–226
89. Triulzi MO, Mattioli R, Signorini G, Cirino D, Esposti D, Aguggini G, Maggi GC (1990) Effects of low-dose diltiazem on isovolumetric relaxation and contraction. G Ital Cardiol 20:1137–1143
90. Corelli F, Manetti F, Taft A, Campiani G, Nacci V, Botta M (1997) Diltiazem-like calcium entry blockers: a hypothesis of the receptor-binding site based on a comparative molecular field analysis model. J Med Chem 40:125–131
91. Campiani G, Garofalo A, Fiorini I, Botta M, Nacci V, Taft A, Chiarini A, Budriest R, Bruni G, Romeo MR (1995) Pyrrolo[2,1-c][1,4]benzothiazines: synthesis, structure–activity relationships, molecular modeling studies, and cardiovascular activity. J Med Chem 38:4393–4410
92. Kimball SD, Floyd DM, Das J, Hunt JT, Krapcho J, Rovnyak G, Duff KJ, Lee VG, Moquin RV, Turk CF, Hedberg SA, Moreland S, Brittain RJ, McMullen DM, Normandin DE, Cucinotta GG (1992) Benzazepinone calcium channel blockers. 4. Structure–activity overview and intracellular binding site. J Med Chem 35:780–793
93. Inoue H, Konda M, Hashiyama T, Otsuka H, Takahashi K, Gaino M, Date T, Aoe K, Takeda M, Murata S, Narita H, Nagao T (1991) Synthesis of halogen-substituted 1,5-benzothiazepine derivatives and their vasodilating and hypotensive activities. J Med Chem 34:675–687
94. Floyd DM, Kimball SD, Krapcho J, Das J, Turk CF, Moquin RV, Lago MW, Duff KJ, Lee VG, White RE, Ridgewell RE, Moreland S, Brittain RJ, Normandin DE, Hedberg SA, Cucinotta GG (1992) Benzazepinone calcium channel blockers. 2. Structure activity and drug metabolism studies leading to potent antihypertensive agents. Comparison with benzothiazepinones. J Med Chem 35:756–772
95. Das J, Floyd DM, Kimball SD, Duff KJ, Vu TC, Lago MW, Moquin RV, Lee VG, Gougoutas JZ, Malley MF, Moreland S, Brittain RJ, Hedberg SA, Cucinotta GG (1992) Benzazepinone calcium channel blockers. 3. Synthesis and structure–activity studies of 3-alkylbenzazepinones. J Med Chem 35:773–780
96. Clozel J, Ertel E, Ertel SJ (1997) Discovery and main pharmacological properties of mibefradil (Ro 40–5967), the first selective T-type calcium channel blocker. J Hypertens 15:S17–S25
97. Van der Vring J, Cleophas T, Van der Wall E, Niemeyer M (1999) T-channel-selective calcium channel blockade: a promising therapeutic possibility, only preliminarily tested so far: a review of published data. Am J Ther 6:229–233
98. Benardeau A, Ertel E (1997) Selective block of myocardial T-type calcium channels by mibefradil: A comparison with the 1,4- dihydropyridine amlodipine. Adis International Chester, UK
99. Ertel SI, Ertel EA, Clozel JP (1997) T-type Ca^{2+} channels and pharmacological blockade: potential pathophysiological relevance. Cardiovasc Drugs Ther 11:723–739
100. Kobrin I, Bieska G, Charlon V, Lindberg E, Pordy R (1998) Anti-anginal and anti-ischemic effects of mibefradil, a new T-typecCalcium channel antagonist. Cardiology 89:23–32
101. Asirvatham S, Sebastian C, Thadani U (1998) Choosing the most appropriate treatment for stable angina: safety considerations. Drug Saf 19:23–44

102. Jeong JA, Cho H, Yeon Jung S, Kang HB, Park JY, Kim J, Joon DJ, Lee JY (2010) 3D QSAR studies on 3,4-dihydroquinazolines as T-type calcium channel blocker by comparative molecular similarity indices analysis (CoMSIA). Bioorg Med Chem Lett 20:38–41
103. Seo HN, Choi JY, Choe YJ, Kim Y, Rhim H, Lee SH, Kim J, Joo DJ, Lee JY (2007) Discovery of potent T-type calcium channel blocker. Bioorg Med Chem Lett 17:5740–5743
104. Heo JH, Seo HN, Choe YJ, Kim S, Oh CR, Kim YD, Rhim H, Choo DJ, Kim J, Lee JY (2008) Synthesis and evaluation of α, α'-disubstituted phenylacetate derivatives for T-type calcium channel blockers. Bioorg Med Chem Lett 18:4424–4427
105. Park JH, Choi JK, Lee E, Lee JK, Rhim H, Seo SH, Kim Y, Doddareddy MR, Pae AN, Kang J, Roh EJ (2007) Lead discovery and optimization of T-type calcium channel blockers. Bioorg Med Chem 15:1409–1419
106. Doddareddy MR, Choo H, Cho YS, Rhim H, Koh HY, Lee J-H, Jeong S-W, Pae AN (2007) 3D pharmacophore based virtual screening of T-type calcium channel blockers. Bioorg Med Chem 15:1091–1105
107. Jo MN, Seo HJ, Kim Y, Seo SH, Rhim H, Cho YS, Cha JH, Koh HY, Choo H, Pae AN (2007) Novel T-type calcium channel blockers: dioxoquinazoline carboxamide derivatives. Bioorg Med Chem 15:365–373
108. Ku IW, Cho S, Doddareddy MR, Jang MS, Keum G, Lee JH, Chung BY, Kim Y, Rhim H, Kang SB (2006) Morpholin-2-one derivatives as novel selective T-type Ca^{2+} channel blockers. Bioorg Med Chem Lett 16:5244–5248
109. Papaioannou S, Panzer-Knodle S, Yang PC (1987) Calcium channel blockers: correlation among receptor binding, calcium uptake and contractility in vitro. J Pharmacol Exp Ther 241:91–96
110. Gupta SP (2006) QSAR studies on calcium channel blockers. In: Gupta SP (ed) QSAR and modeling studies in heterocyclic drugs II, 1st edn. Springer, Germany
111. Gaviraghi G (1989) Lacidipine, a new 1,4-dihydropyridine calcium channel antagonist possessing a potent and long lasting antihypertensive activity. Trends Med Chem 12:675–690
112. Kimball SD, Hunt JT, Barrish JC, Das J, Floyd DM, Lago MW, Lee VG, Spergel SH, Moreland S, Hedberg SA, Gougoutas JZ, Malley MF, Lau WF (1993) 1-Benzazepin-2-one calcium channel blockers-VI. Receptor-binding model and possible relationship to desmethoxyverapamil. Bioorg Med Chem 1:285–307

Therapeutic Potential of N-Type Voltage-Gated Ca^{2+} Channel

C. Gopi Mohan, Ashish Pandey, and Jignesh Mungalpara

Contents

Abstract Voltage-gated N-type Ca^{2+} channels (NCCs) play dominant roles in neuropathic pain and cerebral ischemia. Ion channel therapeutics for many pathophysiological conditions exists, which include: affective disorders, allergic disorders, autoimmune diseases, epilepsy, hypertension, insomnia, pain, anesthesia, anxiety, and stroke. Experimentally, it was well established that NCC inhibitory activity is essential for the treatment of chronic neuropathic pain and stroke. A major obstacle with these membrane proteins is that the atomic resolution experimental structures are not available to understand the mode of small molecule binding at its active sites. This article mainly focuses on Ca^{2+} channel blockers (CCBs), especially for NCCs, wherein lie some of the opportunities and advantages associated with these channels as drug target.

Keywords N-type voltage-gated Ca^{2+} channel • Ziconotide • Neuropathic pain • Stroke • Descriptor • QSAR

C.G. Mohan (✉)
Department of Pharmacoinformatics, National Institute of Pharmaceutical Education and Research, Sector 67, S.A.S. Nagar, Punjab 160 062, India
e-mail: cmohan@niper.ac.in; cgopimohan@yahoo.com

S.P. Gupta (ed.), *Ion Channels and Their Inhibitors*,
DOI 10.1007/978-3-642-19922-6_10,

Abbreviations

CCBs	Ca^{2+} channel blockers
DRG	Dorsal root ganglion
GFA	Genetic function approximation
LCC	L-type Ca^{2+} channel
NCC	N-type Ca^{2+} channel
P/QCC	P- and Q-type Ca^{2+} channel
QSAR	Quantitative structure-activity relationship
RCC	R-type Ca^{2+} channel
TCC	T-type Ca^{2+} channel
VGCCs	Voltage-gated Ca^{2+} channels

1 Introduction

N-type Ca^{2+} channels (NCCs) are associated with central and peripheral neurons, being located on the presynaptic nerve terminals. These channels regulate the Ca^{2+} flux subserving depolarization-evoked release of neurotransmitter from presynaptic endings. At the presynaptic nerve terminal, voltage-gated Ca^{2+} channels (VGCCs) open in response to action potentials to allow an influx of Ca^{2+} ions. The influx is a graded process varying in a linear manner with the frequency of action potentials. These in turn lead to release of various neurotransmitters that diffuse across the synaptic cleft to the postsynaptic membrane and binds to their specific receptors.

Neurotransmission in the central and peripheral nervous system is mainly controlled by NCCs. NCC was identified as promising and selective druggable target for the treatment of pain because it mediates the neurotransmission of pain signals in the spinal cord. It is also well known that NCCs play an important role in stroke disease in which modification in the intracellular Ca^{2+} signaling during neuronal ischemia could be inhibited by blocking NCC and thereby preventing neuronal death [1, 2]. Ligand-gated NCCs open or close in response to the binding of the ligand or small signaling molecule such as Prialt (synthetic version of omega-conotoxin-GVIA), an FDA-approved drug for chronic pain treatment. Prialt is a potent and selective NCC blocker. Some drugs are known to stabilize or destabilize the NCC open state. Ligand plugging at the ligand sensing residues of NCC will stabilize/destabilize its open state gating mechanism and therefore could play an important role in the ion channelopathies [3–16].

Neuronal VGCCs are integral multimeric protein complexes found in presynaptic membrane of neurons that mediate the selective passage of specific ions or molecules across a cell membrane. Free intracellular Ca^{2+} is the most common signal transduction element in cells [17]. An electrochemical gradient exists between an extracellular and intracellular (cytoplasmic) Ca^{2+} concentrations and further these enter the cytosol either through plasma membrane VGCCs or is released from the intracellular pools. These channels are important in a diverse range of physiological processes, including signal transmission in the nervous system, sensory perception,

and regulation of vital systems, such as circulation. Under normal physiological conditions, ion channels permit the orderly movement of ions across both plasma and intracellular cell membranes. A number of disease states as well as cell death also occur under pathologic conditions in which the disorderly movement of ions through these channels dominates. The aberrant elevation of intracellular Ca^{2+} levels through altered Ca^{2+} channel function is related to a variety of serious human pathophysiological conditions, including cardiovascular diseases, muscle disorders, acute or chronic pain, epilepsy, cerebellar ataxia, migraine, mood disorders, and certain types of cancer [18]. Nowycky et al. by studying the Ca^{2+} current in dorsal root ganglion (DRG) neurons gave the functional identification of NCC for the first time and its use in pain research. The drug toward blocking this target further took 20 years by the discovery of Priat by USA and Europe for the treatment of chronic pain [19].

NCC is located predominantly in neurons and is associated with a variety of neuronal responses, including neurodegeneration. Experimental autoimmune encephalomyelitis study in mice by Tokuhara et al. recently concluded the role of NCC in mice neurodegeneration [20]. This channel role in cardiovascular disease was also well known [21]. Neuropathic pain behavioral models in animal showed that NCC blockers when administered via spinal cord attenuates hyperalgesia and allodynia (pain due to stimulus) by mechanical, chemical, and thermal way of stimulation [22]. Further, this Ca^{2+} channel antagonist blockers are responsible for the hyperexcitability of dorsal horn neurons and behavioral peripheral nerve damage (hyperalgesia) seen in the animal models of inflammatory pain [23]. It was further established by Saegusa et al. that NCC was a key target for continuous (persistent) pain by studying three strains of α_{1B} gene knockout mice with elevated neural processes of encoding and noxious stimuli caused due to tissue or nerve injury [5].

Recent studies show that a ubiquitous form of G-protein modulation involves an inhibition of classical voltage-dependent regulation of mammalian Cav2.1 and Cav2.2 (NCC) channels [24]. VGCCs also affect the sensory neurons and many animals have these neurons activated preferentially by stimuli with the potential to cause tissue damage. In humans and other mammals, such sensory neurons are called nociceptors and generate signals interpreted by the central nervous system as pain. Thus, antagonist binding to NCC decreases the pain related neurotransmitters leading to the suppression of the signals causing neuropathic pain [1, 25]. Further, capsaicin-sensitive dorsal root ganglion (DRG) neurons express a unique Cav2.2 splicing form, raising the possibility of developing drugs that preferentially target NCCs in primary afferent neurons. On the contrary, it remains to be determined whether this splice variant is also expressed in human DRG neurons and whether the encoded α_{1B} subunit is localized at primary afferent neuron terminals, where they would regulate neurotransmission [26].

Furthermore, it is also possible to develop a use-dependent blocker that selectively regulates the DRG-specific NCCs. Success in that endeavor should produce an analgesic with an even better safety profile. An important concern, however, are those DRG neurons also express the more ubiquitous form of α_{1B} subunits, in addition to the specific variant. Which variant underlies synaptic transmission in the setting of persistent pain remains to be determined. In any case, a more general use-dependent blocker may be useful for alleviating pain as sympathetic postganglionic neurotransmission is predominantly mediated through NCCs [1, 2].

2 Overview of Neuronal Voltage-Gated Ca^{2+} Channels

Neuronal VGCCs are group of large multi-subunit ion channels with permeability to the ion Ca^{2+} in response to membrane potential changes due to excitation of neurons [27]. They constitute one of a group of superfamily of ion channels showing sequence, topological and functional similarity [28]. These ion channels are designated as voltage dependent in response to activation (open state) at depolarized or inactivation (close state) at polarized membrane potentials. Excited neuronal cells allow the entry of Ca^{2+} in response to membrane depolarization, resulting in muscular contraction, hormone and neuro-transmitter release, cellular motility, cellular growth and regulation, cellular damage and death and finally its survival.

VGCCs are well-studied membrane proteins and lot of information was available using electrophysiological, biochemical, pharmacological, and molecular biology techniques. Based on the pharmacological studies, further categorization of the channel family into L-, N-, P-, Q-, R-, and T- has been done. Also, in accordance with the electrophysiological nature, these channels are classified into two types: (a) high voltage-activated channels belonging to L-, N-, P-/Q-, and R-types, and require higher depolarization current to be activated; (b) low voltage-activated channel belonging to T-type which requires lower depolarization current to be activated. These ion channels differ in function, activation/inactivation voltage, conductance and sensitivity toward various drugs and toxins [29–31].

The biochemical and pharmacological significance of these five ion channels toward disease cause is also well known. (a) L-type Ca^{2+} channels (LCCs) have high activation threshold and have four subunit genes – $Ca_v1.1$, $Ca_v1.2$, $Ca_v1.3$, and $Ca_v1.4$ (α_{1C}, α_{1D}, α_{1S} and α_{1F}). These channels express in neurons, endocrine, skeletal muscle, and cardiovascular system, mainly responsible for cardiac disorders. Specific LCC blockers are discovered, which include different classes such as dihydropyridines, phenylalkylamines, and benzothiazepines. (b) P- and Q-type Ca^{2+} channels (P/Q CCs) have high activation threshold and have one subunit gene – $Ca_v2.1$ (α_{1A}). These channels mainly express in neurons, and was responsible for epilepsy and migraine symptoms. Specific P/QCC blockers are discovered, which include ω-agatoxin IVA, ω-conotoxin MVIIC and ω-conotoxin GVIA. (c) NCCs have high activation threshold and have one subunit gene – $Ca_v2.2$ (α_{1B}). These channels mainly express in neurons, and was responsible for pain symptoms. Specific NCC blockers are discovered, which include ω-conotoxin MVIIA, Prialt® and AM336. (d) R-type Ca^{2+} channels (RCCs) have high activation threshold and have one subunit gene – $Ca_v2.3$ (α_{1E}). These channels mainly express in neurons, and were responsible for diabetes symptoms. SNX-482 is a clinically validated specific RCC blocker. (e) T-type Ca^{2+} channels (TCCs) have low activation threshold and have three subunit genes – $Ca_v3.1$, $Ca_v3.2$, and $Ca_v3.3$ (α_{1G}, α_{1H}, and α_{1I}). These channels mainly expresses in neurons, smooth muscle and sinoatrial node, and were responsible for arrhythmias, epilepsy, and pain. Specific TCC blockers are discovered, which include nickel ethosuximide, zonisamide, mibefradil, and kurotoxin.

3 Structure and Mechanism of Action of N-Type Voltage-Gated Ca^{2+} Channels

Neuronal NCCs are complex protein machinery with several different distinct regulatory subunits composed of α_1, α_2-δ, β, and γ subunits. NCC is mainly encoded by Cav2.2 gene, the pore forming α_{1B} subunit and which in turn contains the ligand sensing residues. This subunit is essential for NCC functions, and which in turn control the channel properties. α_{1B} subunit is primarily expressed in the neuron of spinal cord, that is at the terminals of peptidergic primary afferent neurons and projecting to the superficial laminae of its dorsal horn [32].

The α_1 subunit pore with molecular mass of 190 kDa is the primary hydrophobic subunit gene necessary for channel functioning, and it incorporates the conduction pore, the voltage sensor and gating apparatus, with known sites of channel regulation by second messengers, drugs, and toxins [33]. This subunit is characterized by four homologous **I–IV** domains having six transmembrane helices (**S1–S6**) each. The voltage sensor of the channel lies at **S4** segment and each third and fourth amino acid of this segment contains positive arginine and lysine residue [34]. Transmembrane segments **S5** and **S6** in each domain have different pore loops, which controls its ion conductance and selectivity. In each pore loop due to the negatively charged residues such as glutamate is exquisitely Ca^{2+} selective. The channel pore called P-region is created by four glutamate residues located centrally in the Ca^{2+} channel of α_1 subunit gene. The movement of Ca^{2+} between pore and cell occurs, that is in the middle of the pore. Ca^{2+} is then shifted into the cell after binding of second Ca^{2+} in the pore region. The auxiliary subunits α_2-δ, β and γ subunit genes present in these ion channels modulate the properties of the NCC complex [35, 36] (Fig. 1).

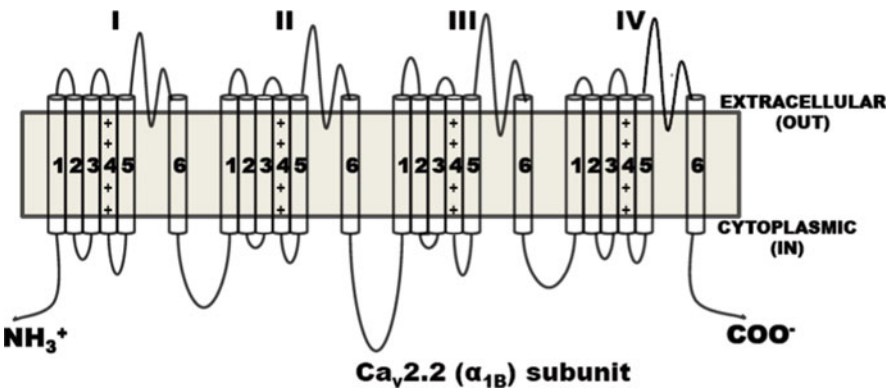

Fig. 1 Schematic representation of α_{1B} subunit of voltage-gated Ca^{2+} channels. The pore-forming α_{1B} subunit has four repeat domains (**I–IV**) connected by linker regions, each repeat domain has six transmembrane segments (**1–6**)

Inflammation and injury of a nerve will directly lead to the upregulation of the α_{1B} subunit. It was also well known that the toxins that block NCC affect the peptidergic primary afferent neuronal function by reducing the release of the glutamate and neuropeptides from its terminals [37]. The dorsal horn neuron stimulus activity was also controlled by this process and it was mainly affected with the injured nerve identified in the rat model system [38]. Recently, it was also established that α_{1B} subunit gene knockout mice showed various abnormalities in neurophysiological functions, such as locomotor activity, memory loss, and sensorimotor gating [39].

4 Review of Literature/Patent Survey on NCC Blockers

Selective NCC blockers could be used as therapeutic agent for the treatment of pain. Blockade of NCCs has recently been shown for the treatment of the chronic pain associated with cancer, AIDS, and neuropathy. Several drugs (or NCC blockers) are in different stages of drug discovery program, and is depicted in Table 1.

1. Ziconotide (also known as SNX111 or Prialt) an FDA approved drug is a potent and selective NCC blocker and is a synthetic version of ω-Conotoxin MVIIA derived from marine snail *Conus magus*. It was administered intrathecally and act as a novel nonopioid for the treatment of chronic pain [40]. This drug has demonstrated efficacy in animal models of traumatic brain injury, focal cerebral ischemia, and chronic pain [41, 42]. However, to minimize the adverse effect of this drug ,it was administered only via intrathecal route.
2. Morphine (also known as avinza, roxanol) is a potent narcotic pain reliever used to treat moderate to severe pain. It is found in opium plant and is produced early in its life cycle. It acts directly in the central nervous system for pain relief. However, morphine has a high potential for physiological dependence, addiction, and tolerance due to binding to opioid receptors. Adverse effects of this drug include respiratory depression, renal failure, and constipation [43].
3. Gabapentin (also known as neurontin) drug was developed for the treatment of epilepsy, but is now widely used to relieve neuropathic pain. This drug is a useful alternative in the treatment of a number of different neuropathic pain syndromes, including diabetic neuropathy, postherpetic neuralgia, trigeminal neuralgia and migraine. In vitro study showed that it binds to the NCC α_2-δ subunit for its down regulation [44, 45].
4. NMED160: The lead compound developed by Neuromed company hopes for the new generation of pain killers. NMED160 is in phase-II clinical trial, which directly blocks the NCC by decreasing the Ca^{2+} concentrations in the neuron and releasing the neurotransmitters from synaptic vesicles [46, 47].
5. ω-Conotoxin CVID (also known as AM336) is a 27 amino acid peptide isolated from the venom of Conus catus and is a selective NCC blocker with high

Table 1 Current status of N-type Ca^{2+} channel blockers

Drug/chemical structure	Use	Stage	Side effects
Ziconotide/Prialt™ H-Cys-Lys-Gly-Lys-Gly-Ala-Lys-Cys-Ser-Arg-Leu-Met-Tyr-Asp-Cys-Cys-Thr-Gly-Ser-Cys-Arg-Ser-Gly-Lys-Cys-NH_2	Neuropathic pain and cancer pain	Clinical	Hypotension, sedation, confusion, ataxia, and memory impairment
Morphine 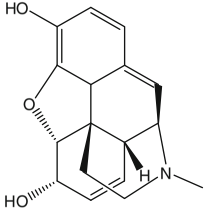	Chronic, neuropathic and inflammatory pain	Clinical	Constipation, narcotic and addictive effects, as well as the development of tolerance
Gabapentin (Neurontin) 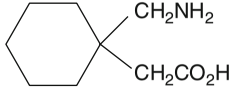	Neuropathic pain	Clinical	Hyperkinesia, dizziness, somnolence, and peripheral edema

(continued)

Table 1 (continued)

Drug/chemical structure	Use	Stage	Side effects
NMED160 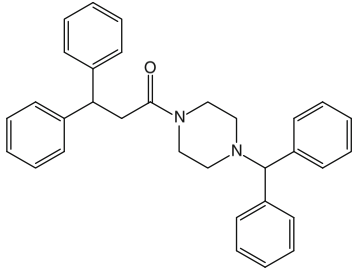	Chronic, neuropathic pain, Postherpetic neuralgia and diabetic neuropathy	Phase II	None identified
ω-Conotoxin CVID H-Cys-Lys-Ser-Lys-Gly-Ala-Lys-Cys-Ser-Lys-Leu-Met-Tyr-Asp-Cys-Cys-Ser-Gly-Ser-Cys-Gly-Thr-Val-Gly-Arg-Cys-NH_2	Neuropathic pain and chronic pain	Phase II	Unknown
ZC-88 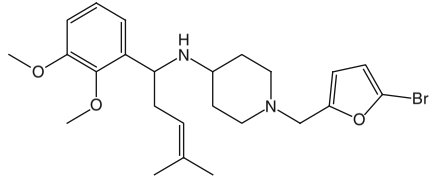	Neuropathic pain	Preclinical	Unknown

therapeutic index. Chronic pain associated with cancer disease could be effective by treating it intrathecally with this peptide [48, 49].

6. ZC-88: A novel nonpeptide NCC blocker is found to be very useful for the treatment of acute and neuropathic pain. Recently, Meng et al. have synthesized compound ZC88, which inhibited Ca^{2+} currents mediated by NCC with high potency and high selectivity. It blocked recombinant human NCC transiently expressed in HEK-293 cells with 0.45 ± 0.09 μM of IC_{50} value [50]. This compound had notable oral analgesia and antiallodynia for acute and neuropathic pain. It can be used alone or in combination with opioids because it enhanced morphine analgesia while preventing morphine-induced tolerance and physical dependence.

Pharmaceutical companies have patented many NCC blockers for the treatment of neuropathic pain and cerebral ischemia. Some of these NCC patent reports are depicted in Table 2 [1, 50]. Antihypertensive drug cilnidipine was reported by Takahara et al. group which is a 1,4-dihydropyridine derived long acting dual CCB, which inhibits both LCC and NCC [51]. Yamamoto et al. group has recently discovered novel series of 1,4-dihydro-pyridines and cyproheptadines as potent

Table 2 Some patent reports on selective N-type Ca^{2+} channel blockers

Compound	NCC activity	Patent no./year	Experimental assay/technique
Pfizer 2	0.048 μM	WO 07125398/2007	In vitro assay using HEK293 cells transfected with NCC. A patch clamp technique was used
Neuromed 1(NMED-160, MK-6721)	0.04 μM	WO 01045709/2001 WO 06105670/2006	
Neuromed 2	0.17 μM	WO 04089377/2004	
Neuromed 3	0.14 μM	WO 07071035/2007	
Neuromed 4	0.09 μM	WO 0804318/2008	
Neuromed 5	0.06 μM	WO 04089922/2004	
Neuromed 6	0.38 μM	WO 04105750/2004	
Neuromed 7	0.32 μM	WO 08031227/2008	
Neuromed 8	–	US 7507760/2009	
Formula I	>20 μM	WO/2010/014257	
Merck 1	Not available	WO 07084394/2007	Not available
Merck 2	Not available	WO 08066803/2008	
Merck 3	Not available	WO 07075524/2007	
Merck 4	Not available	WO 08133867/2008	
Euro-Celtique 1	0.13 μM	WO07110449/2007	In vitro assay using IMR32 human neuroblastoma cells
Euro-Celtique 2	0.39 μM	WO06040181/2006	
Euro-Celtique 3	0.10 μM	WO07118853/2007	
Euro-Celtique- Shionogi 1	0.19 μM	WO07118854/2007	
Euro-Celtique- Shionogi 2	0.080 μM	WO08008398/2008	
Euro-Celtique- Shionogi 3	0.210 μM	WO08150447/2008	
Purdue 1	0.46 μM	WO08124118/2008	
Euro-Celtique 4	0.34 μM	WO07085357/2007	
Euro-Celtique 5	0.23 μM	WO07028638/2007	

and selective NCC blockers [52]. This group also performed SAR study on 2-, 5-, and 6-position of 1,4-dihydropyridine derivatives to identify selective and an injectable NCC blockers with high aqueous solubility [53]. Structure–activity study of L-cysteine-based NCC blockers was carried out by Seko et al. and selectivity toward this channel over LCC was established [54].

Lars et al. also reported recently, synthesis and SAR of novel 2-arylthiazolidinones as selective NCC blockers [55]. Selective NCC blockers belonging to 4-amino-piperidine derivatives were analyzed by Zhang et al. for potent analgesic activity in animal models [56]. Tendori et al. have performed design, synthesis, and preliminary pharmacological evaluation of 4-aminopiperidine derivatives containing the structural motifs of verapamil and flunarizine as NCC blockers for the treatment of pain [57]. Gerald et al. performed flunarizine and lomerizine scaffold-based design and synthesis of potent NCC blockers, which showed good efficacy toward central nervous system in rat seizure model [58]. Structure–activity relationship study of diphenylpiperazine NCC inhibitors exhibiting both antiallodynic and antihyperalgesic activity was carried out by Hassan et al. for the treatment of neuropathic pain in the spinal nerve ligation model of rat [59] (Table 2).

5 Chemoinformatics Study on NCC Blockers

In silico techniques such as QSAR modeling, molecular docking, pharmacophore mapping, and virtual screening have proven their usefulness in pharmaceutical research for the selection/identification and/or design/optimization of new chemical entities. QSAR is one of the most important areas in chemoinformatics and its advances have widened the scope of rational drug design and the search for the mechanism of drug action. It is a well-established fact that the chemical and pharmacological effects of a compound are closely related to its physicochemical properties, which can be calculated by various methods from the molecular structure. Once a reliable QSAR model is created, it is possible to predict the activity of new molecules, and to learn, which structural factors play an important role in the modeled biological response. A reliable QSAR model can also identify and describe important structural features of the molecules that are relevant to variations in molecular activities. These models are useful because they rationalize a large number of experimental observations and allow for saving both time and money in the drug discovery process. In addition, in silico methods can expand screenings to molecules that do not exist physically in the chemical collections, therefore compensating for some of the most important limitations of the high-throughput methods. Several excellent case studies and review articles were published in this field of research [60–68]. Gupta et al. developed 2D-QSAR models for diverse classes of CCBs. These models have the ability to identify and describe important physicochemical features of the molecules that underpin variations in its molecular activity [69, 70].

The pharmacophoric features of NCC blockers are case specific and depend on the studied class of compounds. There exists structurally diverse class of NCC blockers having different scaffolds with no representative structural moiety, which includes (a) peptide and L-cysteine based moiety, (b) aryl heterocyclic moiety, (c) arylsulfonamide moiety, (d) benzhydryl moiety, (e) branched tert-butyl or isopropyl moiety, (f) piperazine and 4-aminopiperidine moiety, (g) 1,4-dihydropyridine moiety, (h) tetrahydro isoquinolines, and (i) cyproheptadine derivatives. The general observation of this diverse class of compounds showed commonly the lipophilic character and the presence of single basic nitrogen in the structure [1].

Over the past few decades, a variety of in silico models for NCC blockers have been developed by different research groups to improve selectivity and ADME/T properties. Recently, we have developed robust 2D-QSAR model to determine the biological activity of different scaffolds of 104 nonpeptidyl derivatives acting as NCC blockers. The NCC blocking potency (IC_{50}) values were measured under the same experimental conditions using a fluorescence-based Ca^{2+} flux assay in IMR32 human neuroblastoma cells [71].

2D-QSAR analysis was performed to explore the structure–activity relationship of different scaffolds of nonpeptidyl derivatives acting as NCC blockers. These blockers possess a variety of scaffolds (**A**, **B**, **C**, **D**, **E** and **F**), di-substituted with different R and X groups and is presented in Fig. 2.

Recently, genetic function algorithm (GFA) has gained great popularity in QSAR research. In this study, GFA method developed by Rogers and Hopfinger [72] was employed to select the relevant descriptors and to generate different QSAR models. Sensitivity analysis on QSAR models was then performed, and the best model developed can be used for predicting test set compounds that were not included in the training set compounds.

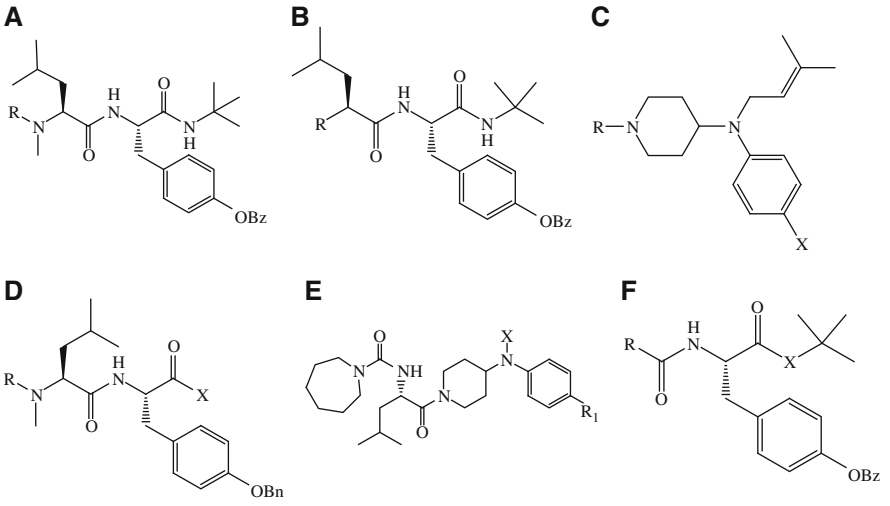

Fig. 2 Six different scaffolds (**A–F**) of N-type Ca^{2+} channel blockers (From [71]. With permission from Springer)

Three classes of descriptors: electrotopological, thermodynamic, and structural were considered for statistical fitting of NCC blockers using the GFA methodology, implemented in Cerius2 software [73]. The electrotopological descriptors are numerical values computed for each atom in a compound and which encode information about both topological environments of that atom and electronic interactions due to all other atoms in the compound. The topological relationship is based on the graph distance to each atom. The electronic aspect is based on intrinsic state and perturbation due to intrinsic state differences between atoms in the compound [74, 75]. Thermodynamic descriptor describes energy of compounds and their conversions. Selection of descriptors is based on their correlation with NCC blocking activity and capability of producing multiple linear regression models with moderate correlation coefficients. A statistically meaningful QSAR model was constructed by checking the variation of different statistical parameters against the number of descriptors. Details of the descriptors, QSAR equations, and analysis are available in our previously published work [71].

The QSAR model was created on a training set of 83 NCC blockers, and validated by a test set of 21 NCC blockers. The model was developed using Atype_C_24, Atype_N_68, Rotlbonds, S_sssN, and ADME_Solubility information-rich descriptors, which play an important role in determining NCC blocking activity. Among these, Atype_C_24, Rotlbonds, and S_sssN descriptors correlated positively with activity, while Atype_N_68 and ADME_Solubility descriptors correlated negatively with NCC blocking activity. These descriptors provided insight into the physicochemical requirements necessary for designing potent NCC blockers.

The robustness of the developed 2D-QSAR models obtained by GFA method was evaluated using a cross-validation strategy involving different techniques. This model was further validated using the leave-one-out cross-validation approach, Fischer statistics, Y-randomization test, and predictions based on the test data set [76, 77]. Y-randomization test confirms whether the model is obtained by chance correlation, and is a true structure–activity relationship to validate the adequacy of the training set compounds. The resulting descriptors produced by QSAR model were used to identify physicochemical features relevant to NCC blocking activity. The predictive properties of the developed model were more rigorously tested by predicting the NCC blocking potency of external test set of 21 compounds, details available elsewhere [71].

2D-QSAR model is statistically significant and explains more than 95% of the variance in the actual (experimental) activity with good predictive power [71]. The structural and electrotopological index descriptors were found to play a major role in determining NCC blocking activity. The atom-type descriptors and rotational bond highlight the significance of spatial aspects in designing these blockers. The influence of electrotopological descriptor S_sssN was promising, and showed that the tertiary nitrogen with its linear aliphatic amine contributions must be taken into account when designing new inhibitors against this channel [71]. Analysis of atom-wise contributions to hydrophobicity will probably help to appropriately take into account those atom types that are essential for determining NCC blocking activity.

Type, definition, and meaning of these five descriptors are described below along with their importance in understanding the NCC blocking activity.

(a) Rotlbonds is a structural descriptor and indicates number of rotational bonds in a compound. The molecular activity and the number of rotatable bonds in the studied compounds can be broadly correlated, and this descriptor showed positive correlation with NCC blocking activity in QSAR model. On the basis of number of rotatable bonds, the "Opera" rule needs to be specified, which in turn contribute to the structural flexibility of the compound required for attaining bioactive conformation for drug-like compounds [78]. (b) Thermodynamic descriptor, Atype_C_24 is one of the atom types AlogP descriptor that appeared in QSAR model. In this descriptor, the C atom in the compound is linked in R– –CR– –R manner, where R represents any group linked through carbon and "– –" represents aromatic bonds as in benzene or delocalized bonds like the N–O bond of a nitro group [79, 80]. Atype descriptors are thermodynamic descriptors defining the presence of that type of atom in the compound. Various atom type AlogP descriptors can be used to calculate the logP of compounds. In this strategy, halogens and hydrogen are classified according to the hybridization and oxidation state of the carbon to which they are bonded; carbon atoms are classified by their hybridization state and the chemical nature of their neighboring atoms. In other words, the aromaticity associated with the C atom as part of the aromatic ring is favorable for NCC blocking activity. Thus, the positive slope of the Atype_C_24 descriptor in QSAR model revealed that NCC blocking activity increases with an increase in hydrophobicity associated with this carbon. (c) Another thermodynamic descriptor S_sssN also appeared in NCC QSAR model, and is defined as the summation of the electrotopological indices for all the N atoms present in a compound that is connected by three single bonds except hydrogen. Zhihua et al. [74] showed that for peptide analogues electrotopological descriptors have both excellent structural selectivity and activity estimation. The numerical values of electrotopological descriptors computed for each atom in a compound encode information about both the topological environment of that atom and electronic interactions due to all other atoms in the compound. The topological relationship is based on the graph distance to each atom. The electronic aspect is based on the intrinsic state and perturbation due to the intrinsic state differences between atoms in the compound [74, 75]. The developed NCC QSAR model revealed a positive correlation with the descriptor S_sssN, suggesting that the nature of the electronic environment in this compound is necessary for potent NCC blocking activity.

The other two descriptors ADME_Solubility and Atype_N_68 selected by QSAR model exhibited a negative correlation with the NCC blocking activity, as discussed in detail below. (d) ADME_Solubility belongs to the ADME set of descriptors, and is defined as the base 10 logarithm of the molar solubility of each compound in water, predicted by linear regression methodology [81]. The presence of this descriptor in QSAR model was correlated with a negative contribution toward NCC blocking activity. (e) Atype_N_68 descriptor is of atom-type and is defined as N present in an Al_3N context in the compound. Al represents aliphatic groups and the N atom linked with the three aliphatic groups in the compound (tertiary nature). The negative slope of this descriptor in QSAR model revealed that NCC blocking activity decreases with an increase in hydrophobicity associated with this nitrogen [71].

The most potent compounds are present in the scaffold D group (**D1** and **D2**), shown in Fig. 3. The contribution of the electronic environment of the descriptor S_sssN in these two compounds has similar chemical features, as reflected in its R– and X– substitutions. The presence of this descriptor is very important for the potent activity of these compounds, which was further confirmed by the positive slope in QSAR model [71]. Further, the functional groups attached at the R region in compounds **D1** and **D2** have aromatic features, and do not completely follow the nature of the chemical environment of the Atype_N_68 descriptor. In other words, compound **D1** has aliphatic amine groups, which are secondary in nature and do not strictly follow the Al_3N manner. In support of this observation, this descriptor also showed a negative slope in QSAR model [71].

The scaffold D group also has the least potent compound **D3** shown in Fig. 3 with an IC_{50} value of 13 μM, which is 1,000-fold less potent than compound **D1**. The presence of an Atype_N_68 descriptor type chemical feature might be the key point determining the low activity of compound **D3**. In compound **D3**, the R-Me group substitution is strictly in accordance with the chemical nature of the Atype_N_68 descriptor. This compound also has two other substitutions with the same chemical features in the X-region, favoring lower activity [71, 82].

We also analyzed the contribution of different descriptor values in QSAR model for S_sssN and Atype_N_68 descriptors, w.r.t the most potent compounds **D1** and **D2** as well as that of the least potent compound **D3**. These values were used mainly for the development of QSAR model and are very significant in distinguishing between potent and less potent NCC blockers. The details of these analyses are reported earlier [71].

2D-QSAR modeling can help in determining which parts of a compound can be modified to increase affinity and efficacy, providing valuable guidance in the drug

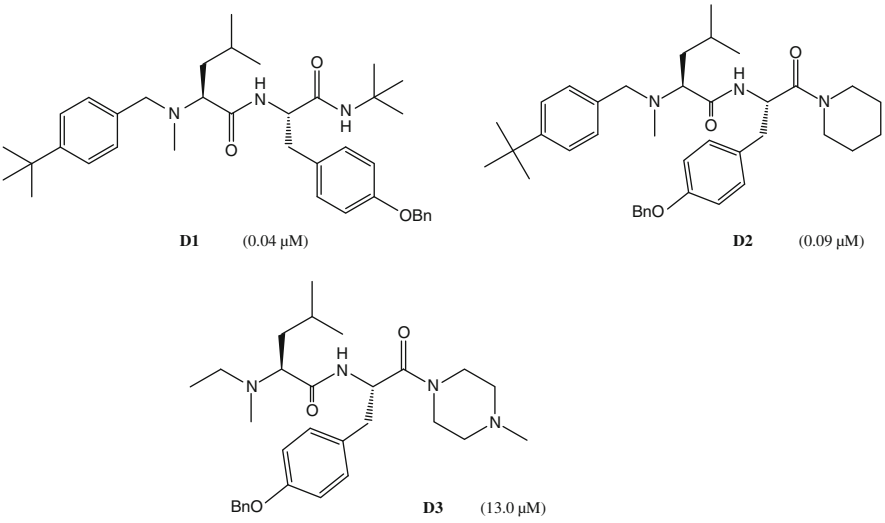

Fig. 3 Chemical structure of the two most potent N-type Ca^{2+} channel blockers **D1** and **D2**, and least potent blocker **D3** (From [82]. With permission from Elsevier)

discovery process [69–72, 83, 84]. These models are useful because they rationalize a large number of experimental observations, and allow saving of both time and money in the drug design process, and represent a step forward in the in silico identification of potent NCC blockers.

The lessons learned from the QSAR analysis is that mapping the chemical space of known NCC blockers has shed some light on the structural aspects of ligands consistent with the channel blocker profile. Also, we have noticed that large number of diverse class of NCC blockers have high flexible linkers and connect various molecular fragments. Due to the high flexibility of the NCC blockers, the bioactive conformation adopted seems to be compatible with the large binding pore region in the channel. Thus, blocker rigidification seems to be a proper solution for overcoming the channel complexity.

Also, much information exists for blockers of NCC with different structural diversity. The ongoing medicinal chemistry optimization program to synthesize potent leads has direct impact on this information. The computational model based on literature data therefore provides a potentially valuable tool for discovery chemistry as future compounds may be synthesized that are potent NCC blockers. The scope of our 2D-QSAR model [71] is interesting in light of the complexity of the NCC states. Possibilities for additional physicochemical features not covered by our QSAR models are entirely plausible given the complexity of the NCC, its state-dependent conformational changes, and its interactions with the membrane and other proteins. Furthermore, factors such as membrane permeation required for accessing the intracellular lumen of the NCC and possible shifts in local p*K*a due to changes in membrane potential further complicate the problem of predicting NCC inhibitory activity. The ability to locate and describe these alternative NCC active sites is likely to come from a concerted effort of in vitro, in vivo, and in silico experiments such as site-directed mutagenesis, radioligand competition assays, theoretical channel modeling, and ultimately membrane structural biology.

The present results can be used to flag commercial libraries overly enriched with predicted NCC platform-specific channel blockers. In addition to this the in vitro and in vivo models are very labor-intensive, expensive, and not widely available. Nevertheless, it is hoped that our 2D-QSAR model can be used as a preliminary guidance for explaining NCC liabilities in early lead candidates as well as for designing out properties that promote NCC blocking in such compounds [71].

6 Need for NCC Blockers

Pain is an unpleasant sensory and emotional experience associated with actual or potential tissue damage. Depending on the etiology and pathophysiology, it is categorized as acute pain and chronic pain. Acute pain is self-limiting and serves as protective biological function by acting as a warning of on-going tissue damage, while chronic pain is itself a disease process. Although acute pain may occur with cancer and neurological diseases. Neuropathic pain is a common type of chronic

nonmalignant pain and remains a clinical challenge for treatment. Pharmacotherapy is the mainstay for treating neuropathic pain. The numerous analgesic compounds currently available are largely ineffective for chronic nerve pain and can control many short-term aches and pains. Even the most potent painkillers available, known as narcotics or opioids, cannot adequately treat some people's lasting pain. Medications from several different drug classes are used to treat neuropathic pain, including topical agents, tricyclic antidepressants, anticonvulsants, and nonopioid analgesics. Anticonvulsant drugs for epilepsy sometime are used to reduce the pain by decreasing the nerve cell excitability, but have serious side effects such as lethargy, fatigue, clouding of mental state and weight gain [85–87].

The treatment of chronic and neuropathic pain remains an area of utmost priority. NCC has long been recognized as suitable targets for pain management. Strategies for direct inhibition of NCC by peptide toxins and small organic blockers have been realized only recently. Moreover, potential ways to target specifically and selectively the NCC are not fully exploited. One of the main reasons could be due to the nonavailability of the experimental structure of NCC [1].

The most selective inhibitors of NCC known to date do not cross the blood–brain barrier. So synthetically feasible small drug-like compounds, which can selectively inhibit NCC was essential for the treatment of pain in different diseases. Further, to be maximally useful in treatment, it is also helpful to assess the side reactions (adverse drug action), which might occur. Thus, in addition of being able to modulate a particular Ca^{2+} channel, it is desirable that the compound has very low activity with respect to the hERG K^+ channel inhibition. Compounds that block this channel with high potency may cause cardiotoxicity, which are fatal [63]. Similarly, it would be undesirable for the compound to inhibit Cytochrome P450 enzymes, since these enzymes are required for drug detoxification. Finally, the compound will be evaluated for Ca^{2+} ion channel-type specificity by comparing its activity among various other types of Ca^{2+} channels, as described earlier, and specificity for one particular channel type is preferred. The compounds which progress through these ADME/T tests successfully are then examined in animal models as actual drug candidates [88, 89].

7 Conclusions and Future Prospective

The voltage-dependent NCCs act as an important target in the pain pathway. Several NCC blocking small-molecule compounds and their clinical as well as preclinical efficacies have been tested and reported. Inhibitory activity of all currently remerging small molecule NCC blockers is mostly within the submicromolar to micromolar range, which are not comparable to those of peptide drugs. It still remains to be determined whether the inhibitory activity of these organic blockers can lead to an efficacious clinical potential similar to ziconotide, and how their unique selectivity/specificity over other type of channel improves the ADME/T profile and efficacy in human.

References

1. Yamamoto T, Takahara A (2009) Recent updates of N-type calcium channel blockers with therapeutic potential for neuropathic pain and stroke. Curr Top Med Chem 9:377–395
2. McGivern JG (2006) Targeting N-type and T-type calcium channels for the treatment of pain. Drug Discov Today 11:245–253
3. Hirning LD, Fox AP, McCleskey EW et al (1988) Dominant role of N-type Ca^{2+} channels in evoked release of norepinephrine from sympathetic neurons. Science 239:57–61
4. Saegusa H, Kurihara T, Zong S et al (2001) Suppression of inflammatory and neuropathic pain symptoms in mice lacking the N-type Ca^{2+} channel. EMBO J 20:2349–2356
5. Saegusa H, Matsuda Y, Tanabe T (2002) Effects of ablation of N- and R-type Ca^{2+} channels on pain transmission. Neurosci Res 43:1–7
6. Snutch TP (2005) Targeting chronic and neuropathic pain: the N-type calcium channel comes of age. NeuroRx 2:662–670
7. Wermeling DP, Berger JR (2006) Ziconotide infusion for severe chronic pain: case series of patients with neuropathic pain. Pharmacotherapy 26:395–402
8. Feng ZP, Hamid J, Doering C et al (2001) Residue Gly1326 of the N-type calcium channel α_{1B} subunit controls reversibility of ω-conotoxin GVIA and MVIIA block. J Biol Chem 276:15728–15735
9. Ellinor PT, Zhang JF, Horne WA et al (1994) Structural determinants of the blockade of N-type calcium channels by a peptide neurotoxin. Nature 372:272–275
10. Liang H, Elmslie KS (2002) Rapid and reversible block of N-type calcium channels (CaV 2.2) by ω-conotoxin GVIA in the absence of divalent cations. J Neurosci 22:8884–8890
11. Yarotskyy V, Elmslie KS (2009) ω-Conotoxin GVIA alters gating charge movement of N-type (CaV2.2) calcium channels. J Neurophysiol 101:332–340
12. Buraei Z, Anghelescu M, Elmslie KS (2005) Slowed N-type calcium channel (CaV2.2) deactivation by the cyclin-dependent kinase inhibitor roscovitine. Biophys J 89:1681–1691
13. Buraei Z, Elmslie KS (2008) The separation of antagonist from agonist effects of trisubstituted purines on CaV2.2 (N-type) channels. J Neurochem 105:1450–1461
14. Buraei Z, Schofield G, Elmslie KS (2007) Roscovitine differentially affects CaV2 and Kv channels by binding to the open state. Neuropharmacology 52:883–894
15. DeStefino NR, Pilato AA, Dittrich M et al (2010) (R)-Roscovitine prolongs the mean open time of unitary N-type calcium channel currents. Neuroscience 167:838–849
16. Yarotskyy V, Elmslie KS (2007) Roscovitine a cyclin-dependent kinase inhibitor, affects several gating mechanisms to inhibit cardiac L-type (Ca(V)1.2) calcium channels. Br J Pharmacol 152:386–395
17. Carafoli E, Santella L, Branca D et al (2001) Generation, control, and processing of cellular calcium signals. Crit Rev Biochem Mol Biol 36:107–260
18. Snutch TP, Larry RS (2009) Voltage-gated calcium channels, Encyclopedia of neuroscience. Oxford Academic Press, Oxford, pp 427–441
19. Nowycky MC, Fox AP, Tsien RW (1985) Three types of neuronal calcium channel with different calcium agonist sensitivity. Nature 316:440–443
20. Tokuhara N, Namiki K, Uesugi M et al (2010) N-type calcium channel in the pathogenesis of experimental autoimmune encephalomyelitis. J Biol Chem 285(43):33294–33306
21. Petrashevskaya NN, Ishii M, D'Souza K et al (2011) Presynaptic stimulus-release and postsynaptic compensatory changes in mice lacking the N-type calcium channel α_{1B}-subunit. Auton Neurosci 160(1–2):9–15
22. Yaksh TL (2006) Calcium channels as therapeutic targets in neuropathic pain. J Pain 7:S13–S30
23. Vanegas H, Schaible H (2000) Effects of antagonists to high-threshold calcium channels upon spinal mechanisms of pain, hyperalgesia and allodynia. Pain 85:9–18

24. Huang X, Senatore A, Dawson TF et al (2010) G-proteins modulate invertebrate synaptic calcium channel (LCa(v)2) differently from the classical voltage-dependent regulation of mammalian Ca(v)2.1 and Ca(v)2.2 channels. J Exp Biol 15:2094–2103
25. Goodman MB (2003) Sensation is painless. Trends Neurosci 26:643–645
26. Bell TJ, Thaler C, Castiglioni AJ et al (2004) Cell specific alternative splicing increases calcium channel current density in the pain pathway. Neuron 41:127–138
27. Van PF, Minor DL (2006) The structural biology of voltage-gated calcium channel function and regulation. Biochem Soc Trans 34:887–893
28. Catterall WA, Striessnig J, Snutch TP et al (2003) International Union of Pharmacology XL. Compendium of voltage-gated ion channels: calcium channels. Pharmacol Rev 55:579–581
29. Catterall WA (2000) Structure and regulation of Voltage-gated Ca^{2+} channels. Annu Rev Cell Dev Biol 16:521–555
30. Ertel EA, Campbell KP, Harpold MM et al (2000) Nomenclature of voltage-gated calcium channels. Neuron 25:533–535
31. Catterall WA, Perez-Reyes E, Snutch TP et al (2005) International union of pharmacology XLVIII. Nomenclature and structure-function relationships of voltage-gated calcium channels. Pharmacol Rev 57:411–425
32. Cao Yu-Qing (2006) Voltage-gated calcium channels and pain. Pain 126:5–9
33. Moosmang S, Lenhardt P, Haider N et al (2005) Mouse models to study L-type calcium channel function. Pharmacol Ther 106:347–355
34. Dolphin AC (2006) A short history of voltage-gated calcium channels. Br J Pharmacol 147: S56–S62
35. Chen YH, Li MH, Zhang Y et al (2004) Structural basis of the α_1-β subunit interaction of voltage-gated Ca^{2+} channels. Nature 429:675–680
36. Lin-ling H, Yun Z, Yu-hang C et al (2007) Functional modularity of the *β*-subunit of voltage-gated Ca^{2+} channels. Biophys J 93:834–845
37. McGivern JG, McDonough SI (2004) Voltage-gated calcium channels as targets for the treatment of chronic pain. Curr Drug Targets CNS Neurol Disord 3:457–478
38. Matthews EA, Dickenson AH (2001) Effects of spinally delivered N- and P-type voltage-dependent calcium channel antagonists on dorsal horn neuronal responses in a rat model of neuropathy. Pain 92:235–246
39. Takahashi E, Tan-No K, Tadano T (2010) Behavioral and neurochemical characterization of mice deficient in the N-type Ca^{2+} channel α_{1B} subunit. Behav Brain Res 208:224–230
40. Bowersox SS, Luther R (1998) Pharmacotherapeutic potential of omega-conotoxin MVIIA (SNX-111), an N-type neuronal calcium channel blocker found in the venom of Conus magus. Toxicon 36:1651–1658
41. Bowersox SS, Gadbois T, Singh T et al (1996) Selective N-type neuronal voltage-sensitive calcium channel blocker, SNX-111, produces spinal anti-nociception in rat models of acute, persistent and neuropathic pain. J Pharmacol Exp Ther 279:1243–1249
42. Schmidtko A, Lötsch J, Freynhagen R et al (2010) Ziconotide for treatment of severe chronic pain. Lancet 375:1569–1577
43. Scott DA, Wright CE, Angus JA (2002) Actions of intrathecal omega-conotoxins CVID, GVIA, MVIIA, and morphine in acute and neuropathic pain in the rat. Eur J Pharmacol 451:279–286
44. Vega-Hernández A, Felix R (2002) Down-regulation of N-type voltage-activated Ca^{2+} channels by gabapentin. Cell Mol Neurobiol 22:185–190
45. Field MJ, Hughes J, Singh L (2000) Further evidence for the role of the $\alpha_2\delta$ subunit of voltage dependent calcium channels in models of neuropathic pain. Br J Pharmacol 131:282–286
46. Snutch TP (2001) Substituted piperazine and piperidine calcium channel blockers. WO 01045709
47. Snutch TP (2006) Composition comprising a combination of a nonpeptidyl N-type calcium channel blocker and a second compound e.g. opioid-useful for ameliorating pain. WO 06105670

48. Smith MT, Cabot PJ, Ross FB et al (2002) The novel N-type calcium channel blocker, AM336, produces potent dose-dependent antinociception after intrathecal dosing in rats and inhibits substance P release in rat spinal cord slices. Pain 96:119–127
49. Meng GE, Ning WU, Zhang C et al (2008) Analgesic activity of ZC88, a novel N-type voltage-dependent calcium channel blocker, and its modulation of morphine analgesia, tolerance and dependence. Eur J Pharmacol 586:130–138
50. http://www.scirus.com
51. Takahara A, Fujita S, Moki K et al (2003) Neuronal Ca^{2+} channel blocking action of an antihypertensive drug, cilnidipine, IMR-32 human neuroblastoma cells. Hypertens Res 26:743–747
52. Yamamoto T, Niwa S, Iwayama S et al (2006) Discovery, structure–activity relationship study, and oral analgesic efficacy of cyproheptadine derivatives possessing N-type calcium channel inhibitory activity. Bioorg Med Chem 14:5333–5339
53. Yamamoto T, Niwa S, Ohno S et al (2008) The structure–activity relationship study on 2-, 5-and 6-position of the water soluble 1, 4-dihydropyridine derivatives blocking N-type calcium channels. Bioorg Med Chem Lett 18:4813–4816
54. Seko T, Kato M, Kohno H (2002) Structure–activity study of L-cysteine-based N-type calcium channel blockers: optimization of N- and C-terminal substituents. Bioorg Med Chem Lett 12:915–918
55. Knutsen LJS, Hobbs CJ, Earnshaw CG et al (2007) Synthesis and SAR of novel 2-aryl thiazolidinones as selective analgesic N-type calcium channel blockers. Bioorg Med Chem Lett 17:662–667
56. Zhang S, Su R, Zhang C et al (2008) C101 a novel 4-amino-piperidine derivative selectively blocks N-type calcium channels. Eur J Pharmacol 587:42–47
57. Teodori E, Baldi E, Dei S et al (2004) Design, synthesis, and preliminary pharmacological evaluation of 4- aminopiperidine derivatives as N-type calcium channel blockers active on pain and neuropathic pain. J Med Chem 47:6070–6081
58. Gerald WZ, Zhong-Ping F, Lingyun Z et al (2009) Scaffold-based design and synthesis of potent N-type calcium channel blockers. Bioorg Med Chem Lett 19:6467–6472
59. Hassan P, Zhong-Ping F, Yanbing D et al (2010) Structure–activity relationships of diphenyl-piperazine N-type calcium channel inhibitors. Bioorg Med Chem Lett 20:1378–1383
60. Hansch C, Hoekman D, Leo A et al (2002) Chem-Bioinformatics: Comparative QSAR at the interface between chemistry and biology. Chem Rev 102:783–812
61. Verma RP, Hansch C (2006) Cytotoxicity of organic compounds against ovarian cancer cells: A quantitative structure-activity relationship study. Mol Pharm 3:441–450
62. Hansch C, Verma RP (2008) Understanding tubulin/microtubule-taxane interactions: a quantitative structure–activity relationship study. Mol Pharm 5:151–161
63. Garg D, Gandhi T, Mohan CG (2008) Exploring QSTR and toxicophore of hERG K^+ channel blockers using GFA and HypoGen techniques. J Mol Graph Model 26:966–976
64. Awale M, Mohan CG (2008) Molecular docking guided 3D-QSAR CoMFA analysis of N-4-pyrimidinyl-1H-indazol-4-amine Inhibitors of Leukocyte-specific protein tyrosine kinase. J Mol Model 14:937–947
65. Gupta SP (2007) Quantitative structure-activity relationship studies on zinc-containing metalloproteinase inhibitors. Chem Rev 107:3042–3087
66. Alvesalo JK, Siiskonen A, Vainio MJ et al (2006) Similarity based virtual screening: a tool for targeted library design. J Med Chem 7:2353–2356
67. Burger A, Abraham DJ (2003) Burger's medicinal chemistry and drug discovery. Wiley, New York
68. McInnes C (2007) Virtual screening strategies in drug discovery. Curr Opin Chem Biol 11:494–502
69. Gupta SP (2006) QSAR studies on calcium channel blockers. In: Gupta RR (Series Editor), Gupta SP (Volume Editor) Topics in heterocyclic chemistry, vol 4; QSAR and molecular modeling studies in heterocyclic drugs II. Springer, Berlin

70. Saini L, Gupta SP, Kumar Satluri VS (2009) A QSAR study on some series of sodium and potassium channel blockers. Med Chem 5:570–576
71. Mungalpara J, Pandey A, Jain V et al (2010) Molecular modeling and QSAR analysis on some structurally diverse N-type calcium channel blockers. J Mol Model 16:629–644 (references cited therein)
72. Rogers D, Hopfinger AJ (1994) Application of genetic function approximation to quantitative structure–activity relationships and quantitative structure-property relationships. J Chem Inf Comput Sci 34:854–866
73. Cerius2, Version 4.10 (2005) San Diego, CA
74. Zhihua L, Yuzhang W, Xuejun Q et al (2002) Use of a novel electrotopological descriptor for the prediction of biological activity of peptide analogues. Int J Pept Res Ther 9:273–281
75. Hall LH, Kier LB (1995) Electrotopological state indices for atom types: a novel combination of electronic, topological, and valence state information. J Chem Inf Comput Sci 35:1039–1045
76. Rucker C, Rucker G, Meringer M (2007) y-Randomization and its variants in QSPR/QSAR. J Chem Inf Model 47:2345–2357
77. Golbraikh A, Shen M, Xiao Z et al (2003) Rational selection of training and test sets for the development of validated QSAR models. J Comput Aid Mol Des 17:241–253
78. Oprea TI, Allu TK, Fara DC (2007) Lead-like, drug-like or "Pub-like": how different are they? J Comput Aid Mol Des 21:113–119
79. Ghose AK, Crippen GM (1987) Atomic physicochemical parameters for three-dimensional-structure-directed quantitative structure-activity relationships. 2. Modeling dispersive and hydrophobic interactions. J Chem Inf Comput Sci 27:21–35
80. Viswanadhan VN, Ghose AK, Reyankar GR et al (1989) Atomic physico-chemical parameters for three-dimensional-structure directed quantitative structure-activity relationships. 2. Modeling dispersive and hydrophobic interactions. J Chem Inf Comput Sci 29:163–172
81. Cheng A, Merz K Jr (2003) Prediction of aqueous solubility of a diverse set of compounds using quantitative structure–property relationships. J Med Chem 46:3572–3580
82. Ryder RT, Hu LY, Rafferty MF et al (1999) Multiple parallel synthesis of N, N dialkyl dipeptidylamines as N-type calcium channel blockers. Bioorg Med Chem Lett 9:1813–1818
83. Verma RP, Hansch C (2009) Camptothecins: a SAR/QSAR study. Chem Rev 109:213–235
84. Hajjo R, Grulke CM, Golbraikh A et al (2010) Development, validation, and use of quantitative structure-activity relationship models of 5-hydroxytryptamine (2B) receptor ligands to identify novel receptor binders and putative valvulopathic compounds among common drugs. J Med Chem 53(21):7573–7586
85. Diana CC, Jean-François D (2010) Grand challenge for ion channels: an underexploited resource for therapeutics. Front Pharmacol. doi:10.3389/fphar.2010.00113
86. Barrow JC, Duffy JL (2010) Voltage-gated calcium channel antagonists for the central nervous system. Annu Rep Med Chem 45:2–18
87. Elena C, Simona F, Laura F et al (2010) Ion channel blockers for the treatment of neuropathic pain. Future Med Chem 2:803–842
88. Adelina MV, Thomas GO, Paul TA (2010) Toward a comprehensive molecular design framework for reduced hazard. Chem Rev 110:5845–5882
89. Mohan CG, Tamanna G, Divita G et al (2007) Computer assisted methods in chemical toxicity prediction. Mini Rev Med Chem 7:499–507

Chloride Ion Channels: Structure, Functions, and Blockers

Satya P. Gupta and Preet K. Kaur

Contents

Abstract Chloride ion channels have been found to play crucial roles in the development of human diseases, for example, mutations in the genes encoding Cl^- channels lead to a variety of deleterious diseases in muscle, kidney, bone, and brain, including myotonia congenita, dystrophia myotonica, cystic fibrosis, osteopetrosis, and epilepsy, and similarly their activation is supposed to be responsible for the progression of glioma in the brain and the growth of malaria-parasite in the red blood cells. Thus, the study of the structure, function, and blockers of

S.P. Gupta (✉)
Department of Applied Sciences, Meerut Institute of Engineering and Technology, Meerut 250005, India
e-mail: spgbits@gmail.com

S.P. Gupta (ed.), *Ion Channels and Their Inhibitors*,
DOI 10.1007/978-3-642-19922-6_11, © Springer-Verlag Berlin Heidelberg 2011

Cl^- channels seems to be of great importance. This article therefore presents all important classes of Cl^- channels with a detail of their structures, functions, and blockers.

Keywords Chloride ion channels • Ion channels • Chloride ion channel blockers • CLC chloride channels • Cystic fibrosis transmembrane conductance regulator • CaCC channels • Ligand-gated Cl^- channels • Chloride intracellular channels • Bestrophins

Abbreviations

CaCC	Ca^{2+}-activated chloride Cl^- channels
CFTR	Cystic fibrosis transmembrane conductance regulator
CLCs	Cl^- channels
CLICs	Chloride intracellular channels
CTB	Cynotriphenylborate
Cyclic-AMP	Cyclic adenosine monophosphate
Cyclic-GMP	Cyclic guanosine monophosphate
DIDS	4,4′-Diisothiocyanostilbene-2,2′-disulfonate
DNDS	4,4′-Dinitrodisulfonic stilbene
ENaC	Epithelial Na^+ conductance
ER	Epithelium reticulum
GABA	γ-Aminobutyric acid
GST	Glutathione S transferase
HEPES	4-(2-Hydroxyethyl)-1-piperazineethanesulfonic acid
IAA	Indanylooxyacetic acid
LGICs	Ligand-gated ion channels
MOPS	3-(N-morpholino)propanesulfonic acid
NBFs	Nucleotide binding folds
ORCCs	Outward rectifying chloride channels
PTN	Picrotin
PTX	Picrotoxin
PTZ	Pentylenetetylenetetrazole
SITS	4-Acetamide-4′-isothiocyanostilbene-2,2′-disulfonate
TMs	Transmembrane domains
WT	Wild type

1 Introduction

Ion channels are the channels situated in the cell membrane that allow the ions, such as Na^+, K^+, Ca^{2+}, Cl^- to pass from one side of the membrane to the other side. Thus, they constitute the crucial components of the living cells and figure in a wide

variety of biological processes that involve changes in the cells. Such processes are, for example, cardiac, skeletal, and smooth muscle contraction, epithelial transport of nutrient ions, T-cell activation, and pancreatic β-cell insulin release. The overactivation of these channels leads to several diseases and hence their inhibitors constitute several important classes of drugs.

Ion channels have been named depending upon what ion they let pass (e.g., Na^+, K^+, Ca^{2+}, Cl^-). Among them, chloride ion channels are pore-forming membrane proteins that allow the passive transport of Cl^- across biological membranes. They are ubiquitously expressed in almost all eukaryotic cells [1]. Voltage-gated and ligand-gated ion channels represent major classes of pharmacological receptors [2]. Voltage-gated ion channels open and close in response to membrane potential and ligand-gated ion channels (LGICs), also called ionotropic receptors, open in response to specific ligand molecules binding to the extracellular domains of the receptor protein. Ligand binding causes a conformational change in the structure of the channel protein that ultimately leads to the opening of the channel gate and the subsequent ion flux across the plasma membrane. Chloride ion channels involve both the mechanism, voltage-gated and ligand-gated, to transport the ions.

Chloride ion channels have been found to play crucial roles in the development of human diseases [3]. Mutations in the genes encoding Cl^- channels have been found to be responsible for the development of a variety of deleterious diseases in muscle, kidney, bone, and brain, including myotonia congenita, dystrophia myotonica, cystic fibrosis, osteopetrosis, and epilepsy [3]. The activation of Cl^- channels has been found to be responsible for several diseases. There is growing evidence that the progression of glioma in the brain and the growth of the malaria-parasite in the red blood cells may be mediated through Cl^- channel activation [4–8]. Thus, the study of structure, function, and blockers of Cl^- channels seems to be of paramount importance. This article presents a review on all such aspects of this important class of ion channels.

2 Classification of Cl^- Channels

Chloride ion channels have been classified according to their gating mechanisms, which may depend on changes in the membrane electrical potential, activation of a protein kinase, increase in intracellular Ca^{2+} levels, and binding of a ligand. Thus, there are four groups of Cl^- channels termed as CLC chloride channels, cystic fibrosis transmembrane conductance regulator (CFTR), Ca^{2+}-activated Cl^- channels (CaCC channels), and ligand-gated Cl^- channels, respectively. Although the Cl^- channels can also be activated by an increase in cell volume, extracellular acidification, the degree of phosphorylation, and the binding of ATP, only CLC, CFTR, and γ-aminobutyric acid (GABA)-activated (a ligand-gated) Cl^- channels have been well recognized [9]. However, a new class of Cl^- channels, known as chloride intracellular channels (CLICs), has also been reported [10, 11]. CLICs have been found to be widely expressed in different intracellular compartments,

having distinct properties, such as the presence of a single transmembrane domain and the dimorphic existence: either as a soluble globular protein or as an integral membrane protein. They are relatively new class of putative ion channel proteins that differ from other classes of channels in their primary structure, and in the transmembrane region of their tertiary structure. We now thus discuss here all important classes of Cl^- channels as mentioned.

2.1 The CLC Chloride Channels

CLC Cl^- channels form a large gene family that is found in bacteria, archae, and eukaryotes. They constitute the only class of Cl^- channels that are conserved from bacteria to man. Mammals have nine different CLC genes, which, based on homology, are grouped into three branches. The first branch contains ClC-1, ClC-2, ClC-Ka, and ClC-Kb that exert their function in the plasma membrane. The second branch is composed of ClC-3, ClC-4, and ClC-5, and the third branch has ClC-6 and ClC-7. These two branches function primarily in intracellular membranes.

All CLC Cl^- channels have a dimeric structure formed from two homologous pore forming proteins having molecular weights between ~60 and 110 kDa. This dimeric structure of CLC channels was deduced from electrophysiological analysis of wild-type (WT) and mutant channels [12–16], using sedimentation analysis and chemical cross-linking [14, 17], which has now been confirmed by crystal structures [18, 19]. However, this dimeric structure of Cl^- channels was first indicated by the biophysical analysis of a channel reconstituted from *Torpedo* electric organ [12]. The compelling evidence for a dimeric structure of CLC channels was provided by single-channel analysis of mutant/WT ClC-0 heteromers [15, 16] as well as of ClC-0/ClC-1 and ClC-0/ClC-2 concatemers [20]. Even a bacterial CLC protein obtained from *E. coli* was shown to be a dimmer [21]. Some CLC-proteins (e.g., ClC-1 and ClC-2) can form heterodimers [20, 22] in vitro, but it is not clear whether this also happens in vivo.

By a detailed biophysical study, Miller [23] proposed a "double-barrel" model for ClC-0 channels, which stated that this channel has two identical pores, which gate independently, but which can also be closed together by a slower, common gate. Also, there is a common "gate" that closes both the pores at the same time. ClC-1 and ClC-2 were also reported to behave as "double-barreled" channels [22, 24]. A brief review of CLC channel gating and the "double barrel" model has been presented by Estévez and Jentsch [25] and by Jentsch et al. [9].

2.1.1 Topological Features of CLC Channels

A definitive picture of topological features of CLC channels has been identified by their crystal structure [18]. Some previous biochemical studies on CLC topology

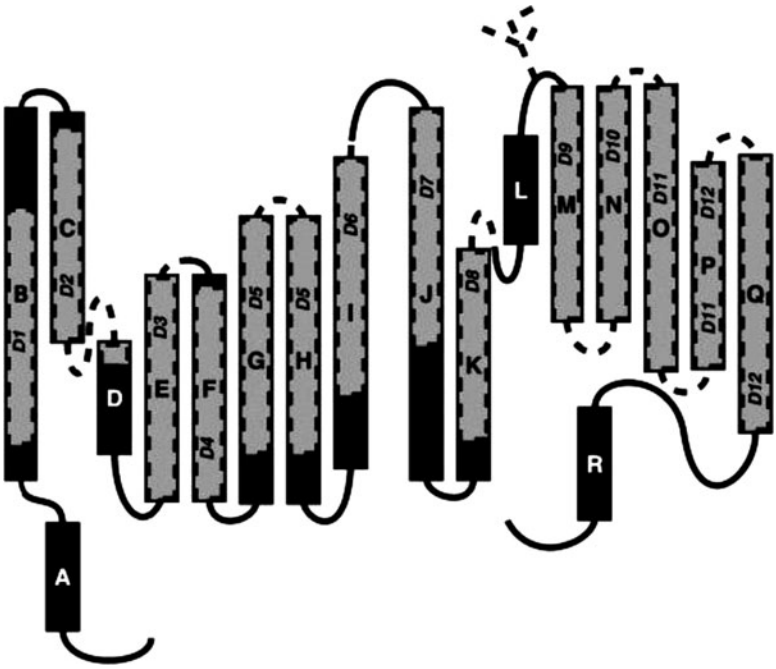

Fig. 1 A schematic representation of CLC channels as deduced from bacterial crystal structure study [18]. A to R refer to new nomenclature of helices, while D1 to D12 refer to the old one. The old model had the helices as indicated by *shaded areas* and *dashed lines*. Reprinted with permission from [9]. Copyright 2002 the American Physiological Society

had given a very confusing picture. The crystal structure study by Dutzler et al. [18] on two bacterial proteins (*Ec*ClC from *E. coli* and *St*ClC from *S. typhimurium*) pictured out a dimer with two identical subunits, each of which encloses a pore. Based on this bacterial study, the membrane topology of CLC channels can be schematically represented as Fig. 1 [9]. Each CLC subunit is composed of 18 α-helices, most of which do not cross the membrane entirely. Each subunit has an internal structural repeat, for example, helix B corresponds to helix J; C corresponds to K, and so on, and the two repeated halves have an antiparallel orientation, and are directly linked between helices I and J. In the dimeric "double-barreled" structure of CLC channels as seen in the crystal, the two repeated halves of each monomer contact each other at helices C and K, and H and P, respectively. The H–P interaction is supposed to be strong enough for channel assembly, as when the channel was split between helices J and L, or L and M, respectively, coexpression of the fragments resulted in functional channels.

The helices H and P (also P and H) exist in the center of the channel and face each other at the interface between the monomers. Helices H and P link the two repeated halves within the each monomer and, likewise, helices I and Q (and Q and I) make intersubunit contacts. Thus, several helices are observed to make contacts between the two subunits. The cytoplasmic helix A, which is resolved in

only one of the two subunits, has been revealed in the crystal structure coming close to the cytoplasmic end of the helix R of the other subunit. However, the two monomers of the CLC channel are tilted by 45° towards each other. With all such observations, however, the biochemical topology studies of CLC channels remain inconclusive, because of which sometimes complications arise in interpreting the effects of mutations [26].

2.1.2 The Pore, Gating, and Cl^- Permeation of CLC Channels

Although it is stated that the dimeric structure of CLC channels have two pores, but which protein segments line the pores have not yet been fully identified. The CLC pore is assumed to be formed by a single subunit [20], where it must be lined by different, nonhomologous parts of a single protein. This is in contrast to K^+ channels, where four identical or homologous "P loops" contribute to the permeation pathway. From the crystal structure study, it has been found that the various regions of the protein come together to form the pore. Four anti-parallel helices extend from the inside and the outside into the center plane of the membrane and the Cl^- is coordinated by residues at the ends of these residues, which contain highly conserved regions from the amino terminals of helix D (GSGIP), helix F (GREGP), helix N (GIFAP), and an amino acid from helix R (Ty445, *St*ClC numbering) [25].

From some transplantation experiments, it was however hypothesized that the region between helices E and F directly lines the pore [27], but its role in permeation and gating is poorly understood.

Regarding the gating of CLC channels, it is said that most CLC proteins that can be expressed functionally show voltage-dependent gating [9]. The charged amino acids in CLC trans-membrane domains are supposed to act as voltage sensors, and it has been indeed proposed that an aspartic acid at the extracellular end of helix B acts as a voltage sensor in ClC-1 [28]. However, the most thorough study on gating has been made for ClC-0 because of its relatively high channel conductance (~10 ps) and relatively simple gating [9]. It has fast gating that is two-state process with monoexponential kinetics. The ClC-0 opening is promoted by its substrate Cl^-. An unusual gating model for ClC-0 has also been proposed by Pusch et al. [29] in which the binding of Cl^- to a site deep within the pore promotes the opening (voltage-independent) of the channel. This results in voltage-dependent gating, as chloride ions have to travel along the electric field to reach this site. The voltage-dependent gating of many CLCs is strongly modulated by extracellular anions and pH [29–35].

The binding of Cl^- to the channels involves the nitrogen and oxygen atoms of the protein. The ions are coordinated with nitrogen atoms of main chain amino acid amide groups of Ile 356, Phe 357 (helix N) and with the oxygen atoms of the side chain of Ser107 (helix D) and Tyr 445 (helix R). The oxygen atom of Ser107 is also involved in the formation of a hydrogen bond with the accompanying Ile109 of the same conserved region, allowing a higher degree of polarization. The Cl^- permeation, however, can be blocked when the side chain of a glutamate residue at the start of helix F projects into the pore on the extracellular side from the chloride binding site.

This phenomenon, however, provides the structural basis for the "fast" Cl^--dependent gating of CLC pores [29, 30]. It is possible that Cl^- opens the gate by dislodging the side chain. The glutamate is conserved in nearly all CLC proteins, with the notable exception of ClC-K channels, where it is replaced by valine or leucine. Although several studies support such a role of glutamate in gating, it cannot be generalized.

2.1.3 Specification of CLC Family Members

The CLC family consists of nine separate genes, ClC-1,-2, . . ., -7, ClC-Ka and ClC-Kb. Based on the homology and function, they are grouped into three clusters. The first cluster consists of ClC-1, ClC-2, ClC-Ka and ClC-Kb, the second one consists of ClC-3, ClC-4 and ClC-5, and the third one consists of only ClC-6 and ClC-7. While the members of the first cluster exert their function in the plasma membrane, those of second and third function primarily in intracellular membranes. A brief description of tissue distribution, presumed functions and the human diseases associated with each member is given below.

ClC-1: A muscle-specific Cl^- channel, found in skeletal muscle, stabilizes the membrane voltage, and its mutational inactivation leads to myotonia in humans and mice [36, 37].

ClC-2: A broadly expressed channel activated by hyperpolarization, cell swelling, and acidic pH. Its role is not very clear but a role of it in transepithelial transport is suggested from the testicular and retinal degeneration in mice from its disruption [38].

ClC-Ka/Kb: These are two renal Cl^- channels that function (in a heteromeric complex with barttin, a β-subunit of Cl^- channel [39]) in transepithelial transport in the kidney and the ear. The mutations in them or in their β-subunit barttin cause Bartter Syndrome associated with kidney failure and deafness [40, 41].

ClC-3: It is expressed in endosomes in many cell types and in synaptic vesicles. Mutations in ClC-3 in mice result in neurogeneration [42].

ClC-4: It is a poorly characterized vesicular channel, not much is known about it.

ClC-5: It is expressed primarily in the renal proximal tubule where it co-localizes with markers of early apical endosomes [43, 44].

Mutations in ClC-5 lead to Dent's disease, a renal defect associated with low-molecular-weight proteinuria, hyperphosphaturia, hypercalicuria, and aminoacidiuria [45]. Probably similar to ClC-3, ClC-5 provides a shunt for the H^+-ATPase that is necessary for the efficient acidification of endosomes.

ClC-6: It is expressed in late endosomes in the nervous system and its disruption results in neurogeneration with pathological features of lysosomal storage disease [42, 44].

ClC-7: It is a lysosomal Cl^- channel, also expressed in late endosomes [44]. It accounts for the major Cl^- permeability of lysosomes [46]. Mutations in ClC-7 leads to osteoporosis in mice and humans [47, 48], and osteoclasts derived from patients harboring ClC-7 mutations show defective bone resorption [49, 50]. ClC-7 leads to acidification of lysosome, as a result an acid flux was characterized in

control human ostereoclasts [50]. Loss of ClC-7 leads to lysosomal storage and neurodegeneration [51].

2.2 Cystic Fibrosis Transmembrane Conductance Regulator

CFTR is the first anion channel to be identified by positional cloning. It is a cyclic-AMP activated plasma membrane chloride channel that has also been assumed to function as a chloride channel in intracellular organelles, where it could contribute to support acidification along the exocytic and endocytic pathways [52–54]. However, it has been observed that while CFTR may function as a Cl^- channel in some intracellular membranes, the organellar acidification is not dependent on CFTR and that organellar pH is not abnormal in cystic fibrosis [44].

Mutations in CFTR leads to disease cystic fibrosis. However, what are the other functions of CFTR in intracellular membranes and whether alterations in these functions contribute to the defects in cystic fibrosis are not well understood. Several experiments were done to establish ion channel function of CFTR [55–57]. CFTR is now known to be a voltage-independent anion channel, which requires the presence of hydrolyzable nucleoside triphosphates for its efficient activity [9].

A spliced form of CFTR is found in cardiac muscle [58, 59]. In fact, the protein kinase A-regulated cardiac Cl^- channel has been found to resemble CFTR [58] and alternative splicing of CFTR Cl^- channel in heart has been studied [59].

CFTR has been found to act as a regulator of other ion channels, for example, Na^+ [60] and Cl^- [61, 62]. The epithelial Na^+ conductance (ENaC) is coexpressed with CFTR in the apical membrane of most epithelia [63], and CFTR and outward rectifying chloride channels (ORCCs) have been observed to be distinct proteins with a regulatory relationship [62]. Egan et al. [61] found that the defective regulation of ORCCs by protein kinase A could be corrected by insertion of CFTR.

As far as the structure of CFTR is concerned, it has been found that it has 12 transmembrane domains (TMs), two nucleotide binding folds (NBFs), and a regulatory R domain (Fig. 2) [9]. It is the only member of the large gene family of ABC transporters that is known to function as an ion channel. Its opening is controlled by interacellular ATP and through phosphorylation by cAMP- and cGMP-dependent kinases. The two NBFs of CFTR differ in their functional characteristics. While NBF1 is required for channel opening and determines the closed time of the channel, NBF2 regulates the channel's opening time, but is not required for channel gating [9].

2.3 Ca^{2+}-Activated Chloride Channels (CaCC Channels)

CaCC channels are thought to regulate the tonus of smooth muscle and to modulate excitability by generating after potentials in neurons and muscle cells. In fact, they

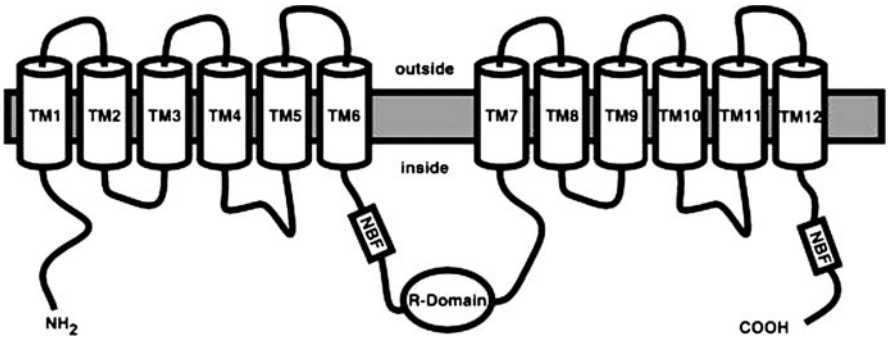

Fig. 2 A schematic representation of cystic fibrosis transmembrane conductance regulator (CFTR) that has 12 transmembranes (TMs), two nucleotide binding folds (NBFs), and a regulatory R domain. Reprinted with permission from [9]. Copyright 2002 the American Physiological Society

are found in many cell types, for example, epithelial cells [64, 65], neurons [66–68], cardiac cells [69], smooth muscle cells [70], and blood cells [71–73]. An important role of these channels is played in epithelial cells where they act as transepithelial transporter [74].

Some Cl^- channels are activated by extracellular calcium ions, for example, cloned renal Cl^- channels [75, 76] and certain of those found in *Xenopus* oocytes [77]. In most of the cases the activation of Cl^- channels by Ca^{2+} involves the phosphorylation by Ca^{2+}/calmudulin-dependent protein kinase II, for example, in human T84 and H-29 colonic cells [78, 79], in normal and cystic fibrosis airway epithelial cells [73], and in *Xenopus laevis* oocytes [80]. However, in certain cases the phosphorylation was not found to be involved in the activation of Cl^- channels by Ca^{2+}, for example, in parotid secretory cells [78] and rat submandibular acinar cells [81]. In addition, however, the phosphorylation by the Ca^{2+}/calmodulin-dependent protein kinase II may also be involved in inactivation of Cl^- channels by Ca^{2+} as observed by Wang and Kotlikoff [82] in smooth muscle.

2.4 Ligand-Gated Cl^- Channels

The GABA and glycine (Gly) receptors that belong to the family of LGICs act as Cl^- channels. The LGICs, also known as ionotropic receptors, open in response to specific ligand molecules binding to extracellular domain of the receptor protein. Ligand binding causes a conformational change in the structure of the channel protein that ultimately leads to the opening of the channel gate and subsequent ion flux across the plasma membrane.

The LGICs are pentameric proteins, in which each subunit has a large extracellular domain at the N-end, four transmembrane (TM) segments, and an

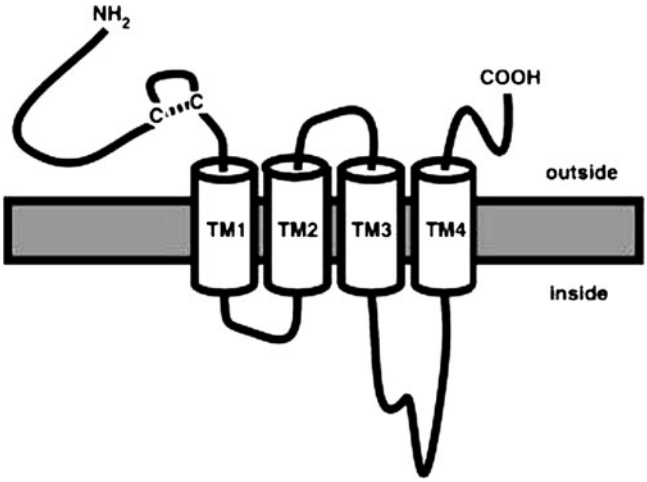

Fig. 3 A diagrammatic model of ligand-gated ion channels. These channels are pentameric proteins, in which each subunit has a large extracellular domain at the N-end, four transmembrane (TM) segments, and an intracellular (TM3–TM4) loop. Reprinted with permission from [9]. Copyright 2002 the American Physiological Society

interacellular (TM3–TM4) loop (Fig. 3) [9]. GABA and glycine receptors respond to the inhibitory neurotransmitters by opening a chloride-selective central pore lined with five TM2 segments. The central pore of LGICs is the only functional domain for which structure-function relationships are relatively well understood due to numerous electrophysiological, pharmacological, mutagenesis, and molecular modeling studies [83]. There is a consensus that five TM2 segments, predominantly in the α-helical conformations, contribute to the structure of this central pore [84–86]. In a drug-receptor binding study with GABA and glycine receptors, Zhorov and Bregestovski [83] found that the binding of the compounds such as cyanotriphenylborate (CTB) and picrotoxin (PTX) in the cytoplasmic half of the pore is stabilized by van der Waals interactions with five TM2 segments. A few more observations made by these authors in this study provided the support to general pore structure of LGICs as discussed.

Although both GABA and glycine receptors are ligand-gated Cl^- channels, they widely differ in their molecular structures, expressions, functional properties, and disruption effects.

2.4.1 Molecular Structures

Out of the three different types of GABA receptors ($GABA_A$, $GABA_B$, and $GABA_C$), only $GABA_A$ and $GABA_C$ receptors act as Cl^- channels [87, 88] and $GABA_B$ receptors are G-protein-coupled receptors [89]. However, as Cl^- channels $GABA_A$ receptors have been most widely discussed. These GABA receptors are

pentameric with 6α, 3β, and 3γ subunit isoforms [90]. On the contrary, the glycine receptors have been found to be a pentameric assembly of ~48 kDa α_1 subunit [91] and 58 kDa β subunits [92]. To date, in humans α_1 to α_4 and β subunits have been characterized.

2.4.2 Expression

GABA receptors are expressed in central as well as peripheral nervous systems, while glycine receptors are prominently expressed in the spinal cord and the medulla. They are also found in the retina [93], adrenal gland [94], kidney [95], liver [96], and sperm [97]. GABA receptors are also found in nonneuronal tissue where their function is not very clear. GABA and glycine receptors have been found to often coexist in spinal cord neurons [98–100].

2.4.3 Functions

Both GABA and glycine receptors were found to be permeable to several ions in the order $SCN^- > Br^- > Cl^- > F^-$ with only a small difference that the former are much more permeable to Cl^- against F^- than the latter. Further, the glycine receptors have also been found to be permeable to NO_3^- ($>I^-$) but not the GABA receptors [9]. However, the GABA receptors have been shown to be additionally permeable to HCO_3^- with a permeability of ~20% of Cl^-.

2.4.4 Disorders Associated

The disruption in GABA receptors has been found to produce epilepsy [101]. Recently, mutations in the γ_2-subunit have been identified in patients suffering from epilepsy [102, 103]. However, not one but several disorders have been found to be associated with mutations in glycine receptors, for example, hunching of shoulders, flexure of arms, and clenching of fists [9].

2.5 Chloride Intracellular Channels (CLICs)

The CLICs are the proteins that function as intracellular chloride channels. The term CLIC was derived from "Chloride Interacellular Channel" [104], and it was proposed that CLICs were the first proteins to function as interacellular chloride channels [105]. The first CLIC to be described was a 64 kDa protein (p64, now known as CLIC5B) isolated by Landry et al. [106] from bovine kidney membrane

fractions. The expression of recombinant CLIC5B in cultured cells led to an increased channel activity in whole cell membrane preparations, and the modification of the protein altered the activity [107, 108].

However, there are several other members in the CLIC family of proteins, which have been termed as CLIC1, 2, 3, 4, 5, and 6 [109, 110]. There exists a high degree of similarity in their C-termini, but their N-termini are divergent in both length and sequence. In addition to these six CLICs, which are mostly found in vertebrates [109], there are a few more which are found in invertebrates, for example, *Dm*CLIC (in *Drosophila melanogaster*), EXC4 and EXL1 (in *Caenorhabditis elegans*) and *At*DGAR1-4 (in *Arabidopsis thaliana*) [11].

2.5.1 Structure of CLICs

All CLICs share structural homology with members of omega glutathione S transferase (GST) superfamily [110, 111]. Unlike other ion channels, they all exist in dimorphic form: either as a soluble globular protein, or as an integral membrane protein suggested to form functional ion channels. The functional ion channels are formed by undergoing a structural transition from the water-soluble form. This transition is, however, a complex process, which is due to the many degrees of freedom and the balance between enthalpic and entropic contribution to the free energy from the polypeptide chain and solvent molecules. To form a functional channel in the membrane by any CLIC protein, it is predicted that there should be at least four molecules, since CLIC proteins have only one transmembrane domain and thus a single molecule cannot form a functional ion channel. Positively charged residues form two selectivity rings in the pore region of the channel indicating their importance in maintaining selectivity.

2.5.2 Biophysical Properties of CLICs

Because of the unavailability of method to directly access intracellular organelles and due to limited electrophysiological techniques for examining intracellular ion channels, no detailed study on the biophysical properties of CLICs so far could be made. So far all electrophysiological studies carried out in planar bilayers have indicated that CLIC proteins predominantly form non-selective ion channels [112–115] with different conductance levels. However, all CLICs form functional ion channels that vary in their conductance in different systems and within the same system [115]. The single putative transmembrane domain present in them lines the pore region of the channels, targets the protein to the membrane, and plays an active role in ion transport. However, it is suggested that CLICs may be functional only in specific cholesterol-rich microdomains in membranes. These

domains facilitate the insertion and proper refolding of CLICs to form functional channels.

2.5.3 Functions of CLICs

There are several hypotheses regarding the functions of CLICs. According to one hypothesis, the CLICs can function as ion channels, while another hypothesis is that they possess other functions in the cell, which do not appear to be related to channel activity. CLICs are also supposed to be multifunctional proteins that can transition between the integral membrane forms, which support ion channel activity, and the soluble globular forms, that may support regulation of various cell processes, such as structure of the cytoskeleton or modulation of gene expression. Control of their distribution between soluble globular and integral membrane forms is central to the understanding of their mode of function [44].

CLICs behave as atypical ion channels and function as intracellular ion channels with limited physiological roles. They are implicated in several important functions, such as membrane trafficking, cytoskeletal function, apoptosis, cell cycle control, mitosis, and differentiation [11]. However, there is limited evidence to believe that they function as Cl^- channels in intracellular membranes. There are only three systems for which some reports are available for their function as Cl^- channels: CLIC1 in nuclear membrane, CLIC4 in vesicles along the intracellular tubulogenic pathway, and CLIC5B in osteoclast ruffled membrane.

2.6 Bestrophins

Bestrophins are a group of four proteins, which have been found to support Cl^- channel activity when overexpressed in cell expression system [116, 117]. Some studies on mutagenesis, in which mutation of the bestrophin causes discrete changes in the associated channel activity, led to assume that they themselves function as channels [44]. The first member of the bestrophin family, bestrophin 1, is assumed to primarily reside in epithelium reticulum (ER) and not in the plasma membrane [118]. An observation that bestrophin 1 modulates both Ca^{2+} release and uptake from interacellular stores, presumably ER, leads to assume that bestrophin functions as an ER chloride channel, which could provide counter ion movement during cycles of Ca^{2+} release and uptake [117]. However, it is only an indirect evidence to say that bestrophin functions as a channel in the ER; it only suggests that bestrophin facilitates only Ca^{2+} movement. The identification of bestrophin 1 as the site of mutation in the Best's disease, a form of early onset macular degeneration [116, 117], simply supports a Ca^{2+}-activated chloride current in the basal membrane of the retinal pigment epithelium. It hardly provides any direct evidence that bestrophin 1 itself functions as chloride ion channel [119].

3 Human Diseases Related to Chloride Ion Channels

The mutations in Cl^- channels have been found to be responsible for the development of a number of deleterious diseases in muscle, kidney, bone, and brain, including myotonia congenita, dystrophia, cystic fibrosis, osteopetrosis, and epilepsy. Not only the mutations, but activation also of these channels has been responsible for the development of certain diseases, such as the progression of glioma in the brain and the growth of the malaria parasite in the red blood cells [120–123]. In addition, it has also been found that a loss of Cl^- channel activity may also mediate the development of chronic pancreatitis, bronchiectasis, congenital bilateral aplasia of vas deferens, alcoholism, cataract, and Best's disease [3]. The development of the various forms of cystic fibrosis (CF) and Bartter syndrome has been attributed to the defective Cl^- transport in epithelial cells [124]. Mutations in α-1 subunit of inhibitory glycine receptor have been found to cause the dominant neurological disorder, hyperekplexia [125–128]. All such human diseases thus known to be associated with the abnormality in Cl^- channels have been well described by Puljak and Kilic [3]. They can be briefly mentioned here as follows.

ClC-1: Myotonia congenita Becker [36], myotonia congenita Thomsen [129], dystrophia myotonica 1 [130, 131], and dystrophia myotonica 2 [130, 132]

ClC-2: Childhood absence epilepsy type 3, juvenile absence epilepsy, juvenile myoclonic epilepsy, and epilepsy with grand mal [133], and seizures on awakening

ClC-Kb: Bartter syndrome III [40]

ClC-Ka, ClC-Kb (Barttin): Bartter syndrome IV or BSND [134, 135]

ClC-5: Dent's disease [136–138]

ClC-7: Autosomal dominant osteopetrosis [139] and autosomal recessive osteopetrosis [140]

CFTR: Cystic fibrosis [141], idiopathic chronic pancreatitis [142–144], bronchiectasis [145–148], and congenital bilateral absence of vas deferens [149–152]

Bestrophin: Best's disease [153–155], adult-onset vitelliform [156], macular and concentric annular macular dystrophy [156]

Unknown: Cataract [157–160]

$GABA_A$: Juvenile myoclonic epilepsy [161], childhood absence epilepsy type 2 [103], generalized epilepsy with febrile seizures plus severe myoclonic epilepsy in infancy [162], alcoholism [163, 164], and insomnia [165]

GlyR: Hereditary hyperekplexia [125–128]

Association of these diseases with Cl^- channels suggests that these channels may be novel targets for the development of useful drugs for a broad spectrum of diseases.

4 Chloride Ion Channel Blockers

The Cl^- channels are usually present in the neurons and muscle cells and in epithelial cells. While in neurons and muscle cells they regulate the excitability, in the epithelial cells they mediate the transepithelial transport of salt and water.

As already discussed, the activation of Cl^- channels lead to variety of human diseases; therefore, the study of their inhibitors is of paramount importance.

The chloride channel blockers can be grouped according to their targets: (1) agents acting at the neuronal chloride channels; (2) agents acting with chloride channels in muscle cells; and (3) agents interfering with the channels in epithelial cells. A brief description of all these groups is as follows.

4.1 Agents Acting at the Neuronal Chloride Channels (GABA and Glycine Receptors)

So far the well studied GABA receptor channel blockers are picrotoxin – a mixture of picrotoxinum (**1**, PTX) and picrotin (**2**, PTN) – pentylenetetrazole (**3**, PTZ), bicuculline (**4**) and some bicyclic phosphates [9, 166], and the only known glycine receptor channel blocker is cyanotriphenylborate (**5**,CTB) [83], which can be used to distinguish receptors containing α_1- or α_2-subunit, as the α_2-subunit is relatively insensitive to CTB.

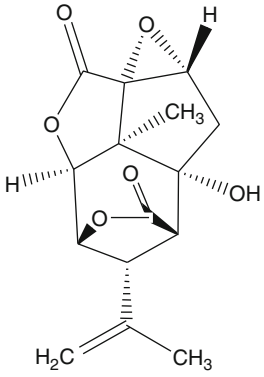

1, Picrotoxinin/Picrotoxinum

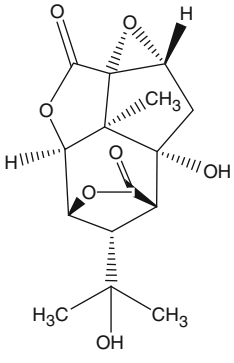

2, Picrotin

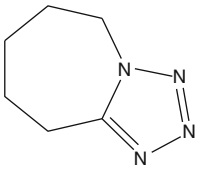

3, Pentylenetetrazole

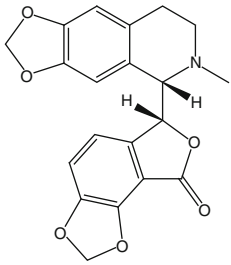

4, Bicuculline

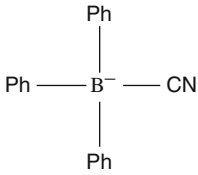

5, Cyanotriphenylborate

4.2 Agents Acting with Chloride Channels in Muscle Cells

In a review, Bretag [167] discussed four groups of compounds that act as chloride channel blockers in striated muscle cells: (1) polycyclics, (2) benzoates, (3) phenoxyacetates, and (4) sulfonates and sulfonamides. The representative compounds of these groups can be cited as anthracene-9-carboxylate (**6**, 9-Ac), furosemide (**7**), ethacrynic acid (**8**), and stilbene disulfonate (**9**), respectively. Further, two sulfonic acid stilbene derivatives, 4-acetamide-4′-isothiocyanostilbene-2,2′-disulfonate (SITS) and 4,4′-diisothiocyanostilbene-2,2′-disulfonate (DIDS), were also assumed to interfere with chloride channels in smooth muscle cells in analogy to their effects in *Torpedo* electric organ chloride channel [168].

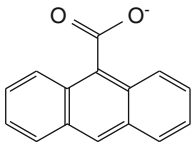

6, Anthracene-9-carboxylate

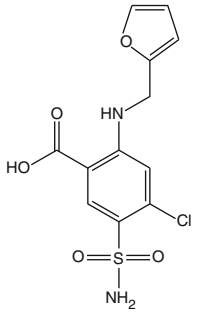

7, Furosemide

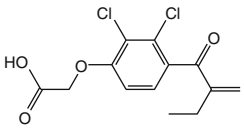

8, Ethacrynic acid

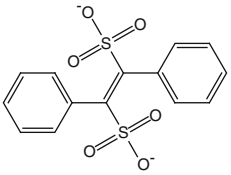

9, Stilbene disulfonate

4.3 Agents Acting on Epithelial Chloride Channels

Chloride permeation through CFTR channel in epithelial cells can be inhibited by a broad range of organic anions that enter the pore from its cytoplasmic end and physically occlude it [169, 170]. Some of the important examples of such anions may be diphenylamine carboxylate (**10**) [171], gluconate (**11**) [172], and glibenclamide (**12**) [173]. The interaction of the anions with CFTR channel involves electrostatic interaction with a positively charged amino acid side chain that lines the pore, K95 [174]. The CFTR channel has also been found to be potentially inhibited by arachidonic acid (**13**) [175], involving the electrostatic interaction with positively charged amino acid side chains located within the chloride ion permeation pathway K95 and R303 [176]. While K95 is located in the first transmembrane region of the CFTR protein and is supposed to form part of the wider inner vestibule of the channel pore [174], R303 is thought to be situated at the very intracellular end of the fifth transmembrane region to be the part of the

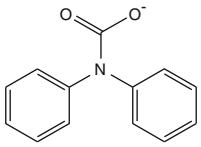

10, Diphenylamine carboxylate

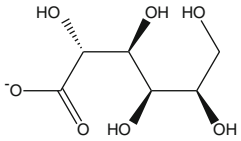

11, Gluconate

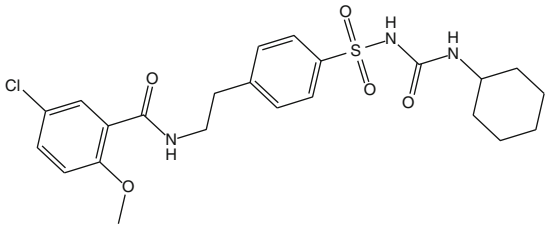

12, Glibenclamide

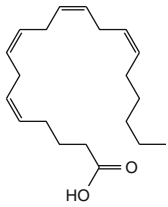

13, Arachidonic acid

cytoplasmic mouth of the pore, where it can attract the Cl^- into the pore by a surface charge mechanism [177]. Thus, arachidonic acid is thought to enter the cytoplasmic end of the channel pore to inhibit the CFTR Cl^- currents, most likely by physically occluding the Cl^- permeation pathway [176]. According to Linsdell [174], however, other negatively charged substances, too, such as sulfonyl ureas, disulfonic stilbenes, indazoles, arylaminobenzoates, and conjugated bile salts, inhibit CFTR Cl^- currents by interacting electrostatically with K95 and blocking the open channel. However, while the inhibition by these substances is weakened by the depolarization of the membrane potential [169, 174] and increase in extracellular Cl^- concentration, the arachidonic inhibition is practically independent of both membrane potential and Cl^- concentration [175].

In general, all anion channels can be blocked by many unrelated classes of compounds, bearing a negative charge at physiological pH. Even many small anions, for example, HEPES (4-(2-hydroxyethyl)-1-piperazineethanesulfonic acid) and MOPS (3-(N-morpholino)propanesulfonic acid) buffers, have been found to block Cl^- channels [178, 179]. Transition metal cations, such as Zn^{2+}, Cd^{2+}, La^{3+}, Gd^{3+} can also block anion channels; for example, Zn^{2+} has been found to block ClC-1 [180, 181] and the GABA receptor [182, 183], and Cd^{2+} has been often used to block ClC-2 channel [184–186].

4.4 Agents Acting on Other Cl^- Channels

As discussed in the preceding section, some members of ClC channels could be blocked by Zn^{2+} and Cd^{2+} ions. The inhibitors for the other chloride channels are not so well studied. However, the Ca^{2+}-activated chloride channels in mammalian cells were found to be inhibited by niflumic and flufenamic acids (**14**,**15**) [187] as well as by 5-nitro-2-(3-phenylpropylamino)benzoic acid (**16**, NPPB). In addition, the disulfonic stilbene DIDS has also been found to potentially block the CaCC in mammalian cells. For CLIC channels, indanylooxyacetic acid (**17**, IAA-94) was found to be a potential blocker. This could block CLIC-1-induced currents [188]. In addition, disulfonic stilbene DNDS (4,4′-dinitrodisulfonic stilbene and TS-TM-calix(4)arene were also found to block p64-induced currents [108].

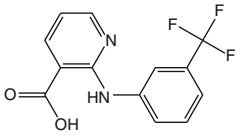

14, Niflumic acid

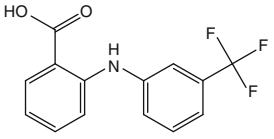

15, Flufenamic acid

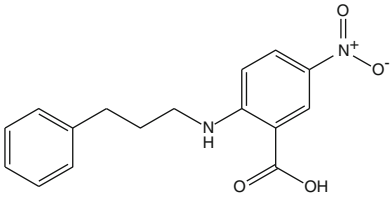

16, 5-Nitro-2-(3-phenylpropylamino)benzoic acid

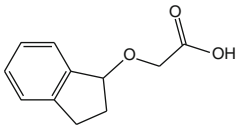

17, Indanylooxyacetic acid

4.5 Other Cl^- Transporting Systems and Their Blockers

In addition to the above important classes of Cl^- channels and their blockers described in the preceding sections, there are some other systems by which chloride ions can be transported, for example, $Na^{2+}/2Cl^-/K^+$ carrier and apolar cells. A brief description of these two and their blockers are given below.

4.5.1 $Na^{2+}/2Cl^-/K^+$ Carrier

$Na^{2+}/2Cl^-/K^+$ carrier was detected by Geck et al. [189] to be another Cl^- transport system. This system is found in many polar and apolar cells [166, 190]. It was so far believed to be only a primary pump, sensitive to furosemide (**18**)-like substances, but now it has been found to also act as a secondary active chloride carrier. Thus, the chloride transport can be blocked by all furosemide-like substances, for example, furosemide (**18**), piretanide (**19**), triflocine (**20**), and torasemide (**21**), which can interact with $Na^{2+}/2Cl^-/K^+$ carrier in epithelial cells. This carrier acts as transepithelial transporter of NaCl, and is found together with Cl^- channels on the opposite cell membranes [191].

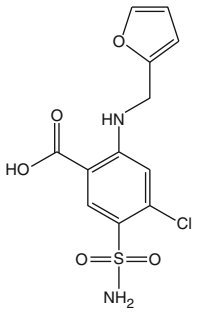

18, Furosemide

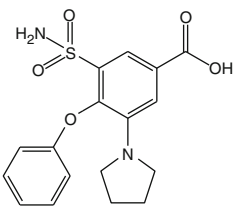

19, Piretanide

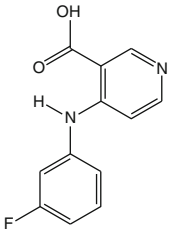

20, Triflocine

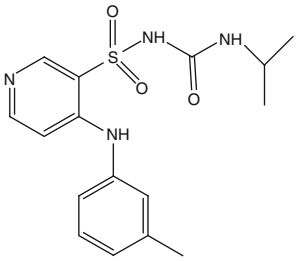

21, Torasemide

4.5.2 Apolar Cells

The red blood cells also act as Cl^- transporters, where the Cl^- flux occurs via the band 3 protein, a form of bicarbonate/chloride exchange system [192]. This protein is assumed to perform electroneutral anion exchange and to also permit the channeling of Cl^-. Its activity may thus be blocked by the compounds related to stilbene, furosemide, and arylbenzoate classes.

4.6 Mechanism of Action of Anionic Channel Blockers

As discussed in a review by Greger [166], all Cl^- channel blockers are essentially converted into anionic form at physiological pH, in which the anionic group is usually a carboxylate. All compounds also possess an amino bridge and an apolar residue. The amino bridge is supposed to be necessary; it cannot be replaced by any other group, such as oxygen, phosphorus, or carbon. The amino bridge may probably be essential because of its ability to form a hydrogen bond acting as a hydrogen-bond donor. An apolar group may be essential to have any hydrophobic interaction with the receptor. In some group of compounds, the distances between the amino and apolar groups and between amino and carboxylate groups are very critical, for example, in the group of NPPB (**16**) derivatives, the optimal spacer between the phenyl ring and the amino group was a propyl group. Replacing this

spacer by a butyl or ethyl led to dramatic reduction in the potency of the compounds. In the case of NPPB class of compounds, which also have a nitro group at the meta-position with respect to carboxylate group, the distance between this nitro group and the carboxylate group was also found to be important. These observations lead to suggest that chloride channel blockers interact with several sites of the channel.

However, this nitro group is found to be possessed by only the chloride channel blockers. The blockers of $Na^{2+}/2Cl^{-}/K^{+}$ carrier contain instead a sulfonamide group as in furosemide (**18**) and piretanide (**19**), or a pyridine ring as in triflocine (**20**) and torasemide (**21**). All other groups, namely, a carboxylate group, an amino group, and an apolar moiety are commonly essential for both the classes of blockers [166].

5 Conclusion

Chloride ion channels have been found to play crucial roles in the development of human diseases. They have been classified into different groups based on their gating mechanisms that depend on changes in the membrane electrical potential, activation of a protein kinase, increase in intracellular Ca^{2+} levels and binding of a ligand. Thus, there are four groups of Cl^{-} channels termed chloride ion channels (CLC channels), cystic fibrosis transmembrane regulator (CFTR), Ca^{2+}-activated chloride (CaCC) channels, and ligand-gated chloride ion channels (LGICs). However, a new class of Cl^{-} channels known as CLICs has also been reported. Further, another class of Cl^{-} channels is constituted of bestrophins, a group of proteins, which have been found to support Cl^{-} channel activity when overexpressed in cell expression.

CLC chloride channels constitute the only class of Cl^{-} channels that are conserved from bacteria to man. The crystal structure of two bacterial proteins pictured out a dimer with two identical subunits, each composed of 18 α-helices, most of which do not cross the membrane entirely. CFTR is a cyclic-AMP activated plasma membrane chloride channel that has also been assumed to function as a chloride channel in intracellular organelles. CFTR has been found to act as a regulator of other ion channels, for example, Na^{+} and Cl^{-}. As far as its structure is concerned, it has been found to possess 12 transmembrane domains, two NBFs, and a regulatory R domain. The Ca^{2+}-activated chloride channels (CaCC Channels) are found in many cell types, for example, epithelial cells, neurons, cardiac cells, smooth muscle cells, and blood cells. They play an important role in epithelial cells as a transepithelial transporter. The ligand-gated Cl^{-} channels (LGICs) open in response to specific ligand molecules binding to extracellular domain of the receptor protein. The two important LGICs are pentameric proteins, in which each subunit has a large extracellular domain at the N-end, four transmembrane segments, and an intracellular loop (Fig. 3). The LGICs are also called ionotropic receptors.

The CLICs are the proteins that function as intracellular chloride ion channels. There are several members in CLIC family of proteins. All CLICs share structural

homology with members of omega GST superfamily. Unlike other ion channels, they exist in dimorphic form: either a soluble globular protein, or as an integral membrane protein suggested to form functional ion channels. Bestrophins are a group of four proteins, which have been found to support Cl^- channel activity. The first member of this family, bestrophin 1, is relatively well studied and has been shown to support Ca^{2+}-activated chloride current in the basal membrane of the retinal pigment epithelium. There is no evidence that it itself functions as a chloride ion channel. It is assumed to primarily reside in epithelium reticulum and not in the plasma membrane.

Number of diseases have been found to be related to the abnormality of Cl^- channels, for example, the mutations in them lead to several deleterious diseases in muscle, kidney, bone, and brain, including mytonia congenita, dystrophia, cystic fibrosis, osteopetrosis, and epilepsy, their activation may lead to progression of glioma in the brain and the growth of malaria parasite in the red blood cells, and the loss of their activity may mediate the development of chronic pancreatitis, bronchiectasis, congenital bilateral aplasia of vas deferens, alcoholism, cataract, and Best's disease. Thus, the blockers of Cl^- channels may be developed as useful therapeutic agents against many of these diseases. So far there are drugs such as picrotoxin, a mixture of picrotoxinin (**1**) and picrotin (**2**), acting as blocker of GABA receptor, and cyanotriphenylborate (**5**) acting as the blocker of glycine receptors. Some polycyclics, benzoates, phenoxyacetates, and sulfonates and sulfonamides have been found to block Cl^- channels in muscle cells, and broad range of anionic ions such as diphenylamine carboxylate (**10**), gluconate (**11**), and glibenclamide (**12**), have been found to block CFTR channel in epithelial cells. Disulfonic stilbene DIDS has been found to potentially block the CaCC in mammalian cells, and indanylooxyacetic acid (**17**) is a potential blocker of CLIC channels.

Thus, this article presents all important aspects of Cl^- channels, which may help the medicinal chemists to develop important drugs for many diseases.

References

1. Nilius B, Droogmans G (2003) Amazing chloride channels: an overview. Acta Physiol Scand 177:119–147
2. Hille B (1991) Ion channels, 2nd edn. Sinauer Associates, Sunderland, MA
3. Puljak L, Kilic G (2006) Emerging roles of chloride channels in human diseases. Biochim Biophys Acta 1762:404–413
4. Merzak A, Pilkington GJ (1997) Molecular and cellular pathology of intrinsic brain tumours. Cancer Metastasis Rev 16:155–177
5. Ransom CB, O'Neal JT, Sontheimer H (2001) Volume-activated chloride currents contribute to the resting conductance and invasive migration of human glioma cells. J Neurosci 21: 7674–7683
6. Romisch K (2005) Protein targeting from malaria parasites to host erythrocytes. Traffic 6:706–709
7. Breman JG, Alilio MS, Mills A (2004) Conquering the intolerable burden of malaria: what's new, what's needed: a summary. Am J Trop Med Hyg 71:1–15

8. Martin RE, Henry RI, Abbey JL et al (2005) The 'permeome' of the malaria parasite: an overview of the membrane transport proteins of *Plasmodium falciparum*. Genome Biol 6: R26
9. Jentsch TJ, Stein V, Weinreich F et al (2002) Molecular structure and physiological function of chloride channels. Physiol Rev 82:503–568
10. Landry DW, Reitman M, Cragoe EJ Jr et al (1987) Epithelial chloride channel. Development of inhibitory ligands. J Gen Physiol 90:779–798
11. Singh H (2010) Two decades with dimorphic chloride intracellular channels (CLICs). FEBS Lett 584:2112–2121
12. Miller C, White MM (1984) Dimeric structure of single chloride channels from *Torpedo* electroplax. Proc Natl Acad Sci USA 81:2772–2775
13. Bauer CK, Steinmeyer K, Schwarz JR et al (1991) Completely functional double-barreled chloride channel expressed from a single *Torpedo* cDNA. Proc Natl Acad Sci USA 88: 11052–11056
14. Middleton RE, Pheasant DJ, Miller C (1994) Purification, reconstitution, and subunit composition of a voltage-gated chloride channel from *Torpedo* electroplax. Biochemistry 33: 13189–13198
15. Middleton RE, Pheasant DJ, Miller C (1996) Homodimeric architecture of a CLC-type chloride ion channel. Nature 383:337–340
16. Ludewig U, Pusch M, Jentsch TJ (1996) Two physically distinct pores in the dimeric ClC-0 chloride channel. Nature 383:340–343
17. Fahlke C, Knittle T, Gurnett CA et al (1997) Subunit stoichiometry of human muscle chloride channels. J Gen Physiol 109:93–104
18. Dutzler A, Campbell EB, Cadene M et al (2002) X-ray structure of a ClC chloride channel at 3.0 Å reveals the molecular basis of anion selectivity. Nature 415:287–294
19. Mindell JA, Maduke M, Miller C et al (2001) Projection structure of a CLC type chloride channel at 6.5 Å resolution. Nature 409:219–223
20. Weinreich F, Jentsch TJ (2001) Pores formed by single subunits in mixed dimers of different ClC chloride channels. J Biol Chem 276:2347–2353
21. Maduke M, Pheasant DJ, Miller C (1999) High-level expression, functional reconstitution, and quaternary structure of a prokaryotic ClC-type chloride channel. J Gen Physiol 114: 713–722
22. Lorenz C, Pusch M, Jentsch TJ (1996) Heteromultimeric ClC chloride channel with novel properties. Proc Natl Acad Sci USA 93:13362–13366
23. Miller C (1982) Open-state substructure of single chloride channels from *Torpedo electroplax*. Philos Trans R Soc Lond B Biol Sci 299:401–411
24. Saviane C, Conti F, Push M (1999) The muscle chloride channel ClC-1 has a double-barreled appearance that is differentially affected in dominant and recessive myotonia. J Gen Physiol 113:457–468
25. Estévez R, Jentsch TJ (2002) CLC chloride channels: correlating structure with function. Curr Opin Struct Biol 12:531–539
26. Schmidt-Rose T, Jentsch TJ (1997) Transmembrane topology of a CLC chloride channel. Proc Natl Acad Sci USA 94:7633–7638
27. Fahlke C, Yu HT, Beck CL et al (1997) Pore-forming segments in voltage-gated chloride channels. Nature 390:529–532
28. Fahlke C, Rüdel R, Mitrovic N et al (1995) An aspartic acid residue important for voltage-dependent gating of human muscle chloride channels. Neuron 15:463–472
29. Pusch M, Ludewig U, Rehfeldt A et al (1995) Gating of the voltage-dependent chloride channel ClC-0 by the permeant anion. Nature 373:527–531
30. Chen TY, Miller C (1996) Nonequilibrium gating and voltage dependence of the ClC-0 Cl^- channel. J Gen Physiol 108:237–250
31. Hanke W, Miller C (1983) Single chloride channels from *Torpedo electroplax*. Activation by proteins. J Gen Physiol 82:25–45

32. Richard EA, Miller C (1990) Steady-state coupling of ion-channel conformations to a transmembrane ion gradient. Science 247:1208–1210
33. Rychkov GY, Pusch M, Astill DS et al (1996) Concentration and pH dependence of skeletal muscle chloride channel ClC-1. J Physiol (Lond) 497:423–435
34. Rychkov GY, Pusch M, Roberts ML et al (1998) Permeation and block of the skeletal muscle chloride channel, ClC-1, by foreign anions. J Gen Physiol 111:653–665
35. Schriever AM, Friedrich T, Pusch M et al (1999) ClC chloride channels in *Caenorhabditis elegans*. J Biol Chem 274:34238–34244
36. Koch MC, Steinmeyer K, Lorenz C et al (1992) The skeletal muscle chloride channel in dominant and recessive human myotonia. Science 257:797–800
37. Steinmeyer K, Klocke R, Ortland C et al (1991) Inactivation of muscle chloride channel by transposon insertion in myotonic mice. Nature 354:304–308
38. Bösl MR, Stein V, Hübner C et al (2001) Male germ cells and photoreceptors, both dependent on close cell–cell interactions, degenerate upon ClC-2 Cl^- channel disruption. EMBO J 20:1289–1299
39. Estévez R, Better T, Stein V et al (2001) Barttin is a Cl^--channel beta-subunit crucial for renal Cl^--reassertion and inner ear K^+-secretion. Nature 414:558–561
40. Simon DB, Bindra RS, Mansfield TA et al (1997) Mutations in the chloride channel gene, *CLCNKB,* cause Barter's syndrome type III. Nat Genet 17:171–178
41. Birkenhäger R, Otto E, Schürmann MJ et al (2001) Mutation of BSND causes Bartter syndrome with sensorineural deafness and kidney failure. Nat Genet 29:310–314
42. Jentsch TJ (2007) Chloride and the endosomal-lysosomal pathway: emerging roles of CLC chloride transporters. J Physiol 578:633–640
43. Gunther W, Luchow A, Cluzeaud F, Vandewalle A et al (1998) ClC-5, the chloride channel mutated in Dent's disease, colocalizes with the proton pump in endocytotically active kidney cells. Proc Natl Acad Sci USA 95:8075–8080
44. Edwards JC, Kahl CR (2010) Chloride channels of intracellular membranes. FEBS Lett 584: 2102–2111
45. Plans V, Rickheit G, Jentsch TJ (2009) Physiological roles of CLC Cl(−)/H(+) exchangers in renal proximal tubules. Pflugers Arch 458:23–37
46. Graves AR, Curran PK, Smith CL et al (2008) The Cl^-/H^+antiporter ClC-7 is the primary chloride permeation pathway in lysosomes. Nature 453:788–792
47. Kornak U, Casper D, Bösl MR et al (2001) Loss of the ClC-7 chloride channel leads to osteopetrosis in mice and man. Cell 104:205–215
48. Frattini A, Pangrazio A, Susani L et al (2003) Chloride channel ClCN7 mutations are responsible for severe, recessive, dominant, and intermediate osteopetrosis. J Bone Miner Res 18:1740–1747
49. Chu K, Snyder R, Econs MJ (2006) Disease status in autosomal dominant osteopetrosis type 2 is determined by osteoclastic properties. J Bone Miner Res 21:1089–1097
50. Henriksen K, Gram J, Neutzsky-Wulff AV et al (2009) Characterization of acid flux in osteoclasts from patients harboring a G215R mutation in ClC-7. Biochem Biophys Res Commun 378:804–809
51. Kasper D, Planells-Cases R, Fuhrman JC et al (2005) Loss of the chloride channel ClC-7 leads to lysosomal storage disease and neurodegeneration. EMBO J 24:1079–1091
52. Barasch J, Kiss B, Prince A et al (1991) Defective acidification of intracellular organelles in cystic fibrosis. Nature 352:70–73
53. Barriere H, Bagdany M, Bossard F et al (2009) Revisiting the role of cystic fibrosis transmembrane conductance regulator and counterion permeability in the pH regulation of endocytic organelles. Mol Biol Cell 20:3125–3141
54. Haggie PM, Verkman AS (2009) Defective organellar acidification as a cause of cystic fibrosis lung disease: reexamination of a recurring hypothesis. Am J Physiol Lung Cell Mol Physiol 296:L859–L867
55. Anderson MP, Gregory RJ, Thomson S et al (1991) Demonstration that CFTR is a chloride channel by alteration of its anion selectivity. Science 253:202–205

56. Bear CE, Li CH, Kartner N et al (1992) Purification and functional reconstitution of the cystic fibrosis transmembrane conductance regulator (CFTR). Cell 68:809–818
57. Sheppard DN, Rich DP, Ostedgaard LS et al (1993) Mutations in CFTR associated with mild-disease-form Cl^- channels with altered pore properties. Nature 362:160–164
58. Nagel G, Hwang TC, Nastiuk KL et al (1992) The protein kinase A-regulated Cl^- channel resembles the cystic fibrosis transmembrane conductance regulator. Nature 360:81–84
59. Horowitz B, Tsung SS, Hart P et al (1993) Alternative splicing of CFTR Cl^- channels in heart. Am J Physiol Heart Circ Physiol 264:H2214–H2220
60. Boucher RC, Stutts MJ, Knowles MR (1986) Na^+ transport in cystic fibrosis respiratory epithelia. Abnormal basal rate and response to adenylate cyclase activation. J Clin Invest 78:1245–1252
61. Egan M, Flotte T, Afione S et al (1992) Defective regulation of outwardly rectifying Cl^- channels by protein kinase A corrected by insertion of CFTR. Nature 358:581–584
62. Gabriel SE, Clarke LL, Boucher RC et al (1993) CFTR and outward rectifying chloride channels are distinct proteins with a regulatory relationship. Nature 363:263–266
63. Alvarez DLRD, Canessa CM, Fyfe GK et al (2000) Structure and regulation of amiloride-sensitive sodium channels. Annu Rev Physiol 62:573–594
64. Peterson OH (1992) Stimulus-secretion coupling: cytoplasmic calcium signals and the control of ion channels in exocrine acinar cells. J Physiol (Lond) 448:1–51
65. Peterson OH, Philpott HG (1980) Mouse pancreatic acinar cells: the anion selectivity of the acetylcholine-opened chloride pathway. J Physiol (Lond) 306:481–492
66. Frings S, Reuter D, Kleene SJ (2000) Neuronal Ca^{2+}-activated Cl^- channels: homing in on an elusive channel species. Prog Neurobiol 60:247–289
67. Mayer ML (1985) A calcium-activated chloride current generates the after-depolarization of rat sensory neurons in culture. J Physiol (Lond) 364:217–239
68. Scott RH, Sutton KG, Griffin A et al (1995) Aspects of calcium-activated chloride currents: a neuronal perspective. Pharmacol Ther 66:535–565
69. Sorota S (1999) Insights into the structure, distribution and function of the cardiac chloride channels. Cardiovasc Res 42:361–376
70. Pacaud P, Loirand G, Lavie JL et al (1989) Calcium-activated chloride current in rat vascular smooth muscle cells in short-term primary culture. Pfügers Arch 413:629–636
71. Nishimoto I, Wagner JA, Schulman H et al (1991) Regulation of Cl^- channels by multifunctional CaM kinase. Neuron 6:547–555
72. Schumann MA, Gardner P, Raffin TA (1993) Recombinant human tumor necrosis factor alpha induces calcium oscillation and calcium-activated chloride current in human neutrophils. The role of calcium/calmodulin-dependent protein kinase. J Boil Chem 268: 2134–2140
73. Wagner JA, Cozens AL, Schulman H et al (1991) Activation of chloride channels in normal and cystic fibrosis airway epithelial cells by multifunctional calcium/calmodulin-dependent protein kinase. Nature 349:793–796
74. Kidd JF, Thorn P (2000) Intracellular Ca^{2+} and Cl^- channel activation in secretory cells. Annu Rev Physiol 62:493–513
75. Uchida S, Sasaki S, Nitika K et al (1995) Localization and functional characterization of rat kidney-specific chloride channel, ClC-K1. J Clin Invest 95:104–113
76. Waldegger S, Jentsch TJ (2000) Functional and structural analysis of ClC-K chloride channels involved in renal disease. J Biol Chem 275:24527–24533
77. Reifarth FW, Amasheh S, Clauss W et al (1997) The Ca^{2+}-inactivated Cl^- channel at work: selectivity, blocker kinetics and transport visualization. J Membr Biol 155:95–104
78. Arreola J, Melvin JE, Begenisich T (1998) Differences in the regulation of Ca^{2+}-activated Cl^- channels in colonic and parotid secretory cells. Am J Physiol Cell Physiol 274: C161–C166
79. Morris AP, Frizzel RA (1993) Ca^{2+}-dependent Cl^- channels in undifferentiated human colonic cells (HT-29).II. Regulation and rundown. Am J Physiol Cell Physiol 264: C977–C985

80. Dascal N, Gillo B, Lass Y (1985) Role of calcium mobilization in mediation of acetylcholine-evoked chloride currents in *Xenopus laevis* oocytes. J Physiol (Lond) 366:299–313
81. Ishikawa T (1996) A bicarbonate-and weak acid-permeable chloride conductance controlled by cytosolic Ca^{2+} and ATP in rat submandibular acinar cells. J Membr Biol 153:147–159
82. Wang YX, Kotlikoff MI (1997) Inactivation of calcium-activated chloride channels in smooth muscle by calcium/calmodulin-dependent protein kinase. Proc Natl Acad Sci USA 94:14918–14923
83. Zhorov BS, Bregestovski PD (2000) Chloride channels of glycine and GABA receptors with blockers: Monte Carlo minimization and structure-activity relationships. Biophys J 78:1786–1803
84. Changeux JP, Galzi JL, Devillers-Thiery A et al (1992) The functional architecture of the acetylcholine nicotinic receptor explored by affinity labelling and site-directed mutagenesis. Q Rev Biophys 25:395–432
85. Galzi JL, Changeux JP (1995) Neuronic nicotinic receptors: molecular organization and regulations. Neuropharmacology 34:563–582
86. Karlin A, Akabas MH (1995) Toward a structural basis for the function of nicotinic acetylcholine receptors and their cousins. Neuron 15:1231–1244
87. Bormann J, Hamill OP, Sakmann B (1987) Mechanism of anion permeation through channels gated by glycine and gamma-aminobutyric acid in mouse cultured spinal neurons. J Physiol (Lond) 385:243–286
88. Polenzani L, Woodward RM, Miledi R (1991) Expression of mammalian gamma-aminobutyric acid receptors with distinct pharmacology in *Xenopus oocytes*. Proc Natl Acad Sci USA 88:4318–4322
89. Kaupmann K, Huggel K, Heid J et al (1997) Expression cloning of $GABA_B$ receptors uncovers similarity to metabotropic glutamate receptor. Nature 386:239–246
90. Sieghart W (1995) Structure and pharmacology of gamma-aminobutyric acids A receptor subtypes. Pharmacol Rev 47:181–234
91. Grenningloh G, Gundelfinger E, Schmitt B et al (1987) Glycine vs GABA receptors. Nature 330:25–26
92. Grenningloh G, Pribilla I, Prior P et al (1990) Cloning and expression of the 58 kd beta subunit of the inhibitory glycine receptor. Neuron 4:963–970
93. Greferath U, Brandstatter H, Wassle H et al (1994) Differential expression of glycine receptor subunits in the retina of the rat: a study using immunohistochemistry and in situ hybridization. Vis Neurosci 11:721–729
94. Yadid G, Goldstein DS, Pacak K et al (1995) Functional alpha 3-glycine receptors in rat adrenal. Eur J Pharmacol 288:399–401
95. Miller GW, Schnellmann RG (1994) A putative cytoprotective receptor in the kidney: relation to the neuronal strychnine-sensitive glycine receptor. Life Sci 55:27–34
96. Ikejima K, Qu W, Stachlewitz RF et al (1997) Kupffer cells contain a glycine-gated chloride channel. Am J Physiol Gastrointest Liver Physiol 272:G1581–G1586
97. Meizel S (1997) Amino acid neurotransmitter receptor/chloride channels of mammalian sperm and the acrosome reaction. Biol Reprod 56:569–574
98. Bohlhalter S, Mohler H, Fritschy JM (1994) Inhibitory neurotransmission in rat spinal cord: co-localization of glycine- and $GABA_A$-receptors at GABAergic synaptic contacts demonstrated by triple immunofluoroscence staining. Brain Res 642:59–69
99. Furuyama T, Sato M, Sato K et al (1992) Co-expression of glycine receptor beta subunit and $GABA_A$ receptor gamma subunit mRNA in the rat dorsal root ganglion cells. Brain Res 12: 335–338
100. Todd AJ, Sullivan AC (1990) Light microscope study of the coexistence of GABA-like and glycine-like immunoreactivities in the spinal cord of the rat. J Comp Neurol 296:496–505
101. Olisen RW, Delorey TM, Gordey M et al (1999) GABA receptor function and epilepsy. Adv Neurol 79:499–510

102. Baulac S, Huberfeld G, Gourfinkel-An I et al (2001) First genetic evidence of GABA(A) receptor dysfunction in epilepsy: a mutation in the gamma2-subunit gene. Nat Genet 28: 46–48
103. Wallace RH, Marini C, Petrou S et al (2001) Mutant GABA(A) receptor gamma2-subunit in childhood absence epilepsy and febrile seizures. Nat Genet 28:49–52
104. Heiss NS, Poustka A (1997) Genomic structure of a novel chloride channel gene, CLIC2, in Xq28. Genomics 45:224–228
105. Landry D, Sullivan S, Nicolaides M et al (1993) Molecular cloning and characterization of p64, a chloride channel protein from kidney microsomes. J Biol Chem 268:14948–14955
106. Landry DW, Akabas MH, Redhead C et al (1989) Purification and reconstitution of chloride channels from kidney and trachea. Science 244:1469–1472
107. Edwards JC, Kapadia S (2000) Regulation of the bovine kidney microsomal chloride channel p64 by p59fyn, a Src family tyrosine kinase. J Biol Chem 275:31826–31832
108. Edwards JC, Tulk B, Schlesinger PH (1998) Functional expression of p64, an intracellular chloride channel protein. J Membr Biol 163:119–127
109. Ashley RH (2003) Challenging accepted ion channel biology: p64 and the CLIC family of putative intracellular anion channel proteins (review). Mol Membr Biol 20:1–11
110. Cromer BA, Morton CJ, Board PG et al (2002) From glutathione transferase to pore in a CLIC. Eur Biophys J 31:356–364
111. Littler DR, Harrop SJ, Goodchild SC et al (2010) The enigma of the CLIC proteins: ion channels, redox proteins, enzymes, scaffolding proteins? FEBS Lett 584:2093–2101
112. Elter A, Hartel A, Sieben C et al (2007) A plant homolog of animal chloride intracellular channels (CLICs) generates an ion conductance in heterologous systems. J Biol Chem 282: 8786–8792
113. Singh H, Ashley RH (2007) CLIC4 (p64H1) and its putative transmembrane domain form poorly selective, redox-regulated ion channels. Mol Membr Biol 24:41–52
114. Singh H, Ashley RH (2006) Redox regulation of CLIC1 by cysteine residues associated with the putative channel pore. Biophys J 90:1628–1638
115. Singh H, Cousin MA, Ashley RH (2007) Functional reconstitution of mammalian 'chloride intracellular channels' CLIC1, CLIC4 and CLIC5 reveals differential regulation by cytoskeletal actin. FEBS J 274:6306–6316
116. Hartzell HC, Qu Z, Yu K et al (2008) Molecular physiology of bestrophins: multifunctional membrane proteins linked to Best disease and other retinopathies. Physiol Rev 88:639–672
117. Kunzelmann K, Kongsuphol P, Aldehni F et al (2009) Bestrophin and TMEM16-Ca(2+) activated Cl(−) channels with different functions. Cell Calcium 46:233–241
118. Barro-Soria R, Aldehni F, Almaca J et al (2010) ER-localized bestrophin 1 activates Ca(2+)-dependent ion channels TMEM16A and SK4 possibly by acting as a counterion channel. Pflügers Arch. doi:10.1007/s0042400907450
119. Marmorstein LY, Wu J, McLaughlin P et al (2006) The light peak of the electroretinogram is dependent on voltage-gated calcium channels and antagonized by bestrophin (best-1). J Gen Physiol 127:577–589
120. Soroceanu L, Manning TJ, Sontheimer H (1999) Modulation of glioma cell migration and invasion using Cl(−) and K(+) ion channel blockers. J Neurosci 19:5942–5954
121. Olsen ML, Schade S, Lyons SA et al (2003) Expression of voltage-gated chloride channels in human glioma cells. J Neurosci 23:5572–5582
122. Alkhalil A, Cohn JV, Wagner MA et al (2004) Plasmodium falciparum likely encodes the principal anion channel on infected human erythrocytes. Blood 104:4279–4286
123. Kirk K, Horner HA, Elford BC et al (1994) Transport of diverse substrates into malaria-infected erythrocytes via a pathway showing functional characteristics of a chloride channel. J Biol Chem 269:3339–3347
124. Jentsch TJ, Maritzen T, Zdebik AA (2005) Chloride channel diseases resulting from impaired transepithelial transport or vesicular function. J Clin Invest 115:2039–2046

125. Rees MI, Lewis TM, Kwok JB et al (2002) Hyperekplexia associated with compound heterozygote mutations in the beta-subunit of the human inhibitory glycine receptor (GLRB). Hum Mol Genet 11:853–860
126. Zhou L, Chillag KL, Nigro MA (2002) Hyperekplexia: a treatable neurogenetic disease. Brain Dev 24:669–674
127. Shiang R, Ryan SG, Zhu YZ et al (1993) Mutations in the alpha 1 subunit of the inhibitory glycine receptor cause the dominant neurologic disorder, hyperekplexia. Nat Genet 5: 351–358
128. Rees MI, Andrew M, Jawad S et al (1994) Evidence for recessive as well as dominant forms of startle disease (hyperekplexia) caused by mutations in the alpha 1 subunit of the inhibitory glycine receptor. Hum Mol Genet 3:2175–2179
129. Steinmeyer K, Lorenz C, Pusch M et al (1994) Multimeric structure of ClC-1 chloride channel revealed by mutations in dominant myotonia congenita (Thomsen). EMBO J 13: 737–743
130. Mankodi A, Urbinati CR, Yuan QP et al (2001) Muscleblind localizes to nuclear foci of aberrant RNA in myotonic dystrophy types 1 and 2. Hum Mol Genet 10:2165–2170
131. Charlet BN, Savkur RS, Singh G et al (2002) Loss of the muscle-specific chloride channel in type 1 myotonic dystrophy due to misregulated alternative splicing. Mol Cell 10:45–53
132. Mankodi A, Takahashi MP, Jiang H et al (2002) Expanded CUG repeats trigger aberrant splicing of ClC-1 chloride channel pre-mRNA and hyperexcitability of skeletal muscle in myotonic dystrophy. Mol Cell 10:35–44
133. Haug K, Warnstedt M, Alekov AK et al (2003) Mutations in CLCN2 encoding a voltage-gated chloride channel are associated with idiopathic generalized epilepsies. Nat Genet 33: 527–532
134. Schlingmann KP, Konrad M, Jeck N et al (2004) Salt wasting and deafness resulting from mutations in two chloride channels. N Engl J Med 350:1314–1319
135. Birkenhager R, Otto E, Schurmann MJ et al (2001) Mutation of BSND causes Bartter syndrome with sensorineural deafness and kidney failure. Nat Genet 29:310–314
136. Lloyd SE, Pearce SH, Fisher SE et al (1996) A common molecular basis for three inherited kidney stone diseases. Nature 379:445–449
137. Fisher SE, Black GC, Lloyd SE et al (1994) Isolation and partial characterization of a chloride channel gene which is expressed in kidney and is a candidate for Dent's disease (an X-linked hereditary nephrolithiasis). Hum Mol Genet 3:2053–2059
138. Fisher SE, van Bakel I, Lloyd SE et al (1995) Cloning and characterization of CLCN5, the human kidney chloride channel gene implicated in Dent disease (an X-linked hereditary nephrolithiasis). Genomics 29:598–606
139. Cleiren E, Benichou O, Van Hul E et al (2001) Albers–Schonberg disease (autosomal dominant osteopetrosis, type II) results from mutations in the ClCN7 chloride channel gene. Hum Mol Genet 10:2861–2867
140. Kornak U, Kasper D, Bosl MR et al (2001) Loss of the ClC-7 chloride channel leads to osteopetrosis in mice and man. Cell 104:205–215
141. Riordan JR, Rommens JM, Kerem B et al (1989) Identification of the cystic fibrosis gene: cloning and characterization of complementary DNA. Science 245:1066–1073
142. Cohn JA, Friedman KJ, Noone PG et al (1998) Relation between mutations of the cystic fibrosis gene and idiopathic pancreatitis. N Engl J Med 339:653–658
143. Sharer N, Schwarz M, Malone G et al (1998) Mutations of the cystic fibrosis gene in patients with chronic pancreatitis. N Engl J Med 339:645–652
144. Weiss FU, Simon P, Bogdanova N et al (2005) Complete cystic fibrosis transmembrane conductance regulator gene sequencing in patients with idiopathic chronic pancreatitis and controls. Gut 54:1456–1460
145. Ninis VN, Kylync MO, Kandemir M et al (2003) High frequency of T9 and CFTR mutations in children with idiopathic bronchiectasis. J Med Genet 40:530–535
146. Bombieri C, Benetazzo M, Saccomani A et al (1998) Complete mutational screening of the CFTR gene in 120 patients with pulmonary disease. Hum Genet 103:718–722

147. Andrieux J, Audrezet MP, Frachon I et al (2002) Quantification of CFTR splice variants in adults with disseminated bronchiectasis, using the TaqMan fluorogenic detection system. Clin Genet 62:60–67
148. Casals T, De-Gracia J, Gallego M et al (2004) Bronchiectasis in adult patients: an expression of heterozygosity for CFTR gene mutations. Clin Genet 65:490–495
149. Chillon M, Casals T, Mercier B et al (1995) Mutations in the cystic fibrosis gene in patients with congenital absence of the vas deferens. N Engl J Med 332:1475–1480
150. Daudin M, Bieth E, Bujan L et al (2000) Congenital bilateral absence of the vas deferens: clinical characteristics, biological parameters, cystic fibrosis transmembrane conductance regulator gene mutations, and implications for genetic counseling. Fertil Steril 74: 1164–1174
151. Kaplan E, Shwachman H, Perlmutter AD et al (1968) Reproductive failure in males with cystic fibrosis. N Engl J Med 279:65–69
152. Augarten A, Yahav Y, Kerem BS et al (1994) Congenital bilateral absence of vas deferens in the absence of cystic fibrosis. Lancet 344:1473–1474
153. Sun H, Tsunenari T, Yau KW et al (2002) The vitelliform macular dystrophy protein defines a new family of chloride channels. Proc Natl Acad Sci USA 99:4008–4013
154. Petrukhin K, Koisti MJ, Bakall B et al (1998) Identification of the gene responsible for Best macular dystrophy. Nat Genet 19:241–247
155. Marquardt A, Stohr H, Passmore LA et al (1998) Mutations in a novel gene, VMD2, encoding a protein of unknown properties cause juvenile-onset vitelliform macular dystrophy (Best's disease). Hum Mol Genet 7:1517–1525
156. Allikmets R, Seddon JM, Bernstein PS et al (1999) Evaluation of the Best disease gene in patients with age-related macular degeneration and other maculopathies. Hum Genet 104: 449–453
157. Zhang JJ, Jacob TJ (1994) ATP-activated chloride channel inhibited by an antibody to P glycoprotein. Am J Physiol 267:C1095–C1102
158. Zhang JJ, Jacob TJ (1996) Volume regulation in the bovine lens and cataract. The involvement of chloride channels. J Clin Invest 97:971–978
159. Zhang JJ, Jacob TJ, Valverde MA et al (1994) Tamoxifen blocks chloride channels. A possible mechanism for cataract formation. J Clin Invest 94:1690–1697
160. Young MA, Tunstall MJ, Kistler J et al (2000) Blocking chloride channels in the rat lens: localized changes in tissue hydration support the existence of a circulating chloride flux. Invest Ophthalmol Visual Sci 41:3049–3055
161. Cossette P, Liu L, Brisebois K et al (2002) Mutation of GABRA1 in an autosomal dominant form of juvenile myoclonic epilepsy. Nat Genet 31:184–189
162. Harkin LA, Bowser DN, Dibbens LM et al (2002) Truncation of the GABA(A)-receptor gamma2 subunit in a family with generalized epilepsy with febrile seizures plus. Am J Hum Genet 70:530–536
163. Lappalainen J, Krupitsky E, Remizov M et al (2005) Association between alcoholism and gamma-amino butyric acid alpha2 receptor subtype in a Russian population, Alcohol. Clin Exp Res 29:493–498
164. Edenberg HJ, Dick DM, Xuei X et al (2004) Variations in GABRA2, encoding the alpha2 subunit of the GABA(A) receptor, are associated with alcohol dependence and with brain oscillations. Am J Hum Genet 74:705–714
165. Buhr A, Bianchi MT, Baur R et al (2002) Functional characterization of the new human GABA(A) receptor mutation beta3(R192H). Hum Genet 111:154–160
166. Greger R (1983) Chloride channel blockers. Methods Enzymol 191:793–810
167. Bretag AH (1987) Muscle chloride channels. Physiol Rev 67:618–724
168. Miller C, White MM (1984) Dimeric structure of single chloride channels from *Torpedo* Electroplax. Proct Natl Acad Sci USA 81:2772–2775
169. Cai Z, Scott-Ward TS, Li H et al (2004) Strategies to investigate the mechanism of action of CFTR modulators. J Cyst Fibros 3:141–147

170. Linsdell P (2006) Mechanism of chloride permeation in the cystic fibrosis transmembrane conductance regulator chloride channel. Exp Physiol 91:123–129
171. McDonough S, Davidson N, Lester HA et al (1994) Novel pore-lining residues in CFTR that govern permeation and open-channel block. Neuron 13:623–634
172. Linsdell P, Hanrahan JW (1996) Flickery block of single CFTR chloride channels by intracellular anions and osmolytes. Am J Physiol Cell Physiol 271:C628–C634
173. Sheppard DN, Robinson KA (1997) Mechanism of glibenclamide inhibition of cystic fibrosis transmembrane conductance regulator Cl^- channels expressed in a murine cell line. J Physiol (Lond) 503:333–346
174. Linsdell P (2005) Location of a common inhibitor binding site in the cytoplasmic vestibule of the cystic fibrosis transmembrane conductance regulator chloride channel pore. J Biol Chem 280:8945–8950
175. Linsdell P (2000) Inhibition of cystic fibrosis transmembrane conductance regulator chloride channel currents by arachidonic acid. Can J Physiol Pharm 78:490–499
176. Zhou JJ, Linsdell P (2007) Molecular mechanism of arachidonic acid inhibition of the CFTR chloride channel. Eur J Pharmacol 563:88–91
177. St. Aubin CN, Linsdell P (2006) Positive charges at the intracellular mouth of the pore regulate anion conduction in the CFTR chloride channel. J Gen Physiol 128:535–545
178. Ishihara H, Welsh MJ (1997) Block by MOPS reveals a conformation change in the CFTR pore produced by ATP hydrolysis. Am J Physiol Cell Physiol 273:C1278–C1289
179. Yamamoto D, Suzuki N (1987) Blockage of chloride channels by HEPES buffer. Proc R Soc Lond B Bio Sci 23:93–100
180. Kürz L, Wagner S, George AL et al (1997) Probing the major skeletal muscle chloride channel with Zn^{2+} and other sulfhydryl-reactive compounds. Pflügers Arch 433:357–363
181. Kürz LL, Klink H, Jacob I et al (1999) Identification of three cysteines as targets for the Zn^{2+} blockade of the human skeletal muscle chloride channel. J Biol Chem 274:11687–11692
182. Horenstein J, Akabas MH (1998) Location of a high affinity Zn^{2+} binding site in the channel of alpha1beta1 gamma-aminobutyric acid A receptors. Mol Pharmacol 53:870–877
183. Wooltorton JR, McDonald BJ, Moss SJ et al (1997) Identification of a Zn^{2+} binding site on the murine $GABA_A$ receptor complex: dependence on the second transmembrane domain of beta subunits. J Physiol (Lond) 505:633–640
184. Blaisdell CJ, Edmonds RD, Wang XT et al (2000) pH-regulated chloride secretion in fetal lung epithelia. Am J Physiol Lung Cell Mol Physiol 278:L1248–L1255
185. Chesnoy-Marchais D, Fritsch J (1994) Activation of hyperpolarization and atypical osmosensitivity of a Cl^- current in rat osteoblastic cells. J Membr Biol 140:173–188
186. Clark S, Jordt SE, Jentsch TJ et al (1998) Characterization of the hyperpolarization- activated chloride current in dissociated rat sympathetic neurons. J Physiol (Lond) 506:665–678
187. White MM, Aylwin M (1990) Niflumic and flufenamic acids are potent reversible blockers of Ca^{2+}-activated Cl^- channels in *Xenopus* oocytes. Mol Pharmacol 37:720–724
188. Tulk BM, Edwards JC (1998) Ncc27, a homolog of intracellular Cl^- channel p64, is expressed in brush border of renal proximal tubule. Am J Physiol Renal Physiol 274: F1140–F1149
189. Geck P, Pietrzyk C, Burckhardt BC et al (1980) Electrically silent cotransport of Na^+, K^+ and Cl^- in ehrlich cells. Biochim Biophys Acta 600:432–447
190. Ellory JC, Dunham PB, Logue PJ et al (1982) Anion dependent cation transport in erythrocytes. Philos Trans R Soc Lond B Biol Sci 299:483–495
191. Greger R (1985) Ion transport mechanisms in thick ascending limb of Henle's loop of mammalian nephron. Physiol Rev 65:760–797
192. Passow H (1986) Molecular aspects of band 3 protein-mediated anion transport across the red blood cell membrane. Rev Physiol Biochem Pharmacol 103:61–203

Index

S.P. Gupta (ed.), *Ion Channels and Their Inhibitors*,
DOI 10.1007/978-3-642-19922-6,